SPRINGER NATURE
Sustainable Development Goals Series

Connecting the Goals

Huadong Guo

Big Earth Data in Support of the Sustainable Development Goals (2022) - China

Science Press
Beijing

OPEN ACCESS

Springer

Sustainable Development Goals Series

The **Sustainable Development Goals Series** is Springer Nature's inaugural cross-imprint book series that addresses and supports the United Nations' seventeen Sustainable Development Goals. The series fosters comprehensive research focused on these global targets and endeavours to address some of society's greatest grand challenges. The SDGs are inherently multidisciplinary, and they bring people working across different fields together and working towards a common goal. In this spirit, the Sustainable Development Goals series is the first at Springer Nature to publish books under both the Springer and Palgrave Macmillan imprints, bringing the strengths of our imprints together.

The Sustainable Development Goals Series is organized into eighteen subseries: one subseries based around each of the seventeen respective Sustainable Development Goals, and an eighteenth subseries, "Connecting the Goals", which serves as a home for volumes addressing multiple goals or studying the SDGs as a whole. Each subseries is guided by an expert Subseries Advisor with years or decades of experience studying and addressing core components of their respective Goal.

The SDG Series has a remit as broad as the SDGs themselves, and contributions are welcome from scientists, academics, policymakers, and researchers working in fields related to any of the seventeen goals. If you are interested in contributing a monograph or curated volume to the series, please contact the Publishers: Zachary Romano [Springer; zachary.romano@springer.com] and Rachael Ballard [Palgrave Macmillan; rachael.ballard@palgrave.com].

Huadong Guo

Big Earth Data in Support of the Sustainable Development Goals (2022) - China

Science Press
Beijing

Springer

Huadong Guo
International Research Center of Big
Data for Sustainable Development
Goals (CBAS)
Chinese Academy of Sciences
Aerospace Information Research
Institute
Beijing, China

ISSN 2523-3084 ISSN 2523-3092 (electronic)
Sustainable Development Goals Series
ISBN 978-981-97-4230-1 ISBN 978-981-97-4231-8 (eBook)
https://doi.org/10.1007/978-981-97-4231-8

Jointly published with Science Press
The print edition is not for sale in China mainland. Customers from China mainland please order the print book from: Science Press.
ISBN of the Co-Publisher's edition: 978-7-03-074647-4

This Springer imprint is published by the registered company Springer Nature Singapore Pte Ltd.
The registered company address is: 152 Beach Road, #21-01/04 Gateway East, Singapore 189721, Singapore

Editorial Board

Principle Authors (in alphabetical order of last name):

Min Cao	Min Chen	Yu Chen	Xuefeng Cui
Jinwei Dong	Shibo Fang	Huadong Guo	Licheng Guo
Haixu He	Xiyong Hou	Chunlin Huang	Jinxia Huang
Lei Huang	Liqiang Ji	Li Jia	Mingming Jia
Min Jiang	Yunzhong Jiang	Xiangbin Kong	Cheng Li
Dong Li	Mengqian Li	Xiaojie Li	Xiaosong Li
Zengyuan Li	Dong Liang	Congtian Lin	Gang Liu
Nanjiang Liu	Saimiao Liu	Wenliang Liu	Xiaojie Liu
Xin Liu	Yafei Liu	Zhe Liu	Jing Lu
Linlin Lu	Shanlong Lu	Yingcheng Lu	Lei Luo
Caihong Ma	Zhenzhen Ma	Yong Pang	Hailong Piao
Haibao Ren	Xiaoli Shen	Yusheng Shi	Xiaoyu Song
Zhongchang Sun	Yixian Tang	Yu Tian	Chao Wang
Futao Wang	Hao Wang	Litao Wang	Mingquan Wu
Liwei Xie	Jinyong Xu	Dongmei Yan	Jining Yan
Shiling Yang	Qingzhen Yao	Huichun Ye	Jinjun You
Yongqiang Yu	Fangfang Zhang	Hailong Zhang	Li Zhang
Wen Zhang	Yan Zhang	Yusi Zhang	Zhonghao Zhang
Yan Zhou	Zhengxi Zhou	Lanwei Zhu	Lijun Zuo

Foreword

Transforming Our World: The 2030 Agenda for Sustainable Development (hereinafter referred to as the 2030 Agenda) draws a grand blueprint for global sustainable development from three dimensions: the economy, society, and the environment. However, problems such as lack of data, unbalanced development, and mutual constraints between goals pose major challenges to the implementation of the United Nations (UN) Sustainable Development Goals (SDGs). At the same time, the impact of climate change has intensified, the COVID-19 pandemic has been repeatedly prolonged, and regional tensions have intensified, which have greatly increased the difficulty of implementing and realizing the 2030 Agenda. Therefore, in 2021, President Xi Jinping proposed a global development initiative at the 76th session of the UN General Assembly to accelerate the implementation of the 2030 Agenda and promote stronger, greener, and healthier development.

Also in 2021, the Sustainable Development Goals Report clearly pointed out that data are a resource for rebuilding and accelerating the realization of the SDGs, and it is more important than ever to obtain and master timely, high-quality data. To this end, the Secretary-General of the UN proposed a data strategy to promote the acquisition of more relevant, disaggregated, timely data to track, predict, and accelerate the implementation of the SDGs so that we can transform data and information into insights, and in turn transform and optimize the decision-making process.

The international comparability and availability of data have improved as digitization has accelerated across the globe, but gaps in geographic coverage and timeliness of SDG data remain across sectors, and innovative approaches are urgently needed to fill these gaps. One such innovation is Big Earth Data technology, which integrates Earth science, information science, and space technology. It has macroscopic, dynamic monitoring capabilities and can greatly improve data acquisition, providing important support for the realization of the SDGs.

On September 22, 2020, President Xi Jinping announced at the 75th session of the UN General Assembly that China would establish the International Research Center of Big Data for Sustainable Development Goals (CBAS). On September 6, 2021, CBAS was officially established as the world's first international scientific research institution dedicated to using big data to serve the 2030 Agenda. Since its establishment, the center has provided SDG indicator assessments to the world by researching and

building a big data platform for the SDGs, launching and operating a sustainable development science satellite (SDGSAT-1), and carrying out research on technical methods of Big Earth Data for SDG monitoring and evaluation to actively contribute to the implementation of the 2030 Agenda.

From 2019 to 2021, the Chinese Academy of Sciences (CAS) took the lead in compiling the annual report on "Big Earth Data in Support of the Sustainable Development Goals" for three consecutive years, accumulatively contributing 207 case studies on monitoring and evaluating SDGs, including 178 data products, 103 methods and models, and 154 decision support guidelines or action items, showing China's exploration and practice of Big Earth Data technology to support national sustainable development.

"Big Earth Data in Support of the Sustainable Development Goals (2022)—China" continues to focus on the seven SDGs and multi-indicator intersections of Zero Hunger, Clean Water and Sanitation, Sustainable Cities and Communities, Climate Action, Life Below Water, and Life on Land. This report presents in-depth research on interrelationships, trade-offs, and coordination roles for measuring SDG indicators, including the prospect of expanding the goal of affordable clean energy (SDG 7) and comprehensive regional research on the SDGs according to regional characteristics. On the basis of the numerous studies presented in this report, it concludes with recommendations to heed the changes in China's ecological environment, integrate and innovate on the basis of four-year case results, conduct a comprehensive assessment of 56 environmental indicators, and monitor China's progress on the SDGs.

This report organizes more than 170 scientific research personnel from more than 40 units in scientific research institutes and universities. It brings together the latest research results in the field of big data for sustainable development. The leaders and agencies of CAS have given great support, the comrades on the writing team have worked hard, and I would like to express my heartfelt thanks.

Huadong Guo (Beijing, China)
Director-General of the International
Research Center of Big Data for
Sustainable Development Goals

Member of the 10-Member group
of the United Nations Sustainable
Development Goals Technology Facilitation Mechanism
(2018–2021)

Executive Summary

This report presents 39 case studies that utilize the strengths and characteristics of big data to address seven Sustainable Development Goals (SDGs): SDG 2 Zero Hunger, SDG 6 Clean Water and Sanitation, SDG 7 Affordable and Clean Energy, SDG 11 Sustainable Cities and Communities, SDG 13 Climate Action, SDG 14 Life Below Water, and SDG 15 Life on Land. The case studies focus on 20 targets of these seven SDGs and the intersection and synthesis of multiple SDG indicators. The research in this report demonstrates monitoring and assessment results at two scales: national and representative areas of China. The data products, methods, models, and decision support guidelines presented in the report showcase innovative practices of big data to support the implementation of the SDGs and provide scientific references for decision-making departments.

Regarding SDG 2, Zero Hunger, this report focuses on improving agricultural productivity, sustainable food production, and halving food waste. The case studies identified the spatiotemporal change in soil organic carbon density of cropland, produced a dataset of carbon emissions for cropping systems in counties at the national scale, monitored soil organic carbon, and proposed a saline-alkali land identification and classification model for Northeast China up to 35 years. Based on the analysis of the above data, it was found that in Western Jilin, one of the world's three largest saline-alkali lands, restoration projects including "Vegetation of Saline and Alkali Land" and "Major Project in West Jilin Province" have reduced the area of saline-alkali land and promoted grain production. From 2015 to 2020, the soil organic carbon density of cropland increased by 3.4%. Agricultural carbon emissions per unit value have declined over the past decade, with high carbon emissions per unit area in the Yangtze-Huai River Basin, Jianghan Plain, and Sichuan Basin.

For SDG 6, Clean Water and Sanitation, this report presents research results on drinking water safety, environmental water quality, water use efficiency, water pressure, and integrated water resources management (IWRM) at the provincial level in China. The case studies include an improved comprehensive evaluation of drinking water source quality, a crop water use efficiency assessment based on multi-source data combined with crop growth data, a set of quantitative assessment tools for water resources management at the provincial level, an SDG 6 composite index, datasets on the proportion of water bodies with good water quality in China (excluding Hong

Kong, Macao, and Taiwan) in 2015 and 2020, the water use efficiency of China's three major grain crops from 2010 to 2019, and the level of water stress in China from 2010 to 2020. Last, China's provincial progress toward SDG 6 was evaluated. The results are of great value for understanding the provincial implementation of SDG 6, identifying problems and gaps, and informing strategies for accelerating the measurement of SDG 6 indicators.

In terms of SDG 7, Affordable and Clean Energy, the case studies in this report utilized Big Earth Data technology to examine spatiotemporal distribution changes in solar power stations in China, as well as the spatiotemporal monitoring and analysis of high energy-consuming industries. Datasets on the distribution of solar power stations and high energy-consuming industrial sites were generated, providing information on their spatiotemporal changes. These case studies reflect, from different perspectives, the effectiveness of China's photovoltaics (PV) power station construction and high energy-consumption industrial infrastructure in recent years.

In terms of SDG 11, Sustainable Cities and Communities, this report focuses on four themes: monitoring and evaluating the urbanization process, urban disaster response, the urban environment, and comprehensive assessments of SDG 11 indicators. The case studies developed several data products, including datasets on urban built-up areas in prefecture-level cities, the annual average deformation rate of the national surface, SDG 11.5 indicator values at the prefectural/municipal level, China's $PM_{2.5}$ population exposure intensity index, $PM_{2.5}$ population-weighted average annual exposure concentration, and an average life expectancy indicator dataset of representative cities in China. These products together can calculate and assess five SDG 11 indicators. Based on analysis of the above data, the case studies present several findings. It was found that from 2015 to 2020, the overall land use efficiency of Chinese cities above the prefecture level was low, and there were significant differences in land use efficiency at different geographic units; the implementation of the Sendai Framework has achieved some success in China, and the impacts of natural disasters in China are generally light and continue the trend of mitigation; from 2000 to 2020, China's overall $PM_{2.5}$ population-weighted average annual exposure concentration peaked in 2013 and then showed a rapidly declining trend; and the average life expectancy in China's megacities, supercities, and cities in the eastern coastal areas, has already reached the level of middle- and high-income countries; however, there are apparent differences in the health level of populations in different regions and city sizes.

The research in this report produced several more datasets to calculate and evaluate four indicators of SDG 13, Climate Action (SDG 13.1.1, SDG 13.1.2, SDG 13.1.3, SDG 13.2.2). The case studies focus on strengthening disaster resistance and climate change response, creating data products on soil moisture content, disaster prevention and mitigation policies, and methane (CH_4) emission. In view of the serious waterlogging in China in 2021, one case study compared the occurrence area and degree of waterlogging in China from July to December 2021 with that in 2016, 2017, 2018, and 2020, providing a scientific basis for disaster prevention and reduction of waterlogging. Another case study recognized that China has established a complete national disaster reduction system in accordance with the Sendai

Framework, with 100% of provincial governments adopting and implementing local disaster risk reduction systems. Another case study found that from 2015 to 2020, China's annual average comprehensive CH_4 emissions were 60.46 Tg, with a trend of decreasing first and then increasing. Energy activity, ruminants, and rice were the three main sources of emissions.

Regarding SDG 14, Life Below Water, this report focuses on reducing marine pollution (SDG 14.1), protecting marine and coastal ecosystems (SDG 14.2), and conserving at least 10% of coastal and marine areas (SDG 14.5). Seven case studies produced and applied spatial datasets to SDG 14, including field observations of nutrient concentrations in the coastal waters of Eastern China from 1978 to 2019, spatiotemporal datasets of green tide biomass in the Yellow Sea of China, 10 m resolution datasets on the spatial distribution of China's coastal tidal flats in 2015 and 2020, harmful algal bloom (red tide) event dataset in the coastal waters of the East China Sea from 1933 to 2017, aggregated typhoon protection values of coastal wetlands in China from 2010 to 2020, remote sensing monitoring data on the development and utilization of spatial resources in China's coastal zone from 2000 to 2020, products related to China's coastal reclamation (returning enclosures to sea and wetlands) from 2010 to 2020, and corresponding analytical methods, models, and decision support guidelines for supporting applications. These research results reflect the effectiveness of China's implementation of marine scientific management in recent years from different aspects.

Regarding SDG 15, Life on Land, this report focuses on four targets: ecosystem conservation, restoration, and sustainable use (SDG 15.1); land degradation and restoration (SDG 15.3); halting the loss of biodiversity (SDG 15.5); and the prevention of invasion of exotic species (SDG 15.8). The case studies for SDG 15 produced land cover and vegetation cover products in areas protected by China's natural forest resources protection project (Tianbao Project) from 2000 to 2020. This report also presents an accurate biodiversity monitoring system using big data to estimate the population size and spatial distribution of woody species in Qianjiangyuan National Park. Three indicators were proposed to assess the prevention and control effects of ten invasive agricultural pests and their potential damage levels in China, along with their potential levels of harm, and to predict their potential distribution. The findings indicate that the Tianbao Project has effectively protected and restored forest resources in conservation areas. Another case study found that the degradation of black soil in Northeast China is relatively small, but it is urgent to take effective measures to carry out scientific protection. Another proposed that specific conservation objectives and strategies can be formulated for different species, especially rare and endangered species and endemic species, laying the foundation for the precise management and conservation of the national park. These research outcomes can provide data and decision-making support for the achievement of SDG 15 in China and also serve as a demonstration and reference for other countries.

Regarding interactions among the SDGs and integrated evaluations, analysis was carried out on synergistic and trade-off relationships among the SDGs at the provincial scale in China. The findings show that in most

provincial administrative regions, SDG 6 and SDG 15 are more susceptible to trade-offs from other SDGs. Of all these regions, relationships of 27% of the trade-off indicator pairs have changed to synergistic ones, and about another 18% of the trade-off indicator pairs have seen their trade-off intensity mitigated. Through a correlation analysis of long-term time-series data of food–water–air quality in Northeast China based on Big Earth Data, it was found that the trade-off between food production (SDG 2) and water security (SDG 6) is gradually easing. Through the integrated evaluation of the transportation industry in China, it shows that China performed well in the transportation facility target (SDG 9.1) from 2000 to 2020. The findings of the SDG regional integrated evaluation on typical provinces and cities in China show that since 2015, Hainan Province has made great progress in developing an "ecological civilization", with high scores on SDG 15 and significant improvement in SDG 2 and SDG 11. Many of the 70 indicators evaluated in Lincang, Yunnan Province, saw progress made or were close to the target. The sustainable development index of ecotourism carrying capacity in the Lijiang River Basin of Guilin, Guangxi Province, rose from 0.457 in 2010 to 0.711 in 2020. The above analytical results can inform efforts in Chinese regions with different characteristics in prioritizing development goals and mitigating the SDG indicator trade-offs that exist in development.

Contents

Acronyms

AD	Activity Density
AOD	Aerosol Optical Depth
AWU	Agricultural Water Use
BCELoss	Binary Cross-Entropy Loss Function
BPC	Built-up Area Per Capita
BRI	Belt and Road Initiative
CAF	Chinese Academy of Forestry
CAM4	Community Atmospheric Model 4.0
CAS	Chinese Academy of Sciences
CASEarth	Big Earth Data Science Engineering Program
CCDC	Continuous Change Detection and Classification
CH_4	Methane
CMIP6	Coupled Model Intercomparison Project Phase 6
COD	Chemical Oxygen Demand
CSP	Concentrated Solar Power
CSs	Coherent Scatterers
CTERN	Chinese Terrain Ecosystem Research Network
CZI	Coastal Zone Imager
DBH	Diameter at Breast Height
DEM	Digital Elevation Model
DIN	Dissolved Inorganic Nitrogen
EC	Electrical Conductivity
ECC	Ecotourism Carrying Capacity
ECHO	Ecological, Hydrological, Economical, and Energy
EDGS	Equivalent Density of Groundwater Stations
EF	Emission Factor
EF-LUE	Evaporative Fraction Light Use Efficiency
ENM	Ecological Niche Model
ESD	Enhanced Spectral Diversity
ESI	Enhanced Salinity Index
ET	Evapotranspiration
ETM+	Enhanced Thematic Mapper Plus
EVS	Explained Variance Score
FAO	Food and Agriculture Organization
fAPAR	Fraction of Absorbed Photosynthetically Active Radiation
FLW	Food Loss and Waste

FVC	Fractional Vegetation Coverage
GDP	Gross Domestic Product
GEE	Google Earth Engine
GEOHAB	Global Ecology and Oceanography of Harmful Algal Blooms
GFED	Global Fire Emissions Database
GIS	Geographic Information System
GPCP	Global Precipitation Climatology Project
GPM	Global Precipitation Measurement
GPP	Gross Primary Production
GPWv4	Gridded Population of the World Version 4
GRACE	Gravity Recovery and Climate Experiment
GRP	Gross Regional Product
GULUC	Global Urban Land Use/Cover
HABs	Harmful Algal Blooms
HDI	Human Development Index
IGSNRR	Institute of Geographic Sciences and Natural Resources Research
IMAGE-GNM	Integrated Model to Assess the Global Environment-Global Nutrient Model
InSAR	Interferometric Synthetic Aperture Radar
IPCC	Intergovernmental Panel on Climate Change
IWRM	Integrated water Resources Management
LASSO	Least Absolute Shrinkage and Selection Operator
LASSO-LARS	Least Absolute Shrinkage and Selection Operator-Least Angle Regression
LASSO Regression	Least Absolute Shrinkage and Selection Operator Regression
LC	Land Cover
LCR	Land Consumption Rate
LCRPGR	Ratio of Land Consumption Rate to Population Growth Rate
LEB	Life Expectancy at Birth
LiDAR	Light Detection and Ranging
LightGBM	Light Gradient Boosting Machine
LMDI	Logarithmic Mean Divisia Index
LOICZ	Land-Ocean Interactions in the Coastal Zone
LOOCV	Leave-One-Out Cross-Validation
LUCC	Land Use/Cover Change
MAE	Mean Absolute Error
MAPE	Mean Absolute Percentage Error
MCI	Multiple Cropping Index
MDGs	Millennium Development Goals
MEIC	Multi-resolution Emission Inventory for China
MFA	Material Flow Analysis
MIROC	Model for Interdisciplinary Research on Climate
mNDWI	Modified Normalized Difference Water Index
MODIS	Moderate-Resolution Imaging Spectroradiometer
MSE	Mean Squared Error

MSI	Multi-Spectral Instrument
MSIC	Maximum Spectral Index Composite
MSPA	Morphological Spatial Pattern Analysis
NASA	National Aeronautics and Space Administration
NDVI	Normalized Difference Vegetation Index
NFPP	Nature Forest Protection Project
NPP	Net Primary Productivity
NSIDC	National Snow and Ice Data Center
NUA	New Urban Agenda
PFTZ	Pilot Free Trade Zone
PGR	Population Growth Rate
PM	Particulate Matter
POI	Point of Interest
PV	Photovoltaics
RCPs	Representative Concentration Pathways
RF	Random Forest
RMSE	Root mean Squared Error
RMSLE	Root mean Squared Logarithmic Error
RUSLE	Revised Universal Soil Loss Equation
SAI	Scaled Algae Index
SDGs	Sustainable Development Goals
SDSN	Sustainable Development Solutions Network
SMAP	Soil Moisture Active and Passive
SSPs	Shared Socio-Economic Pathways
SWA	Surface Water Area
SWIR	Short-Wavelength Infrared
TM	Thematic Mapper
TM5-FASST	TM5-FAst Scenario Screening Tool
TOC	Total Organic Carbon
TWS	Terrestrial Water Storage
UNEP	United Nations Environment Programme
USDA	United States Department of Agriculture
USGS	United States Geological Survey
VB	Virtual Baseline
VIIRS	Visible Infrared Imaging Radiometer Suite
VPD	Vapor Pressure Deficit
WHO	World Health Organization
WTO	World Trade Organization
WUE	Water Use Efficiency

1 Introduction

The 17 Sustainable Development Goals (SDGs) adopted by the United Nations (UN) as part of the 2030 Agenda constitute a global framework for achieving sustainable development. They have become a strategic priority and the focus of action for countries worldwide. However, almost halfway into the 2030 Agenda process, its implementation has been seriously hindered by climate change and the COVID-19 pandemic, with global progress in individual goals even facing setbacks. The goals will not be achieved by 2030 unless their implementation is accelerated. In 2021, about one-tenth of the world's population went hungry; more than three billion people had health risks due to scarce data on the water quality of rivers, lakes, and groundwater; globally, 733 million people still lacked access to electricity; cities were hard hit by the COVID-19 pandemic; four key climate change indicators—global greenhouse gas concentrations, sea-level rise, ocean heat, and ocean acidification—hit record highs; increasing ocean acidification, eutrophication, and plastic pollution put the livelihoods of billions of people at risk; and continuing global deforestation, land and ecosystem degradation, and the loss of biodiversity posed major threats to human survival and sustainable development (UN 2022; Sachs et al. 2022).

Science, technology, and innovation can help address these major challenges, primarily to support assessment at national and local scales and inform policymaking by enhancing data capacity for SDG monitoring and evaluation. The Sustainable Development Goals Report 2022 points out that the pandemic has delayed the development of new national statistical plans worldwide, and there are still considerable gaps in the geographical coverage and timeliness of global data on indicators (UN 2022). Meanwhile, the current indicator data are primarily of coarse-grained statistical values, with the time resolution mostly being "annual" and the spatial resolution mostly "national", incapable of disaggregation by geographical location, population distribution, and environmental differences, which is crucial to thoroughly assessing the regional differences in SDG progress and identifying those lagging. Thus, they are not enough to effectively inform subnational government decision-making. According to estimates from the Organisation for Economic Co-operation and Development, 105 out of the 169 SDG targets will be challenging to achieve without sufficiently engaging subnational governments.[1] Many are environmental targets sensitive to spatiotemporal changes among these targets.

As the core of digital technology, big data has become an important engine of digital transformation across societies. Big Earth Data, a key part of big data, mainly composed of

[1] OECD. The Short and Winding Road to 2030: Measuring Distance to the SDG Targets. https://www.oecd.org/wise/theshort-and-winding-road-to-2030-af4b630d-en.htm. 5 June 2023.

H. Guo, *Big Earth Data in Support of the Sustainable Development Goals (2022) - China*, Sustainable Development Goals Series, https://doi.org/10.1007/978-981-97-4231-8_1

Earth observation and geospatial data, has the advantages of easy acquisition, timely updates, more objective results, and higher resolution. Moreover, it covers different spatial scales and geographical locations free from administrative fragmentation, allowing a more accurate assessment of SDG indicator progress and prompt detection of problems. In addition, its role in analyzing the complex interactions and co-evolution between nature and social systems will contribute to the overall understanding and achievement of the SDGs.

The seven SDGs of Zero Hunger (SDG 2), Clean Water and Sanitation (SDG 6), Affordable and Clean Energy (SDG 7), Sustainable Cities and Communities (SDG 11), Climate Action (SDG 14), Life Below Water (SDG 14), and Life on Land (SDG 15) are closely related to Earth's surface environments and human activity, and can be directly measured and evaluated by using Big Earth Data. With its interdisciplinary strengths, CAS has gathered a wide variety of Big Earth Data, including satellite remote sensing images, geospatial data, social media data, and statistical data for these seven SDGs. CAS has developed innovative technologies and methods for big data processing and analysis based on cloud computing, such as the production of global public data products, the monitoring and evaluation of SDG indicators at multiple scales, and multi-indicator trade-off-and-synergy analysis, to provide data, methods, and information for SDG-related progress assessment, multidisciplinary research, and multilevel decision-making.

The reports on Big Earth Data in Support of the Sustainable Development Goals have been released annually since 2019. In terms of filling the data gap, the reports provide high-quality data products previously lacking for monitoring SDG indicators, for example, the dataset on the prevalence of stunting among children under five in China. They also provide additional background and analytical data for a deeper understanding of the progress and drivers for indicators. This includes long-term time-series data products on global land use classification. In terms of methods and models, they offer new ways for more timely and detailed assessment and prediction of SDG indicators, such as a high-precision inversion model of global crop intensity and a rapid extraction method for global urban impervious surfaces. They also present scientific evidence for decision support, including the tracking and assessment of China's land degradation neutrality and its contribution to the world, and the assessment of the dynamic change in water bodies in Ramsar sites, which can inform policymaking on improving the global synergy and comparability of indicators and addressing cross-border sustainable development issues. In 2022, in the context of climate change, the report adds a chapter that looks at SDG 7, Affordable and Clean Energy, and its monitoring and assessment based on Big Earth Data, and explores the interactions between climate change and food systems, the carbon sequestration effect of desertification control, and the change in the marine physical environment under global warming.

The 2022 report focuses on updates and extensions, new methodologies and indicators, the tracking and evaluation of SDG implementation, the study of interactions among multiple SDGs, and coordinated development in light of those interactions. Based on the datasets from the 2019–2022 reports, with reference to the explicit thresholds for SDGs and their quantitative targets defined by UN agencies and international organizations, this year's report assesses China's progress in 56 environmental sustainable development indicators between 2010 and 2021 (UNEP 2021) (Fig. 1.1). Some quantitative findings on the progress include exploratory results of applying critical big data processing, analytics, and other innovative methods.

In summary, by the end of 2021, China's environmental indicators had improved substantially compared with those in 2015 (the starting year of the 2030 Agenda). Approaching the midpoint of 2030, nearly half of the 56 assessed environmental indicators have been met ahead of schedule, laying a good foundation for achieving all SDGs by 2030 (Guo 2022). The results show that between 2010 and 2015, 38 indicators improved continuously, while five

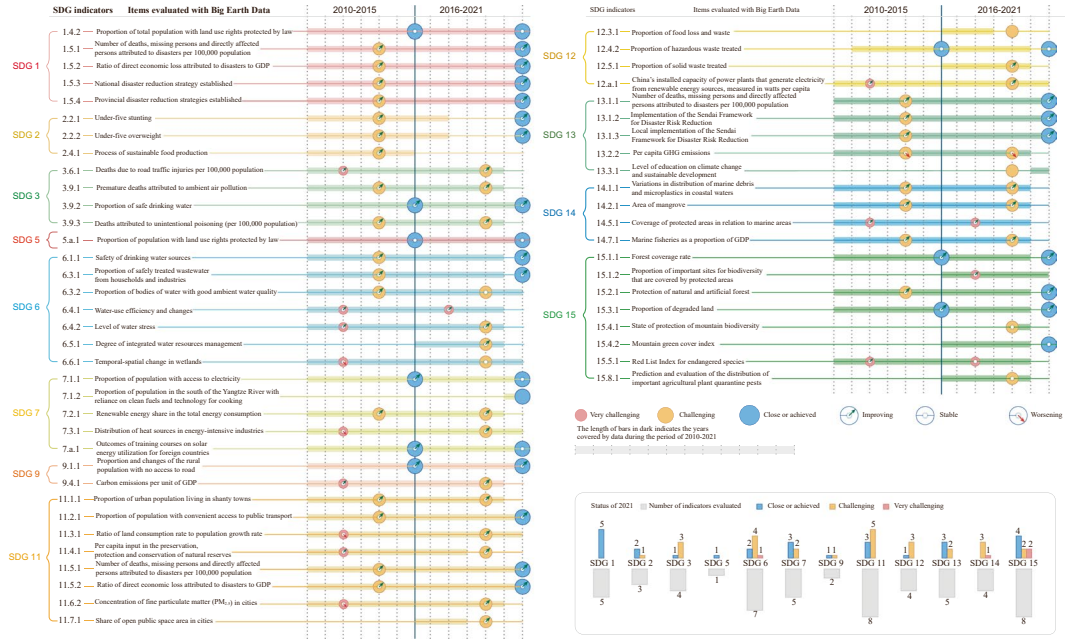

Fig. 1.1 China's progress on the SDGs, evaluated using Big Earth Data

deteriorated. Between 2016 and 2021, 40 indicators improved continuously. In 2015, nine indicators were close or achieved; by 2021, that number had risen to 26. Among all the indicators assessed, China stands out in disaster prevention and mitigation, safe drinking water, renewable energy, road traffic, and forest protection, but needs to do more regarding greenhouse gas emissions and biodiversity protection.

The book is divided into chapters. This chapter introduces the report, Chaps. 2–8 provide examples of using Big Earth Data to measure and monitor the progress of the seven SDGs, Chap. 9 provides new insights into the interactions among the SDGs and integrated evaluations, and Chap. 10 summarizes the report and future prospects.

References

Guo HD (2022) Big Earth Data in support of the Sustainable Development Goals (2021): China. Science Press and EDP Sciences, Beijing

Sachs J, Lafortune G, Kroll C, et al (2022) From crisis to sustainable development: the SDGs as roadmap to 2030 and beyond. Sustainable development report 2022. Cambridge University Press, Cambridge. https://s3.amazonaws.com/sustainabledevelopment.report/2022/2022-sustainable-development-report.pdf. 2 June 2022

UN (2022) The Sustainable Development Goals Report 2022. UN, New York. https://unstats.un.org/sdgs/report/2022. 7 July 2022

UNEP (2021) Measuring progress: environment and SDGs. https://www.unep.org/resources/publication/measuring-progress-environmentand-sdgs.

SDG 2 Zero Hunger

2

2.1 Background

The goal of Zero Hunger is the foundation for sustainable development. Currently, global progress on SDG 2 has deviated from its original trajectory and remains significantly short of being achieved. After five consecutive years of stabilization, the global proportion of hungry people increased from 8.4 to 10.4% in 2020 alone (FAO 2021). Undernutrition in all forms remains a challenge, with malnutrition rates rising from 8.0% in 2019 to 9.8% in 2021. The increasingly frequent and intensifying regional conflicts, climate change, and the slowdown in economic development as three major driving factors are still accelerating global food insecurity (FAO et al. 2022). Furthermore, food systems are threatening global water resources, biodiversity, and critical ecosystems due to large-scale and high-intensity resource and environmental depletion and exploitation.

In September 2021, the UN convened the global Food Systems Summit with an objective of elevating the global consensus on the significance of food system transformation and clarifying that it will contribute to achieving the SDGs by promoting human health and improving the environment of the planet. The UN Secretary-General stated in his address to the summit that food system transformation will be critical in facilitating the global recovery from the pandemic. The five action tracks considered necessary for transformation are ensuring access to safe and nutritious food for all, shifting to sustainable consumption patterns, promoting production with a positive impact on nature, promoting equitable livelihoods, and developing resilience to vulnerabilities, shocks, and stresses, with innovation being the critical lever for change. As an important area of innovation, improving agricultural productivity, sustainable food production, and halving food waste serves as an effective way to secure nutritional access and promote positive impacts on nature, which is essential to mitigate the risk of hunger and achieve global food security.

In previous years, this report has presented long-term time-series spatiotemporal analysis and related pathway analysis at the national scale in China for child growth stunting, the sustainable and intensive utilization of arable land, and sustainable food production in the 2019–2021 reports using Big Earth Data technology. For the 2022 report, this chapter will continue to conduct case studies from the directions of increasing agricultural productivity and sustainable food production, focusing on two specific goals, SDG 2.3 and SDG 2.4, while taking into account the specific goal of halving food waste (SDG 12.3), to support the assessment of progress toward China's Zero Hunger goal.

H. Guo, *Big Earth Data in Support of the Sustainable Development Goals (2022) - China*,
Sustainable Development Goals Series, https://doi.org/10.1007/978-981-97-4231-8_2

2.2 Main Contributions

This chapter presents the monitoring and assessment results for SDG 2 indicators via five case studies around three specific targets that contributed to China's achievements in data products, methods and models, and decision support (Table 2.1).

2.3 Case Studies

2.3.1 Monitoring and Assessing Saline-Alkali Land Improvement and Utilization in Western Jilin Province

Target: SDG 2.3: By 2030, double the agricultural productivity and incomes of small-scale food producers, in particular women, indigenous peoples, family farmers, pastoralists, and fishers, including through secure and equal access to land, other productive resources and inputs, knowledge, financial services, markets, and opportunities for value addition and non-farm employment.

2.3.1.1 Background

Soil salinization is a global issue that hinders the sustainable development of agriculture and rural economies and is a major factor affecting agricultural development. One of the three regions with the most saline-alkali land worldwide is located in the western part of Jilin Province, which accounts for 19% of the total area of black soil in Northeast China. Moreover, over 80% of the saline-alkali land in the black soil region is classified as an area for governance (Zhang et al. 2010). Analyzing the distribution and changes in soil salinization grades over time can provide essential data for studying the causes of soil salinization and evaluating the effectiveness of improvement programs.

2.3.1.2 Data

- Landsat-5 thematic mapper images from 1985, 1990, 1995, 2000, 2005, and 2010, and Landsat-8 OLI images from 2015 and 2020.
- Land use data from 1985, 2000, and 2020.
- Digital elevation model (DEM), vector data of administrative divisions.
- Field survey sample data, industry sector statistics, and monitoring data.

2.3.1.3 Methods

The methods used in the studies mentioned include the use of remote sensing data from Landsat TM, enhanced thematic mapper plus (ETM+), OLI, and other satellite series to assess soil salinity dynamics in different regions over time. The studies also utilized cloud platforms for big data processing and integrated classification algorithms and machine learning models for recognizing and classifying soil salinization.

In a study by Bannari and Al-Ali (2020), Landsat TM, ETM+, and OLI data were used to assess the impacts of climate change on soil salinity dynamics in arid landscapes in Kuwait from 1987 to 2017. Tran et al. (2019) used a spatial regression algorithm and an enhanced salinity index (ESI) based on Landsat time-series images from 1989 to 2018 to explore the salinity dynamics of the Mekong Delta.

In a study focusing on the western part of Northeast China, remote sensing images from Landsat satellites were used as data sources for recognizing and classifying soil salinization. Field survey data were combined with the remote sensing data, and the random forest (RF) method was used for classification and result verification. The overall classification accuracy was reported as 91%. The soil EC inversion model was established using field survey sampling data and satellite remote sensing imagery from different years (Li et al. 2022; Dong et al. 2021). The degree of soil salinization was graded based on the United States Department of Agriculture (USDA) standard (Table 2.2) from Richards (1954). The study also combined

Table 2.1 Case studies and their main contributions

Targets	Cases	Contributions
SDG 2.3 By 2030, double the agricultural productivity and incomes of small-scale food producers, in particular women, indigenous peoples, family farmers, pastoralists, and fishers, including through secure and equal access to land, other productive resources and inputs, knowledge, financial services, markets, and opportunities for value addition and non-farm employment	Monitoring and assessing saline-alkali land improvement and utilization in western Jilin Province	**Data product:** Dataset of soil salinization levels in western Jilin Province from 1985 to 2020 **Method and model:** Integrated classification algorithms and machine learning models were used to construct a soil electrical conductivity (EC) inversion model **Decision support:** Data support for the improvement, utilization, and reclamation of saline-alkali land, and a reference for the development and graded assessment of agricultural production potential
SDG 2.4 By 2030, ensure sustainable food production systems and implement resilient agricultural practices that increase productivity and production, that help maintain ecosystems, that strengthen capacity for adaptation to climate change, extreme weather, drought, flooding, and other disasters, and that progressively improve land and soil quality	Coupling driving relationship between spatiotemporal change in cultivated soil organic carbon and crop yield in the Beijing-Tianjin-Hebei Urban Agglomeration	**Data product:** Temporal and spatial distribution of soil organic carbon in cultivated land in Beijing, Tianjin, and Hebei in 1980, 2010, and 2020 **Decision support:** The case summarizes the cultivated land management experience policy of carbon and grain cooperative growth, and provides a reference for the implementation of cultivated land protection and grain increase
	Assessment of potential for cropland carbon sequestration in China under global change	**Data product:** Carbon density of Chinese cropland soil in 2015 and 2020 and its future spatial pattern **Method and model:** Indigenous intellectual property rights process-based ecosystem model driven by Big Earth Data **Decision support:** Informing decisions on the sustainable production of crop farming aligned with carbon goals
	Temporal and spatial variations in carbon emissions for cropping systems in China	**Data product:** County-scale carbon emissions for cropping systems in China in 2010, 2015, and 2020 **Method and model:** Combining multi-source data and machine learning methods to achieve the quantitative estimation of county-scale carbon emissions for cropping systems in China **Decision support:** It will provide a scientific basis for understanding the current situation of agricultural carbon emissions at the county level and formulating future policies of carbon emission reduction
SDG 12.3 By 2030, halve per capita global food waste at the retail and consumer levels and reduce food losses along production and supply chains, including postharvest losses	Food Loss and Waste and its Reduction Pathways in China	**Data product:** Research dataset on food loss and waste (FLW) in China's food supply chain, 2014–2018 **Decision support:** Provide a scientific basis for formulating effective management policies to reduce FLW

Table 2.2 Classification of soil salinization grades (USDA)

EC_e (dS/m)	Soil classification	Vegetation response
0–2	Low salinity	No salt damage to crops
2–4	Medium salinity	Yields of extremely salt-sensitive crops may be affected
4–8	Very high salinity	Yields of salt-sensitive crops suffer
>8	Excessively high salinity	Severely affects yields, only very few halophyte crops grow

land use data to analyze the feature transformation of saline-alkali land and the importance of meteorological and geomorphological factors in the change in saline-alkali land areas. These studies demonstrate the use of remote sensing data, machine learning models, and classification algorithms to monitor and analyze temporal changes in soil salinity dynamics in different regions, providing valuable insights into the impacts of climate change and other factors on soil salinization.

2.3.1.4 Results and Analysis

Temporal Variation in the Saline-Alkali Land Area in Western Jilin Province

From a spatial distribution perspective, saline soil is mainly concentrated in the central part of the study area, including Da'an, Qian'an, and Zhenlai, with these areas experiencing relatively severe soil salinization. In terms of the temporal distribution of saline soil, the degree of soil salinization has changed continuously over time, showing a trend of initially increasing and then gradually decreasing.

Based on changes in the total area of saline soil, we can divide the three decades into two stages: an increasing trend in the total area from 1985 to 2000, followed by a decreasing trend from 2001 to 2020. This corresponds to the implementation period of the government's saline soil reconstruction project, with the first stage being the natural state (1985–2000) and the second stage being the transformed state (2001–2020). In summary, the total area of natural saline soil showed an increasing trend, while the total area of transformed saline soil showed a decreasing trend.

Before 2010, among the four kinds of saline soil, the area of severely saline soil was the largest—significantly larger than the other three kinds of saline soil. In 2000, the area of severely saline soil and solonchak/solonctz reached the maximum value in 35 years. With the implementation of the renovation project, the degree of soil salinization was mainly mild or moderate after 2010 (Figs. 2.1 and 2.2).

Analysis of the Change Rate of Saline-Alkali Land

Based on the changes in area, the total area of saline-alkali land showed the highest increase from 1990 to 1995, and the largest decrease from 2015 to 2020. The area of solonchak/solonetz and severely saline soil increased from 1985 to 1995, but had been decreasing since 2000. The area of mildly saline soil decreased prior to 2010, but had been increasing from 2010 to 2015.

In terms of dynamic changes in the area, solonchak/solonetz exhibited the greatest change from 1990 to 1995, while mildly saline soil experienced a significant change of 297.71% from 2010 to 2015 (Fig. 2.3).

Analysis of Saline-Alkali Land and Land Use Conversion

The changing regions of saline-alkali land and non-saline-alkali land were overlaid with land use data to analyze the direction of transfer of saline-alkali land. The two stages of the total area change in saline-alkali land, i.e., the natural state (1985–2000) and the transformed state (2001–2020), were combined to obtain the percentage of mutual transformation between different land features and saline-alkali land during these two stages, as shown in Fig. 2.4.

Fig. 2.1 Distribution of saline-alkali land in western Jilin Province from 1985 to 2020

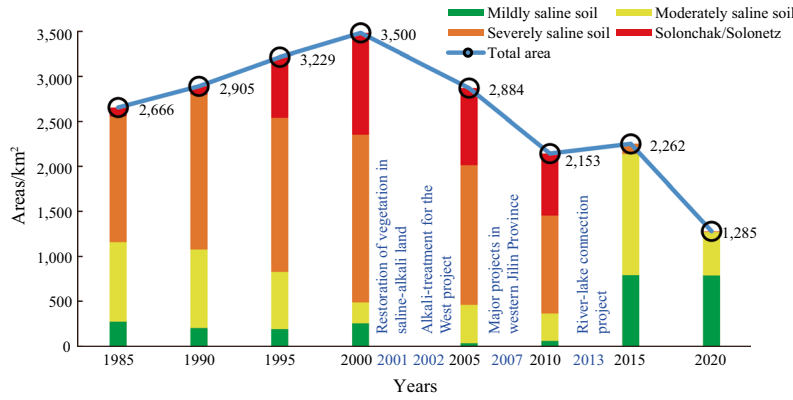

Fig. 2.2 Area of different grades of saline-alkali land in western Jilin Province

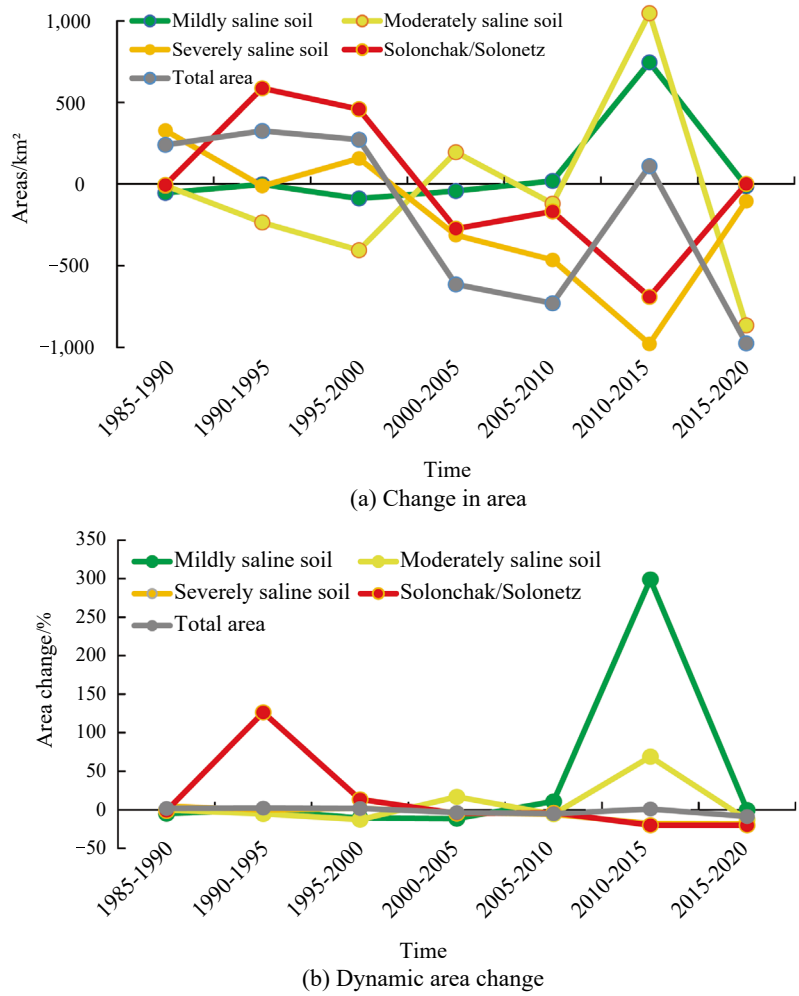

Fig. 2.3 Variation and dynamic trends of the saline-alkali land area

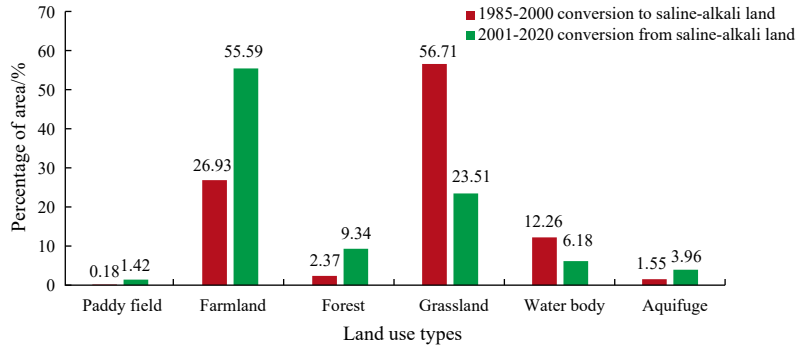

Fig. 2.4 Land use types for the conversion of saline-alkaline land from 1985 to 2020

Figure 2.4 illustrates that 56.71 and 26.93% of the increases in saline-alkali land from 1985 to 2000 were attributed to the conversion of grassland and farmland, which had a detrimental impact on the development of animal husbandry and agriculture and could result in social and economic losses if not controlled. From 2001 to 2020, 55.59% of saline-alkali land was converted to farmland and 23.51% to grassland. In 2002, the "Alkali-treatment for the West project" was launched, and in 2007, the government implemented the "Major projects in western Jilin Province" plan. With the implementation and transformation of these projects, large areas of saline-alkali land were converted into farmland and grassland through artificial intervention.

Influencing Factors of Saline-Alkali Land Area

An RF model was established with the saline-alkali land area as the dependent variable, and total population, evaporation, burying of groundwater, difference of water table, DEM, slope, and aspect as independent variables. The importance of these variables was calculated, and the results are shown in Fig. 2.5. By comparing the natural state (1985–2000) with the transformed state (2001–2020), it was observed that the importance of all meteorological elements, burying of groundwater, and geomorphic elements decreased, except for the total population, and difference in the water table. These findings indicate that in the natural state, these factors have a significant impact on the area of saline-alkali land. However, in the transformed state, due to artificial disturbance, the importance of these factors is reduced, which is consistent with the objective reality. In other words, human activity has a greater influence on the change in the saline-alkali land area compared with natural conditions, which warrants further consideration.

Highlights

- The spatial distribution pattern and change characteristics of the saline-alkali land in western Jilin Province from 1985 to 2020 were analyzed. The results show that the area of saline-alkali land exhibited an increasing trend from 1985 to 2000, followed by a decreasing trend after 2000. This change in the trend can be attributed to the implementation of government policies and a series of reconstruction projects that reversed the increasing trend of the saline-alkali land area.
- The conversion between saline-alkali land, farmland, and grassland was found to be the most frequent land use change.
- The important influencing factors of the saline-alkali land area before and after the implementation of government improvement measures were evaluated.

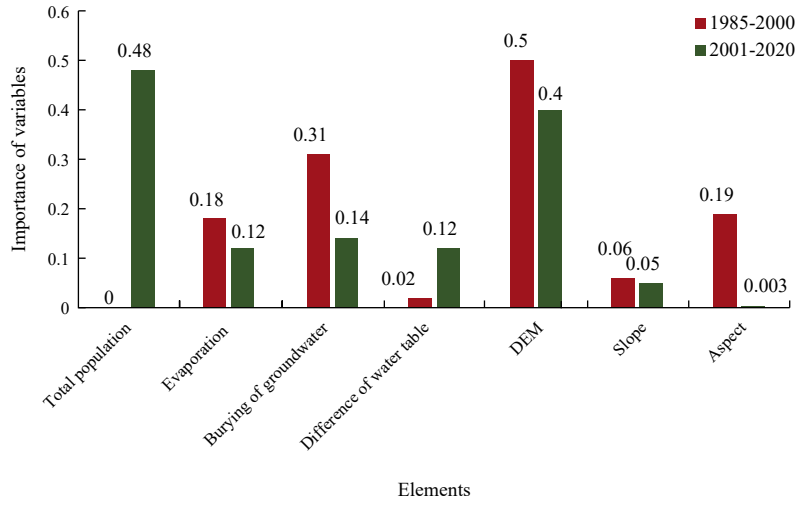

Fig. 2.5 Importance of factors for saline-alkali land area

2.3.1.5 Discussion and Outlook

In this study, recognition algorithms for saline-alkali land and inversion algorithms for soil EC were developed to map the grade distribution of the saline-alkali land in western Jilin Province from 1985 to 2020. These mapping results can provide crucial scientific data for evaluating progress toward SDG 2.4, which focuses on sustainable agriculture and aims to ensure sustainable food production systems and implement resilient agricultural practices.

(1)The area of saline-alkali land in western Jilin Province increased significantly during the natural state period of 1985–2000, but decreased during the transformed state period of 2001–2020, indicating the significant impact of saline-alkali land treatment projects.
(2)Farmland and grassland were the main land features that were frequently converted to saline-alkali land.
(3)Natural conditions such as geomorphic elements and groundwater are important factors contributing to soil salinization, and human activity can mitigate their influence. We recommend increasing positive transformation activity and reducing destructive activity such as overgrazing.

2.3.2 Coupling Driving Relationship Between Spatiotemporal Change in Cultivated Soil Organic Carbon and Crop Yield in the Beijing-Tianjin-Hebei Urban Agglomeration

Target: SDG 2.4: By 2030, ensure sustainable food production systems and implement resilient agricultural practices that increase productivity and production, that help maintain ecosystems, that strengthen capacity for adaptation to climate change, extreme weather, drought, flooding, and other disasters, and that progressively improve land and soil quality.

2.3.2.1 Background

In September 2015, world leaders adopted the 2030 Agenda at the historic UN Summit, which stated that by 2030, we must ensure the establishment of a sustainable food production system and the implementation of disaster-resistant farming methods to improve productivity and output, help maintain ecosystems, strengthen the ability to adapt to climate change, extreme weather, drought, floods, and other disasters, and gradually improve land and soil quality.

To realize a sustainable grain production system, it is necessary to improve grain output and farmland quality in coordination. At present, however, the rapid growth of grain output is often at the expense of the decline of arable land quality. How to ensure stable production while increasing production sustainably has become an urgent problem to be solved.

The research team formed the latest (2020) atlas of topsoil organic carbon in farmland in the Beijing-Tianjin-Hebei Urban Agglomeration and combined the data with previous work results through long-term monitoring of grain yield and cultivated land organic carbon. The work explored the temporal and spatial variation and coupling driving relationship between them. Based on the data of the second national soil survey, combining with the key time nodes of the major transformation of land use patterns in China after the twenty-first century, the research team summarized the experience of farmland management in the representative area of Beijing-Tianjin-Hebei, where the grain yield and organic carbon of cultivated land were synergistically improved.

2.3.2.2 Data

- DEM, land use data, soil type data, and remote sensing meteorological data (1980, 2010, and 2020), provided by the Data Center of the CAS and National Earth System Science Data Center, with a spatial resolution of 1,000 m.
- Data of the second national soil survey, 161 field samples collected in 2010, 187 field samples collected in 2018, and 595 field samples collected in 2020 were used, and the data on the soil organic carbon content in the field samples were obtained by the potassium dichromate external heating method.
- Planting area and yield data of grain crops in the counties of Beijing, Tianjin, and Hebei (1980, 2010, and 2020) were obtained by consulting the statistical yearbook of each city.

2.3.2.3 Methods

Soil organic carbon was measured by the potassium dichromate external heating method, for which the RF model was selected to interpolate the soil organic carbon content of arable land in Beijing, Tianjin, and Hebei. RF is an integrated learning method, and the final prediction result is generally the average of K classified regression tree:

$$\hat{\theta}^K(x) = \frac{1}{K} \cdot \sum_{k=1}^{K} t_k^*(x) \tag{2.1}$$

where t_k^* is the k-th classification regression tree, $\hat{\theta}^K$ is the result of prediction, K is the number of regression tree, and x is the predictive variable.

Soil profile points were divided into a training set and a verification set. RF learns the relationship between variables and auxiliary variables through the training set, and verifies the accuracy of the learning relationship through the verification set, so the model was verified by leave-one-out cross-validation (LOOCV), and the verification indices included model efficiency (R^2), root mean square error (RMSE), and mean absolute error (MAE).

The interpolation results of organic carbon and grain yield data were sorted in Excel, and the degree of coupling coordination was calculated. Finally, the result was connected with an ArcGIS layer to form an atlas of the organic carbon content, the yield, and the coupling coordination degree, and a comparative analysis was made.

2.3.2.4 Results and Analysis

Temporal and Spatial Changes in the Organic Carbon Content in Cultivated Soil Surfaces

The spatial change in the organic carbon content in cultivated soil in Beijing, Tianjin, and Hebei is shown in Fig. 2.6. In 1980, the spatial distribution of soil organic carbon in arable land had no obvious regularity, and its spatial variability was great. The content of soil organic carbon in the piedmont area and coastal area of the Taihang Mountains is obviously higher than that in other areas. In 2010, the soil organic carbon content in the Beijing-Tianjin-Hebei Urban Agglomeration showed obvious differences

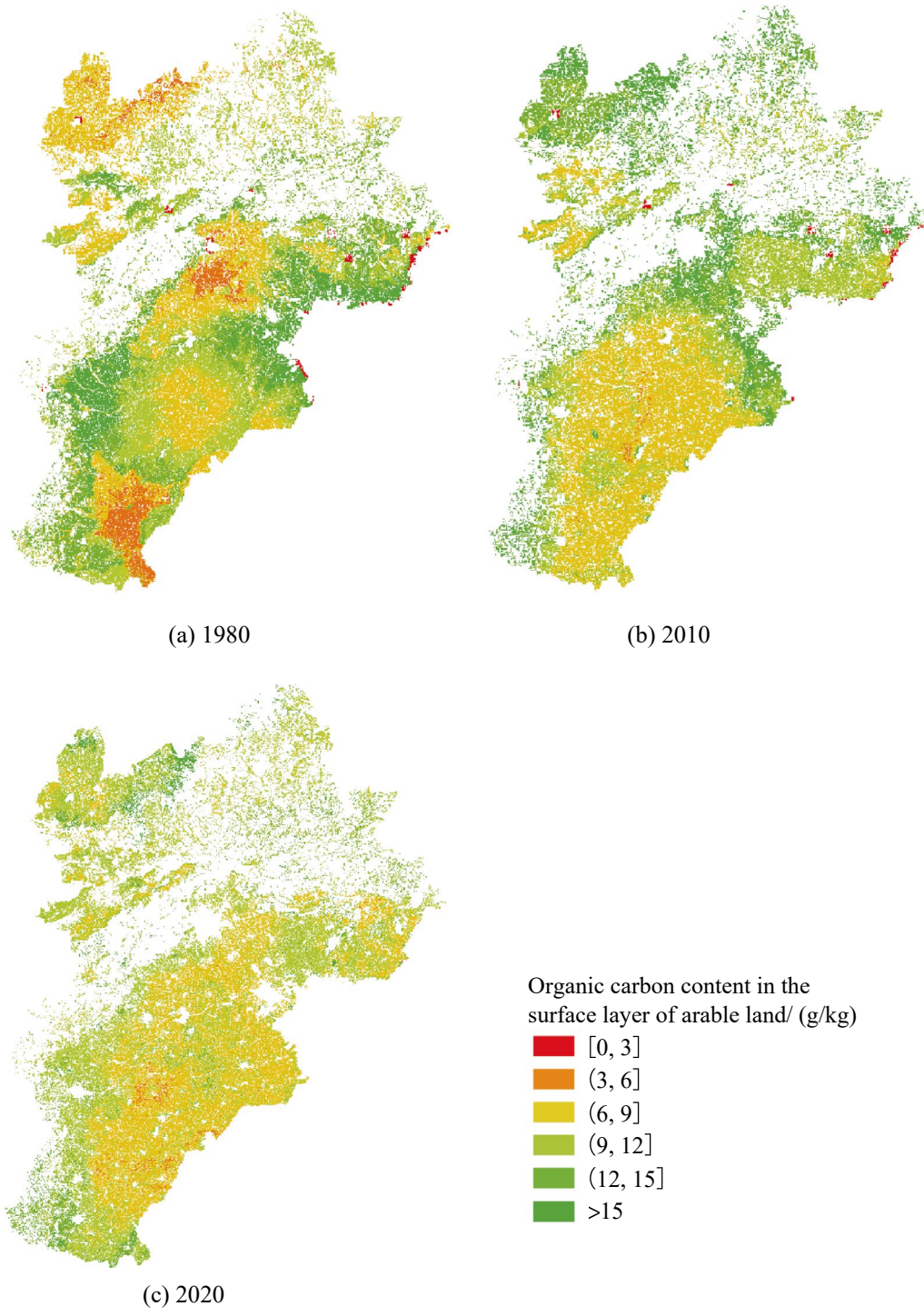

Fig. 2.6 Map of the organic carbon content in the surface layer of arable land

between the north and the south, and the organic carbon content in the northern region was significantly higher than that in the southern region. In 2020, the overall spatial variability of arable land organic carbon in the Beijing-Tianjin-Hebei Urban Agglomeration was significantly reduced. Taking the Taihang Mountains and Yanshan Mountains as the boundary, the distribution pattern of soil organic carbon in the Beijing-Tianjin-Hebei Urban Agglomeration was divided into two parts. The organic carbon content of arable land in the south of the mountain range was slightly lower than that in the north of the mountain range, forming a distribution pattern that was high in the northwest and low in the southeast.

Temporal and Spatial Changes in the Grain Output in the Beijing-Tianjin-Hebei Urban Agglomeration

The temporal and spatial evolution of the grain output in Beijing, Tianjin, and Hebei is shown in Fig. 2.7. In 1980, the grain output of each region was at a low level, and the output was relatively average. From 1980 to 2010, the grain output increased obviously, and the average output increased from 100,000 tons to 190,000 tons, especially in the double cropping area. At this time, the high-yield grain counties were concentrated in the double cropping area.

By 2020, the grain production level in the Beijing-Tianjin-Hebei Urban Agglomeration did not increase significantly compared with 2010, but it is worth noting that the grain production level in the northern region increased significantly, the grain production level around Beijing further decreased, and the difference in the grain production level within the Beijing-Tianjin-Hebei Urban Agglomeration gradually became obvious, while the difference between the north part and south part of Hebei province shrank.

Coupling Analysis of Topsoil Organic Carbon and Crop Yield in the Beijing-Tianjin-Hebei Urban Agglomeration

The coupling relationship between the topsoil organic carbon content and the grain yield is shown in Fig. 2.8. In 1980, the coupling relationship between the organic carbon content and the grain yield was mainly moderate coupling and high coupling, and the low coupling was mainly concentrated in the double cropping area in the southeastern region. From 1980 to 2010, the coupling degree of carbon and grain in the Beijing-Tianjin-Hebei Urban Agglomeration was divided, and the moderate coupling in the northern and southern regions decreased to low coupling, while the moderate coupling in the middle increased to high coupling. The coupling degree was obviously divided into different boundaries, and the coupling degree in northwestern and southeastern regions was significantly lower than that in other regions. From 2010 to 2020, the coupling degree of many places increased by one level, and the coupling relationship between carbon and grain in the northern region improved clearly, but the coupling relationship in most areas in the southern region was still at a low level. To sum up, the coupling relationship between carbon and grain in the annual double cropping area in the southeast of Beijing, Tianjin, and Hebei is always in a state of low coupling, and the sustainable development of local agricultural production is facing more severe challenges.

Analysis of the Strategy of the Synergistic Promotion of the Soil Organic Carbon Content and Grain Yield—Taking Quzhou as an Example

Quzhou County is located in the southeast of the Beijing, Tianjin, and Hebei regions, with a large agricultural population, strong land use intensity, and a high proportion of agricultural output value. It is a typical representative of intensive agricultural areas. Therefore, taking Quzhou as an example, the team summarized the synergistic relationship between the soil organic carbon content and the grain yield by analyzing the changes in carbon grain in the Quzhou area.

Taking small-scale counties as the research object, we can observe the temporal variation in the soil organic carbon content more accurately. From 1980 to 1999, the organic carbon

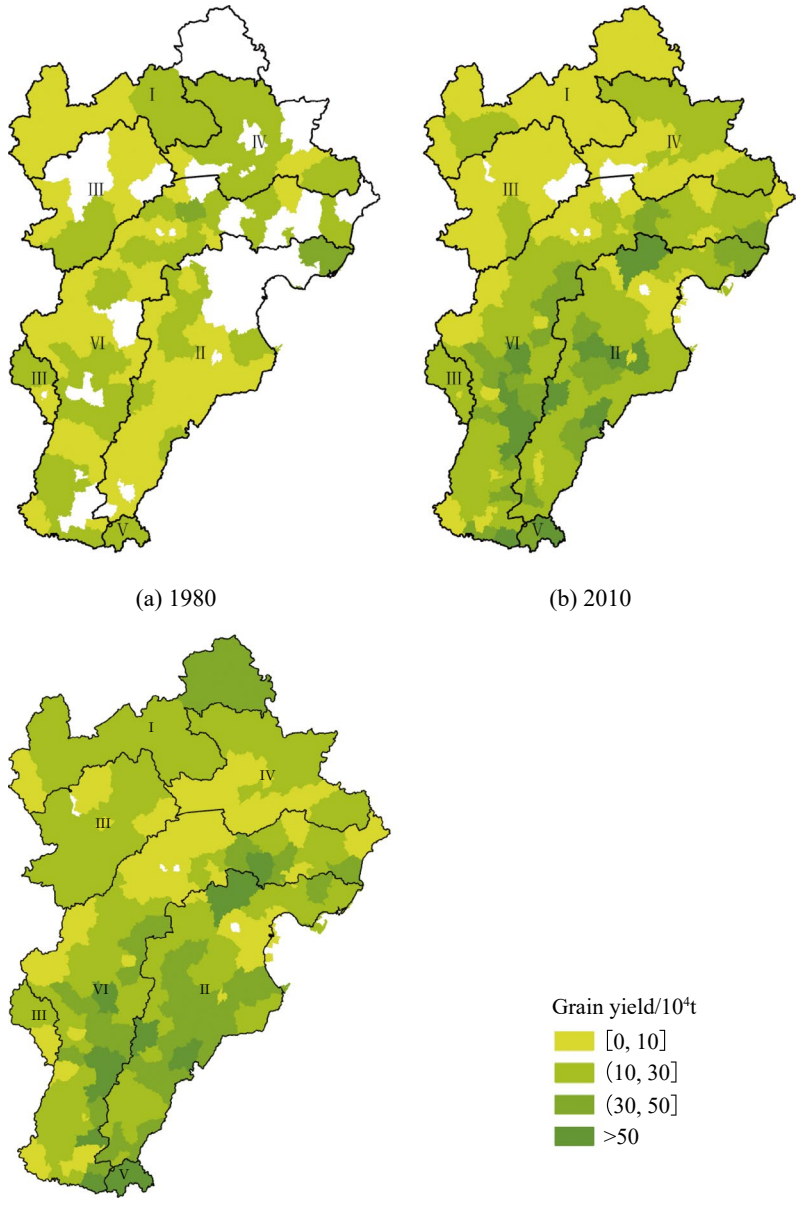

Fig. 2.7 Changes in grain output in Beijing, Tianjin, and Hebei. *Note* I. Semi-arid and cool-loving crops are harvested once a year in the mountainous area of the northern Shanxi Plateau; II. The region where irrigated land is cropped twice a year and dry land is cropped once a year in the plain area where Heilonggang lacks water; III. One-year-one-cropping restoration area in the semi-humid area of eastern Shanxi; IV. One-year cropping area in the semi-arid temperate regions of western Jilin, southeastern Inner Mongolia, and northern Hebei; V. Areas where grain crops are harvested twice a year and cotton is harvested once a year in irrigated land in the low plains of northwestern Shandong and northern Henan; VI. Intercropping, planting in irrigated land with two crops a year and one crop in dry land with one crop a year in the piedmont plain of Yanshan Mountains and Taihang Mountains

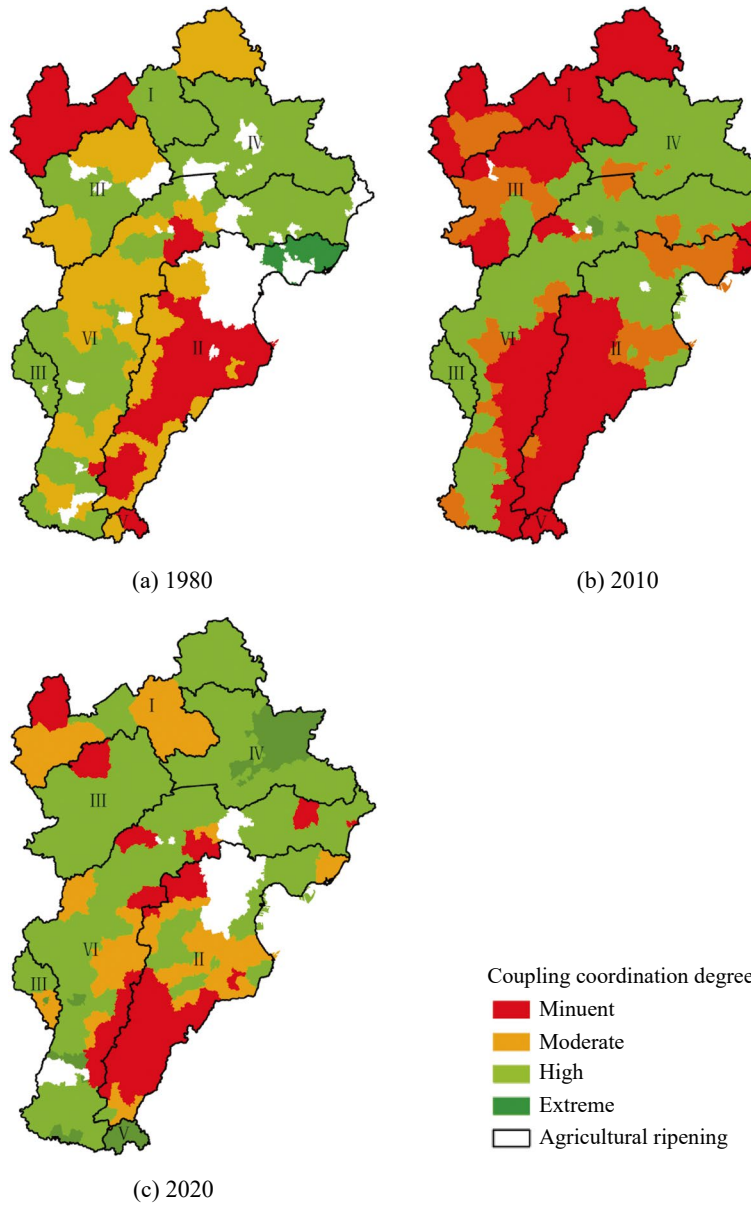

Fig. 2.8 Coupling relationship between the topsoil organic carbon content and crop yield of arable land in Beijing-Tianjin-Hebei. *Note* I. Semi-arid and cool-loving crops are harvested once a year in the mountainous area of the northern Shanxi Plateau; II. Region where irrigated land is cropped twice a year and dry land is cropped once a year in the plain area where Heilonggang lacks water; III. One-year-one-cropping restoration area in the semi-humid area of eastern Shanxi; IV. One-year cropping area in the semi-arid temperate regions of western Jilin, southeastern Inner Mongolia, and northern Hebei; V. Areas where grain crops are harvested twice a year and cotton is harvested once a year in irrigated land in the low plains of northwestern Shandong and northern Henan; VI. Intercropping, planting in irrigated land with two crops a year and one crop in dry land with one crop a year in the piedmont plain of the Yanshan Mountains and Taihang Mountains

content in Quzhou County increased from (4.91 ± 1.3) g/kg to (6.91 ± 1.6) g/kg. From 2000 to 2018, the organic carbon content of arable land increased from (6.95 ± 1.61) g/kg to (10.56 ± 2.4) g/kg. In the past 40 years, the organic carbon content of arable land in Quzhou County has been increasing, and the difference in the organic carbon content of arable land within the county is also gradually expanding.

While the soil organic carbon content steadily increased, the grain output of Quzhou County also increased from 84,000 tons in 1980 to 402,000 tons in 2020, realizing the simultaneous improvement of arable land quality and grain output.

To sum up, Quzhou County provides a successful case for the synergistic improvement of soil organic carbon content and grain yield. In the 1980s, Quzhou County was still a typical saline-alkali area. Researchers and scholars established a comprehensive saline-alkali control area, actively carried out water conservancy, land leveling, drainage, salt washing, and other low- and medium-yield farmland reconstruction projects, leveled the farmland with fluctuating surfaces to facilitate water and fertilizer runoff, dug deep open channels or underground culverts in the farmland, and drained and washed the salt seeping into the soil by underground drainage to reduce the salt content in the soil and restore the soil fertility. At the same time, combined with soil fertility technology, straw returning and scientific fertilization were actively carried out. The straw returning technology directly increased the content of organic matter in soil and improved the soil structure. The comprehensive application of organic fertilizer and inorganic fertilizer further promoted the mineralization of organic nitrogen, enhanced fertilizer efficiency, and opened the prelude to increasing yield and improving soil fertility in Quzhou. In 1988, state leaders inspected Quzhou and spoke highly of the local agricultural development. With the support of state policies, Quzhou's experience went to the entire country, which promoted regional governance and economic development.

There is an inseparable relationship between the improvement of grain yield and the improvement of farmland fertility. How to increase the yield without consuming too much soil fertility and ensure that the soil fertility is maintained at a certain level or even improved in coordination with the yield is the key to realizing the sustainable production of farmland. Faced with this problem, the Chinese government has put forward a series of policies and measures, such as land consolidation, the transformation of medium- and low-yield fields, soil testing, and formula fertilization. Under the guidance of national policies, agricultural producers and operators actively implement farmland protection policies; improve the quality of farmland, scientific engineering, field management, and other measures; build an aboveground-underground carbon cycle; and drive soil organic carbon to increase and stabilize crop production.

Highlights

- This case study analyzed the changes in topsoil organic carbon content, grain yield, and their degree of coupling in Beijing-Tianjin-Hebei farmland from 1980 to 2020.
- A map was created for organic carbon content in the topsoil of farmland in Beijing, Tianjin, and Hebei.
- Taking Quzhou County as a specific research area, this case study summarized the experience with farmland management policies of carbon and cooperative grain growth, providing a reference for the implementation of farmland protection and grain increase.

2.3.2.5 Discussion and Outlook

In this case, spatiotemporal distribution maps of topsoil organic carbon in Beijing-Tianjin-Hebei farmland in 1980, 2010, and 2020 were produced by using 943 field observations and satellite remote sensing data combined with statistical yearbooks. The temporal and spatial changes were analyzed for topsoil organic carbon content, grain yield, and the degree of

coupling between carbon and grain in farmland across three periods, and the experience of farmland management was summarized. Therefore, SDG 2.4, monitoring farmland and analyzing spatiotemporal processes, was reached successfully.

There is a close relationship between soil organic carbon and grain yield, and at the same time, both are influenced by human management. Therefore, in the future, if we can collect multi-period soil data, we can reflect the changes in soil organic carbon and grain yield in a certain area with a small time-step, while taking into account local policies, human activity, and other factors. We can explore the coupling relationship between organic carbon and yield in more detail, reveal the driving mechanism behind it from the perspective of macro-control, and clarify the turning point of soil organic carbon content, grain yield, and the degree of coupling, as well as corresponding policy measures, so as to understand the influence of macro-control on agricultural production at a deeper level and provide a reference for farmland protection.

2.3.3 Assessment of Potential for Cropland Carbon Sequestration in China Under Global Change

Target: SDG 2.4: By 2030, ensure sustainable food production systems and implement resilient agricultural practices that increase productivity and production, that help maintain ecosystems, that strengthen capacity for adaptation to climate change, extreme weather, drought, flooding, and other disasters, and that progressively improve land and soil quality.

2.3.3.1 Background

Ensuring food security is the foundation of global sustainable development and an important issue. Sustainable food production is the basis for achieving food security and an effective measure to address global challenges such as climate change, land degradation, and ecological degradation. This case study establishes a set of cropland soil sink assessment methods and datasets based on our data and independent intellectual property rights models in order to assess SDG 2.4.1, soil health, the most important indicator of cropland soil organic carbon density, and its changes. The study is meant to help achieve the overall goal of food security and reducing carbon emissions in China in the next four decades by dynamically assessing China's cropland soil sink under future climate change scenarios. This will provide quantitative decision-making advice and technical support for the transformation of China's agriculture into environmentally sustainable modern agriculture.

2.3.3.2 Data

- Land use data were obtained from the 2015 and 2020 land use raster datasets with 1 km resolution provided by the Resource and Environment Science and Data Center, CAS. The primary categories include cropland, forestland, grassland, water, residential land, and unused land, among which cropland is subdivided into paddy land and dry land.
- Historical meteorological data came from the China Meteorological Administration and include daily maximum and minimum temperatures, precipitation, and relative humidity for 663 meteorological stations in China from 2015 to 2020.
- Future meteorological data were obtained from four scenarios of climate change (SSP1-2.6/SSP2-4.5/SSP3-7.0/SSP5-8.5) of the FGOALS-g3 model under the Scenario Model Intercomparison Project (ScenarioMIP) of the Coupled Model Intercomparison Project Phase 6 (CMIP6) of the Institute of Atmospheric Physics, CAS, with daily maximum temperature, minimum temperature, precipitation, and radiation in the time range of 2021–2060.

2.3.3.3 Methods

In this case, the Agro-C model was calibrated and validated using yield data of four grain

Table 2.3 Spatial data and management data

Data types		Content	Original formats
Spatial data	Climate	Temperature, precipitation	Raster
	Soil	Organic carbon content, bulk density, clay content, total nitrogen, pH	Raster
	Remote sensing	Spatial distribution of paddy land and dry land	Raster
	Cropping system	Spatial distribution of agricultural cropping systems	Shape
Management data	Country statistics	Nitrogen fertilizer application in the irrigated area, Crop sown area and yield	Excel Table
	Provincial statistics	Nitrogen fertilizer application for different crops	Excel Table
	Other management	Provincial straw returning rate and minimum tillage and no-tillage area	Excel Table

crops (rice, wheat, corn, and soybean), the validated Agro-C model was driven by management scenarios to simulate the spatial distribution of yield changes of the four grain crops and soil density during grain crop production, and the current situation simulated the spatial distribution of soil organic carbon density on cropland in China in 2015 and 2020. The simulations used actual cropland management data.

Under future climate change scenarios, the cropland soil carbon sink potential for food crop production in China in 2030 and 2060 was assessed using the Agro-C model and baseline/optimized cropland management scenarios. The data involved in this case and their original formats are shown in Table 2.3.

2.3.3.4 Results and Analysis

Simulation of Current Changes in Cropland Soil Organic Carbon Density

The overall pattern of cropland soil organic carbon density in major agricultural regions in China shows the highest in Northeast China and slightly higher in the North China Plain than in the Sichuan Basin, and the soil organic carbon density in China's cropland soils at 0–30 cm depth increased from 41.34 tC/ha in 2015 to 42.72 tC/ha in 2020. The changed spatial pattern of soil organic carbon density shows that there was a decrease in Northeast China and an increase in the North China Plain. The most direct reason is the high yield of winter wheat and summer maize rotation in the North China Plain, and the relatively high proportion of straw returning to fields, which is attributed to the substantial extension of the application of crop machine harvesting, especially in the North China Plain (Fig. 2.9).

Future Cropland Carbon Sink Projections Under the Baseline Management Scenario

The baseline scenario is designed by the current management scenario of China's cropland, which includes the average crop yield in the last five years, the proportion of straw returning to fields at the 2020 level, the amount of organic fertilizer, and the minimum tillage and no-tillage area of cropland at the 2020 level. Using the climate projections (SSP1-2.6/SSP2-4.5/SSP3-7.0/SSP5-8.5) of the CAS FGOALS-g3 model, the Agro-C model was driven to estimate the changes in soil organic carbon density of China's cropland in 2030 and 2060 (Fig. 2.10). The spatial pattern of carbon density changes in both years is similar, with a general trend of decreasing in Northeast China and increasing in the North China Plain. Compared with that in 2030, the proportion of decreased grids in Northeast China decreases and the intensity of increases in the North China Plain becomes weaker in 2060.

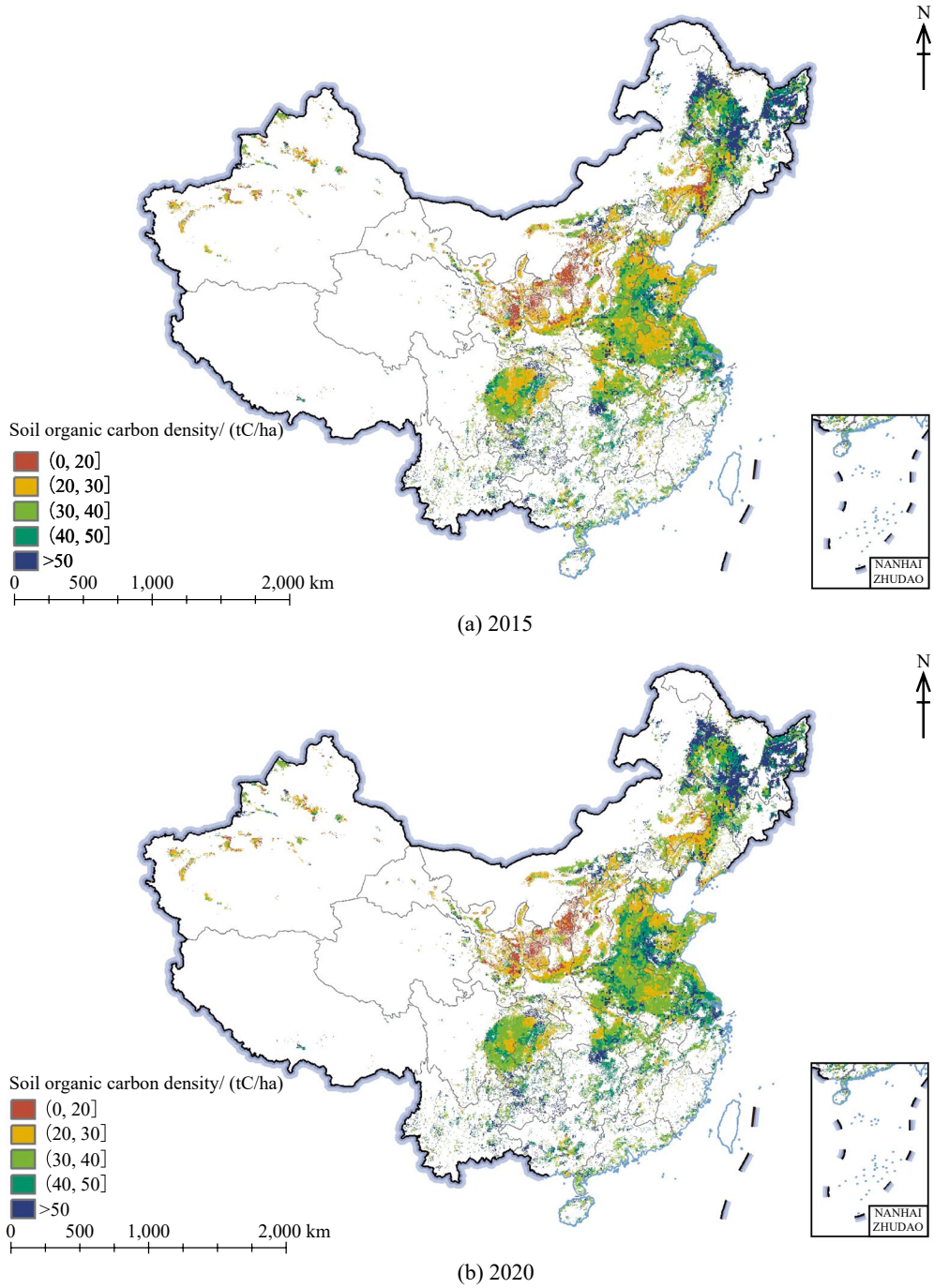

Fig. 2.9 Spatial pattern of soil organic carbon density in China's cropland in 2015 and 2020. *Note* No data for Hong Kong, Macao, and Taiwan

In the context of climate change, the impact of China's cropland management policies and planning implementation on cropland was evaluated, the future cropland management scenarios were integrated, and the management portfolio was designed by a future optimization scenario. The

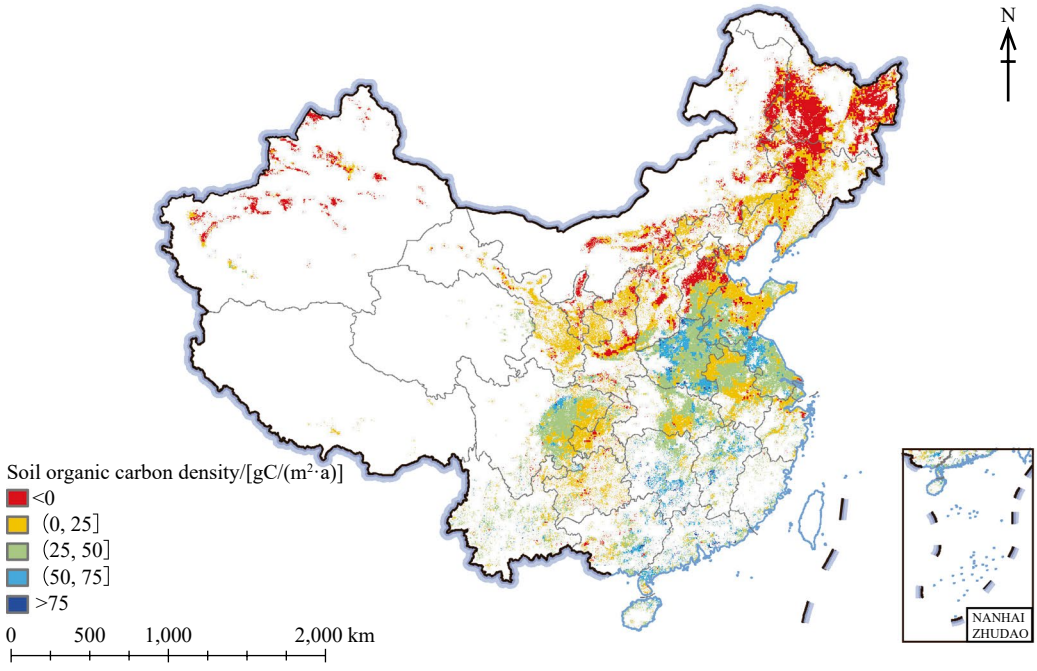

(a) 2030

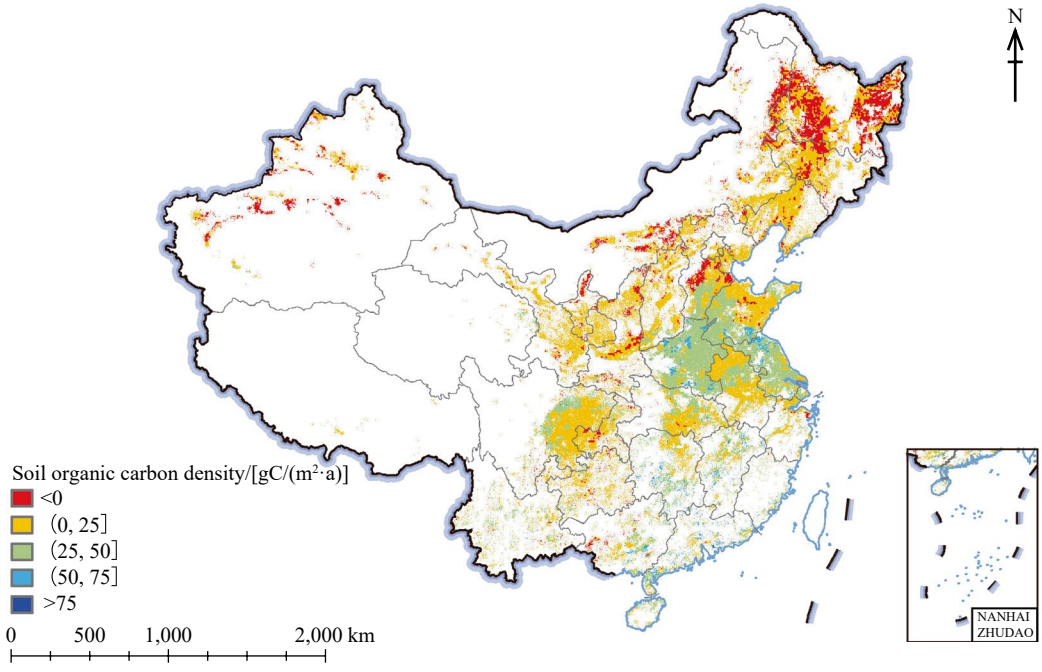

(b) 2060

Fig. 2.10 Changes in the soil organic carbon density of cropland in 2030 and 2060 under the baseline management scenario. *Note* No data for Hong Kong, Macao, and Taiwan

manure amount is derived from the Chinese Academy of Agricultural Sciences, which is based on the future changes in livestock breeding and livestock pollution coefficients. We assume the proportion of the whole livestock manure returning to fields remains unchanged; the amount of livestock manure entering cropland first rises and then falls, and the highest amount of livestock manure in 2043 is 7.24% higher than that in 2020. The proportion of straw returning to fields for the future optimization scenario is derived from the Chinese Academy of Agricultural Sciences. The proportion of straw returning to the field in China increases year by year, achieving 55.6% in 2025, and remains stable at this proportion until 2060. No-tillage area is derived from the Northeast Black Soil Conservation Tillage Action Plan (2020–2025), and the implementation of conservation tillage in the Northeast will achieve 9.33 million hectares by 2025, accounting for 36.8% of the Northeast cropland area. The cropland area and irrigated area in the future optimization scenario are maintained at the 2020 level. Figure 2.11 shows the mean values of carbon intensity changes in Chinese cropland simulated by the four SSP climate change scenarios under the optimization scenario, whose inter annual variability and spatial pattern are similar to the baseline management scenario shown by Fig. 2.10, but the carbon sink intensity is higher than that of the baseline management scenario.

Figure 2.12 shows the temporal dynamics of China's cropland soil carbon sink under two different management scenarios. The two-line chart represents the inter annual variation in China's cropland carbon sink under the four climate change scenarios in the baseline management scenario (Fig. 2.12a) and the optimization management scenario (Fig. 2.12b). The minimum threshold of China's cropland carbon sink is 15 TgC/a under the baseline management scenario and 20 TgC/a under the optimized management scenario in the next 40 years.

Highlights

- A domestic ecosystem model driven by Big Earth Data was created for China based on intellectual property rights processes.
- Spatiotemporal processes of carbon density changes were analyzed for Chinese cropland soils with a high spatial resolution SDG indicator.
- Chinese cropland soils will be a carbon sink for the next 40 years, but the intensity of the sink will decrease year by year. Compared with climate change scenarios, differentiated cropland management scenarios profoundly shape cropland soil carbon sinks.

2.3.3.5 Discussion and Outlook

In this case study, an ecosystem model driven by Big Earth Data was independently developed based on intellectual property rights processes. The study simulated and analyzed the spatiotemporal patterns of soil organic carbon changes in croplands at a high spatial resolution in China. Soil organic carbon stocks in the cultivated layer of Chinese cropland increased by 3.4% from 2015 to 2020. Chinese cropland soils will continue to serve as a carbon sink in the future, but with weakening intensity, and the optimized cropland management practices can increase the carbon sink intensity. For the continued assessment of the future carbon sink capacity of cropland soils, future studies must examine the effects of changes in China's agricultural cropping system and multiple crop index on the carbon sink capacity of cropland soils.

This case study explores greenhouse gas emission reduction assessment methods focused on the production of major food crops in order to achieve the overall goals of China's food security and carbon emissions reduction in the next 40 years. The study used an independent ecosystem model based on intellectual property rights processes and Big Earth Data to achieve a dynamic assessment of China's food production and greenhouse gas emission reduction under future climate change scenarios. This case study provides quantitative decision-making advice and technical support for China's plantations and local strategic solutions at the scale of provinces and municipalities for local carbon emissions reduction.

Case 2.3.2 uses soil organic carbon field observations and the RF method to obtain spatial

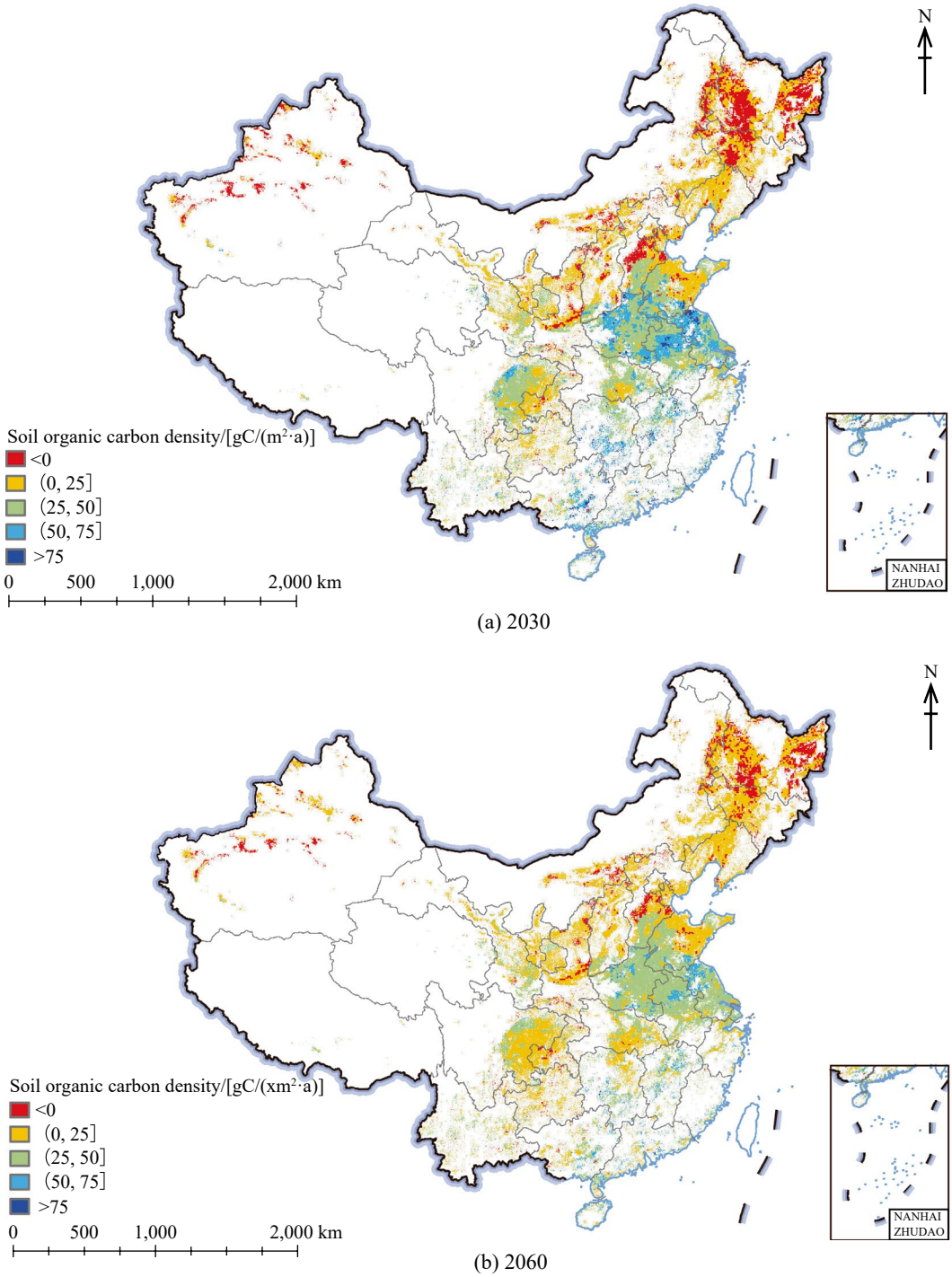

Fig. 2.11 Changes in the soil organic carbon density of cropland in 2030 and 2060 under the optimized management scenario. *Note* No data for Hong Kong, Macao, and Taiwan

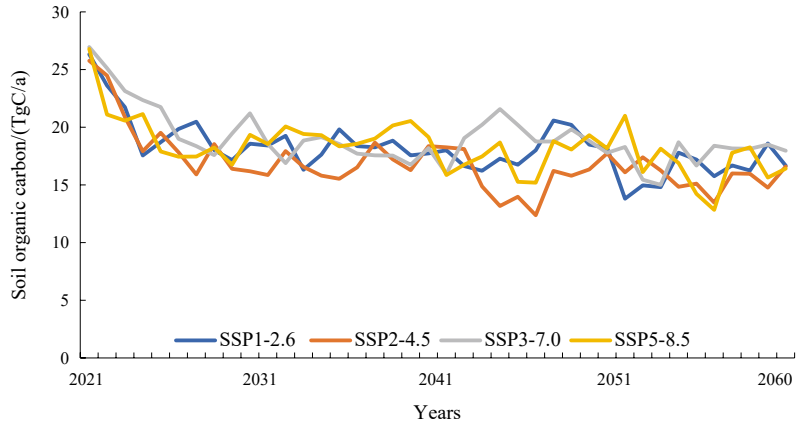

(a) The baseline management scenario

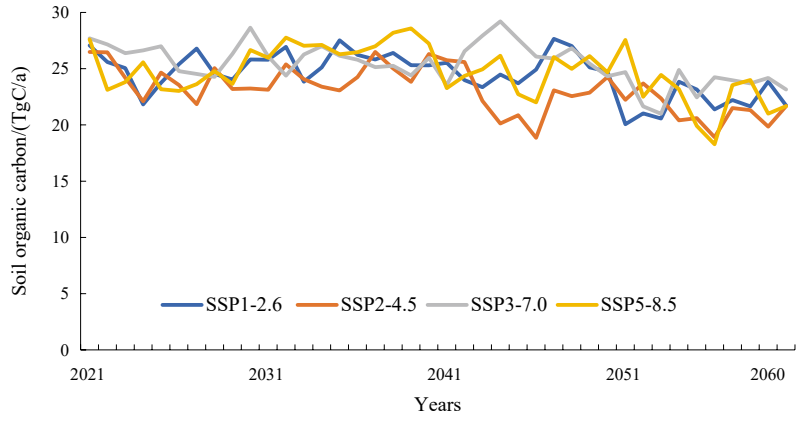

(b) The optimization management scenario

Fig. 2.12 Temporal dynamics of carbon sink in cropland soils for the baseline and optimization management scenarios

patterns of soil organic carbon, and Case 2.3.3 uses the initial spatial patterns of soil organic carbon obtained from observations and a process model to estimate the temporal changes in soil organic carbon. Case 2.3.2 is a method to obtain spatial patterns of soil organic carbon with higher spatial resolution with less input from field observations; Case 2.3.3 uses the process model to assess the driving mechanisms of temporal changes in soil organic carbon and to evaluate the soil carbon sequestration potential under climate change conditions. Cases 2.3.2 and 2.3.3 provide more details on the spatial pattern and temporal dynamics of soil organic carbon, respectively; the coupling of methods from both cases can be used in the future to obtain new methods to assess the spatiotemporal dynamics of soil organic carbon in more detail.

2.3.4 Temporal and Spatial Variations in Carbon Emissions for Cropping Systems in China

Target: SDG 2.4: By 2030, ensure sustainable food production systems and implement resilient agricultural practices that increase productivity and production, that help maintain

ecosystems, that strengthen capacity for adaptation to climate change, extreme weather, drought, flooding, and other disasters, and that progressively improve land and soil quality.

2.3.4.1 Background

The estimation of carbon emissions for cropping systems is an important element of SDG 2.4—establishing a sustainable food production system—and is closely related to China's strategy for reducing carbon emissions. In recent decades, agricultural production has been growing rapidly, and carbon emissions from cropping systems have been increasing at a significant rate and have taken up an important role in agricultural greenhouse gas emissions (Hong et al. 2021). On the one hand, the quantity and quality of soil organic carbon in the cultivated layer largely determine regional crop yields (Lal 2020) and are governed by soil temperature and moisture conditions. Meanwhile, reducing exogenous carbon inputs and accelerating erosion and leaching in the context of climate change can contribute to the loss of soil organic carbon (Crowther et al. 2016). On the other hand, there is a very complex interaction between emissions of multiple greenhouse gases from cropland and management. As crop yields increase, crop residues increase significantly; however, more crop residues will stimulate CH_4 production and emissions in rice fields (Liang et al. 2021). Meanwhile, drainage in the middle of the rice-growing season can suppress CH_4 production, but may stimulate N_2O emissions (Zou et al. 2009). Although more N fertilizer application increases crop yields and improves the soil organic carbon content, the applied N fertilizer also stimulates increased soil N_2O emissions (Bolinder et al. 2006). Thus, greenhouse gas emissions caused by crop cultivation depend largely on local environmental conditions and management practices, and the potential for agricultural greenhouse gas emission reduction varies across regions (Powlson et al. 2011).

Most of the current studies understand carbon emissions for cropping systems, that is, it is believed that carbon emissions for cropping systems mainly characterize the carbon emission effects of greenhouse gases directly or indirectly caused by human production activities in the production process of crops (Ding et al. 2022). However, the comparability of carbon emission estimation results between different cropping systems is not high due to estimation methods and spatiotemporal scales, which makes it difficult to provide a scientific basis for a strategy on reducing carbon emissions and policy formulation for SDG targets. Therefore, it is necessary to develop county-scale carbon emission datasets in China based on big data technology, and explore the spatiotemporal patterns of carbon emissions in different time periods to improve the accuracy of the results (Guo 2020).

2.3.4.2 Data

- Carbon emission data for cropping systems in China at the provincial scale from 1978 to 2016 (Liang et al. 2021).
- Gross primary productivity data from 2000 to 2020, provided by the University of New Hampshire, USA, with a spatial resolution of 5 km.
- Cultivation distribution data of major crops (e.g., early rice, single-season rice, wheat and maize) in China since 2000, provided by Beijing Normal University, China, with a spatial resolution of 1 km.
- Land use/land cover data in China from 1985 to 2020, provided by the Aerospace Information Research Institute, CAS, with a spatial resolution of 30 m.
- Nighttime light data in China from 2000 to 2020, with a spatial resolution of 1 km (Li et al. 2020).
- Climate data (e.g., precipitation, radiation, etc.) from 2000 to 2020, provided by the National Meteorological Information Center of the China Meteorological Administration.
- Statistical data in China at the provincial scale from 2010 to 2020.
- Carbon emission data of China's plantation industry in 2010, provided by the Aerospace Information Research Institute, CAS, with a spatial resolution of 8 km.

2.3.4.3 Methods

The methods are as follows: (1) collecting satellite data, statistical data, and carbon emission data for cropping systems; (2) evaluating the influence of natural and anthropogenic factors on carbon emissions for cropping systems at the provincial scale, and then determining the main factors affecting carbon emissions using the RF method; and (3) using carbon emissions for cropping systems at the provincial scale as the dependent variable and screened natural and anthropogenic factors as the independent variables. Carbon emissions for cropping systems at the county scale were obtained by the downscaling method and then the spatiotemporal patterns of carbon emissions for cropping systems at the county scale in China were analyzed for 2010, 2015, and 2020.

Combined with the agricultural production practices in the study period, a carbon emission intensity index was designed as carbon emission intensity per unit of crop yield. We analyzed the characteristics of this index so as to provide scientific support for government departments to formulate future strategies for reducing carbon emissions.

2.3.4.4 Results and Analysis

China's county-scale carbon emissions for cropping systems in 2010, 2015, and 2020 are shown in Fig. 2.13a–c. There is an obvious spatial heterogeneity in the county-scale carbon emissions for cropping systems, with an overall distribution pattern of higher in the south and east and lower in the west and north. Among them, Jiangsu, Henan, Hubei, Hunan, Sichuan, and Guangdong have higher carbon emissions per unit area. In particular, the regions with carbon emissions per unit area exceeding 200 t CO_2-eq/km^2 are mainly concentrated in the Yangtze-Huai River Basin, the Jianghan Plain, and the Sichuan Basin.

Overall, China's county-scale carbon emissions per unit area for cropping systems showed a stage-specific difference (Fig. 2.13d–f). Compared with those in 2010 and 2015, the county-scale carbon emissions per unit area increased by about 13.19 and 6.44% in 2020, respectively; while the county-scale carbon emissions per unit area in 2015 increased by about 6.34% compared with that in 2010, indicating an increasing trend of county-scale carbon emissions in China in those 10 years. The areas with larger increases are mainly located in some provinces in the northeast and south.

Combined with the changes in crop yield in China during the study period, the carbon emission intensity, i.e., carbon emission intensity per unit of yield, was proposed, and the results are shown in Fig. 2.14. The crop yield showed a rapidly increasing trend ($p<0.05$) during the study period, and thus the carbon emission intensity per unit of yield also showed some variation differences. Specifically, the carbon emission intensity per unit of yield showed a decreasing trend until 2016, with a decrease of about 13.61%. However, the carbon emission intensity per unit of yield has remained stable since 2016.

Carbon emission data for 2010 (Fig. 2.15a) was also obtained from the Aerospace Information Research Institute, CAS, to further verify the estimation of carbon emissions from China's cropping systems based on machine learning methods. The estimation results of different methods compared with the prediction result based on the machine learning methods (Fig. 2.15b) indicate that there is an obvious spatial heterogeneity in China's carbon emissions for cropping systems, and the overall spatial differences are higher in the south and east and lower in the west and north. However, there are some differences in the estimation results due to the different boundary conditions between the two datasets.

Highlights

- Using Big Earth Data and machine learning methods, carbon emission data for cropping systems in China were produced at the county scale for 2010, 2015, and 2020, enabling the monitoring of carbon emissions with high temporal and spatial resolution.
- In the past ten years, China's agricultural carbon emissions per unit area have continued

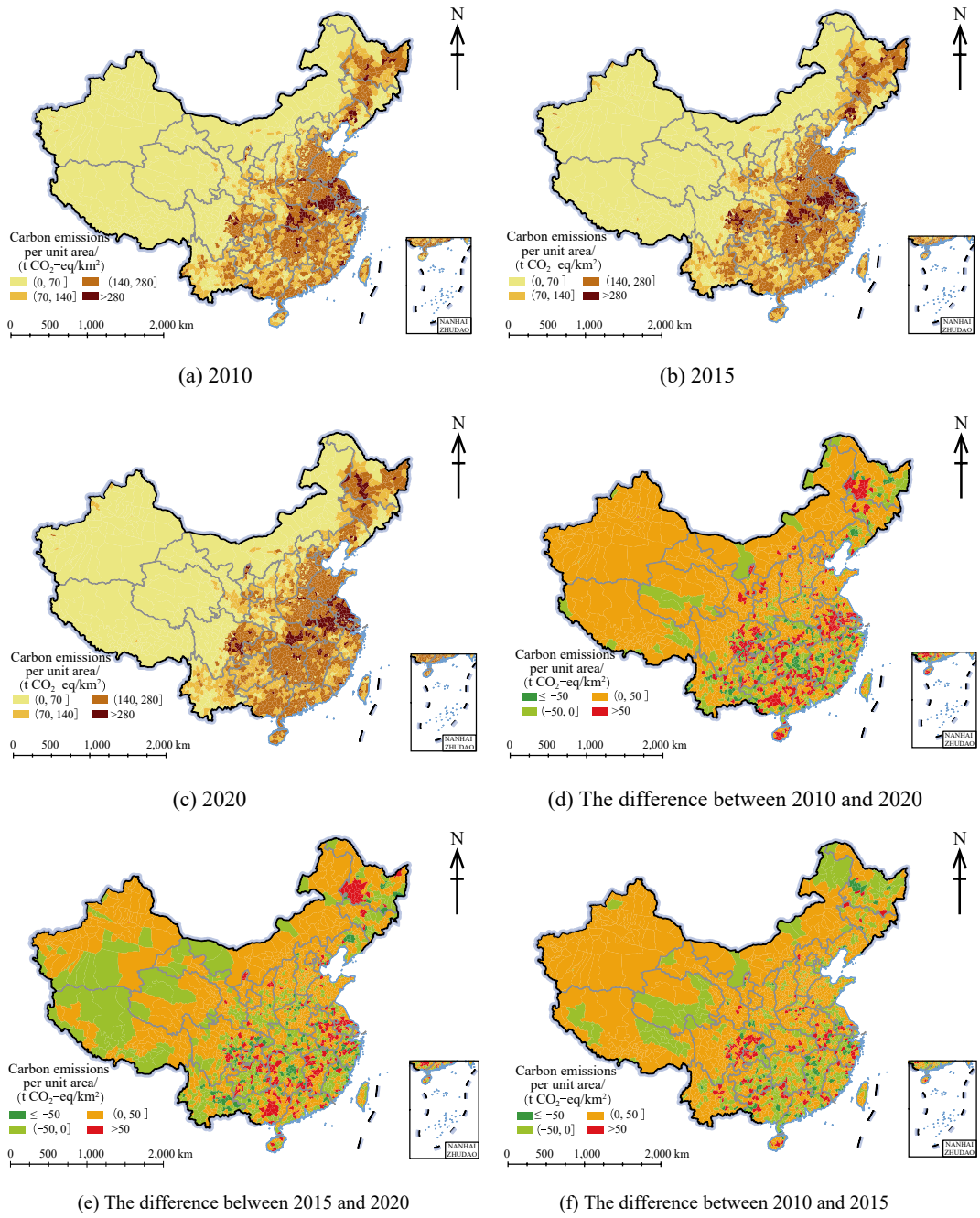

Fig. 2.13 County-scale carbon emissions for cropping systems in China in 2010, 2015, and 2020

to decline, while carbon emissions per unit yield have remained stable. Higher carbon emissions per unit area were observed in the Yangtze-Huai River Basin, the Jianghan Plain, and the Sichuan Basin.

2.3.4.5 Discussion and Outlook

This case used multi-source data and machine learning methods to produce a dataset of county-scale carbon emissions for cropping systems in China for 2010, 2015, and 2020 to provide

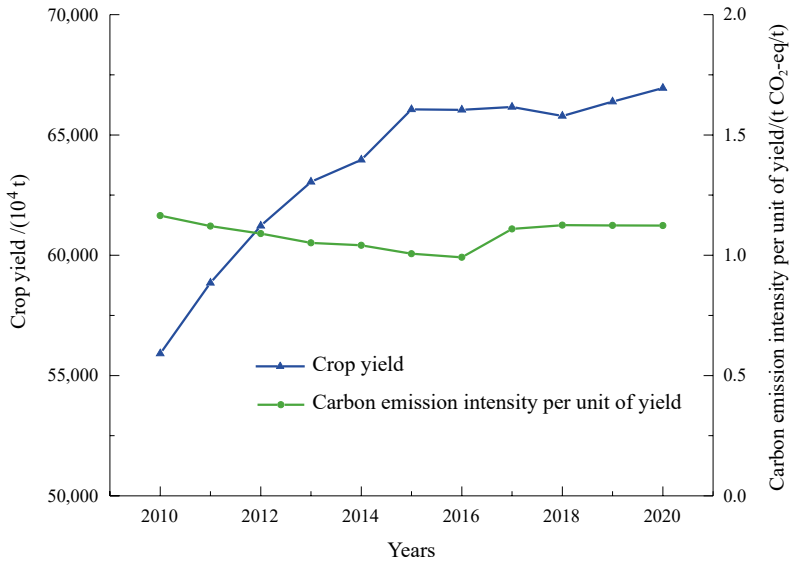

Fig. 2.14 Curves of the national crop yield and carbon emission intensity per unit of yield from 2010 to 2020

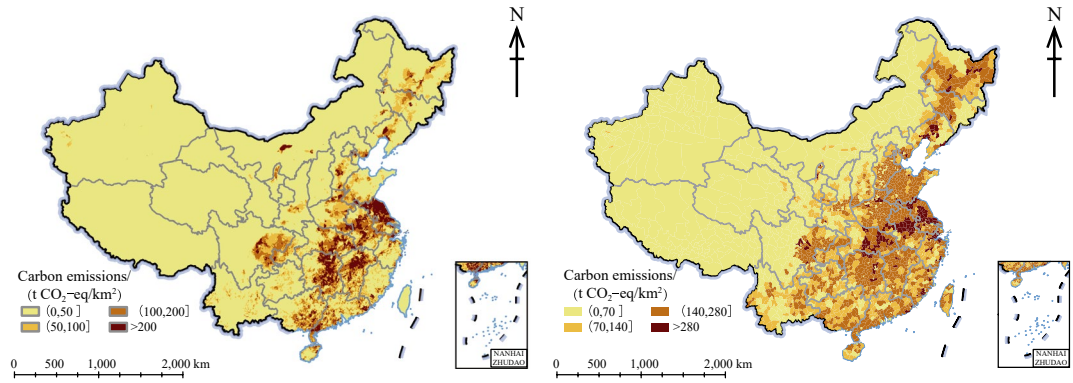

(a) 2010-reference (b) 2010-prediction

Fig. 2.15 Spatial distribution of reference and prediction data in 2010

important scientific data for the evaluation of SDG 2.4 at the national scale.

This case found that: (1) there is an obvious spatial heterogeneity in China's county-scale carbon emissions for cropping systems, with an overall distribution pattern higher in the south and east and lower in the west and north. Compared with 2015, the county-scale carbon emissions per unit area in 2020 increased by 6.44%. (2) China's crop yield increased in the past decade, but the carbon emissions per unit of yield were basically stable.

It should be noted that since China's strategy on reducing carbon emissions was proposed, the country has formulated relevant policies and action guidelines. However, there is an obvious spatial heterogeneity in carbon emissions for cropping systems at the county scale due to different socio-economic, and geographic conditions and cropping patterns. Therefore, scientific conservation and governance efforts should be increased in the future in order to achieve a lower level of carbon emission growth by 2030.

2.3.5 Food Loss and Waste and Its Reduction Pathways in China

Target: SDG 12.3: By 2030, halve per capita global food waste at the retail and consumer levels and reduce food losses along production and supply chains, including postharvest losses.

2.3.5.1 Background

Food loss and waste (FLW) is a global problem. One-third of the food produced in the world is wasted every year, amounting to 1.3 billion tons (Gustavsson et al. 2011). SDG 12.3 calls for reducing FLW and is closely related to food security (SDG 1), nutrition and health (SDG 2), resources and environment (SDG 6, SDG 13, SDG 14, and SDG 15), socio-economic development (SDG 8), and other SDGs (FAO 2019; Springmann et al. 2018; Xue et al. 2017). FLW reduction is critical in a world where food security is being challenged by the COVID-19 pandemic, international political instability, and climate change.

The problem of FLW in China has attracted great attention from the government and the public, but so far there is still a lack of research to comprehensively account from the perspective of the entire food supply chain. It is necessary to conduct a quantitative study from the perspective of the food supply chain, including production, postharvest handling and storage, processing, distribution, retailing, and consumption, and integrate primary survey data and indirect data from literature to improve accuracy and scientificity.

2.3.5.2 Data

- Data of major food supply chain loss and waste surveys conducted in 35 major grain-producing counties in 16 provinces during 2014–2018.
- Survey data of household food waste among rural households in Jinan City, Weifang City, and Dezhou City, Shandong Province, and urban households in Zhengzhou City, Henan Province, in 2017 and 2018, respectively.
- Survey data of food waste from eating out in four typical cities (Beijing, Shanghai, Chengdu and Lhasa) in 2013 and 2015, respectively.
- With "food loss" and "food waste" as keywords, 107 Chinese and English literature datasets were selected.

2.3.5.3 Methods

The food supply chain is commonly categorized into six major stages: production, postharvest handling and storage, processing, distribution, retailing, and consumption. We used the Food and Agriculture Organization (FAO) definition of FLW: food loss refers to the decrease in edible food quantity that is intended for human consumption, occurring during production, postharvest handling and storage, and processing; food waste refers to food discarded at the distribution, retailing, and consumption stages by relevant actors including consumers. Based on a large scale of field surveys and the material flow analysis (MFA) approach, combined with literature review, statistical analysis, and scenario analysis, we focused on the Chinese food system to reveal the mass flow and FLW in the food system, and assessed the efficiency of the Chinese food system.

2.3.5.4 Results and Analysis

From the mass balance of different agrifood products along the entire supply chain from production to consumption in China (Fig. 2.16), the total amount of FLW in the entire food supply chain in China reached 349 million tons during 2014–2018, accounting for 27% of the total food production (direct to consumers). While this share is still lower than that in the United States (30–40%) (U.S. Food and Drug Administration 2019), the total quantity of FLW is phenomenal and makes up about a quarter of the world's total FLW.

The largest amount of FLW was found at the postharvest handling and storage stage with a share of 45% in the total amount of FLW (Fig. 2.17a) much higher than that in industrialized countries such as the United Kingdom (UK) and Japan. This suggests a huge potential

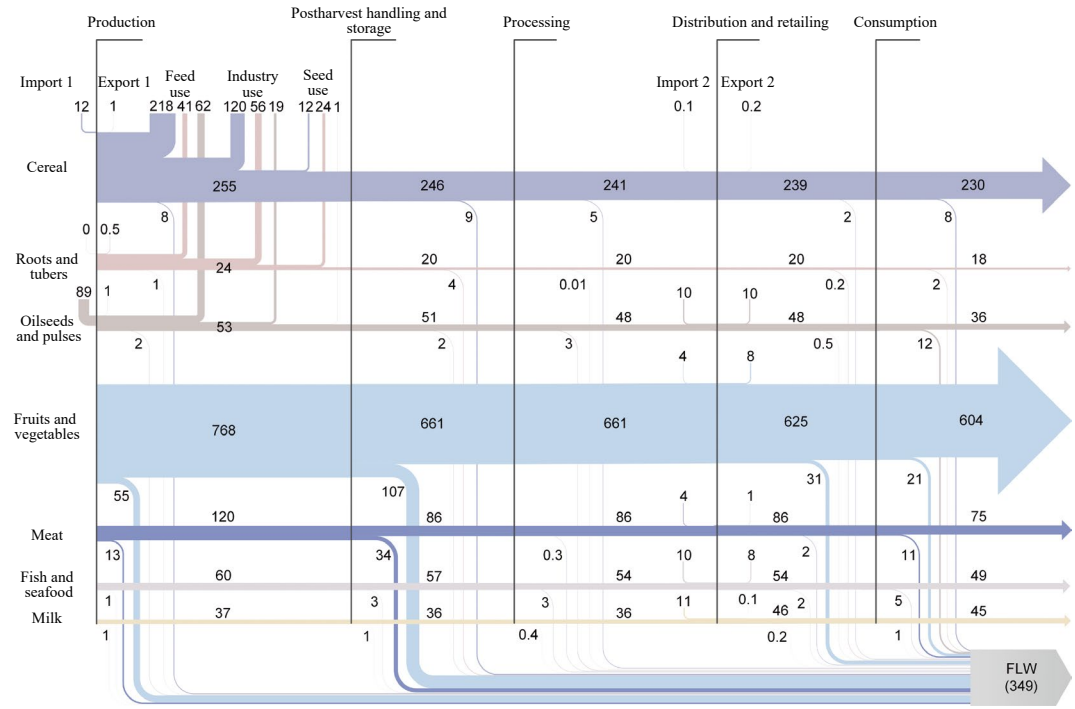

Fig. 2.16 Food flow in China's supply chain from farm to fork. *Note* The number represents the flow value for each stage in the food supply chain; data are annual averages for the period 2014–2018. Values are in Mt

for cutting FLW in China (and in other developing countries) with more advanced technologies (for example, for threshing) and better infrastructure development (for example, for grain storage) in the future. The production stage also contributes to 24% of the total FLW. This is mainly caused by insects, diseases, and mechanical damage in harvesting. The consumption stage also contributes substantially to the total FLW (17%). It is noteworthy that out-of-home food waste accounts for 13% of the total FLW, far exceeding household food waste (4%). The high share of out-of-home food waste in China reflects both the increasing dining-out frequency (related to continuing urbanization and growing household income) and certain food cultures and traditions (for example, overordering for hosted meals in restaurants due to *mianzi*, the tradition of showing hospitality) in China.

From a food category perspective, fruits and vegetables take up the highest share of the total amount of FLW (62%) along the entire chain, followed by meat (17%), cereal (9%), and oilseeds and pulses (5%), and potatoes and milk have relatively small amounts of loss and waste (Fig. 2.17b,c). Fruits and vegetables also dominate (over 30%) among all food categories at each stage of the supply chain, especially for retailing (making up almost 86% of the total FLW at this stage), which basically reflects the perishable nature of fruits and vegetables.

Figure 2.18a presents how the shares of FLW at different stages along the supply chain in China compare with selected countries primarily based on secondary data from statistics and/or literature. China and South Africa have over half of FLW occurring at the production and postharvest handling and storage stages. But for the five industrialized countries/regions, the consumption stage contributes the most to the total FLW. This is related to different levels of economic development and eating habits. When the household food waste composition was compared (Fig. 2.18b), fruit and vegetable waste dominated (over 30%) among all food categories in all countries. The share of other food categories,

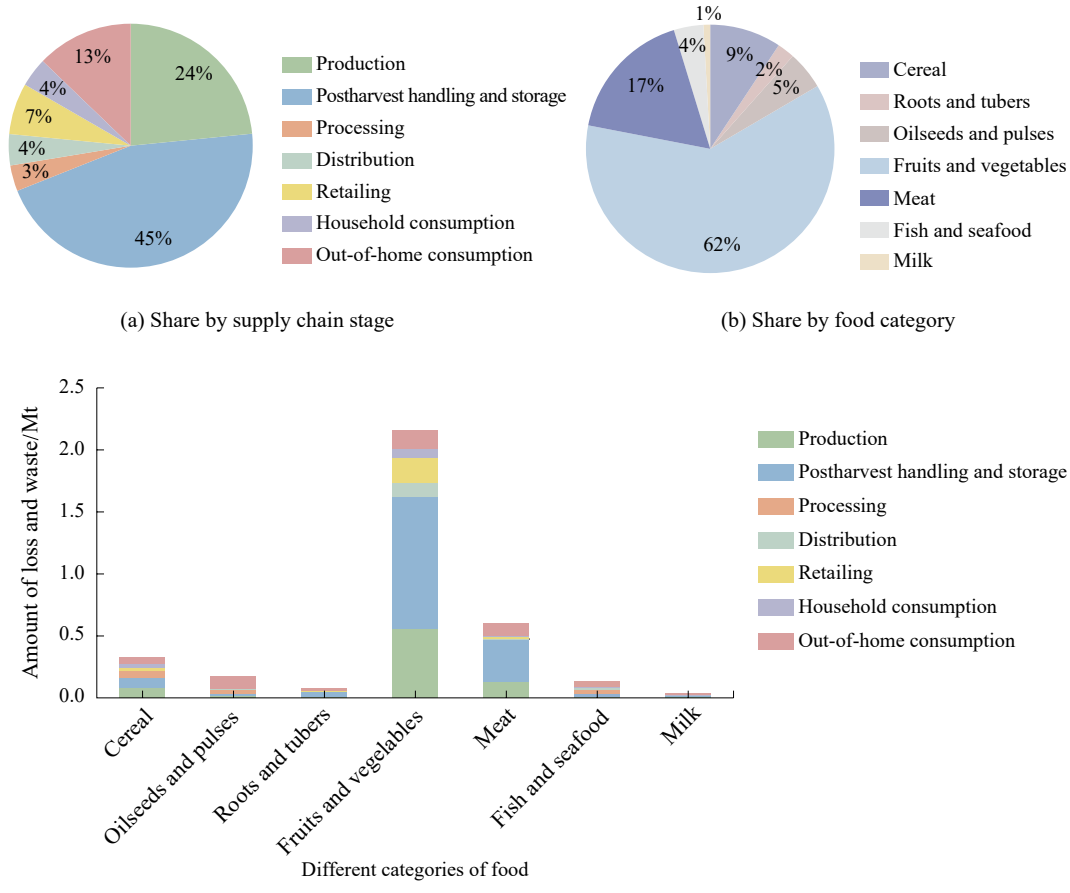

(a) Share by supply chain stage

(b) Share by food category

(c) The amount of loss and waste of different category of food

Fig. 2.17 Estimated FLW in China (annual average for the period 2014–2018)

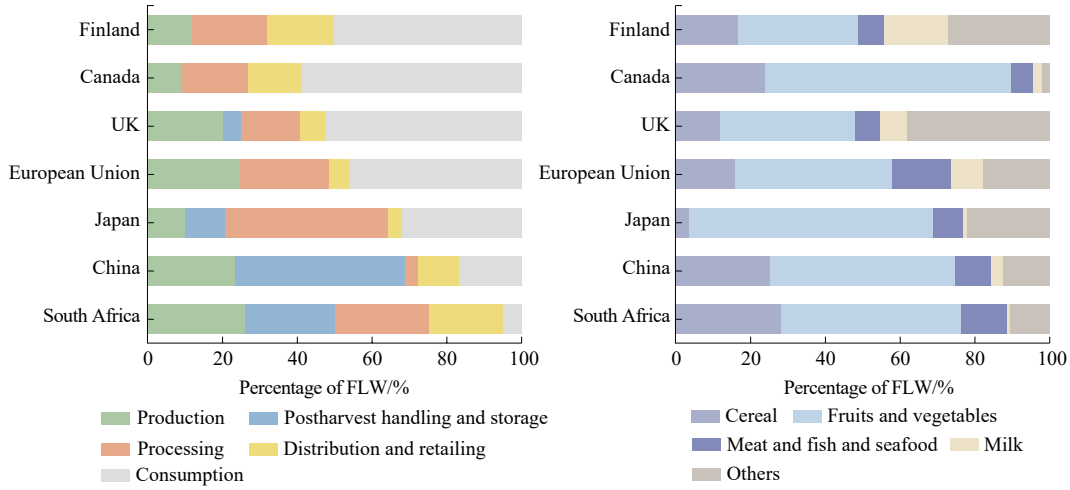

(a) Percentage of total FLW by food supply chain stage

(b) Percentage of FLW by food category for household food waste

Fig. 2.18 Comparison of FLW between China and other countries and organizations

however, reflects variations in the dietary structure, the urbanization level, and the household income of different countries.

Highlights

- Based on the MFA approach, from the perspective of the food supply chain, we used large-scale field surveys and literature data over six years to quantify the FLW of major agrifood products along the entire farm-to-fork chain in China.
- During 2014–2018, 27% of food annually produced for human consumption in the country (349 ± 4 Mt) was lost or wasted; 45% of this is associated with postharvest handling and storage, and 13% with out-of-home consumption activity. These results highlight the importance of better primary data to inform FLW reduction actions and ensure food security and sustainability.

2.3.5.5 Discussion and Outlook

Our study, based on large-scale field work conducted over six years plus a comprehensive literature review and synthesis, provides an estimate of the patterns and magnitudes of FLW along China's food supply chain. Our results provide a step forward in addressing relevant data gaps in China, the world's most populous country. These data provide a good basis to further discuss the role that reducing FLW can play in combating hunger, increasing resource efficiency and lowering environmental burdens. This study was published in *Nature Food* in July 2021 and was selected as a highlight report by *Nature*. The research results are of great significance for the implementation of the Anti-food Waste Law of the People's Republic of China, the improvement of national food security, the promotion of the sustainable development of the food system, and the realization of the "dual carbon goals".

This study showed the following. (1) In the entire food system, a total of 349 Mt food was lost or wasted, that is, approximately 27% of China's total food produced for humans did not make it into human stomachs annually during 2014–2018. China faces a daunting task in reducing FLW. (2) The postharvest handling and storage stage had a share of 45% in the total amount of FLW, and food waste at the consumption stage also accounted for 17%. An FLW reduction action platform involving multi-stakeholders such as processing companies, retailers, farmers, and other relevant entities should be established to act positively on FLW mitigation strategies (modified from Xue et al. 2021).

2.4 Summary

This chapter showcased the use of Big Earth Data to monitor and study indicators of SDG 2, Zero Hunger, in three aspects—improving agricultural productivity, sustainable food production, and halving food waste—at two scales—China and representative subnational regions. As compared with the reports in the previous three years, we expanded the monitoring of SDG 2.4.1 (soil degradation, soil fertility-related sub-indicators) on the scale of China or representative areas, and conducted a thematic study on sustainable food production in the context of climate change on the scale of China specific to SDG 2.4. On the basis of the studies in this chapter, we found that:

(1) Western Jilin, one of the three largest saline-alkali soil areas globally, accounted for 19% of the total area of the northeastern black soil region, and the monitoring revealed a decreasing trend of saline-alkali land area in this region after 2000, mainly influenced by a series of transformative projects such as the "Major projects in western Jilin Province" and the "Alkali-treatment for the West project".
(2) The average value of soil organic carbon density in 0–30 cm of farmland soils in China increased from 41.34 tC/ha in 2015 to 42.72 tC/ha in 2020, the increase of farmland soil carbon in the Beijing-Tianjin-Hebei Urban Agglomeration was the most obvious, and the soil carbon and food production in parts of the region showed a simultaneous increase

in the 40 years. The carbon sink of farmland soil was seen while the carbon emission of the plantation industry showed an increase from 2010 to 2020, yet the carbon emission per unit of production was basically stable.

(3) The total FLW in China accounted for 27% of the total food production (direct for consumer consumption) between 2014–2018 and occurred primarily at the postharvest handling and storage stage, and the adoption of advanced technology and infrastructure in the food distribution process would help reduce food loss.

We will continue to explore the capabilities of Big Earth Data in food security monitoring and assessment in the future, to identify sensitive areas and constraining factors, and to provide a scientific basis for proposing pathways to achieve Zero Hunger.

References

Bannari A, Al-Ali ZM (2020) Assessing climate change impact on soil salinity dynamics between 1987–2017 in arid landscape using Landsat TM, ETM+ and OLI data. Remote Sens 12(17):2794

Bolinder MA, Vandenbygaart AJ, Gregorich EG et al (2006) Modelling soil organic carbon stock change for estimating whole-farm greenhouse gas emissions. Can J Soil Sci 86(3):419–429

Crowther TW, Todd-Brown KEO, Rowe CW et al (2016) Quantifying global soil carbon losses in response to warming. Nature 540(7631):104–108

Ding BG, Zhao Y, Deng JH (2022) Calculation, decoupling effects and driving factors of carbon emission from planting industry in China. Chin J Agric Resour Regional Plann 43(5): 1–11 (in Chinese)

Dong G, Zhao FY, Chen JQ et al (2021) Land uses changed the dynamics and controls of carbon-water exchanges in alkali-saline Songnen Plain of Northeast China. Ecol Ind 133:108353

FAO, IFAD, UNICEF, et al (2022) The state of food security and nutrition in the world 2022. Repurposing Food and Agricultural Policies to Make Healthy Diets More Affordable. Rome, FAO

FAO (2019) The State of Food and Agriculture 2019. https://www.fao.org/publications/home/faoflagship-publications/the-state-of-food-and-agriculture/2019/en. 29 August 2023

FAO (2021) Tracking progress on food and agriculture-related SDG indicators 2021: a report on the indicators under FAO custodianship. Food and Agriculture Organization of the United Nations, Rome

Guo HD (2020) Big Earth Data in Support of the Sustainable Development Goals (2019). Science Press and EDP Sciences, Beijing

Gustavsson J, Cederberg C, Sonesson U et al (2011) Global food losses and food waste: extent, causes and prevention. FAO, Rome

Hong CP, Burney JA, Pongratz J et al (2021) Global and regional drivers of land-use emissions in 1961–2017. Nature 589(7843):554–561

Lal R (2020) Soil organic matter content and crop yield. J Soil Water Conserv 75(2):27A-32A

Li XC, Zhou YY, Zhao M et al (2020) A harmonized global nighttime light dataset 1992–2018. Scientific Data 7:168

Li XJ, Sun YS, Chen XP et al (2022) Saline-sodic soil EC retrieval based on box-cox transformation and machine learning. IEEE J Sel Top Appl Earth Obs Remote Sens 15:1692–1700

Liang DJ, Lu X, Zhuang MH et al (2021) China's greenhouse gas emissions for cropping systems from 1978–2016. Sci Data 8:171

Powlson DS, Whitmore AP, Goulding KWT (2011) Soil carbon sequestration to mitigate climate change: a critical re-examination to identify the true and the false. Eur J Soil Sci 62(1):42–55

Richards LA (1954) Diagnosis and improvement of saline and alkali soils (No. 60). US Government Printing Office. LWW 78(2): 154.

Springmann M, Clark M, Mason-D'Croz D et al (2018) Options for keeping the food system within environmental limits. Nature 562(7728):519–525

Tran TV, Tran DX, Myint SW et al (2019) Examining spatiotemporal salinity dynamics in the Mekong River Delta using Landsat time-series imagery and a spatial regression approach. Sci Total Environ 687:1087–1097

U.S. Food and Drug Administration (2019) How to cut food waste and maintain food safety. https://www.fda.gov/media/101389/download

Xue L, Liu G, Parfitt J et al (2017) Missing food, missing data? A critical review of global food losses and food waste data. Environ Sci Technol 51(12):6618–6633

Xue L, Liu XJ, Lu SJ et al (2021) China's food loss and waste embodies increasing environmental impacts. Nature Food 2(7):519–528

Zhang S W, Yang J C, Li Y, et al (2010) Changes of saline-alkali land in Northeast China and its causes since the mid-1950s. J Nat Resour 25(3): 435–442 (in Chinese)

Zou J, Huang Y, Qin Y et al (2009) Changes in fertilizer-induced direct N_2O emissions from paddy fields during rice-growing season in China between 1950s and 1990s. Glob Change Biol 15(1):229–242

SDG 6 Clean Water and Sanitation

3

3.1 Background

"Ensuring availability and sustainable management of water and sanitation for all" is at the core of SDG 6. UN-Water, in its comprehensive assessment report issued in 2021, pointed out that the world was already off track on SDG 6 even before the outbreak of the COVID-19 pandemic (UN-Water 2021). There are still 2 billion people in the world without access to safe drinking water and 3.6 billion people without access to safe sanitation facilities. In addition, 2.3 billion people lack soap and basic handwashing facilities at home. Most wastewater is discharged untreated. One-fifth of the world's river basins are undergoing rapid changes, and 80% of wetland ecosystems have been lost. In the next nine years, we need to move four times faster in some areas to meet SDG 6 on time (Harlin et al. 2021).

In the SDG 6 progress report released by UN-Water in 2021, the status of implementing SDG 6 worldwide was systematically reviewed and analyzed through individual indicators: wastewater treatment (SDG 6.3.1), ambient water quality (SDG 6.3.2), change in water use efficiency (SDG 6.4.1), level of water stress (SDG 6.4.2), degree of integrated water resources management (SDG 6.5.1), transboundary water cooperation (SDG 6.5.2), and freshwater ecosystems (SDG 6.6.1). However, there were huge gaps in the data used in the report. In addition, national-level data are inadequate in accurately informing decision-making. Therefore, urgent actions need to be taken in the following two aspects: first, strengthen data collection at the national and local levels; second, inform decision-makers on practical actions.

Big Earth Data technology, making rapid advances in recent years, has dramatically improved the capacities for monitoring and evaluating SDG 6. Through remote sensing, regular revisits, and rapid information extraction, such technology enables high spatiotemporal resolution monitoring of relevant indicators, producing more accurate and comprehensive evaluation results at a lower cost and shorter time (Lu et al. 2021). In the past three years, with the support of Big Earth Data, national-scale monitoring was carried out for water quality improvement, water use efficiency (WUE) improvement, IWRM, and change in water-related ecosystems, and an evaluation was conducted on the effectiveness of the implementation of integrated management of water quality, water quantity, and water ecosystems in China. Nevertheless, the role of these studies in informing policies is weakened due to the lack of understanding of the differences in indicator progress in different administrative regions within the country. This chapter systematically evaluates the provincial-level implementation of SDG 6 in China, covering safe drinking water, ambient water quality, WUE, level of water stress, IWRM, freshwater

H. Guo, *Big Earth Data in Support of the Sustainable Development Goals (2022) - China*,
Sustainable Development Goals Series, https://doi.org/10.1007/978-981-97-4231-8_3

ecosystems, and integrated assessments. The results are of great value for understanding the provincial implementation of SDG 6, identifying problems and gaps, and informing strategies for accelerating the realization of SDG 6.

3.2 Main Contributions

The main contributions of the six case studies in this chapter include datasets of the proportion of water bodies with good ambient water quality at the provincial level in China, WUE of China's three major grain crops, the degree of water stress in China, the methods of an improved comprehensive evaluation of water quality in drinking water sources, the combination of multi-source data and methods such as crop WUE assessment during crop growth, the quantitative assessment of water resources management tools in different provinces, and decision support for the construction and management of drinking water sources at the provincial level in China, as well as the assessment of the status of IWRM (Table 3.1).

3.3 Case Studies

3.3.1 Water Quality Monitoring and Assessment of Drinking Water Sources in China

Target: SDG 6.1: The proportion of the population benefiting from secure managed drinking water services.

3.3.1.1 Background

Water resources are the basic resources to support economic, social, and ecological sustainable development. Among the 17 SDGs of the 2030 Agenda, five of them are related to water. The intensification of climate change and the delay of the COVID-19 pandemic have highlighted the importance and urgency of achieving the water goals of the UN 2030 Agenda. One of the 17 SDGs is to ensure that all people have access to "Clean Water and Sanitation" by 2030 (SDG 6).

Ensuring safe drinking water is a fundamental requirement for people's livelihoods, and it is closely related to the health of the population. It is imperative to address the issue of drinking water safety with great importance, considering it from the strategic perspective of building a comprehensive well-off society and achieving the sustainable development of the Chinese nation. Water quality is a crucial aspect of guaranteeing the safety of drinking water. The Outline of the "Healthy China 2030" plan clearly states that it is necessary to promote the construction of drinking water source areas that meet safety standards, and the main indicator for the construction of the "Healthy China" is the proportion of surface water quality reaching Class III water bodies or better. On the basis of reaching 70% in 2020, continuous improvement will be achieved by 2030. Therefore, the monitoring and assessment of the water quality of drinking water sources will help to improve the ability to ensure the safety of drinking water, protect people's safety of drinking water, and provide strong support for the integrated management of water resources and sustainable development.

This study is based on the SDGs and indicator framework of SDG 6 (Clean Water and Sanitation), and develops an algorithmic toolset that can meet the needs of monitoring and assessing indicators of the water quality safety of surface drinking water sources related to SDG 6.1 in 2015 and 2020.

3.3.1.2 Data

- Online water quality monitoring station data for surface drinking water sources from the National Water Resources monitoring Capacity Building Project for 2015 and 2020, involving a total of 30 provinces (autonomous regions and municipalities), not including Hong Kong, Macao, Taiwan, and Heilongjiang Province, and the time scale was updated every 4 h.

Table 3.1 Case studies and their main contributions

Targets	Tier classification	Cases	Contributions
SDG 6.1 By 2030, achieve universal and equitable access to safe and affordable drinking water for all	Tier I	Water Quality Monitoring and Assessment of Drinking Water Sources in China	**Method:** Improved method for the comprehensive evaluation of drinking water source water quality **Decision support:** Support the evaluation of the effectiveness of the construction and management of drinking water sources at the provincial level in China
SDG 6.3 By 2030, improve water quality by reducing pollution, eliminating dumping and minimizing release of hazardous chemicals and materials, halving the proportion of untreated wastewater, and substantially increasing recycling and safe reuse globally	Tier II	Proportion of water bodies with good ambient water quality in China's provinces and change assessment in 2015 and 2020	**Data product:** Dataset of the proportion of water bodies with good ambient water quality for rivers, lakes (reservoirs), water sources, and total water bodies in 31 provincial administrative regions in China in 2015 and 2020 **Decision support:** Support the effective evaluation of surface water and groundwater environmental treatment at the provincial level in China
SDG 6.4 By 2030, substantially increase water use efficiency across all sectors and ensure sustainable withdrawals and supply of freshwater to address water scarcity and substantially reduce the number of people suffering from water scarcity	Tier I	Assessment of change in water use efficiency of three major grain crops in China	**Method:** Evaluation method based on multi-source data combined with the crop growth process **Data Product:** Dataset of WUE of three major grain crops in China from 2010 to 2019, yearly, 1 km spatial resolution
	Tire I	Changes in and drivers of water stress in China from 2010 to 2030	**Data product:** China water stress dataset, between 2010–2020, by month, with spatial resolution 0.5° **Decision support:** Inform industrial restructuring policies under the scenarios of climate change and water resources constraints

(continued)

Table 3.1 (continued)

Targets	Tier classification	Cases	Contributions
SDG 6.5 By 2030, implement integrated water resources management at all levels, including through transboundary cooperation as appropriate	Tier I	Assessment of Data Supporting Capacity for Provincial Integrated Water Resources Management in China	**Method:** Quantitative assessment method for implementation of water resources management tools by province **Decision support:** Inform the assessment of the status of IWRM at the provincial scale in China
SDG 6 Ensure availability and sustainable management of water and sanitation for all	–	Comprehensive assessment of China's SDG 6 progress from 2015 to 2020	**Method:** Sustainability index of water resources development and protection **Decision support:** Inform the assessment of progress in clean water and sanitation facilities at the provincial level in China

- Longitude and latitude data of online monitoring stations for water quality of surface drinking water sources.
- Evaluation based on the Environmental Quality Standard for Surface Water (GB 3838–2002).
- Water Resources Bulletins of 31 provinces, autonomous regions, and municipalities (excluding Hong Kong, Macao, and Taiwan) in 2015.
- Report on the State of the Ecology and Environment of 31 provinces, autonomous regions, and municipalities (excluding Hong Kong, Macao and Taiwan) in 2020.

3.3.1.3 Methods

In this study, a big data cleaning method based on the AdaBoost algorithm (Xie 2021) was first used to clean data from online monitoring data on surface drinking water sources, then the water quality of the sources was evaluated by the BP neural network (Kong et al. 2017; Li et al. 2015), and the spatiotemporal changes in the sources in 2015 and 2020 were compared and analyzed according to the system clustering method based on the square Euclidean distance and Spearman rank correlation coefficient method (Xie et al. 2022).

The steps are as follows.

1. A total of five indicators of surface water quality—dissolved oxygen, permanganate index, ammonia nitrogen, total phosphorus, and total nitrogen—were selected, and the water quality was set to meet the safety standards of Class III water or above, referring to the Environmental Quality Standard for Surface Water (GB 3838-2002).
2. For the problem of abnormal data in the process of online water quality monitoring, a big data cleaning method based on the AdaBoost algorithm was used. We first used the isolated forest algorithm (IF algorithm) to quickly and accurately identify and reject abnormal water quality data, and then interpolated the missing dataset of water quality through the AdaBoost algorithm to further improve data accuracy.
3. Based on the above water quality online monitoring data cleaning results, we analyzed the water quality safety of surface drinking water sources in 2015 and 2020.
4. To quantitatively analyze the spatiotemporal changes in water quality of surface drinking water sources monitored online in 2015 and 2020, we first used the system clustering method based on Euclidean distance squared to partition the water quality compliance rate of drinking water sources, and then used the Spearman rank correlation coefficient method to compare and analyze each monitoring index.

3.3.1.4 Results and Analysis

Distribution of Online Monitoring Stations for Water Quality at Drinking Water Sources

The current situation of water quality pollution in drinking water is not uncommon. In order to ensure the safety of the water supply for the public, it is necessary to start with standardized and accurate water quality monitoring. This can be achieved with online monitoring technology.

According to the national water resources monitoring capacity from the station network data, the number of online monitoring stations in 2020 increased from 118 in 2015 to 489, by three times. The frequency of online water quality monitoring is once every four hours, which improves the water quality monitoring and warning capabilities of drinking water source areas (Fig. 3.1).

Spatial Clustering Analysis of Water Quality in Drinking Water Sources

The water quality threshold of drinking water sources met the standards of Class III water and above. Conducting a statistical analysis of water quality compliance at various online monitoring stations, we spatially clustered the compliance rates for each province, and classified drinking water sources into three zones: the first zone (80% to 100%), the second zone (60% to 80%), and the third zone (0% to 60%).

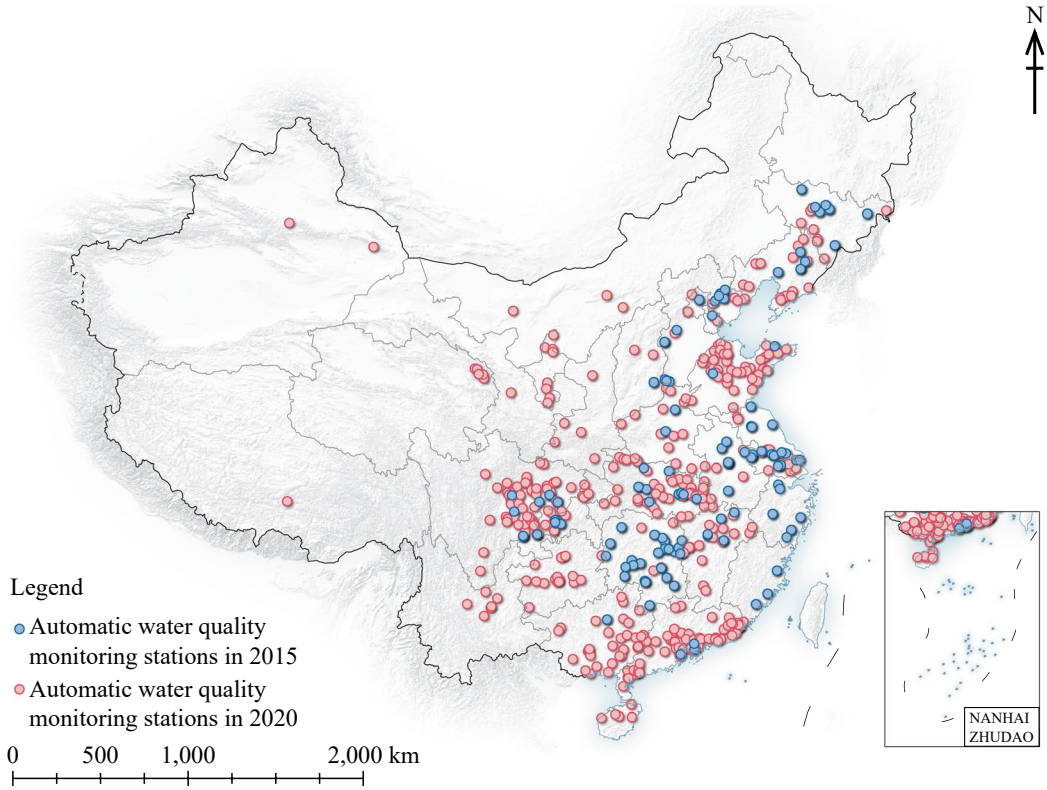

Fig. 3.1 Distribution of automatic water quality monitoring stations in drinking water sources in 2015 and 2020 in China. *Note* No data for Hong Kong, Macao, Taiwan, and Heilongjiang

In 2015, the first category consisted of 17 provinces (including autonomous regions and municipalities) including Hainan, Gansu, and Beijing, while the second category consisted of 10 provinces including Anhui, Sichuan, and Chongqing. The third category comprised four provinces, including Shanxi, Zhejiang, and Shandong. In 2020, except for Hebei Province, all 30 other provinces fell under the first category, as illustrated in Fig. 3.2.

Analysis of Changes in Water Quality Monitoring Indicators for Drinking Water Sources

Water quality monitoring itself must meet certain timeliness requirements. Traditional manual sampling and analysis have relatively low efficiency, but the emergence of online water quality monitoring technology has significantly improved monitoring efficiency. The online water quality monitoring project examined in this case study mainly includes the following two parts: (1) routine indicators used for the most basic monitoring of water quality, including pH, water temperature, dissolved oxygen, EC, and turbidity, and (2) total amount of pollutants. The monitoring of the five parameters of water quality can only form a general understanding of the water environment. In order to have more comprehensive information and more targeted water environment protection, it is also necessary to monitor the total amount of pollutants. The material indicators to be monitored include the permanganate index, nitrogen, and phosphorus.

This study is based on the data of existing online monitoring stations for surface drinking water source water quality. The monitoring indicators are mainly dissolved oxygen, permanganate index, ammonia nitrogen, total phosphorus, and total nitrogen. The growth rate is used to

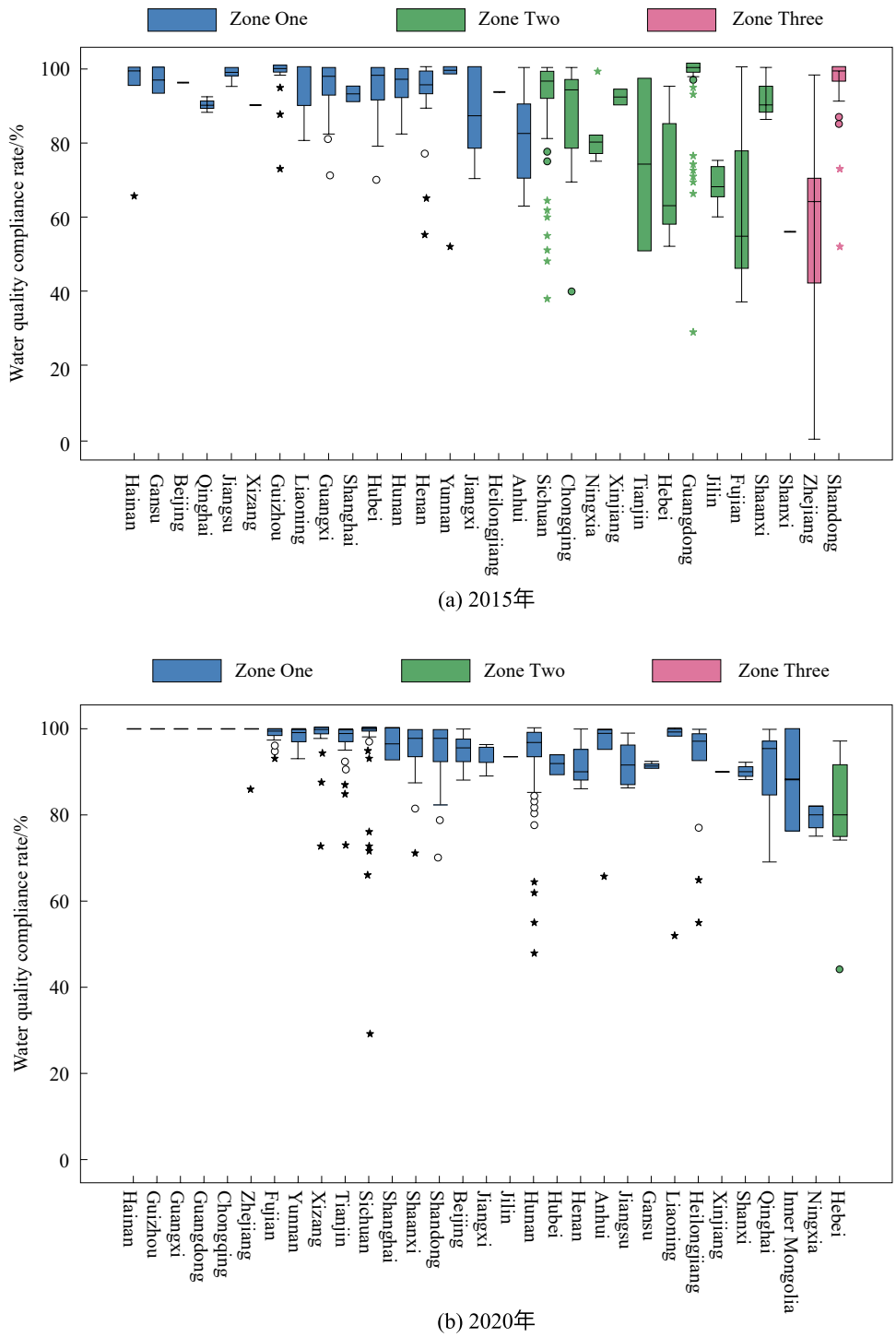

Fig. 3.2 Comparison of cluster analysis results of the spatial distribution of water quality in drinking water sources in 2015 and 2020. *Note* ★ and ○ represent outliers after clustering

evaluate the changes in water quality monitoring indicators in 2020 compared with 2015. The expression is:

$$\text{Growth rate} = (\text{2020 target value} - \text{2015 target value})/\text{2015 target value} \times 100\% \quad (3.1)$$

1. **Dissolved Oxygen**
   In 2020, the compliance rate of dissolved oxygen at monitoring stations was 99%, showing a growth rate of 3% compared to 2015. Hebei and Jilin had the highest growth rates in dissolved oxygen compliance, reaching 14%. Following were Shanxi and Ningxia, with growth rates of 13% and 11%, respectively.
2. **Permanganate Index**
   In 2020, the compliance rate of permanganate index at monitoring stations was 99%, showing a growth rate of 3% compared to 2015. Jilin had the highest growth rate in permanganate index compliance, reaching 13%. Following were Tianjin, Shanxi, Jiangxi, and Hunan, with a growth rate of 11%. Next were Inner Mongolia and Chongqing, with growth rates of 10% and 8%, respectively.
3. **Ammonia Nitrogen**
   In 2020, the compliance rate of ammonia nitrogen at monitoring stations was 95%, showing a growth rate of 9% compared to 2015. Inner Mongolia had the highest growth rate in ammonia nitrogen compliance, exceeding 100%. Following were Shanxi and Shaanxi, with a growth rate of 52%. Next was Tianjin, with a growth rate of 35%.
4. **Total Phosphorus**
   In 2020, the compliance rate of total phosphorus at monitoring stations was 98%, showing a growth rate of 11% compared to 2015. Shandong had the highest growth rate in total phosphorus compliance, reaching 90%. Following were Shanxi and Fujian, with growth rates of 72% and 55%, respectively. Next was Guangdong, with a growth rate of 40%.
5. **Total Nitrogen**
   In 2020, the compliance rate of total nitrogen at monitoring stations was 98%, showing a growth rate of 8% compared to 2015. Zhejiang had the highest growth rate in total nitrogen compliance, reaching 78%. Following were Shanxi and Jilin, with growth rates of 49% and 44%, respectively (Figure 3.3).

Water Quality and Safety Evaluation Results of Drinking Water Sources

Based on the water quality data from the online monitoring stations developed under the National Water Resources monitoring Capacity Building Project, the safety compliance rate reached 94% in 2020. Five provinces (municipalities) including Beijing, Tianjin, Jilin, Shanghai, and Zhejiang achieved a 100% compliance rate for the safety of surface drinking water sources. Following were three provinces, Jiangsu, Jiangxi, and Hunan, with a 99% compliance rate. Furthermore, a total of twenty provinces including Shandong, Guangdong, Guizhou, Gansu, Guangxi, Liaoning, Hubei, Fujian, Heilongjiang, Xinjiang, Shanxi, Anhui, Hainan, Yunnan, Shaanxi, Henan, Chongqing, Sichuan, Xizang, and Qinghai achieved a safety compliance rate of over 90%. Compared to 2015, the compliance rate of surface drinking water source area safety increased by 16%, with improvements observed in the compliance rates of all provinces. Among them, Inner Mongolia had the highest growth rate in the compliance rate, exceeding 100%, showcasing the most prominent improvement. Following was Shandong, with an 85% increase in the compliance rate and Zhejiang at 79% (Fig. 3.4).

Highlights

- Through the implementation of the National Water Resources Monitoring Capacity Building Project, China's water quality monitoring significantly improved, and the number of online monitoring stations in 2020 compared with 2015 increased by three times.
- Through monitoring, it has been observed that in 2020, China's surface drinking water source areas showed varying degrees of improvement in compliance rates for

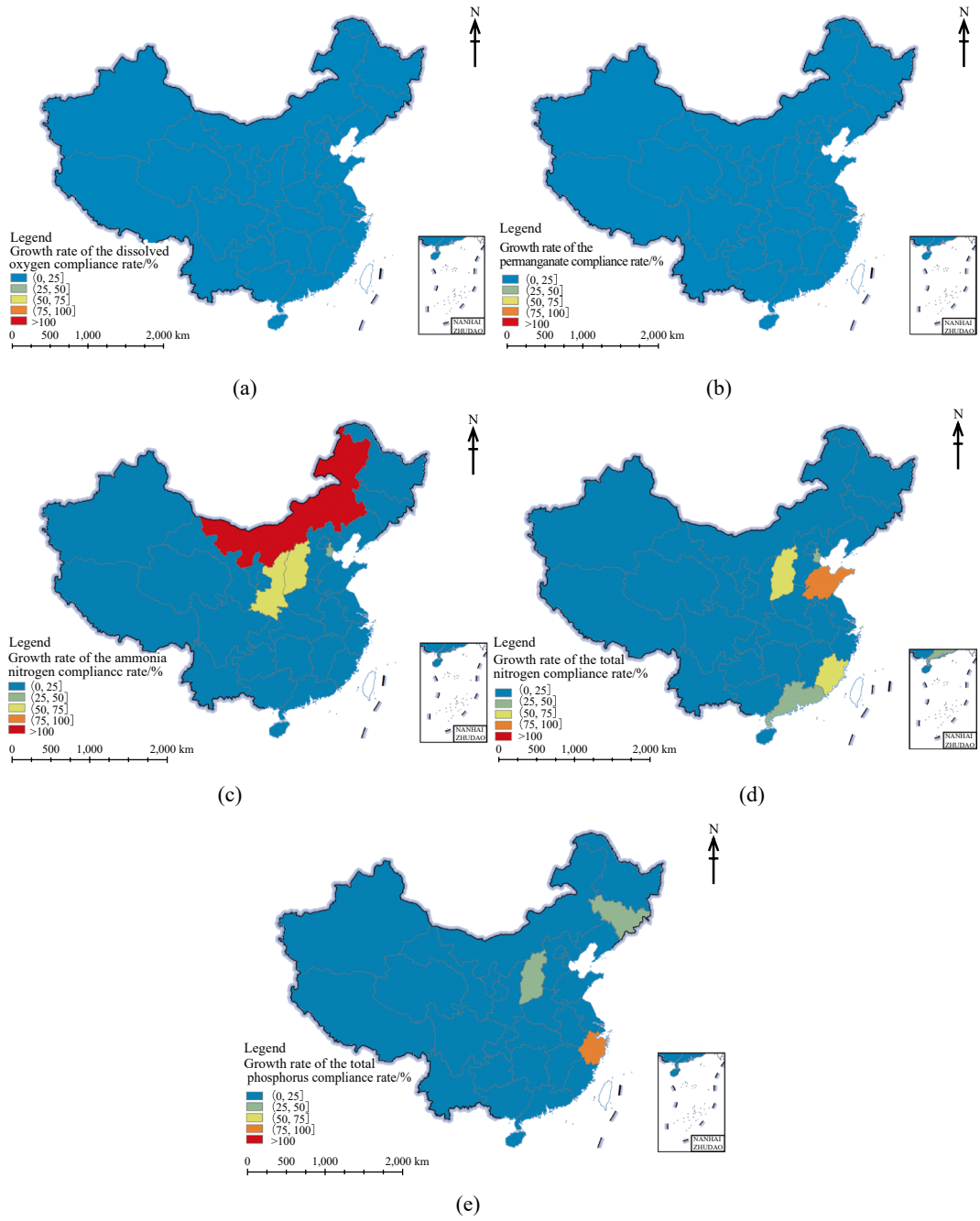

Fig. 3.3 Change rates of water quality monitoring indicators in China's drinking water sources in 2020 relative to 2015. *Note* No data for Hong Kong, Macao, and Taiwan

automatic monitoring indicators, including dissolved oxygen, permanganate index, ammonia nitrogen, total phosphorus, and total nitrogen, compared to 2015. The compliance rate for total phosphorus had the highest growth rate, reaching 11%, indicating a significant enhancement in water source quality.

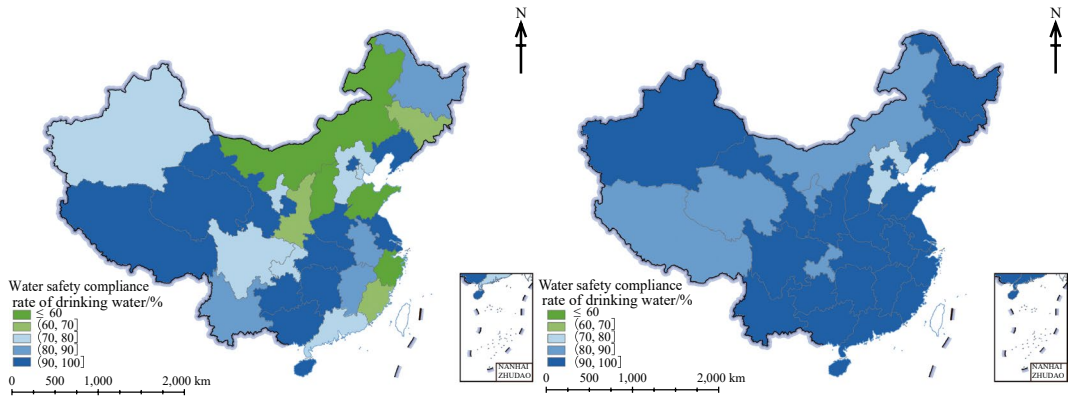

(a) 2015 (b) 2020

Fig. 3.4 Spatial distribution of water quality safety compliance rates in China's drinking water sources in 2015 and 2020. *Note* No data for Hong Kong, Macao, and Taiwan

- Based on the assessment of monitoring results, in 2020, the safety compliance rate of drinking water sources in 31 provinces across the nation (excluding data from Hong Kong, Macao, and Taiwan) showed improvement compared to 2015, with a growth rate of 16%. This signifies a continuous enhancement in China's capacity to ensure safe drinking water.

3.3.1.5 Discussion and Outlook

This study is based on research conducted using online monitoring data of drinking water sources under the National Water Resources monitoring Capacity Building Project. Data for certain provinces were either missing or lacked representativeness due to the absence of monitoring sites or the inclusion of unrepresentative sites. For these provinces, the data in this study were calibrated using bulletin data from the same year. This study draws the following conclusions.

1. In 2020, the number of online monitoring stations for surface drinking water sources increased by more than three times compared to 2015, and the monitoring and safety assurance capabilities of drinking water sources have been continuously enhanced.
2. In 2020, the compliance rates of online monitoring indicators for surface drinking water sources, including dissolved oxygen, permanganate index, ammonia nitrogen, total phosphorus, and total nitrogen, showed varying degrees of improvement compared to 2015. The compliance rate for total phosphorus had the highest growth rate, reaching 11%, signifying a significant improvement in water source area quality.
3. In 2020, the compliance rate of drinking water source area safety improved compared to 2015, with a growth rate of 16%, demonstrating a continuous enhancement in China's capacity to ensure safe drinking water.

Considering that some of the monitoring stations established in 2015 may face operational and other issues, and might not have been able to maintain functionality by 2020, a comparison between the results from the same monitoring stations in 2015 and 2020 was not feasible. This limitation introduces a certain degree of uncertainty into the results, and this clarification is important. Based on the assessment of available data, the water quality of surface drinking water sources showed significant improvement from 2015 to 2020. However, challenges remain in some regions regarding water quality, indicating

the need to strengthen governance measures and regulatory efforts. Enhancing the security and protection of China's drinking water sources will provide robust support for comprehensive water resources management and sustainable development. In light of this, the following recommendations are proposed.

First, to address the issue of uncertainty in water quality assessment due to insufficient or less representative monitoring stations, it is suggested to incorporate local monitoring networks into the assessment process. This will enhance the ability to identify spatial variations in water quality, thereby improving the precision of targeted strategies.

Second, regular assessments of the environmental conditions of water sources should be conducted, continually enhancing the capacity for risk prevention, control, and emergency response.

3.3.2 Proportion of Water Bodies with Good Ambient Water Quality in China's Provinces and Change Assessment in 2015 and 2020

Target: SDG 6.3: By 2030, improve water quality by reducing pollution, eliminating dumping and minimizing release of hazardous chemicals and materials, halving the proportion of untreated wastewater, and substantially increasing recycling and safe reuse globally.

3.3.2.1 Background

Goal 6 of the UN 2030 Agenda reflects the significant increase in global attention to water, and progress toward the goal can be measured by SDG 6.3.2, proportion of water bodies with good ambient water quality, and SDG 6.6.1, change in the extent of water-related ecosystems over time.

In 2015, the State Council of China issued the Action Plan for Prevention and Control of Water Pollution. The plan proposes that the proportion of excellent water quality (up to or better than Class III) in the seven major river basins has reached more than 70%, including the Yangtze River, Yellow River, Pearl River, Songhua River, Huaihe River, Haihe River, and Liaohe River. Black and odorous water bodies in urban built-up areas at the prefecture level or above were controlled within 10% by 2020. By 2030, the overall proportion of excellent water quality in the seven major river basins in China will reach over 75%, while black and odorous water bodies in urban built-up areas will be eliminated, and the overall proportion of centralized drinking water sources in cities reaching or surpassing Class III will be around 95%. The plan has important guiding significance for the prevention and control of water pollution in China, as well as the protection and construction of beautiful rivers and lakes.

At present, China's water environment problems are still very prominent, mainly manifested in poor water quality in some water bodies, the imbalanced supply and demand of water resources, severe damage to water ecology, and multiple hidden dangers in the water environment. All provinces (autonomous regions and municipalities, excluding Hong Kong, Macao, and Taiwan) have carried out water quality monitoring and report, but there is a lack of intercomparison and analysis among provinces. This study will fill in the gap in this field and provide data and decision-making support for formulating water pollution prevention and control policies for all provinces.

3.3.2.2 Data

- China Environmental Statement 2015 for 31 provinces (autonomous regions and municipalities, excluding Hong Kong, Macao, and Taiwan).
- China Ecology and Environment Statement 2020 in China for 31 provinces (autonomous regions and municipalities, excluding Hong Kong, Macao, and Taiwan).
- Water quality data for 2019, 2020, and 2021 were obtained via the National Groundwater

Monitoring Project (Ministry of National Resources of the People's Republic of China).

3.3.2.3 Methods

Surface Water Quality Evaluation Method

This study first collected the China Environmental Statement 2015 and China Ecology and Environment Statement 2020 in China from 31 provinces (autonomous regions and municipalities). Then, the total number (or cross-section) and the number with good quality of rivers, lakes (reservoirs), and water sources in each province were extracted from the above bulletins, and the missing data were supplemented through data review and consultation surveys. The data were digitized to form a water quality database. Finally, the statistics, analysis, and mapping of the data were conducted to obtain overall good proportionality, changes, inter-provincial comparisons, spatial distribution characteristics, and temporal variation patterns of rivers, lakes, and water sources in all provinces of China in 2015 and 2020.

The calculation formula for the proportion of water bodies with good quality (P_W) in rivers, lakes, and water sources is as follows:

$$P_W = N_G/N_T \times 100\% \tag{3.2}$$

where N_G and N_T refer to the number of water bodies (or cross sections) with good quality and the total number (or cross sections), where good-quality is defined as classes I–III for water quality classification.

The overall proportion of good-quality water bodies (P_{W-T}) for each province was calculated using the weighted average of rivers, lakes (reservoirs), and water sources. The formula is as follows:

$$P_{W-T} = \frac{N_G^R}{N_T^3} \times P_{W-R} + \frac{N_G^L}{N_T^3} \times P_{W-L} + \frac{N_G^S}{N_T^3} \times P_{W-S} \tag{3.3}$$

where $N_T^3 = N_T^R + N_T^L + N_T^S$; N_T^R, N_T^L and N_T^S represent the total number of rivers, lakes (reservoirs), and water sources; N_G^R, N_G^L, and N_G^S represent the number of good-quality water bodies of rivers, lakes (reservoirs), and water sources; and P_{W-R}, P_{W-L} and P_{W-S} represent the proportion of water bodies (or cross sections) with good quality of rivers, lakes (reservoirs), and water sources.

Comparing the data on the proportion of water bodies with good quality between 2015 and 2020, the calculation method for the change amount ($P_{\mathrm{w}}^{2015-2020}$) over the five years is as follows:

$$P_w^{2015-2020} = P_w^{2020} - P_w^{2015} \tag{3.4}$$

where P_w^{2015} and P_w^{2020} represent the proportion of water bodies with good quality in 2015 and 2020, respectively.

Assessment Methods of Groundwater Quality

According to the Standard for Groundwater Quality (GB/T 14848—2017), each water quality index of the monitoring stations was assessed as an F_i factor (Table 3.2).

According to the Nemerow index method (Ni and Feng 2018), a comprehensive evaluation was produced using formulas (3.5) and (3.6), thus yielding an F value:

$$F = \sqrt{\overline{F}^2 + F_{\max}^2/2} \tag{3.5}$$

$$\overline{F} = \frac{1}{n}\sum_{i=1}^{n} F_i \tag{3.6}$$

where F_i represents the evaluation result of the i-th water quality indicator; $F_{\max}$ is the maximum of F_i; and n represents the number of indicators participating in comprehensive evaluation.

By defining the F value, the quality assessment was classified for each monitoring well (Table 3.3).

The evaluation results show that groundwater of classes I–III has relatively low chemical

Table 3.2 Single indicator evaluation level F_i value

Individual index assessment	I	II	III	IV	V
F_i	0	1	3	6	10

Table 3.3 Comprehensive evaluation results of groundwater quality at monitoring stations

Comprehensive evaluation classes	I	II	III	IV	V
F	<0.8	0.8–2.5	2.5–4.25	4.25–7.2	>7.2

components and is suitable as a centralized drinking water source and industrial and agricultural water. These are defined in this study as "excellent". Class IV groundwater, which has a high chemical component content, is suitable for agriculture and some industrial use, and can be used as domestic drinking water after proper treatment. It is defined as "good" in this study. Class V groundwater is not suitable for drinking and is defined as "inferior".

3.3.2.4 Results and Analysis

Inter-Provincial Comparison of Surface Water Bodies with Good Quality

In 2015, there were seven provinces with over 90% of water bodies with good water quality, five with 80%–90%, thirteen with 60%–80%, and six with less than 60%. In 2020, the water quality in most provinces improved significantly, with a significant increase in the proportion of water bodies with good water quality exceeding 90% in seventeen provinces and a decrease in the number of provinces with water quality below 60% to two provinces. The top three water bodies with good water quality in 2015 and 2020 were Xizang, Fujian, and Guizhou, at nearly 100%. In 2015 and 2020, Tianjin and Beijing ranked in the bottom three, while Shanghai and Inner Mongolia respectively entered the bottom three in 2015 and 2020 (Fig. 3.5).

Spatial Distribution of Surface Water Bodies with Good Quality in All Provinces of China

In 2015, surface water bodies with good quality in all provinces of China showed circular distribution characteristics. The water quality shows a gradual improvement trend from North China to the outside. Beijing, Tianjin, Hebei, and Shanxi in North China, and Liaoning in Northeast China have the worst water quality. Those with a good water quality ratio of over 90% are mainly

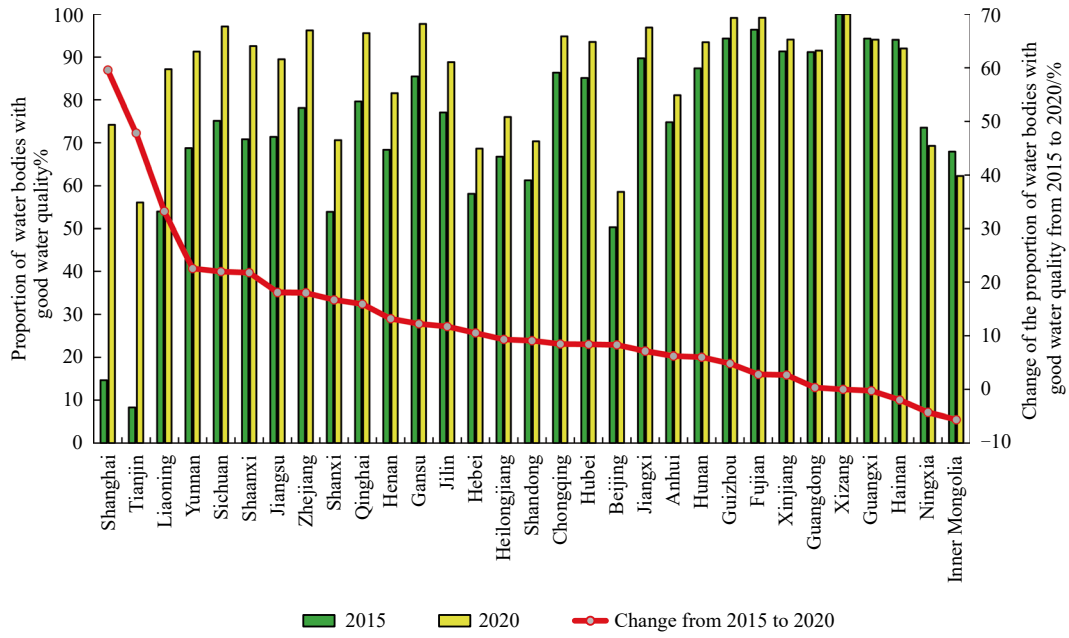

Fig. 3.5 Proportion and changes in surface water bodies with good quality in all provinces (autonomous regions, municipalities, excluding Hong Kong, Macao, and Taiwan) of China in 2015 and 2020

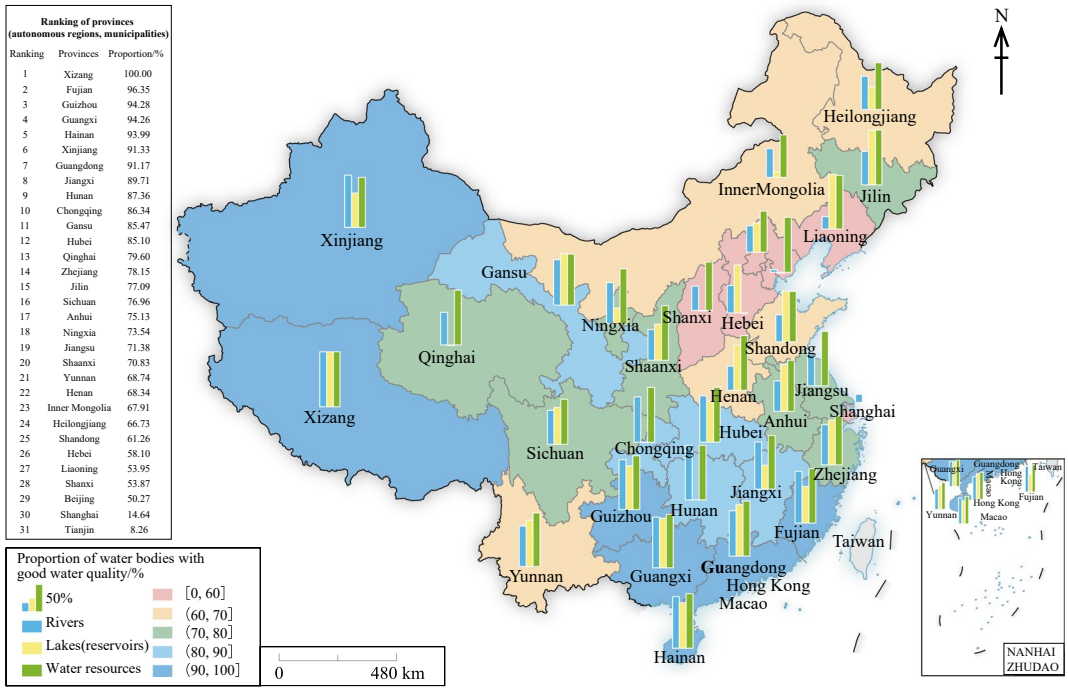

Fig. 3.6 Spatial distribution pattern of surface water bodies with good quality in all provinces of China in 2015. *Note* Some data on rivers, lakes (reservoirs), and water sources are missing, shown as −1% in the bar chart. No data for Hong Kong, Macao, and Taiwan

distributed in Xinjiang in northwestern China, Xizang and Guizhou in southwestern China, as well as Fujian, Guangdong, Guangxi, and Hainan along the southern coast (Fig. 3.6).

In 2020, the provinces with poor water quality were significantly reduced, with only Beijing and Tianjin having a proportion of surface water bodies with good quality below 60%. The proportion of surface water bodies with good quality in 17 provinces exceeded 90%, accounting for about two-thirds of China's total land area. The overall improvement in water quality was significant (Fig. 3.7).

In terms of water body types, the water quality of water sources is generally good, followed by rivers, and the water quality of lakes (reservoirs) is weak and still needs significant improvement.

Changes in the Proportion of Surface Water Bodies with Good Quality in All Provinces of China from 2015 to 2020

From 2015 to 2020, the water quality of most provinces in China showed a trend of improvement, with 26 experiencing an increase in the proportion of surface water bodies with good quality and only four experiencing a decrease, while Xizang maintained 100% excellence. The proportion of water bodies with good quality in the provinces along the Northeast-Southwest (Heilongjiang to Yunnan) that originally had poor water quality increased, resulting in a significant improvement. The water quality improvement in Inner Mongolia, Ningxia, Xinjiang, and several coastal provinces was relatively small, and even slightly deteriorated. In terms of provincial distribution, from 2015 to 2020, Shanghai, Tianjin, and Liaoning achieved the most improvement in water quality, especially with less than 20% of surface water bodies with good quality in Shanghai and Tianjin in 2015 whose water quality situation was very poor, but both of them had significant improvements in 2020, with the proportion of water bodies with good quality reaching 74.21% and 56.07%, respectively. The water quality in Guangxi, Hainan, Ningxia, and Inner Mongolia slightly deteriorated, while others improved.

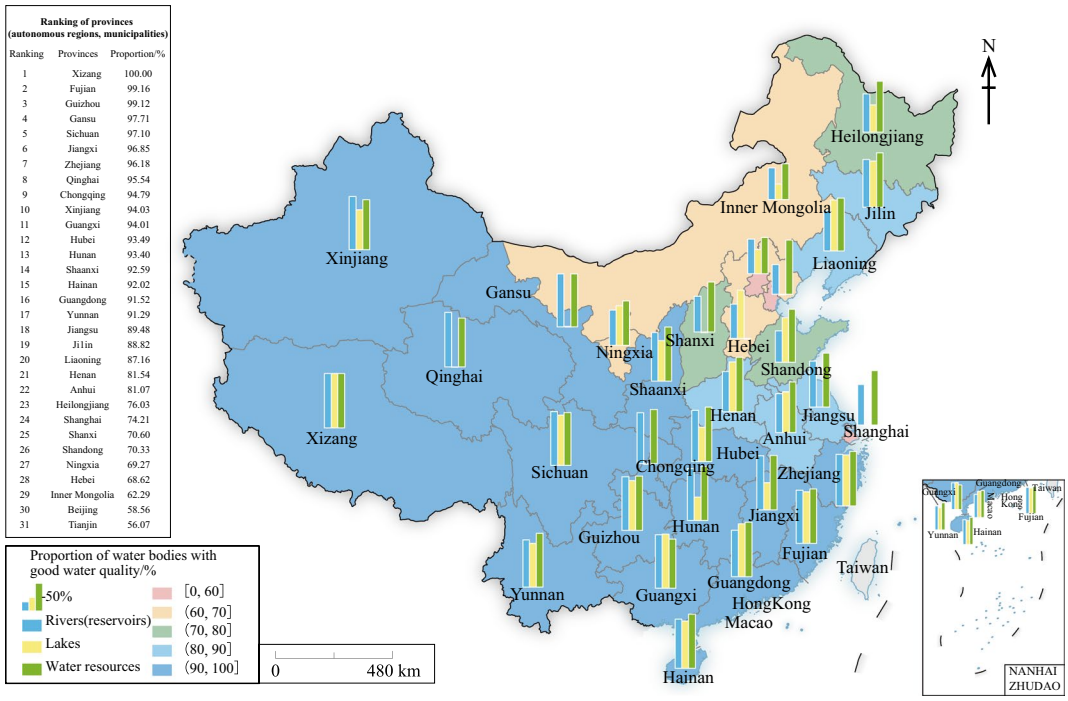

Fig. 3.7 Spatial distribution pattern of surface water bodies with good quality in all provinces of China in 2020. *Note* Some data on rivers, lakes (reservoirs), and water sources are missing, shown as −1% in the bar chart. No data for Hong Kong, Macao, and Taiwan

In terms of water body types, the improvement of water quality in rivers and lakes (reservoirs) was significant, especially in rivers, indicating that provinces had achieved good results in extensively controlling river pollution. The water quality of water sources has always been good, and it has maintained a stable and positive trend over the five years (Fig. 3.8).

General Groundwater Quality of China from 2019 to 2021

Groundwater quality assessment resulted in mainly class IV for all 10,171 monitoring wells, at around 67.86%; class V came second, taking approximately 17.93%; while classes I–III took about 14.21%. From 2019 to 2021, there was a drop in the proportion for class V, yet, classes I–III rose with fluctuation (Table 3.4). For individual wells, 11.78% were upgraded from lower classes, while 9.92% were downgraded from higher classes, and 78.29% stayed unchanged from 2019 to 2021.

The main groups that affect water quality are manganese, iron, total hardness, total dissolved solids, sodium, sulfide, chloride, ammonia, sulfate, iodide, and fluoride. For manganese, 48% of the monitoring wells exceeded the class IV threshold, meaning that nearly half of the groundwater contains manganese higher than 1.5 mg/L, which is the threshold value of class IV. In more than 20% of monitoring wells, iron, total hardness, total dissolved solids, and sodium are greater than their class IV thresholds. Fluoride and iodine are the elements that are closely related to endemic diseases mainly in the Northeast China Plain, North China Plain, and Plains in Northwest China. The rates of these two elements exceeding the thresholds are about 15% and 18%, respectively.

General Groundwater Quality of All Provinces from 2019 to 2021

The groundwater quality of each province of China generally presents a gradually

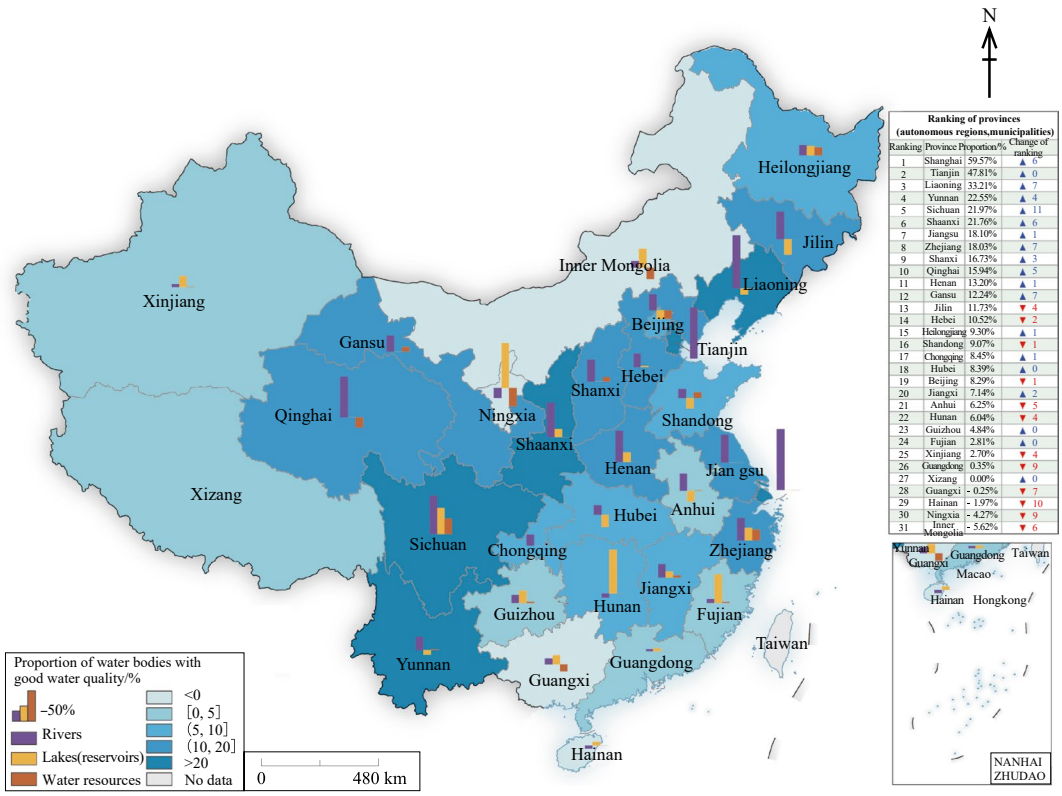

Fig. 3.8 Changes in the proportion of surface water bodies with good quality in all provinces of China from 2015 to 2020. *Note* Some data on rivers, lakes (reservoirs), and water sources are missing, shown as −1% in the bar chart

Table 3.4 Proportion of water quality evaluation results at national groundwater monitoring wells (unit: %)

Years	Excellent			Good	Inferior
	Class I	Class II	Class III	Class IV	Class V
2019	2.48	10.33	1.55	66.88	18.76
2020	3.11	9.44	1.00	68.80	17.65
2021	3.36	10.24	1.12	67.89	17.39

deteriorating trend, as the population grows from west to east. Coastal provinces are in a worse scenario than inland ones. Groundwater quality in the northeastern and northwestern provinces is mainly affected by congenital factors, and is assessed as class IV. The proportion of Class V in North to East China is relatively high, due to being severely affected by human activity (Fig. 3.9).

The groundwater quality assessment results of groundwater monitoring stations in all provinces were mainly stable, except for those in North, East, Northwest, and Southwest China from 2019 to 2021. The groundwater quality in Guizhou, Hunan, Henan, and Guangdong tended to get better; nevertheless, the groundwater quality in Jiangsu, Anhui, Jiangxi, Ningxia, Hebei, Liaoning, Jilin, and Tianjin worsened in the three years (Fig. 3.10).

Policy Recommendations

The regions with poor surface water quality (including Tianjin, Beijing, Inner Mongolia, Hebei, Ningxia, Shandong, Shanxi, Shanghai, and Heilongjiang), as well as Guangxi, Hainan, Ningxia, and Inner Mongolia with deteriorating water quality, need to strengthen water

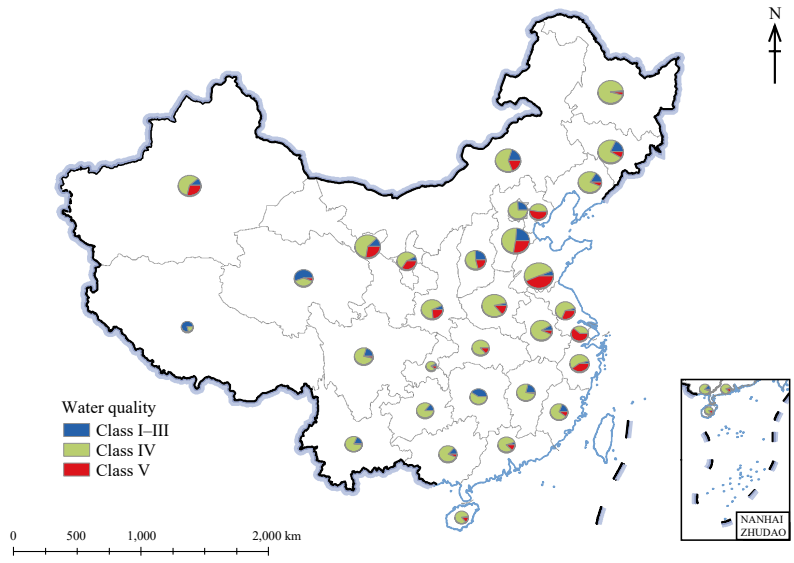

(a) 2019

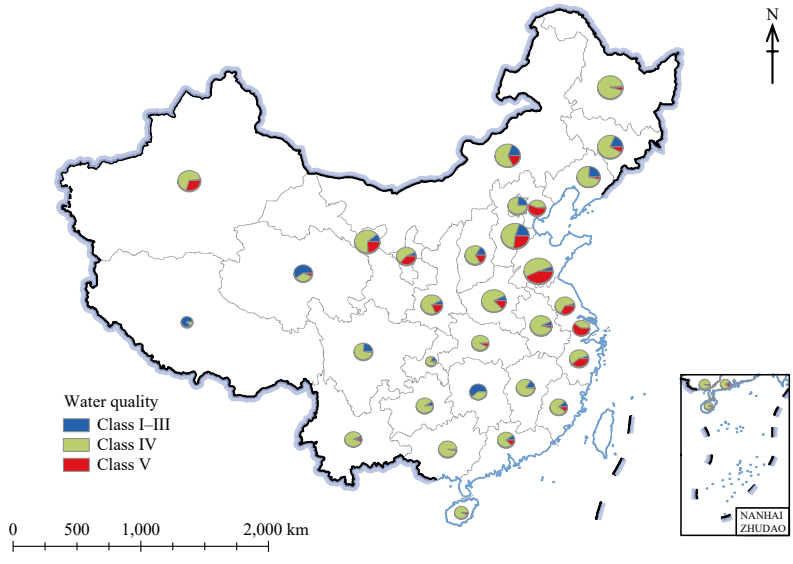

(b) 2020

Fig. 3.9 Assessment results at groundwater monitoring wells at the provincial level from 2019 to 2021. *Note* No data for Hong Kong, Macao, and Taiwan

environment protection and governance efforts, curb the downward trend, and continuously increase the proportion of surface water bodies with good quality. Provinces with a good water quality ratio exceeding 90% (Xizang, Fujian, Guizhou, Gansu, Sichuan, Jiangxi, Zhejiang, Qinghai, Chongqing, Xinjiang, Guangxi, Hubei, Hunan, Shaanxi, Hainan, Guangdong, Yunnan) and provinces with significant water pollution control results in the five years (Shanghai, Tianjin, Liaoning, Yunnan, Sichuan, Shaanxi) still need to maintain their original water environment protection and control measures to prevent water quality deterioration.

The reasons for changes in groundwater quality are relatively complex, and in addition to

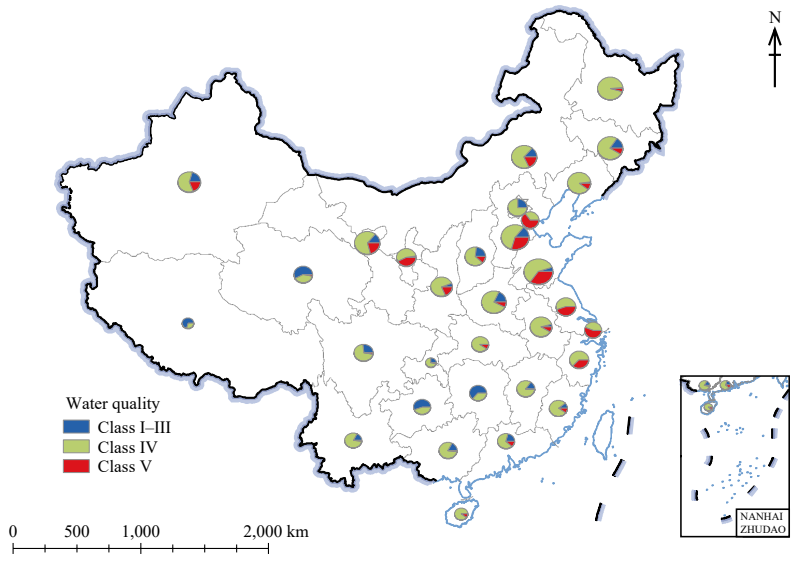

(c) 2021

(continued)

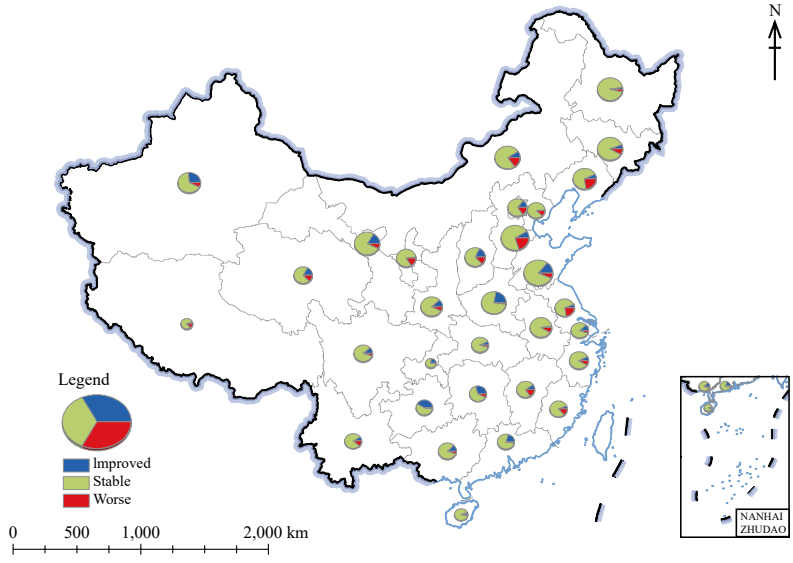

Fig. 3.10 Change in assessment results at groundwater monitoring sites at the provincial level between 2019 and 2021. *Note* No data for Hong Kong, Macao, and Taiwan

congenital factors, the impact of human activity on groundwater cannot be ignored. The groundwater quality in the lower reaches of the Yellow River in Henan, Shandong, and other regions, and in the Pearl River Basin in Guizhou, Guangxi, Hunan, Guangdong, and other regions has improved. Benefiting from the ecological protection and high-quality development of the Yellow River Basin and Pearl River Basin and other policies, we should continue to strengthen pollution control and environmental protection, especially the adjustment of the proportion

of water use, and the control of production and domestic waste discharge. In areas around the Bohai Sea, such as Liaoning, Tianjin, and Hebei, there is a trend of deterioration in groundwater quality. In densely populated areas, especially those with frequent industrial and agricultural production and human activity, it is necessary to plan the intensity of groundwater extraction reasonably, continue to implement ecological water replenishment policies, and thus slow down and prevent water quality changes caused by groundwater level decline. Meanwhile, it is necessary to be vigilant about the leaching effect of heavy precipitation on the existing pollutants in the vertical recharge paths of the atmosphere, soil, and aeration zone during the process of groundwater recharge, in order to prevent surface environmental pollution components from entering groundwater through recharge channels.

Highlights

- For the first time, a provincial-level evaluation and analysis were conducted on the quality of surface water bodies and groundwater in 31 provinces (autonomous regions and municipalities, excluding Hong Kong, Macao, and Taiwan), providing scientific data and decision-making support for provincial-level water protection and pollution prevention.
- Most provinces in China have shown an overall improvement in surface water bodies and groundwater quality, which indicates significant effectiveness in water pollution control. Among them, the water quality of water sources is generally good, the water quality of rivers, and lakes (reservoirs) has significantly improved, and the groundwater quality is mainly stable.

3.3.2.5 Discussion and Outlook

From 2015 to 2020, the provinces with a proportion of good-quality surface water bodies exceeding 90% increased from seven to seventeen, accounting for about two-thirds of China's total land area. The overall improvement in water quality was significant. The water quality of rivers and lakes (reservoirs) significantly improved, especially in rivers, indicating that provinces had achieved good results in vigorously controlling river pollution. The quality of water sources was always good during the study period, and it has maintained a stable and positive trend over the five years. The information produced in this case study provides support for the evaluation of water environment protection and governance policies over the past few years. Horizontal comparisons between provinces urge lagging provinces to increase policy support. The results provide decision-making support for the implementation of new policies and measures for water environment protection and governance in the future.

Groundwater quality is related to the safe supply of drinking water sources. The comprehensive assessment resulted in class IV for most of China from 2019 to 2021. The proportion of class V water was slightly higher than that of classes I–III. The main substances affecting the water quality were inferior components such as manganese, iron, total hardness, total dissolved solids, and sodium. The groundwater quality of each province of China generally presented a gradually deteriorating trend from west to east. Coastal regions were in a worse scenario than inland areas. Over the three years, the groundwater quality assessment results across the country were mainly stable. The groundwater quality in South China has improved, while the groundwater quality in regions such as East China, North China, and Northeast China has deteriorated. This study analyzed the national groundwater quality as well as the quality and distribution of the main impact indicators, summarized the provincial groundwater quality status, and the changes between 2019 and 2021, which could provide important scientific data for evaluating SDG 6.3.2 on a national scale.

3.3.3 Assessment of Change in Water Use Efficiency of Three Major Grain Crops in China

Target: SDG 6.4: By 2030, substantially increase water use efficiency across all sectors and ensure sustainable

withdrawals and supply of freshwater to address water scarcity and substantially reduce the number of people suffering from water scarcity.

3.3.3.1 Background

China's three major grain crops, including rice, maize, and wheat, account for more than 80% of the total sown area of grain crops and play an important role in food production and consumption. However, the large amount of water required for grain production, combined with high water consumption due to evapotranspiration (ET), has led to ecological and environmental problems, such as water shortages, which has restricted sustainable agricultural development. Improving the cropland water use efficiency (WUE) is a key measure to achieve water-efficient agriculture and promote sustainable agricultural development.

Cropland WUE is a commonly used indicator to assess agricultural WUE, which refers to the biomass or yield produced by a unit of water, and can reflect the efficiency of water use from an output perspective. Cropland WUE can comprehensively reflect the trade-off between grain production and water consumption by cropland, and is an effective indicator for guiding the sustainable use of regional agricultural water resources. Multi-source remote sensing data and other Earth observation big data can provide spatial information to support the assessment of temporal and spatial changes in agricultural WUE and related SDGs, with better coverage, timeliness, and update frequency than statistical data-based evaluation methods. However, research on the quantitative assessment of cropland WUE using remote sensing observations is still in its early stages, and related studies still face significant challenges. At the same time, SDG 6.4.1 "change in water-use efficiency over time" is also a key indicator of SDG 6.4, but long-term global and regional cropland WUE datasets are still lacking.

This study aims to develop a method for estimating cropland WUE using multi-source data to address the current lack of agricultural WUE data. This study evaluates the WUE of three major grain crops in China (wheat, maize, and rice) and their interannual variations, and provides technical support for promoting sustainable agricultural development in China.

3.3.3.2 Data

- Gross primary production (GPP) and ET data for all crops in China from 2001 to 2019, with a spatial resolution of 1 km and a temporal resolution of 1 day.
- Remotely sensed high-resolution phenology data for China's three major grain crops (wheat, maize, and rice) from 2001 to 2019, with a spatial resolution of 1 km and a temporal resolution of 1 day.
- Crop growth and soil moisture data with a 10-day observation interval from agricultural meteorological stations in China.
- Provincial-level statistics on the area and yield of the three major grain crops (wheat, maize, and rice) in China from 2001 to 2019.
- Global irrigated area dataset (Meier et al. 2018) with a spatial resolution of 1 km, which provides information on the distribution of irrigated farmland worldwide.

3.3.3.3 Methods

WUE can be expressed as the ratio of crop yield per unit area to ET (i.e., water consumption per unit area). ET is calculated using the ETMonitor model (Hu and Jia 2015; Zheng et al. 2022) driven by multi-source remote sensing data and atmospheric reanalysis data ERA5. The ETMonitor model comprehensively considers the major physical processes that affect ET, such as energy balance, water balance, and vegetation physiology. The accuracy of ETMonitor is superior to other existing ET products and has the advantage of high spatiotemporal resolution. The data have been released through the CASEarth Data Sharing and Service Portal.[1]

The crop yield was estimated based on cropland GPP combined with crop phenology and

[1] https://data.casearth.cn/sdo/detail/6253cddc819aec49731a4bc2.

provincial crop yield statistics. Cropland GPP was estimated using the Evaporative Fraction Light Use Efficiency (EF-LUE) model driven by remote sensing data (Du et al. 2022). The specific methods are as follows: (1) The EF-LUE model, which considers soil water stress in addition to the air temperature constraint and water vapor pressure deficit (VPD) constraint, was used to estimate crop GPP. The GPP obtained from carbon flux data collected from the eddy covariance flux tower observation network of ChinaFlux was used to optimize the model parameters for maximum light-use efficiency, air temperature constraint factor, and water VPD factor to improve the accuracy of crop GPP estimation. (2) The high-resolution phenology dataset of China's three major grain crops (obtained from remote sensing data) was corrected using 10-day crop growth and soil moisture data from agricultural meteorological stations in China to improve the accuracy of the remotely sensed crop phenology data and thus the accuracy of the estimation of cumulative GPP and ET estimation during the crop growing season. (3) The harvest indices of the three major grain crops were estimated annually at the provincial level by combining provincial statistics on crop yield and cumulative GPP during the growing season. This approach can greatly reflect the influence of scientific and technological advances and farmland management practices on crop yield, and improve the accuracy of crop yield estimates.

The yield and ET (i.e., crop water consumption) of China's three major grain crops were estimated using the above method by combining remote sensing observations of surface parameters [soil moisture, leaf area index, the fraction of absorbed photosynthetically active radiation (fAPAR), etc.], phenological data, and statistical data, and the spatiotemporal distribution of WUE for these crops was obtained with high accuracy.

As for the analysis method, this study first used the least squares method to obtain the average annual rate of change of WUE, ET, and the yield of three major grain crops. The annual rate of change was then multiplied by the total number of years (18 years) and divided by the values of WUE, ET, and yield of the initial year (i.e., 2001) to obtain the magnitude of changes between 2001 and 2019. The differential equation method was used to quantitatively decompose the contribution rate of ET and yield changes to the trend of WUE change.

3.3.3.4 Results and Analysis

According to the spatial distribution of the WUE of the three major grain crops (Fig. 3.11), the WUE of wheat in North China and Central China is relatively high, while the WUE of wheat in Southwest China is relatively low. The WUE of maize in Northeast China and East China is relatively high, while it is relatively low in Southwest and South China. The WUE of rice in Central China and Northeast China is relatively high, while it is relatively low in the Southwest, South, and North China. Such spatial patterns are influenced by factors such as climate, terrain, cropping structure, and agricultural infrastructure.

The WUE of the three major grain crops in China showed a significant increasing trend from 2001 to 2019 (Fig. 3.12), among which the WUE of wheat increased by 33.4% [0.024 kg/(m^3·a)], WUE of maize increased by 20.0% [0.016 kg/(m^3·a)], and WUE of rice increased by 14.1% [0.014 kg/(m^3·a)]. From the regional perspective, the WUE of the three major grain crops in each geographical region also showed an increasing trend, but the increasing rate was different (Figs. 3.13 and 3.14). The WUE of wheat showed a larger increase in North China, East China, and Central China, and a smaller increase in Southwest China. The WUE of maize showed a faster increase in North China and Northeast China, and a relatively slower increase in Central China and East China. The WUE of rice generally showed a significant increasing trend in Central China, East China, and South China, and a smaller increase in Northeast China and Northwest China.

According to the analysis of the contribution rate of changes in crop WUE to changes in crop ET and yield, the increase in crop yield is the main factor driving the increase in the

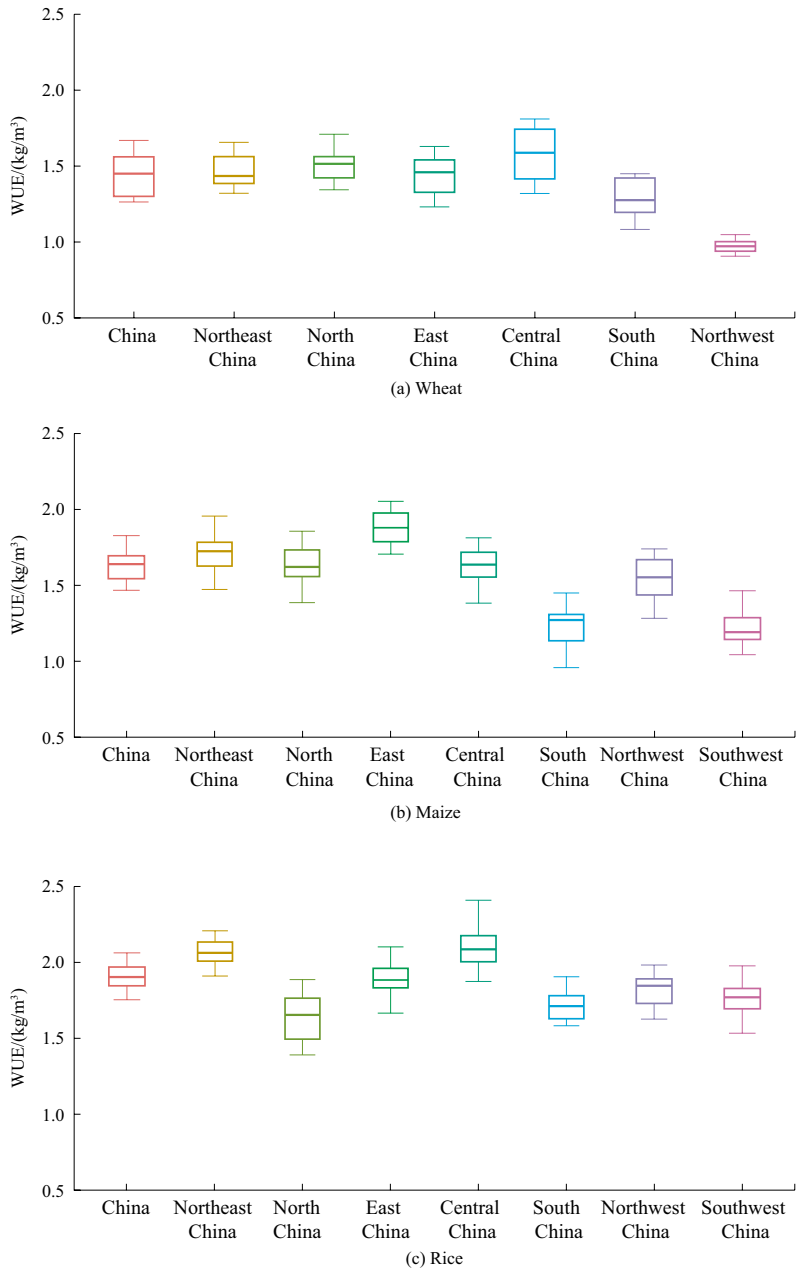

Fig. 3.11 Statistics on the WUE of the three major grain crops in China and in the major geographical regions from 2001 to 2019

WUE of the three major grain crops in China and in different geographical regions. Although ET shows an increasing trend, the contribution of ET change to the change in WUE is relatively small compared to the contribution of yield change (Figs. 3.12 and 3.14). The significant increase in grain yield is not accompanied by a synchronous increase in water consumption per unit area, which is due to the significant improvement in agricultural technology, agricultural infrastructure, water-saving irrigation, and agricultural water management

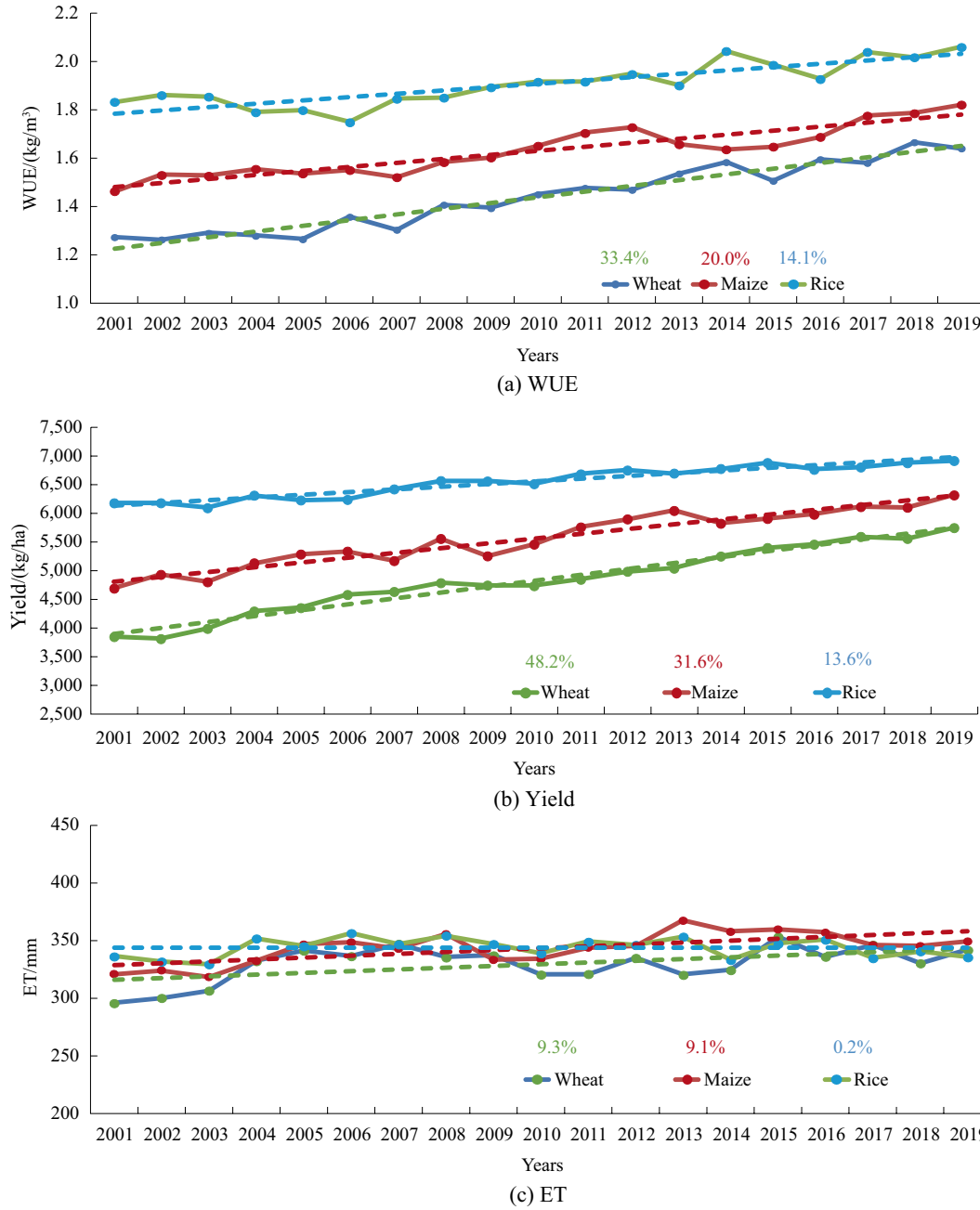

Fig. 3.12 Interannual variation and trends of WUE, yield, and ET of the three major grain crops in China from 2001 to 2019. *Note* The percentages in the figure represent the increase rate from 2001 to 2019

technology, all of which are beneficial to the sustainable development of grain production in China.

The multi-year average and increase rate of wheat WUE in Southwest China are relatively small, which may be due to the fact that wheat is not the main grain crop in this region, and the quality of cultivated land for growing wheat is relatively poor (e.g., dry land and hilly farmland) with insufficient agricultural management

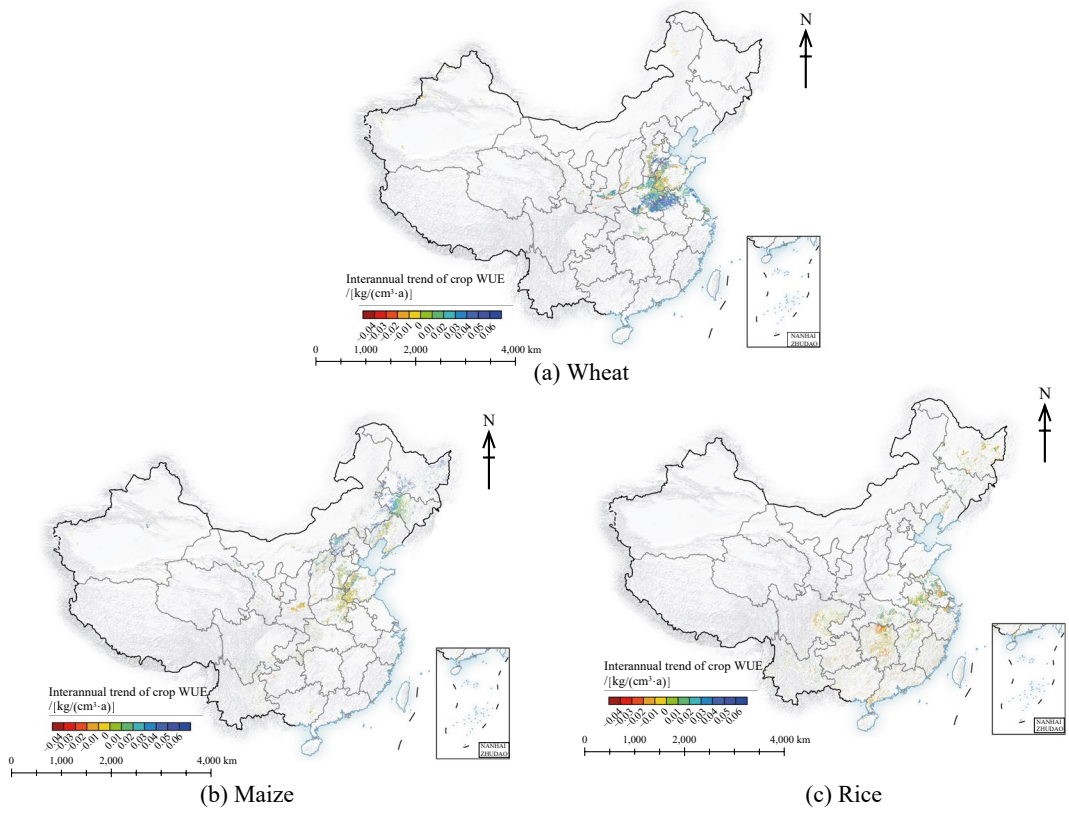

Fig. 3.13 Spatial distribution of the WUE trends of the three major grain crops in China from 2001 to 2019

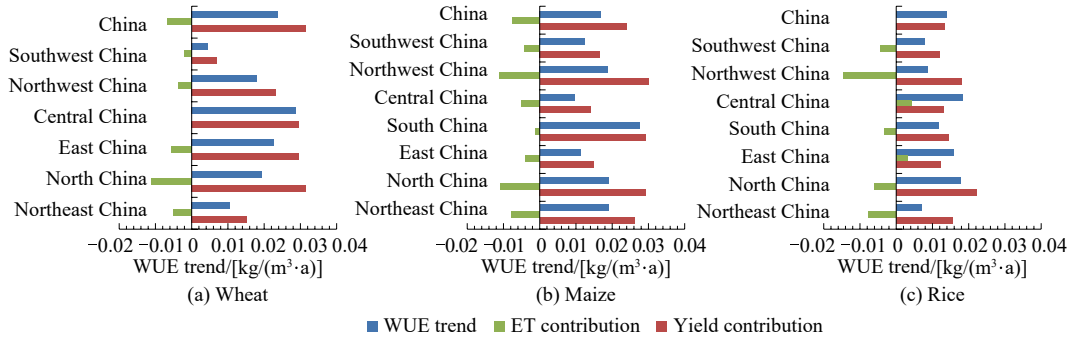

Fig. 3.14 Contribution of changes in yield and ET to the trend of WUE from 2001 to 2019 for the three major grain crops in China and in each geographical region. *Note* A positive value of yield contribution indicates that the trend of yield is consistent with that of WUE, and a negative value indicates that the trend is opposite. A positive value of ET contribution indicates that the trend of ET is opposite to that of WUE, and a negative value indicates that the trend of ET is consistent with that of WUE. If the absolute value of yield contribution is greater than the absolute value of ET contribution, it means that the contribution of the yield change to the trend of WUE is large, and vice versa, the contribution of ET change to the trend of WUE change is large

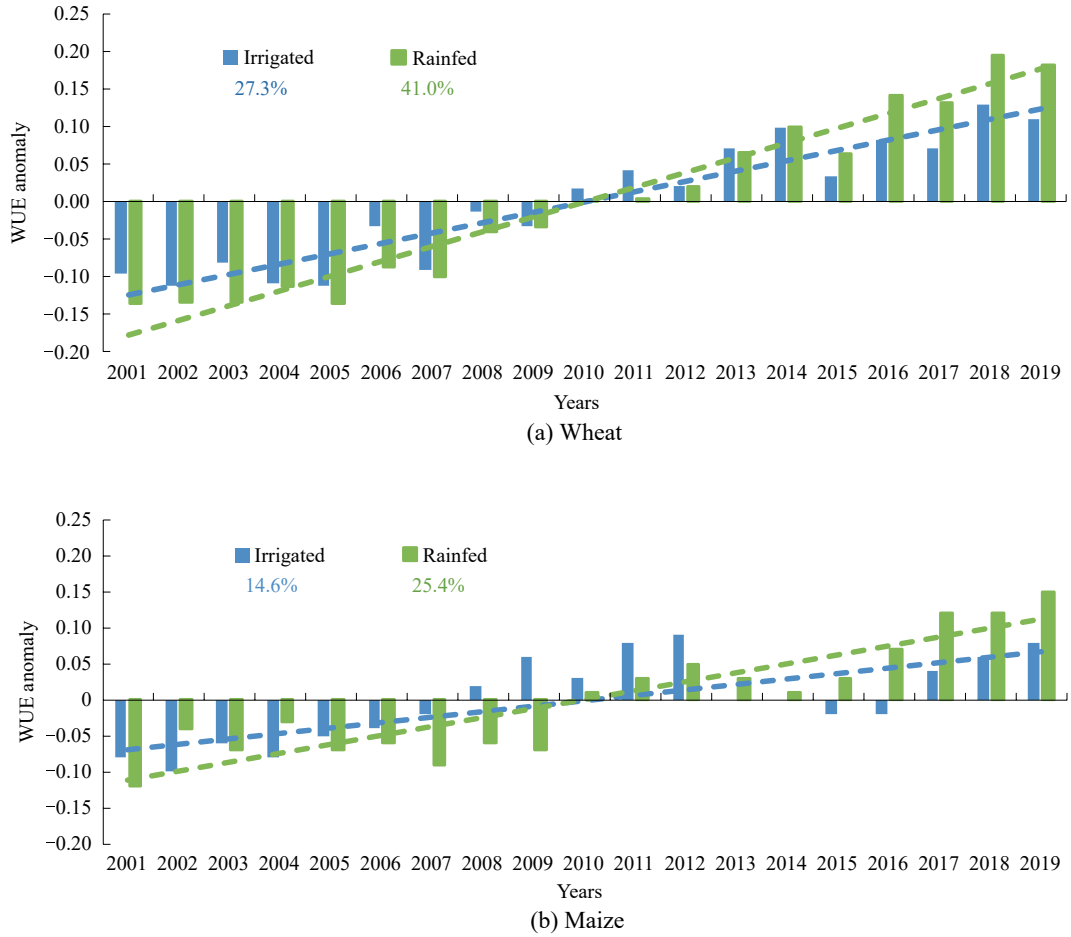

Fig. 3.15 WUE anomalies of irrigated and rainfed crops (wheat and maize) from 2001 to 2019. *Note* The percentages in the figure represent the increased rate of crop WUE between 2001 and 2019

and infrastructure investment, resulting in a lower increase rate of wheat yield, thus reducing the increase rate of WUE. The low increase in WUE for maize in East and Central China is also mainly due to the relatively small increase in yield, which may be related to the fact that maize is not the main grain crop in these two regions, resulting in less investment in agricultural management and infrastructure. Central and Northeast China are the main rice-producing areas in China, with high rice yields and relatively high WUE. However, compared with Central China, the increase in WUE for rice in Northeast China is relatively small because the increase in ET is relatively large compared with the increase in yield. This is related to factors such as temperature increase and the rapid expansion of rice-paddy fields in this region (the quality and yield of newly added rice-paddy fields are generally lower than those of long-term cultivated rice-paddy fields, and the irrigation water consumption is not lower than that of long-term cultivated rice-paddy fields, thus affecting the increase of rice WUE).

From the perspective of rainfed and irrigated crops (considering only wheat and maize), both rainfed and irrigated crops showed an upward trend in WUE over the 20 years (Fig. 3.15). The WUE of rainfed wheat and maize is lower than that of irrigated wheat and maize, but the increase in the WUE of rainfed crops (41.0% for rainfed wheat and 25.4% for rainfed maize) is higher than that of irrigated crops (27.3% for

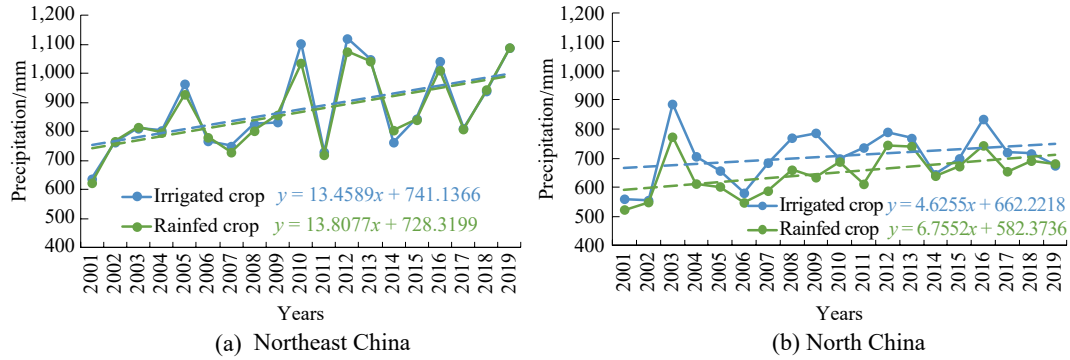

(a) Northeast China (b) North China

Fig. 3.16 Annual precipitation of irrigated and rainfed farmlands in Northeast China and North China from 2001 to 2019

irrigated wheat and 14.6% for irrigated maize). A possible reason is that rainfed crops are more sensitive to precipitation than irrigated crops. Crop yield has been improved due to advances in agricultural technology and farmland management practices (such as seed improvement, agronomic technology, mulching for moisture and heat retention, soil and water conservation, etc.). In addition, precipitation in the concentrated rainfed cropland areas, such as Northeast China and North China, showed a slightly increasing trend (Fig. 3.16). With the improvement in water conditions, the yield of rainfed crops increased more than that of irrigated crops, and the increase of the WUE of rainfed crops was higher than that of irrigated crops.

Highlights

- An innovative crop WUE assessment method based on multi-source data combined with crop growth information was developed, and WUE datasets on the three major grain crops (rice, maize, and wheat) in China from 2001 to 2019 were produced, providing scientific data support for the monitoring and evaluation of SDG 6.4.1 in agricultural areas of China.
- The WUE of the three major grain crops in China showed an increasing trend from 2001 to 2019, with an increase of 33.4% for wheat, 20.0% for maize, and 14.1% for rice. The increase in WUE was mainly caused by the increase in yield, which benefited from the advances in agricultural science and technology, the improvement of agricultural infrastructure conditions, and the improvement of water-saving irrigation technology.

3.3.3.5 Discussion and Outlook

This study developed a crop WUE assessment method based on crop growth information using multi-source data. By using remote sensing ET data and crop yield estimates, the WUE and its interannual changes in the three major grain crops (wheat, maize, and rice) in China from 2001 to 2019 were estimated and analyzed. It is of great significance to accurately grasp the historical process and current level of the WUE of these major grain crops in China, and to support sustainable grain production and sustainable water resources utilization. At the same time, this study provides a calculation and evaluation method and dataset for SDG 6.4.1, "change in water-use efficiency over time", demonstrating China's commitment to improving agricultural WUE. The analysis results and datasets can also provide methodological guidance and data support for achieving other SDG targets, such as those in SDG 2 and SDG 15.

This study showed the following. (1) From 2001 to 2019, the WUE of China's three major crops, wheat, maize, and rice, increased significantly, with wheat WUE increasing by 33.4%, maize WUE by 20.0%, and rice WUE by 14.1%. However, there were spatial differences in the

trends. (2) The contribution rates of the crop yield change to the change in WUE of three major crops were greater than that of ET. This was due to factors such as agricultural technological progress, significant improvement in agricultural infrastructure conditions, and the promotion of water-saving irrigation and agricultural water management technologies. (3) The increase in the WUE of rainfed cropland was higher than that of irrigated cropland. The possible reason was that rainfed cropland is more sensitive to precipitation given the improvement of crop yield due to progress in agricultural science and technology, changes in farmland management practices, and other factors. The increase in precipitation in the concentrated rainfed areas led to better water conditions. The yield increase of rainfed cropland was higher than that of irrigated cropland, which further promoted the improvement of the WUE of rainfed cropland.

However, the improvement in cropland WUE did not necessarily mean a decrease in total crop water consumption, as total crop water consumption was also affected by the crop planting area. From the statistical data, the sowing area of wheat and rice did not change significantly from 2001 to 2019, while the sowing area of maize increased significantly due to factors such as market prices, national policies, and climate change.

In recent years, climate change altered the spatiotemporal distribution of water and heat resources in China, including the extension of the crop growing season, the expansion of crop cultivation to higher latitudes and elevations, and the expansion of planting areas for warm-loving, overwintering, and cool-climate crops. In the future, the crop planting areas may continue to expand, increasing pressure on water resources and exacerbating problems such as the mismatch of water and heat resources for crop cultivation and land degradation. For example, in Northeast China, the expansion of rice-growing areas due to factors such as climate change, agricultural policy reforms, and advances in farming techniques led to increased demand for irrigation water. This, in turn, limited the increase in rice WUE in the region.

In the future, it is necessary to further optimize planting structures and cultivation practices, strengthen the construction of agricultural water conservancy facilities, promote water-saving measures in agriculture, strengthen the transformation of low-yielding fields, make better use of water and heat resources, and prevent the excessive development and use of water and soil resources. This will help achieve a higher level of food security and water resources security.

3.3.4 Changes and Drivers of Water Stress in China from 2010 to 2030

Target: SDG 6.4: By 2030, substantially increase water use efficiency across all sectors and ensure sustainable withdrawals and supply of freshwater to address water scarcity and substantially reduce the number of people suffering from water scarcity.

3.3.4.1 Background

Water is at the core of sustainable development in human society, and water scarcity is one of the most serious threats to sustainable development. Severe water shortages can have devastating effects on the environment and hinder economic and social development. The level of water stress is defined as the ratio of freshwater withdrawals to available freshwater resources, also known as water withdrawal intensity, which is an important indicator for measuring SDG 6.4. China is a populous country with 1.4 billion people, and the scarcity and uneven distribution of water resources are fundamental characteristics of the country's water situation. Water scarcity is a major constraint on economic and social development. With continuous population growth, economic expansion, and global climate change, the water scarcity situation in China remains severe. The contradiction between water supply and demand is still prominent, which is not conducive to achieving the SDGs. To solve China's increasingly complex water resources problems, it must rely on institutions,

policies, and reforms to achieve the efficient and effective protection and utilization of water resources.

In 2012, China began to implement the strictest water resources management system with the aim of building a water-saving society, strengthening demand management, and maintaining the sustainability of water resources. Promoting the construction of a water-saving society and comprehensively improving the efficiency and effectiveness of water resources utilization are important goals of China's 14th Five-Year Plan and an important content of ecological civilization construction. The Intergovernmental Panel on Climate Change Sixth Assessment Report (IPCC AR6), released in 2021, used a set of new emission scenarios driven by different socio-economic models—the shared socio-economic pathways (SSPs)—developed by the CMIP6 climate model to replace the representative concentration pathways (RCPs). The setting of the SSP scenarios is based on the current national and regional situations and development plans to obtain specific socio-economic development scenarios.

Within the framework of the UN SDGs, a comprehensive understanding of the spatiotemporal differences and drivers of water stress in China from 2010 to 2030 can contribute to the formulation of water resources-related policies, which are of great significance for the construction of a water-saving society and sustainable development.

3.3.4.2 Data

- Remote sensing data include GPM precipitation, ETMonitor ET, and GRACE terrestrial water storage changes, with a spatiotemporal resolution of 0.5° monthly.
- Statistical data include water-related data from annual water resources bulletins, and population and economic data from China Statistical Yearbooks collected at the provincial level.
- Model simulation data include meteorological data, population and GDP data from the MIROC6 model SSP1-2.6, SSP2-4.5, SSP3-7.0, SSP4-6.0, and SSP5-8.5[2] scenarios, and water withdrawal use data simulated by the Water GAP v2.2d hydrological model, with a spatiotemporal resolution of 0.5° monthly (Müller Schmied et al. 2020).

3.3.4.3 Methods

According to the definition of SDG 6.4.2 by FAO (2018), the formula for calculating the water stress level (WS, %) is as follows:

$$\mathrm{WS} = \frac{\mathrm{TFWW}}{\mathrm{TRWR} - \mathrm{EFR}} \times 100 \qquad (3.7)$$

where TFWW is the total freshwater withdrawal by all economic sectors, including agriculture, industry, household, and eco-environment, but excluding the water supply from wastewater treatment and reuse, rainwater usage, and seawater desalination projects. TRWR refers to the total renewable freshwater resources, and EFR is the environmental water requirements. TFWW and TRWR data for provincial administrative regions from 2010 to 2020 were obtained from water resources bulletins and extended to a monthly gridded scale using remote sensing data and model simulation data. TRWR—EFR represents the available water resources obtained by multiplying TRWR by the ratio of available water resources to calculate water stress levels from 2010 to 2020 (Wang et al. 2006). To estimate water stress levels in future scenarios from 2020 to 2030, agricultural irrigation water use was estimated using the Penman–Monteith equation-based ET model, industrial water use was estimated using the quota method, and domestic water use was estimated by multiplying per capita water use by the population density. TRWR and EFR were obtained by simulating runoff and minimum runoff using a hydrological model. Water stress levels were classified as: 0–25% no stress, 25–50% low water stress, 50–75% moderate water stress, 75–100% high water stress, and >100% extremely high water stress.

[2] Sustainable development path SSP1-2.6, middle-of-the-road path SSP2-4.5, regional competition path SSP3-7.0, uneven path SSP4-6.0, and traditional fossil fuel-based path SSP5-8.5.

In order to analyze the driving factors of changes in water stress levels from 2010 to 2020, the factor decomposition method was used to decompose the driving factors of water stress levels into climate factors and water use factors. Climate factors include precipitation and ET based on water balance, while water use factors include population, economy (GDP), and technology (water use per unit of GDP). The contribution values of each driver were calculated using the logarithmic mean divisia index (LMDI) method.

To estimate water stress levels in future scenarios, the latest standard of future socio-economic development scenarios based on IPCC-SSPs was used. Five typical SSP development scenarios were referenced, including the sustainable development pathway SSP1, the middle-of-the-road pathway SSP2, the regional competition pathway SSP3, the unequal pathway SSP4, and the fossil fuel dominant pathway SSP5. The elements used to construct the future socio-economic development scenarios include population and human resources, economic development, lifestyles, human development, environment and natural resources, policies and institutions, and technological development. A simulation model was developed to simulate socio-economic development to obtain the national and regional socio-economic elements and meteorological data from 2020 to 2030 under five future scenarios (SSP1-2.6, SSP2-4.5, SSP3-7.0, SSP4-6.0, and SSP5-8.5). Hydrological and water resources-related elements in China were simulated, including ET, surface runoff, groundwater flow, agricultural irrigation water, industrial water, domestic water, and ecological environment water.

3.3.4.4 Results and Analysis

Changes in Water Stress Levels and Climate Drivers in China from 2010 to 2020

The overall water stress level in China was 58% in 2020, decreased from 71% in 2010 and 66% in 2015, and was in a medium water stress level. The regions of Beijing, Tianjin, Hebei, Shanxi, and Henan in North China, Shandong, Jiangsu, and Shanghai in East China, and Xinjiang and Ningxia in Northwest China were in an extremely high water stress level (Fig. 3.17), indicating that the natural water resources in

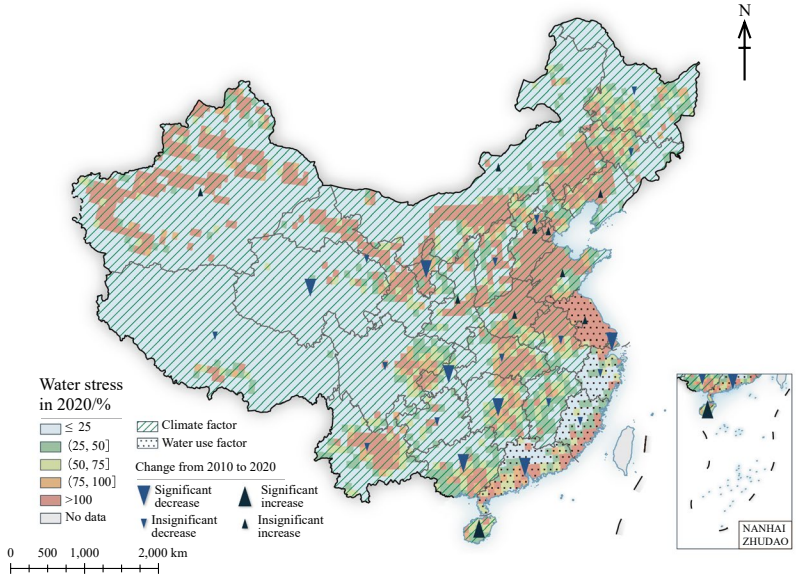

Fig. 3.17 Spatial distribution and change in water stress in China

these regions cannot meet the regional water use demand. Meanwhile, the water stress level in provincial capitals and economically developed cities or regions was higher than that in other areas. The areas with an extremely high water stress level accounted for 19% of the total national area and affected about 800 million people.

From 2010 to 2020, the overall water stress level and the extremely high water stress areas showed a significant downward trend. At the provincial level, except for Hainan, the water stress level in the other provinces showed a decreasing trend or a nonsignificant increase (Fig. 3.17). The provinces with nonsignificant increases included Tianjin, Hebei, Inner Mongolia, Liaoning, Jiangsu, Shandong, Henan, Shaanxi, and Xinjiang, which are also areas with high water stress levels. The increasing trend of water stress is not conducive to regional sustainable development.

Climate change and water use together contribute to changes in water stress levels. Most provinces and regions, as well as the national level, are mainly driven by climate change, while Jiangsu, Zhejiang, Fujian, and Guangdong in Southeast China were mainly driven by changes in water use (Fig. 3.17). Climatic factors determine the availability of water resources, and the significant downward trend in water stress at the national level is mainly attributed to a 70% contribution from climatic wetting and a 30% contribution from water use reduction. Among the climatic drivers, precipitation is the dominant factor. ET is the water consumption process in the water cycle, which plays an important role in the changes in water resources in arid and semi-arid regions in Northern China.

Seasonal Variations in Water Stress in China and the Impact of Droughts

Under the condition of water resources management without considering hydraulic engineering planning such as reservoir storage, the overall water stress level in China is higher in summer (June to August) than in other seasons (Fig. 3.18a), and the season with maximum water stress changes by region (Fig. 3.18b). In regions with high water stress, such as North China and Xinjiang, the peak occurs in the second quarter (April–June). These regions are also important agricultural areas in China, where large amounts of irrigation water are needed to grow crops in spring and where drought is prone to occur due to low precipitation. As a result, available water resources are limited, leading to high water stress. In Northeast China, most provinces in the western regions except Xinjiang, and Central China, the highest water stress occurs in the third quarter (July to September). Although there is more precipitation in the summer, large amounts of water are needed for industry, agriculture, and households, resulting in high water stress. Southwest China and South China have the highest water stress in the first and fourth quarters, respectively. These regions in Southern China can provide sufficient heat for crops to grow, so crops can be harvested two or three times a year, resulting in a large amount of agricultural water use (AWU). In addition, low precipitation in autumn and winter also leads to high water stress.

There is a strong correlation between water stress and the standardized precipitation drought index (Fig. 3.18c), meaning that water stress is exacerbated during drought and high-temperature events.

Drivers of Water Use Changes in China

From a sectoral perspective, water use changes in Northeast and South China were mainly driven by a decrease in industrial water use (Fig. 3.19a), which contributed more than 50% of the total water use change in Jilin, Heilongjiang, Shanghai, Fujian, Hubei, Hunan, Guangdong, and Fujian. In most provinces in Northern China, the decrease in AWU dominated the total water use change, accounting for more than 50% in Hebei, Liaoning, Shandong, Qinghai, and Ningxia.

In terms of demographic, economic, and technological factors, economy and technology were the dominant drivers. Economic development increases water use, but technological progress restrains the increase (Fig. 3.19b). The contribution of population growth to water use

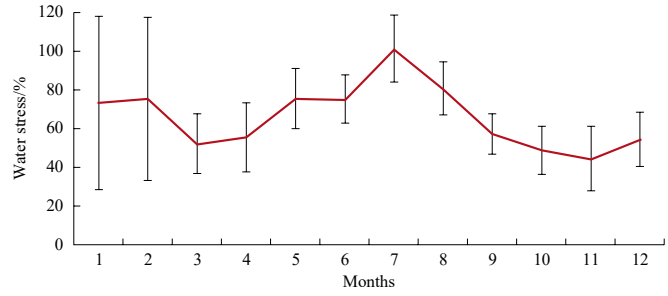

(a) Monthly distribution of water stress in China

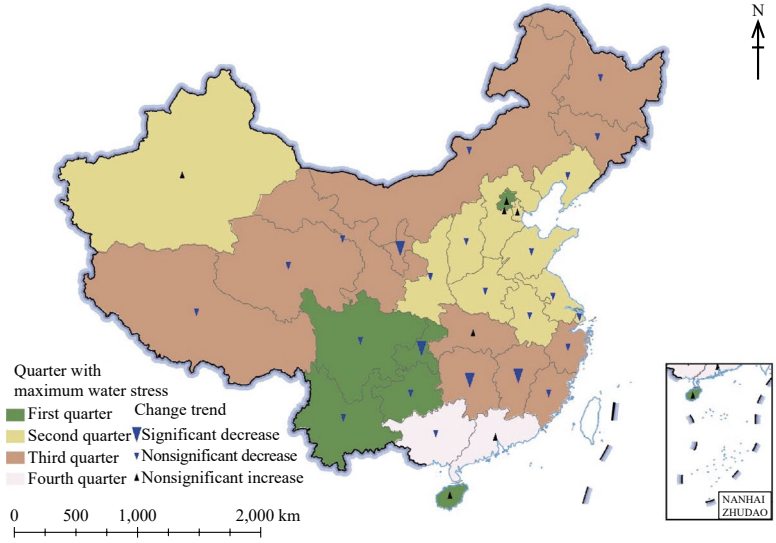

(b) Quarterly spatial distribution of maximum water stress
Note: No data for Taiwan province

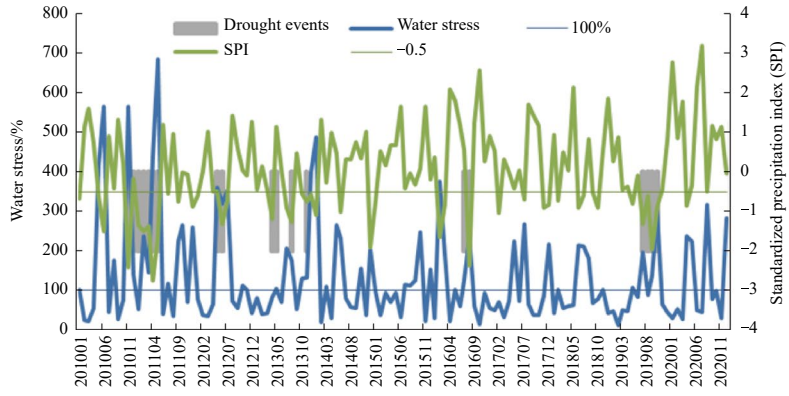

(c) Temporal evolution of water stress and standardized precipitation index (taking Anhui as an example)

Fig. 3.18 Monthly distribution of water stress in China, quarterly spatial distribution of maximum water stress, and temporal evolution of water stress and standardized precipitation index from 2010 to 2020

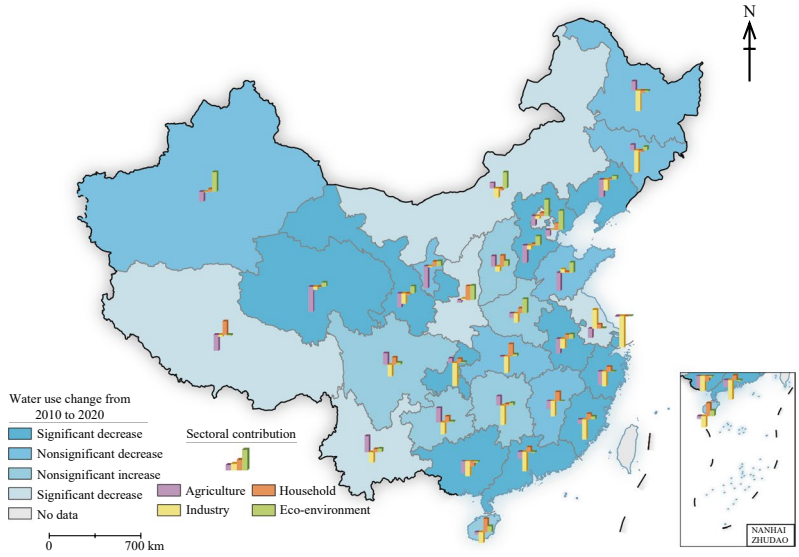

(a) Contributions of water use change driven by sectoral water use change

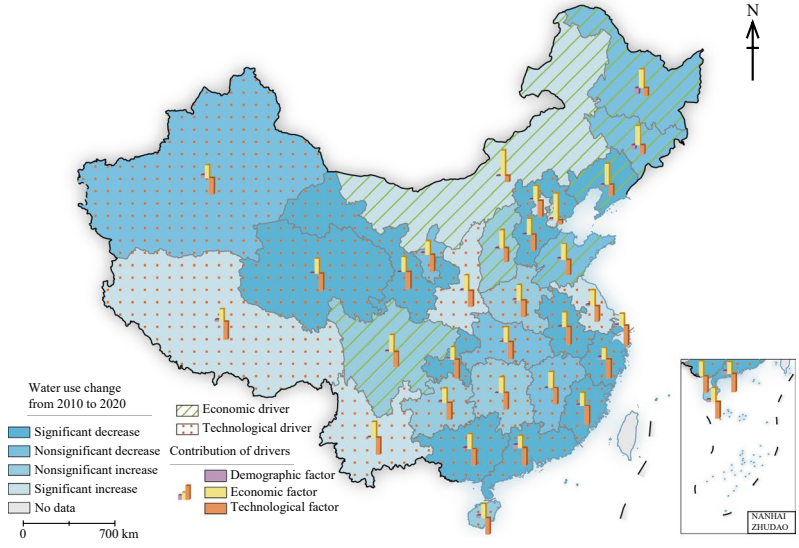

(b) Contributions of water use change driven by demographic, economic, and technological factors

Fig. 3.19 Contributions of water use change driven by sectoral water use change and by demographic, economic, and technological factors

increases in each province was less than 10%. In the southern and western provinces where water use has decreased, technological progress played an essential role in water use reduction; while in Xizang, Yunnan, Guizhou, Hunan, Shaanxi, Henan, Jiangsu, Sichuan, Shanxi, and Inner Mongolia, the combined effect of population and economic growth led to an increase in water use. In Northeast China, the decreased population and advanced technology restrained water use. Generally, technological progress has been the most significant driver of water use changes.

Simulation of China's Water Stress Levels from 2020 to 2030 Under Multiple Scenarios

With the ecological, hydrological, economical, and energy (EHEE) model and different emission scenarios from CMIP6, China's regional hydrological simulation was conducted under new emission scenarios driven by different socio-economic models, namely: sustainable development path SSP1-2.6, middle-of-the-road path SSP2-4.5, regional competition path SSP3-7.0, uneven path SSP4-6.0, and traditional fossil fuel-based path SSP5-8.5. The simulations included ET, surface runoff, groundwater flow, and future water resources demand based on historical simulations of food, water, and energy demand. Finally, SDG 6.4.2 was calculated.

Under all scenarios, China's regional water stress levels will decrease from 2020 to 2030, with the lowest water stress level under the sustainable development scenario (SSP1-2.6) (Table 3.5). The regions with higher water stress levels will be Beijing, Tianjin, Shandong, Jiangsu, and in the western region, Ningxia (Fig. 3.20).

Highlights

- Water stress in China was at a medium level and showed a decreasing change trend from 2010 to 2020, and most provinces in China had a decreasing or nonsignificant increasing trend. The decreasing trend of water stress is attributed to the increase in available water resources due to climate change and the decrease in water use. Technological progress is the main driving force to suppress the increase in water use.
- Based on future climate and socio-economic scenarios, a hydrological model was used to simulate the water stress level in each province of China under different socio-economic patterns. The results show that the water stress in China is expected to decrease from 2020 to 2030. The main driving factors are increased precipitation and economic slowdown.

3.3.4.5 Discussion and Outlook

This study monitored and simulated the spatiotemporal changes of water stress in China from 2010 to 2030, and analyzed the driving factors of water stress changes in China. From 2010 to 2020, the overall water stress in China decreased and remained at a medium level. Technological progress and wetting climate were the main drivers of the decrease in water stress. Under future climate and socio-economic scenarios, water stress in China is expected to continue to decrease from 2020 to 2030, with the lowest level of water stress under the sustainable development scenario (SSP1-2.6). This study focused mainly on assessing changes in water stress under the natural endowment of water resources. More factors such as net water withdrawal, reservoir storage, engineering water diversion, and water recycling should be further considered in the future. In addition, other uncertain factors that influence socio-economic conditions, such as the COVID-19 pandemic and wars, should also be included in the future scenario.

The availability of water resources is uncertain under climate change. As water demand increases due to population growth and economic development, water conservation remains the most important way to mitigate water stress. Technological progress is an important means of reducing water consumption. In order to reduce water stress and achieve the sustainable use of water resources, it is necessary to further promote and strictly enforce the strictest water resources management policies, raise public awareness of water resources protection and conservation, develop high-precision monitoring

Table 3.5 Water stress levels in China under different SSPs in 2020 and 2030 (unit: %)

Different SSPs	SSP1-2.6	SSP2-4.5	SSP3-7.0	SSP4-6.0	SSP5-8.5
2020	58	72	74	67	68
2030	57	57	71	63	60

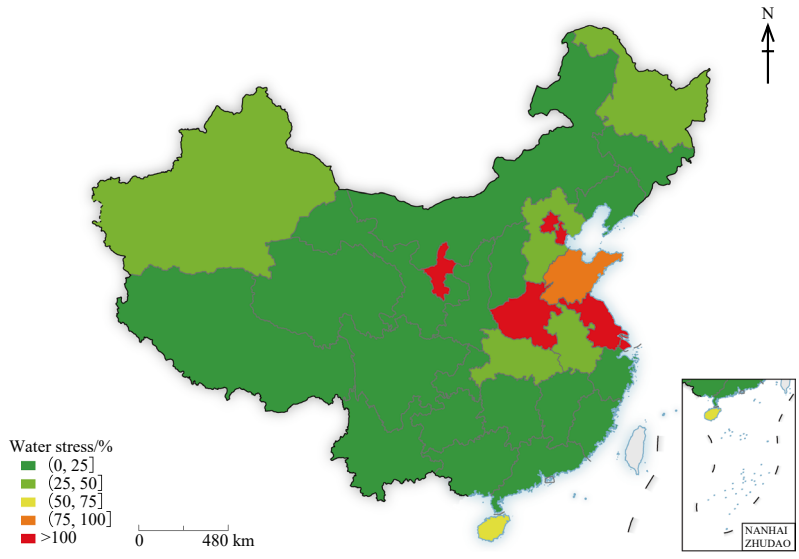

(a) SSP1-2.6

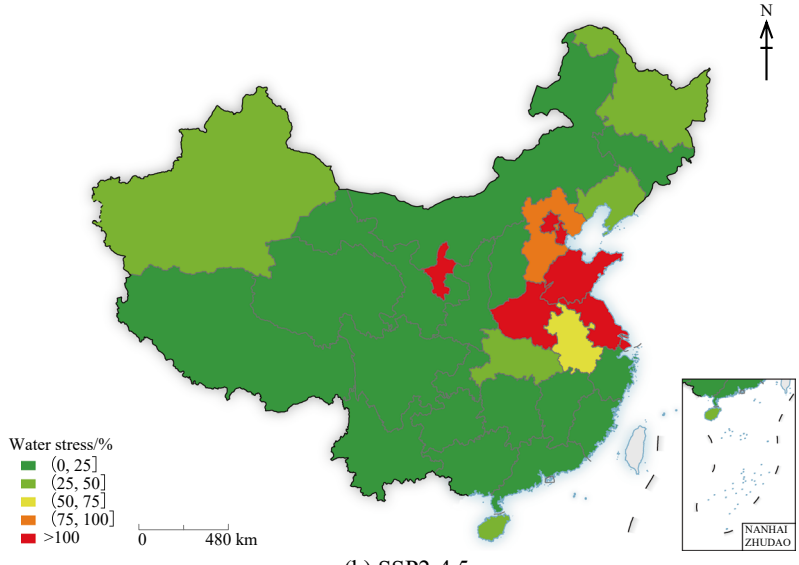

(b) SSP2-4.5

Fig. 3.20 Multi-scenario simulation results of water stress in China in 2030. *Note* No data for Hong Kong, Macao, and Taiwan

and evaluation methods and technologies based on multiple data sources, improve AWU efficiency by developing water-saving irrigation technologies, and reduce water consumption in high-water-consuming industries through measures such as technological transformation, the adjustment of industrial structure, and changes in water use time. The proportion of industries with low water use efficiency should be reduced, while the proportion of high-tech industries should be increased to optimize the allocation of water resources. Necessary water transfer projects should be constructed, and existing projects, such as the South-to-North Water Transfer Project, should be operated conscientiously. Environmental flow is the amount of freshwater

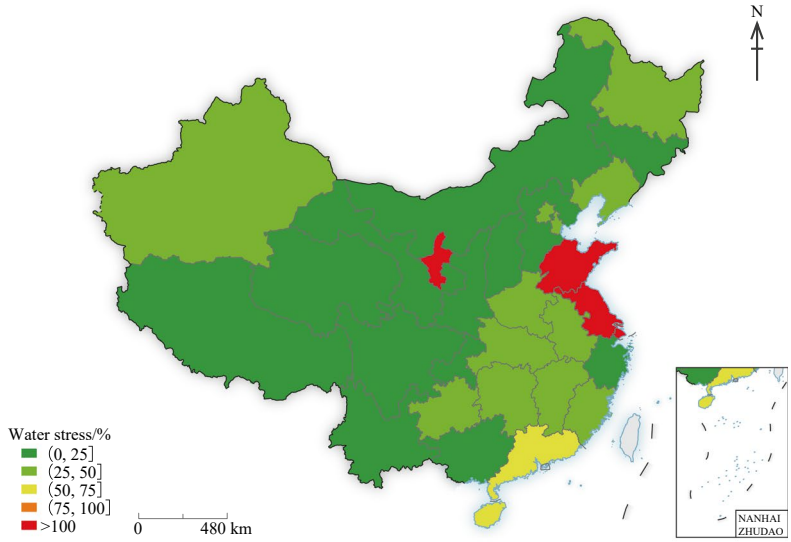

(c) SSP3-7.0

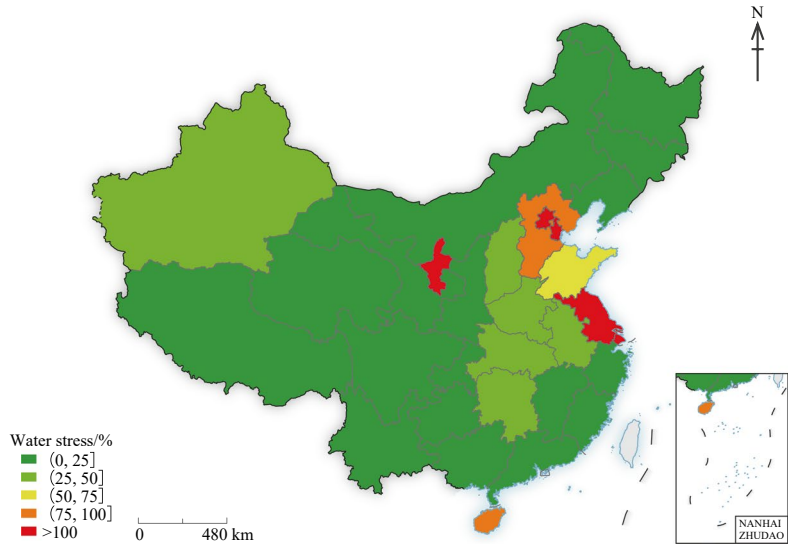

(d) SSP4-6.0

(continued)

required to sustain freshwater ecosystems and the human livelihoods and health that depend on them. The amount of environmental flow directly affects the results of water stress calculation. The amount of environmental flow is closely related to natural conditions, ecological diversity, and management policies. While ensuring water use, it is of great importance to reasonably maintain environmental flow for the sustainability of the ecological environment.

3.3.5 Assessment of Data Supporting Capacity for Provincial Integrated Water Resources Management in China

Target: SDG 6.5: By 2030, implement integrated water resources management at all levels, including through transboundary cooperation as appropriate.

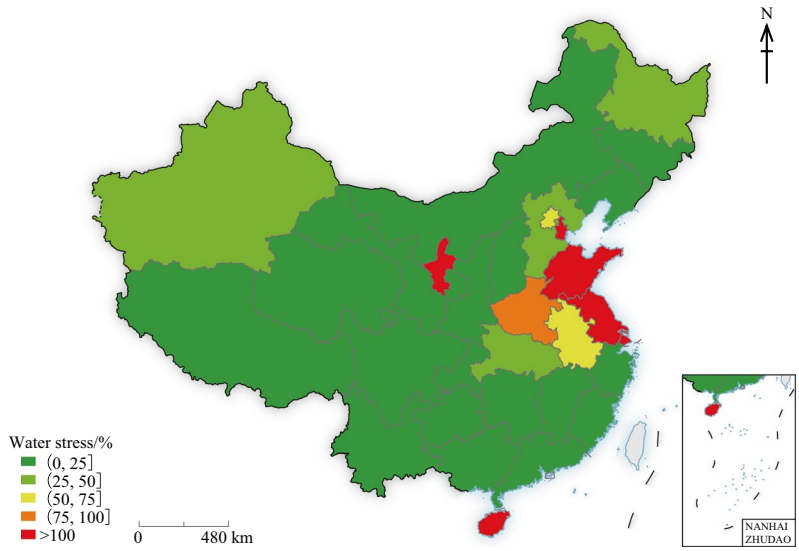

(e) SSP5-8.5

(continued)

3.3.5.1 Background

Since the 1990s, integrated water resources management (IWRM) has been widely accepted around the world as an effective and important approach to achieving sustainable water resources development and conservation, and has been incorporated into the UN SDGs. The degree of IWRM implementation, SDG 6.5.1, is assessed through four key aspects: enabling environment, institutions and participation, management instruments, and financing.

In recent years, China has carried out IWRM deeply and gradually formed a relatively sound water resources management system and a water resources administrative mechanism with Chinese characteristics. Especially in terms of management instruments, the government has implemented the strictest water resources management system and the water use statistics and survey system (in trial), strengthened the construction of basic monitoring instruments continuously, improved the layout of the hydrological station network, completed the National Water Resources Monitoring Capacity Building Project, and started a direct reporting management system for national water use statistics and surveys, which have effectively served the implementation of the management system and strongly supported the improvement of the degree of IWRM implementation.

At present, there is little research on SDG 6.5.1 evaluation methods, and the studies are often simplified, omissive, or qualitative (Bhaduri et al. 2016; Ladel et al. 2020). There is no report on the assessment of data supporting capacity for IWRM. In the context of increasingly advanced hydrology and water resources monitoring tools, based on the connotations of SDG 6.5.1 and the actual situation in China, this case study integrates hydrology and water resources monitoring and statistics data, extracts localized indicators, improves the original subjective qualitative assessment to objective quantitative assessment, compares the spatial differences of the data supporting capacity for IWRM, and puts forward targeted suggestions for improvement, which can provide support to facilitate the measurement of SDG 6.5.1, and is also a beneficial attempt to apply big data to support SDGs related to water security.

3.3.5.2 Data

- Hydrological station data and groundwater station data in 2017 and 2020 are from the Annual Report of National Hydrological

Statistics and 2020 Statistic Bulletin on China Water Activities.
- Statistical data of water supply and consumption in 2017 and 2020 are from China Water Resources Bulletins.
- Water quality monitoring data for water source areas and water supply and consumption monitoring data from 2017 and 2020 are from the National Water Resources Monitoring Capacity Building Project.
- Survey data on water use are from 2020 from the direct reporting management system for the National Water Use Statistics and Survey.

3.3.5.3 Methods

In the guideline "Step-by-step Methodology for Monitoring Integrated Water Resources Management (6.5.1)" (UN Environment 2016) from the United Nations Environment Programme (UNEP), the assessment of water resources management instruments covered several aspects including the national monitoring of water availability, the sustainable and efficient management of water use, pollution control, the management of water-related ecosystems, management instruments to reduce impacts of water-related disasters, basin management instruments, aquifer management instruments, and data and information sharing within countries. Based on the situation of hydrology and water resources monitoring and statistics and the content of water resources management in China, an assessment index of data supporting capacity for IWRM was set up to assess five aspects, including water availability management, water use management, water source area management, aquifer management, and data validity (Table 3.6).

The equivalent density values of the hydrological station network and groundwater station network are proposed for indicators of hydrological monitoring capacity in order to eliminate the influence of physical geography, resource endowment, socio-economic development, and human activity on the setting of hydrological monitoring stations. These indicators make the data comparable among provinces when measuring their capacity to support resource management and aquifer management.

According to the minimum density requirements for hydrological station construction from the World Meteorological Organization (WMO) (World Meteorological Organization 2008) and

Table 3.6 Assessment index of data supporting capacity for IWRM in China

Nos.	Types	Indicators	Connotations
1	Water availability management	Equivalent density of the hydrological station network	Equivalent watershed area controlled by one hydrological station
2	Water use management	Monitoring rate of water use	Proportion of the monitored quantity of water use to the total quantity of water use
3	Water source area management	Monitoring rate of water source quality	Proportion of the number of major water sources in which water quality monitoring is carried out to the total number of major water sources
4	Aquifer management	Equivalent density of the groundwater station network	Number of groundwater monitoring stations per unit equivalent area
5	Data validity	Reporting completeness rate of monitoring sites	Proportion of the number of monitoring sites with complete reported data in each month to the total number of monitoring sites

Technical Regulations for Hydrologic Network Design (SL 34—2013), the regions with different topographical conditions and degrees of human activity were all converted into the plain equivalent area. The equivalent density of the hydrological station network is calculated as follows:

$$\mathrm{EDHS} = \frac{\mathrm{EAHSD}}{\mathrm{NHS}} = \frac{\begin{array}{c}\mathrm{PA} + w_{\mathrm{h}} \times \mathrm{HA} + w_{\mathrm{m}} \times \mathrm{MA} + w_{\mathrm{cp}} \\ \times \mathrm{CPA} + w_{\mathrm{c}} \times \mathrm{CA} + w_{\mathrm{a}} \times \mathrm{AA}\end{array}}{\mathrm{NHS}} \tag{3.8}$$

where EDHS is the equivalent density of the hydrological station network; EAHSD is the equivalent area of hydrological stations that should be constructed; NHS is the total number of hydrological stations; PA, HA, MA, CPA, CA, and AA are the area of plain, hill, mountain, plateau, coastal and arid regions, respectively; and w_{h}, w_{m}, w_{cp}, w_{c}, and w_{a} are the area conversion coefficient of hill, mountain, plateau, coastal, and arid regions relative to plain, respectively. According to the multiple of hydrological station density requirements in a certain type of region to that in the plain region, w_{h}, w_{m}, w_{cp}, w_{c}, and w_{a} were set as 1, 1.88, 0.375, 0.68, and 0.09, respectively, while w_{m} of remote mountainous regions was set as 0.375.

As required by the Technical Code for Groundwater Monitoring (GB/T 51040—2014), groundwater monitoring stations in China are mainly constructed in plain areas. In addition, the density needs to be increased in special types of areas such as urban built-up areas, groundwater over-extraction areas, sea (salt) water intrusion areas, and land subsidence areas. Based on the density requirement of groundwater monitoring stations and the actual situation of groundwater management in China, the area of plain regions with different exploitation degrees and special type regions were all converted into the equivalent area of the plain regions with medium exploitation degrees. The equivalent density of the groundwater station network was calculated as follows:

$$\mathrm{EDGS} = \frac{\mathrm{NGS}}{\mathrm{EAGSD}} = \frac{\mathrm{NGS}}{w_{\mathrm{p}} \times \mathrm{PA} + w_{\mathrm{s}} \times \mathrm{SA}}$$

$$w_{\mathrm{s}} = 4 - w_{\mathrm{p}} \tag{3.9}$$

s.t.

$$\begin{cases} \text{when } K < 0.3,\ w_{\mathrm{p}} = 0.5 \\ \text{when } 0.3 \le K < 0.7,\ w_{\mathrm{p}} = 1 \\ \text{when } 0.7 \le K \le 1,\ w_{\mathrm{p}} = 2 \\ \text{when } K > 1,\ w_{\mathrm{p}} = 2.5 \end{cases}$$

where EDGS is the equivalent density of the groundwater station network; NGS is the total number of groundwater exploitation quantity and groundwater level monitoring stations; EAGSD is the equivalent area of groundwater monitoring stations that should be constructed; PA and SA are the areas of the plain region and the special type region respectively; w_{p} and w_{s} are the area conversion coefficients of the plain region with different exploitation degrees and the special type region relative to the plain region moderately exploited, respectively; and K is the exploitation coefficient, i.e., the ratio of the exploitation quantity to the exploitable quantity. When $K<0.3$, it is a weakly exploited region; when $0.3 \le K<0.7$, it is a moderately exploited plain region; when $0.7 \le K \le 1$, it is a strongly exploited plain region; and when $K>1$, it is an overexploited plain region. Because the groundwater station density requirement in the special type of region is about four times that of the moderately exploited plain region and the special type of region is mostly plain, it is necessary to deduct the duplicate part of the requirements for station construction in the plain region. Then, $w_{\mathrm{s}}=4–w_{\mathrm{p}}$.

3.3.5.4 Results and Analysis

Data Supporting Capacity for IWRM in China

Assessment results of data supporting capacity for IWRM in China in 2017 and 2020 are shown in Table 3.7. First, the result suggests that the supporting capacities of all kinds of data for IWRM in China from 2017 to 2020 have made progress to different degrees. The monitoring rate of water use, which reflects water use

Table 3.7 Assessment results of data supporting capacity for IWRM in China in 2017 and 2020

Nos.	Types	Indicators	2017	2020	Degrees of progress/%
1	Water availability management	Equivalent density of the hydrological station network/ (km^2/station)	299.6	259.9	13.3
2	Water use management	Monitoring rate of water use/%	27.1	62.2	129.5
3	Water source area management	Monitoring rate of water source quality/%	26.9	100.0	271.7
4	Aquifer management	Equivalent density of the groundwater station network /(station/10^3 km^2)	8.4	13.8	64.3
5	Data validity	Reporting completeness rate of monitoring sites/%	56.6	93.0	64.3

management data supporting capacity, and the monitoring rate of water source quality, which reflects water source area management data supporting capacity, improved significantly, from 27.1% and 26.9% in 2017 to 62.2% and 100.0% in 2020, respectively. The degrees of progress in these two indicators are 129.5% and 271.7%, respectively. This indicates that China has made rapid progress in the monitoring of water use and water source areas, which is closely related to the promotion of the strictest water resources management system, the completion of the national water resources monitoring capacity building project, and the implementation of the water use statistics and survey system (in trial). Second, with the strengthening of groundwater management in China in recent years, the data supporting capacity of aquifer management has made obvious progress. The equivalent density of the groundwater station network increased from 8.4 stations/10^3 km^2 in 2017 to 13.8 stations/10^3 km^2 in 2020, with a progress degree of 64.3%. Additionally, not only has the hydrological and water resources monitoring network been further improved, but the data validity has also been greatly enhanced. The reporting completeness rate of monitoring sites increased from 56.6% in 2017 to 93.0% in 2020, with a progress degree of 64.3%. Finally, compared with other indicators, the progress of the equivalent density of the hydrological station network is relatively small, only 13.3%. The main reason is that the development time and foundation of hydrological monitoring are earlier and better than water resources monitoring. The hydrological station network has been basically completed. The main construction task of the hydrological station network in recent years is to supplement and perfect it, so the progress is relatively small.

Data Supporting Capacity for Provincial IWRM

The evaluation results of the data supporting capacity for provincial IWRM in China in 2017 and 2020 are shown in Fig. 3.21. The result shows that the water quality of all major water sources in China was monitored in 2020, and there is little difference among provinces in terms of the reporting completeness rate of monitoring sites. But other indicators still show an inter-provincial imbalance. The equivalent density of the hydrological station network is characterized by being large in the southeast and small in the northwest, with the largest value in Shanghai and the smallest value in Qinghai, which are 15.5 km^2/station and 2343.1 km^2/station, respectively. The monitoring rate of water use is characterized by being high in the north and low in the south, with the highest value in Ningxia and the lowest value in Hebei, which are 84.2% and 33.7%, respectively. The equivalent density of the groundwater station network has the characteristics of being large in the north and small in the south, with the largest value in Beijing and the smallest value in Xinjiang, which are 80.7 station/10^3 km^2 and 1.5 station/10^3 km^2, respectively.

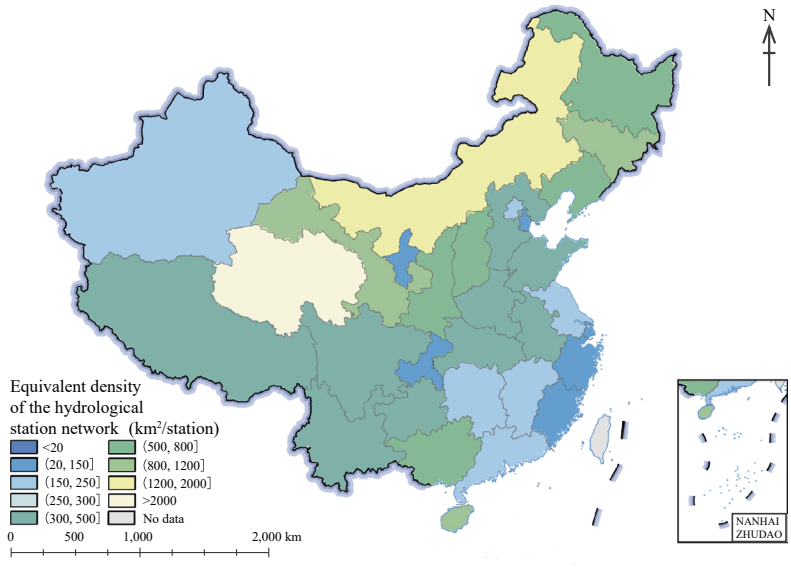

(a) Equivalent density of the hydrological station network in 2017

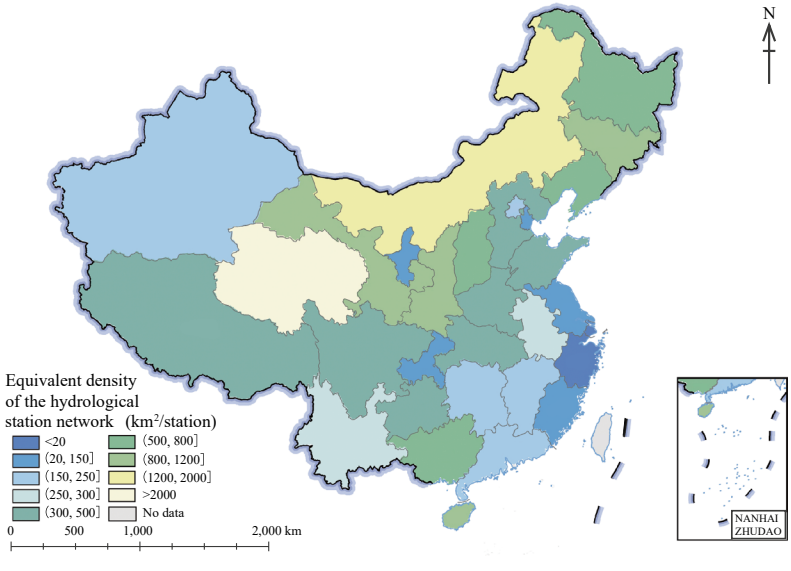

(b) Equivalent density of the hydrological station network in 2020

Fig. 3.21 Data supporting capacity for provincial IWRM in China. *Note* There are no actual monitoring data in Heilongjiang and Xizang, and their evaluation results are the average values of the evaluation results in Northeast China (Liaoning and Jilin) and Southwest China (Yunnan, Guizhou, and Sichuan), respectively. Hong Kong, Macao, and Taiwan were not evaluated due to the lack of data

Overall, differences in the data supporting capacity for IWRM in different provinces are closely related to the water resources endowment conditions, socio-economic development status, and the characteristics of water resources development and utilization. The more water resources and the higher socio-economic level the province has, the stronger data supporting capacity is for water availability management, while the fewer water resources the province

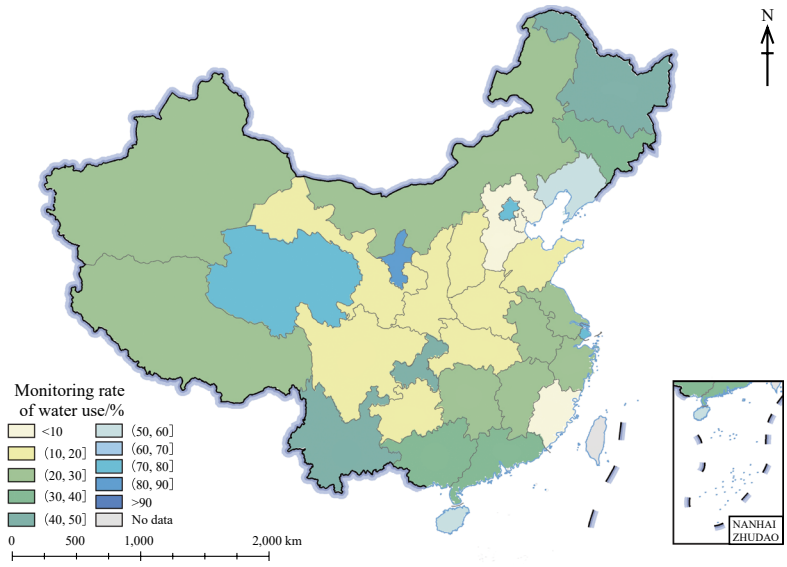

(c) Monitoring rate of water use in 2017

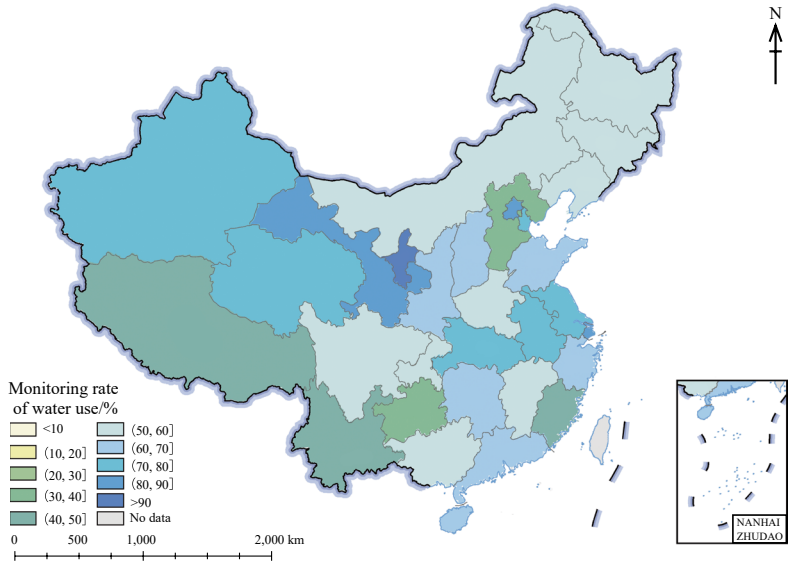

(d) Monitoring rate of water use in 2020

(continued)

has, the stronger the data supporting capacity is for water use management. Also, less surface water, more overexploited groundwater, and a more sensitive groundwater environment in a province lead to a stronger data supporting capability for aquifer management. The data validity of water resources monitoring in each province has been greatly improved, benefiting from the development of the National Water Resources Monitoring Capacity Building Project, the construction of the direct reporting management system for water use statistics and surveys, and the increase in local investment in construction and management of water resources monitoring. However, Sichuan and Qinghai are still clearly lagging behind.

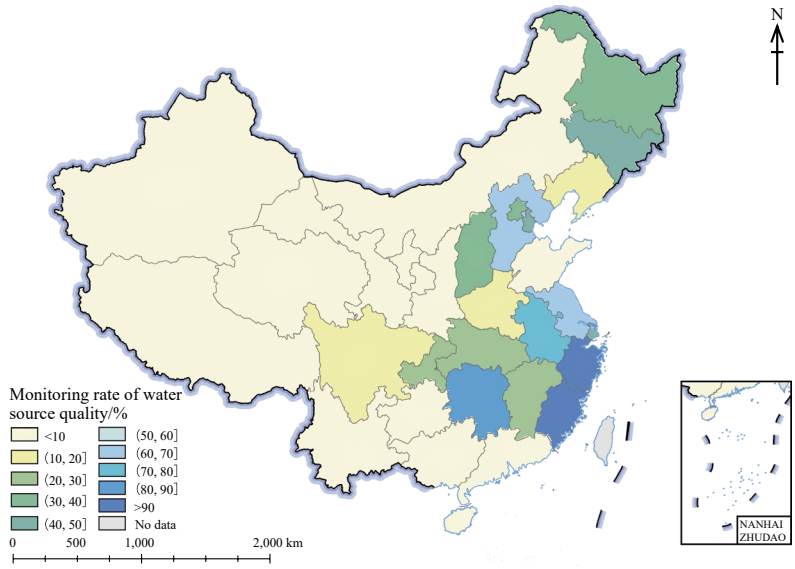

(e) Monitoring rate of water source quality in 2017

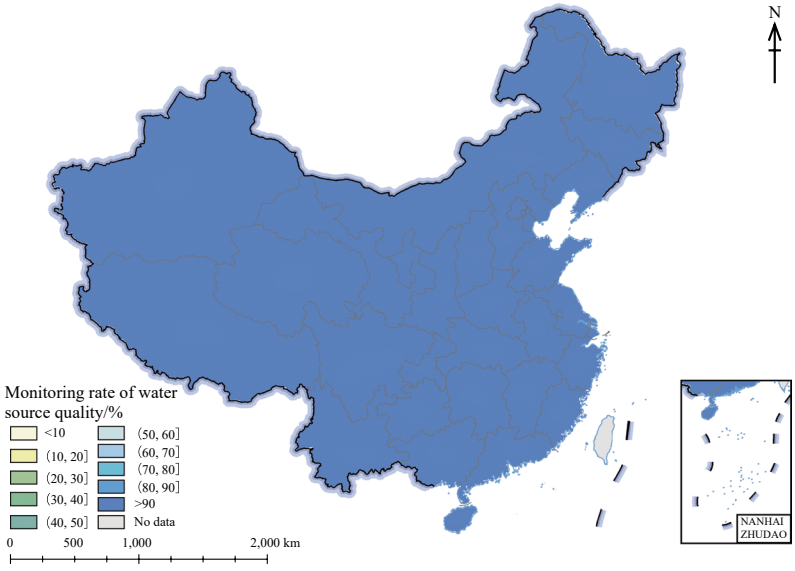

(f) Monitoring rate of water source quality in 2020

(continued)

A comprehensive ranking was obtained by adding the rank of all types of data supporting capacities by province. The results show that Beijing, Zhejiang, and Shanghai rank in the top three, indicating that their data supporting capacities are the strongest. Jilin, Yunnan, and Xizang are lagging behind in comprehensive ranking, and all three provinces have low monitoring rates of water use. Furthermore, the equivalent density of the hydrological station network in Jilin, the equivalent density of the groundwater station network in Yunnan, and the monitoring rate of water use in Xizang are all lower than others, which results in the lagging rank of these provinces. In the future, it is necessary to strengthen investment in the construction, management, and maintenance of monitoring infrastructure.

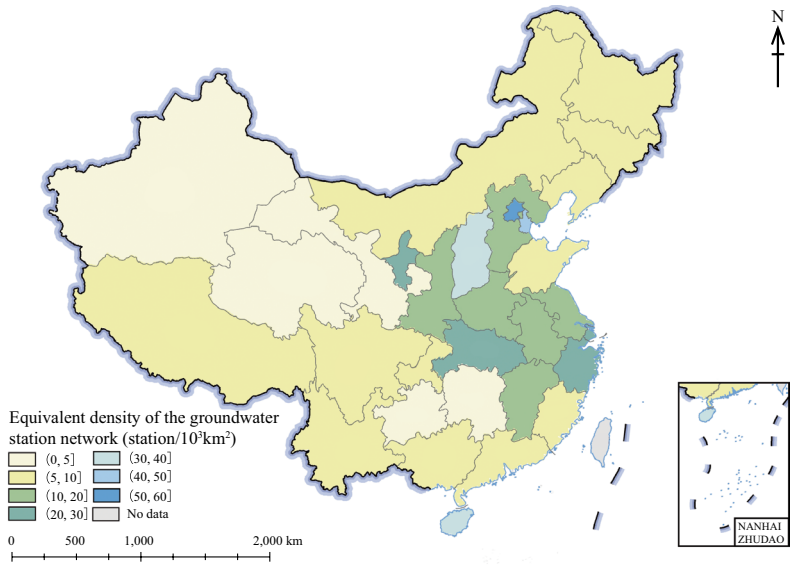

(g) Equivalent density of the groundwater station network in 2017

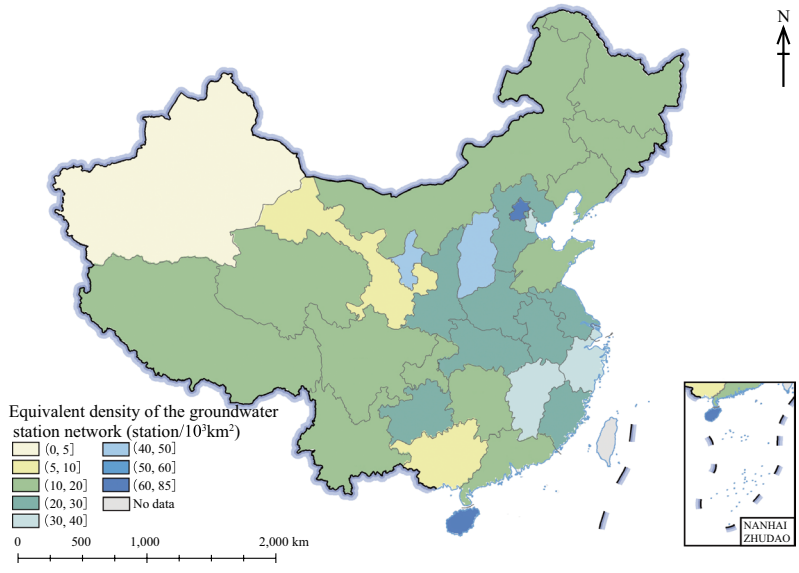

(h) Equivalent density of the groundwater station network in 2020

(continued)

Highlights

- Based on the connotations of SDG 6.5.1 and the actual situation in China, this case integrates hydrology and water resources monitoring and statistics data, extracts localization indicators, and evaluates the data supporting capacity for provincial IWRM in China quantitatively, which can overcome the shortcomings of the qualitative questionnaire methods used in the past.
- Supporting capacities of all types of data for IWRM in China from 2017 to 2020 have made progress to different degrees. The data supporting capacity of water source management and water use management improved

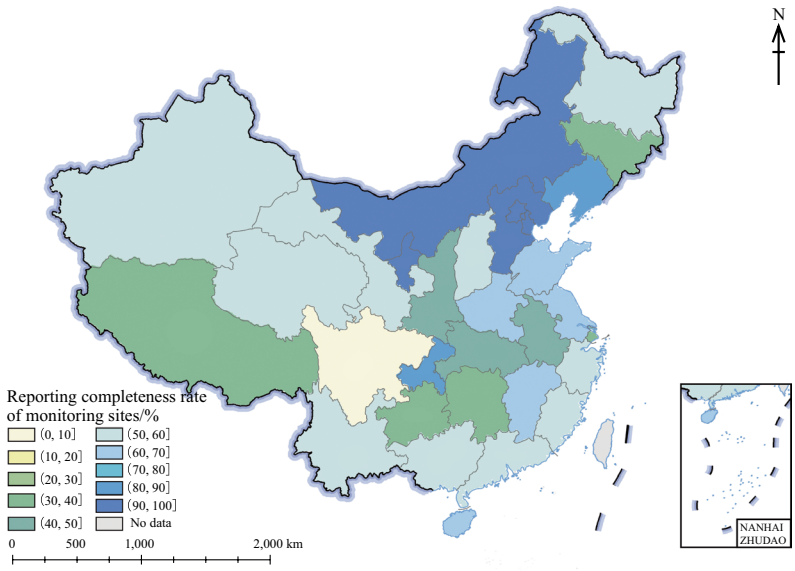

(i) Reporting completeness rate of monitoring sites in 2017

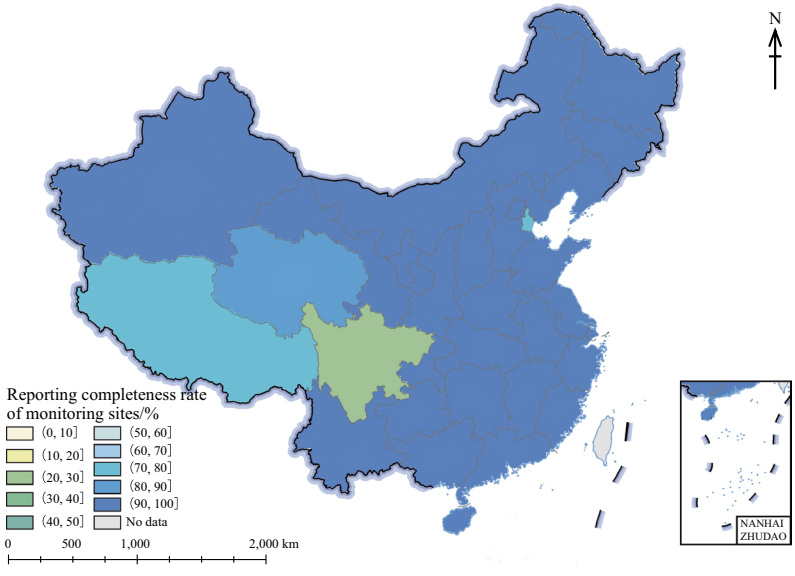

(j) Reporting completeness rate of monitoring sites in 2020

(continued)

significantly. Monitoring rates of water use and water source quality increased from 27.1% and 26.9% in 2017 to 62.2% and 100.0% in 2020, respectively.

- In 2020, all major water sources in China were monitored, with little difference in data validity among provinces. There were significant differences in data supporting capacities for water availability, water use, and aquifer management among provinces, which are closely related to water resources endowment, socio-economic development, and the characteristics of water resources development and utilization.
- In the comprehensive provincial ranking of the data supporting capacity for IWRM, the top three were Beijing, Zhejiang, and Shanghai, indicating that their data

supporting capacities were the strongest, while Jilin, Yunnan, and Xizang lagged behind. It is suggested to strengthen water use monitoring and automatic monitoring combined with remote sensing, and to use the water use data conversed by electricity use to improve data supporting capacity.

3.3.5.5 Discussion and Outlook

Based on the index content of SDG 6.5.1, this case proposed local indicators from the aspects of water availability management, water use management, water source area management, aquifer management, and data validity, quantitatively assessed the data supporting capacity and progress of IWRM in China, and also analyzed provincial differences. The study overcomes the deficiency of the questionnaire method, which causes differences in measurement standards among respondents' subjective knowledge and feelings, and provides a basis and technical support for improving the ability of water resources monitoring and IWRM in China.

The comprehensive ranking results show that the provinces with remote geographical locations and low socio-economic development levels have weak data supporting capacities for IWRM, generally. It is suggested to increase the investment in basic monitoring facilities in the future, strengthen the construction and maintenance of automatic monitoring facilities, and improve the data supporting capacity by using new technologies such as satellite remote sensing and unmanned aerial vehicles.

The analysis results show that the imbalance of water use monitoring rates is more prominent, and all the provinces with low overall ranking have low monitoring rates of water use. At present, water users above the designated scale have been monitored in each province. In the future, it is necessary to increase the monitoring coverage, and focus on strengthening the mechanism of calculating the water consumption of small water users based on typical monitoring to improve the accuracy of water use monitoring for the users below the designated scale. A variety of calculations should be carried out through other non-water resources data for indicators with weak monitoring, such as converting electricity use for pumps into water use data, and checking department and total water use through population, economy, and land use.

Suggestions

1. Improve automatic monitoring and regional information monitoring capabilities, and enhance the national monitoring capacity of water availability. Western regions with a low-density hydrological station network, such as Xinjiang, Xizang, and Qinghai, should focus on strengthening the construction of automatic hydrological monitoring to increase coverage under the condition of reducing accuracy requirements, which can improve water resources monitoring in key water source areas of China, and reduce the difficulty of operation and maintenance.
   Meanwhile, satellite remote sensing and other advanced technologies should be used to strengthen the monitoring of surface rainfall, groundwater, and lake water storage and improve the accuracy of water cycle monitoring and water balance analysis.
2. Improve the accuracy of current water use monitoring, and establish a scientific calculation system to support the measurement of SDG 6 targets (e.g., SDG 6.4, improving WUE). At present, the water resources monitoring system has basically completed large-scale water user monitoring, but small-scale water users have not been monitored yet. The cost of complete monitoring is high, and the management is difficult. Therefore, in regions with high water scarcity and low water use monitoring such as North China, the mechanism for calculating the water consumption of small water users through typical monitoring should be strengthened to improve the accuracy of water use monitoring for the users below the designated scale. A conversion method utilizing electricity consumption and socio-economic data to estimate total water consumption should also be used.
3. Improve big data analysis capabilities. The accuracy and frequency of monitoring should

be improved through big data analysis in those regions with small total water consumption but high water use intensity and high cost and output of water resources utilization, such as the Yangtze River Delta, the Pearl River Delta, and the Beijing-Tianjin region. For example, correlation analysis between water consumption monitoring and social and economic information such as population, product output, economic volume, and material flow should be strengthened to improve the verification of water use monitoring and services for water use control and water resources management.

4. Improve data assimilation analysis and consistency and balance relationship processing, and enhance the ability of data applications to support IWRM. Currently, the input of water resources monitoring is large, but the output effect is insufficient to support water resources management. The main shortcoming lies in the lack of a close relationship between water resources monitoring data and businesses, inconsistency between different types of data, and insufficient integration and analysis with data in other fields. A relationship must be established between various types of monitoring and water resources management, and carry out data assimilation, validity, and consistency analysis for different types of monitoring data. Further research should be conducted on multi-source data fusion methods to support water resources management.

3.3.6 Comprehensive Assessment of China's SDG 6 Progress from 2015 to 2020

Target: SDG 6.1: By 2030, achieve universal and equitable access to safe and affordable drinking water for all;
SDG 6.3: By 2030, improve water quality by reducing pollution, eliminating dumping and minimizing release of hazardous chemicals and materials, halving the proportion of untreated wastewater, and substantially increasing recycling and safe reuse globally;
SDG 6.4: By 2030, substantially increase water use efficiency across all sectors and ensure sustainable withdrawals and supply of freshwater to address water scarcity and substantially reduce the number of people suffering from water scarcity;
SDG 6.5: By 2030, implement integrated water resources management at all levels, including through transboundary cooperation as appropriate;
SDG 6.6: By 2020, protect and restore water-related ecosystems, including mountains, forests, wetlands, rivers, aquifers, and lakes.

3.3.6.1 Background

This case study examines the period 2015–2020 to comprehensively evaluate the positive role of various water-related policies in promoting the realization of the SDGs during the 13th Five-Year Plan period. It provides scientific suggestions for further optimizing policies during the 14th Five-Year Plan period, avoiding policy conflicts and isolated policies caused by overlapping sectoral interests (Weitz et al. 2018), and accelerating the realization of the 2030 Agenda.

Water resources are essential to the survival of life. They support the operation of human societies and economies, and maintain the development of natural ecosystems. The UN 2030 Agenda explicitly calls for "ensure availability and sustainable management of water and sanitation for all" in SDG 6. The realization of SDG 6 is an important foundation for the realization of other SDGs, especially SDGs 3, 5, 7, 8, 10, 11, 12, and 15. Indirectly affected SDGs include SDGs 1, 2, 9, 14, and 16 (Requejo-Castro et al. 2020; Cernev and Fenner 2020). It provides the means to develop and protect natural processes and contributes to the improvement of human

well-being. According to the UN Sustainable Development Report 2022, over 85% of the world's wetlands have been lost, and more than 733 million people have lived in countries with high or severe water stress (2019) in the last 300 years. At the current rate, 1.6 billion people will lack access to safe drinking water, 2.8 billion people will lack access to safe sanitation, and 1.9 billion will lack access to basic hand hygiene facilities by 2030, requiring a fourfold increase in the current rate of progress to reach the 2030 targets for water, sanitation, and hygiene. Therefore, a comprehensive assessment of the implementation status and progress rate of SDG 6 is crucial to the realization of the 2030 Agenda in the region.

With the rapid development of China's economy and the continuous increase in population, alleviating the contradiction between the supply and demand of water resources and promoting the sustainable utilization of water resources have become important bottlenecks restricting China's economic and social development. Ensuring the sustainable use of water resources is not only an important basis for promoting regional development, but also a necessary prerequisite for realizing the construction of a beautiful China. To ensure the sustainable use of water resources, we should not only optimize the allocation of water resources and improve their utilization efficiency, but also maintain healthy development of the water environment and water-related ecosystems. However, there are no studies on the comprehensive level, regional difference, and spatial distribution of sustainable water resources development in China by using a comprehensive evaluation index method combining multiple indicators. At present, it is urgent to comprehensively evaluate the current situation of the sustainable development of water resources in China and explore the existing problems in water resources protection. This would increase our understanding of the changes necessary to achieve SDG 6 and improve the level of sustainability, and would furthermore have great significance for promoting a beautiful China and global sustainable development.

3.3.6.2 Data

This case study is based on the SDG 6 indicator data of 31 provinces generated by other case studies related to SDG 6, including SDG 6.1.1, SDG 6.3.2, SDG 6.4.2, and SDG 6.5.1, combined with statistical data and remote sensing data, to comprehensively study the progress and change trends of an SDG 6 composite index. Specific data sources are as follows.

- Data for four SDG 6 indicators came from other studies in this report: SDG 6.1.1, SDG 6.3.2, SDG 6.4.2, SDG 6.5.1. Data for SDG 6.1.1 were derived from the case on "Water quality monitoring and assessment of drinking water sources in China", data for SDG 6.3.2 were derived from the case on "Proportion of water bodies with good ambient water quality in China's provinces and change assessment in 2015 and 2020", SDG 6.4.2 data came from "Changes in and drivers of water stress in China from 2010 to 2030", and the data for SDG 6.5.1 from "Assessment of data supporting capacity for provincial integrated water resources management in China" (this case's study period began in 2017 instead of 2015).
- SDG 6.3.1 data came from the China Urban Construction Statistical Yearbook (2015, 2020).
- SDG 6.4.1 data were calculated using the China Statistical Yearbook (2016, 2021) and China Water Resources Bulletin (2015, 2020).
- SDG 6.6.1 assessment data came from the "Remote sensing monitoring dataset of land use and land cover in China" (CNLUCC) and CAS Mangroves 2.0 dataset.

3.3.6.3 Methods

This case study involves the measurement of five targets and seven indicators of SDG 6 and its composite index (Table 3.8). Data and results for SDG 6.1.1, SDG 6.3.2, SDG 6.4.2, and SDG 6.5.1 were adopted from other studies in this report. SDG 6.1.1 uses the standard water quality of centralized drinking water sources and the safe drinking water level of the region.

Table 3.8 An indicator list for the sustainable state index of water resources development and protection

Goal	Targets	Indicators	Indicator names	Indicator directions
SDG 6 Clean water and sanitation	SDG 6.1	SDG 6.1.1	Proportion of the population using safely managed drinking water services	Positive
	SDG 6.3	SDG 6.3.1	Proportion of domestic and industrial wastewater flows safely treated	Positive
		SDG 6.3.2	Proportion of bodies of water with good ambient water quality	Positive
	SDG 6.4	SDG 6.4.1	Change in water use efficiency over time	Positive
		SDG 6.4.2	Level of water stress: freshwater withdrawal as a proportion of available freshwater resources	Negative
	SDG 6.5	SDG 6.5.1	Degree of integrated water resources management	Positive
	SDG 6.6	SDG 6.6.1	Change in the extent of water-related ecosystems over time	Positive

SDG 6.5.1, the comprehensive management level index of water resources in provinces and regions, was obtained by the calculation of five indicators in the case study. SDG 6.3.1, the sewage treatment ratio of each province (autonomous region, municipality), was calculated with data from the China Urban Construction Statistical Yearbook (2015, 2020). SDG 6.4.1 and SDG 6.6.1 are based on the UN metadata method (United Nations Statistics Division 2022). SDG 6.4.1 is calculated using GDP, water consumption, and the proportion of rainfed agricultural area of three industries by province and city in the China Statistical Yearbook and Water Resources Bulletin. SDG 6.6.1 adopts the area of river channels, lakes, reservoir pits, permanent glacial snow, mud flats, tidal flats, and marshlands in the "Remote sensing monitoring dataset of land use and land cover in China" and the provincial mangrove area in China in CAS Mangroves 2.0 dataset.

The SDG 6 composite index adopts a comprehensive evaluation method, and each target index adopts the extreme value method to normalize the evaluation and accounting results of the indicators according to the positive and negative directions of the above seven indicators (Xu et al. 2020), and calculates the target index based on the results of the indicators. The 2030 Agenda has three characteristics of universality, integrity, and indivisibility, and the realization of each target is of the same importance. Therefore, the weight assignment was carried out according to the method of equal weight of each target and equal weight of each indicator in the target. The five targets are divided into 0.2 weights. Based on the indices and weights of the above five targets, the SDG 6 composite index of the provinces and regions in 2015 and 2020 were calculated, and the realization and changes in SDG 6 of the provinces and regions were analyzed through the SDG 6 composite index.

3.3.6.4 Results and Analysis

The sustainable development level of water resources was significantly improved during 2015–2020 in China, with the SDG 6 composite index rising from 0.51 in 2015 to 0.66 in 2020. Significant progress was made in all indicators of SDG 6, with SDG 6.1.1 ("proportion of the population using safely managed drinking water services") increasing from 70.09% to 97.03%. SDG 6.3.1 ("proportion of domestic and industrial wastewater flows safely treated") increased from 87.67% to 97.46%, and the sewage treatment rate in all provinces was above 95.31% in 2020. SDG 6.3.2 ("proportion of bodies of water with good ambient water quality") increased

Table 3.9 Changes in the state of sustainability of water resources development and protection and SDG 6 indicators from 2015 to 2020

Indicators	Indicator names	2015	2020
SDG 6.1.1	Proportion of the population using safely managed drinking water services	70.09%	97.03%
SDG 6.3.1	Proportion of domestic and industrial wastewater flows safely treated	87.67%	97.46%
SDG 6.3.2	Proportion of bodies of water with good ambient water quality	72.67%	85.35%
SDG 6.4.1	Water use efficiency (yuan/m^3)	116.72	161.73
SDG 6.4.2	Level of water stress: freshwater withdrawal as a proportion of available freshwater resources	148.73%	139.11%
SDG 6.5.1	Degree of integrated water resources management	0.44	0.74
SDG 6.6.1	Change in the extent of water-related ecosystems over time	1.75%	12.70%
SDG 6 composite index	Sustainability index of water resources development and protection	0.51	0.66

from 72.67% to 85.35%. SDG 6.4.1 ("change in water-use efficiency over time") increased from 116.72 yuan per cubic meter to 161.73 yuan per cubic meter. The WUE of agriculture, industry, and the service industry all improved, and the corresponding national WUE increased by 4.62%, 46.20%, and 32.83%, respectively. SDG 6.4.2 ("level of water stress: freshwater withdrawal as a proportion of available freshwater resources") decreased from 148.73% to 139.11%. SDG 6.5.1 ("degree of integrated water resources management") increased from 0.44 to 0.74. SDG 6.6.1 ("change in the extent of water-related ecosystems over time") increased from 1.75% to 12.70% (Table 3.9).

The spatial differences in SDG 6 indicators are obvious (Figs. 3.22 and 3.23). In 2015, the safety level of drinking water in Eastern China was higher than that in Western China. The proportion of the population using safely managed drinking water services in 21 provinces reached 100% in 2020. The undeveloped regions have better water environment quality, and the top five provinces for proportion of domestic and industrial wastewater flows safely treated are Henan, Hebei, Hainan, Guangxi, and Shanxi. The top five provinces of proportion of bodies of water with good ambient water quality are Sichuan, Gansu, Guizhou, Fujian, and Xizang. In addition, the sewage treatment rates in Xizang and Qinghai have increased by 404.85% and 58.91%, respectively. The rate of meeting the standard of surface water quality in Shanghai and Tianjin increased significantly, at 406.90% and 578.81%, respectively. The spatial distribution of WUE is contrary to that of the water environment. The economically developed provinces have higher WUE, and the top five provinces are Chongqing, Shanghai, Zhejiang, Tianjin, and Beijing, while the bottom five provinces are Xinjiang, Heilongjiang, Ningxia, Xizang, and Guangxi. In addition, the WUE of Fujian, Anhui, Guizhou, and Beijing has improved rapidly, with an increase of over 70%. The change in WUE in Hebei, Jiangsu, and other provinces is related to the adjustment of the industrial structure. The water stress in Ningxia, Shanxi, Shandong, Henan, Xinjiang, Beijing, Hebei, Tianjin, Jiangsu, and Shanghai all exceeded 100%. In 2020, the water stress reached 1020.44% in Ningxia. The degree of integrated water resources management was generally improved in all provinces and regions, and the degree of integrated water resources management to the east of the Hu Line was higher than that in the west. The area of water-related ecosystems in each province increased, and the area of water-related ecosystems to the

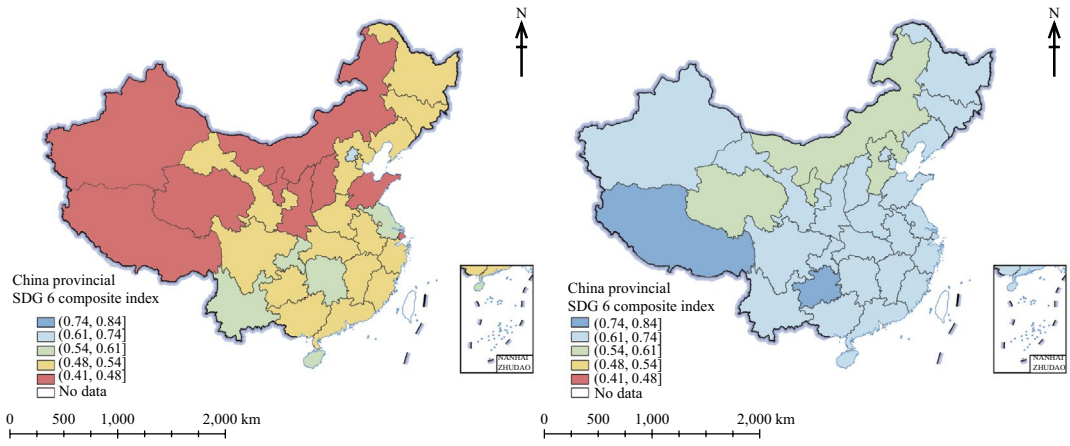

Fig. 3.22 Spatial distribution map of the SDG 6 composite index in 2015 and 2020

west of the Hu Line generally increased, while the area of water-related ecosystems decreased mainly to the east of the Hu Line.

The SDG 6 composite index differs significantly among provinces. The regions with a higher index are distributed in Xizang and Guizhou, which have better ecological environments, and Beijing, Shandong, Chongqing, and Zhejiang, which have had faster development. The regions with a lower index are mostly economically underdeveloped regions. In 2015, the regions with a low comprehensive index were distributed in Inner Mongolia, Ningxia, Shanghai, Shaanxi, Shandong, Shanxi, Xinjiang, Xizang, and Qinghai, while the SDG 6 composite indices of Ningxia, Inner Mongolia, Hebei, Qinghai were low in 2020.

The SDG 6 composite index of all provinces in China showed an increasing trend (Figs. 3.24 and 3.25), among which the SDG 6 composite indices of Xizang, Guizhou, and Shandong increased significantly by more than 50%, and that of Xizang reached 78.52%. The increase in the SDG 6 composite index in Xizang was related to the improvement of the regional sewage treatment rate and the area of water-related ecosystems. The increase in the indices in Guizhou and Shandong was related to the significant increase in the proportion of local safe drinking water use.

At present, there are significant differences in the level of sustainable water resources development among provinces in China, and there are different problems among regions. The economically developed provinces are mostly challenged in the water environment (SDG 6.3) and water-related ecosystems (SDG 6.6), while the less economically developed provinces generally have low WUE (SDG 6.4), and some regional individual indicators show a downward trend.

Highlights

- Based on the results of case studies in this report and other multi-source data, a sustainability index was constructed for water resources development and protection (SDG 6 composite index) to provide a comprehensive assessment of the progress toward SDG 6 from 2015 to 2020 at the national and provincial levels. The results show that the SDG 6 composite index increased from 0.51 to 0.66, and the level of sustainable water resources management was significantly improved.
- The SDG 6 composite index of all provinces increased to different degrees, among which the indices of Xizang, Guizhou, and Shandong increased by more than 50%. There are significant differences in the sustainable

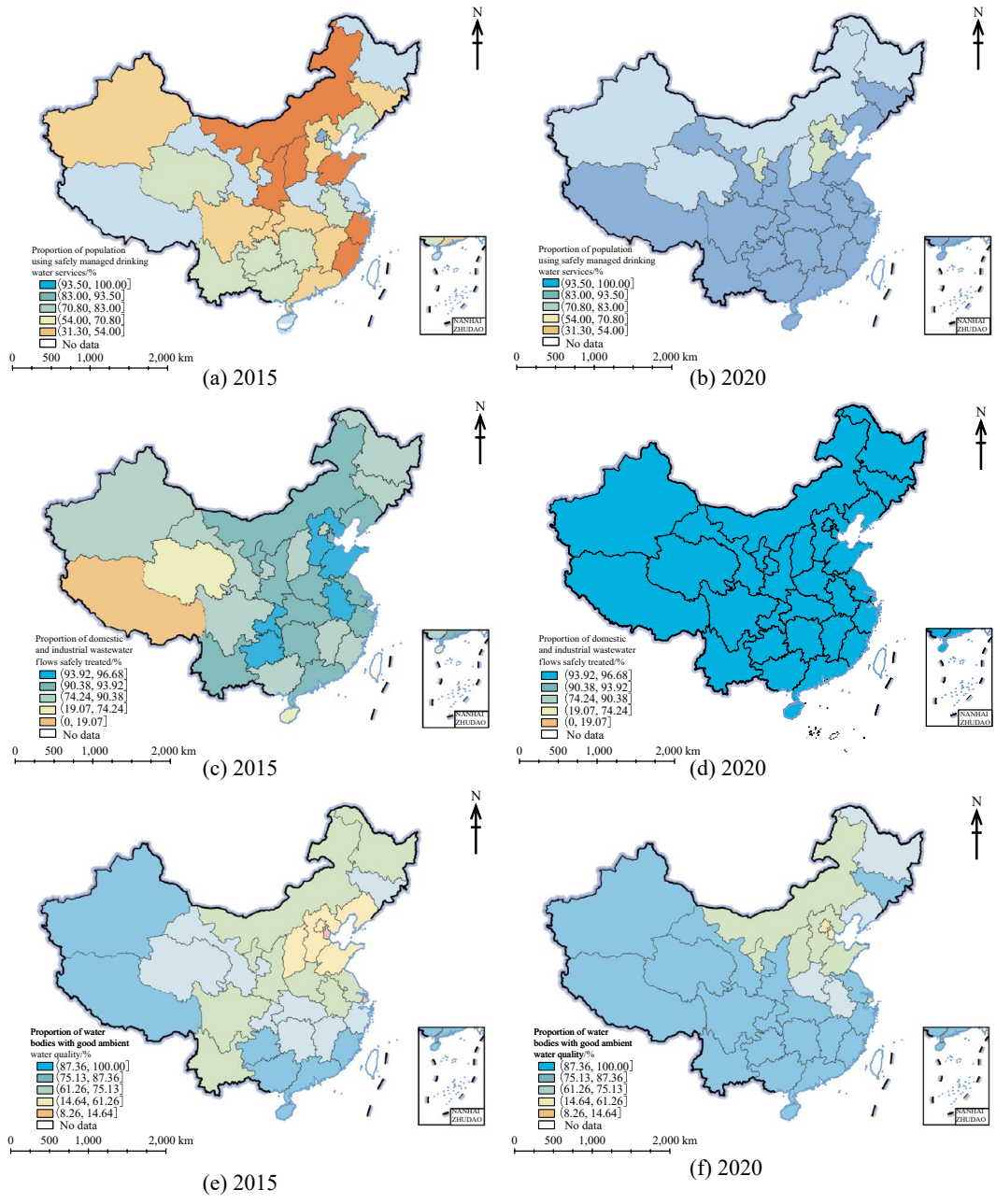

Fig. 3.23 Spatial distribution map of SDG 6 indicators in 2015 and 2020

development level of water resources among China's provinces. The economically developed provinces are mostly challenged in the water environment (SDG 6.3) and water-related ecosystems (SDG 6.6), while the economically undeveloped provinces generally have low WUE (SDG 6.4), and individual indicators show a downward trend in some regions. It is necessary to analyze the specific development problems according to the natural conditions and resource endowments of each province, in order to formulate an optimization path for the realization of SDG 6 in each region.

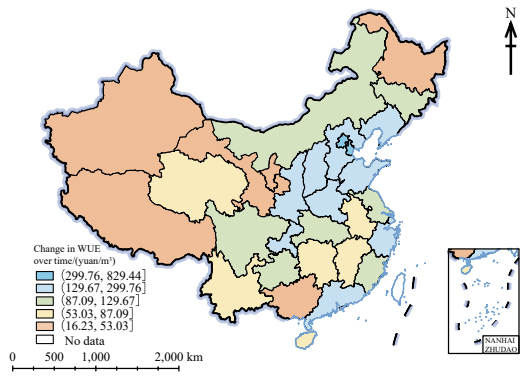

(g) 2015

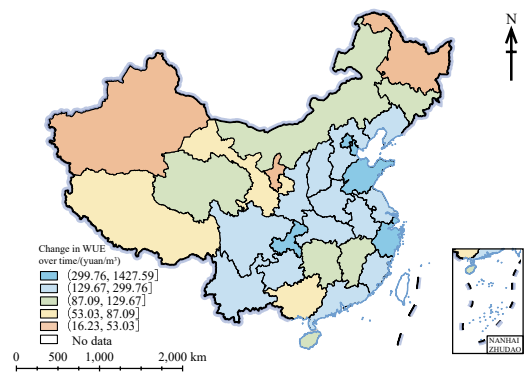

(h) 2020

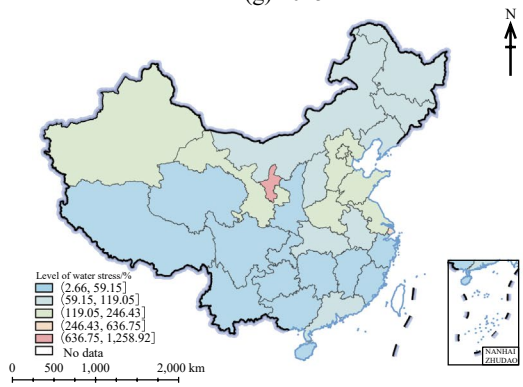

(i) 2015

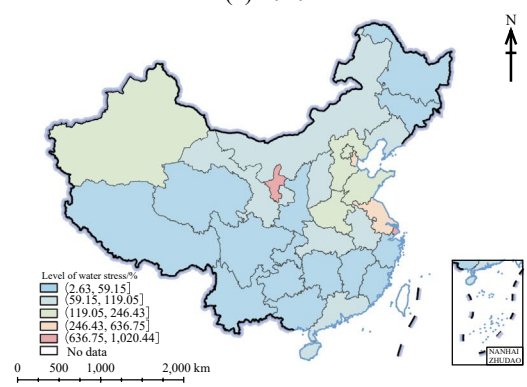

(j) 2020

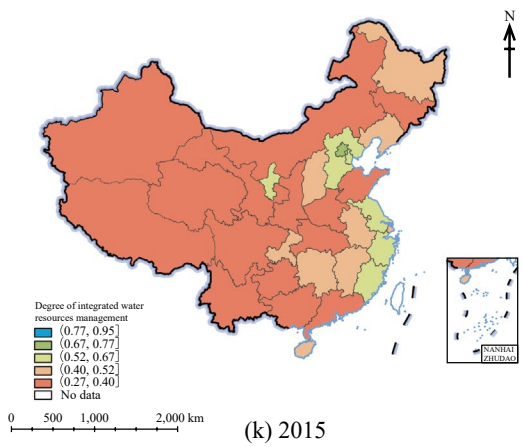

(k) 2015

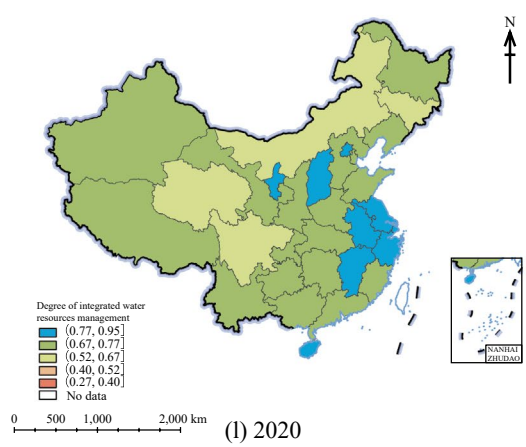

(l) 2020

(continued)

3.3.6.5 Discussion and Outlook

In this case study, five targets and seven indicators of SDG 6 in 2015 and 2020 were used to carry out a multi-index evaluation of SDG 6 in 2015 and 2020 at the provincial level, calculate the SDG 6 composite index, and analyze the realization and changes in SDG 6 in the provinces and regions. The sustainable development level of water resources in China significantly improved during 2015–2020, mainly attributable to the strictest water resources management system implemented by the Chinese government in recent years. The total water utilization and WUE control system, combined with the promotion of a water-saving society, has continuously improved WUE in all provinces (SDG

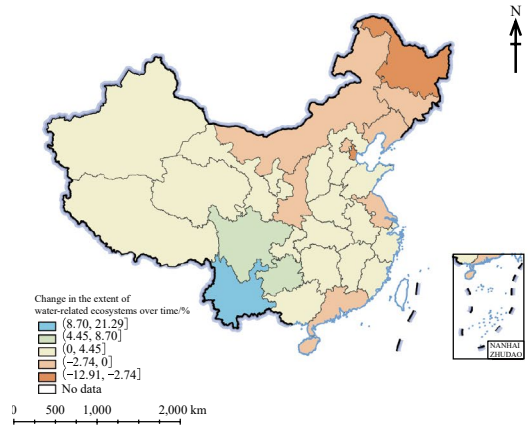

(m) 2015

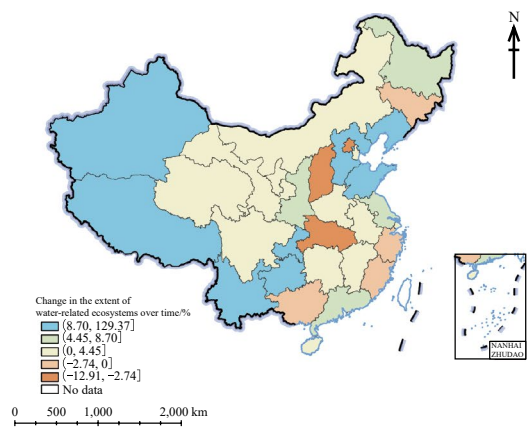

(n) 2020

(continued)

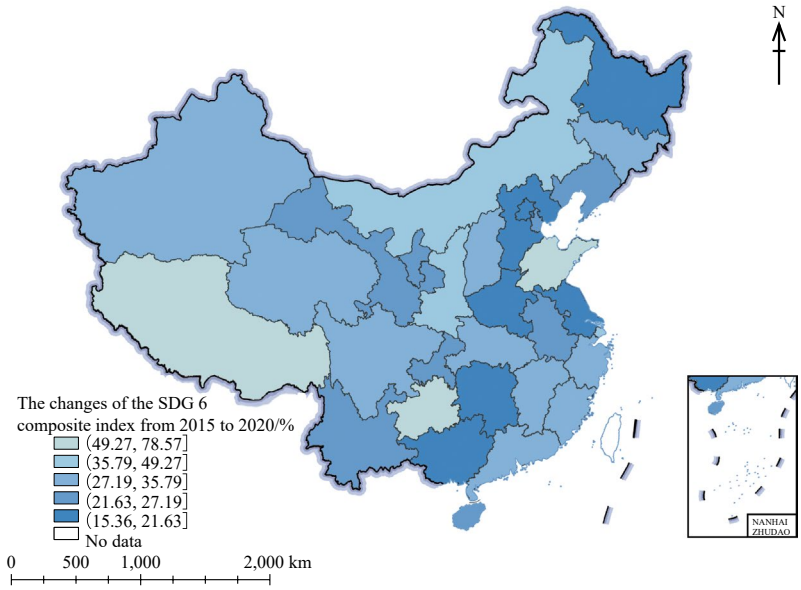

Fig. 3.24 Changes in the SDG 6 composite index from 2015 to 2020

6.4), and the water function zone pollution limitation system has promoted the improvement of the water quality (SDG 6.3) and the protection and restoration of water-related ecosystems (SDG 6.6). The continuous improvement of the water resources management responsibility and assessment system has improved national water resources management (SDG 6.5). In addition, in view of drinking water safety (SDG 6.1), a project has been implemented to consolidate and improve drinking water safety in rural areas, which comprehensively improves the quality of drinking water sources for residents and ensures the quantity and convenience of domestic water. At the same time, since 2017, China has launched a "toilet revolution" to solve rural public health problems (SDG 6.2) and continuously improve the living environment. The combination of policies is comprehensively advancing China's progress toward SDG 6.

In view of the different characteristics of the sustainable development level of each region, it is necessary to analyze the specific development problems according to the

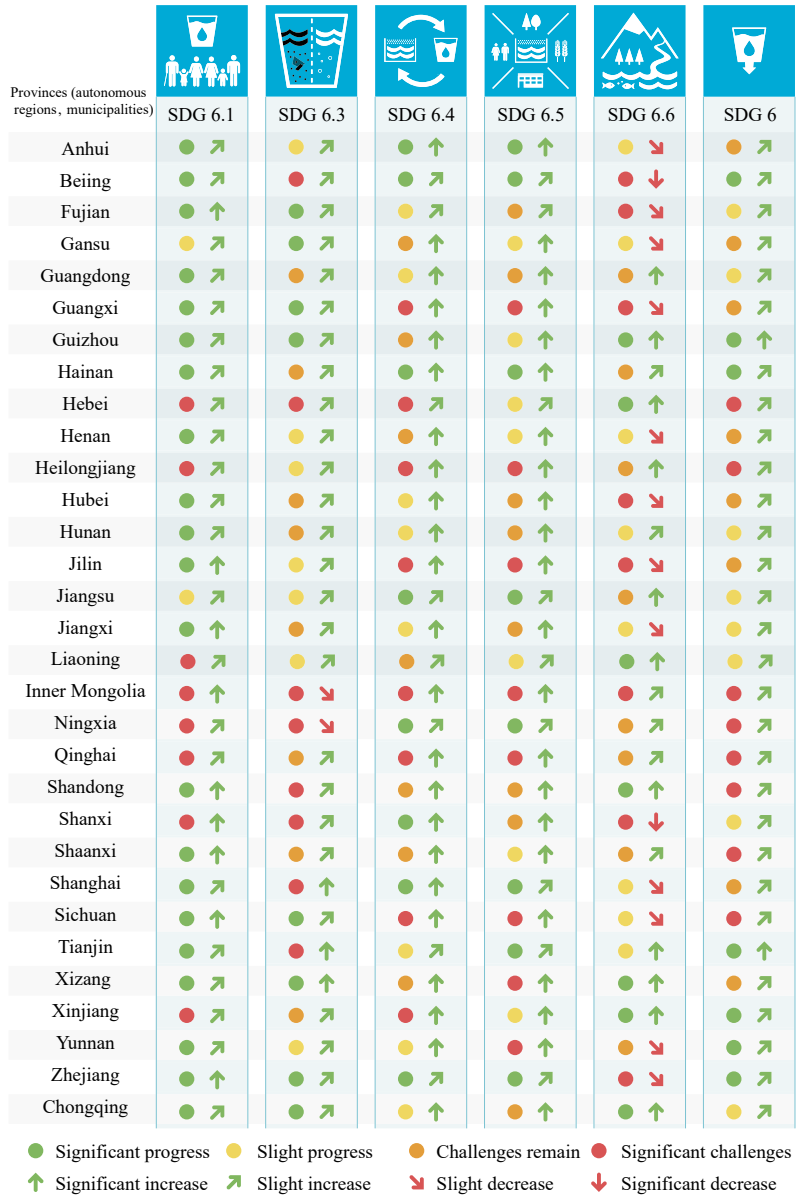

Fig. 3.25 Progress and trends of SDG 6 from 2015 to 2020

natural geographical conditions and resource endowments of each province to formulate an optimization path for each region, which provides reference for the formulation of an SDG 6 action plan for each province. At the same time, the future plan is to further integrate multi-source data to make specific suggestions for solving the problem of monitoring and evaluating indicators (such as coverage of SDG 6.2, environmental sanitation facilities) that lack clear evaluation data and evaluation methods, carrying out a more comprehensive assessment of the status quo of SDG 6, further improving the spatial accuracy and time range of data, and specifying the problems and challenges faced by various regions.

3.4 Summary

This chapter comprehensively used multi-source data, such as satellite remote sensing imagery, ground observation station networks, and statistical surveys, to assess the consumption of safe drinking water, improvement of water environments, improvement of WUE, reduction of water stress, integrated management of water resources, and the overall realization of clean water and sanitation goals of various provinces in China. The case studies addressed the lack of both single-indicator monitoring and comprehensive assessments of SDG 6 at the national and provincial level, which has led to unclear progress toward SDG 6. This report draws the following understandings and conclusions.

1. From 2015 to 2020, the proportion of safe drinking water in the country has increased significantly.
2. Compared to 2015, the proportion of water bodies with good water quality in 26 provinces of China increased in 2020, with one province remaining unchanged and four showing a slight decrease. From 2019 to 2021, the water quality assessment results of groundwater monitoring stations in all provinces of China were mainly stable.
3. From 2001 to 2019, the WUE of China's three major grain crops (wheat, corn, and rice) showed a significant increase. From 2010 to 2020, the national water stress and the area occupied by high water stress showed a significant decrease, though it is highly likely that China's water stress will increase in the future.
4. From 2017 to 2020, the implementation of water resources management tools in various provinces in China progressed to different degrees, and the management of water sources and water supply made significant progress. The amount of resources, water supply, and the implementation of aquifer management vary greatly from province to province, and are closely related to the conditions of water resources endowment, social and economic development, and the characteristics of water resources development and utilization.
5. The SDG 6 composite index of all provinces in the country shows an increasing trend, but the spatial difference is obvious. The sustainable development of water resources varies significantly among provinces, presenting distinct challenges for economically developed and underdeveloped regions. Economically developed regions encounter numerous issues related to their water environment and ecology, whereas economically underdeveloped regions tend to exhibit lower efficiency in water usage.

Overall, from 2015 to 2020, China made significant progress on all indicators of SDG 6. The three targets of SDG 6.1, SDG 6.3, and SDG 6.5 in China's provinces have improved significantly and are close to achieving the 2030 goal, while SDG 6.4 is still more than halfway to being achieved.

References

Bhaduri A, Bogardi J, Siddiqi A et al (2016) Achieving sustainable development goals from a water perspective. Front Environ Sci 4:64

Cernev T, Fenner R (2020) The importance of achieving foundational Sustainable Development Goals in reducing global risk. Futures 115:102492

Du DD, Zheng CL, Jia L et al (2022) Estimation of global cropland gross primary production from satellite observations by integrating water availability variable in light-use-efficiency model. Remote Sensing 14(7):1722

FAO (2018) Progress on level of water stress—global baseline for SDG 6 indicator 6.4.2 2018. http://www.fao.org/3/CA1592EN/ca1592en.pdf [2023-06-08]

Harlin J, Alabaster G, Slaymaker T, et al (2021) In need of speed: data can accelerate progress towards water and sanitation for all. https://sdg.iisd.org/commentary/guest-articles/in-need-of-speed-data-can-accelerate-progress-towards-water-and-sanitation-for-all/ [2023-6-8]

Hu GC, Jia L (2015) Monitoring of evapotranspiration in a semi-arid inland river basin by combining microwave and optical remote sensing observations. Remote Sensing 7(3):3056–3087

Jiang YZ (2016) Strengthen the construction of water resources monitoring capabilities and provide support

for the dual control action of water resources. China Water Resources 13:7–9 (in Chinese)
Kong G, Wang OJ, Huang Q (2017) Evaluation of groundwater quality in Changping piedmont plain of bering based on BP neural network. Trans Chin Soc Agric Eng 33(Supp.1):150–156, 389 (in Chinese)
Kroll C, Warchold A, Pradhan P (2019) Sustainable development goals (SDGs): are we successful in turning trade-offs into synergies? Palgrave Commun 5:140
Ladel J, Mehta M, Gulemvuga G, et al (2020) Water policy on SDG6.5 implementation: progress in integrated & transboundary water resources management implementation. World Water Policy 6(1):115–133
Li L, Zhou JL, Zhao F (2015) Application of the BP neural network model on shallow groundwater quality evaluation in Yanqi Country in Xinjiang. Environ Prot Xinjiang 37(3):40–43 (in Chinese)
Lu S L, Jia L, Jiang YZ, et al (2021) Progress and prospect on monitoring and evaluation of United Nations SDG 6 (clean water and sanitation) target. Bull Chin Acad Sci 36(8):904–913 (in Chinese)
Meier J, Zabel F, Mauser W (2018) A global approach to estimate irrigated areas—a comparison between different data and statistics. Hydrol Earth Syst Sci 22:1119–1133
Müller Schmied H, Cáceres D, Eisner S, et al (2020) The global water resources and use model WaterGAP v2.2d–Standard model output. PANGAEA
Ni T X, Feng L (2018) Comparison and analysis of two kinds of correction of Nemerow index method in groundwater quality evaluation and their application. Ground Water 40(6):8–11, 53 (in Chinese)
Requejo-Castro D, Giné-Garriga R, Pérez-Foguet A (2020) Data-driven Bayesian network modelling to explore the relationships between SDG 6 and the 2030 Agenda. Sci Total Environ 710:136014
UN Environment (2016) Step-by-step methodology for monitoring integrated water resources management (6.5.1). https://www.unwater.org/publications/step-step-methodology-monitoring-integrated-water-resources-management-6-5-1/ [2016-12-30]
UN (2022). The sustainable development goals report 2022. UN, New York https://unstats.un.org/sdgs/report/2022 [2022-07-07]
United Nations Statistics Division (2022) SDG indicator metadata. UN, New York. Available online https://unstats.un.org/sdgs/metadata/ [2023-08-08]
UN-Water (2021) Summary progress update 2021 SDG 6 water and sanitation for all. Version: 1 March 2021. Switzerland, Geneva
Wang JS, Zhong HP, Geng LH, et al (2006) Available water resources in China. Adv Water Sci 17(4):549–553 (in Chinese)
Weitz N, Carlsen H, Nilsson M et al (2018) Towards systemic and contextual priority setting for implementing the 2030 Agenda. Sustain Sci 13(2):531–548
World Meteorological Organization (2008) Guide to hydrological practices (Volume I: Hydrology–from measurement to hydrological information). https://unstats.un.org/unsd/envaccounting/waterGuidelines/Material/WMO_Guide_168_Vol_I_en_hydrological_practices.pdf [2023-02-15]
Xie WS, Huang DK, Lu HJ et al (2022) Variation trend and spatio-temporal distribution of river manganese pollution in the cluster area of electrolytic manganese industry. Environ Chem 41(1):315–326 (in Chinese)
Xie YK (2021) Research on water use anomaly monitoring based on isolated forest algorithm. Beijing University of Posts and Telecommunications (in Chinese)
Xu ZC, Chau SN, Chen XZ et al (2020) Assessing progress towards sustainable development over space and time. Nature 577(7788):74–78
Zheng CL, Jia L, Hu GC et al (2019) Earth observations-based evapotranspiration in northeastern Thailand. Remote Sensing 11(2):138
Zheng CL, Jia L, Hu GC (2022) Global land surface evapotranspiration monitoring by ETMonitor model driven by multi-source satellite earth observations. J Hydrol 613:128444. https://doi.org/10.1016/j.jhydrol.2022.128444

SDG 7 Affordable and Clean Energy

4

4.1 Background

Energy is a global issue of common concern today, at the heart of almost every major challenge and opportunity. Since the Industrial Revolution, fossil fuels such as coal, oil, and natural gas have been the main sources of electricity production and for meeting the basic needs of human life. In 2019, only slightly more than 11.4% of energy came from non-nuclear renewable sources. The combustion of fossil fuels produces a large amount of greenhouse gases, causing harmful and significant impacts on the climate and ecological environment essential to human survival. Over the past half-century, global energy consumption has been increasing every year. With the growth of wealth and the development of markets, the demand for energy is becoming increasingly greater. Sufficient energy must be provided to meet the demand in order to drive global development and improve living standards.

To address global climate change, the transition from fossil fuels to green and low-carbon energy has become a global consensus. To promote global energy transformation, 193 member states of the UN officially adopted the SDGs and their corresponding targets at the UN Sustainable Development Summit in September 2015. SDG 7 calls for "affordable, reliable, sustainable and modern energy for all" by 2030 and is one of the 17 goals of the UN 2030 Agenda, which will open up a new world full of opportunities for billions of people. The targets of SDG 7 cover energy supply, renewable energy, energy efficiency improvement, and international energy cooperation, and its three core targets are:

- Ensure universal access to affordable, reliable, and modern energy services.
- Increase substantially the share of renewable energy in the global energy mix.
- Double the global rate of improvement in energy efficiency.

The energy industry is vigorously promoting the clean and low-carbon transformation of the energy structure, and vigorously developing renewable clean energy such as wind power and PV, which has become an important measure for countries to accelerate green development and build a clean, low-carbon, safe, and efficient energy system. China adheres to the concept of ecological civilization and attaches great importance to the development of renewable energy. It has taken a series of measures to cope with climate change and made significant achievements in the field of clean energy. China's installed capacity of renewable energy has been ranked first in the world for consecutive years, and the development of wind power and PV power generation industries has promoted the large-scale application of renewable energy power generation worldwide. From a domestic perspective,

H. Guo, *Big Earth Data in Support of the Sustainable Development Goals (2022) - China*,
Sustainable Development Goals Series, https://doi.org/10.1007/978-981-97-4231-8_4

energy conservation and carbon emission reduction are in line with the concept of ecological civilization; from an international perspective, the net-zero CO_2 emissions trend is unstoppable, and China is a major emitter of carbon emissions. Its role in global climate governance is indispensable. Active participation not only reflects its responsibilities as a major country, but also has significant implications for enhancing its power in international discourse.

The National Development and Reform Commission and the National Energy Administration issued the "Opinions on Improving the System, Mechanism and Policy Measures for Green Energy and Low-carbon Transformation" on February 10, 2022, proposing to promote the construction of an energy supply system mainly composed of clean and low-carbon energy. With a focus on desert and arid regions, efforts will be accelerated to promote the construction of large-scale wind and PV power generation bases. As a strategic emerging industry of national importance, PV has become one of China's strategic emerging industries with international competitive advantages and is widely recognized as one of the most promising renewable clean energy sources. Developing the PV industry is of great significance for adjusting the energy structure, promoting the energy production and consumption revolution, and promoting the construction of an ecological civilization. Under the global development initiative and South–South cooperation framework, China has actively assisted other countries, especially developing countries, in achieving SDG 7 through international energy cooperation such as investment, construction, equipment supply, and training, making significant contributions to global achievement of SDG 7.

It is of great significance to track and evaluate the global progress' of SDG 7 in a timely and accurate manner for policy formulation and project implementation to achieve SDG 7 in various countries. International organizations such as the International Energy Agency have jointly published annual global SDG 7 tracking reports since 2017, but the evaluation of SDG 7 progress still faces challenges such as data gaps and lagging updates. Developing a new generation of SDG 7 tracking and evaluation methods based on Big Earth Data technology has become an international research hotspot. This chapter aims to use Big Earth Data technology such as remote sensing and geographic information systems (GIS) to periodically obtain and comprehensively analyze global multi-source data, improve global Big Earth Data monitoring and evaluation methods for SDG 7, evaluate the progress of each indicator of SDG 7, and provide scientific data support for achieving SDG 7 worldwide.

4.2 Main Contributions

In order to address the energy crisis and global climate change, increase the proportion of renewable energy in the global energy structure, and double the global energy efficiency improvement rate and other SDGs, the advantages of various remote sensing technologies and GIS will be fully utilized to provide monitoring and evaluation methods for SDG 7. This chapter mainly focuses on two targets, SDG 7.2 and SDG 7.3, and contributes to the global monitoring of China's data products for SDG 7 indicators (Table 4.1).

Table 4.1 Case studies and their main contributions

Targets	Cases	Contributions
SDG 7.2 By 2030, increase substantially the share of renewable energy in the global energy mix	Construction and spatiotemporal distribution analysis of PV power stations in China	**Data product:** Chinese PV power station distribution dataset for 2015 and 2020
SDG 7.3 By 2030, double the global rate of improvement in energy efficiency	Spatiotemporal monitoring and analysis of China's high energy-consuming industries	**Data product:** Chinese high energy-consuming industry distribution dataset for 2012 and 2020

4.3 Case Studies

4.3.1 Construction and Spatiotemporal Distribution Analysis of PV Power Stations in China

Target: SDG 7.2: By 2030, increase substantially the share of renewable energy in the global energy mix.

4.3.1.1 Background

To achieve a better and more sustainable future blueprint, the UN has proposed SDG 7.2, which aims to significantly increase the proportion of renewable energy in the global energy structure by 2030 to ensure that everyone has access to affordable, reliable, and sustainable modern energy as the most available form of renewable energy. Solar energy has enormous potential for replacing fossil fuels to reduce greenhouse gas emissions and mitigate climate change, and PV technology can convert solar energy into electricity by using large solar cell arrays. With the rapid development of PV technology and industry, the cost of PV power generation has been reduced to the same level as traditional fossil fuel power plants, and PV and concentrated solar power (CSP) have become driving forces for renewable energy power growth. The National Energy Administration further proposed that the proportion of non-fossil energy consumption in the country should reach 25% by 2030, and the target for wind and PV installed capacities should be over 1.2 billion kilowatts. The national strategic needs provide new opportunities and challenges for the development of new energy, such as PV power generation and wind power generation. Rapid and accurate acquisition of the spatial distribution of national PV is of great significance for the future planning of PV power stations.

4.3.1.2 Data

- Sentinel-2 A/B data with a spatial resolution of 10 m.
- Gaofen-2 satellite images with a spatial resolution of 0.8 m (Panchromatic band) and 4 m (Multispectral bands).
- China land cover data with a spatial resolution of 30 m in 2015.
- Vector boundaries of Chinese provinces, autonomous regions, and municipalities.
- Statistical data related to PV power generation released by the National Energy Administration.
- Consultation reports released by chinapower.com.cn (organized by China Electric Power Promotion Council).

4.3.1.3 Methods

This study constructed a PV power station extraction model based on Google Earth Engine (GEE) and a deep learning model (Deeplab V3+). This study utilized two periods of Sentinel-2 images in 2015 and 2020 as the basis of remote sensing data sources, supplemented by historical image data from Google Earth and Tiandi Map. Two periods of PV power stations were extracted. The training sample set for PV power stations was mainly selected based on the national PV power station construction progress released by the National Energy Administration; large, centralized PV power station data provided by Wikipedia; and high-resolution image data such as Gaofen-2, which includes countries such as China, India, the United States, France, Vietnam, and Spain, ensuring the reliability and diversity of sample sources. Afterward, the images in the selected area were labeled by visual interpretation to create a preliminary PV power station sample set. The interpretation sign of PV power stations on remote sensing images was established, and the main features include color, texture, shape, size, and geographic location. The created sample set was subsequently augmented with data to further expand the sample set. The established training sample set mainly comes from large-scale PV power stations, and the accurate and comprehensive land cover contained in it further ensures the quality of the samples.

Using the sample database of PV power stations as input, we obtained the PV power

plant extraction model by training the Deeplab V3+network. The Deeplab series is a series of semantic segmentation algorithms proposed by Google. Among them, Deeplab V3+introduced the encoder–decoder architecture of networks such as Feature Pyramid Network (FPN) to achieve the fusion of Feature Map across blocks, and used group convolution to accelerate training. During training, the epoch was fixed at 100, the learning rate was fixed at 0.001, and the batch size was fixed at 12. The polynomial decay method was used to iteratively decrease the learning rate during training, with a decay factor of 0.9. In order to avoid overfitting, the weight decay coefficient was set to 0.0005. The optimization method used stochastic gradient descent, and the momentum was set to 0.9 to regulate learning. In this solution, extracting PV power plants was regarded as a binary semantic segmentation problem, so the binary cross-entropy loss function (BCELoss) was used as the loss function for this network. Based on the trained PV power plant extraction model and the small-scale images generated by the sliding window segmentation algorithm with coordinate information, the PV power plant area in the small-scale images could be accurately extracted. The extraction results were reassembled based on the coordinate information to accurately extract PV power plant areas nationwide. The accuracy of the extraction results was evaluated in conjunction with manually interpreted data. The results show that the overall accuracy of the model is 98.76%, and the Kappa coefficient is 0.87, indicating that the model has a good recognition effect for PV power plants.

4.3.1.4 Results and Analysis

Distribution of China's PV Power Plants

The total area of existing PV systems in China was 4,483.3 km^2 in 2020. The spatial distribution of PV power plants is shown in Fig. 4.1(a). In order to conduct a more detailed analysis of the distribution of PV systems, the proportion of the PV area on the east and west sides of the Hu Line was calculated separately. The eastern region of the Hu Line accounts for 57.4% of the PV area, mainly distributed in the densely populated and solar-rich North China Plain and East China region. Small- and medium-sized PV systems and distributed PV systems are the main types, and their distribution density is influenced by factors such as topography and PV subsidy policies. The western region accounts for approximately 42.6% of the PV area, mainly consisting of large PV power plants and solar thermal power stations. PV installations are mainly distributed in Northwest and North China, consistent with the annual statistical data from the National Energy Administration. The provinces with a high proportion of PV areas are Xinjiang, Inner Mongolia, and Ningxia, with 518 km^2, 420 km^2, and 406 km^2, respectively, accounting for 12%, 9%, and 9% of the country's total PV area [Fig. 4.1(b)-(c)]. These regions have abundant solar energy resources, sparse vegetation, and low population density. Grassland and wasteland are the main underlying surfaces of centralized solar PV power plants, accounting for 31% and 16%, respectively (Fig. 4.2). Distributed PV power plants are mainly located on built-up land, supplemented by small amounts of forest and barren land around villages and towns, which may be due to restrictions on the installation of PV panels due to vegetation cover. Overall, the selection of PV power plant sites in China follows two trends: resource orientation, with a focus on western and northwestern regions of China with suitable natural conditions such as high elevation, abundant solar resource, low population density, and less demand for electricity; and demand orientation, with a focus on eastern coastal provinces of China with lower elevation, high population density, developed industry, and greater demand for energy. The Sichuan Basin and Heilongjiang have low solar energy resources due to climate, topography, and latitude, thus limiting the development of PV power generation, with only sporadic PV power plants.

Spatiotemporal Distribution Changes of China's PV Power Plants

As the world's largest developing country and a major contributor to carbon emissions, China also faces challenges in reducing carbon emissions in the coming years. PV technology, as

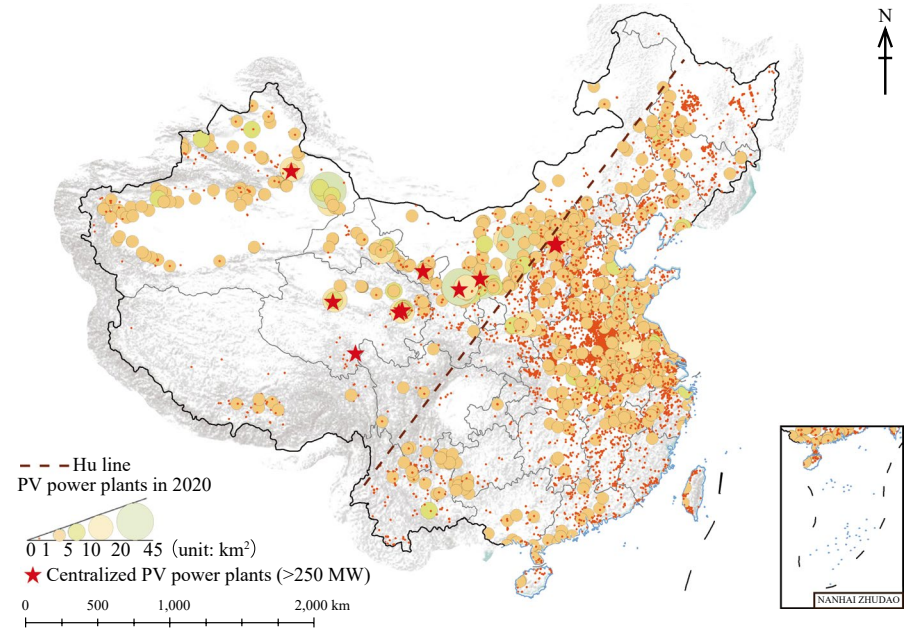

(a) Spatial distribution

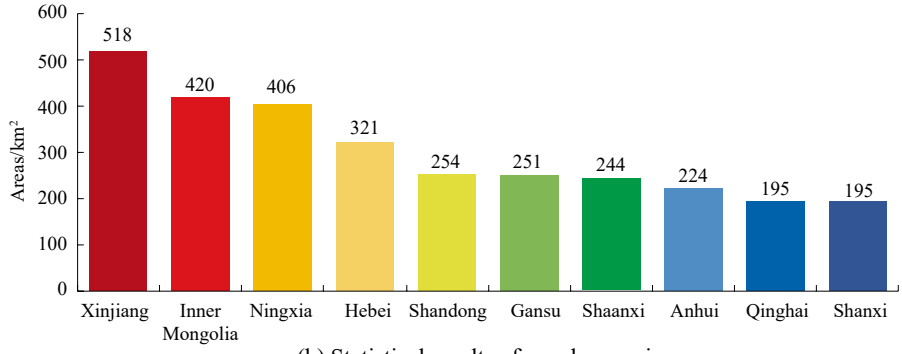

(b) Statistical results of area by province

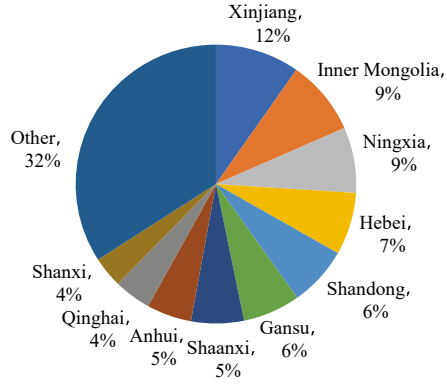

(c) Proportion of area by province

Fig. 4.1 China's PV power plants in 2020

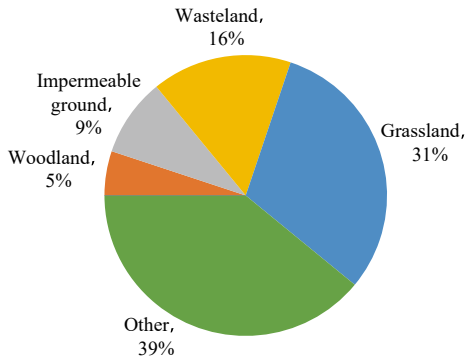

Fig. 4.2 Distribution of China's PV power plants with different land cover types in 2020

an effective solution to mitigate the impacts of climate change, is increasingly being used worldwide to replace fossil fuel-based electricity generation and minimize greenhouse gas emissions. From 2015 to 2020, driven by economic development and national policies, China became the country with the highest cumulative installed capacity and the fastest construction speed of PV power generation in the world. Combining the results of the PV installed capacity of the National Energy Administration and this study's analysis of PV power station areas, it was found that in the five years, the total area of China's PV power stations increased by 1,177 km^2, and the newly added PV power generation capacity connected to the grid was 210 million kilowatts. The newly added PV area was mainly distributed in the "Three-North" regions, accounting for 54% of the country's total new PV area [Fig. 4.3(a)]. Liaoning, Inner Mongolia, Shandong, and Ningxia ranked at the top in terms of the newly added PV area, with increases of 109 km^2, 97 km^2, 85 km^2, and 81 km^2 respectively, accounting for 10%, 9%, 8%, and 7%, respectively. Hebei, Shaanxi, Jiangsu, Anhui, and Hubei had similar increases in area, ranging from 40 to 74 km^2, and accounting for between 3 and 7%.

Highlight

- Using Google Earth Engine and Sentinel-2 imagery, a machine learning method was introduced to independently identify the PV power stations in China in 2015 and 2020. Over the five-year period, China's total installed area of PV power stations increased by 1,177 km^2, and the cumulative installed capacity of PV power increased by 210 million kilowatts. Many of the new PV installations were distributed in the "Three-North" regions, accounting for 54% of the country's total new PV area. In 2020, China's cumulative installed capacity of PV power ranked first in the world, surpassing the total of the European Union and the United States. In the eastern and western areas of the Hu Line, PV power station distribution accounted for 57.4% and 42.6%, respectively. In the western area, large-scale centralized PV power generation was the focus, while in the eastern area, small-scale and distributed PV power generation was the main focus, driven by local solar resource endowments, terrain, and policies, among other factors. The provinces with the highest installed capacity of PV power were Xinjiang, Inner Mongolia, and Ningxia, in the northwestern region, accounting for 12%, 9%, and 9% of the country's total, respectively. The development of PV power generation in Heilongjiang and Sichuan Basin was limited due to their climate, complex terrain, latitude, and weak solar energy resources.

4.3.1.5 Discussion and Outlook

This study developed an automatic extraction method for PV power plants based on Google Earth Engine combined with deep learning methods. High-resolution Sentinel-2 images were used as inputs to achieve high-precision extraction of China's PV power plants in 2015 and 2020. Datasets on the distribution and area of China's PV power plants in 2015 and 2020 were successfully established. The method combines the efficiency of deep learning methods and the accuracy of visual interpretation. The model, based on Deeplab V3+, performed well in extracting PV power plants, with a producer accuracy of 84.25% and an overall accuracy of over 98.76%.

Through this study, it was found that PV power stations in China are mainly distributed

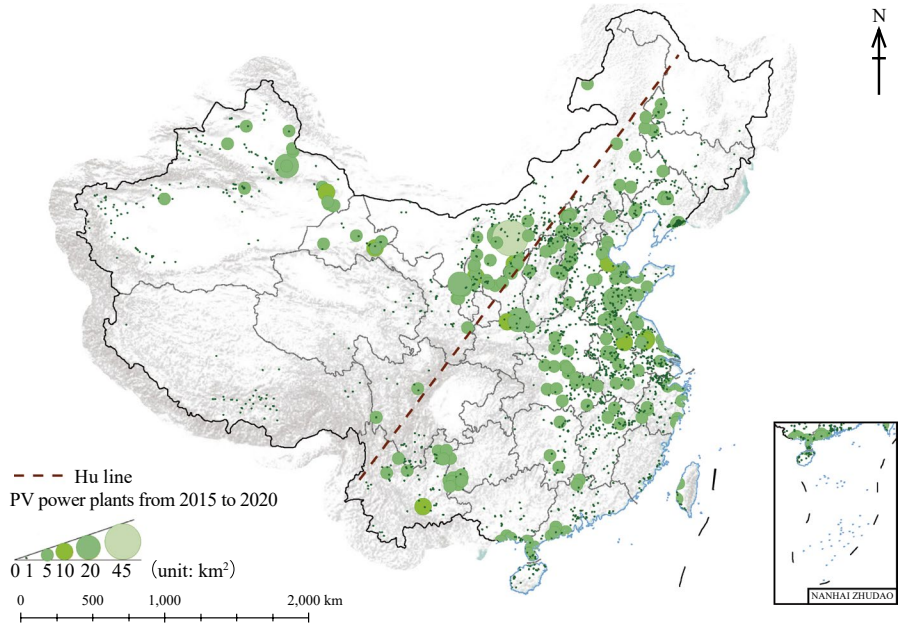

(a) Spatial distribution

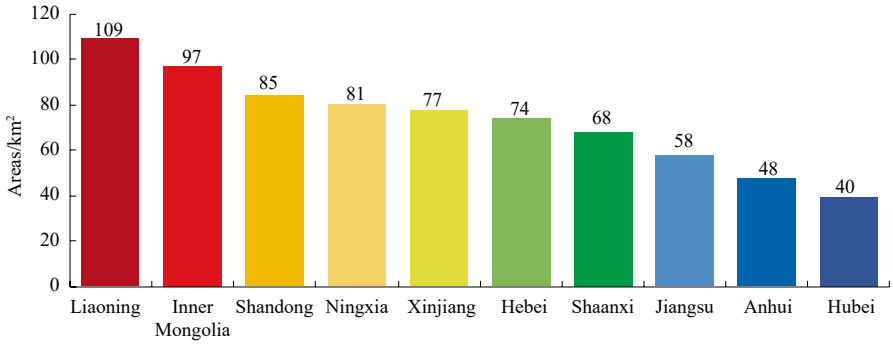

(b) Statistical results of area by the top ten provinces

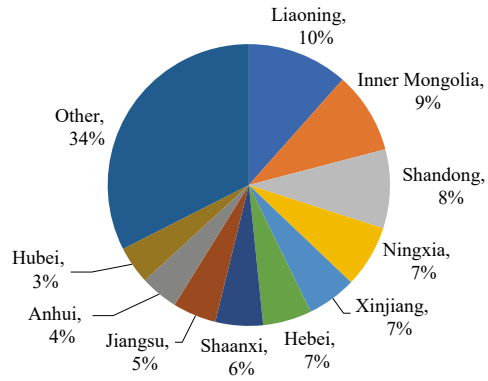

(c) Proportion of area by the top ten provinces

Fig. 4.3 China's newly added PV stations between 2015 and 2020

in the North China Plain, the East China region, and the western regions of Xinjiang, Ningxia, and Inner Mongolia, which are rich in solar energy resources. CSP plants were mainly distributed in Xinjiang, Gansu, and Qinghai. The PV proportion to the east and west of the Hu Line is approximately 57.4% and 42.6%, respectively. From 2015 to 2020, the total area of PV power plants in China increased by 1,177 km^2, of which Liaoning, Inner Mongolia, Shandong, Ningxia, Xinjiang, and Hebei provinces in Northeast, Northwest, and North China accounted for 48% of the country's new area.

The dataset produced by this study can provide training samples for subsequent research to further improve the model accuracy and identify future PV power plants. The spatiotemporal distribution patterns of PV power plants in the two phases can provide important scientific data for the reasonable planning and site selection of PV power plants and the evaluation of SDG 7.2 at the national scale.

4.3.2 Spatiotemporal Monitoring and Analysis of China's High Energy-Consuming Industries

Target: SDG 7.3: By 2030, double the global rate of improvement in energy efficiency.

4.3.2.1 Background

Improving energy efficiency is one of the main ways to achieve large-scale CO_2 reduction. In 2022, China's "Action Plan for Improving Industrial Energy Efficiency" proposed that by 2025, the energy consumption per unit of the added value of industrial units above the designated size will decrease by 13.5% compared to 2020. High energy-consuming industries such as steel, petrochemical, and non-ferrous metals are key areas of China's energy efficiency improvement action plans. The spatiotemporal variation characteristics of heat sources in China's high energy-consuming industries can characterize their spatiotemporal distribution pattern and reflect the comprehensive changes in energy utilization efficiency and the effectiveness of industrial optimization and energy upgrades. Its indicator data are an important basis for evaluating the progress of implementing SDG 7.3 and can provide key data support for China's specific compliance actions under the Paris Agreement.

This study is based on Big Earth Data, such as long-term satellite remote sensing and field research, to revolve around China's industrial structure adjustment policies. A long-term dataset of China's high energy-consuming industries from 2012 to 2021 was developed. A remote sensing spatiotemporal monitoring and analysis method for China's high energy-consuming industries was also proposed. It provides data support for improving energy efficiency in key industries in China. The data in this study can provide an important scientific basis for the evaluation of SDG 7.3 at the national scale and can serve as an important reference for evaluating SDG 8.4, SDG 9.2, SDG 12.2, and SDG 13.3. It provides independent scientific data and support for China to actively respond to the upgrading of the "structure adjustment and capacity reduction" industrial model, improve the atmospheric environment, promote the global sustainable development process, and build a community with a shared future for humankind.

4.3.2.2 Data

- Active fire/hotspot data from the Visible Infrared Imaging Radiometer Suite (VIIRS) onboard the Suomi National Polar-Orbiting Partnership (NPP) satellite, ranging from 2012 to 2021.
- High-resolution satellite image data such as that from Google Earth from 2012 to 2021.
- Point of interest (POI) information database from 2012 to 2021.
- Corresponding statistical data and published information on the adjustment and transformation of high energy-consuming industries in China.

4.3.2.3 Methods

Due to "fixed location and continuous time" characteristics in the operation of high

energy-consuming industrial heat source enterprises, they exhibit persistent, abnormally high-temperature radiation in remote sensing images. A combination model based on spatiotemporal density segmentation and machine learning (Ma et al. 2018) was adopted to identify high energy-consuming industries in China. The main process includes selecting long-term active thermal anomaly data, building heat source objects by using the spatiotemporal density segmentation method, identifying multiple thermal information characteristics of heat source objects, using an RF method to identify and analyze heat source objects in high energy-consuming industries, and combining high-resolution satellite image data from Google Earth, POI information, and field research to check and correct the identification results.

This study focuses on the problem of identifying high energy-consuming industries in China. We selected remotely sensed active thermal anomaly data from 2012 to 2021, and used technology based on spatiotemporal density segmentation and machine learning to identify the number of high energy-consuming industries (Ma et al. 2018). Totally, 4,411 high energy-consuming industrial sites in China from 2012 to 2021 were identified. After manual testing and field investigation, the overall recognition accuracy reached 95%.

4.3.2.4 Results and Analysis

Spatial Distribution Pattern of China's High Energy-Consuming Industries

The spatial distribution of high energy-consuming industries in China from 2012 to 2021 is shown in Fig. 4.4. In 2012, 2015, and 2021, there were 2,973, 3,166, and 2,653 high energy-consuming industries operating, mainly in Benxi-Anshan-Yingkou in Liaoning, Tangshan in Hebei, Handan in Hebei-Anyang in Henan, narrow basins from Taiyuan to Hejin via Linfen, Changzhi in Shanxi, Ordos in Inner Mongolia, and Wuhai and Urumqi in Xinjiang. The high energy-consuming industrial sites in Hebei, Shanxi, Xinjiang, Inner Mongolia, and Shandong provinces (including autonomous regions) account for more than 40% of the total number in China. As of 2021, there is still enough transfer room for high energy-consuming industries in the central, western, and northeastern regions.

Spatiotemporal Distribution Characteristics of China's High Energy-Consuming Industries

Figure 4.5 shows the spatial distribution changes in high energy-consuming industries in China from 2012 to 2021. The number of high energy-consuming industrial sites showed a trend from increasing to decreasing from 2012 to 2021. The number reached a peak in 2014 but by 2021 had decreased by 10.76% compared to 2012. The average annual decrease in the number of high energy-consuming industries from 2012 to 2015 was -2.28%, then 2.88% from 2015 to 2021.

From 2012 to 2015, the number of high energy-consuming industries was mainly distributed in the Northwest, Central China, and South China, which saw an increase (as shown in Fig. 4.5). The reduction trend was most evident in North China. Hebei Province showed the largest reduction.

Between 2015 and 2021, there were only six provinces in South and West China with a net increase. The average increase in the number of high energy-consuming industries was eight in each province. The decreasing trend in economically developed regions such as North and East China was most evident. Compared with the period from 2012 to 2015, the decreasing trend was more pronounced from 2015 to 2021.

On September 10, 2013, the State Council of China issued the Action Plan for Air Pollution Prevention and Control, which promotes "adjusting and optimizing industrial structure, promoting industrial optimization and upgrading". Then a supply-side reform in 2015 was proposed. China has actively implemented industrial transformation, upgrading, and structure adjustment strategies. As of December 31, 2021, the number of high energy-consuming industries in China had decreased by 19.75% compared to 2014. The number of high energy-consuming

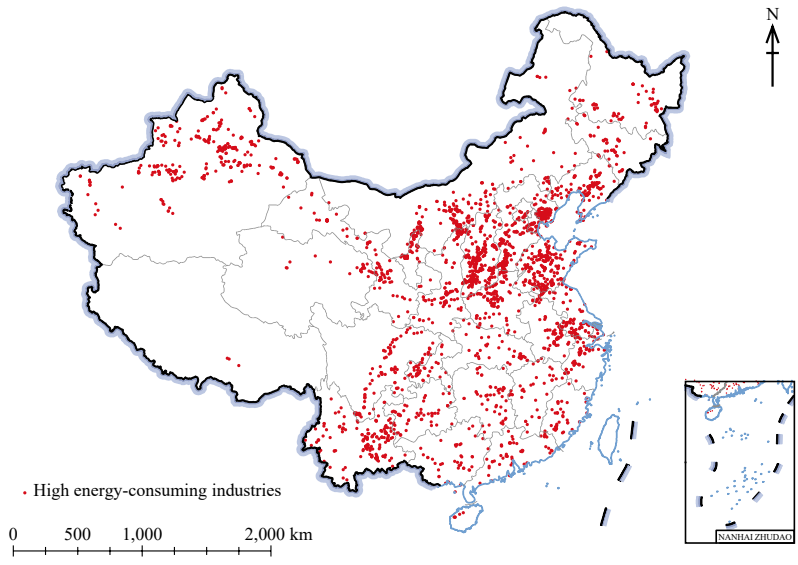

(a) 2012

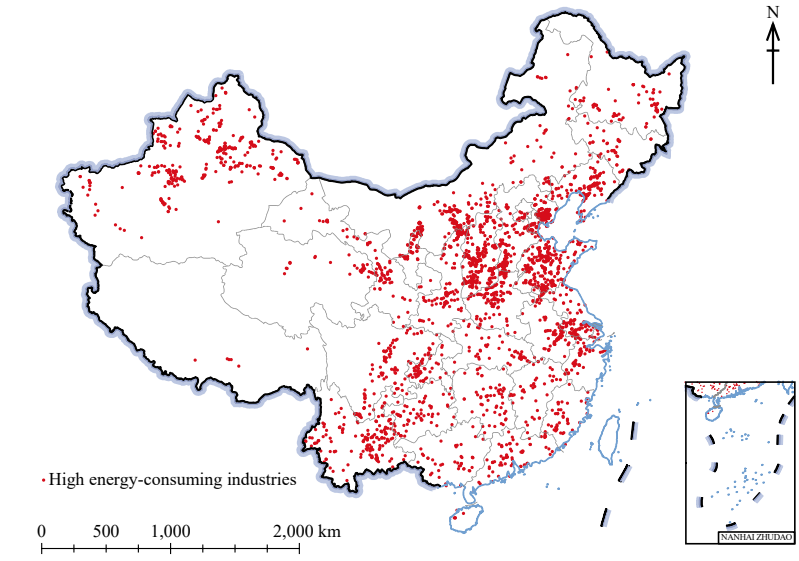

(b) 2015

Fig. 4.4 Spatial distribution and change in China's high energy-consuming industries in major provinces (including autonomous regions) in 2012, 2015, and 2021. *Note* No data for Hong Kong, Macao, and Taiwan

industries in over 80% of provincial administrative regions has shown a downward trend. Between 2012–2015 and 2015–2021, the China Statistical Bulletin showed that high energy-consuming industrial products maintained an average annual growth rate of 8.35% and 5.06%, respectively. This indicates that most of the high energy-consuming enterprises eliminated in China from 2014 to 2021 belong to the "high energy consumption and low production capacity" type. The operating enterprises also effectively improved energy utilization efficiency, and the effect of clean and low-carbon energy transformation was significant.

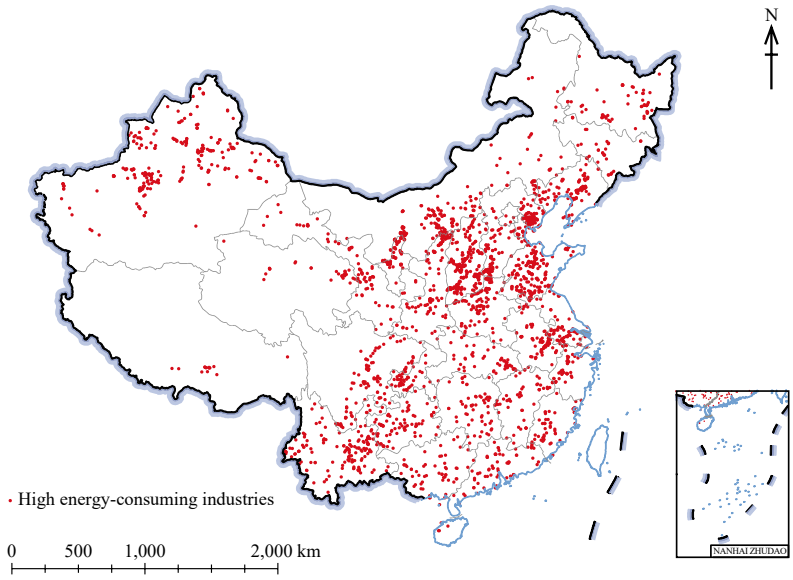

(c) 2021

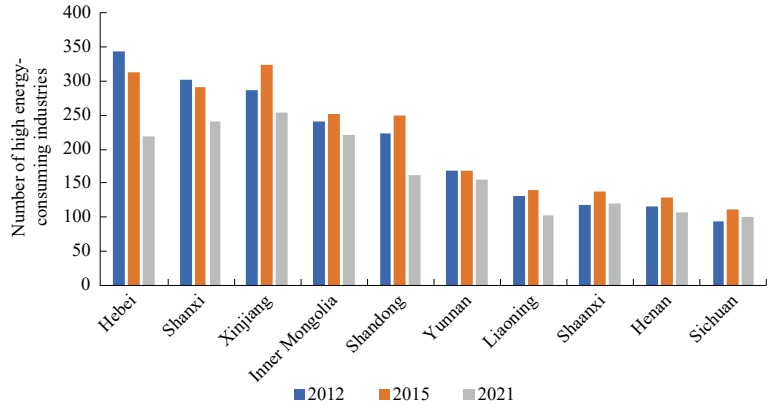

(d) The change of high energy-consuming industries in major provinces (autonomous regions)

(continued)

In 2021, the Energy Consumption Per Unit of GDP in China Decreased by One-Fifth Compared to 2014, Making an Important Contribution to Global Energy Efficiency

The number of high energy-consuming industries is closely related to the changes in energy consumption per unit of GDP in China. The correlation coefficient between the number of high energy-consuming industries and energy consumption per unit of GDP is 0.93 (Fig. 4.6). In 2021, the energy consumption per unit of GDP decreased by one-fifth compared to 2014. In 2014, the number of high energy-consuming industries in China reached its peak, and then decreased year by year, effectively promoting a decrease in energy consumption per unit of GDP in China.

Highlights

- A remote sensing spatiotemporal monitoring and analysis method was constructed for identifying high energy-consuming industries based on spatiotemporal density

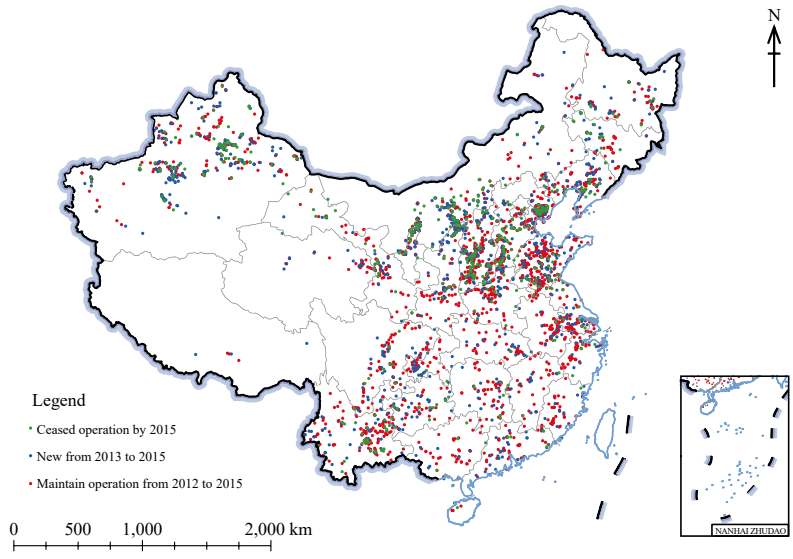

(a) 2012-2015

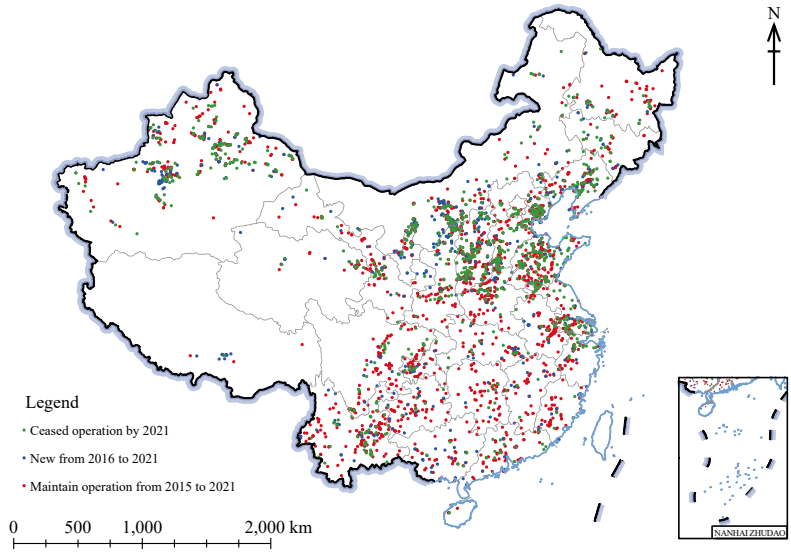

(b) 2015-2021

Fig. 4.5 Spatiotemporal changes in China's high energy-consuming industries from 2012 to 2015 to 2021. *Note* No data for Hong Kong, Macao, and Taiwan

segmentation. A spatial distribution dataset was developed for high energy-consuming industrial sites in China from 2012 to 2021.

- Quantitative evaluation of the effectiveness of China's "structural adjustment and capacity reduction" policy shows that the distribution of high energy-consuming industries in China is characterized by local agglomeration. As of 2021, there was still enough transfer room for high energy-consuming industries in the central, western, and northeastern regions. In 2021, the number of high energy-consuming industries in China decreased by 19.75% compared to 2014. More than 80%

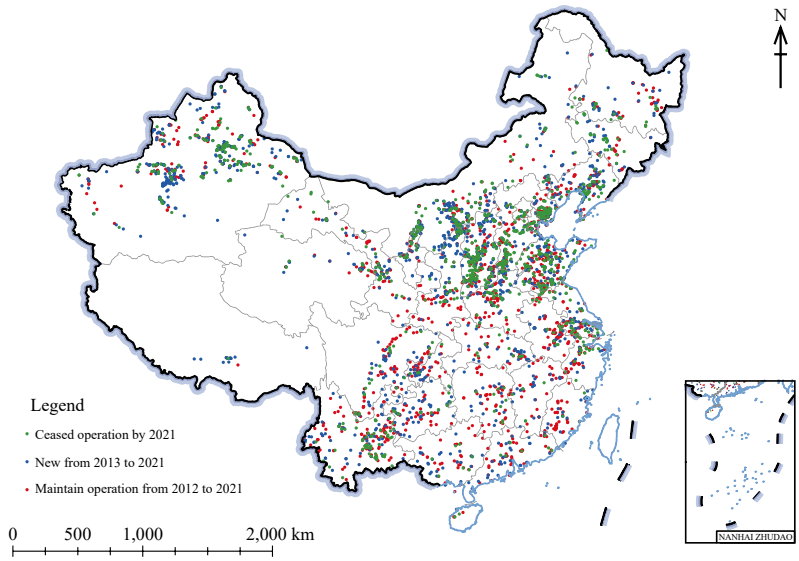

(c) 2012-2021

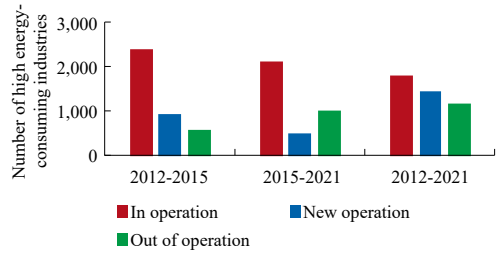

(d)

(continued)

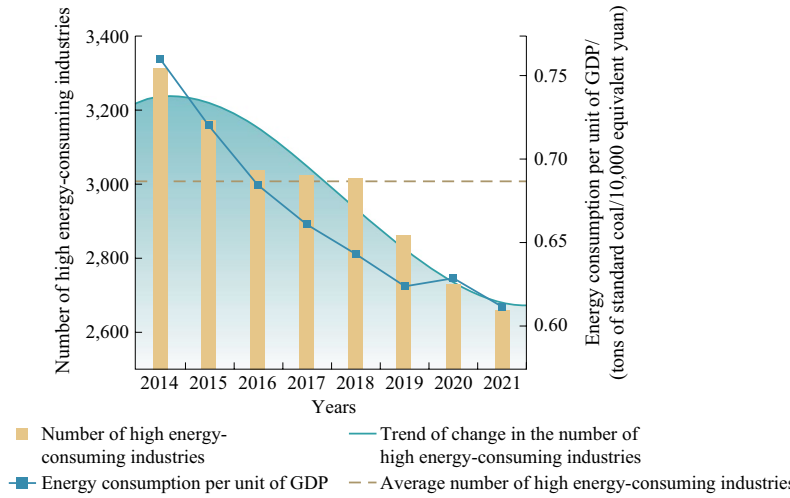

Fig. 4.6 Time variation in energy consumption and energy consumption per unit of GDP in China's high energy-consuming industries from 2014 to 2021

of provincial-level administrative regions showed a downward trend. The number of high energy-consuming industries is closely related to the changes in energy consumption per unit of GDP. The correlation coefficient between the two indicators is 0.93. In 2021, the values of the above two indicators decreased by one-fifth compared to the peak. This means that the change in China's high energy-consuming industries promotes the improvement of global industrial energy efficiency and makes important contributions to the global response to climate change.

4.3.2.5 Discussion and Outlook

In terms of technical methods and data, this study developed a spatiotemporal monitoring and analysis method for China's high energy-consuming industries based on long-term remote sensing thermal anomaly data, integrating spatiotemporal density segmentation and machine learning. A dataset of high energy-consuming industrial sites in China from 2012 to 2021 was developed. The data in this study can provide decision-making support for China's industrial structure adjustment, provide an important scientific basis for the evaluation of SDG 7.3 at the national scale, and serve as the data basis for evaluating SDG 8.4, SDG 9.2, SDG 12.2, and SDG 13.3.

In terms of decision support, this study found that the distribution of high energy-consuming industries in China is characterized by local agglomerations. As of 2021, there was still enough transfer room for high energy-consuming industries in the central, western, and northeastern regions. Compared with 2014, the number of high energy-consuming industries in over 80% of provincial-level administrative regions decreased in 2021. This indicates the continuous optimization and upgrading of China's industrial structure. The number of high energy-consuming industries is closely related to the changes in energy consumption per unit of GDP. The correlation coefficient between the two indicators is 0.93. In 2021, these two indicators saw a reduction by one-fifth compared to their peak values, which has contributed significantly to the enhancement of global industrial energy efficiency and has made important contributions to the worldwide response to climate change. It is of great practical significance to scientifically plan the transformation path of high energy-consuming industries and promote them to move toward a cleaner, more energy-efficient, and lower carbon emission development model. The results of this study not only support the scientific evaluation of SDG 7, but also actively respond to the upgrading of the "structural adjustment and capacity reduction" industrial model, and carbon taxes on domestic and foreign transactions.

4.4 Summary

This chapter focused on monitoring and analysis methods for SDG 7 using Big Earth Data to measure two indicators: renewable energy and energy efficiency. The methods were improved to evaluate China's progress toward SDG 7, which results indicate has been significant.

In terms of data products, one study independently produced China's PV power plant data products for 2015 and 2020, as well as China's high energy-consumption industry products from 2012 to 2021.

In terms of methods and models, high energy-consuming industry recognition technology was developed based on a combination of spatiotemporal density segmentation and machine learning. The SDG 7 indicators were revised and expanded to further improve the SDG indicator system. For example, a long-term dataset of China's high energy-consuming industries from 2012 to 2021 was developed to improve industrial energy efficiency. And the remote sensing spatiotemporal monitoring and analysis method for China's high energy-consuming industries was proposed to provide data support for the energy efficiency improvement of key industries in China.

In terms of decision support, this chapter provided an important scientific basis for the development and layout of new energy such as PV power station construction in China, as well as the energy efficiency evaluation of SDG 7.3. It

can also serve as an important reference for the evaluation of SDG 8.4, SDG 9.2, SDG 12.2, and SDG 13.3. The case studies in this chapter provide independent scientific data on upgrading the "structure adjustment and capacity reduction" industrial model in China. It can support capacity for promoting global sustainable development and building a community with a shared future for humankind, such as by improving the atmospheric environment.

References

Kruitwagen L, Story KT, Friedrich J et al (2021) A global inventory of photovoltaic solar energy generating units. Nature 598:604–610

Liao ML, Zhang Z, Jia J et al (2022) Mapping China's photovoltaic power geographies: Spatial-temporal evolution, provincial competition and low-carbon transition. Renewable Energy 191:251–260

Ma CH, Yang J, Chen F et al (2018) Assessing heavy industrial heat source distribution in China using real-time VIIRS active fire/hotspot data. Sustainability 10(12):4419

Ma CH, Yang J, Xia W et al (2022) A model for expressing industrial information based on object-oriented industrial heat sources detected using multi-source thermal anomaly data in China. Remote Sensing 14(4):835

Zhang XH, Xu M, Wang SJ et al (2022) Mapping photovoltaic power plants in China using Landsat, random forest, and google earth engine. Earth Syst Sci Data 14(8):3743–3755

SDG 11 Sustainable Cities and Communities

5

5.1 Background

Cities are the engine of economic growth, contributing about 60% to global GDP. At the same time, they are the main battleground in our fight against climate change. Cities generate about 70% of the global carbon emissions and use more than 60% of all resources. SDG 11 aims at making cities and human settlements "inclusive, safe, resilient and sustainable", overcoming the challenges of congestion, lack of funds, and infrastructure damage in ways that allow them to continue to thrive and grow, and improving resource use and reducing pollution and poverty as well. However, the average urban solid waste collection rate worldwide was 82% by 2022, and the rate under management in controlled urban facilities was 55%. Only 3% of the 6475 cities in 117 countries and territories around the world do not exceed the threshold of air quality guidelines of the World Health Organization (WHO).

With the development and progress of Earth observation and big data technology, Big Earth Data methods that pull together remote sensing, statistics, and geographic information play an important role in the monitoring and evaluation of SDG 11 indicators, as it is becoming widely used in sustainability evaluations, e.g., the evaluation of urban atmospheric environment, sustainable land use, and social and economic development. In the process of advancing the SDGs, the focus of research work has been shifting from the construction of SDG indicator systems to the monitoring and evaluation of SDG progress.

This chapter centers on four themes under SDG 11—monitoring and evaluating the urbanization process, urban disasters and response, urban environments, and comprehensive assessment of SDG 11 indicators. The case studies draw on research based on the previous three annual reports and use Big Earth Data methods to monitor and evaluate individual and multiple SDG 11 targets, including Chinese cities at the community scale.

5.2 Main Contributions

This chapter evaluates the progress of SDG 11.3, SDG 11.5, and SDG 11.6 in China and provides a comprehensive evaluation of SDG 11. The main contributions are as follows (Table 5.1).

5.3 Case Studies

5.3.1 Changes in Urban Land Use Efficiency in China

Target: SDG 11.3: By 2030, enhance inclusive and sustainable urbanization and capacity for participatory, integrated, and sustainable human settlement planning and management in all countries.

H. Guo, *Big Earth Data in Support of the Sustainable Development Goals (2022) - China*,
Sustainable Development Goals Series, https://doi.org/10.1007/978-981-97-4231-8_5

Table 5.1 Case studies and their main contributions

Targets	Cases	Contributions
SDG 11.3 By 2030, enhance inclusive and sustainable urbanization and capacity for participatory, integrated, and sustainable human settlement planning and management in all countries	Changes in urban land use efficiency in China	**Data product**: Urban built-up area data for 337 cities at the prefecture level in China in 2015 and 2020 **Method and model**: Automatic extraction model for urban built-up areas based on land cover data **Decision support**: Data to quantitatively describe the human-land relationship in the entire country, different regions, and provinces, cities of different scales, and different urban agglomerations, and to provide a reference for the policy of optimization and adjustment of land and population
SDG 11.5 By 2030, significantly reduce the number of deaths and the number of people affected and substantially decrease the direct economic losses relative to the global gross domestic product caused by disasters, including water-related disasters, with a focus on protecting the poor and people in vulnerable situations	Surface movement of China in 2021 based on a space-borne InSAR technique	**Data product**: 2021 InSAR-based annual average surface deformation rate of China **Method and model**: Coherent-Scatterer InSAR (CS-InSAR) **Decision support**: Provide information support and a decision-making reference for urban planning and disaster prevention
	Annual change in soil erosion at the county level in China (2010–2021)	**Data product**: 2010–2021 China county-level soil erosion risk products **Method and model**: Revised Universal Soil Loss Equation (RUSLE) **Decision support**: Provide data support and decision reference for national and local departments to make water and soil conservation planning
	Monitoring of natural disaster risks in China at the prefecture level (2010–2021) and analysis of typhoon disaster risks at the county level (2016–2020)	**Data product**: Dataset of SDG 11.5 indicators for 333 prefecture-level cities in China from 2010 to 2021 **Decision support**: To provide supporting information for decisions on the further improvement of disaster prevention and resilience of cities

(continued)

Table 5.1 (continued)

Targets	Cases	Contributions
SDG 11.6 By 2030, reduce the adverse per capita environmental impact of cities, including by paying special attention to air quality and municipal and other waste management	Assessment of changes in population exposure to typical atmospheric particulate matter in China	**Data product**: A dataset of $PM_{2.5}$ population exposure intensity index for the kilometer grid from 2000 to 2020 and a dataset of $PM_{2.5}$ population-weighted average annual exposure concentration at the prefecture-level city from 2000 to 2020 **Decision support**: A data reference for future air pollution policy formulation in China
SDG 3 Ensure healthy lives and promote well-being for all at all ages SDG 6 Ensure availability and sustainable management of water and sanitation for all SDG 11 Make cities and human settlements inclusive, safe, resilient, and sustainable SDG 11.6 By 2030, reduce the adverse per capita environmental impact of cities, including by paying special attention to air quality and municipal and other waste management SDG 11.7 By 2030, provide universal access to safe, inclusive, and accessible, green and public spaces, in particular, for women and children, older persons, and persons with disabilities	Analysis of the average life expectancy indicator of Chinese cities	**Data product**: Average Life Expectancy Indicator Dataset of China in 2020 **Method and model**: Machine learning models, such as extreme trees **Decision support**: Continuous monitoring and assessment of population health levels of cities in China, providing corresponding research support and policy recommendations for governments and health and management departments at all levels

5.3.1.1 Background

SDG 11.3.1, the ratio of land consumption rate to population growth rate (LCRPGR), is used to quantify the coordination between urban land expansion and population growth and evaluate the urbanization status of population and land. In recent years, scholars from around the world have studied data acquisition and analysis to measure SDG 11.3.1 and have made a series of achievements for the concept of sustainable development and its future progress (Melchiorri et al. 2019; Jiang et al. 2021; Guo et al. 2021).

The urban built-up area data used in the research are mainly based on low-to-medium-resolution urban impervious surface data products, with relatively coarse granularity and significant differences in results. Additionally, the results lack spatial details and tend to overestimate the area of built-up areas, which cannot completely reflect the characteristics of urban–rural development differences. In comparison, high-resolution remote sensing images have the characteristics of distinct feature boundaries and plenty of spatial information, which are useful for urban fine-scale built-up area extraction. Therefore, it is necessary to construct a high-precision urban built-up area delineation method based on high-resolution remote sensing images that are in line with China's actual urban situation and meet application needs, on the basis of fully understanding and respecting the theoretical methods of urban built-up area delineation given by the UN. This will enable a more accurate evaluation of changes in urban land use efficiency in China's urbanization process and provide guidance for urban sustainable development.

5.3.1.2 Data

- Geographical Condition Monitoring data of 337 cities at the prefecture level in China in 2015 and 2020, including land cover data, as well as geographic unit data such as roads, river systems, administrative divisions, and the locations of district/county governments.
- Population data for urban areas from the China Urban Construction Statistical Yearbook for 2015 and 2020.

5.3.1.3 Methods

This study refers to the Regulations on Statistical Division of Urban and Rural Areas (State Letter [2008] No. 60) and uses the geographic data for monitoring conditions from the Ministry of Natural Resources of the People's Republic of China as the basis for constructing an automatic extraction model for urban built-up areas. The geographic national condition monitoring data were obtained through a combination of the manual interpretation of high-resolution remote sensing images with a resolution better than 2 m and field surveys, following unified standards. They have the characteristics of high objectivity and precision and can more accurately reflect the surface coverage information of urban areas. In this study, the parcels divided by roads and river systems were used as the smallest units for extracting urban built-up areas. Then, the proportion of the built-up area within each unit was calculated to determine the actual development situation. Distance iteration clustering was conducted outward from the location of the district (county) government at a distance of 200 m to determine connectivity. Urban built-up areas were extracted based on obtained urban areas, and algorithm models were integrated to achieve the fine, standardized, and automatic extraction of urban built-up areas.

According to the evaluation method of SDG 11.3.1, using the self-produced urban built-up area data and population data from the statistical yearbook, we calculated the ratio between the land consumption rate (LCR) and the population growth rate (PGR), as well as the built-up area per capita (BPC). The calculation formula is as follows:

$$\mathrm{LCRPGR} = \frac{\mathrm{LCR}}{\mathrm{PGR}} = \frac{\mathrm{In}(\mathrm{Urb}_{t+n}/\mathrm{Urb}_t)}{\mathrm{In}\left(\mathrm{Pop}_{t+n}/\mathrm{Pop}_t\right)} \quad (5.1)$$

$$\mathrm{BPC} = \frac{\mathrm{Urb}_t}{\mathrm{Pop}_t} \quad (5.2)$$

where Urb_t denotes the urban built-up area of a city in year t; Urb_{t+n} denotes the urban built-up area of a city in year $t + n$; Pop_t denotes the urban population of a city in year t; and Pop_{t+n} denotes the urban population of a city in the year $t + n$.

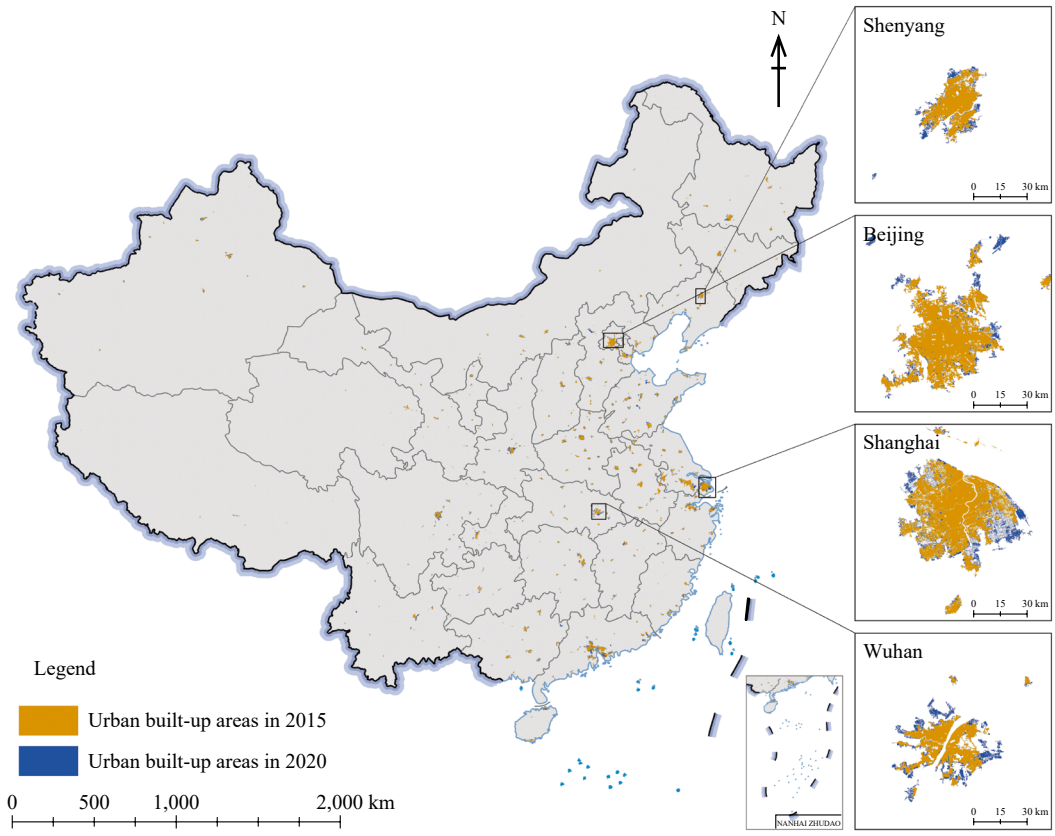

Fig. 5.1 Spatial distribution of urban built-up areas in cities at the prefecture level in China in 2015 and 2020. *Note* No data for Taiwan Province

On this basis, the coordinated relationship between land urbanization and population urbanization was comprehensively measured by calculating LCRPGR and BPC, and the sustainability of urban land use efficiency changes in China from 2015 to 2020 was comprehensively assessed from multiple perspectives of different provinces, regions, and city-scale classes.

5.3.1.4 Results and Analysis

High-Precision Mapping of Urban Built-Up Areas

The distribution of urban built-up areas in China with a 2 m resolution in 2020 is shown in Fig. 5.1. Compared to the analysis of the 30 m Global Urban Land Use/Cover (GULUC) product of Kuang et al. (2021), the average overlap rate between the two products reaches 84%. For the non-overlapping areas, the overlapping remote sensing images showed that the 30 m GULUC product had the problem of misidentifying large rural residential areas and missing a large area of a concentrated construction area. Therefore, the overall accuracy of this product is higher and can better reflect clear boundaries between urban and rural transition zones. Compared with the built-up area data in the China Urban Construction Statistical Yearbook, the overall area statistics of this product are smaller. The R^2 values with the statistical data in 2015 and 2020 are relatively high, at 0.7926 and 0.8623, respectively (Fig. 5.2).

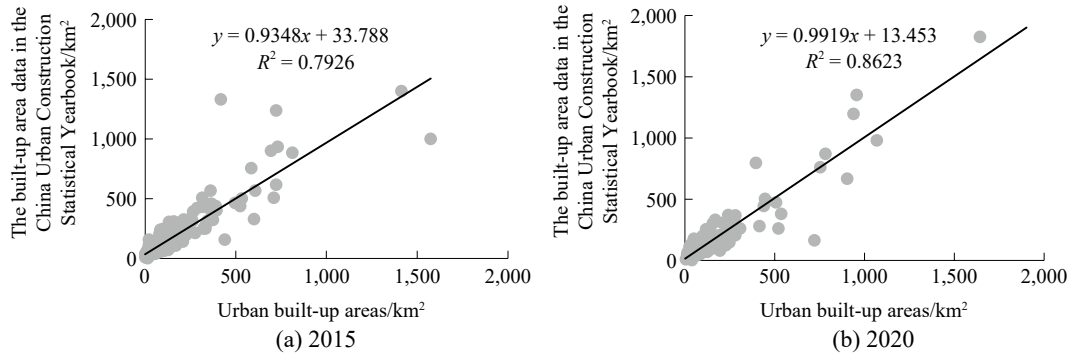

Fig. 5.2 Comparison of the urban built-up area data product in this study with the results of built-up areas in the statistical yearbook

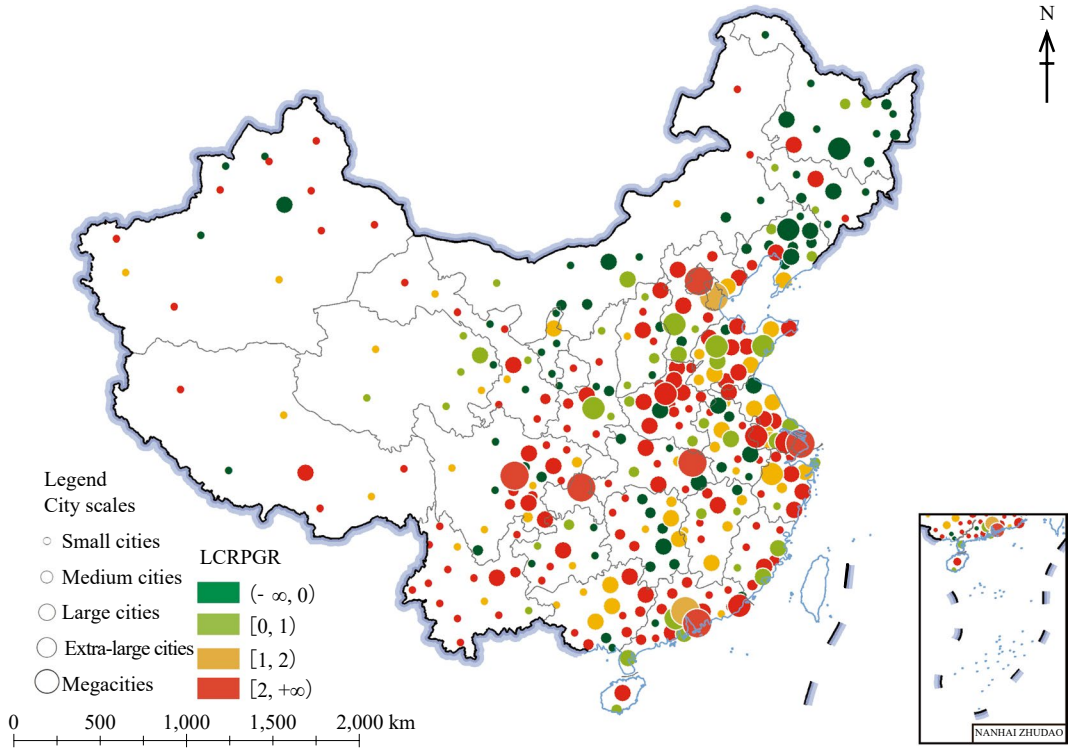

Fig. 5.3 Spatial distribution of LCRPGR in cities at the prefecture level in China from 2015 to 2020. *Note* No data for Taiwan Province

LCRPGR

The spatial distribution of LCRPGR for 337 cities at the prefecture level in China is shown in Fig. 5.3. From 2015 to 2020, the main trend was that land urbanization was faster than population urbanization. Among them, 60% of cities showed that the LCR was more than twice the PGR (LCRPGR > 1), with the most prominent being small and medium cities; 15% of cities showed that the PGR was greater than the LCR (0 < LCRPGR < 1), including the majority of small cities in the eastern and western

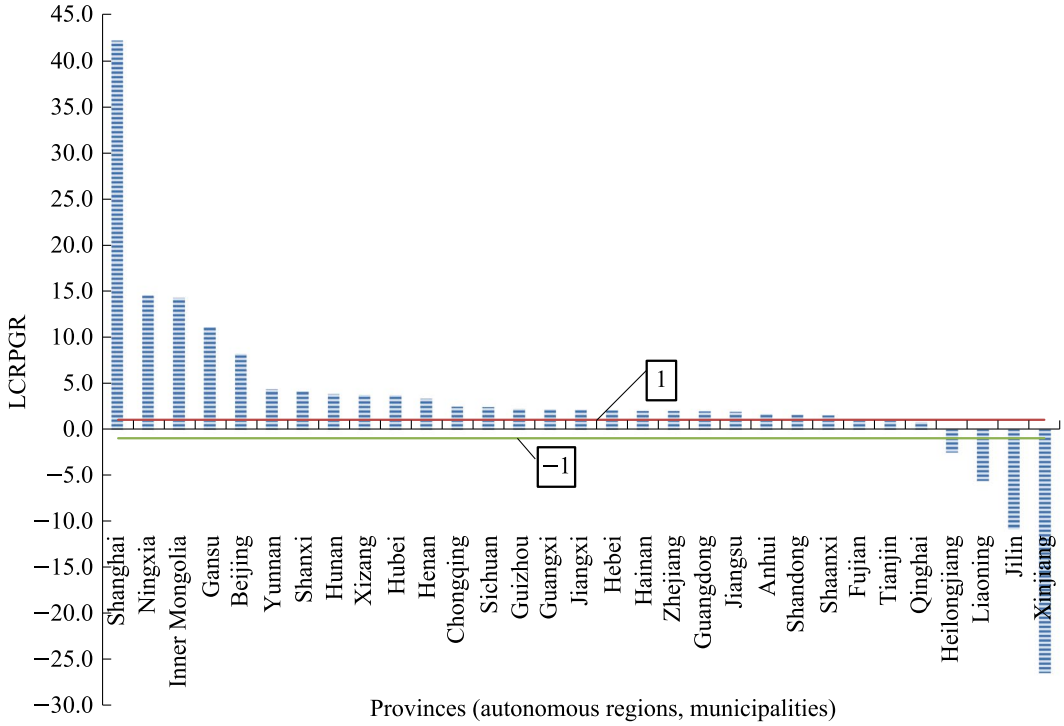

Fig. 5.4 Distribution of LCRPGR in 31 provinces (autonomous regions, municipalities) in China

regions; 23% of cities had an LCRPGR < 0 due to population shrinkage; and 2% of cities had an LCRPGR < 0 due to land shrinkage.

The results of LCRPGR analysis from different regions and city scales (Figs. 5.4 and 5.5) show that the urban land use efficiency significantly differs in different geographical units, with obvious inter-provincial and intra-provincial differences. Four provinces, Xinjiang, Jilin, Liaoning, and Heilongjiang, have negative LCRPGR due to population decline. Qinghai has a PGR higher than the rate of built-up area expansion. Tianjin and Fujian have the highest urban land use efficiency, while other provinces have a higher LCR than the PGR, especially Shanghai with a PGR of only 0.53%, which is much lower than the LCR of 22.44%, and its LCRPGR is much higher than that of other provinces. In terms of regions, there is a pattern of the central region (2.95) > western region (2.58) > eastern region (2.07) > northeastern region (− 4.51), with the northeastern region showing a population decline. In terms of city scales, there is a pattern of small cities (5.25) > medium cities (4.04) > large cities (2.50) > megacities (2.39) > extra-large cities (1.38). This indicates that land urbanization is too fast in the central region, and the land use efficiency of extra-large cities is significantly better than that of other cities. However, other regions and cities of different scales are facing a situation where population urbanization lags behind land urbanization, particularly in the northeastern region and some small cities and medium cities with significant pressure on population urbanization.

BPC

The spatiotemporal evolution of BPC in cities at the prefecture level in China from 2015 to 2020 is shown in Fig. 5.6. Overall, there is a trend of increasing BPC, with only about 12% of cities showing a decreasing trend, mainly in the eastern region for extra-large cities and large cities, and in the western region for small cities. From the results of different

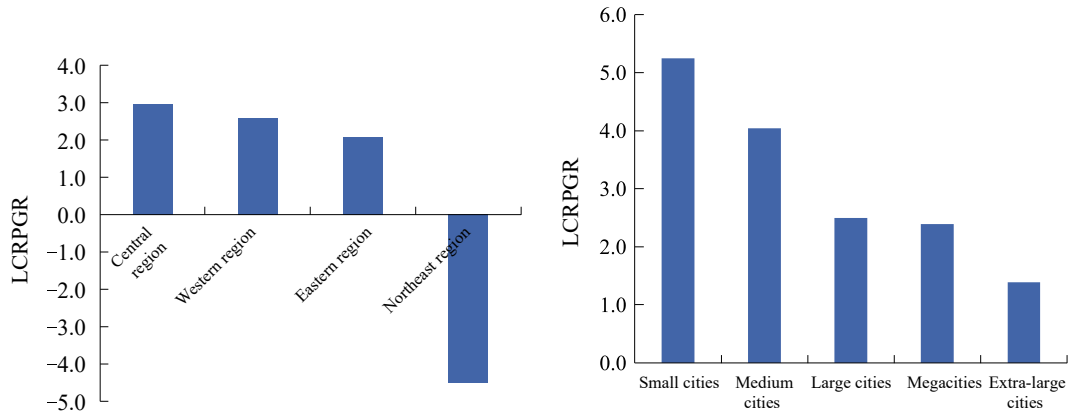

Fig. 5.5 Distribution of LCRPGR in four major regions and cities of different scales in China

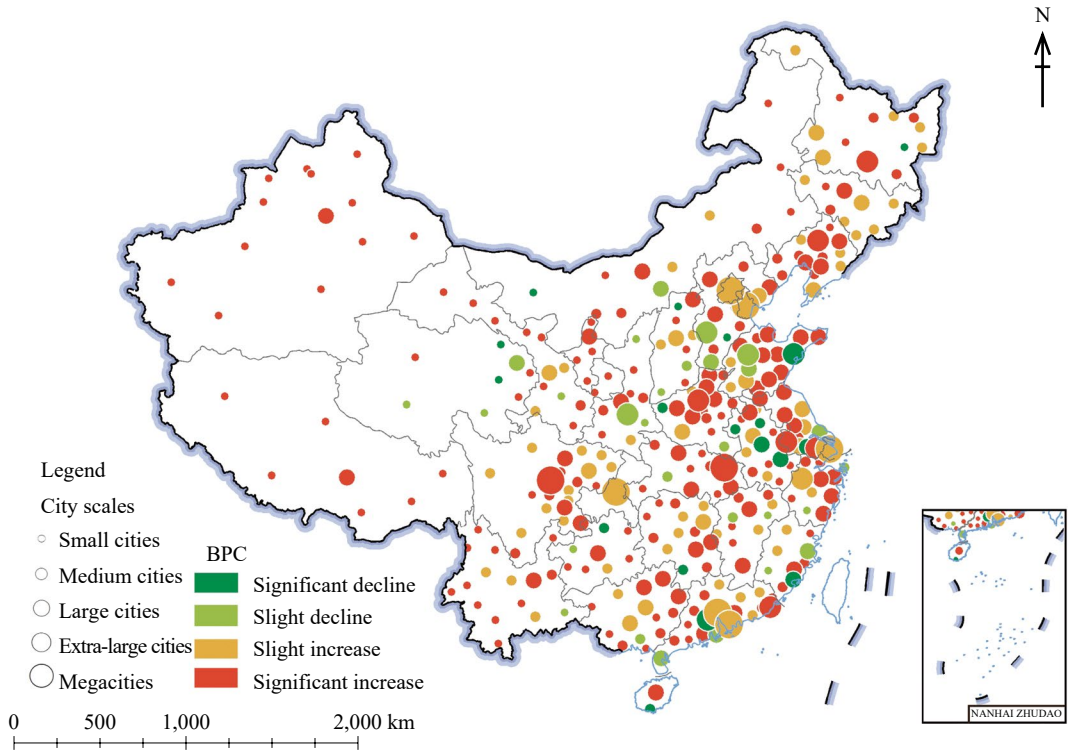

Fig. 5.6 Spatiotemporal evolution of BPC in cities at the prefecture level in China from 2015 to 2020. *Note* No data for Taiwan Province

geographical units, both provincial administrative divisions and regions show an increasing trend, with the increase in the area being highest in the central region, followed by the northeastern, western, and eastern regions. As for the city scales, there is a regular pattern that the lower the scale is, the more significant the increase in the BPC area is.

Highlights

- Using land cover data with a resolution of better than 2 m, we independently produced an urban built-up area product for 337 cities at the prefecture level in China in 2015 and 2020. We also conducted high-precision analysis and mapping of changes in urban land use efficiency in China.
- From 2015 to 2020, the overall urban land use efficiency of cities at the prefecture level in China was low, with significant differences in land use efficiency across different geographic units. The urban land use efficiency in extra-large cities was significantly better than that in other cities, while the northeastern region and some small cities and medium cities faced significant pressures from urbanization.

5.3.1.5 Discussion and Outlook

We developed an automatic extraction model of urban built-up areas based on high-resolution land cover data better than 2 m combined with geographic unit data such as roads, river systems, and the locations of district/county governments. The method was used to independently produce an urban built-up area product for 337 cities in China in 2015 and 2020. By calculating the LCRPGR and BCP indicators, the spatiotemporal variations in urban land use efficiency in China were comprehensively analyzed from multiple perspectives. This analysis provides a reference for the future development of differentiated population and land use control strategies to optimize the land use structure. In the future, the plan is to produce a dataset of urban built-up areas using the methodological model of this study, with low- and medium-resolution land cover data products as the input data source. The results can then be compared and analyzed with the product based on 2 m resolution data from this study to evaluate the effect of the accuracy of the source data on the calculation results for SDG 11.3.1, with the aim of better supporting the monitoring and evaluation of this indicator.

5.3.2 Surface Movement of China in 2021 Based on a Space-Borne InSAR Technique

Target: SDG 11.5: By 2030, significantly reduce the number of deaths and the number of people affected and substantially decrease the direct economic losses relative to global gross domestic product caused by disasters, including water-related disasters, with a focus on protecting the poor and people in vulnerable situations.

5.3.2.1 Background

With the rapid development of urbanization in China, various types of geological disasters have caused significant losses to the economy and society, of which land subsidence is the most influential. China has become one of the most seriously affected countries by land subsidence and has the largest subsidence area in the world. The 2011–2020 National Land Subsidence Prevention and Control Plan pointed out that in the past 40 years, more than 50 cities had suffered from land subsidence disasters in China, distributed in 20 provinces (including autonomous regions and municipalities) such as Beijing, Tianjin, Shanghai, Jiangsu, Hebei, Shanxi, and Inner Mongolia. The economic losses caused by land subsidence exceeded 300 billion yuan, of which Shanghai was the most serious, with the direct economic losses of 14.5 billion yuan and indirect economic losses of 275.4 billion yuan; the direct economic losses caused by land subsidence in the North China Plain reached 40.442 billion yuan, and the indirect economic losses were 292.386 billion yuan. The subsidence surface poses a great threat to civil infrastructure such as roads, railroads, and buildings. Land subsidence also increases flood susceptibility and risk, especially for coastal cities. Land subsidence has become a substantial threat for China to realize the SDGs of the 2030 Agenda.

The methods of surface deformation monitoring mainly include ground-based measurements, such as level measurement and GNSS measurement, and the space-borne interferometric synthetic aperture radar (InSAR) technique. Level measurement and GNSS measurement are based on point measurements, requiring manpower and material resources, and cannot meet the monitoring of ground surface deformation on a national scale. The InSAR technique uses data repeatedly observed by radar satellites, and has the ability to monitor large-scale, continuous surface deformations. However, national-scale surface deformation data have been incomplete due to the huge amount of data processing and the high requirements of computing resources. Therefore, it is necessary to obtain the surface deformation of China by using satellite-borne synthetic aperture radar and Big Earth Data processing methods, in order to improve the accuracy and scientificity of the overall assessment of the national surface deformation.

5.3.2.2 Data

- Sentinel-1 SAR data of 2020 and 2021 over China.
- DEM and vector data of the national administrative divisions.
- WorldPop dataset of the spatial distribution of China's population in 2020 in raster format with 100 m resolution (Bondarenko et al. 2020).

5.3.2.3 Methods

The method of CS-InSAR was applied to processing the Sentinel-1 data of 2020 and 2021 in three steps: TOPS mode SAR image processing, interferogram generation, and time-series InSAR analysis (Duan et al. 2020).

TOPS Mode SAR Image Processing

Based on each burst data in every sub-swath of the Sentinel-1 data, co-registration was carried out in two steps—combining geometric registration (based on external DEM from TanDEM Mission) and the enhanced spectral diversity (ESD) method. After co-registration, the burst data were debursted and spliced to obtain the co-registration SAR data for further InSAR processing.

Interferogram Generation

Optimal interferometric pairs were selected automatically by considering the spatial baseline and coherence, and then, the topography-free interferograms of those selected interferometric pairs were prepared for multi-temporal interferometry processing by using the following equation:

$$\gamma = \frac{\sum_{n=1}^{N}\sum_{m=1}^{M} S_1(n,m)\cdot S_2^*(n,m)\cdot e^{-j\varphi_{topo\_flat}}}{\sqrt{\sum_{n=1}^{N}\sum_{m=1}^{M}|S_1(n,m)|^2\sum_{n=1}^{N}\sum_{m=1}^{M}|S_2(n,m)|^2}} \tag{5.3}$$

where S_1, S_2 are the complex values of the primary and secondary images, respectively; and $\varphi_{\text{topo\_flat}}$ is the topography-related phase.

Time-Series InSAR Analysis

First, the high coherent scatterers (CSs) were selected based on the average coherence of time-series differential interferograms. Then a constant velocity phase model was applied to phase variations between neighboring identified CSs connected by the Delaunary network, where the impact of atmospheric components is assumed to be very similar and so cancels out the difference. Therefore, the phase model can be written as follows:

$$\Delta\phi_{\text{diff}}(m,n,T_i) = \Delta\phi_{\text{mod el}}(m,n,T_i) + \Delta w(m,n,T_i) \tag{5.4}$$

$$\Delta\phi_{\text{model}}(m,n,T_i) = \frac{4\pi}{\lambda}\cdot T_i\cdot\Delta v(m,n) + \frac{4\pi}{\lambda}\frac{B_{\perp i}\cdot\Delta\varepsilon(m,n)}{R_i\cdot\sin\theta_i} \tag{5.5}$$

where m, n are the neighboring identified CSs; and Δv and $\Delta\varepsilon$ are relative velocity and relative elevation between neighboring identified CSs. Since phase values $\Delta\phi_{\text{diff}}$ are wrapped, Δv and $\Delta\varepsilon$ are estimated by maximizing the temporal coherence.

$$\max\gamma_{\text{mod el}}(m,n) = \frac{1}{M}\cdot\left|\sum\nolimits_i \exp\{j\cdot[\Delta\phi_{\text{diff}}(m,n,T_i) - \Delta\phi_{\text{mod el}}(m,n,T_i)]\}\right| \tag{5.6}$$

Once Δv and $\Delta\varepsilon$ are obtained, the phase differences are then unwrapped, and the linear

deformation rates are generated by the network adjustment.

The algorithm of CS-InSAR was parallelized and implemented on the supercomputing system provided by the Big Earth Data Science Engineering Program (CASEarth). The 2021 nationwide land deformation rate was obtained by processing the Sentinel-1 data covering all of China, which consists of 33 tracks, 368 frames, and 109,85 scenes in total.

On the basis of the national land deformation results in 2021, the spatial distribution of the national surface deformation was analyzed, and its effect was analyzed with the population data. Then, compared with the deformation rate of 2020, the annual changes in the national surface deformation from 2020 to 2021 were found.

5.3.2.4 Results and Analysis

The results of the national annual average surface deformation rate in 2021 and the local deformation rate results of Beijing-Tianjin-Hebei, Qinghai-Xizang Plateau, Yulin mining area, and Danba County landslides are shown in Fig. 5.7. According to statistics, from January 2021 to December 2021, 34 provincial-level administrative regions and more than 140 prefecture-level cities across the country experienced different degrees of surface deformation at certain scales. Considering all types of land deformation, extensive ground subsidence caused by excessive groundwater extraction is the most common and most widespread in China. It mainly happens in flatter areas such as alluvial plains (e.g., North China Plain, Yangtze River Delta, Northeast Plain), coastal plains (e.g., Pearl River Delta), or alluvial basins (e.g., Fenwei Basin), where the Beijing-Tianjin-Hebei region of North China Plain is the most developed, and urban subsidence funnel areas have been formed including Beijing; Tianjin; Langfang, Baoding, Hengshui, Xingtai, Handan, and Tangshan in Hebei as shown in Fig. 5.7(b). Besides groundwater extraction, urban expansion and large-scale construction are also factors for urban subsidence. China is rich in underground mineral resources, and the surface deformations caused by underground resource exploitation such as coal mines, oil fields, and natural gas are also one of the main types of surface deformation, such as the underground coal mining in Yulin in Fig. 5.7(d). In addition to the surface deformation caused by human activity, the large area of permafrost distributed on the Qinghai-Xizang Plateau also causes surface deformation during the seasonal freeze–thaw process, and the results of the surface deformation rate on the Qinghai-Xizang Plateau are

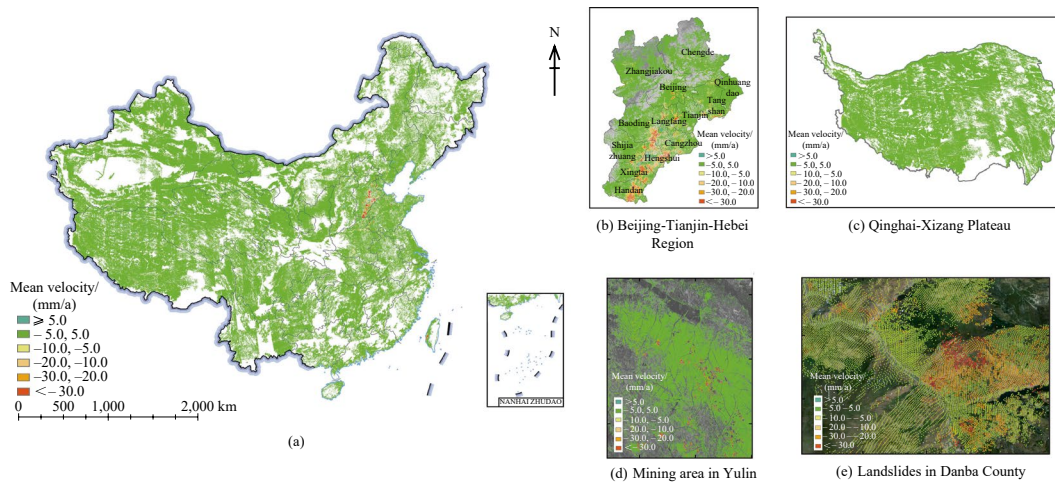

Fig. 5.7 Annual average rate of surface deformation in China in 2021. *Note* The direction of deformation is in the satellite line of sight

shown in Fig. 5.7(c). Being in the transition zone between the first and second terrain steps, Southwest China has complex geological formations and active geological activity, where the surface deformation is mainly in the form of geological hazards such as landslides and debris flows, as shown in Fig. 5.7(e), which is due to landslides in Danba County.

Based on the national annual deformation rate products in 2020 and 2021, the areas with surface deformation rates (satellite line of sight direction) greater than 30 mm/a are considered severe subsidence areas, and the extraction results are shown in Figure 5.8(a)–(b). The severe subsidence area in 2020 was about 6261 km^2, and the severe subsidence area in 2021 was about 6168 km^2, a decrease of 1.49% year-on-year. The surface subsidence is slowing down nationwide, but there is a trend of aggravated subsidence in individual areas, such as around the Yangtze River Basin. Relevant departments should cooperate to monitor and control it.

The population distribution data with 100 m resolution of China in 2020 provided by WorldPop were overlaid with the severe subsidence areas, and the exposed population within a 3 km buffer zone around the severe subsidence areas was calculated to be 84,326,300. The data were created using constrained top-down methods for all countries of the world for 2020 and adjusted to match UN national population estimates.

The severe subsidence area is about 4223.33 km^2 in the North China Plain, which accounted for 68.47% of the national severe subsidence area in 2021, and the exposed population within the 3 km buffer zone around the severe subsidence area in the North China Plain is about 32,074,600, accounting for 38.04% of the total exposed population in the country. The severe subsidence areas in each province of the North China Plain were counted, as shown in Figure 5.8(e). The results show that the severe subsidence areas within the North China Plain in Beijing, Tianjin, Hebei, Anhui, and Shandong all decreased, and those within the North China Plain in Henan and Jiangsu increased to a small extent. In addition, the phenomenon of surface uplift was found in several places of the North China Plain, which is thought to be related to the groundwater utilization control policies, groundwater recharge measures, and the current year's precipitation, including the recharge effect of the South-to-North Water Diversion Project on groundwater in North China.

Highlights

- Based on the supercomputing platform of CASEarth, we independently developed a time-series InSAR processing algorithm applicable to the monitoring of surface deformation at the national scale and used the Sentinel-1 satellite data of China in 2020 and 2021 to process and obtain the national annual average surface deformation rate products.
- The spatial distribution of surface deformation in China in 2021 was analyzed, and the characteristics of surface deformation changes in China between 2020 and 2021 were explored. The results show that the severe subsidence area in 2020 was about 6261 km^2, and that in 2021 was about 6168 km^2, 1.49% lower, and the directly exposed population within 3 km of the severe subsidence area was about 84,326,300.

5.3.2.5 Discussion and Outlook

Based on the supercomputing platform of CASEarth, the developed CS-InSAR technique was applied to processing all the Sentinel-1 data of China in 2021 for the national annual average surface deformation rate products in this study. The spatial distribution characteristics and causal factors of surface subsidence in China in 2021 were summarized, the severe subsidence areas in China in 2020 and 2021 were extracted, and the interannual surface subsidence changes were compared in the North China Plain, where subsidence is the most developed in China. In the future, we plan to conduct longer time-scale observation and analysis of surface deformation across the country to achieve continuous observation and provide a more valuable reference for groundwater management departments and geological disaster emergency departments.

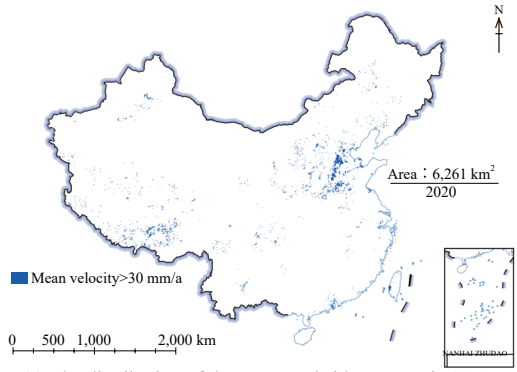

(a) The distribution of the severe subsidence area in 2020

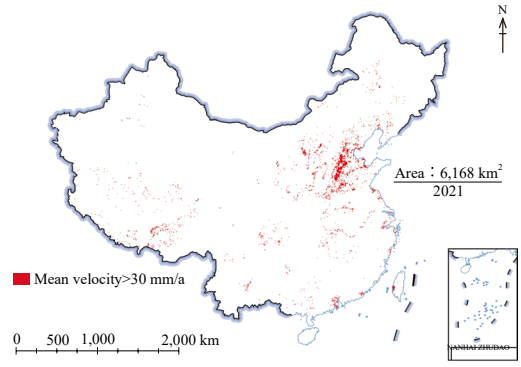

(b) The distribution of the severe subsidence area in 2021

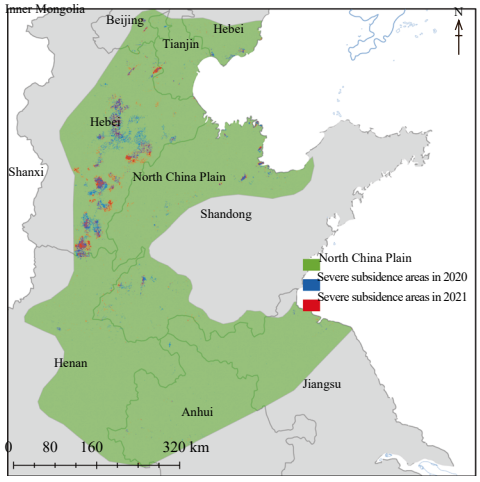

(c) The distribution of severe subsidence area in North China Plain

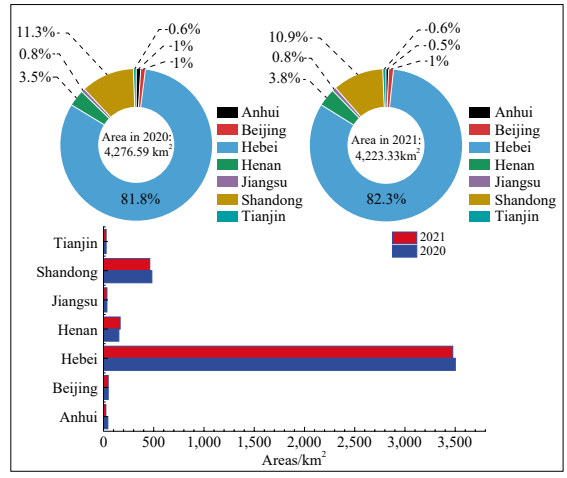

(d) The changes of severe subsidence areas in the provinces (municipalities) of the North China Plain in 2020-2021

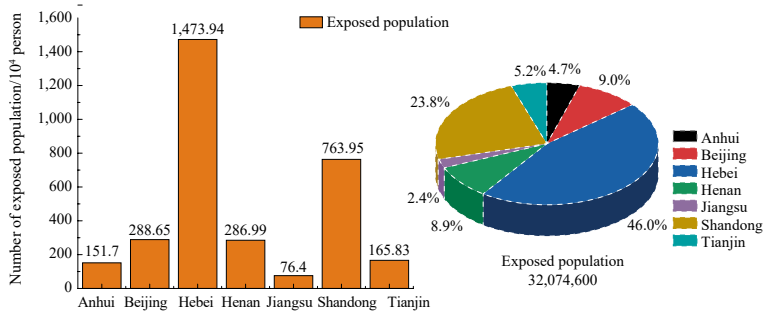

(e) The total exposed population within the 3 km buffer zone around the severe subsidence areas in the provinces (municipalities) of the North China Plain

Fig. 5.8 Spatiotemporal variations in severe subsidence areas in China from 2020 to 2021

5.3.3 Annual Change in Soil Erosion at the County Level in China (2010–2021)

Target: SDG 11.5: By 2030, significantly reduce the number of deaths and the number of people affected and substantially decrease the direct economic losses relative to the global gross domestic product caused by disasters, including water-related disasters, with a focus on protecting the poor and people in vulnerable situations.

5.3.3.1 Background

Urban soil erosion is a universal, global, and urgent problem in the process of urbanization, and it is particularly serious in economically developed or rapidly urbanizing areas of China, where soil erosion is a major challenge for achieving the UN SDGs. Soil erosion status and change patterns are closely related to economic and social development, investment in control measures, and changes in the ecological environment. It is an important basis for the national implementation of SDG 11.5. Data on soil erosion can provide an important basis for national and local authorities to formulate watershed management plans for monitoring areas, improve soil and water conservation regulations, and serve soil and water conservation and regional development.

This case study focuses on the following three points in order to further statistically and verifiably analyze the changes in soil erosion risk trends and the impacts of soil erosion on poverty in China from 2010 to 2021 and to quickly assess the dynamic changes in soil erosion at a high accuracy level.

(1) Map the changes in soil erosion risk in China from 2010 to 2021 and verify the accuracy with the China Soil and Water Conservation Bulletin. The data can support the analysis of trends and changes in soil erosion risk across the country and correlation analysis of economic development levels.

(2) Quantitatively study the temporal and spatial variation of soil erosion risk at the county level in China from 2010 to 2021. This can reveal, at a finer scale, the temporal and spatial patterns of soil erosion from the perspective of spatial visualization.

(3) Discuss the temporal and spatial relationship between soil erosion intensity and economic development in various regions of the country, and redefine the proportion of the poor population in areas with severe soil erosion.

5.3.3.2 Data

- DEM and soil physical and chemical property data.
- Monthly rainfall data (2010–2021), normalized difference vegetation index (NDVI) data, and land cover data.
- Population, GDP, and administrative division vector data from the National Bureau of Statistics.
- Global Disaster Data Platform.

5.3.3.3 Methods

This case study is based on RUSLE with the help of Google Earth Engine to map 2010–2021 China municipal-level soil erosion risk for SDG 11.5. RUSLE is expressed as follows:

$$A = R \times K \times \mathrm{LS} \times C \times P$$

where A is the amount of soil loss [t/(km^2·a)]; R is the rainfall erosivity factor [MJ·mm/(km^2·h·a)]; K is the soil erodibility factor [t·km^2·h/(km^2·MJ·mm)]; LS is the slope length factor (dimensionless); C is the vegetation coverage and management factor (dimensionless); and P is the soil and water conservation measure factor (dimensionless). In this case study, the five factors, R, K, LS, C, and P, were selected to explore the sensitivity of soil erosion and to construct a county-level soil erosion risk classification system in China. The Mann-Kendall nonparametric trend test was used to analyze the change trend of soil erosion risk through a quantitative study of temporal and spatial variation in soil erosion risk at the county level.

5.3.3.4 Results and Analysis

Accuracy Assessment and Analysis of Soil Erosion Products in China

The hydraulic erosion grades (very slight, slight, moderate, and severe or above, as shown in Table 5.2) of each area were predicted by the model and compared with those of the 31 provinces in China's Bulletin of Soil and Water Conservation in 2018, 2019, and 2020 to assess the prediction accuracy (excluding, Hong Kong, Macao, and Taiwan). In terms of the proportion of the national hydraulic erosion area, the provincial average absolute error of the statistical results is about 5%, and the R^2 is 0.774. In the four-type hydraulic erosion grade classification system, the average absolute error of slight erosion is 4.77%, and the average absolute error of moderate soil erosion and severe or above soil erosion is below 2%.

Figure 5.9 shows the distribution of soil erosion in China from 2010 to 2021. According to the statistics from 2021, the area of soil erosion totaled 1.4297 million km^2, accounting for 14.95% of the total land area, of which slight erosion accounted for 76.48%, moderate erosion accounted for 18.11%, and severe or above erosion accounted for 5.41%. The lost area decreased by a total of 0.4264 million km^2. In Fujian, Hainan, Xizang, and Shaanxi, the reduction ratio of the erosion area with severe or above all exceeded 5%. It can be seen from Fig. 5.9 that the areas with severe or above soil erosion are mainly concentrated in Shaanxi, Shanxi, Sichuan, Yunnan, Gansu, Guizhou, and Jiangxi.

Table 5.2 Hydraulic erosion grade classification used in this case study

Grades	Average erosion modulus [t/(km^2·a)]
Very slight	≤ 1000
Slight	(1000, 2500]
Moderate	(2500, 5000]
Severe or above	>5000

Analysis of the Risk Trend of Soil Erosion at the County Level in China

Soil erosion products in China from 2010 to 2021 were used to reveal the effectiveness of measures taken to cope with soil erosion in the country (Fig. 5.10). According to statistics, a total of 2090 counties showed a decreasing trend in soil erosion risk from 2010 to 2021, and the aggregated areas with increasing attenuation trends were mainly in the southern part of the Loess Plateau and other areas. In areas with serious soil erosion, measures have been taken for soil erosion control such as building horizontal terraces, soil and water conservation afforestation, soil and water conservation grass planting, mountain sealing, slope sealing, and the construction of small water conservancy and soil conservation projects, and the country has achieved remarkable results in soil and water conservation.

During 2010–2021, the average soil erosion risk in 33 of the 42 national key protected areas for soil erosion prevention showed a decreasing trend (Fig. 5.11). However, soil erosion in China has not been effectively curbed yet, and there is still a trend of increasing soil erosion in areas such as Northeast China and parts of North China. Conducting the dynamic analysis of soil erosion in China holds significant importance for the prevention and control of soil erosion and the pursuit of building a beautiful China.

Risk Correlation Analysis of Soil Erosion in Impoverished Counties

Soil erosion causes great harm to the ecological environment and economic development. Soil erosion destroys the integrity of the ground, reduces soil fertility, causes hard petrifaction and desertification of land, affects agricultural production, aggravates the occurrence and development of natural disasters such as floods, leads to poverty and the deterioration of production conditions, impedes sustainable economic and social development, and leads to a vicious circle of "the more reclamation, the poorer; the poorer, the more reclamation". According to the distribution of 585 impoverished counties

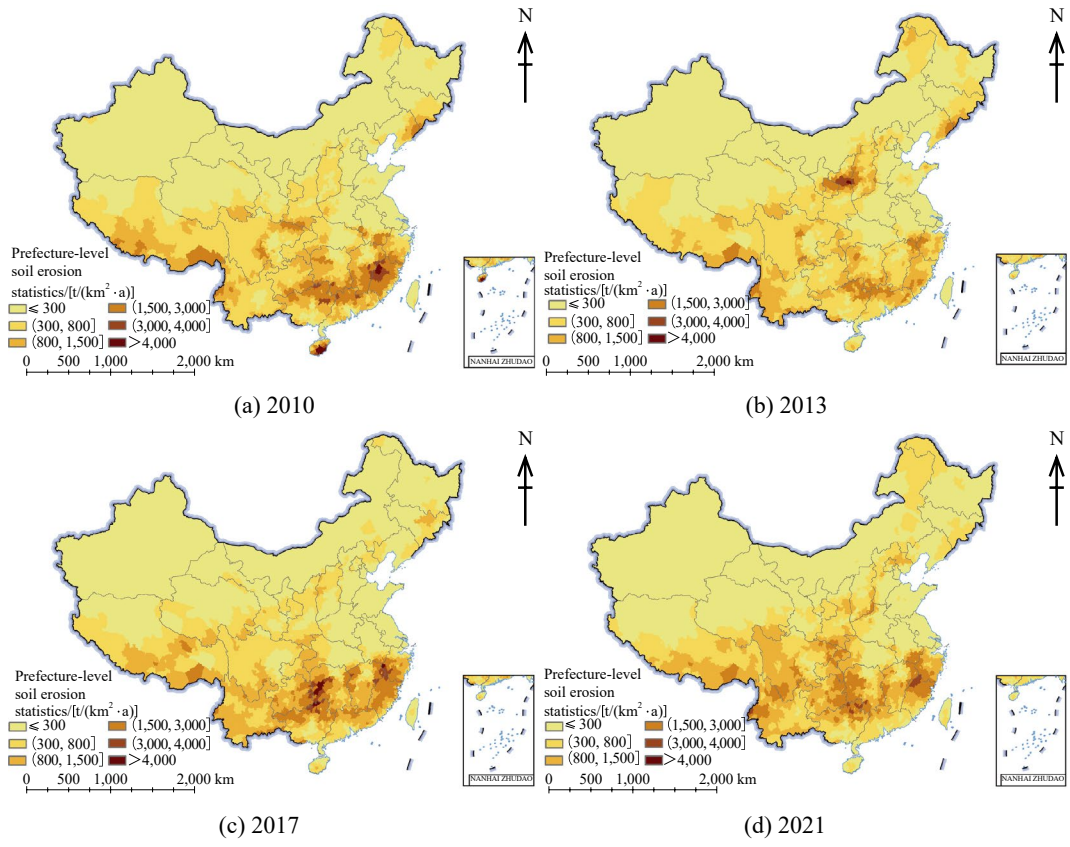

Fig. 5.9 Distribution of soil erosion in China in 2010, 2013, 2017, and 2021

released by the state in 2018 in areas with severe or above soil erosion (soil loss greater than 5000 t/(km^2·a) (Fig. 5.12), 48% of the country's impoverished counties and 55% of the poor population are located in areas with severe or above soil erosion. More than 65% of the impoverished counties in the five provinces (autonomous regions) of Guizhou, Qinghai, Sichuan, Xizang, and Yunnan are located in areas with severe or above soil erosion. Compared with the results in 2008, 76% of the impoverished counties and 74% of the poor population live in areas with severe or above soil erosion. In 2018, the two indicators showed a significant downward trend.

Highlights

- This case study produced 2010–2021 county-level soil erosion risk products for China.
- A quantitative study was conducted to analyze the temporal and spatial variation characteristics of soil erosion risk at the county level in China from 2010 to 2021.
- The aim was to explore the spatial correlation between economic population and soil erosion risk in impoverished counties across the country in 2018.

5.3.3.5 Discussion and Outlook

Through the 2010–2021 China county-level soil erosion risk products, the change trend of China's soil erosion risk was analyzed, helping to accurately control and assess the progress of soil and water conservation in areas with severe soil erosion. Spatial correlation analysis with county-level GDP statistics provides important information support for consolidating the achievements of poverty alleviation and rural

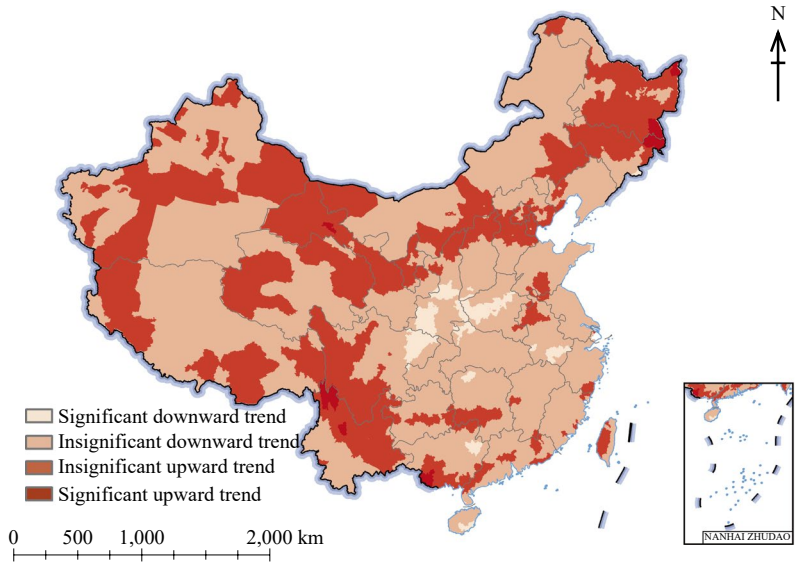

Fig. 5.10 Change trend of soil erosion in counties across the country from 2010 to 2021

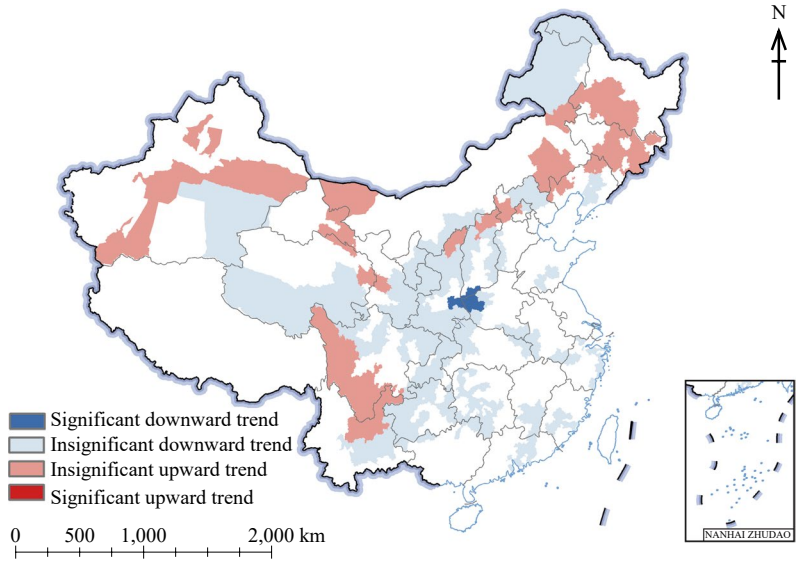

Fig. 5.11 Change trend of 42 national key protected areas for soil erosion prevention from 2010 to 2021. *Note* No data for Taiwan Province

revitalization strategies. Through research statistics, we found that: (1) from 2010 to 2021, the area of soil erosion in most parts of China showed a downward trend, indicating that China has achieved good soil and water conservation results and (2) the current proportion of impoverished counties and poor populations in soil erosion areas shows a downward trend compared with ten years ago, indicating that important progress has been made in soil and water conservation in impoverished areas. With the rapid development of China's urbanization process, improving urban water and soil conservation is one of the key factors for the

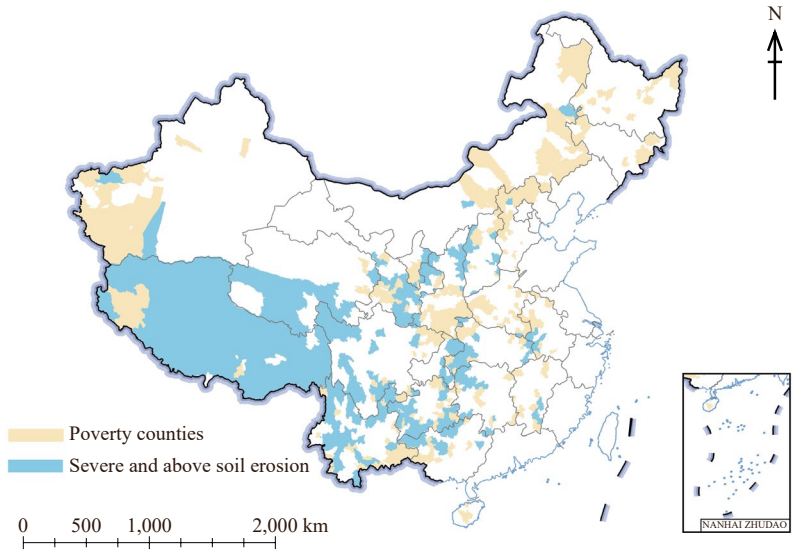

Fig. 5.12 Distribution of impoverished counties and counties with severe or above soil erosion in 2018. *Note* No data for Taiwan Province

comprehensive advancement of an urban ecological civilization. In the future, we should continue to improve the system of water and soil conservation laws and regulations, establish a long-term management mechanism for water and soil conservation, create an expert pool of water and soil conservation talent, promote the informatization and intelligence of soil erosion supervision, and continue to improve the effectiveness of urban water and soil conservation work.

5.3.4 Monitoring of Natural Disaster Risks in China at the Prefecture Level (2010–2021) and Analysis of Typhoon Disaster Risks at the County Level (2016–2020)

Target: SDG 11.5: By 2030, significantly reduce the number of deaths and the number of people affected and substantially decrease the direct economic losses relative to global gross domestic product caused by disasters, including water-related disasters, with a focus on protecting the poor and people in vulnerable situations.

5.3.4.1 Background

Indicators of progress toward SDG 11.5 are important quantitative descriptions of the impacts of disasters on people, economies, and society, and they are also the only quantitative indicators in the seven global targets proposed in the Sendai Framework for Disaster Risk Reduction 2015–2030 (Sendai Framework) (UN 2015, 2021). In this case study, we focused on two indicators of SDG 11.5, namely, SDG 11.5.1 "number of deaths, missing persons and directly affected persons attributed to disasters per 100,000 population" and SDG 11.5.2 "direct economic loss attributed to disasters in relation to global gross domestic product (GDP)". We constructed long-term time-series monitoring datasets of these two indicators at the prefecture level for the entire nation of China and at the county level for critical hazard and vulnerable areas. We aim to provide strong information support for implementing comprehensive regional assessments of SDGs and

demonstrating the effectiveness of disaster prevention and reduction in China and to provide decision support for analyzing the spatial and evolving patterns of disaster risks in China at the prefecture and county levels.

But currently, the temporal and spatial resolution for the dynamic monitoring of SDG 11.5 is limited and incapable of supporting in-depth integrated evaluation at regional and prefecture levels, especially the latter. Based on disaster losses and socio-economic statistics of cities, we extended the temporal resolution of SDG 11.5 to all years since 2010 and the spatial resolution to the prefecture level, which can improve temporal and spatial resolution for monitoring. Specifically, in this case study, we produced a data product of SDG 11.5 indicators at the prefecture level in 2021, to form a continuous and serial dataset of indicators. Meanwhile, for coastal provinces in East and South China, we extended the spatial resolution of the SDG 11.5 indicators of typhoon disasters to the county level, which can provide valuable support for disaster risk assessment using Big Earth Data.

5.3.4.2 Data

- Statistical data on the number of directly affected persons, the number of deaths and missing persons, and direct economic losses attributed to natural disasters from 2010 to 2021, at the national and prefecture levels.
- Statistical data of year-end population and GDP from 2010 to 2021 at the prefecture level, based on data from regional statistical yearbooks.
- Statistical data of year-end population and GDP from 2016 to 2020 at the county level, based on data from regional statistical bulletins.

5.3.4.3 Methods

Based on the datasets of indicator monitoring at the prefecture and county levels, we analyzed natural disaster risks from temporal evolution trends and regional difference characteristics. Key research included the modeling and mapping of historical changes in administrative divisions as well as the analysis of spatiotemporal patterns of disaster risks. Using SDG 11.5 indicators at the prefecture level from 2010 to 2021, we divided risky regions based on the analysis of spatial clustering patterns of indicators, investigated temporal evolution trends and spatial distribution patterns in each region, and presented concluding remarks on the variations in disaster risks in China at the prefecture level. Then, using evaluation results of indicators at the county level, we charted risk maps for typhoon disasters. We performed multi-dimensional disaster risk monitoring by fusing statistical and spatial data, where statistical data were used for indicator evaluation and spatial data were used for thematic maps and regional analysis.

The case study was divided into four stages: data production, data processing, indicator calculation, and result analysis.

(1) Data production. The data on standard administrative divisions, disaster losses, and social-economic statistics were produced, covering the prefecture level from 2010 to 2021 and the county level in vulnerable regions from 2016 to 2020. The data on standard administrative divisions are from the national dataset released by the Ministry of Civil Affairs of the People's Republic of China, the data on disaster losses are from the Ministry of Emergency Management of the People's Republic of China, and the social-economic statistics are from provincial statistical yearbooks.
(2) Data processing. We used the standard administrative division data in 2021 as anchors and constructed modeling and mapping relationships for administrative divisions at the prefecture and county levels. By doing this, interannual disaster loss data, as well as social-economic statistics data, were projected into the same set of administrative divisions, and the data across 2010 to 2021 were all standardized into the same baseline of 2021. After that, the logic, consistency, and completeness of datasets were verified.
(3) Indicator calculation. Using outcomes from the data processing, we finished the calculation and review of three SDG 11.5 indicators

as well as comprehensive disaster indices for vulnerable counties.

(4) Result analysis. We completed the charting of annual thematic maps of monitoring indicators along the indicator dimension and year dimension. Then, the spatial distribution of disaster losses was analyzed in counties vulnerable to typhoons. The aforementioned results were presented in the following case report.

The formulas used in this case study are as follows:

$$\text{Affected persons per } 100,000 \text{ population} = \frac{\text{Number of affected persons}}{\text{Year-end population (in } 10,000 \text{ people)}} \times 10 \tag{5.7}$$

$$\text{Deaths and missing persons per } 100,000 \text{ population} = \frac{\text{Deaths and missing persons}}{\text{Year-end population (in } 10,000 \text{ people)}} \times 10 \tag{5.8}$$

$$\text{Direct economic loss in relation to GDP} = \frac{\text{Direct economic loss (in 100 million yuan)}}{\text{GDP (in 100 million yuan)}} \times 100\% \tag{5.9}$$

$$\text{Direct economic loss in relation to GRP} = \frac{\text{Direct economic loss (in 100 million yuan)}}{\text{GRP (in 100 million yuan)}} \times 100\% \tag{5.10}$$

5.3.4.4 Results and Analysis

Dynamic Monitoring of Natural Disaster Impacts to China

Overall, the two SDG 11.5.1 and SDG 11.5.2 indicators demonstrated an obvious decreasing trend in China from 2010 to 2021, which is shown in Fig. 5.13.

In 2021, the number of affected persons per 100,000 population was 7597, which was the lowest from 2010 to 2020 and decreased by 58.2%, compared with the annual mean from 2010 to 2020. The number of deaths and missing persons per 100,000 population was 0.061, which was the third lowest from 2010 to 2021 (only higher than those in 2018 and 2020) and decreased by 54.7%, compared with the annual mean from 2010 to 2020. Direct economic loss in relation to GDP was 0.29%, which was the second lowest from 2010 to 2021 (only higher than 2018) and decreased by 50.8%, compared with the annual mean from 2010 to 2020.

Monitoring and Analysis of Disaster Impacts at the Prefecture Level in 2021

The temporal and spatial distribution of SDG 11.5.1, that is, the number of affected persons per 100,000 population, at the prefecture level in 2021, is illustrated in Fig. 5.14. In 2021, the overall impact of natural disasters was relatively mitigated, but local regions suffered heavy losses. Due to severe floods caused by extreme rainstorms, Henan, Shanxi, Shaanxi, and Gansu sustained great losses. Local areas in Qinghai were affected by the Maduo earthquake. Among all prefecture-level cities affected by natural disasters, 87% had SDG 11.5.1 values lower than the target (15,000 persons) set by the National Comprehensive Plan on Disaster Prevention and Reduction (2016–2020), while 90.8% of cities had their indicators decreased to historical means from 2010 to 2020, with an average decrease of 78.1%. Heavily impacted areas were mainly distributed in Henan, Shanxi, Shaanxi, and local regions of Qinghai and Xizang.

The temporal and spatial distribution of the other part of SDG 11.5.1, that is, the number of deaths and missing persons per 100,000 population, at the prefecture level in 2021, is illustrated in Fig. 5.14. In 2021, among all prefecture-level cities affected by natural disasters, 94% had their indicators lower than the target (1 person) set by the National Comprehensive Plan on Disaster Prevention and Reduction (2016–2020),

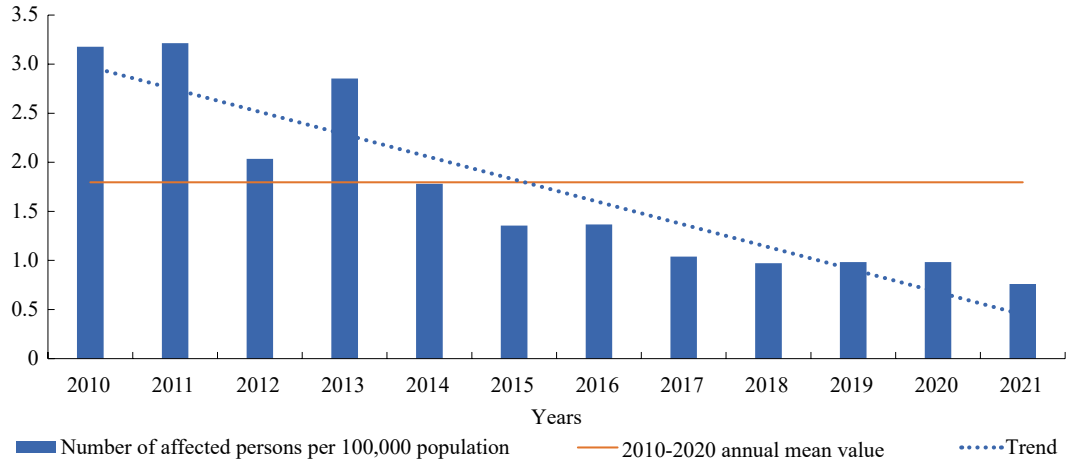

(a) Interannual variation of the number of affected persons per 100,000 population

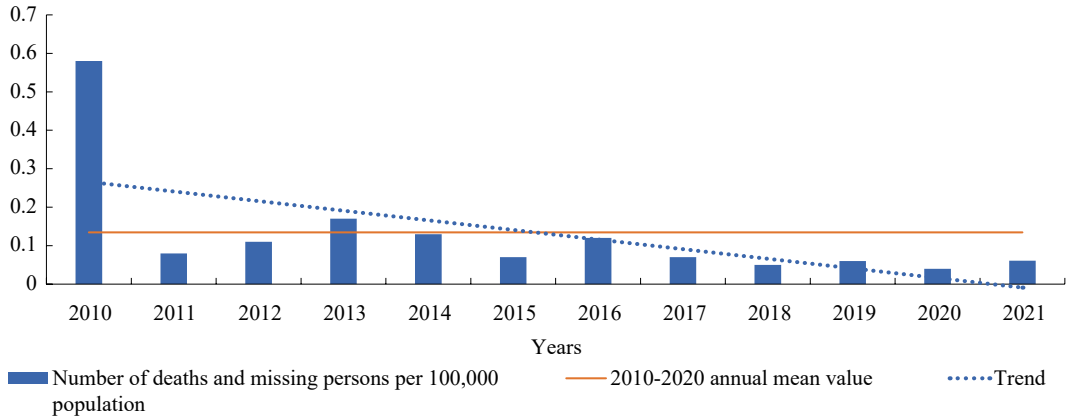

(b) Interannual variation of the number of deaths and missing persons per 100,000 population

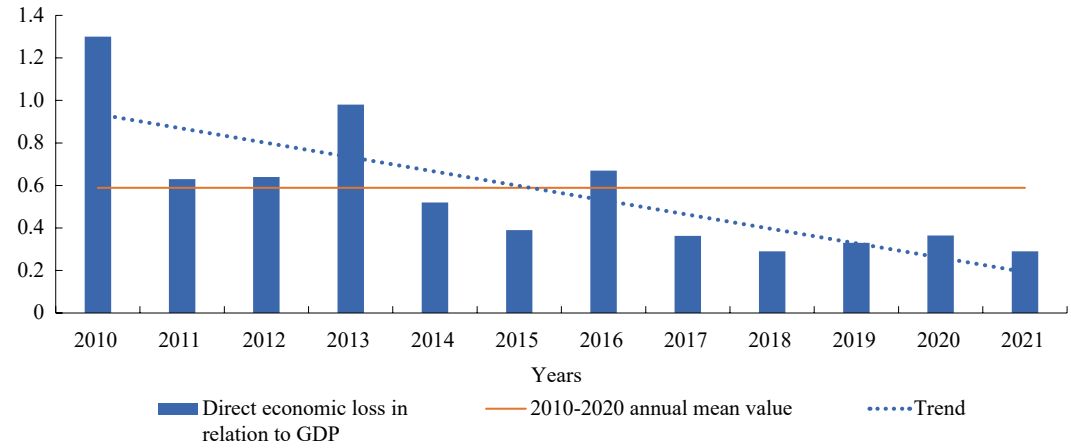

(c) Interannual variation of direct economic losses in relation to GDP

Fig. 5.13 Interannual variation of SDG 11.5 indicators in China from 2010 to 2021

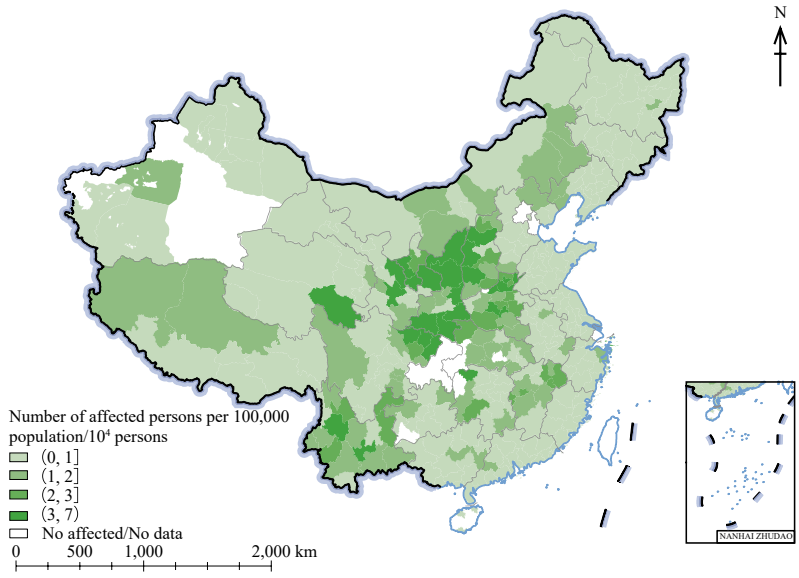

(a) Distribution of the number of affected persons per 100,000 population

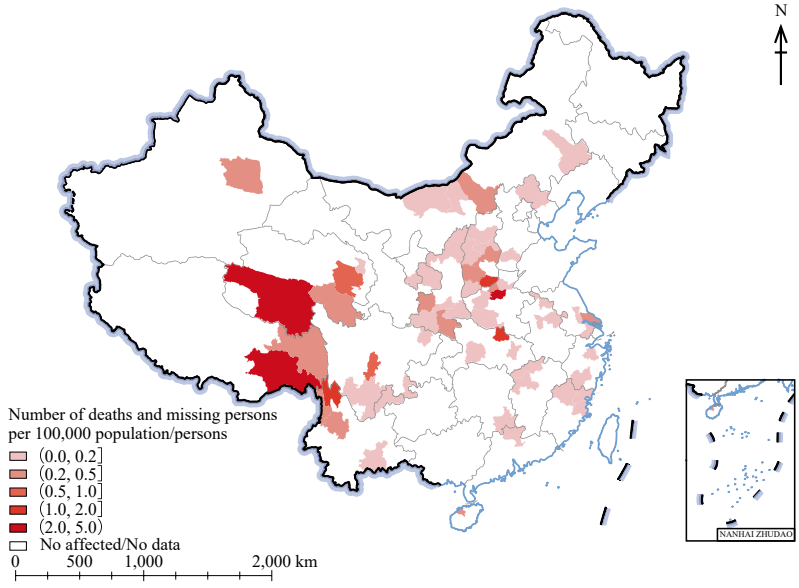

(b) Distribution of the number of deaths and missing persons per 100,000 population

Fig. 5.14 Distribution of the SDG 11.5 indicators at the prefecture level in 2021

while 36.6% of cities had their indicators decreased to historical means from 2010 to 2020, with an average decrease of 51.8%. It should be noted that cities in Henan had obviously high indicators due to great fatalities caused by the extreme storm and flood in July.

The temporal and spatial distribution of SDG 11.5.2, that is, direct economic loss in relation to GRP, at the prefecture level in 2021, is also illustrated in Fig. 5.14. In 2021, among all prefecture-level cities affected by natural disasters, 86% had indicators lower than the target

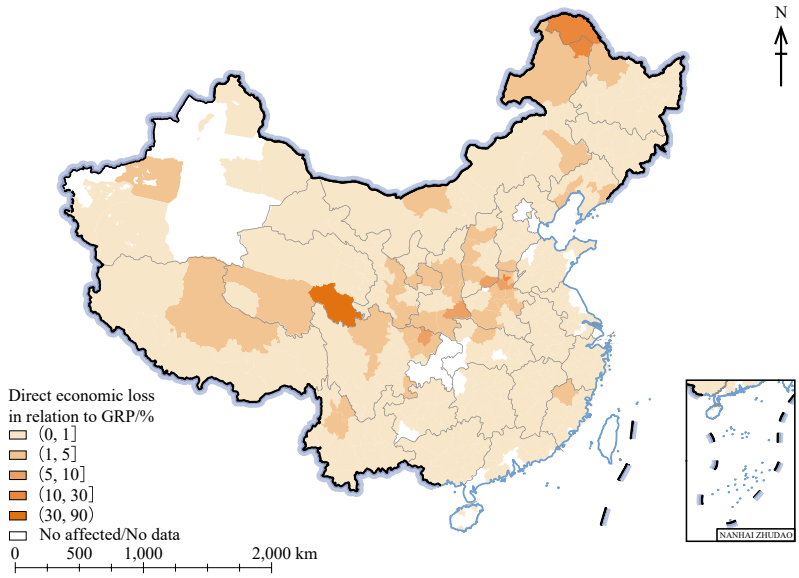

(c) Distribution of direct econmic losses in relation to GRP

(continued)

(1%) set by the National Comprehensive Plan on Disaster Prevention and Reduction (2016–2020), while 83% of cities had their indicators decreased to historical means from 2010 to 2020, with an average decrease of 76.5%. Despite the obvious decrease for most cities in China, northern Henan and local regions in Qinghai saw their SDG 11.5 indicators increased by the impacts of the severe flood in Henan and the Maduo earthquake.

Risk Analysis of Typhoon Disasters at the County Level (2016–2020)

Coastal areas in East and South China have the biggest area of urbanization, the most vigorous economic activity, and the highest density of population. Meanwhile, they are also the most vulnerable regions to tropical cyclones. In this case study, we evaluated the SDG 11.5 indicators of typhoon disasters for counties in this region during the 13th Five-Year Plan period (2016–2020), covering Shanghai, Zhejiang, Jiangsu, Fujian, Guangdong, Guangxi, and Hainan, as demonstrated in Fig. 5.15. Specifically, the number of affected persons per 100,000 population showed that the overall impact of typhoon disasters on people was mitigated, but relative impacts to Fujian, Zhejiang, Hainan, and Guangxi were still heavy. The number of deaths and missing persons per 100,000 population revealed that the highly risky regions with typhoon-caused fatalities mainly distributed in inland mountainous areas, where Guangxi, the west and north of Guangdong, and the west of Fujian had relatively high indicators. Direct economic loss in relation to GRP demonstrated that the overall impact of typhoon disasters on the economy had a mitigating trend, but relative losses in inland areas were high due to weaker developing foundations. Generally speaking, the disaster impact showed an alternating pattern between East and South China. The converging effects of losses and risks were obvious in coastal areas with a high density of population and economy.

Highlights

- A dataset of SDG 11.5 indicators was presented for 333 prefecture-level cities (2010–2021) in China.
- In 2021, the natural disaster impacts on China were continuously mitigated. The

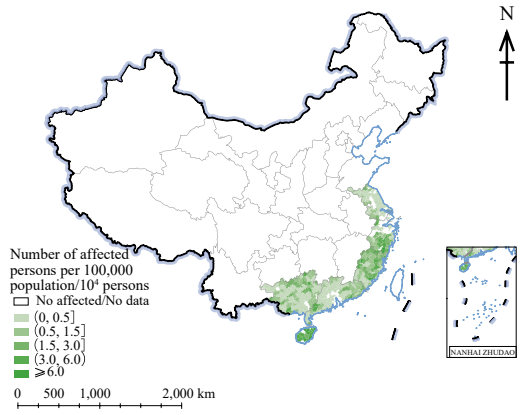

(a) Number of affected persons per 100,000 population in 2016

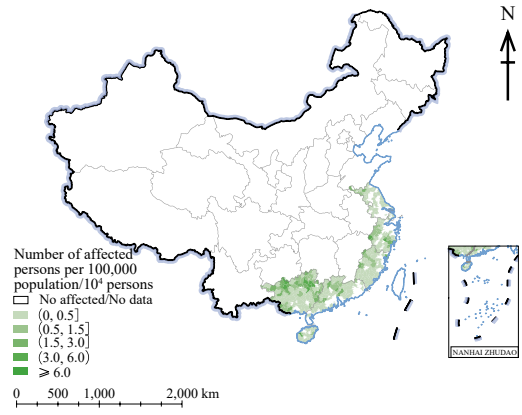

(b) Number of affected persons per 100,000 population in 2020

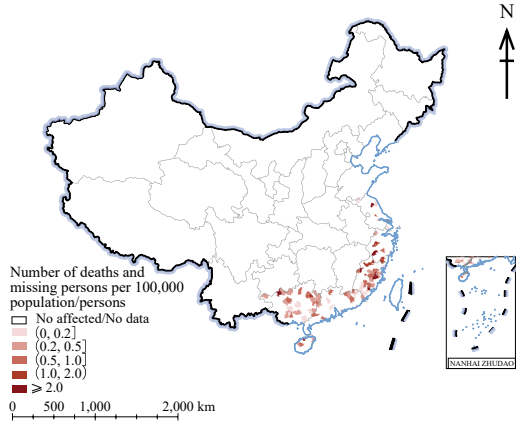

(c) Number of deaths and missing persons per 100,000 population in 2016

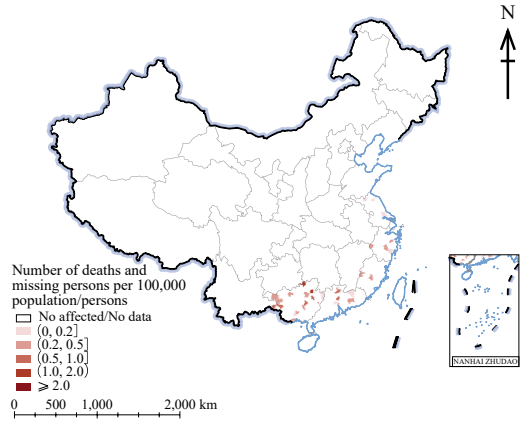

(d) Number of deaths and missing persons per 100,000 population in 2020

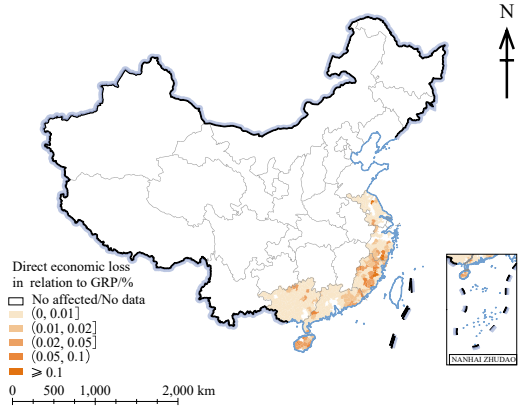

(e) Direct economic losses in relation to GRP in 2016

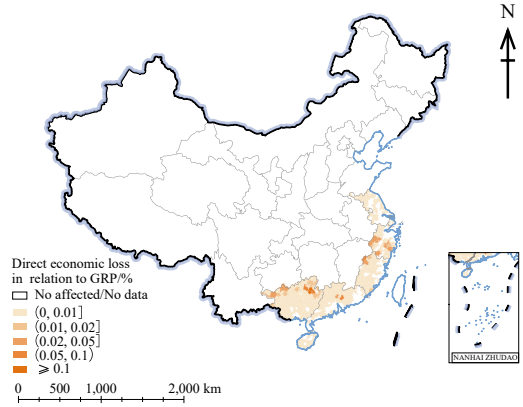

(f) Direct economic losses in relation to GRP in 2020

Fig. 5.15 Monitoring of SDG 11.5 indicators of typhoon disasters at the county level in East and South China from 2016 to 2020

number of directly affected persons per 100,000 population, the number of deaths and missing persons per 100,000 population, and direct economic loss in relation to GDP were reduced by 58.2%, 54.7%, and 50.8%, respectively, compared with the annual means from 2010 to 2020. However, extreme disaster events caused severe impacts on local areas.

- Coastal regions in East and South China with high density of population and economy suffered heavy impacts from typhoon disasters. Inland mountainous areas in Fujian, Guangdong, and Guangxi have greater risks of typhoon disasters.

5.3.4.5 Discussion and Outlook

In 2021, China faced a complicated and critical disaster situation. Extreme weather and climate events happened more frequently, while the relative impacts of disasters showed a mitigating trend, which proved the effectiveness of capability construction on comprehensive disaster prevention and reduction as well as resilience to disasters for cities. Under the background of global climate change, extreme rainstorm events have higher frequency in the north, while the typhoon impacts extend to inland regions, which clearly demonstrates the irregularity of natural disasters. Meanwhile, as to the disaster prevention and resilience capability of cities, southern and coastal regions of China outperform northern and inland regions. Disaster risks in the latter should be highlighted more. The establishment of bottom-line thinking and the strengthening of the ability to respond to extreme disaster events are important measures for reducing urban disaster risks during the 14th Five-Year Plan period.

5.3.5 Assessment of Changes in Population Exposure to Typical Atmospheric Particulate Matter in China

Target: SDG 11.6: By 2030, reduce the adverse per capita environmental impact of cities, including by paying special attention to air quality and municipal and other waste management.

5.3.5.1 Background

In recent years, China has achieved some improvement in air quality. The concentration of various pollutants and the proportion of days exceeding the standard show a downward trend, but China still faces a serious air pollution situation led by atmospheric particulate matter (PM), affecting people's lives and health. Data from the Report on the State of the Ecology and Environment in China 2021 show that there are still 121 cities with ambient air quality exceeding the standard among 339 prefecture-level and above cities in China, accounting for 35.7%. The number of days with $PM_{2.5}$ and PM_{10} as the primary pollutants exceeding the standard accounts for 39.7% and 25.2% of the total number of days, respectively, with $PM_{2.5}$ concentration of 30 $\mu g/m^3$ and PM_{10} concentration of 54 $\mu g/m^3$. The health effects of atmospheric PM involve multiple systems of the body. Several studies have confirmed that there is a statistically significant relationship between $PM_{2.5}$ and numerous diseases (Abdulrahman et al. 2022). Long-term or short-term exposure to atmospheric respirable PM, especially $PM_{2.5}$, can lead to increased cardiopulmonary morbidity, mortality, and overall population mortality (Guo and Wei 2013). A long-term time-series assessment of population exposure to typical atmospheric PM can provide a data reference for future air pollution policy formulation in China and better allow high-quality development in China.

5.3.5.2 Data

- 2000–2020 China High PM_X dataset, spatial resolution 1 km (Wei et al. 2019).
- 2000–2020 WorldPop population count dataset, spatial resolution 1 km.

5.3.5.3 Methods

In this case study, the $PM_{2.5}$ population exposure intensity index and $PM_{2.5}$ population-weighted average annual exposure concentration were

calculated at the grid scale and administrative unit scale, respectively, to assess the trend in population exposure to atmospheric particulate matter (PM) in China.

(1)$PM_{2.5}$ population exposure intensity index:

$$E_j = P_j \times PM_{2.5j} \tag{5.11}$$

The value is used to reflect the absolute annual average intensity of population exposure at the 1 km grid scale, where, j is the j-th spatial unit, E_j is the population exposure intensity in the j^{th} spatial unit, P_j is the number of populations in the j-th spatial unit, and $PM_{2.5j}$ is the annual average $PM_{2.5}$ concentration in the spatial unit j.

Then, Theil-Sen Median slope estimation and Mann–Kendall trend analyses were used to examine the trend in $PM_{2.5}$ population exposure intensity from 2000 to 2020. Theil-Sen Median slope estimation is a robust nonparametric statistical trend calculation method, and Mann–Kendall trend analysis can be further tested for the significance of trends in long-term time-series data.

(2)$PM_{2.5}$ population-weighted average annual exposure concentration:

$$\overline{PM}_{2.5} = \frac{\sum_j PM_{2.5j} P_j}{\sum_j P_j} \tag{5.12}$$

The value is used to reflect the annual exposure concentration per capita on a prefecture-level city scale, where, $\overline{PM}_{2.5}$ is the population-weighted average of $PM_{2.5}$ concentration in the total spatial unit, P_j is the number of populations in the j-th spatial unit, and $PM_{2.5j}$ is the annual average $PM_{2.5}$ concentration in the spatial unit j.

5.3.5.4 Results and Analysis

Spatial Patterns and Trends in $PM_{2.5}$ Population Exposure Intensity in China

Figure 5.16 shows the spatial distribution of $PM_{2.5}$ population exposure intensity index in China in 2000, 2005, 2010, 2015, and 2020. In general, the spatial pattern of population exposure intensity from 2000 to 2020 is relatively stable. The high values are mainly concentrated in North China and the north of East China, which shows a contiguous cluster. Some high-value areas also exist in Chengdu and Chongqing and some regions of the southeastern coast. The high values of population exposure intensity in Northeast China are concentrated in the capital cities of the three northeastern provinces, distributed in a banded pattern along the north–south direction. The high-value clustering areas in the West are mainly in the regions of southern Xinjiang.

The trend of the $PM_{2.5}$ population exposure intensity index in China from 2000 to 2020 reflected by the Mann–Kendall trend analysis is shown in Fig. 5.17. The population exposure intensity in most regions of China shows a decreasing trend, among which the decreasing trend is obvious in South China, Central China, and Northeast China. However, there are still some regions with an increasing trend, among which North China and some regions of the southeastern coast still have an increasing trend, while the southwest of Inner Mongolia, Northwest China, Xizang, and the southwest of Sichuan also have an obvious increasing trend.

Spatial Distribution Patterns and Changes in $PM_{2.5}$ Population-Weighted Average Annual Exposure Concentration in China

At the prefecture-level city scale (Fig. 5.18), the high values of $PM_{2.5}$ population-weighted average annual exposure concentration in China are mainly found in North China and southern Xinjiang, with the former mainly due to emission pollution brought by the high concentration of human production and living, while the latter is due to natural factors such as local sand and dust. During the period from 2000 to 2010, the overall annual average exposure concentration shows an increasing trend, with a significant increase in North China. From 2010 to 2015, the $PM_{2.5}$ population-weighted average annual exposure concentration in most parts of the country began to gradually decrease, with only southern

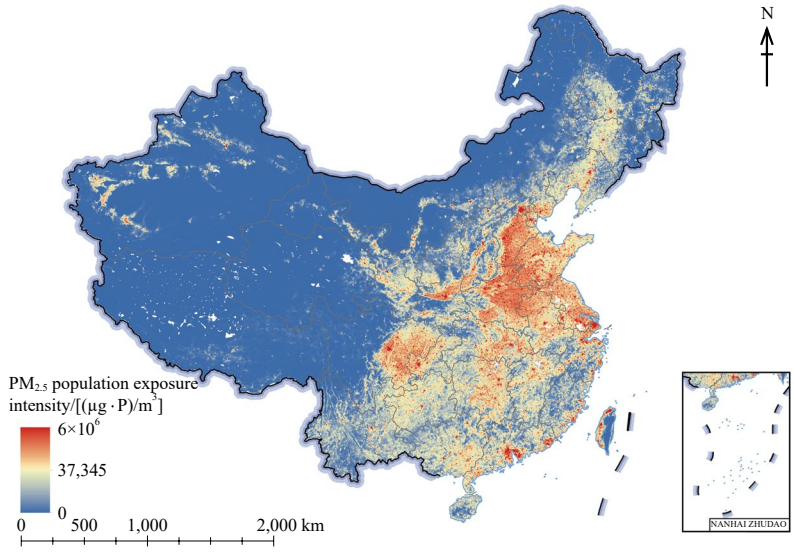

(a) 2000

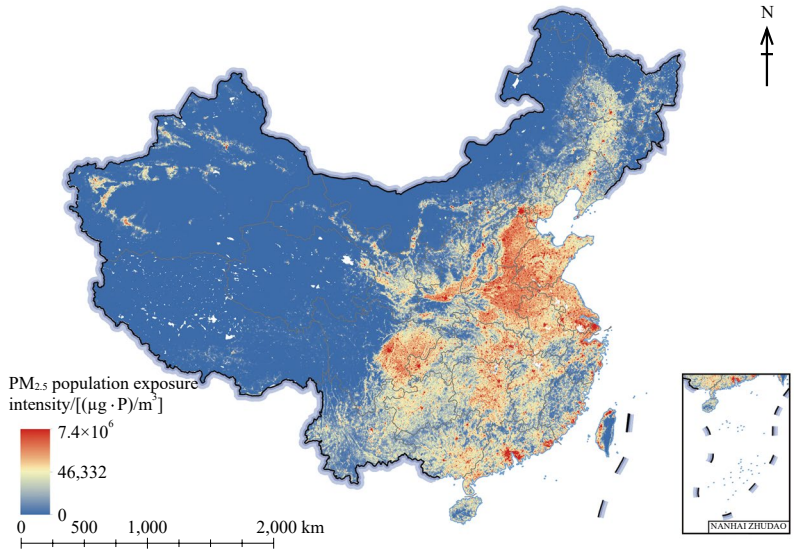

(b) 2005

Fig. 5.16 Spatial distribution of the $PM_{2.5}$ population exposure intensity index in China in 2000, 2005, 2010, 2015, and 2020

Xinjiang showing an increasing trend. After 2015, the $PM_{2.5}$ population-weighted average annual exposure concentration in most regions of China saw a rapidly decreasing trend. North China also began to show the effects of industrial structure adjustment and environmental pollution control, where the $PM_{2.5}$ population-weighted average annual exposure concentration dropped to below 65 65 $\mu g/m^3$ by 2020, while most other regions in China dropped to below 45 $\mu g/m^3$. The absolute high values are only found in the regions of southern Xinjiang.

In terms of the overall national population-weighted average annual exposure concentration (Fig. 5.19), the concentration shows a fluctuating upward trend until 2013, reaching

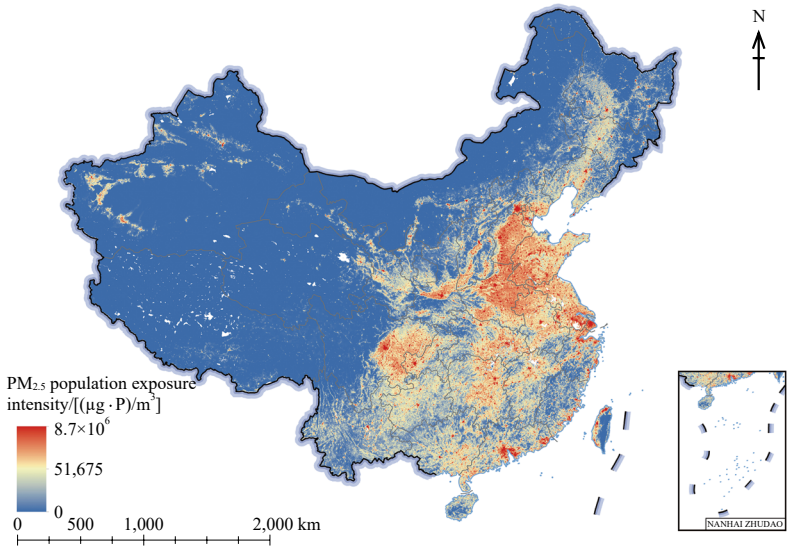

(c) 2010

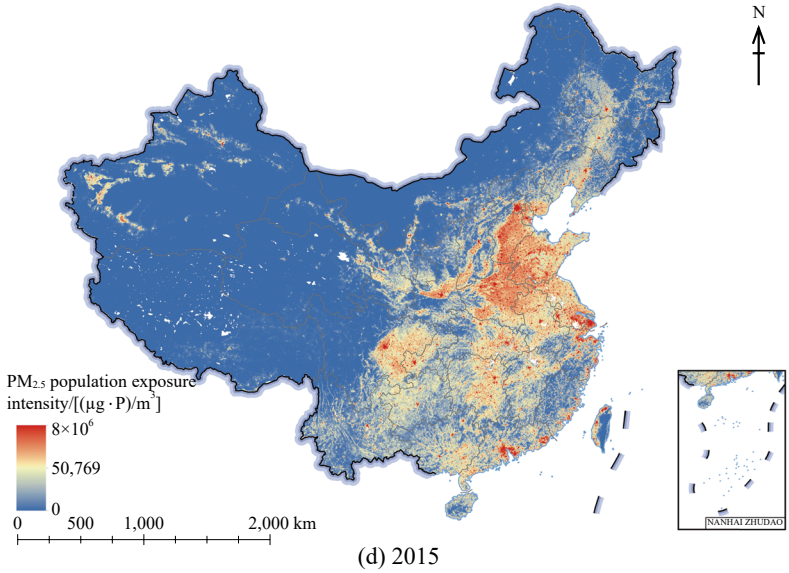

(d) 2015

(continued)

a peak of 65 $\mu g/m^3$ in 2013. To improve air quality and solve people's livelihood problems, the State Council of China issued and implemented the Air Pollution Prevention and Control Action Plan in September 2013, which proposed ten articles and thirty-five key task measures. After 2013, $PM_{2.5}$ population-weighted average annual exposure concentration shows a rapidly decreasing trend, and by 2020 they had dropped to 34 $\mu g/m^3$, lower than the national secondary concentration limit standard (35 $\mu g/m^3$), which shows that China's air control actions have achieved very significant results.

Highlights

- The high values of $PM_{2.5}$ population exposure intensity in China from 2000 to 2020 are concentrated in North China as well as the north of East China. From the perspective of the

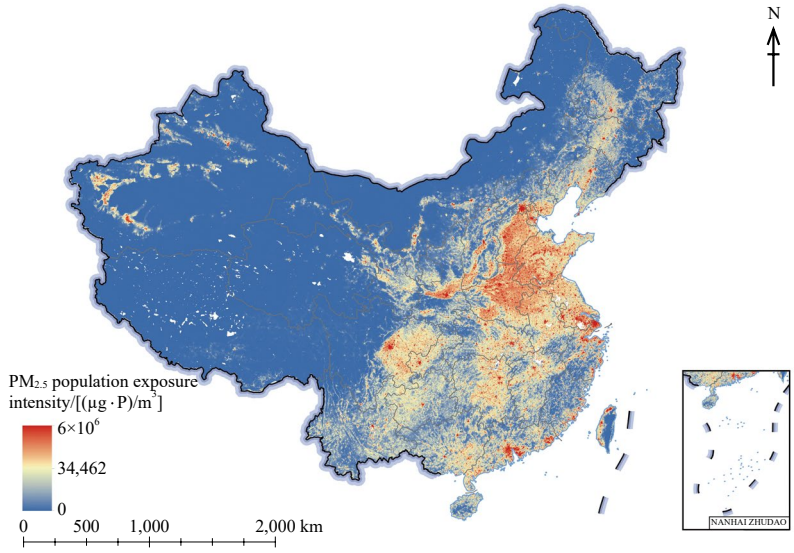

(e) 2020

(continued)

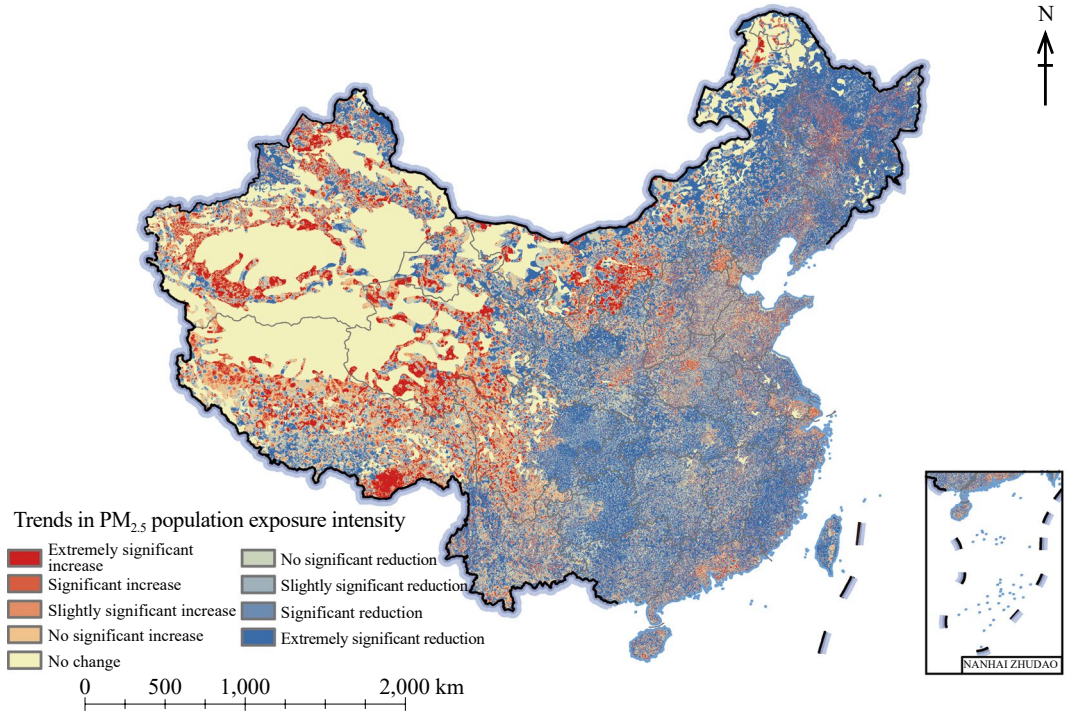

Fig. 5.17 Trend in the $PM_{2.5}$ population exposure intensity index in China from 2000 to 2020

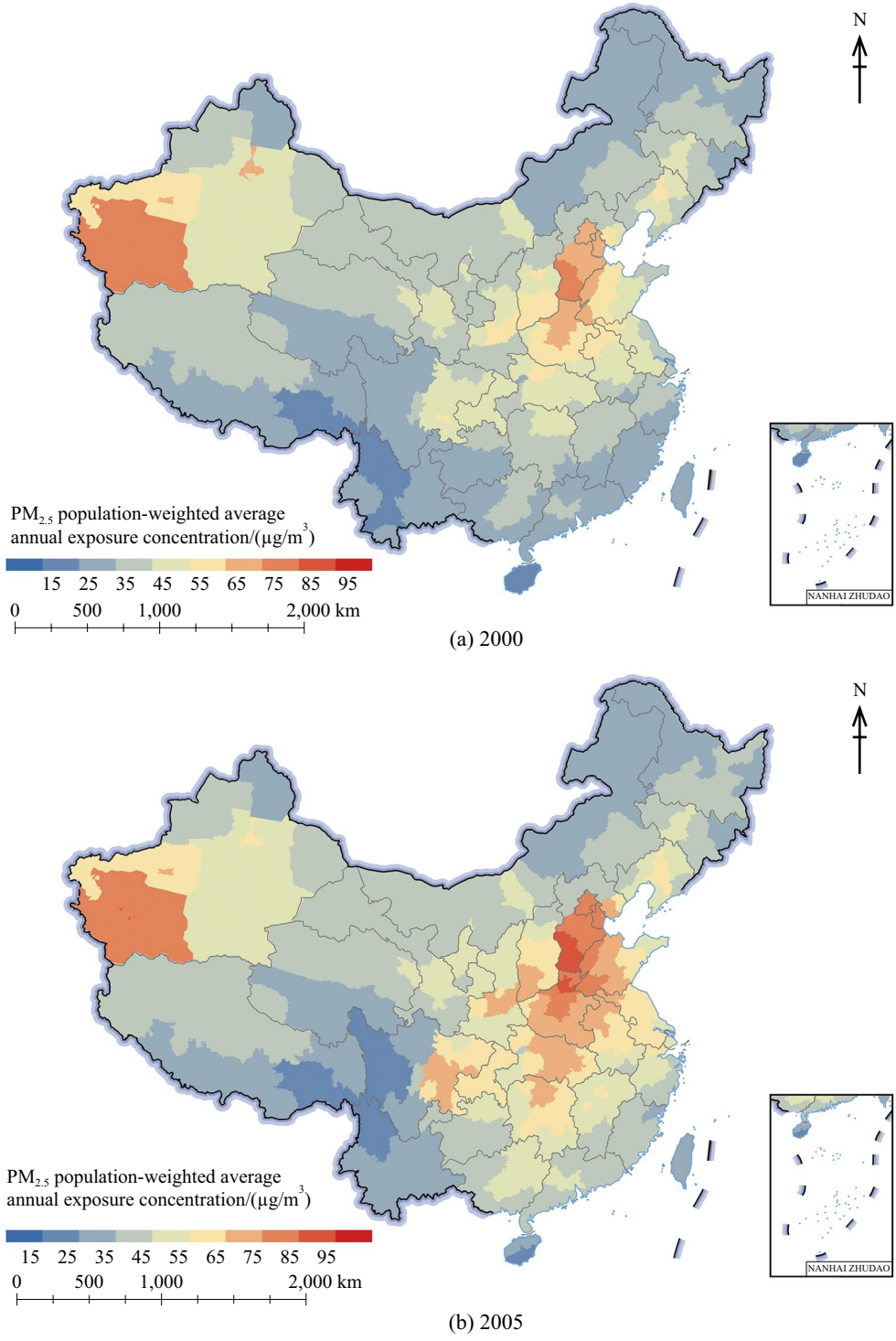

Fig. 5.18 Spatial distribution of $PM_{2.5}$ population-weighted average annual exposure concentration in China in 2000, 2005, 2010, 2015, and 2020

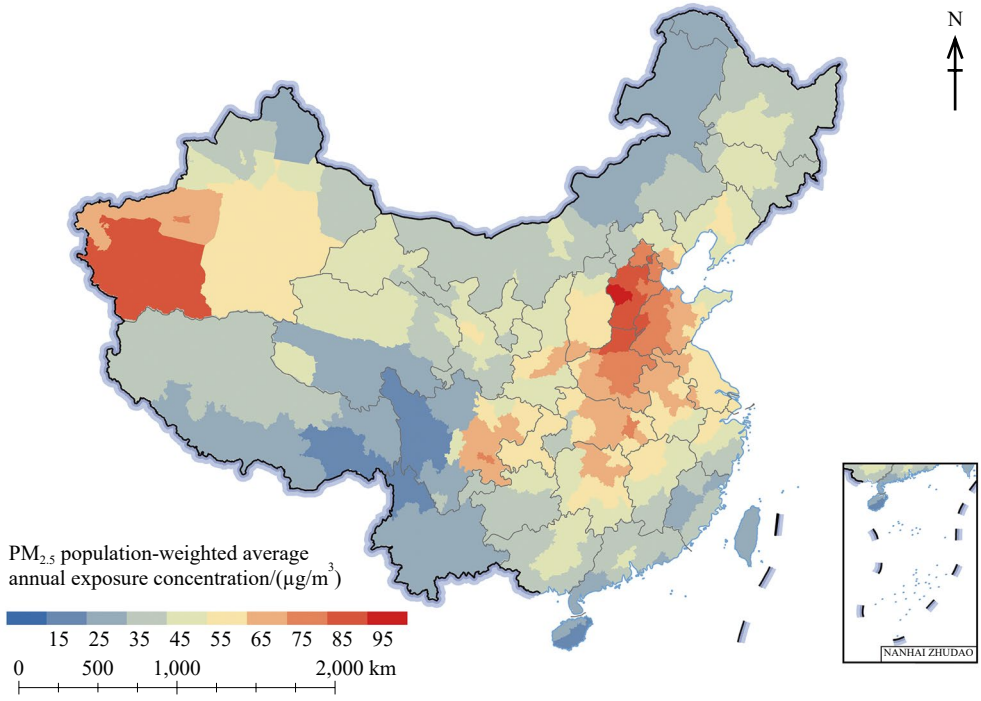

(c) 2010

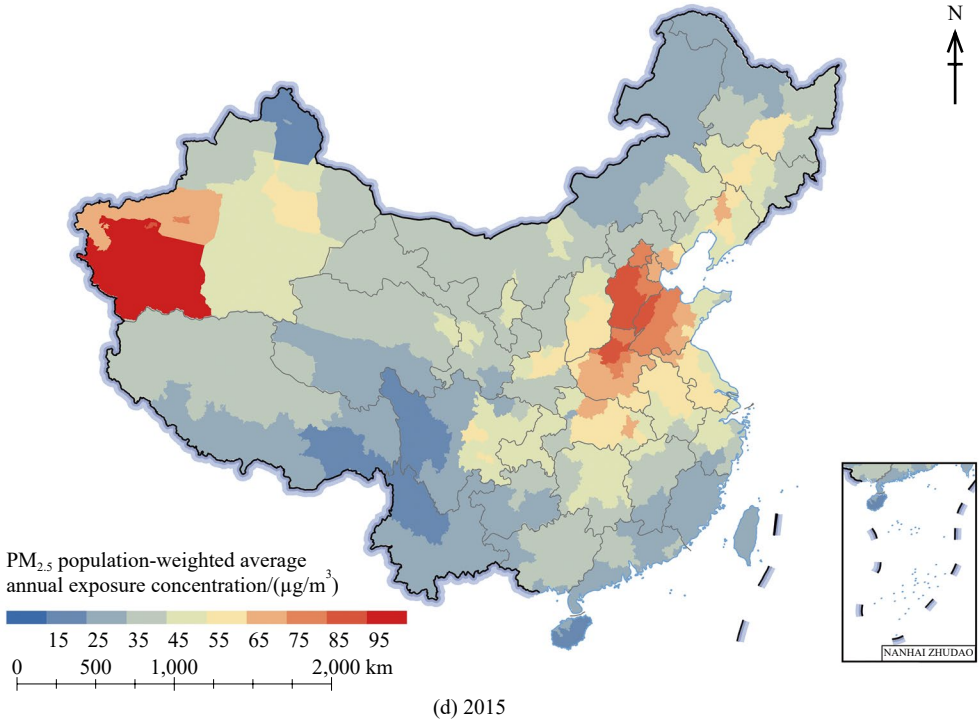

(d) 2015

(continued)

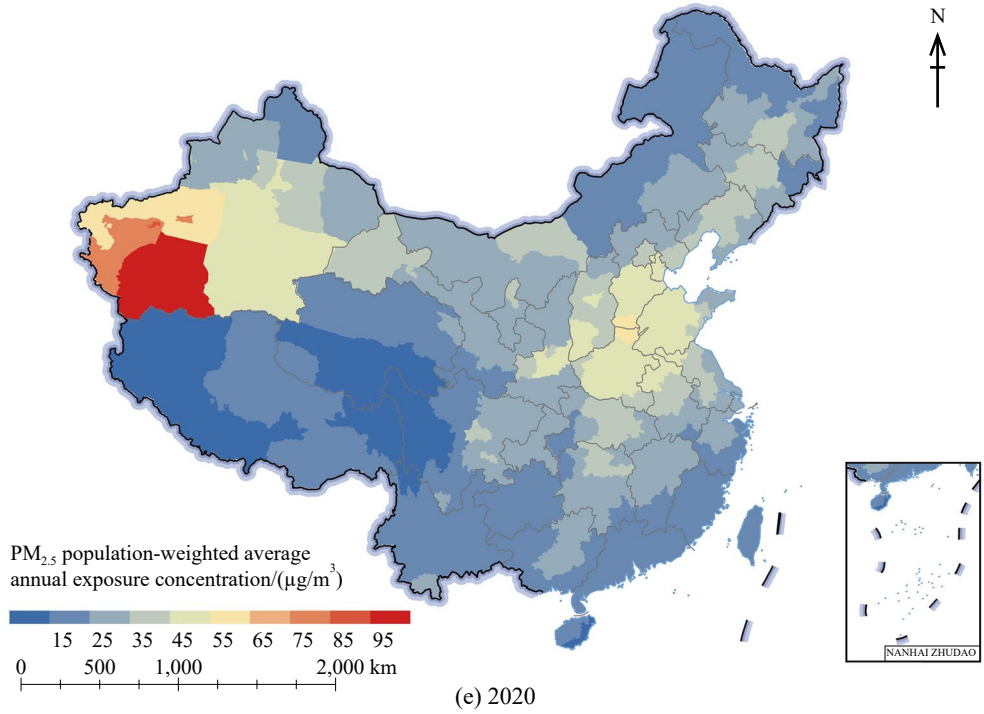

(e) 2020

(continued)

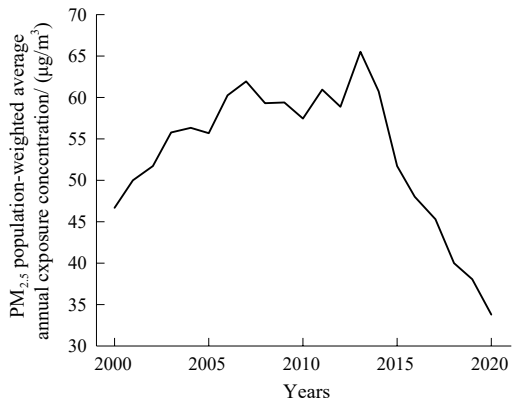

Fig. 5.19 Changes in $PM_{2.5}$ population-weighted average annual exposure concentration in China from 2000 to 2020

overall trend, South and Central China show a significant decreasing trend, while North China and some regions of the southeastern coast still show an increasing trend.

- The overall $PM_{2.5}$ population-weighted average annual exposure concentration in China from 2000 to 2020 shows a rapidly decreasing trend after reaching a peak in 2013 and then falling to 34 $\mu g/m^3$ by 2020, which is below the national secondary concentration limit standard. The exposure concentration of each prefecture-level city also shows a general trend of first increasing and then rapidly decreasing. In 2020, the high values were only concentrated in Southern Xinjiang.
- We compiled a dataset of a $PM_{2.5}$ population exposure intensity index for the kilometer grid from 2000 to 2020 and a dataset of $PM_{2.5}$ population-weighted average annual exposure concentration at the prefecture-level city from 2000 to 2020.

5.3.5.5 Discussion and Outlook

In this case, we used the near-surface $PM_{2.5}$ concentration data (Wei et al. 2019) and Worldpop population count data from remote sensing

inversion, and constructed the $PM_{2.5}$ population exposure intensity index and the $PM_{2.5}$ population-weighted average annual exposure concentration to assess the long-term trend of the $PM_{2.5}$ population exposure in China and generate the dataset. The results indicate that the $PM_{2.5}$ population exposure intensity in most regions of China shows a decreasing trend. The high values appear in North China and the north of East China, with a spatial pattern of a contiguous cluster. The $PM_{2.5}$ population-weighted average annual exposure concentration in most regions of China from 2000 to 2020 shows a trend of first increasing and then rapidly decreasing, with high values only occurring in southern Xinjiang in 2020. The overall $PM_{2.5}$ population-weighted average annual exposure concentration in China peaked in 2013 and then declined rapidly to 34 $\mu g/m^3$ by 2020.

In the future, we plan to analyze the differences in $PM_{2.5}$ exposure among different populations in China, especially the exposure of $PM_{2.5}$ susceptible populations, which gives a more refined assessment of the negative environmental impacts of air quality problems and adds to the research on the causal relationship between air pollution and diseases in China. In addition, we would like to track the new changes in population exposure after 2020 and especially focus on the impacts of the COVID-19 pandemic on typical atmospheric particulate matter in China.

5.3.6 Analysis of the Average Life Expectancy Indicator of Chinese Cities

Target: SDG 3: Ensure healthy lives and promote well-being for all at all ages.
SDG 6: Ensure availability and sustainable management of water and sanitation for all.
SDG 11: Make cities and human settlements inclusive, safe, resilient, and sustainable.
SDG 11.6: By 2030, reduce the adverse per capita environmental impact of cities, including by paying special attention to air quality and municipal and other waste management.
SDG 11.7: By 2030, provide universal access to safe, inclusive, and accessible, green and public spaces, in particular, for women and children, older persons, and persons with disabilities.

5.3.6.1 Background

The UN SDGs and the New Urban Agenda (NUA) all emphasize the importance of health issues during the development of cities, and building healthy cities has become a common goal for all of humanity. There are also several indicators in the SDGs that are highly compatible with the concept of healthy cities. The WHO European Healthy Cities Network proposed a set of healthy city indicators, but no unified standard exists worldwide. In 2018, the National Patriotic Health Campaign Committee of the People's Republic of China researched and developed the National Healthy City Indicator System (2018 edition), but the evaluation sample covered only some cities.

In the existing research and practice, life expectancy at birth (LEB) is an important indicator of a country or region's social health status and an important component of the UN Human Development Index (HDI). China ranks only 85th in the 2020 global HDI results and has space for improvement. China's 12th Five-Year Plan includes life expectancy as one of the core indicators to evaluate the levels of national economic and social development for the first time.

In practice, the average life expectancy indicator is estimated based on mortality information, and the age-specific mortality data are the basis for calculating this indicator. According to public information, the average life expectancy of Chinese residents in 2020 reached 77.93 years, but there are still serious problems with data availability and data quality at different levels of nation, province, and city. Regarding data availability, only national- and provincial-level average life expectancy is published in relevant

statistical yearbooks, and the provincial-level average life expectancy is estimated based on the decennial census data, lacking continuous yearly information. At the city scale, most cities do not provide information on average life expectancy. Regarding data quality, there are different degrees of underreporting of the infant mortality in China's census results (Cui et al. 2013), which impacts the accuracy of the model results. Also, in recent years, large-scale population movements have had a large impact on mortality rates, especially in the middle and young age labor force cohorts. The net inflow of the young labor force brings gains to the average life expectancy of the resident population in developed regions and also leads to some losses in the average life expectancy in outflow regions (Yang and Lu 2019). Therefore, with limited data, it is significant for academic research, urban management, and national sustainable development to construct a unified dataset of city-level average life expectancy with broader coverage through new data-driven research methods.

5.3.6.2 Data

- Self-collected statistical data and social big data of 90 sample cities in China for healthy city assessment in 2020, formed a system of health services, health behaviors, health facilities, and health environment indicators, with more than 60 tertiary calculated indicators, including the local average life expectancy indicators reported by each sample city.
- Basic characteristic indicators of 296 prefecture-level cities in China were collected and calculated independently, then were combined with the statistical data of the seventh census, departmental statistics, Internet positioning big data, remote sensing, and geographic information-related spatial data, and forming five major aspects of the type of city, basic geography, spatial location, economic level, and population structure.
- Statistical indicators on population, economy, health, environment, and facilities were collected and supplemented by the assessment system for 296 cities in China in 2020.

5.3.6.3 Methods

Average life expectancy is affected by multiple factors such as social economy and natural ecology (Bilal et al. 2021), which is a complex nonlinear system problem, and it is difficult to identify and refine the main patterns between input and output indicators by ordinary least squares regression. Technological advances such as machine learning and artificial intelligence can better meet such challenges and provide better tools and solutions for social research represented by the SDGs (Tomašev et al. 2020).

The core technical approach of this case study includes the following key steps. First, a feature engineering approach was adopted to design and define the city description index system, including but not limited to geography, location, administrative level, population, economy, industry, mobility, culture, and other "basic background" conditions of the city. Second, based on the evaluation of healthy cities, we collected and selected representative and critical indicators of healthy city construction measures, including but not limited to health care investment, ecological and environmental management, resident behavioral characteristics, supporting facilities, and other "transformation intervention" features. Finally, by comparing, testing, and validating machine learning models, including feature processing, algorithm selection, and hyperparameter optimization, a model with good generalization and a fitting degree was established, and the inferred results of indicators were output to form a complete dataset of healthy Chinese cities with average life expectancy at the city level in China (Fig. 5.20).

By establishing and comparing various machine learning algorithms and parameter tuning, 11 algorithms were selected, such as RF, light gradient boosting machine (LightGBM), least absolute shrinkage and selection operator (LASSO regression), and ridge regression (Table 5.3). First, the model was trained based on 90 sample cities, and the stability of the model was improved by K-fold cross-validation ($K=5$) due to the shortage of samples. Second, the better forecasting algorithms were compared via performance indices such as RMSE, mean absolute

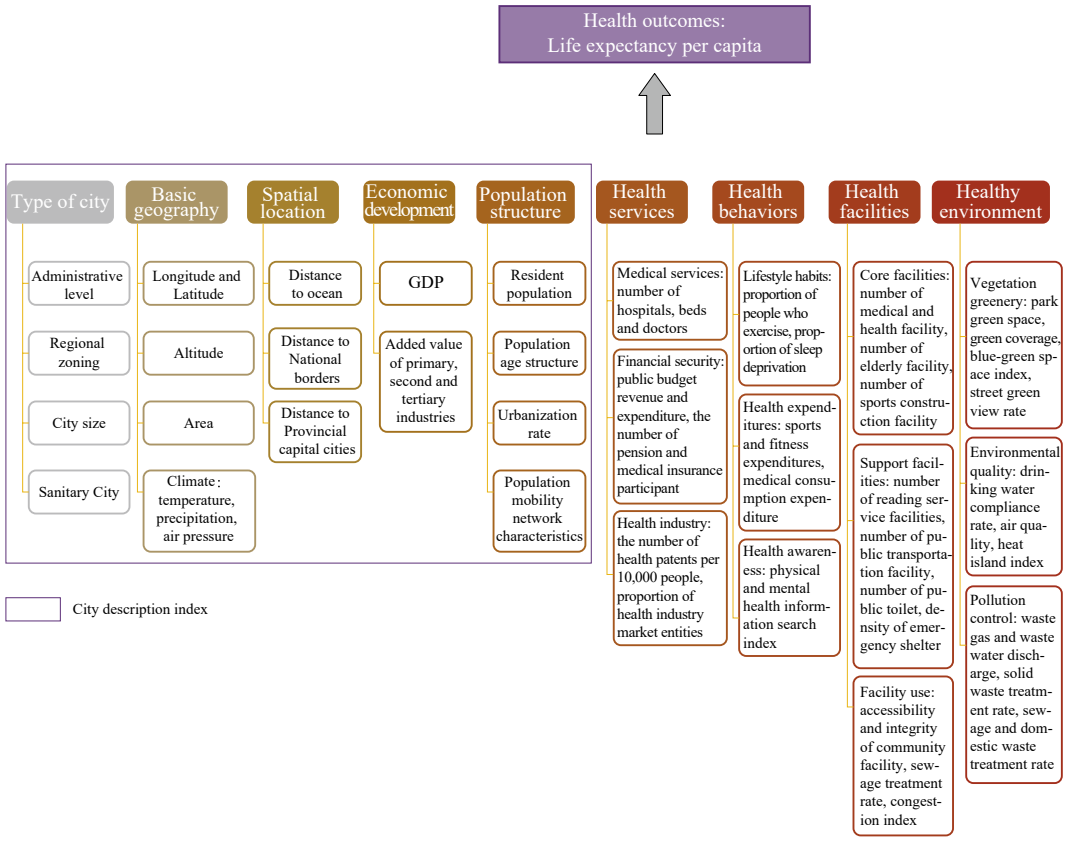

Fig. 5.20 Schematic diagram of characteristic index types

percentage error (MAPE), and the coefficient of determination (R^2 score) of different algorithms.

Different performance metrics have different characteristics and meanings for the effect of algorithm prediction. RMSE can be ranked for minor errors; MAPE of 0% indicates a perfect model, and MAPE greater than 100% indicates an inferior model; the R^2 score can compare the effect of models under different scales by referring to the calculated R^2 value.

The results show that the prediction performances of all algorithms are similar, and the top-ranked algorithms (e.g., extremely randomized trees, RF, gradient-boosted trees, etc.) have the top performance metrics, while the bottom-ranked algorithms [e.g., *K*-nearest neighbors, least absolute shrinkage and selection operator-least angle regression (LASSO-LARS), ordinary least squares] are also in the bottom of the list. The extremely randomized trees algorithm achieved the best performance, with the main performance indicators of RMSE = 1.52, MAE = 1.16, and R^2 score = 0.58. This algorithm predicted the average life expectancy and analyzed the impact factors for 296 cities above the prefecture level.

5.3.6.4 Results and Analysis

Based on the model results, the overall weighted average life expectancy of the total population of 296 cities by size[1] and eight

[1] The division of the city size is carried out in accordance with the State Development [2014] No. 51 Notice of the State Council on Adjusting the Standards for Categorizing City Sizes, and based on the results of the seventh national population census in 2020, the cities are divided into five categories and seven grades with the resident population in urban areas as the statistical caliber.

Table 5.3 Algorithm prediction performance comparison

Machine learning algorithms	Explained variance score (EVS)	MAPE	MAE	Mean squared error (MSE)	RMS	Root mean squared logarithmic error (RMSLE)	R^2	Correlation coefficient
Extremely randomized trees	0.59 (± 0.33)	1.5% (± 0.3%)	1.16 (± 0.25)	2.40 (± 2.12)	1.52 (± 0.62)	0.02 (± 0.01)	0.58 (± 0.34)	0.78 (± 0.23)
RF	0.56 (± 0.27)	1.5% (± 0.4%)	1.22 (± 0.27)	2.61 (± 2.21)	1.59 (± 0.61)	0.02 (± 0.01)	0.55 (± 0.28)	0.76 (± 0.20)
Gradient boosted trees	0.53 (± 0.29)	1.6% (± 0.2%)	1.28 (± 0.14)	2.78 (± 2.04)	1.64 (± 0.56)	0.02 (± 0.01)	0.52 (± 0.30)	0.73 (± 0.21)
LightGBM	0.51 (± 0.33)	1.7% (± 0.3%)	1.32 (± 0.20)	2.92 (± 2.39)	1.68 (± 0.63)	0.02 (± 0.01)	0.49 (± 0.36)	0.71 (± 0.24)
XGBoost	0.50 (± 0.30)	1.6% (± 0.3%)	1.28 (± 0.28)	2.96 (± 1.84)	1.70 (± 0.55)	0.02 (± 0.01)	0.48 (± 0.32)	0.72 (± 0.16)
Ridge (L2) regression	0.46 (± 0.37)	1.6% (± 0.2%)	1.25 (± 0.17)	3.11 (± 1.85)	1.74 (± 0.54)	0.02 (± 0.01)	0.44 (± 0.39)	0.69 (± 0.22)
LASSO (L1) regression	0.42 (± 0.28)	1.7% (± 0.3%)	1.36 (± 0.23)	3.40 (± 1.61)	1.83 (± 0.42)	0.02 (± 0.01)	0.40 (± 0.32)	0.67 (± 0.23)
Decision tree	0.19 (± 0.62)	2.0% (± 0.7%)	1.59 (± 0.53)	4.89 (± 4.09)	2.17 (± 0.89)	0.03 (± 0.01)	0.15 (± 0.66)	0.58 (± 0.34)
K-nearest neighbors ($K=5$)	0.19 (± 0.27)	2.2% (± 0.4%)	1.76 (± 0.31)	5.02 (± 2.61)	2.22 (± 0.55)	0.03 (± 0.01)	0.13 (± 0.35)	0.49 (± 0.17)
LASSO-LARS	− 0.19 (±0.80)	2.6% (± 0.6%)	2.04 (± 0.48)	6.95 (± 2.29)	2.63 (± 0.46)	0.03 (± 0.01)	− 0.26 (± 0.79)	0.49 (± 0.36)
Ordinary least squares	− 0.24 (± 1.04)	2.6% (± 0.7%)	2.08 (± 0.53)	7.26 (± 4.12)	2.67 (± 0.74)	0.03 (± 0.01)	− 0.33 (± 1.07)	0.51 (± 0.41)

economic zones in China in 2020 is shown in Table 5.4. The average life expectancy of cities nationwide is 79.44 years, slightly higher than the national statistical value of 1.51 years. In terms of the city size, megacities and supercities have the highest average life expectancy at 81.81 and 81.82 years, respectively, exceeding the national average by 2.37 and 2.38 years; small cities (Type II) have the lowest average life expectancy at 76.98 years, which is 2.46 years below the national average; and the difference between the highest and lowest values between the groups is 4.84 years (Fig. 5.21). In terms of the eight economic zones, there are more distinct inter-regional differences in average life expectancy; the highest average life expectancy is in the eastern coastal region, reaching 82.29 years; the lowest is in the northwestern region, going 77.85 years; the difference between the highest and lowest economic regions is 4.44 years; regions that are higher than the national average of cities include the eastern coast, the southern coast, the northeast, and the northern coast (Fig. 5.22). The above situation shows that there are still relatively obvious differences in the health level of the population represented by the average life expectancy between cities of different sizes in different regions, which is not conducive to the overall promotion of the Healthy China Action Plan and should be given special attention in future policies.

Regarding spatial distribution, the cities with the highest average life expectancy are clustered in the four major regions of China's economic growth: the Yangtze River Delta, the Pearl River Delta, Beijing-Tianjin-Hebei, and the Chengdu-Chongqing urban agglomeration. In other

Table 5.4 Average life expectancy in cities of China in 2020 (forecasted)

No	Cities	Average life expectancy in 2020/years	No	Cities	Average life expectancy in 2020/years	No	Cities	Average life expectancy in 2020/years
1	Shanghai	84.51	36	Huizhou	80.69	71	Fuxin	79.36
2	Suzhou	84.07	37	Wuhan	80.67	72	Huangshan	79.36
3	Nanjing	83.75	37	Xi'an	80.67	73	Meizhou	79.35
4	Shenzhen	83.48	39	Yantai	80.49	74	Baotou	79.33
5	Wuxi	83.10	40	Yichang	80.43	75	Jincheng	79.32
6	Nantong	83.05	41	Hefei	80.41	75	Mianyang	79.32
7	Changzhou	83.03	42	Quzhou	80.36	77	Taiyuan	79.31
7	Hangzhou	83.03	43	Jinhua	80.35	78	Jiamusi	79.30
9	Guangzhou	83.02	44	Qinhuangdao	80.29	79	Fushun	79.29
10	Dongguan	82.99	44	Harbin	80.29	80	Daqing	79.28
11	Tianjin	82.91	46	Lianyungang	80.26	81	Rizhao	79.27
12	Jiaxing	82.85	47	Panjin	80.25	82	Ma'anshan	79.26
13	Shaoxing	82.84	48	Kunming	80.12	83	Jieyang	79.25
14	Zhenjiang	82.80	49	Lishui	80.06	84	Qitaihe	79.24
15	Zhuhai	82.73	50	Zibo	80.05	85	Mudanjiang	79.22
16	Foshan	82.52	51	Zhengzhou	80.03	86	Weifang	79.20
17	Huzhou	82.01	52	Changsha	79.99	87	Heyuan	79.19
18	Ningbo	81.96	53	Benxi	79.95	88	Liaoyuan	79.18
19	Yangzhou	81.90	53	Huai'an	79.95	88	Shanwei	79.18
20	Taizhou	81.89	53	Shantou	79.95	90	Shijiazhuang	79.16
21	Zhoushan	81.69	56	Yingkou	79.90	91	Tonghua	79.15
22	Wenzhou	81.65	57	Huludao	79.81	91	Chaozhou	79.15
23	Beijing	81.54	58	Qingyuan	79.76	93	Suqian	79.14
24	Weihai	81.49	59	Shaoguan	79.75	94	Tieling	79.13
25	Taizhou	81.37	60	Dandong	79.61	95	Wuhai	79.11
26	Qingdao	81.36	60	Zhaoqing	79.61	95	Jilin	79.11
27	Chengdu	81.29	62	Jinan	79.57	97	Jixi	79.09
28	Hohhot	81.21	63	Liaoyang	79.50	98	Xuancheng	79.08
29	Dalian	81.16	64	Anshan	79.48	99	Chaoyang	79.07
30	Zhongshan	81.03	65	Jinzhou	79.47	99	Shuangyashan	79.07
31	Xiamen	80.96	66	Zhanjiang	79.45	99	Leshan	79.07
32	Shenyang	80.80	67	Changchun	79.44	102	Jinmen	79.05
33	Karamay	80.71	68	Deyang	79.38	103	Hegang	79.04
34	Yancheng	80.70	69	Zhangjiakou	79.37	103	Yunfu	79.04
35	Jiangmen	80.69	69	Fuzhou	79.37	105	Bayan Nur	79.03
106	Baishan	79.01	141	Suihua	78.61	176	Nanchong	78.28
107	Panzhihua	79.00	141	Jiaozuo	78.61	177	Danzhou	78.25

(continued)

Table 5.4 (continued)

No	Cities	Average life expectancy in 2020/years	No	Cities	Average life expectancy in 2020/years	No	Cities	Average life expectancy in 2020/years
108	Zhuzhou	78.99	141	Hami	78.61	178	Suizhou	78.24
108	Yangjiang	78.99	144	Songyuan	78.60	178	Luzhou	78.24
110	Maoming	78.96	145	Quanzhou	78.59	180	Jinzhong	78.23
111	Xinxiang	78.95	146	Liaocheng	78.57	180	Wuzhou	78.23
112	Tangshan	78.94	146	Liuzhou	78.57	182	Qinzhou	78.22
112	Wuhu	78.94	148	Luoyang	78.56	182	Yinchuan	78.22
114	Heihe	78.93	149	Ningde	78.55	184	Cangzhou	78.21
115	Baicheng	78.92	149	Yuxi	78.55	184	Linyi	78.21
115	Qiqihar	78.92	151	Hengshui	78.53	186	Xingtai	78.19
117	Langfang	78.91	152	Ulanqab	78.52	186	Huangshi	78.19
118	Guilin	78.88	152	Jingzhou	78.52	186	Hengyang	78.19
119	Dongying	78.86	152	Chongqing	78.52	189	Jiujiang	78.17
119	Xiangtan	78.86	155	Hulunbuir	78.51	189	Bangzhou	78.17
121	Datong	78.85	156	Xinyu	78.49	191	Luohe	78.16
121	Tongliao	78.85	156	Shiyan	78.49	191	Guigang	78.16
121	Haikou	78.85	156	Nanning	78.49	191	Yibin	78.16
121	Meishan	78.85	159	Ya'an	78.47	194	Nanping	78.15
125	Chizhou	78.84	160	Tongling	78.42	194	Taian	78.15
126	Sanya	78.81	160	Longyan	78.42	196	Xinzhou	78.13
127	Xiangyang	78.80	160	Pingxiang	78.42	196	Kaifeng	78.13
128	Jining	78.79	163	Handan	78.41	198	Dazhou	78.11
129	Baoding	78.78	163	Zigong	78.41	199	Changji	78.09
130	Chengde	78.77	165	Putian	78.38	199	Suzhou	78.09
131	Yangquan	78.74	165	Suining	78.38	201	Hezhou	78.08
131	Nanchang	78.74	167	Lijiang	78.37	202	Yingtan	78.07
131	Guangyuan	78.74	168	Anyang	78.36	203	Baoshan	78.06
131	Liupanshui	78.74	169	Sanming	78.35	204	Xiaogan	78.05
135	Siping	78.72	170	Huainan	78.33	205	Jingdezhen	78.04
135	Zaozhuang	78.72	171	Huaibei	78.30	205	Yiyang	78.04
137	Xuzhou	78.70	171	Zhangzhou	78.30	207	Heze	78.03
138	Yichun	78.69	173	Bengbu	78.29	207	Laibin	78.03
139	Binzhou	78.65	173	Anqing	78.29	209	Chuzhou	78.02
139	Beihai	78.65	175	Hebi	78.28	209	Jiuquan	78.02
211	Baoji	78.01	246	Jiayuguan	77.71	281	Yulin	76.96
212	Chifeng	78.00	247	Nanyang	77.68	282	Zhangye	76.94
212	Dezhou	78.00	247	Zhaotong	77.68	283	Guyuan	76.89
214	Yulin	77.99	249	Yuncheng	77.67	284	Ordos	76.80

(continued)

Table 5.4 (continued)

No	Cities	Average life expectancy in 2020/years	No	Cities	Average life expectancy in 2020/years	No	Cities	Average life expectancy in 2020/years
215	Pu'er	77.98	249	Bozhou	77.67	285	Qujing	76.73
216	Fuzhou	77.97	249	Yichun	77.67	285	Xianyang	76.73
217	Chongzuo	77.96	252	Shangqiu	77.66	287	Longnan	76.65
218	Pingdingshan	77.95	253	Lincang	77.59	288	Jinchang	76.45
218	Yueyang	77.95	254	Xinyang	77.58	289	Xining	76.37
220	Loudi	77.93	255	Puyang	77.57	290	Zunyi	74.41
221	Hechi	77.91	256	Ganzhou	77.56	291	Shannan	73.24
222	Changde	77.87	257	Urumqi	77.53	292	Shigatse	72.97
222	Guang'an	77.87	258	Huaihua	77.52	293	Linzhi	72.82
222	Shizuishan	77.87	259	Tianshui	77.51	294	Nagchu	72.56
225	Zhangjiajie	77.86	260	Shuozhou	77.49	295	Qamdo	72.40
226	Neijiang	77.84	260	Zhoukou	77.49	296	Lhasa	71.27
226	Lanzhou	77.84	262	Anshun	77.48			
228	Lvliang	77.83	262	Pingliang	77.48			
228	Fangchenggang	77.83	264	Ankang	77.47			
230	Bazhong	77.82	265	Baiyin	77.40			
230	Tongchuan	77.82	266	Linfen	77.37			
232	Sanmenxia	77.81	266	Shangluo	77.37			
232	Zhumadian	77.81	268	Bijie	77.36			
232	Ziyang	77.81	268	Hanzhong	77.36			
235	Huanggang	77.80	270	Ji'an	77.32			
236	Lu'an	77.79	271	Wuzhong	77.31			
236	Ezhou	77.79	272	Haidong	77.23			
238	Xianning	77.78	273	Weinan	77.21			
238	Shaoyang	77.78	274	Yan'an	77.18			
240	Fuyang	77.76	275	Tongren	77.17			
240	Xuchang	77.76	276	Qingyang	77.03			
242	Guiyang	77.75	277	Dingxi	77.02			
243	Yongzhou	77.73	278	Turpan	77.00			
244	Baise	77.72	279	Wuwei	76.98			
245	Shangrao	77.71	280	Zhongwei	76.97			

regions, especially some Western cities with higher elevations, harsh natural environments, and lagging economic development levels, the average life expectancy is shorter, and they are key areas to pay attention to (Fig. 5.23).

As shown by the feature importance analysis of the machine learning models, the key factors that determine the average life expectancy in Chinese cities include population age structure, physical geographic environment, health-related

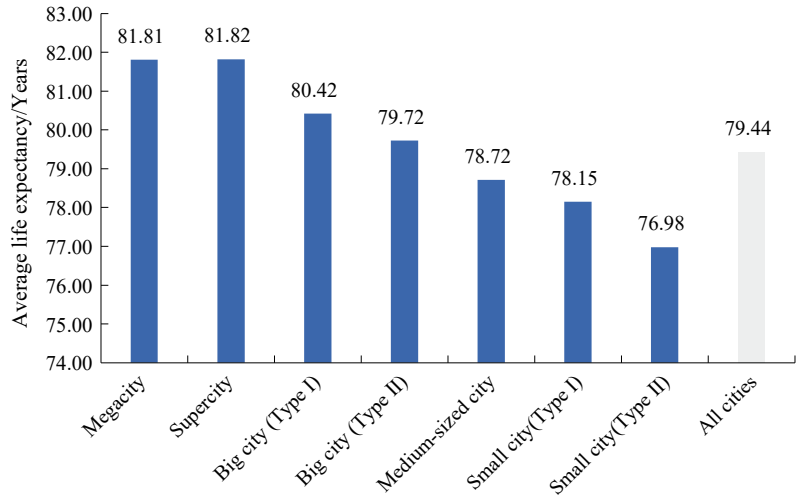

Fig. 5.21 Average life expectancy of various city sizes in seven grades in 2020. *Note* The average life expectancy for each group and all cities is weighted by total population from the seventh national population census

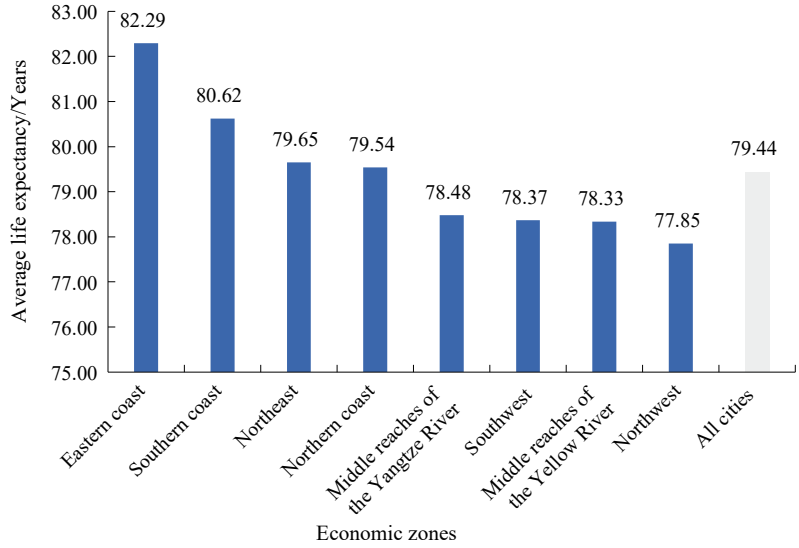

Fig. 5.22 Average life expectancy of the eight economic zones in 2020. *Note* The average life expectancy for each group and all cities is weighted by total population from the seventh national population census

facilities, economic development level, population mobility, and regional history and culture. This reflects the comprehensive and complex nature of the population health and requires multidisciplinary collaboration. At the same time, the models also give the differential impact factor ranking of average life expectancy in different cities, which can provide a data basis for cities to conduct customized and localized academic and policy research to improve local governmental shortcomings and deficiencies.

Highlights

- Big data and information technology have been actively used to collect emerging

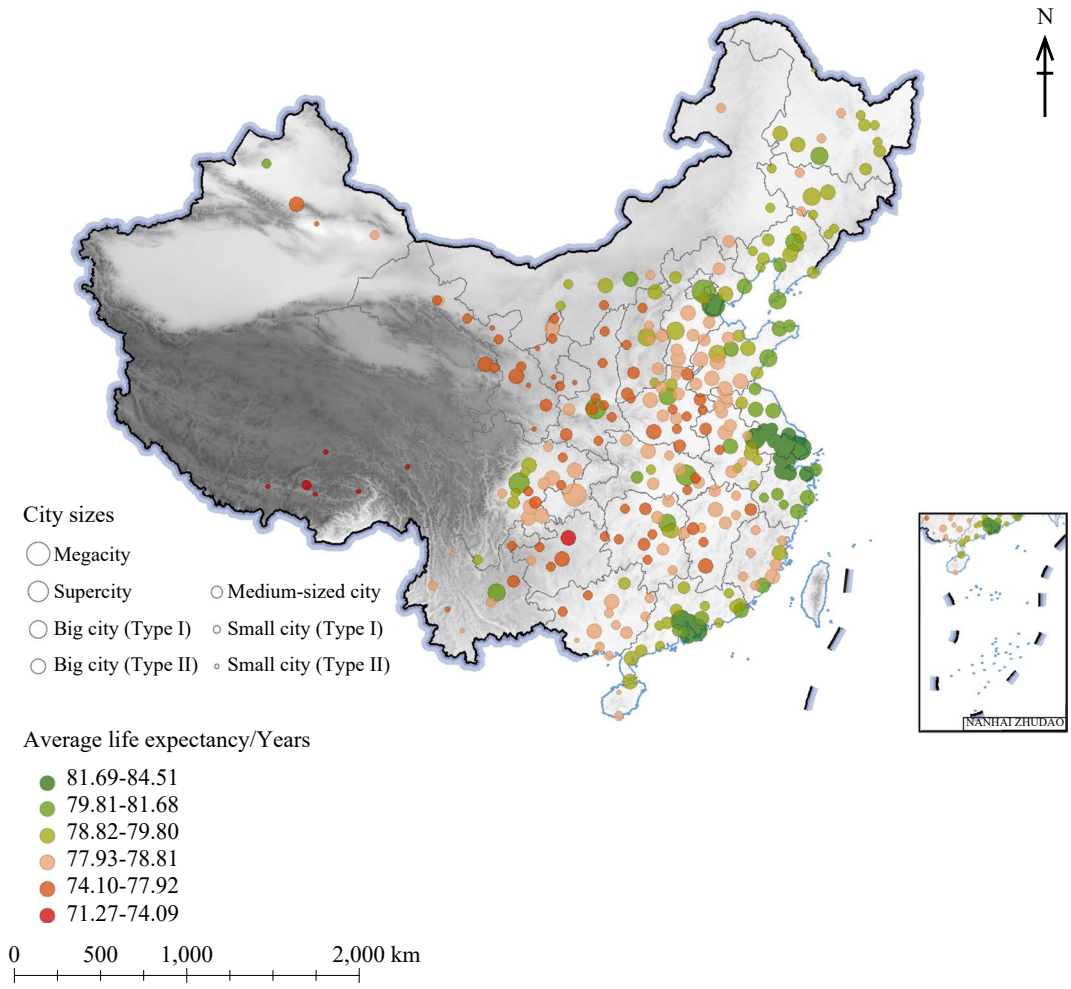

Fig. 5.23 Average life expectancy of all sample cities in China in 2020

multi-source social big data, including population mobility, facility location, remote sensing imagery, and enterprise business registration, and to measure indicators at the national city level, actively expanding the sources of data related to healthy cities based on traditional statistics.

- After integrating government data and social big data and working closely with the National Health Commission of the People's Republic of China and the National Patriotic Health Campaign Committee, we have built a comprehensive third-party healthy city evaluation index system, collecting more than 60 calculated indices and conducting a thorough assessment of the urban health status of major cities in China.
- Based on the assessment of data from sample cities and healthy city-related indicators, the characteristics of 296 prefecture-level cities in China have been created, and big data and machine learning have been innovatively used for methodological exploration to establish, compare, and optimize the machine learning models to predict the average life expectancy of each city, resulting in a city-level average life expectancy prediction dataset for China, which solves the difficult problem of the

general lack of the average life expectancy indicator at the city level in the country. It also provides solid foundations for technical support, such as automated monitoring and forecasting for policy research.

- The relevant research results are regularly released to the public, which, on the one hand, encourages the community to pay attention to urban health issues, and on the other hand provides technical support for national and provincial health committees, healthcare offices at all levels, and the Chinese Center for Disease Control and Prevention to conduct thematic studies, providing an independent third-party evaluation.

5.3.6.5 Discussion and Outlook

By using rich data collection, cleaning, processing, and analysis tools, this case constructs an assessment system of health indicators for 296 prefecture-level cities in China based on the mutual combination of government data, and social big data and predicts the key indicator of average life expectancy at the city level in 2020 using objective and cutting-edge machine learning models, making up for the general lack of this information at the city level.

In the context of the post-pandemic era, the third-party evaluation of urban health is strongly relevant and has long-term strategic significance. Different from the evaluation work carried out by departments and local governments, the indicator analysis of this case, as a third-party scientific and open evaluation result, will be more conducive to tracking the effect of policies related to healthy cities, checking weaknesses and filling shortcomings, becoming an important reference for promoting the modernization, wisdom, and resilience of urban governance, and strongly contributing to the overall process of Healthy China Action Plan.

In the future, we plan to continue to collect and update the evaluation index system of healthy cities, to design an urban health evaluation index system, and to measure relevant specific indicators through a combination of qualitative and quantitative "top-down" and "bottom-up" approaches. It will provide comprehensive data analysis, implement continuous monitoring and evaluation of population health levels in Chinese cities, provide corresponding research support and policy suggestions for governments and health and management departments at all levels, and promote the formation of a good feedback mechanism.

5.4 Summary

This chapter discussed progress in three themes—monitoring and evaluation of the urbanization process, urban disaster and response, and urban environments—while providing a comprehensive evaluation of progress toward SDG 11 in China.

Based on the case studies, we offer the following recommendations.

(1) For urban land use efficiency (SDG 11.3.1), the study found that the northeastern region and some small and medium cities in China faced a major uncoordinated situation from 2015 to 2020. The situation will require rationally planning urban land expansion, optimizing land resource allocation, and avoiding low-level expansion as well as inefficient utilization.
(2) As to SDG 11.5.1 and SDG 11.5.2 for urban disasters, a case study revealed that the relative impacts of natural disasters in China were continuously being mitigated, which demonstrates the effectiveness of capacity building in integrated disaster prevention and mitigation and resilience to natural disasters at the municipal level. However, under the dual background of global climate change and the urbanization rate of China exceeding 65%, it is necessary to further enhance the ability of urban areas to deal with extreme disasters. It is recommended to coordinate the promotion of ecological protection and economic development, continue to improve the system of water and soil conservation laws and regulations, establish a long-term management mechanism for water and soil conservation,

create a soil and water conservation talent expert library, promote the informatization and intelligence of soil erosion supervision, and continuously improve the effectiveness of urban water and soil conservation work.

(3) For the SDG 11.6.2 for $PM_{2.5}$, the study found that the overall annual population-weighted average of $PM_{2.5}$ concentration in China peaked in 2013 and then declined rapidly by 2020. The $PM_{2.5}$ population exposure intensity in most regions of China shows a decreasing trend. Although the results of China's air control actions are remarkable, there is still a distance between the AQG2021 standard proposed by the WHO. More localized anti-pollution policies must be proposed to reduce the adverse per capita environmental impact in the future.

(4) In response to the research need for a comprehensive assessment of SDG 11 indicators, the average life expectancy of cities as a characteristic indicator to analyze the population health level has the following main findings: the average life expectancy of megacities and supercities, and also cities in the eastern coastal region of China has reached the level of middle-and high-income countries, but there are more obvious differences in the health level of populations in different regions and different city sizes. The Health China Initiative in future should focus on the differentiated characteristics of different regions, and comprehensively promote the improvement of urban health based on city policies.

Future studies should understand the transformation toward sustainable urbanization and continue to explore the capacity of digital technology represented by Big Earth Data in monitoring and evaluating sustainable cities and communities, so as to provide scientific solutions to the realization of SDG 11 by filling data gaps, expanding the indicator system, and informing government decision-making.

References

Abdulrahman J, Zhou XD, Liu J et al (2022) Air pollution exposure disparities across US population and income groups. Nature 601(7892):228–233

Bilal U, Hessel P, Perez-Ferrer C et al (2021) Life expectancy and mortality in 363 cities of Latin America. Nat Med 27(3):463–470

Bondarenko M, Kerr D, Sorichetta A et al (2020) Census/projection-disaggregated gridded population datasets, adjusted to match the corresponding UNPD 2020 estimates, for 183 countries in 2020 using Built-Settlement Growth Model outputs. WorldPop. University of Southampton, UK. https://doi.org/10.5258/SOTON/WP00685

Cui HY, Xu L, Li R (2013) An evaluation of data accuracy of the 2010 population census of China. Popul Res 37(1):10–21 (in Chinese)

Duan W, Zhang H, Wang C et al (2020) Multi-temporal InSAR parallel processing for sentinel-1 large-scale surface deformation mapping. Remote Sens 12(22):3749

Guo HD, Chen F, Sun ZC et al (2021) Big earth data: a practice of sustainability science to achieve the sustainable development goals. Sci Bull 66(11):1050–1053

Guo XB, Wei HY (2013) Progress on the health effects of ambient $PM_{2.5}$ pollution. Chin Sci Bull 58:1171–1177 (in Chinese)

Jiang HP, Sun ZC, Guo HD et al (2021) An assessment of urbanization sustainability in China between 1990 and 2015 using land use efficiency indicators. NPJ Urban Sustain 34(1):1–13

Kuang WH, Du GM, Lu DS et al (2021) Global observation of urban expansion and land-cover dynamics using satellite big-data. Sci Bull 66(4):297–300

Melchiorri M, Pesaresi M, Florczyk A et al (2019) Principles and applications of the global human settlement layer as baseline for the land use efficiency indicator–SDG 11.3.1. ISPRS Int J Geo-Inf 8(2):96.

Tomašev N, Cornebise J, Hutter F et al (2020) AI for social good: unlocking the opportunity for positive impact. Nat Commun 11:2468

UN (2015) Sendai framework for disaster risk reduction 2015–2030. UN, Geneva

UN (2021) The sustainable development goals report 2021. UN, New York. https://unstats.un.org/sdgs/report/2021/. Accessed 12 Dec 2021

Wei J, Huang W, Li Z et al (2019) Estimating 1-km-resolution $PM_{2.5}$ concentrations across China using the space-time random forest approach. Remote Sens Environ 231:111221

Yang MX, Lu B (2019) An assessment of mortality and life expectancy for China's provinces: based on the 2010 provincial census data. Popul Res 43(1):18–25 (in Chinese)

SDG 13 Climate Action

6

6.1 Background

Climate change is triggering unpredictable responses on the global land and in the oceans and atmosphere and has a lasting and far-reaching impact on sustainable development and ecological environments (World Meteorological Organization 2022). According to the data released by the EM-DAT international disaster database, disasters and economic losses caused by extreme weather events across the world have increased significantly in the past 20 years. Mitigation of climate change requires all countries to take the most urgent actions to reduce greenhouse gas emissions and increase carbon sinks through forest protection, soil management, and carbon capture (IPCC 2022).

In order to cope with the threats of climate change to the sustainable development of humankind, SDG 13 was established to "take urgent action to combat climate change and its impacts" (hereinafter referred to as "Climate Action"). Targets under this goal include, among others, strengthening resilience to natural disasters, reducing greenhouse gas emissions, and improving education and early warning. China has actively responded to the call for Climate Action by setting its carbon emission reduction and implementing disaster prevention and reduction strategies. Furthermore, in 2022, the Chinese government released the National Climate Change Adaptation Strategy 2035, which proposes to build a climate-resilient society by 2035 by improving climate change monitoring, early warning, and response capabilities.

Currently, among all 17 SDGs, Climate Action suffers the most severe shortage of data (UN 2021). Therefore, this chapter focuses on the four themes of disaster monitoring and reduction, early warning, global land/marine carbon sink estimation, and climate education and describes the use of Big Earth Data methods to generate data products to monitor Climate Action progress and conduct spatiotemporal analysis to support decision-making.

Compared with the previous three annual reports, the big data in this report are of broader scope and spatial scale and with greater relevance to SDG indicators. The progress in China of the four indicators of SDG 13 was assessed, and global-scale disaster and carbon sink data products were generated to make a greater contribution to climate change response and adaptation.

6.2 Main Contributions

This chapter evaluates the progress on two SDG targets, SDG 13.1 and SDG 13.2, using satellite remote sensing, surveying, and statistics through three case studies and provides methods and models for evaluation, and data with spatiotemporal information for SDG 13. The main contributions are as follows (Table 6.1).

H. Guo, *Big Earth Data in Support of the Sustainable Development Goals (2022) - China*,
Sustainable Development Goals Series, https://doi.org/10.1007/978-981-97-4231-8_6

Table 6.1 Case studies and their main contributions

Targets	Cases	Contributions
SDG 13.1 Strengthen resilience and adaptive capacity to climate-related hazards and natural disasters in all countries	Waterlogging and its impacts on wheat seeding and growth in China	**Data product:** Daily soil moisture products that combine observation data from 2,075 automatic soil moisture stations in China and passive microwave remote sensing from 2016 to 2021 **Decision support:** The area of waterlogged cropland in China in 2021 was about 2.6 times the average in previous years. The yield loss can be effectively compensated through fine-scale field management
	Quantitative evaluation of China's disaster prevention and reduction policies under the Climate Action goal	**Data product:** China's disaster prevention and reduction policy dataset **Decision support:** China has developed a full-fledged disaster reduction system using the Sendai Framework
SDG 13.2 Integrate climate change measures into national policies, strategies, and planning	Integrated methane emissions in China	**Data product:** Gridded ($0.1° \times 0.1°$) Chinese CH_4 emission inventory with high spatial resolution **Decision support:** Identify energy activity as the main source of CH_4 to provide a basis for emission reduction

6.3 Case Studies

6.3.1 Waterlogging and Its Impacts on Wheat Seeding and Growth in China

Target: SDG 13.1: Strengthen resilience and adaptive capacity to climate-related hazards and natural disasters in all countries.

6.3.1.1 Background

The influence of waterlogging on crops is second only to drought in China. The occurrence of waterlogging has an important impact on people's lives and the growth and development of crops. From July to December 2021, the precipitation in China was significantly higher than that in previous years. The precipitation in North China and Northeast China reached an observed extreme value, and the precipitation period was concentrated. The duration of waterlogging caused by heavy precipitation is usually longer than the duration of precipitation. Prolonged waterlogging in autumn may result in winter wheat planting failure or delay in sowing, reduced tillering, and poor growth. Therefore, this case makes a detailed analysis of the spatiotemporal distribution of waterlogging and its impacts on winter wheat in China in 2021, so as to provide a scientific basis for disaster prevention and reduction.

6.3.1.2 Data

- Soil moisture data was inversed from Soil Moisture Active and Passive (SMAP) L3 9 km daily soil moisture products from July to September 2016, 2017, 2018, 2020 and from July to December 2021, which were obtained from the National Snow and Ice Data Center (NSIDC).
- The ground observation data of soil moisture were collected from the automatic soil moisture network of the China Meteorological Administration (2075 stations).
- Soil field water capacity data were obtained from the previous calculations of our research group (Wu et al. 2021).
- The cropland data were obtained from China's 0.05° land cover product (1982–2018) released by the National Earth System Science Data Center.
- The winter wheat data were obtained from Sentinel-2 historical images from 2019 to 2021

6.3.1.3 Methods

The extraction method of agricultural waterlogging distribution from 2016 to 2021: Based on the 2075 automatic soil moisture stations in China and SMAP soil moisture products, the high-precision surface soil volume moisture content fusion daily dataset (0–10 cm) of China was produced by using the fusion algorithm model. The accuracy of this dataset was 79% compared with the data of automatic soil moisture stations. Combined with the soil field water capacity data, the soil relative water content was calculated. Waterlogging is considered to occur when the soil relative water content is greater than or equal to 90% for 10 consecutive days (Li et al. 2022). The ratio of total waterlogging days in the study period to the total number of days in the study period was calculated, and the severe distribution area of waterlogging with single waterlogging days greater than 40 was calculated. The area of cropland affected by waterlogging was obtained by superimposing cropland distribution data. At the same time, the statistics of the waterlogging area were calculated. Rice was misjudged as a waterlogged area due to long-term flooding from July to September, so the area of rice was excluded.

The extraction method of winter wheat sown area in 2021: According to the characteristics of a low NDVI value at the seeding stage of winter wheat (mid-September to mid-November), the continuous increase of the NDVI value at the regreening stage of winter wheat (March to mid-April of the next year) and the continuous decline of the NDVI value at the mature harvest stage of winter wheat (late

April to mid-June) and other ground features, the sown area of winter wheat was extracted. Furthermore, the sown area of winter wheat in Shandong was analyzed (Wang et al. 2017). Compared with the statistical yearbook data, the absolute error of the sown area of winter wheat of Shandong in previous years is 4%.

6.3.1.4 Results and Analysis

Spatiotemporal Characteristics of Waterlogging and Its Impacts on Winter Wheat from July to September 2021

During the study period, waterlogging in Northeast China and North China was more serious. Waterlogging mainly occurred in the southwest of Heilongjiang, Hebei, Shandong, and Henan, the middle and lower reaches of the Yangtze River, Sichuan Basin, Jiangsu, and Anhui, among which the largest waterlogging area occurred in the southwest of Heilongjiang, Shandong, and Sichuan Basin, and the longest duration of single waterlogging was more than 40 days. During the study period, the ratio of total waterlogging days to total days was more than 0.8, and the soil was saturated for a long time, resulting in serious waterlogging (Fig. 6.1).

The area of waterlogging was 1.5978×10^6 km^2 from July to September 2021, accounting for about 90% of the total area of cropland, and the area where waterlogging occurred for more than 40 days was 3.06×10^5 km^2. The area of waterlogging in 2021 was significantly higher than that in other years (Fig. 6.2).

The Spatiotemporal Characteristics of Waterlogging and Its Impacts on Crops from October to December 2021

As can be seen from Figs. 6.3 (a) and 6.3 (b), waterlogging mainly occurred in the southeast of Hebei, Shandong, Henan, Jiangsu, Sichuan, and Hubei in 2021. Among them, Shandong, Hubei, and Sichuan had larger waterlogging areas and longer duration.

The area of waterlogging that occurred in the cropland was 8.50×10^5 km^2 from October to December 2021, accounting for 66.7% of the total cropland, and the worst-hit area was 3.79×10^5 km^2. Figure 6.4 shows the area of cropland waterlogging for the provinces that were seriously affected by waterlogging from October to December 2021. Among them, Shandong had the largest waterlogging area, which was about 8.41×10^4 km^2, and the area of waterlogging accounted for 67% of the total cropland. Hubei was seriously affected by waterlogging, and the worst-hit area was 4.71×10^4 km^2.

Effect of Waterlogging on the Sown Area of Winter Wheat (A Case Study in Shandong)

Sentinel-2 satellite data with a spatial resolution of 10 m showed that the sown area of winter wheat in Shandong was 3.73×10^4 km^2 in 2021, accounting for 91.2% of the total sown area in 2020. Waterlogging resulted in a decrease or late sowing of winter wheat in 2021, but the winter wheat production in Shandong still increased steadily. According to the national grain production data released by the National Bureau of Statistics, the total grain production of Shandong in 2022 reached 55 billion kilograms, with an increase of 0.54 billion kilograms compared with the previous year. The total winter wheat production reached 26.41 billion kilograms, with an increase of 45 million kilograms compared with 2021. The main reason is that the government has attached great importance to grain production, increased disaster prevention and reduction measures and the application of high-yield agricultural technologies, continuously increased support for grain production, and improved wheat breeding and cultivation management.

Highlights

- The observation data of 2,075 automatic soil moisture stations in China and SMAP daily soil moisture products were integrated to obtain the high-precision surface soil volume moisture content fusion daily dataset (0–10 cm) with a resolution of 9 km in China.

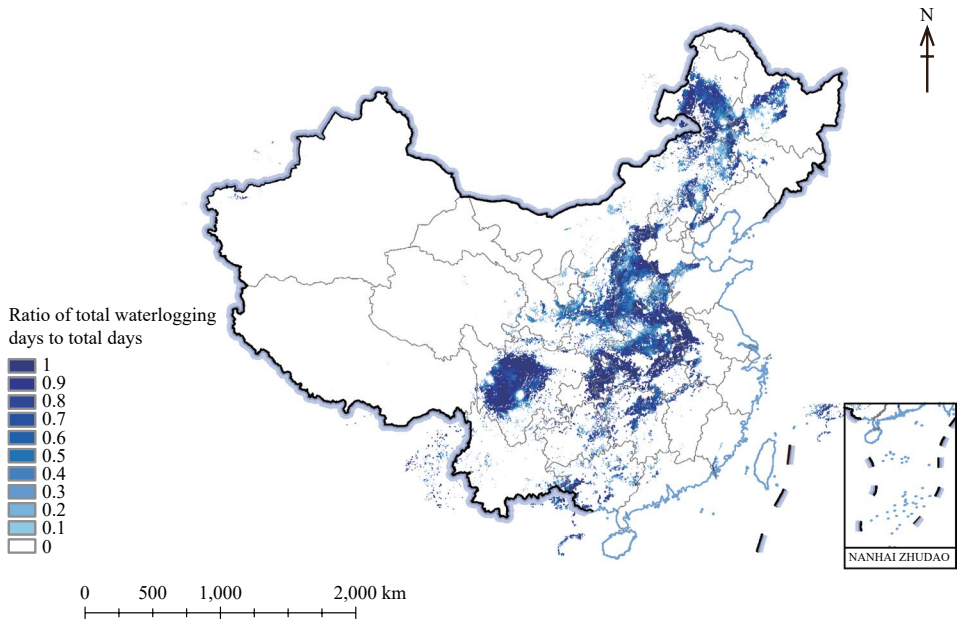

(a) Ratio of total waterlogging days to total days

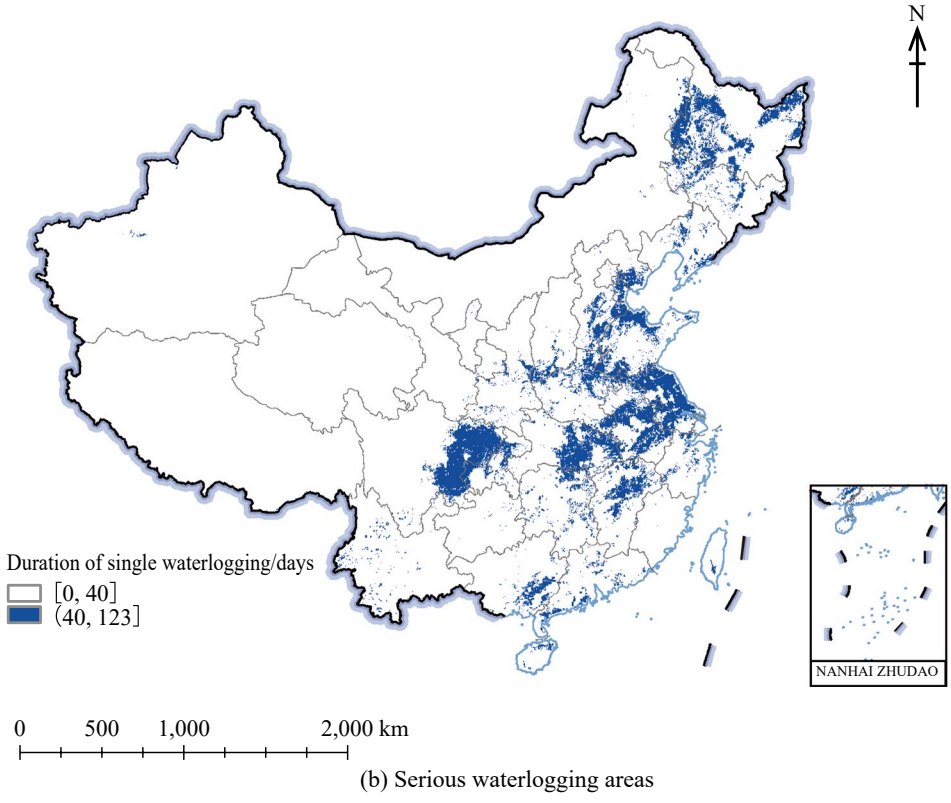

(b) Serious waterlogging areas

Fig. 6.1 Distribution of winter wheat waterlogging from July to September 2021

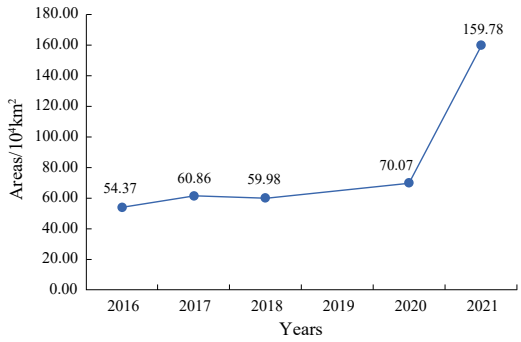

Fig. 6.2 Area of cropland waterlogging in China from July to September from 2016 to 2021

- In view of the serious waterlogging in China in 2021, the occurrence area and degree of waterlogging from July to December 2021 were studied and compared with the waterlogging in 2016, 2017, 2018, and 2020. The results provide a scientific basis for disaster prevention and mitigation of waterlogging.
- The sown area of winter wheat in Shandong in 2021 was about 91.2% of that in 2020.

6.3.1.5 Discussion and Outlook

A high-precision daily dataset of soil moisture in China was developed, with a spatial resolution of 9 km. The monitoring and evaluation technology of waterlogging was developed, and the temporal and spatial distribution of waterlogging in 2021 in China was analyzed to provide technical methods for future waterlogging monitoring. The effect of waterlogging distribution on winter wheat in Shandong in 2021 was analyzed. The results provide important scientific data for the evaluation of SDG 13.1.

6.3.2 Quantitative Evaluation of China's Disaster Prevention and Reduction Policies Under the Climate Action Goal

Target: SDG 13.1: Strengthen resilience and adaptive capacity to climate-related hazards and natural disasters in all countries.

6.3.2.1 Background

In the first two decades of the twenty-first century, the total number of global natural disasters has significantly increased, with a surge in the number of climate-related natural disasters being the main cause. Based on the 2030 Agenda and the global indicator framework for the SDGs, the Sustainable Development Goals Report 2021 includes incomplete data for China in the statistical annex, such as "SDG Indicator13.1.3: Proportion of local governments that adopt and implement local disaster risk reduction strategies in line with national disaster risk reduction strategies", which covers 369 countries (regions) but lacks data for China (as of June 15, 2022).

As a country heavily affected by natural disasters with multiple types and high frequencies, China faces increasing risks of disasters under the backdrop of global warming and extreme weather events. The Chinese government is committed to enhancing the comprehensive disaster prevention and mitigation capacity of the whole of society. It is necessary to timely reflect the strategic-level actions of China in the UN's monitoring indicators, as well as to monitor and evaluate China's disaster prevention and reduction work. This study explores the formulation and calculation of localized indicators for SDG 13.1.2 and SDG 13.1.3, establishes a dataset for China's disaster prevention and reduction policies, grasps the characteristics of China's disaster prevention and reduction policies, and evaluates and monitors China's disaster prevention and reduction strategies in a timely manner, which are of great significance to national disaster prevention, reduction, and relief capacity building.

6.3.2.2 Data

- China's Disaster Prevention and Reduction Policies 2010–2022 (as of May 15, 2022, no data for Hong Kong, Macao, and Taiwan).

6.3.2.3 Methods

To correspond to the SDG indicators, we designed national and provincial policy evaluation indicators for China: national disaster risk

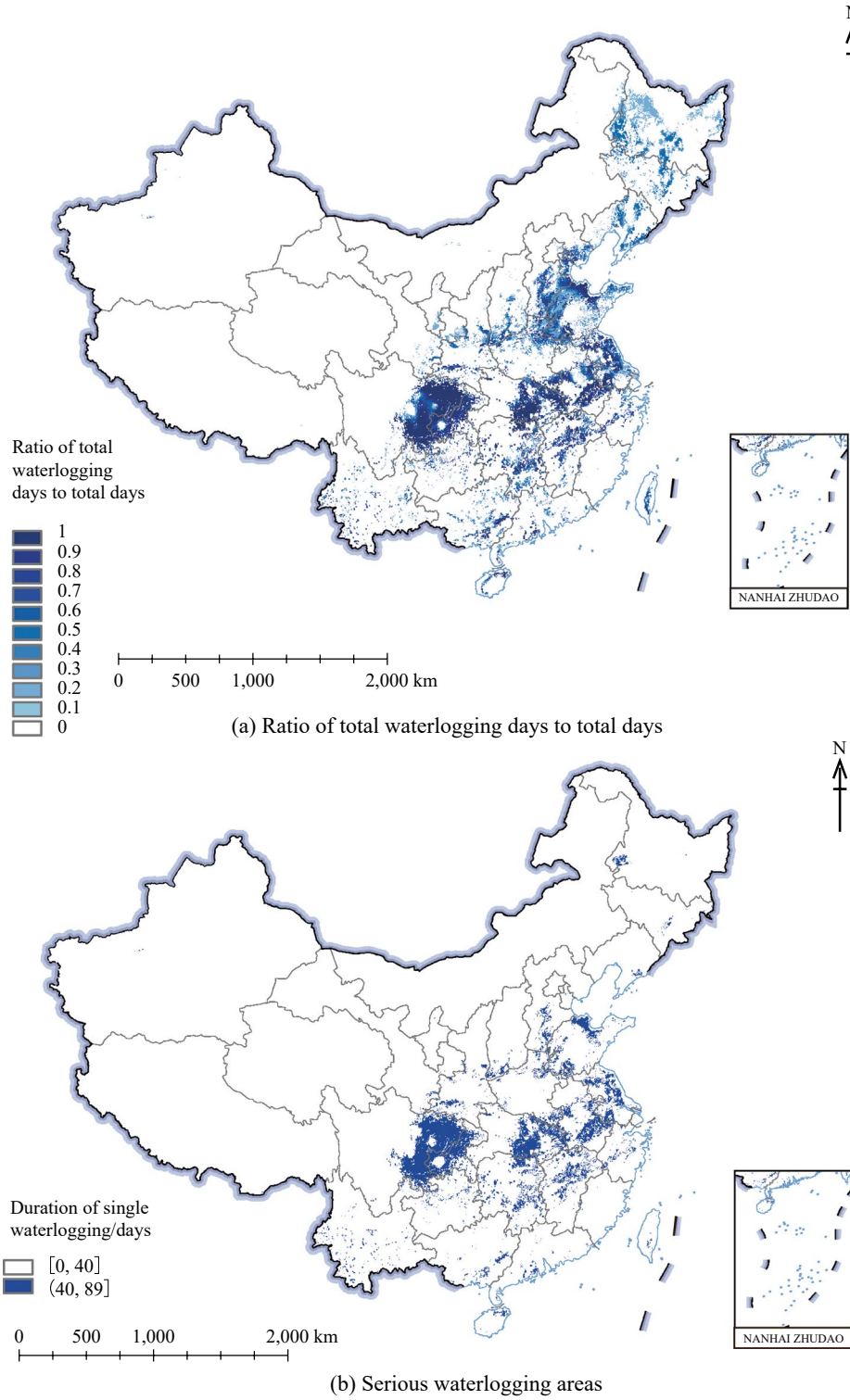

Fig. 6.3 Distribution of winter wheat waterlogging from October to December 2021

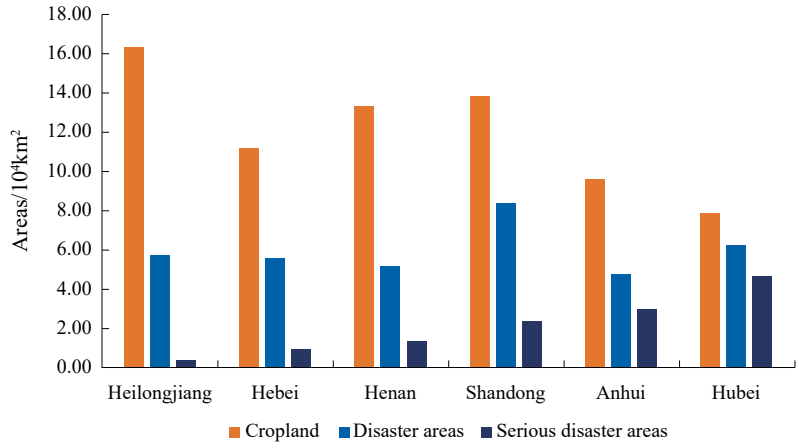

Fig. 6.4 Area of cropland waterlogging for the provinces that were seriously affected by waterlogging from October to December 2021

reduction strategies (SDG 13.1.2) and local disaster risk reduction strategies (SDG 13.1.3).

We collected national and provincial disaster prevention and reduction policies in China and analyzed their spatiotemporal distribution characteristics. Based on the Sendai Framework's four priority action areas and the characteristics of those policies, this study designed four primary indicators, including "enhancing disaster risk awareness", "strengthening disaster risk governance", "improving disaster resilience", and "enhancing disaster preparedness" and 15 sub-indicators. We encoded and classified the strategic planning policies for disaster prevention and reduction strategies, analyzing their content characteristics.

6.3.2.4 Results and Analysis

Spatiotemporal Distribution Characteristics of China's Disaster Prevention and Reduction Policies

From 2010 to 2022, 185 national-level and 909 provincial-level disaster prevention and reduction policies were promulgated in China. In response to the Sendai Framework, the country produced the largest number of national strategies and plans for disaster risk reduction in 2016. By May 15, 2022, China (no data for Hong Kong, Macao, and Taiwan) had adopted relevant strategic plans and local disaster risk reduction strategies in line with the relevant national strategies. Compared with the period from 2010 to 2015, significantly more comprehensive disaster reduction policies were made during 2016–2020.

Content Characteristics of China's Disaster Prevention and Reduction Policies

From 2010 to 2022, national and provincial disaster prevention and reduction policy measures existed in all four priority action areas of the Sendai Framework, with the main focus on enhancing disaster risk awareness and preparedness and measures that correspond to the Sendai Framework's priority areas: understanding disaster risk and enhancing disaster preparedness for effective response and to "Build Back Better" in recovery, rehabilitation, and reconstruction. Compared with the period from 2011 to 2015, China actively promoted the implementation of the Sendai Framework from 2016 to 2020, with particular emphasis on strengthening disaster risk governance and enhancing disaster preparedness. A series of policy measures were formulated, such as enhancing disaster risk management capacity and constructing early warning systems.

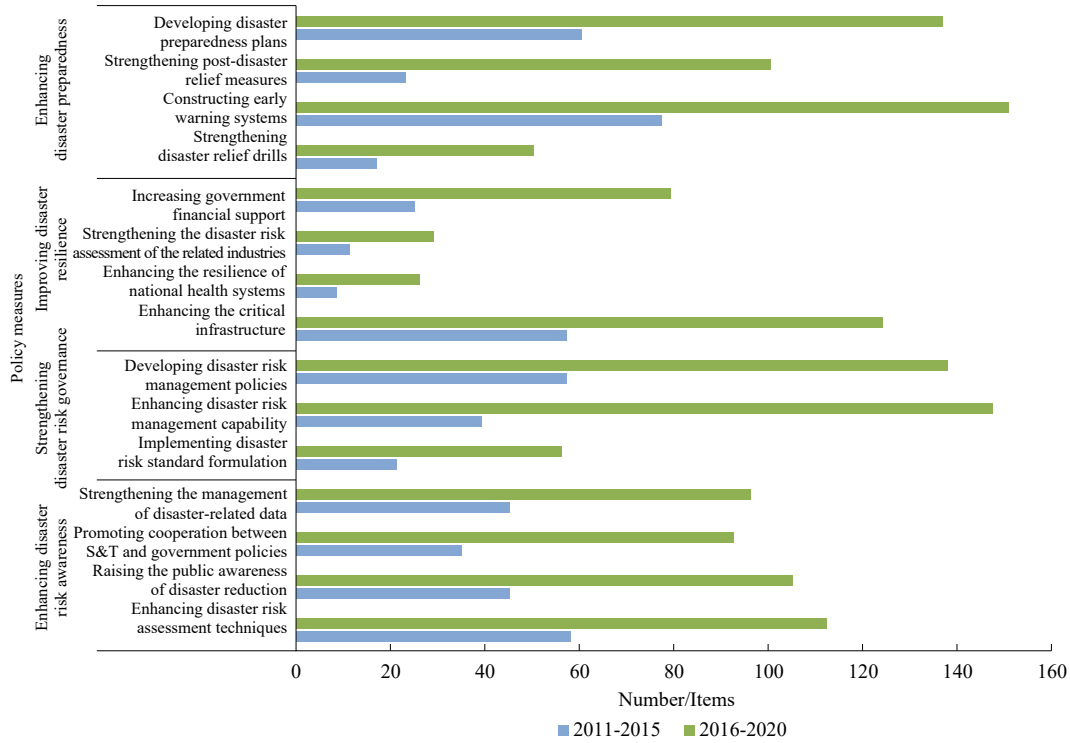

Fig. 6.5 Numbers of disaster prevention and reduction policy measures in China introduced from 2011 to 2015 and from 2016 to 2020

The Chinese strategy for disaster prevention and reduction shifted its stress from post-disaster relief to prevention and preparedness, from targeting a single and specific disaster to comprehensive disaster reduction, and from disaster loss reduction to disaster risk reduction (Fig. 6.5).

Highlights

- This study develops localized measurement and evaluation indicators for China's disaster prevention and reduction policies that are aligned with SDG 13.1.2 and SDG 13.1.3, with the purpose of facilitating the evaluation of China's disaster prevention and mitigation capacity and monitoring processes at the national level.
- This study establishes China's first disaster prevention and reduction policy dataset: China's Disaster Prevention and Reduction Policies 2010–2022.
- Since 2010, China has consistently issued and implemented disaster prevention and reduction strategies, strengthening its ability to resist and adapt to climate-related natural disasters. The country has established a comprehensive national disaster reduction system based on the Sendai Framework, and all provincial governments have adopted and implemented their own disaster risk reduction systems.

6.3.2.5 Discussion and Outlook

This study is oriented to SDG 13.1. Localized evaluation indicators were designed for China's disaster prevention and reduction strategies based on SDG 13.1.2 and SDG 13.1.3, and China's Disaster Prevention and Reduction Policies 2010–2022 were also constructed. Corresponding to SDG 13.1.2, China has been actively implementing disaster risk reduction strategies since the adoption of the Sendai

Framework's indicators. According to SDG 13.1.3, all provincial governments in China have adopted and have been implementing local disaster risk reduction strategies, and a full-fledged disaster reduction system has been built on the basis of the Sendai Framework. In the future, it will be possible to utilize China's remote sensing data to accurately analyze the improvement of disaster prevention and reduction capabilities in various regions.

The indicator design and quantitative evaluation method established in this study can be extended to characteristic analysis in other policy areas that are related to the SDGs, such as climate change.

6.3.3 Integrated Methane Emissions in China

Target: SDG 13.2: Integrate climate change measures into national policies, strategies, and planning.

6.3.3.1 Background

Global warming has led to a series of extreme catastrophic weather, and the significant increase of greenhouse gases in the atmosphere is the most important cause of global warming. CH_4 is one of the most important greenhouse gases, with a high warming effect and strong chemical characteristics. The GOSAT satellite is the world's first satellite dedicated to the observation of greenhouse gas content in the atmosphere and can be used for the real-time monitoring of CH_4 concentration in China and the detection of spatiotemporal changes in the long-term time series. A comprehensive CH_4 emission inventory with high spatial resolution and a monthly time scale can be used to explain the spatiotemporal variability of atmospheric CH_4 concentrations in three dimensions: spatial distribution, temporal variability, and emission source composition. Most of the existing emission inventories are based on the traditional estimation method, which uses national statistics as the main input parameters and cannot reflect the intra-provincial spatial variation and intra-annual temporal variation trends of CH_4 emissions in China.

Therefore, the main content of this case study is based on multi-source remote sensing data. The relationship between CH_4 emission factors and environmental factors is used to improve the traditional estimation methods by incorporating remote sensing data in estimating the comprehensive CH_4 emission inventory in China with high spatiotemporal resolution. In the estimation process, both natural and anthropogenic sources are considered to develop the comprehensive CH_4 emission inventory, which can provide reliable data support for the subsequent study of regional CH_4 balance and atmospheric chemical transport processes. We will develop a comprehensive and detailed CH_4 emission inventory by considering eight emission sources: wetlands (freshwater swamps, peatlands, and salt marshes), vegetation (coniferous forests, broadleaf forests, mixed forests, shrubs, grasslands, and sparse vegetation), rice (double-season rice, single-season rice), ruminants (cattle, sheep, etc.), biomass burning (outdoor and indoor), energy activity (energy extraction processes, fossil fuel combustion), solid waste and wastewater. CH_4 emission inventories quantitatively analyze the spatiotemporal variation characteristics of CH_4 emissions in China, compare them with currently available emission inventories, and discuss and analyze the uncertainties in the estimation process.

6.3.3.2 Data

- Moderate-resolution Imaging Spectroradiometer (MODIS) satellite data: monthly time scale, 0.05° × 0.05° resolution MOD11C3 surface temperature data and MCD12Q1 land cover types.
- Global Precipitation Climatology Project (GPCP): monthly time scale, 2.5° × 2.5° resolution global rainfall data.
- FAO: 10 km × 10 km resolution gridded animal distribution data.
- Global Fire Emissions Database (GFED): monthly time scale, 0.25° × 0.25° resolution NPP and biomass burning data.

- National Earth System Science Data Center: monthly time scale, 1 km × 1 km resolution sunshine hour dataset.
- Remote Sensing Monitoring Dataset of Land Use Status (Paddy Type) and Farmland Maturity at 1 km × 1 km resolution by the Resource and Environment Science and Data Center, CAS.
- 30 arc-seconds × 30 arc-seconds resolution Gridded Population of the World Version 4 (GPWv4) population grid density data.
- 0.1° × 0.1° resolution Emissions Database for Global Atmospheric Research (EDGARv4.3.2) fuel extraction CH_4 emissions.
- China Statistical Yearbook, China Rural Statistical Yearbook, and China Energy Statistical Yearbook.

6.3.3.3 Methods

In this case study, activity data represent the number of individuals emitting CH_4, such as the areas covered by wetlands and rice (m^2), leaf biomass (g), ruminant population (head), energy production [coal (t), oil (t) and natural gas (m^3)], and straw and fuel wood use (t). Activity density (AD) data represent activity data per unit area. The emission factor (EF) indicates the amount of CH_4 emitted per unit of the individual. The monthly AD data and EF data of each emission source are used to estimate CH_4 emissions from wetlands, vegetation, rice, ruminants, biomass burning, energy activity, solid waste, and wastewater sources by remote sensing with high spatiotemporal resolution:

$$E(i,j,t) = \sum_{S}\sum_{C} \mathrm{AD}_{S,C}(i,j,t) \times \mathrm{EF}_{S,C}(i,j,t) \times \left(1 - \mathrm{CF}_{S,C}(i,j,t)\right) \tag{6.1}$$

where i and j denote the image element's horizontal and vertical coordinates, respectively, and t denotes the month; E denotes the CH_4 emissions from the image element (i, j) in the month t; S and C represent each emission source and each emission condition, respectively; AD denotes activity density data (individuals m^{-2}), and EF denotes emission factor data (g CH_4 individual $^{-1}$) (Table 6.2 and Table 6.3); CF represents the recovery rate of CH_4 emissions (for energy activity), oxidation rates (for household waste), or correction factors (for wastewater).

6.3.3.4 Results and Analysis

Estimated CH_4 Emission Inventory in China

Using a combination of MODIS data (MOD11C3, MCD12Q1, and MOD13C2), high spatiotemporal resolution meteorological data (rainfall, sunshine hours), and statistical yearbook data, we estimated multi-source data to obtain the Chinese CH_4 emission inventories from 2015 to 2020 containing the eight emission sources (wetlands, vegetation, rice, ruminants, biomass burning, energy activity, solid waste, and wastewater). The high spatial resolution (0.1° × 0.1°) CH_4 emission inventory (Fig. 6.6) and its statistics (Table 6.4) were obtained for 2020. The next step is to compare the estimated results with the existing emission inventory results, and then the uncertainty of the results will be discussed.

The estimated results show that the total CH_4 emissions in China from 2015 to 2020 were 61.22 Tg, 56.98 Tg, 55.86 Tg, 61.80 Tg, 62.22 Tg, and 64.65 Tg. Energy activity, ruminants, and rice were the main sources of emissions during the period, with average emissions of 19.94 Tg/a, 14.12 Tg/a, and 12.02 Tg/a, respectively. The results of the various CH_4 emission sources estimated in this case are consistent with the EDGAR v5.0 dataset, the People's Republic of China Second Biennial Update Report on Climate Change, and other existing studies. In addition, our estimated CH_4 emissions in China in 2015 are slightly higher than the 2010 emissions estimated by Zhang et al. (2016), indicating that CH_4 emissions in China have shown an increasing trend in recent years, which is consistent with the findings of Du et al. (2018).

Spatiotemporal Distribution Characteristics of CH_4 Emissions in China

The spatial distribution characteristics and temporal variation trends were compared with the

Table 6.2 Parameters related to CH_4 emissions from rice, coal mining, and solid waste disposal in different provinces of China

Provinces	Paddy ER/[kg/(hm^2·d)] (Fu and Yu 2010)			Underground coal mining EF/ (m^3/t) (Peng et al. 2016)	Correction factor for municipal solid waste
	Early	Late	Single-season		
Beijing	—	—	1.26	6.97	0.85
Tianjin	—	—	1.08	—	0.86
Hebei	—	—	1.46	6.97	0.83
Shanxi	—	—	0.63	6.97	0.71
Inner Mongolia	—	—	0.85	5.97	0.78
Liaoning	—	—	0.88	14.4	0.77
Jilin	—	—	0.53	14.4	0.75
Heilongjiang	—	—	0.79	14.4	0.78
Shanghai	1.46	2.75	1.46	—	0.70
Jiangsu	1.89	2.76	1.89	6.22	0.95
Zhejiang	1.69	3.45	1.69	6.22	0.80
Anhui	1.97	2.76	1.97	6.22	0.80
Fujian	0.91	5.26	0.91	6.22	0.81
Jiangxi	1.82	4.58	1.82	6.22	0.77
Shandong	—	—	2.0	6.97	0.85
Henan	—	—	1.7	7.83	0.84
Hubei	2.06	3.9	2.06	7.83	0.80
Hunan	1.73	3.41	1.73	7.83	0.89
Guangdong	1.77	5.16	1.77	7.83	0.89
Guangxi	1.46	4.91	1.46	7.83	0.78
Hainan	1.58	4.94	1.58	—	0.80
Chongqing	0.77	1.85	0.77	21.68	0.91
Sichuan	0.77	1.85	0.77	21.68	0.84
Guizhou	0.6	2.1	0.6	21.68	0.72
Yunnan	0.28	0.76	0.28	—	0.76
Xizang	—	—	0.65	5.97	0.70
Shaanxi	—	—	1.19	5.97	0.70
Gansu	—	—	0.65	5.97	0.78
Qinghai	—	—	—	5.97	0.88
Ningxia	—	—	0.7	5.97	0.77
Xinjiang	—	—	1	5.97	0.70

Note — means no data

remote sensing observation data of atmospheric CH_4 concentration and the estimated monthly CH_4 emission inventories obtained from 2015 to 2020 in China, respectively. The spatiotemporal distribution characteristics of CH_4 emissions from 2015 to 2020 for each source in China by year, the main sources of CH_4 emissions in each province, and the temporal variation trends were analyzed.

Table 6.3 EFs of CH_4 during intestinal fermentation and manure management of different species of livestock in China [Unit: kg/(head·a)]

Temperature		Animals in stock at the end of the year								Slaughter animals		
		Cattle	Cows	Buffalo	Sheep	Pigs	Horses	Donkeys	Camels	Sheep	Cattle	Pigs
Intestinal fermentation		55	68	47	5	1	18	10	46	5	53	1
Manure management	10 °C	1	9	1	0.11	2	1.09	0.6	1.28	0.11	1	2
	11 °C	1	10	1	0.11	2	1.09	0.6	1.28	0.11	1	2
	12 °C	1	10	1	0.11	2	1.09	0.6	1.28	0.11	1	2
	13 °C	1	11	1	0.11	2	1.09	0.6	1.28	0.11	1	2
	14 °C	1	12	1	0.11	2	1.09	0.6	1.28	0.11	1	2
	15 °C	2	13	1	0.16	3	1.64	0.9	1.92	0.16	1.5	3
	16 °C	2	14	1	0.16	3	1.64	0.9	1.92	0.16	1.5	3
	17 °C	2	15	1	0.16	3	1.64	0.9	1.92	0.16	1.5	3
	18 °C	2	16	1	0.16	3	1.64	0.9	1.92	0.16	1.5	3
	19 °C	2	17	1	0.16	4	1.64	0.9	1.92	0.16	1.5	4
	20 °C	2	18	1	0.16	4	1.64	0.9	1.92	0.16	1.5	4
	21 °C	2	20	1	0.16	4	1.64	0.9	1.92	0.16	1.5	4
	22 °C	2	21	1	0.16	5	1.64	0.9	1.92	0.16	1.5	5
	23 °C	2	23	1	0.16	5	1.64	0.9	1.92	0.16	1.5	5
	24 °C	2	24	1	0.16	5	1.64	0.9	1.92	0.16	1.5	5
	25 °C	2	26	1	0.16	6	1.64	0.9	1.92	0.16	1.5	6
	26 °C	2	28	1	0.21	6	2.19	1.2	2.56	0.21	1.5	6
	27 °C	2	31	1	0.21	7	2.19	1.2	2.56	0.21	1.5	7
	28 °C	2	31	1	0.21	7	2.19	1.2	2.56	0.21	1.5	7

Changes in the Spatial Distribution Characteristics of CH_4 Emissions in China

From 2015 to 2020, the spatial distribution characteristics of CH_4 emissions in China changed slowly. Bounded by the Hu Line, the overall spatial distribution pattern of CH_4 emissions in China was high in the southeast and low in the northwest, which was more consistent with the distribution characteristics of population density. CH_4 emissions in the southeast were generally above 4 g/(m^2·a), with the highest CH_4 emissions in Henan, Anhui, and Jiangsu, most of which have exceeded 16 g/(m^2·a); CH_4 emissions in the northwest are generally low, averaging below 1 g/(m^2·a), with only scattered areas of high emissions above 1 g/(m^2·a), which is consistent with the sparse and scattered distribution of population and energy activity in the northwest.

Changes in the Temporal Distribution Characteristics of CH_4 Emissions in China

On the scale of annual average changes in CH_4 emissions, China's CH_4 emissions showed a trend of decreasing and then increasing from 2015 to 2020 (Fig. 6.7), with the lowest in 2017 at 55.86 Tg, where energy activity, rice, and ruminants were the main sources of emissions. CH_4 emissions showed a significant decrease in 2016 and 2017, which was mainly influenced by energy activity and wastewater. Energy activity emissions were mainly related to the significant decrease

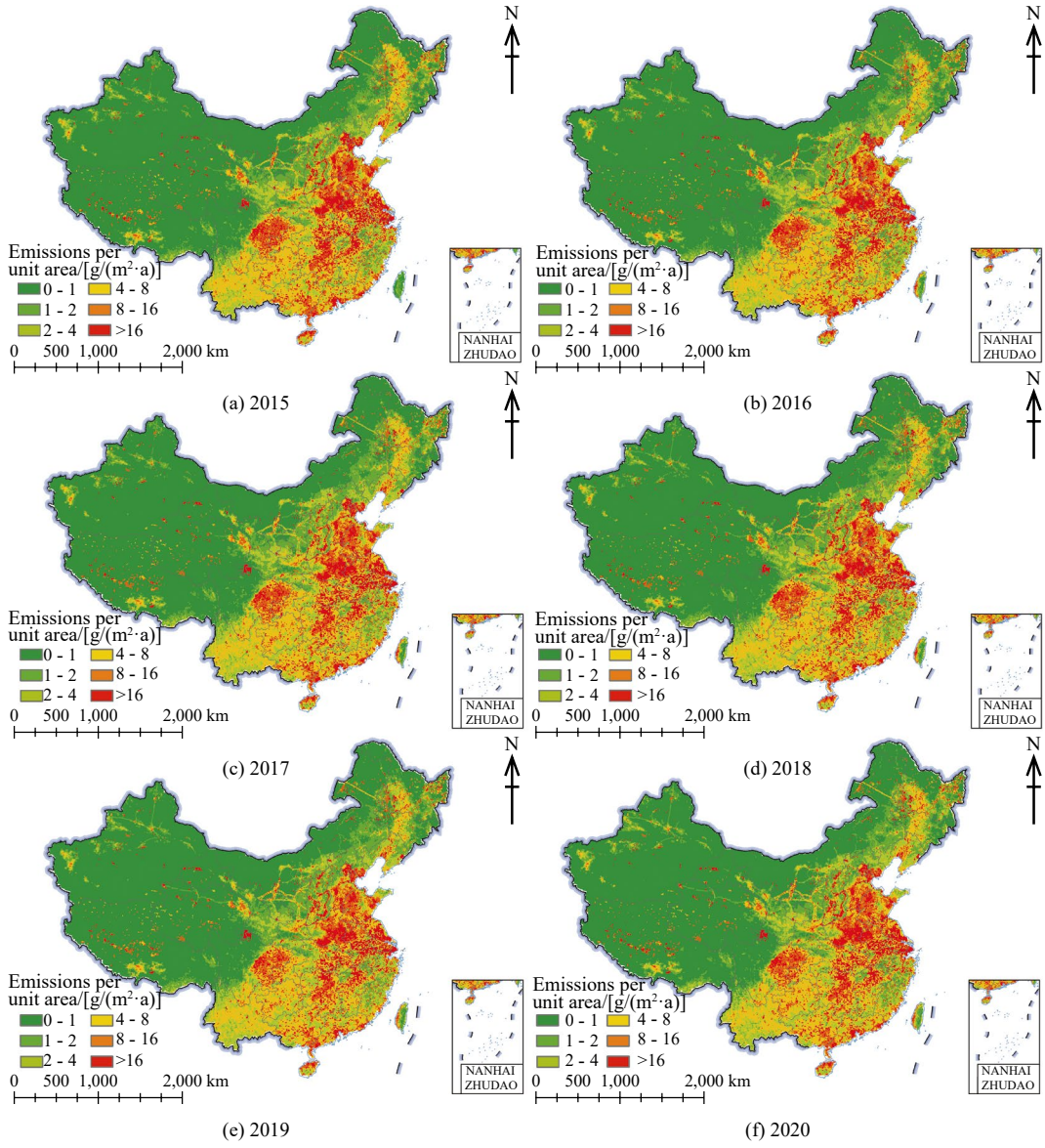

Fig. 6.6 Spatial distribution characteristics of CH_4 emissions in China from 2015 to 2020

in raw coal production in 2016 and 2017 (from 3,746,540,000 t in 2015 to 3,410,600,000 t in 2016 to 3,523,560,000 t in 2017), the decrease in raw coal production is mainly influenced by the structural reform of the supply side in the energy sector in the same period, and the results can indicate that the structural reform of the energy supply side in China was more effective in 2016. As for wastewater CH_4 emission, it is mainly affected by chemical oxygen demand (COD) in wastewater, which was continuously reduced in 2016 and 2017 but surged in 2020, indicating that energy conservation and emission reduction work during the 13th Five-Year Plan is effective but the situation is still severe, and the work of pollution reduction and carbon reduction still cannot be slackened.

From 2015 to 2020, in terms of each emission source, emissions from energy activity first

Table 6.4 Total annual average emissions from the eight CH_4 emission sources in China during 2015–2020 (Unit: Tg)

CH_4 emissions	Years						Average
	2015	2016	2017	2018	2019	2020	
Wetlands	4.13	4.47	4.28	4.31	4.25	4.67	4.35
Vegetation	3.70	3.70	3.72	3.72	3.71	3.71	3.71
Rice	12.16	12.03	11.96	11.95	11.89	12.13	12.02
Ruminants	14.56	14.75	14.62	13.66	13.69	13.41	14.12
Biomass burning	1.39	1.26	1.27	1.21	1.20	1.18	1.25
Energy activity	19.25	16.37	15.53	22.44	22.99	23.05	19.94
Solid waste	2.59	2.74	2.85	2.88	2.86	2.42	2.72
Wastewater	3.44	1.66	1.63	1.63	1.63	4.08	2.34
Total	61.22	56.98	55.86	61.80	62.22	64.65	60.45

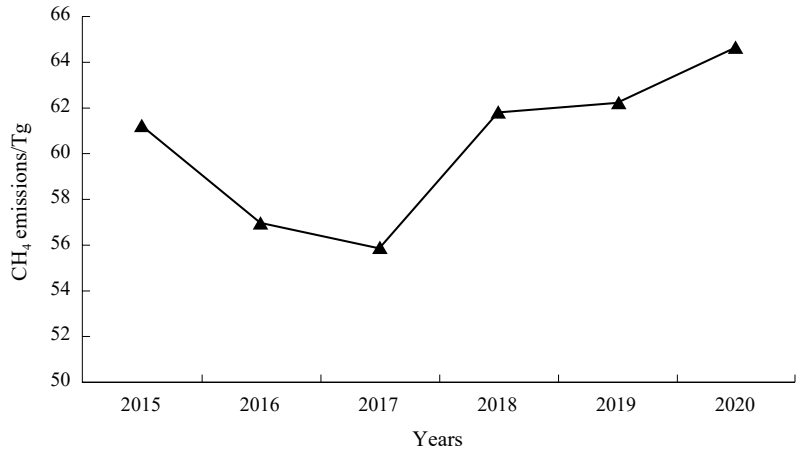

Fig. 6.7 Trends in average CH_4 emissions in China from 2015 to 2020

decreased and then increased, wastewater emissions increased by 128,000 t/a, wetland emissions increased by 108,000 t/a, vegetation emissions increased by 2000 t/a, while reducing emissions by 230,000 t/a for ruminant emissions, 42,000 t/a for biomass burning emissions, and 6000 t/a for rice emissions, respectively. Solid waste emissions were reduced by 34,000 t/a.

In terms of spatial distribution, CH_4 emissions in North China show an increasing trend year by year, mainly due to the increase in emissions from energy activity in Shanxi, Inner Mongolia, Shaanxi, Xinjiang, Henan, and other regions. The decrease in emissions in the south is mainly due to the decrease in emissions from energy activity in Guizhou, Sichuan, Hunan, Zhejiang, Fujian, and other regions.

In the study area, the spatial distribution pattern of the ellipse of CH_4 emissions did not change much from 2015 to 2020, and the center of the ellipse was located in the southwestern part of Henan, with a slight shift toward the northwest [from (111.96°E, 33.24°N) to (111.73°E, 33.71°N)]. This indicates that Henan is the center of high values of CH_4 emissions in the country, which is consistent with the fact that Henan is an important and populous province in China. The azimuth increases from 68.03° to 73.92°, indicating that the share of CH_4 emissions in the southeastern part of China increased year by year (Fig. 6.8).

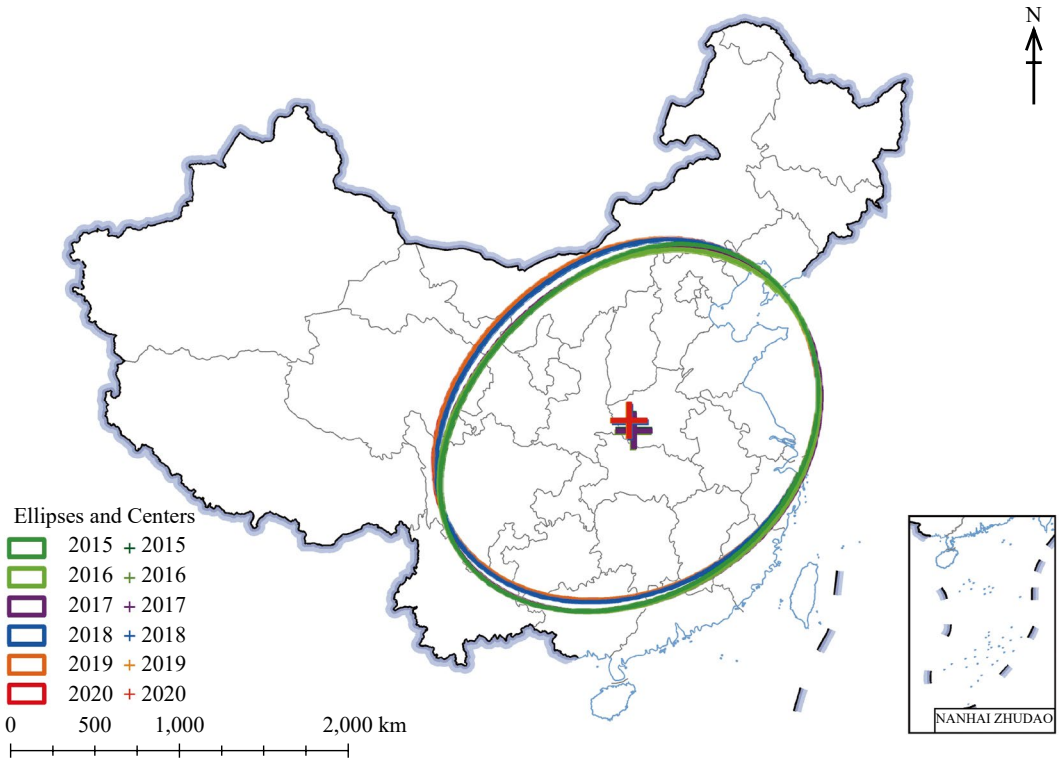

Fig. 6.8 Ellipse distribution of the standard deviation of CH_4 emissions in China for different years from 2015 to 2020

Highlights

- By considering both natural and anthropogenic sources, the integrated and comprehensive CH_4 emission inventory for China was developed, which can provide data support for subsequent studies of regional CH_4 balance and atmospheric chemical transport processes. This case study integrated eight emission sources to develop a comprehensive and detailed CH_4 emission inventory for China, encompassing wetlands (freshwater swamps, peatlands, and salt marshes), vegetation (coniferous forests, broadleaf forests, mixed forests, shrubs, grasslands, and sparse vegetation), rice (double-season rice, single-season rice), ruminants (cattle, cows, buffaloes, sheep, etc.), biomass burning (outdoor and indoor), energy activity (energy extraction processes, fossil fuel combustion), solid waste, and wastewater.
- By combining the obtained gridded (0.1° × 0.1°) Chinese CH_4 emission inventory with high spatial resolution, this case study addressed that the existing inventories cannot truly reflect the spatial variability and seasonal trends of CH_4 emissions. The annual average comprehensive CH_4 emissions in China from 2015 to 2020 were 60.45 Tg. Energy activity, ruminants, and rice are the three major emission sources, with average emissions of 19.94 Tg/a, 14.12 Tg/a, and 12.02 Tg/a, respectively, and the sum of the three is 76.22% of the total emissions. CH_4 emissions in the southeast are generally above 4 g/(m^2·a), with Shandong, Henan, Anhui, and Jiangsu having the highest CH_4 emissions per unit area, with most urban areas in these provinces having exceeded 16 g/(m^2·a); CH_4 emissions in the northwest are generally low and sporadically distributed, averaging less than 1 g/(m^2·a).

6.3.3.5 Discussion and Outlook

This case is based on remote sensing data (MODIS satellite data), high spatiotemporal resolution meteorological data (rainfall, sunshine hours), and statistical yearbook data, and improves the traditional CH_4 emission inventory estimation method, which only relies on the statistical yearbook data. This method has solved the problem that the existing inventories cannot truly reflect the spatial variability and seasonal trends of CH_4 emissions and provided reliable data support for the subsequent study of regional CH_4 balance and atmospheric chemical transport processes.

In addition, in this case, when estimating CH_4 emissions from solid waste, ruminants, energy activity, and other emission sources, monthly data were obtained by averaging because monthly time-scale activity data were not available, so there was no seasonal variation. Future studies can improve this method and include termite, soil, permafrost, and other emission sources to estimate CH_4 emission data that can better reflect the real situation, and also research other estimation methods for CH_4 emission inventories in China to improve the accuracy of CH_4 emission estimation.

6.4 Summary

This chapter focused on the three specific targets of SDG 13 Climate Action and used Big Earth Data to monitor the progress of four indicators of SDG 13 (SDG 13.1.1 Disaster Impact, SDG 13.1.2 National Disaster Reduction Strategy, SDG 13.1.3 Local Disaster Reduction Strategy, and SDG 13.2.2 Greenhouse Gas Emissions) in China, simultaneously developing spatial data products to provide decision-making support for Climate Action.

The research in this chapter indicates the following suggestions:

1. Regarding SDG 13.1.1, SDG 13.1.2, and SDG 13.1.3, research has shown that the impact area of waterlogging in China in extreme years is about 2.6 times that of normal years, and the frequency and intensity of global land heat waves have increased. Although China has established a relatively complete disaster reduction system, the prevention of short-term climate disasters and the early warning of long-term changes cannot be ignored. In the future, it is still necessary to improve disaster resistance, increase technological means, and enhance the ability to withstand more extreme disasters.
2. Regarding SDG 13.2.2, research has shown that China's CH_4 emissions have been fluctuating and increasing in recent years. Energy activity, rice, and ruminants are the main sources of CH_4 emissions in China. Although energy conservation and emission reduction work has achieved great results, the situation remains severe, and there is still no room for slackening in the work of reducing pollution and carbon emissions.

Big Earth Data has shown significant advantages in monitoring the progress of SDG 13 indicators. In the future, it is necessary to explore more greenhouse gas monitoring. Analyzing the education level of climate change and sustainable development through sample surveys may not reflect the true situation of a large education population. In the future, new big data methods need to be explored to obtain more universal samples.

References

Du MX, Zhu QA, Wang XG et al (2018) Estimates and predictions of methane emissions from wastewater in China from 2000 to 2020. Earth's Future 6(2):252–263

IPCC (2022) Climate change 2022: mitigation of climate change. https://www.ipcc.ch/report/ar6/wg3/. 8 Jun 2023

Li MQ, Fang SB, Zhu YC et al (2022) Spatial and temporal distributions of waterlogging disasters in the summer of 2021 in Mainland China and their possible impacts. Nat Remote Sens Bulletin 26(9):1886–1894. https://doi.org/10.11834/jrs.20221782

UN (2021) The sustainable development goals report 2021. UN, New York. https://unstats.un.org/sdgs/report/2021/ 20 Dec 2021

Wang JZ, Tian HF, Wu MQ et al (2017) Rapid mapping of winter wheat in Henan Province. J Geo Inf Sci 19(6):846–853

World Meteorological Organization (2022) State of the global climate 2021. https://public.wmo.int/en/our-mandate/climate/wmo-statement-state-of-global-climate. 6 Jun 2023

Wu D, Li ZH, Zhu YC et al (2021) A new agricultural drought index for monitoring the water stress of winter wheat. Agric Water Manag 244:106599

Zhang B, Yang TR, Chen B et al (2016) China's regional CH_4 emissions: characteristics, interregional transfer and mitigation policies. Appl Energy 184:1184–1195

SDG 14 Life Below Water

7

7.1 Background

Ocean systems are characterized by their large scale, rapid change, and high complexity, making SDG 14 itself a diverse, dynamic, and interconnected system. The effective measurement and monitoring of specific targets is the most important aspect for ensuring the realization of SDG 14. However, there is still difficulty in determining how to measure these targets. Moreover, there is an urgent need to establish scientifically sound and complete data and methodological support systems.

Big Earth Data in the marine field is mainly generated from large marine scientific experimental devices, exploration equipment, remote sensing sensors, socio-economic observations, and computer simulation processes with spatial properties. On one hand, it has the general nature of big data such as being massive, multi-source, heterogeneous, multi-temporal, multi-scale, and non-smooth. On the other hand, it has a strong spatiotemporal and physical correlation among marine elements as well as with data generation methods and sources. Big Earth Data has become a "new key" to our understanding of the ocean and a "new engine" for knowledge discovery. In recent years, Chinese research institutions, universities, and government departments have made great efforts to explore the use of big data and its related technologies and methods to serve the implementation of SDG 14. These institutions have accumulated good practical experience in the production of datasets and construction of assessment models. Following the concept of "innovation, coordination, green, openness, and sharing", this chapter focuses on the three objectives of reducing marine pollution, protecting marine ecosystems, and protecting marine areas. The contents of the chapter include: the fine monitoring of nutrient salinity changes and green tide biomass in China's coastal waters, dynamic monitoring of coastal mudflats, risk assessment of harmful algal blooms (HABs) in the East China Sea, assessment of typhoons in offshore marine wetlands, and the monitoring of the development and utilization of spatial resources in China's coastal zone. We share this experience through typical cases and look forward to jointly promoting the achievement of SDG 14 and building a community with a shared future for humankind.

7.2 Main Contributions

This chapter carries out the monitoring and assessment of indicators related to SDG 14.1, SDG 14.2, and SDG 14.5 in China and its surrounding regions through seven case studies. The main contributions of the chapter are shown in Table 7.1.

H. Guo, *Big Earth Data in Support of the Sustainable Development Goals (2022) - China*,
Sustainable Development Goals Series, https://doi.org/10.1007/978-981-97-4231-8_7

Table 7.1 Case studies and their main contributions

Targets	Tiers	Cases	Contributions
SDG 14.1 By 2025, prevent and significantly reduce marine pollution of all kinds, in particular from land-based activities, including marine debris and nutrient pollution	Tier II	Analysis of long-term variations and trends in nutrient concentrations in the coastal waters of China	**Data product**: Datasets on the field observations of nutrient concentrations in the coastal waters of Eastern China from 1978 to 2019 **Decision support**: Information support for the prevention and control of eutrophication and comprehensive decision-making in the coastal waters of China
		High-precision monitoring of green tide biomass in offshore China through remote sensing	**Data product**: Spatiotemporal datasets of green tide biomass in the Yellow Sea of China **Method and model**: A multi-source remote sensing inversion model of green tide biomass
SDG 14.2 By 2020, sustainably manage and protect marine and coastal ecosystems to avoid significant adverse impacts, including by strengthening their resilience, and take action for their restoration in order to achieve healthy and productive oceans	Tier II	High-precision dynamic monitoring of China's coastal tidal flats	**Data product**: Datasets with a 10 m resolution depicting the spatial distribution of China's coastal tidal flats in 2015 and 2020 **Method and model**: Automated tidal flat extraction using the maximum spectral index composite (MSIC) and Otsu algorithms
		Risk assessment of HABs in the coastal waters of the East China Sea	**Data product**: A dataset containing information on HAB events, commonly referred to as "red tides", in the East China Sea from 1933 to 2017 **Method and model**: A comprehensive HAB disaster risk assessment method was developed that considers the harmfulness of algal blooms and the vulnerability of disaster bearing bodies **Decision support**: This dataset can provide support for the management and disaster mitigation decision-making of HABs in the East China Sea. Additionally, it can offer valuable insights and methods for the risk assessment and management of HAB disasters in other marine regions
		Estimating the economic value of China's coastal wetlands for typhoon protection	**Data product**: Aggregated datasets of typhoon protection values for coastal wetlands in China from 2010–2020 **Method and model**: A linear logarithm environmental economic model for valuing typhoon protection

(continued)

Table 7.1 (continued)

Targets	Tiers	Cases	Contributions
SDG 14.5 By 2020, conserve at least 10 per cent of coastal and marine areas, consistent with national and international law and based on the best available scientific information	Tier I	Dynamic monitoring of the development and utilization of spatial resources in China's coastal zone	**Data product**: Remote sensing monitoring data for the development and utilization of spatial resources in China's coastal zone for the years 2000, 2005, 2010, 2015, and 2020 **Decision support**: Provide information and decision basis for ecological protection and sustainable development and the utilization of spatial resources in the coastal zone
		Dynamic monitoring of China's coastal reclamation and the efforts to return enclosures to the sea and wetlands from 2010 to 2020	**Data product**: Vector data products at a 1:100,000 scale depicting China's coastal reclamation and the return of enclosures to the sea and wetlands during the periods of 2010–2015, 2015–2018, and 2018–2020 **Decision support**: Support the assessment of coastal reclamation control and management effects

7.3 Case Studies

7.3.1 Analysis of Long-Term Variations and Trends in Nutrient Concentrations in the Coastal Waters of China

Target: SDG 14.1: By 2025, prevent and significantly reduce marine pollution of all kinds, in particular from land-based activities, including marine debris and nutrient pollution.

7.3.1.1 Background

Ocean health and sustainable development are the focus of global attention. In response to the growing problems of offshore pollution, the UN has put forward the long-term development goal of safeguarding marine health, protecting and sustainably utilizing ocean and marine resources to promote sustainable development, and preventing and substantially reducing all types of marine pollution by 2025. This also concerns pollution caused by land-based activities, including marine debris pollution and nutrient pollution. The eutrophication of water bodies caused by nitrogen, phosphorus, and other nutrient pollution in estuaries and coastal waters is currently a hot issue and a core research component of some major international programs such as the Land-Ocean Interactions in the Coastal Zone (LOICZ) and Global Ecology and Oceanography of Harmful Algal Blooms (GEOHAB). Nitrogen, phosphorus, and silica nutrients are important biogenic elements in the ocean that are not only the basis of the food chain, but also directly affect the growth and reproduction of marine organisms (Song 2004; Ferreira et al. 2007), which in turn affect the structure and function of the ecosystem (Justić et al. 1995; Yunev et al. 2007). In recent decades, the rapid development of global agriculture and industry has led to major changes in the influx of nutrients into the ocean. This has led to significant changes in the concentration and structure of nutrients and the frequent occurrence of red tides (Anderson et al. 2002; Glibert and Burkholder 2011; Paerl 2006; Yunev et al. 2007), green tides (Liu et al. 2010; Xu et al. 2014b; Zhou et al. 2015), hypoxia (Cai et al. 2011; Kemp et al. 2009; Rabalais et al. 2002, 2014), frequent appearances of jellyfish (Sun 2012; Purcell 2012; Uye 2008; Xian et al. 2005), and other disastrous and abnormal ecological events. As a result, the stability of marine ecosystems is seriously threatened (Tang et al. 2010). Therefore, there is an urgent need to conduct research on the analysis of nutrient concentrations, structural change patterns, and trends under the dual stress of human activity and global climate change in China's coastal waters. This research will provide key theoretical support for the prevention and control of eutrophication as well as ecological and environmental protection.

7.3.1.2 Data

- Continuous-field-observations of NO_3^--N, NO_2^--N, NH_4^+-N, dissolved inorganic phosphorous (DIP), and SiO_3^{2-}-Si in the coastal waters of China from 1978 to 2019. The field observations were obtained from the four seasons in February, May, August, and November of each year from 1978 to 1995, 2013, and 2016. There were field observations for two seasons in winter (January/February) and summer (July/August) in each year from 1996 to 2016. Lastly, there were field observations for at least two seasons in spring, summer, and autumn for each year from 2016 to 2020.
- Statistical data for the total fertilizer application amount, total sewage discharge, sewage treatment rate, and total nitrogen and phosphorus discharge of sewage in China, 1980–2019 (China Statistical Yearbook, 1980–2019, China Environmental Statistical Yearbook, 1999–2019).

7.3.1.3 Methods

In this study, the average values for surface and bottom nutrient concentrations were calculated separately for all stations surveyed in a typical section (Yellow and Bohai Seas) in the Yangtze

River Estuary, South Yellow Sea, and Bohai Sea and for fixed stations in a specific region (the mixing zone of the Yangtze River Estuary). The results were used to represent the surface and bottom nutrient concentrations in the sea at that time. The study used field-measured concentration data for various species of nutrients in the coastal waters of Eastern China to analyze the long-term variations in nutrient concentrations through linear and binomial regression. The statistical data represented the national fertilizer application amount, total sewage discharge, sewage treatment rate, and the total nitrogen and total phosphorus discharge of sewage from 1978 to 2019. The long-term trends in nutrient concentration ratios, N/P and Si/N, were also analyzed and compared with the Redfield ratio.

The study aimed to analyze the influence of various nutrient sources on long-term nutrient changes in the study area. To accomplish this, this study used the Integrated Model to Assess the Global Environment-Global Nutrient Model (IMAGE-GNM) with a spatial resolution of 0.5 by 0.5 degrees. This model was used to comprehensively analyze the total amount of nitrogen and phosphorus in China's coastal waters introduced by external sources, including river input, atmospheric deposition, and mariculture input, and assessed their long-term variations (Wang et al. 2020). The model inputs included land cover and climate change data from the Integrated Model to Assess the Global Environment (IMAGE) model (Stehfest et al. 2014) and hydrological data from the PCRaster Global Water Balance (PCR-GLOBWB) model, including runoff volume, surface water area (SWA), water body type (e.g., rivers, lakes, reservoirs, etc.), water body coverage area, water depth, and water transportation time for different locations in the basin (van Beek et al. 2011). In addition, the IMAGE-GNM aquaculture nutrient budget model was used to estimate the total nitrogen and phosphorus fluxes released from mariculture activities in the sea. Mariculture production data was obtained from the Fisheries Statistics (FishStat) database for the period of 1970–2010 and was used as the input value for estimation. The values were calculated based on the live weight of each aquaculture population in different aquatic environments in the seas of a country or region (FAO 2012). NH_3 and NO_x emission data was obtained from the EDGAR database for the period of 1970–2010 and was used as input values for the TM5-FAst Scenario Screening Tool (TM5-FASST) model to simulate atmospheric nitrogen deposition concentrations in the South Yellow Sea. The nitrogen flux input in the South Yellow Sea was estimated through atmospheric deposition (EDGAR 2019). The distribution of global atmospheric phosphorus deposition concentrations in the South Yellow Sea area was simulated by previous models using the Community Atmospheric Model 4.0 (CAM4) and climate-ocean-wind field coupling model.

7.3.1.4 Results and Analysis

The Nutrient Concentrations in the Coastal Waters of Eastern China Decreased Significantly over the Recent Decade

There were significant differences in the long-term variations and trends of different nutrients in different seas due to their unique sources and controlling factors (Wei et al. 2015; Yang et al. 2018; Wang et al. 2018, 2022; Liu et al. 2022c). On the spatial scale, each nutrient had a significantly higher concentration at the bottom of the sea than on the surface. Additionally, the nearshore area had a higher nutrient concentration than the offshore area, and high concentration values were mainly located in river estuaries. On the seasonal scale, the nutrient concentrations were higher in winter than in summer, which was mainly due to the uptake by phytoplankton. The variation trends of dissolved inorganic nitrogen (DIN) concentrations in the South Yellow Sea and Yangtze River Estuary showed an inflection point over the course of long time scales and shifted from a continuous increase to decrease in value. However, the timing of the inflection point for DIN concentrations differed due to the different sources and controlling factors in various sea areas (Figs. 7.1

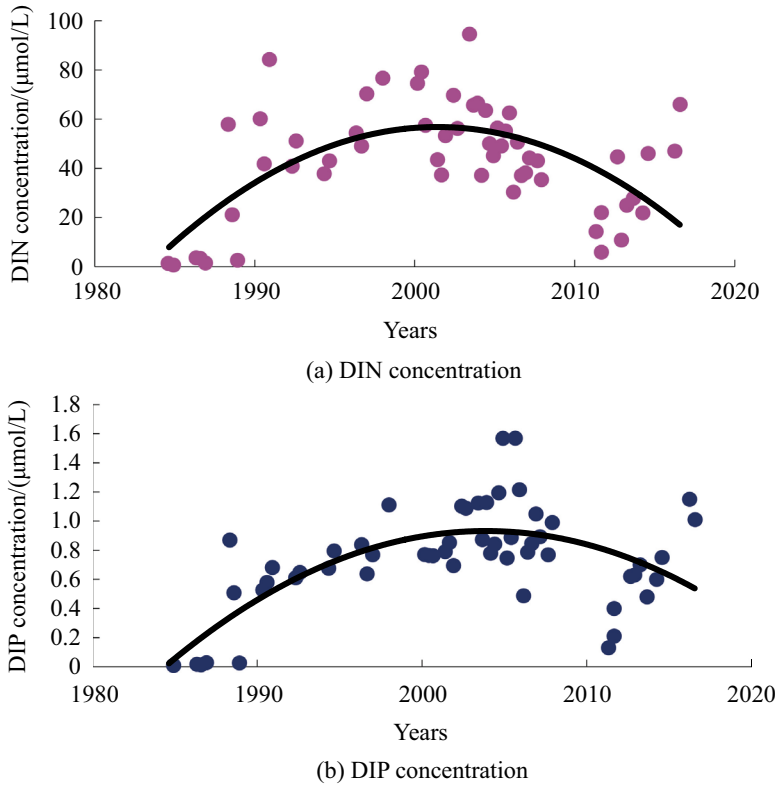

Fig. 7.1 Long-term changes of DIN and DIP in the Yangtze River Estuary

and 7.2). For example, the DIN concentration in the Yangtze River Estuary was mainly affected by input from the Yangtze River, leading to the inflection point for DIN to occur in 2003 (Fig. 7.1). The South Yellow Sea was mainly affected by the input from terrestrial point and non-point sources, leading to the inflection point for the DIN concentration to occur in 2006 (Fig. 7.2). The overall DIP concentration in China's offshore area was observed to be at a low level, and there were significant interannual variations in DIP and silicate with different interannual trends in different sea areas. The DIP concentration in the Yangtze River Estuary showed a long-term trend that first increased and then decreased, while the DIP concentration in the South Yellow Sea showed a long-term fluctuating trend. However, the DIP and silicate nutrient concentrations were observed to decrease significantly in the coastal waters of Eastern China since 2006. The concentrations of DIN, DIP, and silicate were observed to be significantly higher at the bottom of the South Yellow Sea than on the surface. The DIN concentrations on the surface and at the bottom of the South Yellow Sea were found to continuously increase from the 1970s to 2006. The change in concentration reached an inflection point after 2006, shifting from a continuous increase to a decrease in value, with the concentration significantly decreasing in 2006. The DIP concentration generally showed a decreasing trend on the surface, while the concentration at the bottom showed a fluctuating increasing trend from the 1970s to the early 1990s and a decreasing trend after the mid-1990s. The silicate concentrations on the surface and at the bottom of the sea decreased significantly from the 1970s to the end of the 1980s and then slowly increased. The concentrations decreased significantly

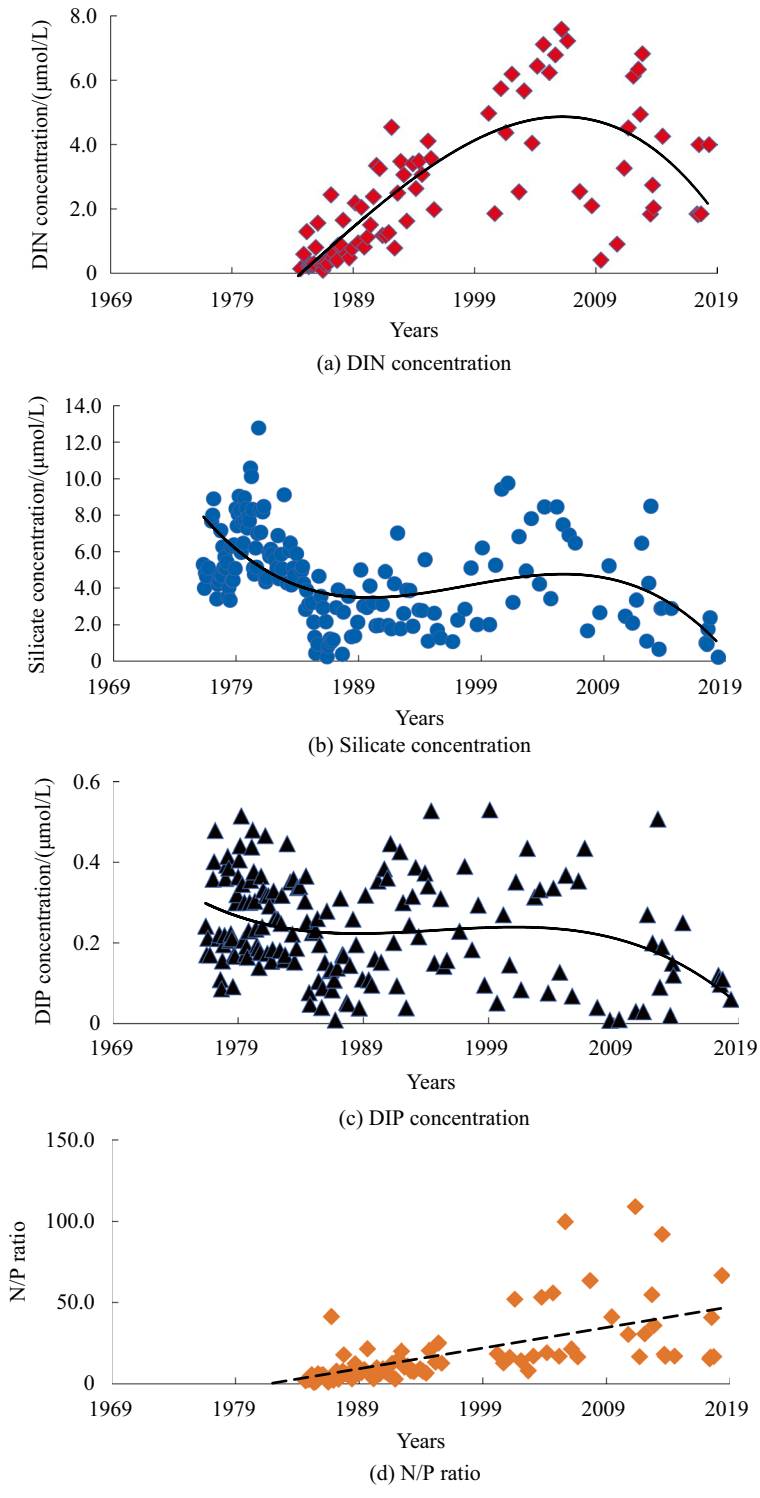

Fig. 7.2 Long-term variations in nutrient concentrations in the South Yellow Sea

after the beginning of the twenty-first century. The N/P ratio increased significantly from the early 1980s to 2006, while the surface N/P ratio began to slightly decrease after 2006. The bottom N/P ratio also showed a decreasing trend after 2011 with significant seasonal variations. The N/P ratio was significantly higher than the Redfield (16:1) ratio after the twenty-first century. The Si/N ratio decreased significantly from the 1980s to 1990s, and has remained low since then. DIN concentrations and N/P ratios have continued to increase in recent decades, while Si/N ratios have been decreasing. In the South Yellow, there was an evolutionary trend resulting in the shift from a nitrogen limitation to potential phosphorus and silicon limitations. Moreover, the nutrient structure deviates from the Redfield ratio, which will inevitably have a significant impact on the dominant species of phytoplankton, and thus affect the structure and function of the ecosystem.

The Reduction in Terrestrial Nitrogen and Phosphorus Inputs Were the Main Cause of the Decrease in Nitrogen and Phosphorus Concentrations in China's Coastal Waters

The study used the IMAGE-GNM model to conduct a comprehensive analysis of the total nitrogen and total phosphorus contributions from external sources, including inputs from rivers and atmospheric deposition and mariculture. Their long-term variations show that the concentration and structure of nutrients in China's coastal waters were highly correlated with terrestrial inputs, and river inputs were the most important among all external sources. The contributions from aquaculture were observed to initially grow at an accelerating rate, but have now declined in recent decades. The inputs from atmospheric deposition and their total nitrogen fluxes have continued to grow. Mariculture was observed to have a lower contribution, but it is currently growing rapidly. In the case of DIN and DIP flux from the river to the sea, natural sources remained unchanged, and the application of agricultural fertilizers and sewage discharge were the most important input sources. The flux in nitrogen and phosphorus from Chinese rivers also changed significantly. The field-measured data from the Yangtze River verified that the decrease in nitrogen and phosphorous inputs from the Yangtze River were consistent with decreasing concentrations of DIN and DIP in China's coastal waters, thus justifying the foregoing analysis. The Chinese government has always attached great importance to the protection and construction of ecological environments, especially over the past decade. China has followed the concept of green development and achieved certain reductions in the application of chemical fertilizer and a slowed increase in sewage discharge. However, there has been a rapid development in the number of sewage treatment plants and auxiliary treatment facilities. In China, the number of sewage treatment plants increased from 80 in 1990 to 6,910 in 2015, and the sewage treatment rate significantly increased from 14% in 1990 to more than 95% in 2018 (Fig. 7.3(a)). The establishment of sewage treatment plants and the significant improvement in the sewage treatment rate have led to a significant reduction in the total nitrogen and phosphorus discharge within sewage. In 2016, the total national nitrogen and phosphorus discharge from sewage decreased by 1/2 and 4/5 respectively compared to 2015, and the total discharge from sewage has remained relatively low and stable since 2016 (Fig. 7.3(b)).

Highlights

- The study analyzed the long-term variation in nutrients and their controlling factors in the Yangtze River Estuary and South Yellow Sea since 1978. The variation in DIN concentrations were found to have an inflection point in the Yangtze River Estuary, South Yellow Sea, and Bohai Sea, which changed from a continuous increase to decrease. DIP and silicate concentrations decreased over the past decade, which was mainly caused by the reduction in terrestrial nitrogen and phosphorus inputs.

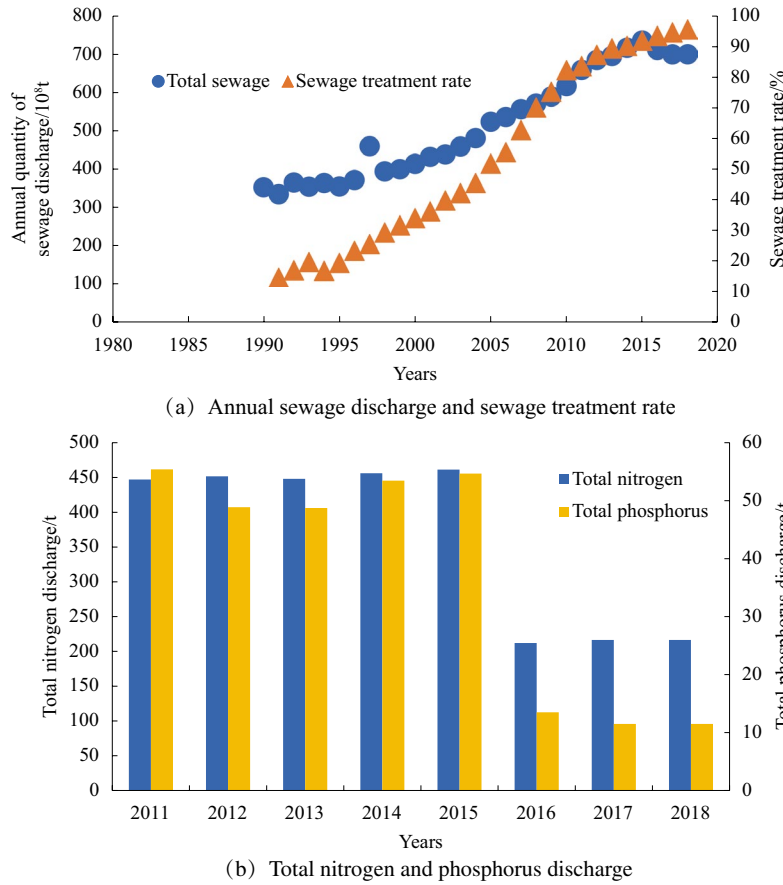

Fig. 7.3 Interannual variations in China's annual quantity sewage discharge, sewage treatment rate, and total nitrogen and phosphorus discharge

7.3.1.5 Discussion and Outlook

The concentration and structure of nutrients in China's coastal waters were highly correlated with terrestrial inputs, while the nitrogen and phosphorus inputs from terrestrial sources mainly depended on agricultural activities and sewage discharge. Nutrient concentrations, mainly DIN, shifted from a continuous increase to decrease in China's coastal waters with notable inflection points. China has achieved remarkable results in environmental protection. The application of fertilizer has been slightly reduced in recent years, while sewage discharge, although still increasing, has slowed down, and the sewage treatment rate has reached over 95%. Therefore, there is a low possibility for the further increase in nutrient inputs into the sea from anthropogenic activities. Additionally, there is a low possibility that nitrogen and phosphorus, especially DIN, will increase in coastal waters. However, the phosphorus limitation may intensify due to the low concentration of phosphorus in China's offshore areas, which is alarming.

The interannual variation in nutrient concentrations, compositions, and sources in China's coastal waters are an essential element for the growth and reproduction of phytoplankton and macroalgae. These factors will inevitably have an important impact on the dominant species and community structure of phytoplankton, which could lead to ecological disasters such as

red tides, green tides, and hypoxia. Their relationships need to be further studied. Further development of this scientific problem requires more relevant data that must be obtained through improved observation methods and continuous long-term field investigations, as well as through further studies that use interdisciplinary approaches and ecosystem dynamics models.

7.3.2 High-Precision Monitoring of Green Tide Biomass in Offshore China Through Remote Sensing

Target: SDG 14.2: By 2020, sustainably manage and protect marine and coastal ecosystems to avoid significant adverse impacts, including by strengthening their resilience, and take action for their restoration in order to achieve healthy and productive oceans.

7.3.2.1 Background

The occurrence of large-scale green tides in China's Yellow Sea has caused serious damage to the marine and coastal ecological environment, aquaculture, and tourism since 2007, and has become a critical eco-environmental problem in the seas around China (Hu 2009; Liu et al. 2010; Xing et al. 2015; Qi et al. 2016; Li et al. 2018). Satellite remote sensing data can provide optimal technical support for the spatiotemporal dynamic monitoring of green tides (Qi et al. 2016; Hu et al. 2017, 2019, 2023; Xing et al. 2019). MODIS, onboard the Terra/Aqua satellites, can provide data that has large coverage and a high temporal resolution. However, the data is insufficient for precise monitoring due to its 250 m spatial resolution. Haiyang-1C/1D (HY-1C/1D) are China's first operational ocean-color satellites. The onboard coastal zone imager (CZI) can provide multi-spectral data that has high spatial (50 m) and temporal (twice in three days) resolutions for monitoring the marine ecological environment, assisting with preventing and reducing marine disasters and maintaining marine rights and interests (Liu et al. 2022b, 2023). Based on HY-1C/1D CZI data from 2019 to 2021, a green tide identification and extraction method was developed for the China Seas under a complex sea surface background using high spatial resolution imagery. The green tide biomass estimates obtained from CZI were cross-validated using optical remote sensing data with different spatial resolutions. The results can clarify the response characteristics of the size of floating algae patches using data with different spatial resolutions. This can reduce uncertainty in the estimation of algae area caused by differences in spatial resolution and can significantly improve the monitoring of green tides in the China Seas. Furthermore, the results can provide theoretical support and advanced applications for the dynamic monitoring of marine floating algae in China and in global seas.

7.3.2.2 Data

- Experimentally simulated spectral dataset of green tide biomass in the China Seas.
- MODIS reflectance products for the 2015–2021 period.
- HY-1C/1D CZI reflectance products for the 2019–2021 period.
- Sentinel-2 multi-spectral instrument (MSI) reflectance products for 2021.

7.3.2.3 Methods

Green Tide Extraction Algorithm for High Spatial Resolution Data in the China Seas

A floating algae identification and extraction algorithm combining the scaled algae (SAI) and virtual baseline (VB) indexes was developed for high-resolution optical remote sensing data, such that from HY-1C/1D CZI (Keesing et al. 2011; Garcia et al. 2013; Xing and Hu 2016). This algorithm is applicable for satellite data lacking the short-wavelength infrared (SWIR) band. The algae signal is enhanced by the VB

index, and the complex sea surface interference information in high spatial resolution data can be effectively removed using SAI. As a result, floating algae can be identified and extracted with high precision. The algorithm has shown good computational and operational efficiency, satisfying the demand for the operational monitoring of floating algae in the China Seas using national autonomous satellites (Liu et al. 2022a).

Remote Sensing Estimation Models of Green Tide Biomass Based on Experimental Observation Data

The modeling analysis of green tide biomass estimation was based on simulation experiments and observation-validation data. The analysis was carried out for different satellite optical loads with consideration of sensor parameters and imaging processes. This model is applicable for MSI, CZI, and MODIS data and was cross-validated with quasi-synchronous multi-source satellite data.

Estimation and Validation of Green Tide Biomass Based on Multi-source Satellite Remote Sensing Data

MSI, CZI, and MODIS optical remote sensing data were preprocessed to produce Rayleigh-corrected reflectance (R_{rc}) products. The resulting data was used for the identification and extraction of green tides, and the production of the spatiotemporal distribution datasets of green tides for the China Seas. Based on this, VB index images were produced and processed through the SAI algorithm, and remote sensing estimation models were used for the estimation of green tide biomass based on different satellite optical data (Fig. 7.4). Finally, the estimation results were cross-validated with the quasi-synchronous MSI, CZI, and MODIS green tide biomass products.

7.3.2.4 Results and Analysis

Differences in the Green Tide Parameters for Multi-source Satellite Remote Sensing Data

A set of quasi-synchronous MSI, CZI, and MODIS data with 10 m, 50 m, and 250 m resolutions, respectively, were used for identifying, extracting, and estimating green tide biomass. The conclusions are provided as follows. (1) The results from the identification and extraction of green tide from multi-source satellite remote sensing data were different in algae pixel areas due to the differences in spatial resolution. The sizes of the green tide pixel areas were 349.7 km^2, 621.7 km^2, and 884.7 km^2, respectively. (2) The inversion of green tide coverage areas reduced the spatial scale differences of pixel areas, and the sizes of the estimated green tide coverage areas were 154.5 km^2, 179.3 km^2, and 188.6 km^2, respectively. Furthermore, the uncertainty caused by different spatial resolutions was also significantly reduced. (3) The green tide biomass for large patches of co-detectable green tides estimated based on MSI, CZI, and MODIS data were 369.9 kilotons, 362.0 kilotons, and 352.6 kilotons, respectively, which further reduced uncertainty (Fig. 7.5).

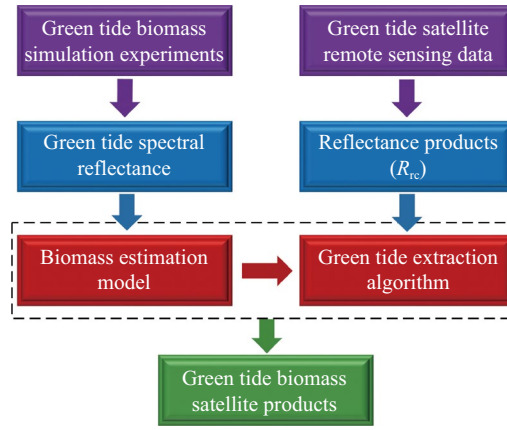

Fig. 7.4 Technology roadmap for satellite remote sensing estimation of green tide biomass in the China Seas

Cross-Validation of Green Tide Biomass Estimation Using Multi-source Satellite Remote Sensing Data

The cross-validation of coverage areas and green tide biomass was performed using the quasi-synchronous MSI, CZI, and MODIS data and 10 km × 10 km grids. The inversion results from the MSI data were used as the true value

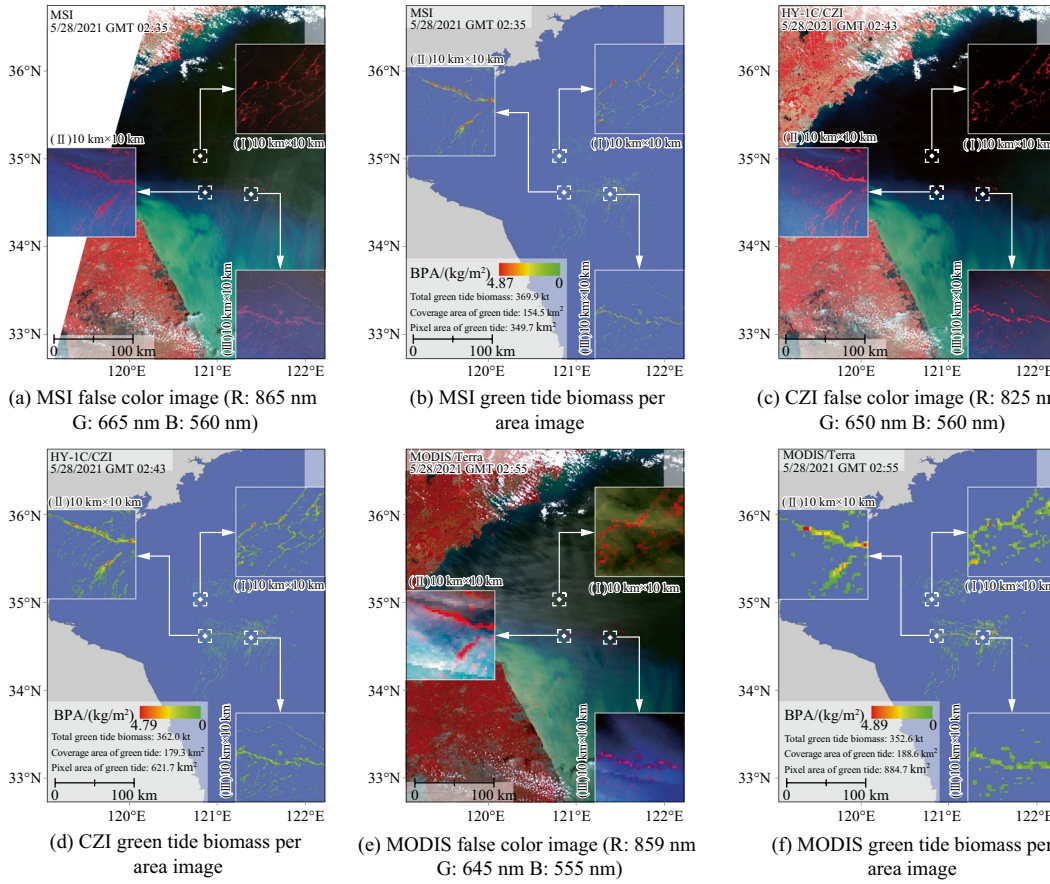

(a) MSI false color image (R: 865 nm G: 665 nm B: 560 nm)

(b) MSI green tide biomass per area image

(c) CZI false color image (R: 825 nm G: 650 nm B: 560 nm)

(d) CZI green tide biomass per area image

(e) MODIS false color image (R: 859 nm G: 645 nm B: 555 nm)

(f) MODIS green tide biomass per area image

Fig. 7.5 Area and biomass estimation of co-detectable green tides in the China Seas based on the quasi-synchronous MSI, CZI, and MODIS data

(the grid statistics for green tides within the white box in Fig. 7.5). The results are as follows. (1) The lower spatial resolution caused higher uncertainties in green tide coverage areas in comparison with the 10 m spatial resolution MSI data. The green tide coverage areas for CZI and MODIS data were overestimated by 15% and 28%, respectively, and the uncertainty of CZI estimation was about one-third of that of MODIS. (2) The green tide biomass estimation based on MSI, CZI, and MODIS data showed a good consistency for co-detectable green tides. The uncertainty for the CZI and MODIS biomass estimation results was about 2% and 7%, respectively, but the uncertainty for MODIS was about three times that of CZI (Fig. 7.6).

Spatiotemporal Distribution of Green Tide Biomass and Its Variation in the China Seas

Based on CZI and MODIS data, the same-day spatiotemporal distribution and variation in green tide biomass in the China Seas showed additional variation in the coverage area and biomass. This was caused by the spatial differentiation of small floating algae patches. Some floating algal patches were too small to be detected by MODIS but could be detected by CZI. In such cases, CZI featured higher estimation results for the green tide coverage area and biomass in comparison to MODIS. This situation displays CZI's strong ability for monitoring green tide patches (Fig. 7.7).

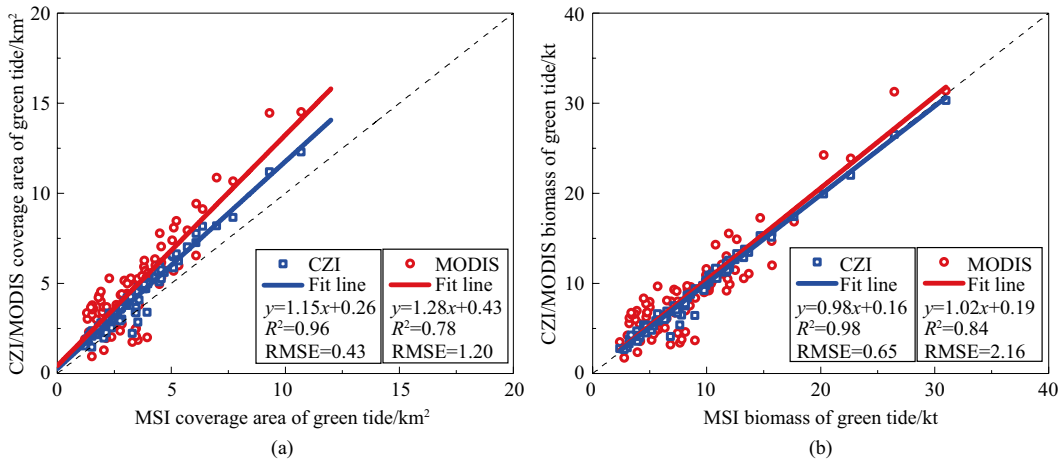

Fig. 7.6 Cross-validation of green tide coverage area and biomass for quasi-synchronous CZI and MODIS data using MSI inversion results as true values

The green tide biomass dataset for 2021 was produced using CZI and MODIS data. The study examined the changes in the green tide coverage area and biomass per area in the China Seas in 2021 (Fig. 7.8). Since CZI has the advantage of higher spatial resolution data in comparison to MODIS, it can provide more accurate green tide coverage areas and biomass parameters, eliminating the uncertainty caused by the overestimation of green tide pixel areas and the omission of small green tide patches by low spatial resolution data. After July 10, 2021, the CZI data showed a greater detection efficiency compared to MODIS data due to its advantage in detecting small green tide patches, indicating that the CZI data was more accurate in monitoring the outbreak and extinction processes of algae.

Highlights

- A method was introduced for estimating green tide biomass using optical remote sensing data. An estimation model was developed for green tide biomass using different optical remote sensing data, which realized the high spatial resolution optical estimation of green tide biomass. The model further clarified the spatial scale differences of algae pixel areas on different satellite images and improved the monitoring and estimation of green tides in the China Seas.
- The study covered temporal and spatial monitoring of varying green tide biomass in the China Seas. Based on multi-source time-series satellite data, green tide monitoring has developed from focusing on the coverage area to biomass estimation. The high-precision green tide biomass data can provide reliable technical support for the monitoring, analysis, and sustainable management of green tides in the China Seas.
- The study demonstrated the application efficiency of China's ocean-color satellites. The CZI onboard China's HY-1C/1D satellites have shown remarkable performance in area monitoring and biomass estimation of offshore floating macroalgae. These platforms can provide quantitative and operational application data with high precision and effectively improve the efficiency of China's satellites in serving SDGs.

7.3.2.5 Discussion and Outlook

National Ocean-Color Satellites Show Fine Monitoring Capability

The CZI sensor onboard China's national ocean-color satellites features a high signal-to-noise

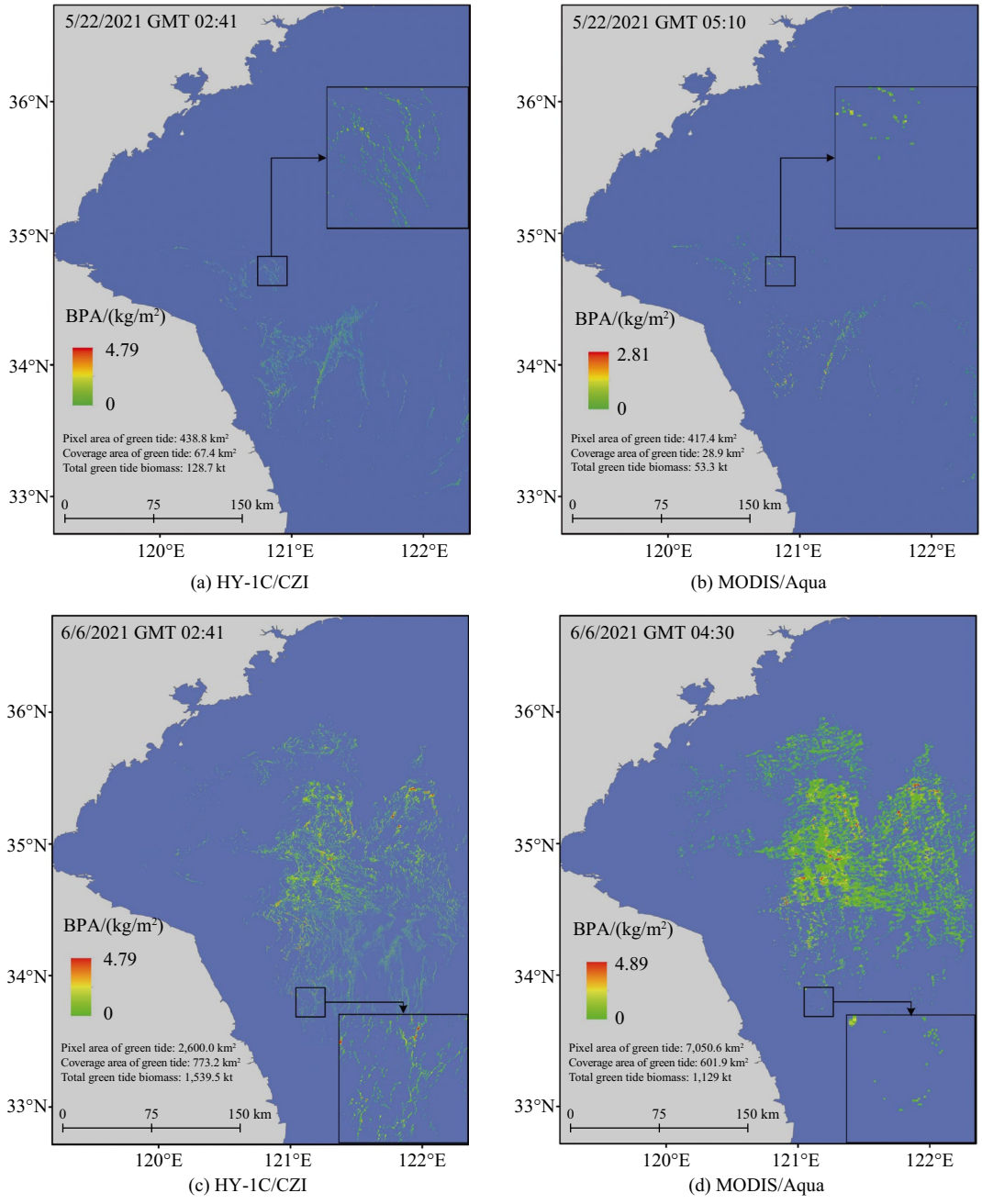

Fig. 7.7 Spatiotemporal distribution of green tide biomass per area in the China Seas based on CZI and MODIS data

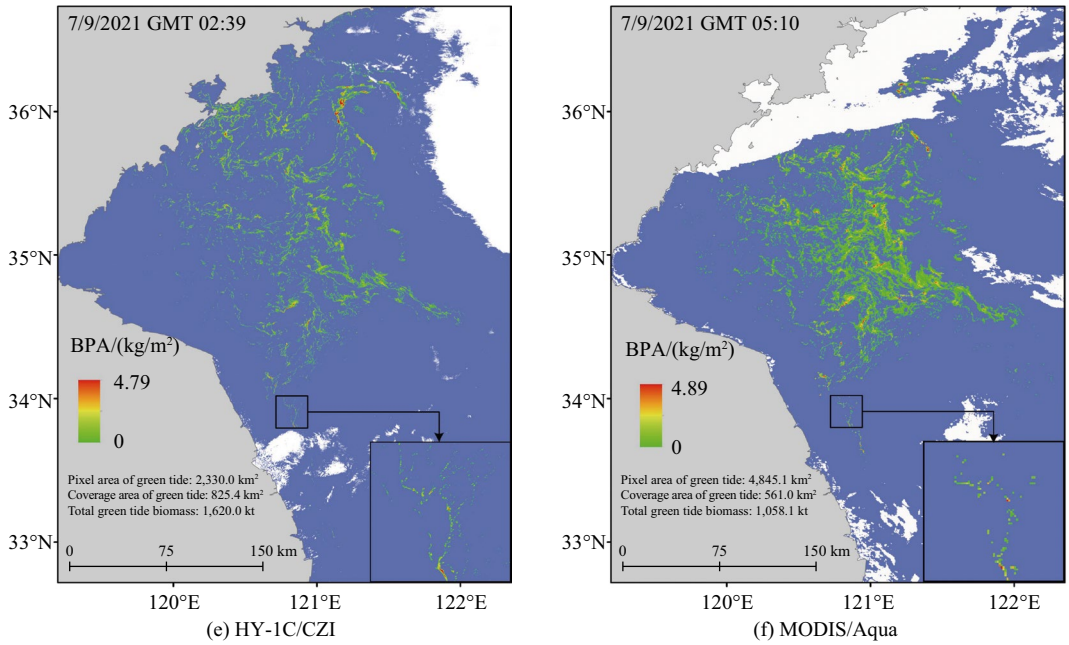

(continued)

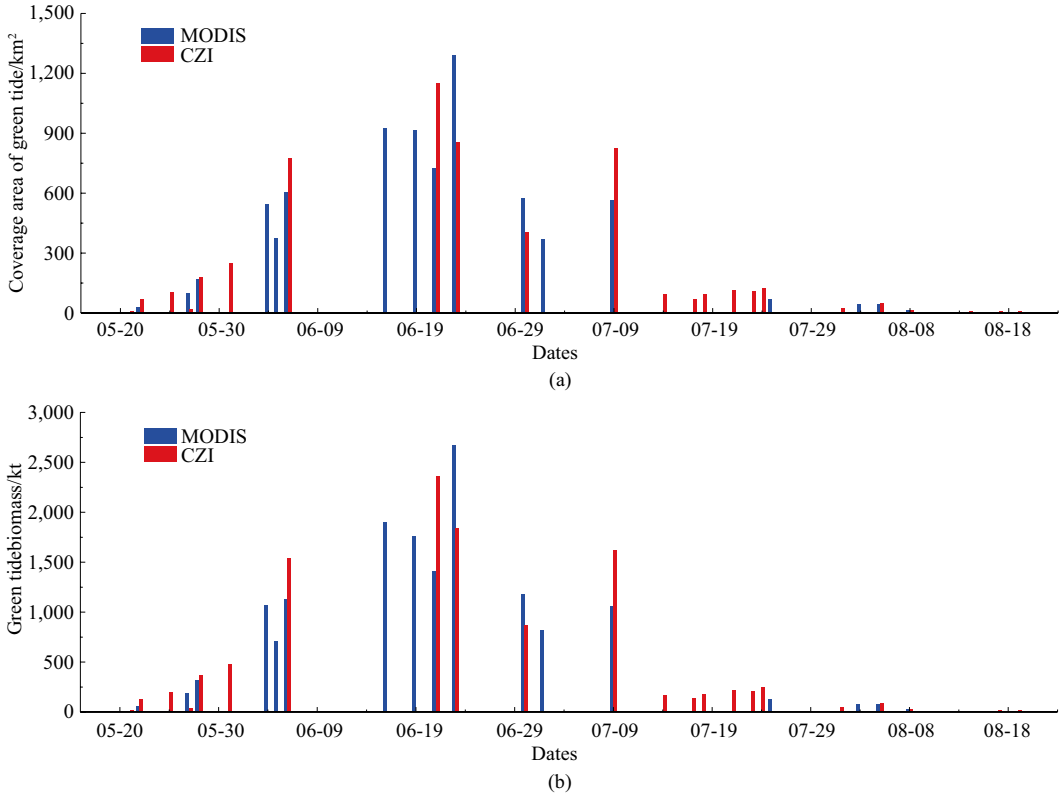

Fig. 7.8 Trends in the green tide coverage area and the total biomass in the China Seas in 2021 based on CZI and MODIS data

ratio and an excellent spatial and spectral resolution. The platform has obvious advantages in the identification, extraction, and biomass estimation of offshore green tides. It can provide more accurate floating algae area and biomass data products and features a strong ability for detecting small green tide patches. The sensor can provide precise data covering the growth, outbreak, and extinction of green tides. Moreover, the HY-1C/1D network can provide observation data with wide coverage and high temporal resolution (twice in three days) and can provide the optimal quantitative data for the operational application of green tides in the China Seas.

Floating Algae Biomass Contributes to the Assessment of Ecological Effects

When combined with marine survey data for carbon, nitrogen, and phosphorus (C, N, P), the satellite remote sensing estimation product for green tide biomass can be used to estimate the C, N, and P of green tides in the China Seas. This can help further assess the ecological and environmental effects of green tides, especially for the assessment of the carbon uptake capacity of large floating algae.

7.3.3 High-Precision Dynamic Monitoring of China's Coastal Tidal Flats

Target: SDG 14.2: By 2020, sustainably manage and protect marine and coastal ecosystems to avoid significant adverse impacts, including by strengthening their resilience, and take action for their restoration in order to achieve healthy and productive oceans.

7.3.3.1 Background

Tidal flats, including intertidal mudflats, rocks, and sands, are non-vegetated transition zones between marine and terrestrial environments that provide unique ecosystem services. For instance, they can defend against storm surge, maintain shorelines, filter pollutants, and promote carbon storage. They also serve as feeding grounds for migrating birds and spawning and nursery habitats for fish and other marine wildlife. Tidal flats are one of the most ecologically and economically important ecosystems; however, they are also globally vulnerable. These areas are highly threatened by tidal reclamation and natural disturbances. Sustainable management of coastal tidal flats has been listed in the SDGs as part of the UN 2030 Agenda. The unique and important ecosystem functions and services that tidal flats provide in coastal regions warrant the necessity of mapping such a particular land cover type with high precision and accuracy. This is necessary to provide essential information for coastal management and facilitate the implementation of SDGs.

With the accelerated economic development of coastal regions, Chinese tidal flats are rapidly changing and facing great challenges. The coastal tidal flats in China have been threatened by noticeable industrialization, urbanization, and aquaculture expansion over the past four decades. Currently, more than 70% of China's medium-to-large cities are located along the coastal zone, which produces over 60% of the national GDP and contributes to 61.5% of the world's aquaculture production (FAO 2016; Ren et al. 2019). More than two-thirds of China's coastlines have been converted into artificial seawalls, causing extensive damage to tidal flats (Ma et al. 2014). The Chinese government has exerted enormous efforts to restore and manage degrading coastal ecosystems to achieve the SDGs related to the sustainable management of coastal resources. Nevertheless, tidal flat reclamation is a key source of enormous economic benefits for local communities. Thus, sustainable strategies are urgently needed for balancing coastal protection and utilization.

This study was based on Big Earth Data and utilized Google Earth Engine to construct dense high-quality time-series image stacks of Sentinel-2 data. The MSIC and Otsu algorithms (i.e., the MSIC-OA) were integrated to build 10 m resolution datasets representing the spatial distribution of China's coastal tidal flats in 2015 and 2020. This study then analyzed the quantitative variation and spatial distribution

characteristics of the tidal flat resources in China. This study offers reliable research methods and data products to support the evaluation of SDG 14, which can contribute to supporting management and policymaking for coastal zones. Furthermore, the study provides baseline data for China to make reasonable protection and scientific development strategies for both tidal flat resources and the whole coastal ecosystem.

7.3.3.2 Data

- Multi-temporal Sentinel-2 multi-spectral images covering the coastal areas of China.
- UAV ground surveys, Gaofen-2 images, and Google Earth images.

7.3.3.3 Methods

In this study, coastal tidal flats were defined as non-vegetated areas between the maximal and minimal tidal inundations, i.e., the highest and lowest tidal waterlines along the shoreline. Thus, to map tidal flats, the key is to obtain spatial distributions of the maximal and minimal water extents between the highest and lowest tides, respectively. To accomplish this, the highest and lowest tide images were synthesized from Sentinel-2 high-quality dense time-series image stacks. Second, binary classification results, i.e., water and non-water, were automatically created from the highest and lowest tide images to derive the maximal and minimal water extents, respectively. Thirdly, we intersected the maximal and minimal water extents to obtain the intertidal zones. Finally, we removed intertidal vegetation and permanent seawater from the intertidal zones and only retained tidal flat areas. The workflow for tidal flat mapping is shown in Fig. 7.9(a). To further explain how the MSIC-OA approach works, we chose the Inner-deep Bay as the case study area. The workflow is described below (Fig. 7.9(b)).

1. Select the modified normalized difference water index (mNDWI) as the spectral index to create a composite of the maximal water extent image (mNDWI-MSIC) (Fig. 7.9(b)). Each pixel in this image has the maximum mNDWI value of times-series pixels for its position.
2. Select NDVI as the spectral index to composite the minimal water extent image (NDVI-MSIC) (Fig. 7.9(b)). Each pixel in this image has the maximum NDVI value of times-series pixels for its own position.
3. Apply the Otsu algorithm to mNDWI-MSIC to obtain the maximal water extent and use the extent to clip the minimal water extent image. Thus, an image of the intertidal area is created that contains seawater, tidal flat, and intertidal vegetation.
4. Apply the Otsu algorithm to the image of the intertidal area in Fig. 7.9(b) to get the maximal intertidal vegetation extent and erase the maximal intertidal vegetation extent. Thus, an image is created that only contains seawater and tidal flats.
5. Lastly, apply the Otsu algorithm to images of tidal flats and water, resulting in the final delineation of tidal flats.

MSIC can ensure the acquisition of information for both the highest and lowest tide from all images, while the Otsu algorithm can automatically divide water and non-water and vegetation and non-vegetation. Thus, the MSIC-OA approach has the advantages of being fast, robust, and fully automatic.

The MSIC-OA approach was applied to obtain the Chinese tidal flat distribution in 2015 and 2020. An accuracy validation was performed using a confusion matrix derived from ground survey samples. A polygon-to-image comparison based on sub-meter resolution images was also used in accuracy verification. The overall classification accuracy for China's coastal tidal flats monitoring results was 92% and 94% for 2015 and 2020, respectively.

7.3.3.4 Results and Analysis

Spatial Distribution and Temporal Dynamics of Tidal Flats in China from 2015 to 2020

Figure 7.10 shows the spatial distribution of coastal tidal flats in China in 2020. China's coastal tidal flats are rich in resources and

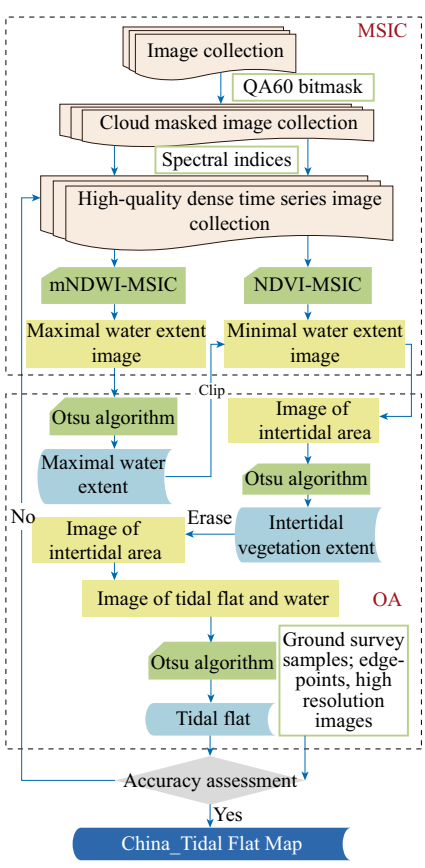

(a) Workflow of the MSIC-OA approach

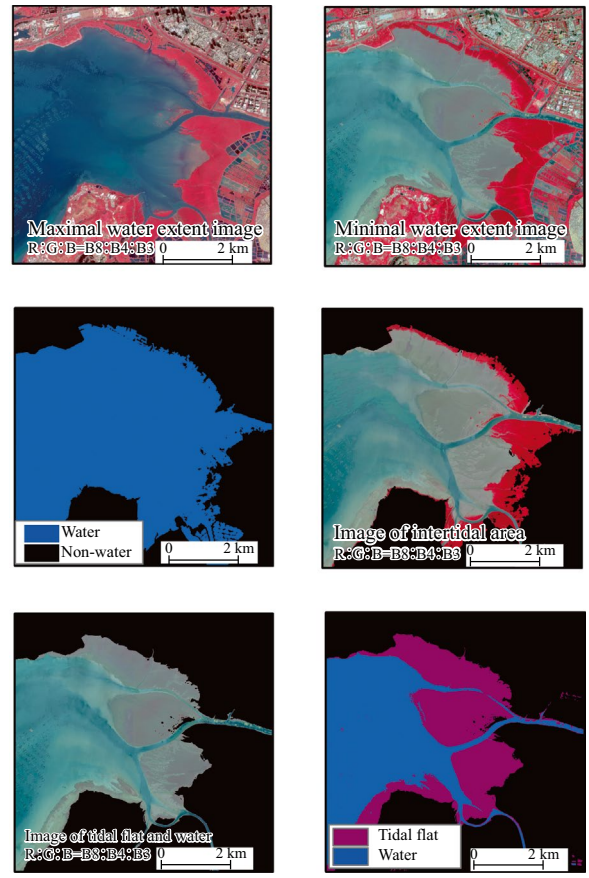

(b) Results of each step while delineating tidal flats in the Inner-deep Bay based on the MSIC-OA approach and time series Sentinel-2 images

Fig. 7.9 Workflow for tidal flat mapping and the results of each step when applying the MSIC-OA to time-series Sentinel-2 images of the Inner-deep Bay

feature a long and narrow patch in the intertidal zone. The four largest patches are situated on the southern coast of Jiangsu Province. The estuarine regions, such as the Liao River, Hai River, Yellow River, Yangtze River, Minjiang River, and Pearl River, have abundant tidal flat resources with intact patches. The results show that China's coastal tidal flats presented an erosion phenomenon as a whole. The coastal tidal flats areas in Zhejiang, Jiangsu, Guangxi, Tianjin, Hebei, and some parts of Shanghai displayed a slightly increasing trend, while the tidal flat patches along the coasts of Shandong, Guangdong, Liaoning, Taiwan, and Fujian showed a slightly decreasing trend.

Coastal Tidal Flat Area and Its Temporal Changes in China from 2015 to 2020

Figure 7.11 displays the changes in the coastal tidal flats within China's main coastal provinces (autonomous regions, municipalities) from 2015 to 2020. The country's coastal tidal flat area declined from 883,342 ha to 858,779 ha, with a decrease of 24,563 ha. In 2015, Jiangsu Province possessed the largest coastal tidal flat area (191,089 ha), followed by Shandong and Liaoning provinces. Together, these three provinces accounted for 49.48% of the total coastal tidal flat area. In comparison, the Tianjin Municipality had the smallest coastal tidal flat area in 2015. In 2020, Jiangsu Province had the

Fig. 7.10 Spatial distribution of coastal tidal flats in China in 2020

largest share of tidal flats (23.77%), followed by Zhejiang, Fujian, Shandong, and Liaoning provinces. These five provinces featured about 73.33% of China's tidal flats, and the Tianjin Municipality had the smallest area of 1.22%. Northern China had a larger area of tidal flats than that of Southern China, and the tidal flats area decreased significantly when moving from Fujian to Hainan Province.

The change in tidal flat area exhibited a significant heterogeneity across different provinces between 2015 and 2020 (Table 7.2). The tidal flat areas showed an obvious erosion trend in Liaoning, Shandong, and Guangdong provinces, which decreased by 10,788 ha (−9.64%), 29,500 ha (−22.00%), and 25,296 ha (−28.95%), respectively. Guangdong Province had the highest degree of erosion at 28.95%, followed by Shandong Province at 22.00%, and Liaoning Province with a relatively lower degree of erosion at 9.64%. In contrast, the tidal flats showed a smaller erosion trend in Fujian and Taiwan provinces, with a decrease of 2,318 ha (−2.13%) and 3,327 ha (−12.84%), respectively. The provinces of Zhejiang and Jiangsu showed a notable expansion trend with an area of 20,004 ha and 13,046 ha, respectively. Zhejiang Province had a high degree of expansion with a relative expansion of 21.47%, while Jiangsu Province had a small degree of expansion with a relative expansion of 6.83%. Guangxi Province showed a significant tidal

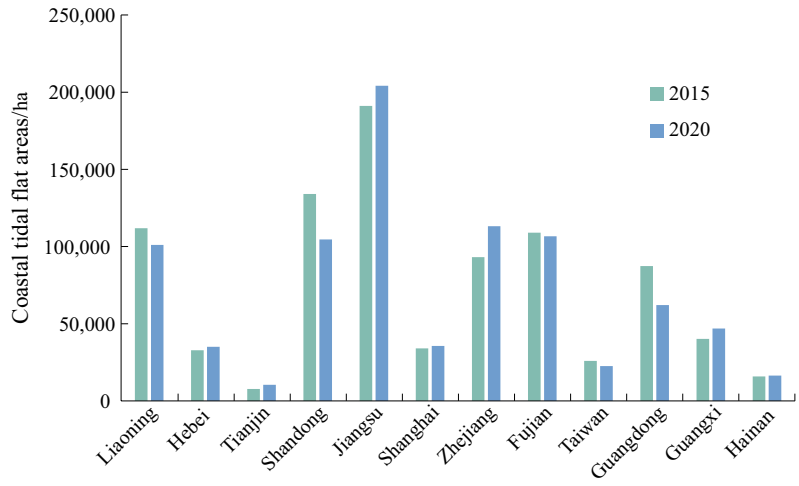

Fig. 7.11 Changes in the tidal flats of China's main coastal provinces (including autonomous regions and municipalities) from 2015 to 2020

Table 7.2 Provincial-level statistics for coastal tidal flat areas and their changes

Provinces	2015/ha	2020/ha	Area changes from 2015 to 2020/ha	Area change percentage from 2015 to 2020/%
Liaoning	111,902	101,114	−10,788	−9.64
Hebei	32,855	35,021	2,166	6.59
Tianjin	7,758	10,474	2,716	35.02
Shandong	134,112	104,612	−29,500	−22.00
Jiangsu	191,089	204,135	13,046	6.83
Shanghai	34,065	35,590	1,525	4.48
Zhejiang	93,188	113,192	20,004	21.47
Fujian	108,988	106,670	−2,318	−2.13
Taiwan	25,904	22,577	−3,327	−12.84
Guangdong	87,374	62,078	−25,296	−28.95
Guangxi	40,201	46,935	6,734	16.75
Hainan	15,907	16,381	474	2.98
Total	883,342	858,779	−24,563	−2.78

flat expansion with an area of 6,734 ha and a relative expansion of 16.75%. Hebei Province, Tianjin Municipality, Shanghai Municipality, and Hainan Province had a slight expansion trend with an expansion of 2,166 ha, 2,716 ha, 1,525 ha, and 474 ha, respectively, among which Tianjin Municipality was the most significant area in China with a change ratio of 35.02%.

Highlights

- In this study, we tracked the variations in coastal tidal flat areas in China between 2015 and 2020, and analyzed the spatial patterns and change characteristics of Chinese tidal flats. Chinese coastal tidal flats were found to feature an overall erosion trend from 2015 to 2020, and the most significant decreasing

trends were in Liaoning, Shandong, and Guangdong provinces. Conversely, the coastal tidal flat areas featured a significant expansion trend in Zhejiang and Jiangsu provinces. China should strengthen the sustainable management and reasonable protection of coastal tidal flat resources.

7.3.3.5 Discussion and Outlook

In terms of methodology and data, the high-quality dense time-series Sentinel-2 image stacks used in this study were constructed based on Google Earth Engine to replace the traditional method of obtaining tidal flat information from single-scene images. In addition, the MSIC-OA method was applied to realize the rapid, robust, and automatic delineation of Chinese coastal tidal flats in 2015 and 2020 with a 10 m resolution. The method can be easily applied to local, regional, continental, and global scales. Specifically, it can obtain a more accurate and robust global coastal tidal flat dataset in comparison to previous datasets, which is suitable for the long-term and intensive monitoring of coastal tidal flat changes. The results of this study can be used to support a broad scope of coastal management and policymaking related to the sustainable use of tidal flats. For example, in alignment with SDG 14, China's State Council made an announcement to enhance coastal protection and control reclamation activities in 2018. Therefore, the updated dataset describing the spatial distribution of coastal tidal flats is essential for decision-making in the selection of coastal development districts. Additionally, the results of this study can also facilitate the efforts for managing relevant coastal ecosystems, such as mangrove afforestation and the control of *Spartina alterniflora* invasion. This study can also be used as baseline data for scientific research, such as studying biodiversity conservation and migratory bird protection, carbon storage estimation, sea-level rise impact, and coastal erosion.

In terms of decision support, this study provides the following conclusions. (1) The coastal tidal flat area has decreased significantly in China since the SDG era (2015), indicating that China should strengthen the rational protection and sustainable management of coastal tidal flats. (2) The erosion of coastal tidal flats mainly occurred in the coastal areas of Liaoning, Shandong, and Guangdong provinces from 2015 to 2020, while expansion mainly occurred in the coastal areas of Zhejiang and Jiangsu provinces. (3) China's coastal tidal flats showed an overall erosion trend from 2015 to 2020, with a total reduction of 24,563 ha. The results of this study can not only support the scientific evaluation of SDG 14.2, but also provide an important scientific basis for the scientific and sustainable development of coastal tidal flat resources in China.

7.3.4 Risk Assessment of HABs in the Coastal Waters of the East China Sea

Target: SDG 14.2: By 2020, sustainably manage and protect marine and coastal ecosystems to avoid significant adverse impacts, including by strengthening their resilience, and take action for their restoration in order to achieve healthy and productive oceans.

7.3.4.1 Background

HABs are the result of the explosive growth of toxic and harmful microalgae, macroalgae, or cyanobacteria in water bodies, and are harmful to aquatic ecosystems and even human health (Berdalet et al. 2017). Cyanobacteria outbreaks, such as *Microcystis*, are the main types of HABs in freshwater environments. Marine HABs include the "red tide" and "brown tide" formed by microalgae, and the "green tide" and "golden tide" formed by macroalgae, etc. (Anderson et al. 2012). HABs in the ocean have the potential to pose a significant threat to human health, ecological integrity, and social and economic development through various mechanisms. These include the production of toxins and their detrimental effects on marine organisms, disruption of marine ecological environments, and the alteration of seawater properties (Anderson

et al. 2015). Thus, HABs are commonly investigated as a significant form of ecological disaster in marine ecosystems due to their considerable impact on the marine environment.

The frequency of HABs has increased significantly in recent decades. Data analysis, such as that presented in the Bulletin of Marine Ecology and Environment Status of China, indicated that the occurrence of HABs in China's coastal waters was infrequent and relatively small in scale prior to the 1990s, and seldomly exceeded several hundred square kilometers. The frequency and geographical extent of HABs have shown a notable escalation since the year 2000. HAB occurrences, which can persist for periods of over a month, are now recorded between 50 and 80 times annually, encompassing thousands and sometimes even tens of thousands of square kilometers. The East China Sea is one of the most prevalent areas for the occurrence of HABs with the largest affected area, which has attracted extensive attention worldwide. Dinoflagellates and diatoms are the main causative groups of HABs in the East China Sea. In recent years, large-scale dinoflagellates such as *Prorocentrum Donghaiense*, *Karenia Mikimotoi*, and *Alexandrium* sp. have experienced frequent outbreaks, leading to serious threats to the development of aquaculture, human health, and ecological security.

The harmful effects of HABs are not only affected by the frequency, scale, diversity, and toxicity of the causative species, but are also closely related to biological resources, aquaculture, coastal tourism, and nuclear power facilities that are vulnerable to HABs. Therefore, the risk assessment of algal bloom disasters is a complex topic. A series of theoretical studies have been carried out to assess the risk of algal bloom disasters, but a complete risk assessment method has not yet been established. Scientific algal bloom risk assessment methods can be developed by analyzing the occurrence of HABs and their harmful effects. They are helpful for deepening the understanding of algal bloom hazard risk, improving prevention awareness and ability, and supporting the sustainable development of the social economy.

7.3.4.2 Data

The data for the marine environments and resources used in this study include the following two aspects.

- Data for HABs in the East China Sea (1933–2017).

The data includes the location, area, duration, causative species, and hazards of HABs.

1. Bulletin of marine environment conditions in China and surrounding provinces and cities in the East China Sea and the Bulletin of China Marine Disasters.
2. China Ocean Yearbook.
3. Investigation and Evaluation of Red Tide Disaster in China (1933–2009) and other literature.

Social and economic data for coastal cities along the East China Sea: The data includes seafood production, mariculture production, tourism, and nuclear power facility distribution within the surrounding provinces and cities bordering the East China Sea. The statistical yearbook data mainly comes from various provinces and cities.

7.3.4.3 Methods

This study considers algal bloom disaster risk assessment as the starting point and establishes a method based on the basic idea of risk assessment, namely: risk = hazard × vulnerability (Risk = $H \times V$), which comprehensively considers the hazards of HABs (H) and the vulnerability of the disaster bearing body (V).

The hazard of HABs was assessed using the historical record of HABs in the East China Sea. Four statistical factors were used, including the frequency, scale, causative species diversity, and toxic algal species status. Based on the statistical data for the four factors, the entropy weight method was used to comprehensively rate the risk of HABs. The HAB hazards in various regions of the East China Sea were divided into five levels.

The vulnerability of the disaster bearing body (V) was analyzed and evaluated from four aspects, including mariculture yield, seafood

yield, coastal tourism, and the distribution of nuclear power facilities. The four factors were graded and assigned based on a hierarchical analysis method, and the vulnerability of the disaster bearing body was evaluated using the comprehensive rating results. The vulnerability of the disaster bearing body in various regions of the East China Sea was divided into three levels.

According to the administrative divisions around the East China Sea, the risk value of algal bloom disasters was calculated based on the assessment results for the risk degree of HABs and the vulnerability degree of the disaster bearing body in each grid. The algal bloom disaster risk was divided into five levels according to the calculation results, and the study produced a spatial distribution map of the algal bloom disaster risk.

7.3.4.4 Results and Analysis

In this study, a total of 1,065 HAB events were recorded from 1933 to 2017 in the East China Sea. The occurrence time, location, scale, causative species classification, toxicity, and harm of algal bloom were sorted, allowing for the construction of a dataset describing the occurrence of HABs in the East China Sea. A total of 81 causative species of HABs were recorded in the East China Sea. Most of the HABs were formed by diatoms and dinoflagellates. Large-scale HABs were mainly caused by *Prorocentrum donghaiense*, *Noctiluca scintillans*, *Skeletonema costatum*, *Karenia Mikimotoi*, and *Alexandrium* sp. Around the year 2000, the causative species showed an evolutionary trend from diatoms to dinoflagellates, and the number of HABs gradually increased. *Prorocentrum donghaiense* and *Karenia mikimotoi* became the dominant species causing algal blooms, which caused serious damage to the development of aquaculture. The spatial distribution characteristics and hotspots of HABs in the East China Sea were analyzed using a GIS platform. HABs in the East China Sea were mainly distributed in the waters adjacent to the Yangtze River Estuary (Fig. 7.12). The occurrence risk of HABs in the East China Sea was examined by integrating their frequency, scale, causative species diversity, and toxic algal species status. The results are shown in Fig. 7.13.

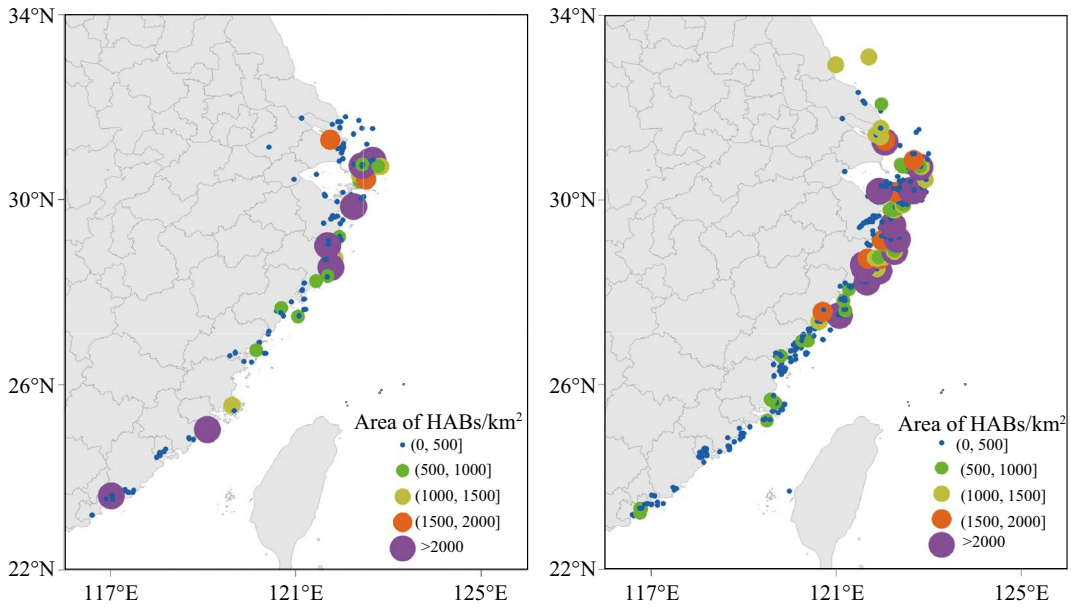

Fig. 7.12 Distribution of HABs in the coastal areas of the East China Sea

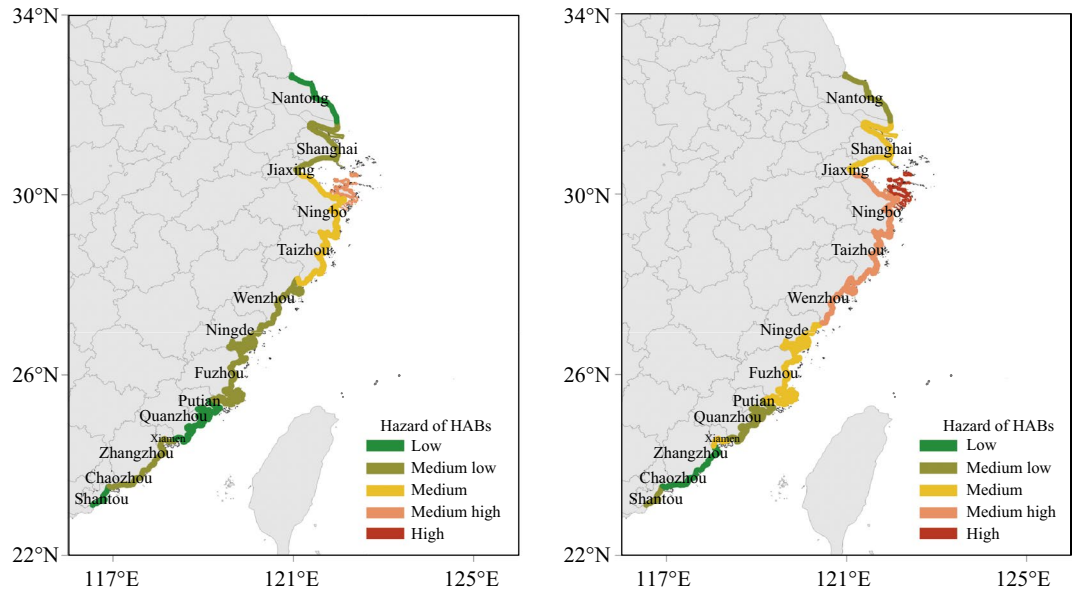

Fig. 7.13 Occurrence risk of HABs in the coastal areas of the East China Sea

The seafood yield, mariculture area, and tourism development were statistically analyzed using the data from provinces and cities located around the East China Sea. The vulnerability of HAB disaster bearing bodies in coastal areas was assessed using classification, and included analysis of the areas in Nantong, Shanghai, Jiaxing, Ningbo, Taizhou, Wenzhou, Ningde, Fuzhou, Putian, Quanzhou, Xiamen, Zhangzhou, Chaozhou, and Shantou. The evaluation results are shown in Fig. 7.14.

The assessment of algal bloom risk in the East China Sea relied on the results obtained from the hazard classification and vulnerability assessment of the entities susceptible to HABs (Fig. 7.15). The findings indicated an increased occurrence of HABs in the East China Sea since the year 2000, with HAB hotspots progressively shifting southward. The coastal areas in the Zhoushan Islands, Fuzhou, Ningbo, Taizhou, Quanzhou, and Xiamen exhibited a relatively high-risk level for algal bloom disasters. This was primarily attributed to the escalation in the HAB hazard and the heightened vulnerability of certain areas, such as the Fuzhou coast, since 2000.

Highlights

- The study constructed a dataset of HABs in the East China Sea from 1933 to 2017. The results show that the causative species of HABs in the East China Sea had an obvious evolutionary trend from diatoms to dinoflagellates around the year 2000, and the hotspot areas for HABs expanded to the southern part of the East China Sea.
- The risk assessment method for algal bloom disasters was established by considering the hazard of HABs and the vulnerability of entities susceptible to HABs. The hazard assessment of HABs was carried out based on four aspects, including frequency, scale, causative species diversity, and toxic algal species status. The vulnerability of the entities susceptible to HABs was carried out from the perspectives of mariculture yield, seafood yield, coastal tourist population, and the distribution of nuclear power facilities.
- The risk assessment results for algal bloom disasters in the East China Sea showed that the HAB risk was relatively high in the

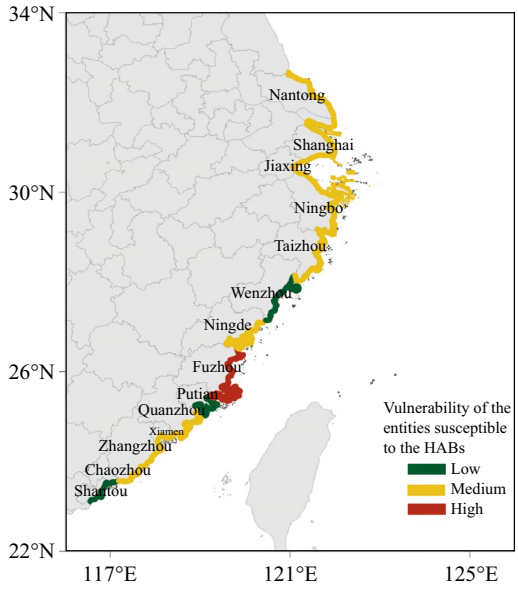

Fig. 7.14 The vulnerability of the entities susceptible to HABs in the East China Sea coastal area

coastal areas of Zhoushan Islands, Fuzhou, Ningbo, Taizhou, Quanzhou, and Xiamen. The evaluation results can offer support for management and disaster reduction strategies concerning HABs in the East China Sea. Furthermore, they can serve as a source of ideas and methods for the risk assessment and management response to algal blooms in other water bodies.

7.3.4.5 Discussion and Outlook

The current monitoring work on the occurrence of HABs in the East China Sea was found to be both systematic and comprehensive. This resource can provide relatively complete data support for the assessment of algal blooms and is conducive to risk assessment. The risk assessment of algal blooms in the East China Sea showed that HABs mainly occurred in the Yangtze River Estuary and its adjacent waters, and there was a trend of southward expansion after 2000. Coastal areas, such as the Zhoushan Islands, Fuzhou, Ningbo, Taizhou, Quanzhou, and Xiamen, featured the highest risk of HABs. The tracking and monitoring of HABs in these areas should be further pursued in future studies. The case evaluation results are expected to provide a basis and guidance for the prevention and control of algal bloom disasters in the East China Sea.

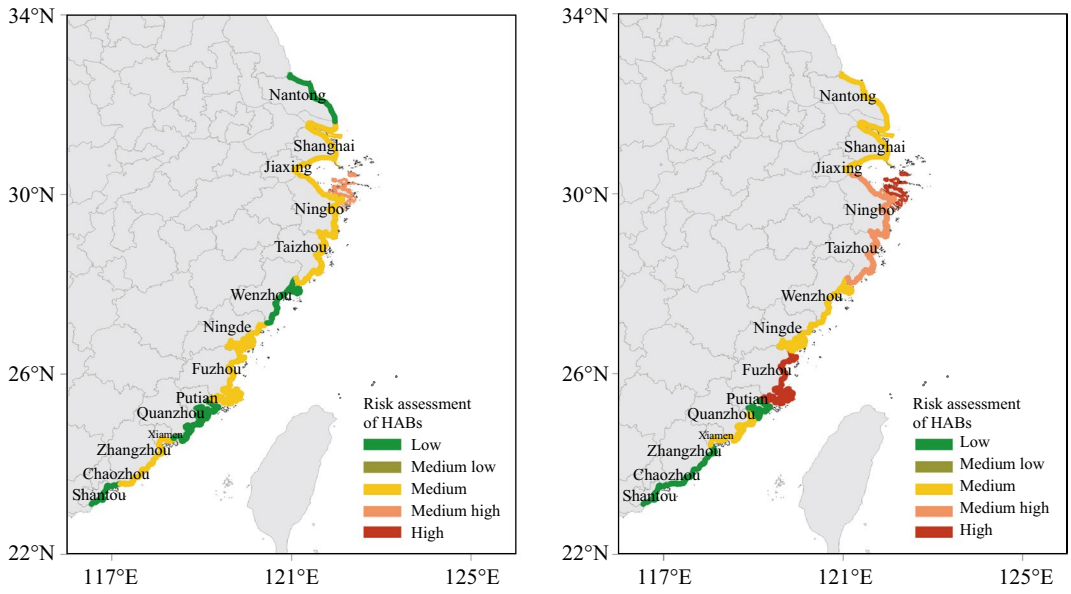

(a) 1933-1999 (b) 2000-2017

Fig. 7.15 Risk assessment results for algal bloom disasters in the coastal areas of the East China Sea

The present study employed data spanning nearly a century for comparative analysis, with data categorized into two distinct periods before and after 2000. It is crucial to acknowledge that this method may potentially obscure valuable information related to the interannual variability of HABs. Additionally, recent years have witnessed a significant surge in attention and efforts directed toward preventing and controlling HABs in various regions, leading to a gradual reduction in their annual occurrence. Hence, it is imperative to undertake further investigations to delve into the interannual variability of HABs in future studies.

The evaluation method established in this study not only considered the hazard of HABs, but also evaluated the vulnerability degree status of HABs based on the algal bloom situation. This approach provides a comprehensive reflection of HAB risk and can be adapted for assessing the risk of other marine algal bloom disasters. The study is anticipated to make a valuable contribution to the sustainable management and protection of marine and coastal ecosystems, aligning with SDG 14.2, by offering insights into algal bloom disaster prevention and control.

7.3.5 Estimating the Economic Value of China's Coastal Wetlands for Typhoon Protection

Target: SDG 14.1: By 2025, prevent and significantly reduce marine pollution of all kinds, in particular from land-based activities, including marine debris and nutrient pollution.

7.3.5.1 Background

Since the advent of global modern satellite monitoring in 1970, China has been identified as one of the countries most affected by typhoons. According to statistics provided by the China Meteorological Administration, a total of 1,120 typhoons landed on China's coasts from 1949 to 2021, with an average occurrence of 15.34 per year (CMA Tropical Cyclone Data Center 2022), resulting in a huge loss of lives and property. For example, Typhoon Mujigae caused direct economic losses reaching up to 2.67 billion yuan in 2016, and took the lives of five people during flooding (State Oceanic Administration 2018). China's low-lying coastal provinces have been continuously impacted by typhoons over long time periods. However, these areas still have insufficient resistance to the flooding caused by typhoons, making the areas prone to huge social impacts and economic losses.

It is well known that coastal wetlands are a natural barrier against typhoons. The coastal wetlands located between the vast ocean and inland highlands include shallow waters and lush vegetation, which can reduce wind speed, lower wave height, and reduce the water levels and flow velocity of flood waters. Consequently, coastal wetlands play an important role in mitigating typhoon impacts on human society through their typhoon protection ecological services (Costanza et al. 2021). China's coastal wetlands are mainly distributed along nine provinces and two municipalities, including Liaoning, Hebei, Shandong, Jiangsu, Zhejiang, Fujian, Guangdong, Hainan, Guangxi, Tianjin, and Shanghai. There are twelve types of coastal wetlands in China that act as a natural barrier against typhoons, including: permanent shallow sea waters, ocean subtidal water beds, coral reefs, rocky coasts, intertidal sand/pebble beaches, intertidal mud/sand beaches, intertidal swamps, mangroves, coastal saltwater lagoons, coastal freshwater lagoons, deltas, and estuaries (Jiang et al. 2015). This case study focused on the types of coastal wetlands defined in land use/cover change (LUCC), including canals, lakes, reservoirs, ponds, tidal flats, beaches, and swamps along China's coasts. The area and ecological functions of coastal wetlands around the world have been constantly decreasing and degrading due to the overexploitation and use of coastal wetlands by human inhabitants. So far, only 14.7% of coastal wetlands in China are protected (Yang et al. 2017). Hence, the quantitative evaluation of the ecological functions of typhoon protection and disaster reduction provided by coastal wetlands is helpful for

strengthening the conservation and restoration of coastal wetlands, improving the capacity of coastal wetlands to resist typhoons, protecting human property and environmental safety, and promoting the sustainability of coastal zone development.

Additionally, compared with their supply of food and raw materials, the typhoon protection provided by coastal wetlands has been ignored for a long time due to the lack of a real trading market. In recent years, domestic and international research has shown that the ecological functions of coastal wetlands such as typhoon protection and disaster reduction are considerable and should not be underestimated. For instance, a regional study by Narayan et al. (2017) showed that wetlands prevented $600 million in property damage resulting from typhoon-induced flooding during Hurricane Sandy. Seriño et al. (2017) found that preserving one ha of mangroves could save human lives and was worth as much as $301,811 during Typhoon Haiyan's impacts on the Visayas coast of the Philippines. However, these studies have been criticized for focusing on a regional scale, using a small sample size, or not adequately considering other influencing factors. Recently, more experts have found that the typhoon protection provided by coastal wetlands is more sustainable and cost-effective compared to traditional seawalls. To provide evidence to support this argument, it is necessary to evaluate and research the typhoon protection provided by coastal wetlands using large samples at the national scale, especially in China. China has a long history of relying on seawalls to prevent and mitigate typhoon disasters. It is important to clarify the value of China's coastal wetlands in typhoon protection in order to compare the economic benefits with seawalls.

7.3.5.2 Data

- Tracks, wind speed, and the durations of typhoons that landed on China's coasts and caused economic losses during 1989–2020 (https://www.saic.com/what-we-do/information-technology/digital-transformation; https://www.jma.go.jp/jma/indexe.html).
- Data on the direct economic losses caused by typhoons (http://www.mnr.gov.cn/sj/sjfw/hy/gbgg/zghyzhgb/index_1.html).
- Population, GDP, and other related social and economic factor datasets (https://data.stats.gov.cn/).
- National 1 km × 1 km land use remote sensing data for 2010, 2015, and 2020 (http://www.dsac.cn/DataProduct/Index/200804).

7.3.5.3 Methods

This case study was based on China's LUCC and long-term time-series datasets (1989–2020), including data for typhoons, economic losses, population, and GDP. An environmental economic model was employed to quantitatively evaluate the ecological function value of typhoon protection provided by China's coastal wetlands, and included landforms defined by the LUCC, such as canals, lakes, reservoirs, ponds, tidal flats, beaches, and swamps. The total economic value of China's coastal wetlands in resisting typhoons, protecting property, and reducing disaster damage was estimated using the annual frequency of typhoon impacts along China's coasts. Following Costanza et al. (2021), a linear logarithm environmental economic model was constructed to evaluate the typhoon protection value of coastal wetlands. The model is given as Eq. (7.1):

$$\ln(\mathrm{TD}_i/\mathrm{GDP}_i) = \alpha + \beta_1 \ln(\mathrm{wetland}_i) + \beta_2 \ln\left(\mathrm{speed}_i\right) + \beta_3 \ln(\mathrm{duration}_i) \tag{7.1}$$

where i is the index for the typhoon; TD_i refers to the total direct economic loss caused by the typhoon (i); GDP_i denotes the potential loss of GDP in the swath of the typhoon (i); $\mathrm{wetland}_i$ represents the area of wetlands in the swath of the typhoon (i); speed_i is the wind speed of the typhoon (i) upon landing; $\mathrm{duration}_i$ is the time duration of the typhoon (I) in hours; α, β_1, β_2, and β_3 are the estimated coefficients. R^2 explains the fitness of the model regression, and the estimated coefficients are judged by the significance level (p). It is expected that $\beta_1 < 0$, $\beta_2 > 0$, $\beta_3 > 0$. Once the coefficients are estimated by ordinary least squares regression, Eq. (7.1) can be

rewritten as a hindcasting model for the overall direct economic losses caused by the typhoon (i):

$$\mathrm{TD}_i = \mathrm{e}^a \times \mathrm{wetland}_i^{\beta 1} \times \mathrm{wind}_i^{\beta 2} \times \mathrm{duration}_i^{\beta 3} \times \mathrm{GDP}_i \quad (7.2)$$

Obviously, in line with Eq. (7.2), it was assumed that the change in the total direct economic loss (TD) was expected to have a linear relationship with GDP, the β_1 power of the wetland area in the swath of typhoon, the β_2 power of the typhoon wind speed, and the β_3 power of the typhoon duration. If the wetland area in the swath of typhoon increases by Q km^2, the change in the total direct economic loss TD can be described as:

$$\Delta\mathrm{TD}_i = \mathrm{e}^a \times [\mathrm{wetland}_i^{\beta 1} - (\mathrm{wetland}_i + Q)^{\beta 1}] \times \mathrm{wind}_i^{\beta 2} \times \mathrm{duration}_i^{\beta 3} \times \mathrm{GDP}_i \quad (7.3)$$

If Q equals 1, Eq. (7.3) can be rewritten as:

$$\Delta\mathrm{TD}_i = \mathrm{e}^a \times [\mathit{wetland}_i^{\beta 1} - (\mathrm{wetland}_i + 1)^{\beta 1}] \times \mathrm{wind}_i^{\beta 2} \times \mathrm{duration}_i^{\beta 3} \times \mathrm{GDP}_i \quad (7.4)$$

$\Delta\mathrm{TD}_i$ is the marginal value of coastal wetlands for typhoon protection, that is, the economic loss avoided by every increase in 1 km^2 of the coastal wetland area in the typhoon swath, all other conditions being equal (i.e., typhoon landfall wind speed, typhoon duration, potential GDP).

7.3.5.4 Results and Analysis

The statistical analysis based on the environmental economic model indicated that more property was protected and the community suffered less economic damage in the typhoon swath area where coastal wetlands were present. The results show that the median value of China's coastal wetlands for typhoon protection and disaster reduction was estimated to be 14.06 million/km^2 yuan. The frequency and intensity of typhoons hitting China are projected to increase with more and more occurrences of extreme weather events under global climate change. Consequently, the typhoon protection function provided by coastal wetlands will become increasingly important and valuable in the future.

Coefficients Estimated by the Linear Logarithm Environmental Economic Model

There were 138 typhoons that impacted China and caused economic losses in the 30-year span from 1989 to 2018. The environmental economic model based on the 138 cases shows that the coefficient of coastal wetlands (Table 7.3) was negative and significant ($\beta_1 = -0.377$), which implies that coastal wetlands played a significant and positive role in mitigating the economic damage caused by typhoons. The total economic damage decreased rapidly with the increase in wetland area. On average, the logarithm of the relative economic loss (i.e., TD/GDP) was expected to decrease or increase by 0.377 for every increase or decrease in the unit area of coastal wetlands in the swath of typhoon. Aside from coastal wetlands, other significant factors affecting the total direct economic loss caused by typhoons included the wind speed and duration. As expected, both typhoon wind speed and duration were positively correlated with the logarithm of the relative economic loss ($\beta_2 = 3.471$, $p<0.01$; $\beta_3 = 1.139$, $p<0.01$). The logarithm of the relative economic loss increased with the increase in wind speed (3.471) and duration (1.139). The relative damage caused by the typhoon increased

Table 7.3 Environmental economic model and coefficient estimation (Liu and Geng 2022)

Model variables	Coefficients estimations
Constant a	−21.877***
Wetland (the area of coastal wetlands in the swath of typhoon)	−0.377***
Speed (landfall wind speed for typhoon)	3.471***
Duration (duration of typhoon)	1.139***

Note ***Indicates 99% of the significance level

with the increase in the speed of the typhoon. The longer the typhoon impacts the coastal area, the greater the total direct economic losses.

Establishing a Value for the Typhoon Protection Function Provided by Coastal Wetlands

Equation (7.4) was used to estimate the marginal value of coastal wetlands in each specific typhoon swath for all 138 historical cases. Through calculation, the marginal value of typhoon protection provided by the coastal wetlands was between 48,900 yuan (Typhoon Lekima in 2001) and 3,459.42 million yuan (Typhoon Sinlaku in 2002) per km^2. The average value was 120.64 million yuan per km^2, and the median value was 14.06 million yuan per km^2. Liu et al. (2019) found that the median value for typhoon protection provided by seawalls was 4.8 million yuan per km. Seawalls not only need a huge amount of money to build, but also require high annual maintenance costs. It is noted that coastal wetlands have significant economic benefits in typhoon protection and disaster reduction. In the context of global climate change, extreme weather events are becoming more and more frequent, and the number of typhoons landing on China's coasts is becoming more extensive. Hence, the ecological functions of typhoon protection provided by coastal wetlands will play a more important role in the future. Meanwhile, it should also be pointed out that the R^2 of the model was 0.59, which means that there was a difference between the observed ln(TD/GDP) and the model prediction for 41% of historical typhoon cases. The model overestimated typhoons causing small economic losses and underestimated typhoons causing large economic losses.

Economic Losses Avoided Through the Typhoon Protection Provided by Coastal Wetlands During the 2010–2020 Period in China

The Bulletin of China Marine Disaster reported that although both the frequency and intensity of typhoons impacting China had increased, the economic losses resulting from typhoons decreased from 2010 to 2020. The country benefited from the conservation and restoration of additional coastal wetlands during the 10-year period, which played an important role in the protection against typhoons. It should be noted that the existing coastal wetlands in the typhoon swath were particularly important in terms of typhoon protection, as nearly 90% of typhoons landed in the southern part of China.

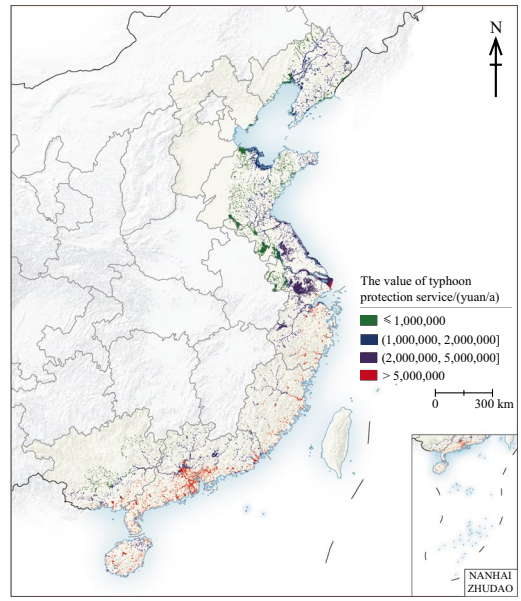

Fig. 7.16 Economic losses that were avoided due to the typhoon protection provided by coastal wetlands in 2020. *Note* No data available for Hong Kong, Macao and Taiwan; Liu and Geng (2022)

As shown in Fig. 7.16, the coastal wetlands in typhoon-prone areas avoided economic damage valued at 92.77 billion yuan in 2010, which increased to 212.2 billion yuan in 2015, and 296.28 billion yuan in 2020 (Fig. 7.16).

Highlights

- The median value of China's coastal wetlands for typhoon protection and disaster reduction was estimated to be 14.06 million yuan per km^2.
- The annual economic losses prevented by coastal wetlands steadily increased between 2010 and 2020.

- In terms of typhoon protection and disaster reduction, coastal wetlands were found to be more environmentally friendly and cost-effective than seawalls.

7.3.5.5 Discussion and Outlook

This case study applied an environmental economic model to comprehensively evaluate the ecological functions of typhoon protection provided by the coastal wetlands across China. Through the frequency and trend of typhoons landing on China's coasts, the annual economic contribution of existing coastal wetlands was conservatively estimated in terms of typhoon protection and disaster reduction. Coastal wetlands not only have significant social benefits in typhoon protection, but also have important ecological functions such as climate regulation, biodiversity support, and ecological product supply. It is suggested that the layout of coastal wetlands should be rationally arranged in terms of their ecological functions, production, and recreation to improve their ecological value to a greater extent and promote sustainable development.

7.3.6 Dynamic Monitoring of the Development and Utilization of Spatial Resources in China's Coastal Zone

Target: SDG 14.5: By 2020, conserve at least 10% of coastal and marine areas, consistent with national and international law and based on the best available scientific information.

7.3.6.1 Background

The coastal zone is defined as the area where the land and sea meet and interact, and includes land and sea areas of a certain width that are close to the coastline. China's coastal zone is located in the eastern part of Asia and on the west coast of the Pacific Ocean and features very strong land-sea interactions. This area is densely populated and has many cities, constituting the engine of China's social and economic development. China's accession to the World Trade Organization (WTO) in 2001 further promoted the rapid social and economic development of China's coastal areas over the past 20 years. As a result, urban expansion and the development and utilization of wetlands in coastal zones have become issues of concern. SDG 14 aims to "conserve and sustainably use the oceans, seas and marine resources for sustainable development". Oceans and coastal areas worldwide provide a wealth of products that are fundamental to human well-being and global food security. However, the breadth and depth of the exploitation and utilization of maritime spatial resources have been significantly enhanced due to the increasing "sea-oriented" characteristics of the population and economy. Therefore, both aspects pose a threat to sustainable development in many coastal areas. In view of the development and utilization of coastal spatial resources, the previous research based on remote sensing techniques have had the following shortcomings, including: relatively few studies focusing on the macro-spatial scale and long-term periods, the insufficient land-sea integration of classification systems and data products, and the insufficient disclosure of the unique laws and mechanisms within the coastal zone. Therefore, concerning China's coastal zone over the past 20 years, this case study aims to monitor the dynamic characteristics of the development and utilization of spatial resources using remote sensing techniques to reveal existing problems and their causes. Moreover, the study puts forward policies and suggestions for the sustainable development and utilization of spatial resources in China's coastal zones.

7.3.6.2 Data

- The initial data was from China's land use data for the year 2000 developed by the Institute of Geographic Sciences and Natural Resources Research, Chinese Academy of Sciences (IGSNRR, CAS). The data has a spatial accuracy and scale of 1:100,000. A subset of this data was created by clipping out the coastal areas.

- Time-series Landsat satellite images captured by various sensors. Landsat-7 ETM+ imagery for the year 2000, Landsat-5 TM imagery for 2005 and 2010, and Landsat-8 OLI imagery for 2015 and 2020 were chosen as the primary data sources for time-series land use and land cover classification. The United States Geological Survey (USGS) and the Geospatial Data Cloud provide free download services for these images. The images with a more concentrated capturing time in the growing season, and no or few cloud coverage (<6%) were selected and downloaded for each year. Multiple temporal phases of Landsat images were synergistically used to improve the classification accuracy for a small number of scenes. Overall, about 60 scenes of specific Landsat images were used for each of the five years.
- High-resolution Google Earth imagery was used to collect validation samples and to assist in the determination of the land use/cover type.

7.3.6.3 Methods

A land use classification system for China's coastal zone (LUCS_CZ, Table 7.4) was established based on characteristics of the development and utilization of spatial resources as well as the recognition ability of Landsat multi-spectral satellite images (Di et al. 2014). It is a two-level system, with 8 types for the first level and 24 types for the second level. The study aimed to fully reveal the relationships between land and sea in the coastal zone and the dynamics of spatial resource development and utilization. In terms of the spatial extent of land use mapping, the land area was bounded by the administrative district of the coastal prefecture-level city. The sea area was determined by the union of a 10 m isobath and 10 km buffer zone for the coastline, including the entire area of Hainan and Taiwan and their surrounding islands and waters. This spatial extent featured a total area of about 745,800 km^2. Next, the 1:100,000 scale land use data established by IGSNRR, CAS (Liu et al. 2003) was chosen to clip out the data for this spatial extent. Then, the boundaries and attributes of land use polygons were modified through visual interpretation in ArcGIS software according to the features of Landsat images in 2000 and the classification criteria for LUCS_CZ. Finally, the land use data for China's coastal zone was obtained for the year 2000. Furthermore, using the features from 2005 Landsat imagery, the land use data for China's coastal zone in 2000 were updated to that of 2005 by interpreting the areas that changed during the five-year period (Hou et al. 2018a). As mentioned above, the land use data for China's coastal zone was obtained for the periods of 2010, 2015, and 2020. Finally, a five-year interval land use dataset was established for China's coastal zone for the period between 2000 and 2020.

Validation samples for 2010, 2015, and 2020 were collected using high-resolution Google Earth imagery, and the accuracy of

Table 7.4 Land use classification system for China's coastal zone (LUCS_CZ)

First level	Second level
1-Farmland	11-Paddy; 12-Dry land
2-Forest	21-Forest; 22-Woods; 23-Shrub; 24-Other forest
3-Grassland	31-Dense grass; 32-Moderate grass; 33-Sparse grass
4-Built-up area	41-City; 42-Rural settlement; 43-Isolated industrial-mining
5-Inland freshwaters	51-Rivers; 52-Lakes; 53- Reservoirs and ponds; 54- Bottomland
6-Coastal wetland	61-Beach and shore; 62-Estuarine waters; 63-Estuarine delta; 64-Coastal lagoons; 65-Shallow water
7-Human-made wetland	71-Salt pan; 72-Mariculture
8-Unused land	81-Unused land

Table 7.5 Accuracy of land use classification results

Years	Amounts of samples	Overall accuracy/%	Kappa coefficients
2020	16,456	94.12	0.9247
2015	16,418	93.98	0.9229
2010	13,013	95.16	0.9357

coastal land use mapping was analyzed for the eight first-level land use types (Table 7.5). The results show that the overall accuracy varied from 93.98% to 95.16% for the three years, and the Kappa coefficient was between 0.9229 and 0.9357. The results prove that a very high accuracy was achieved for coastal land use mapping.

Figure 7.17 shows the results from the land use mapping of China's coastal zone. The land use classification was simplified to highlight the fundamental characteristics and dynamics of spatial resource development and utilization in coastal areas. This process worked by merging most of the second-level land use types according to the characteristics of the coastal zone. Only the "shallow water" type was juxtaposed with the eight first-level land use types. In other

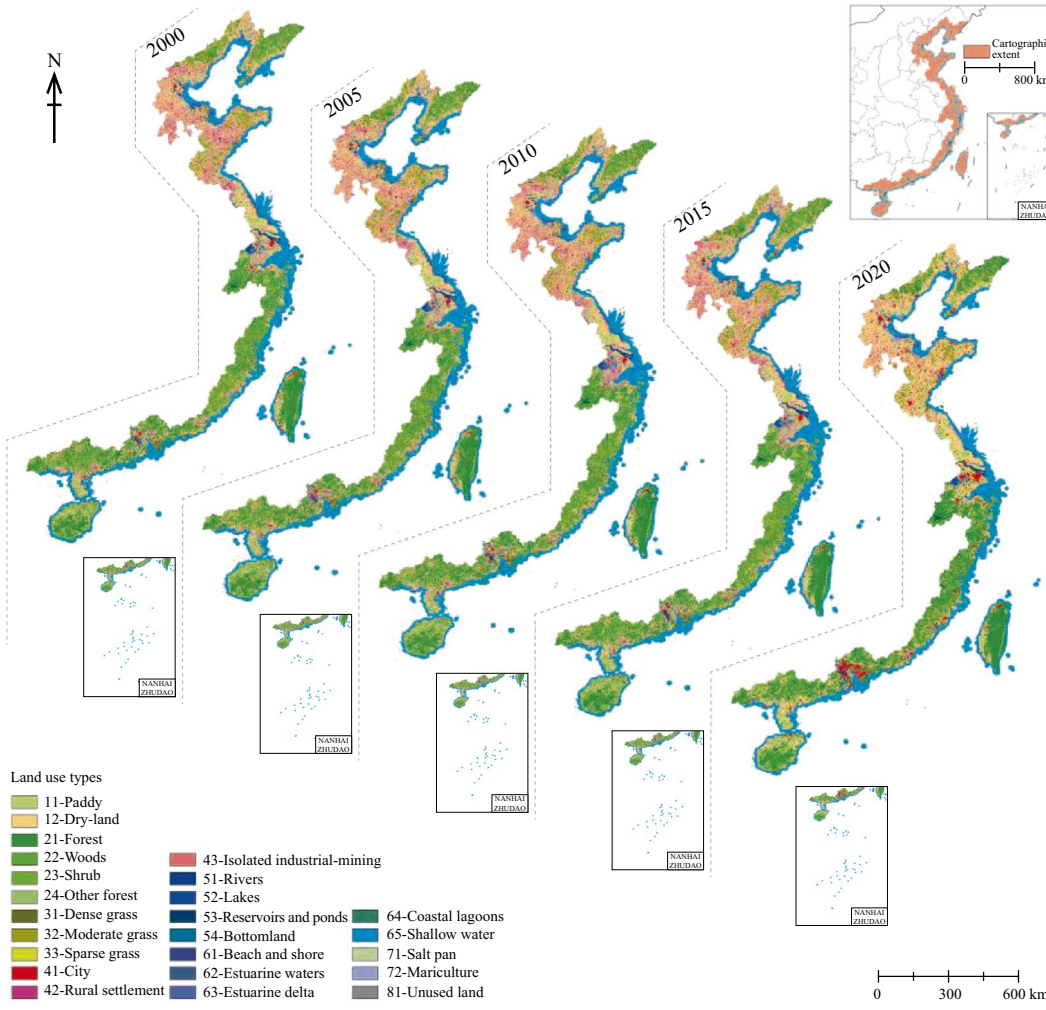

Fig. 7.17 Land use mapping of China's coastal zone using remote sensing techniques

words, a total of nine types, including farmlands, forests, grasslands, built-up areas, inland freshwaters, coastal wetlands, shallow waters, human-made wetlands, and unused land were targeted to analyze the characteristics and dynamics of spatial resources in China's coastal zone.

7.3.6.4 Results and Analysis

Spatial Patterns of Coastal Spatial Resource Development and Utilization

As shown in Fig. 7.17, there were very complex spatial patterns of coastal spatial resource development and utilization. Specifically, the north–south difference was very prominent at the macro-spatial scale. The coastal area in South China had a much wider distribution of paddies, forests, and inland freshwaters, while the coastal area in North China had a more prominent distribution of dry land and coastal wetland. There were also significant gradient characteristics between land and sea. The dominant combination of various land use types gradually changed from "farmland-forest-grassland-inland freshwaters" to "human-made wetland-coastal wetland-shallow water" when moving from land to sea. In addition, whether in the northern or southern coastal zone, the built-up area was mainly embedded in the form of patches of various sizes in other types, showing a macro-scale discreting and medium-scale agglomerating spatial pattern.

Structural Characteristics of Coastal Spatial Resource Development and Utilization

As shown in Fig. 7.17, the macro-spatial pattern of spatial resource development and utilization in China's coastal zone was relatively stable over the past 20 years. Correspondingly, the distribution areas and the proportions of various land use types, i.e., the quantitative structure of spatial resource development and utilization, were generally stable. Taking 2020 as an example (Fig. 7.18), nine land use types were sorted in descending order based on their area size, including: farmland, forest, shallow water, built-up area, grassland, inland freshwaters, human-made wetland, coastal wetland, and unused land.

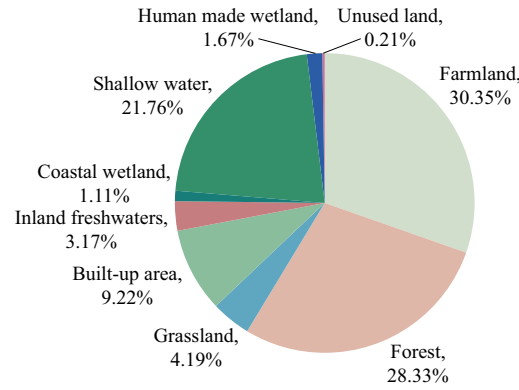

Fig. 7.18 Structural characteristics of spatial resource development and utilization in China's coastal zone

Among the nine types, farmlands, forests, shallow waters, and built-up areas were the four most dominant types with their total areas accounting for 89.66% of the coastal zone in China.

Quantitative Changes in Coastal Spatial Resource Development and Utilization

As shown in Fig. 7.19, the following quantitative changes in spatial resource development and utilization occurred in China's coastal zone from 2000 to 2020. The three most widely distributed types, namely farmland, forest, and shallow water, had a continuous decrease in the distribution area, while the distribution areas for built-up areas and human-made wetlands continued to increase. The areas of other land use types were characterized by fluctuation but were observed to decrease overall.

Transfer Characteristics Among the Multiple Types of Coastal Spatial Resource Development and Utilization

All nine land use types featured complex area transfers during the 20-year period (Table 7.6). The spatial areas with multiple types of transfers accounted for 7.23% of the entire coastal zone. In terms of the specific transfers among various types, farmland→built-up area, forest→built-up area, shallow water→coastal wetland, shallow water→built-up area, and coastal wetland→human-made wetland were the most widely distributed. The interchange between farmland and forest, and farmland and

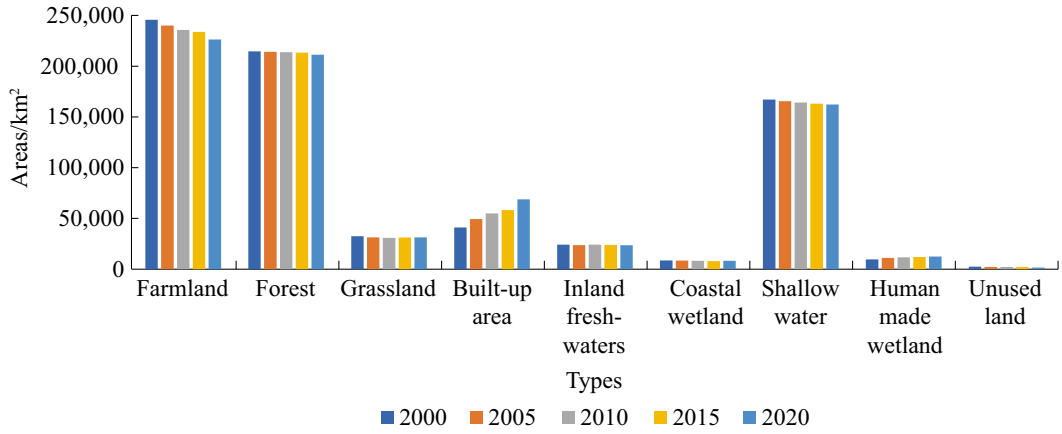

Fig. 7.19 Quantitative changes in the coastal spatial resource development and utilization in China's coastal zone

Table 7.6 Land use area transfer matrix in China's coastal zone (unit: km^2)

Land use types	1-Farm-land	2-Forest	3-Grass-land	4-Built-up Area	5-Inland freshwa-ters	6-Coastal wetland	7-Shal-low water	8-Human made wetland	9-Unused land
1-Farmland	220,943	1,306	544	19,395	2,047	22	1	1,321	133
2-Forest	1,448	208,242	845	3,347	393	8	4	168	113
3-Grassland	769	1,240	28,462	1,008	324	89	3	470	58
4-Built-up area	485	107	48	40,051	132	17	3	237	12
5-Inland freshwaters	1,384	119	262	1,300	19,686	403	18	881	60
6-Coastal wetland	219	98	324	556	290	4,936	638	1,494	57
7- Shallow water	140	66	283	1,519	431	2,490	161,527	555	114
8-Human-made wetland	380	26	380	1,297	229	115	11	7,087	107
9-Unused land	570	79	104	289	87	175	53	216	933

inland freshwaters had more significance in the land areas located away from the sea. However, in coastal areas, human-made wetlands played an "intermediate role" in the conversion process of coastal wetland→built-up area and shallow water→built-up area.

Highlights

- The study created a dataset using remote sensing techniques that describe the development and utilization of spatial resources in China's coastal zone in 2000, 2005, 2010, 2015, and 2020. Its advantages include land-sea integration, a detailed classification system, and high accuracy.
- The study revealed the basic characteristics of the development and utilization of spatial resources in China's coastal zone from 2000 to 2020, including the spatial patterns, structural characteristics, temporal changes, and area transfers among multiple types.
- The study analyzed the key influencing factors and mechanisms affecting the pattern and process of the development and utilization of spatial resources in China's coastal zone.

7.3.6.5 Discussion and Outlook

The development and utilization of spatial resources in China's coastal zone were more prominent during the 2000 to 2020 period. This mainly manifested as the expansion of built-up areas (the occupation of farmland, forest, shallow water, etc.) and the increase in human-made wetlands (mainly the occupation of coastal wetlands). In this context, the loss of farmland and various types of ecological spaces (coastal wetlands, etc.) and the efficiency of production and living spaces in urban and rural areas (for example, ghost towns) have gradually become more significant problems in China's coastal zone. In general, there were various factors influencing the processes and characteristics of spatial resource development and utilization in China's coastal zone during the 20-year period. However, three aspects must be emphasized, namely: the strong drive for regional development strategies, the significant disturbance caused by the global financial crisis, and the constraints produced by "ecological civilization" construction policies.

1. The Outline of the Five-Year Plan for National Economic and Social Development has been an important factor in driving economic and social development at national and regional levels. Moreover, nearly 30 regional development strategies were launched or implemented in coastal provinces, autonomous regions, and municipalities over the past 20 years. The implementation of these strategies has become an important driver of the continuous growth of the built-up area and the massive reclamation of farmlands, forests, coastal wetlands, and shallow waters.
2. The outbreak of the global financial crisis in 2008 had significant impacts on spatial resource development and utilization in China's coastal zone (Du et al. 2022). The increase in the built-up area in 2010–2015 only accounted for 11.85% of the total increase over the 20-year period, which was much lower than that in other periods. However, the global financial crisis had no significant inhibitory effect on the development and utilization of coastal wetlands and shallow waters. The occupation of coastal wetlands and shallow waters was only slightly lower in 2010–2015 than in 2000–2005, but much higher than that in 2005–2010 and 2015–2020 (Du et al. 2022).
3. Since the 18th National Congress of the Communist Party of China, the national promotion of an ecological civilization as well as coastal wetland restoration measures has effectively curbed the occupation of coastal wetlands and shallow waters and significantly reversed the decline of coastal wetlands. The land use dataset employed in this study confirmed the remarkable restoration of coastal wetlands during 2015–2020. The distribution area in 2020 had almost recovered to the previous areal extent in 2010.

China's coastal zone has been an important engine area for economic and social development, a key region for promoting the construction of the Belt and Road Initiative (BRI), and an important area for reducing carbon emissions. Therefore, in the future, it is necessary to give more emphasis to the comprehensive advantages of remote sensing big data, cloud computing, artificial intelligence, and other technologies for strengthening research in the following ways: (1) to continuously monitor and analyze the evolutionary characteristics of the development, utilization, and protection of spatial resources in China's coastal zone; (2) to strengthen the dynamic monitoring of key land use types such as coastal wetlands, built-up areas, and farmlands; (3) to strengthen the dynamic monitoring of critical zones such as estuaries and deltas, including the Bohai Rim, Guangdong-Hong Kong-Macao Greater Bay Area, and the Beibu Gulf; and (4) to strengthen the high-precision and intensive temporal monitoring and evaluation of typical problems such as coastal erosion, the ecological restoration of beaches, and storm surges.

7.3.7 Dynamic Monitoring of China's Coastal Reclamation and the Efforts to Return Enclosures to the Sea and Wetlands from 2010 to 2020

Target: SDG 14.5: By 2020, conserve at least 10% of coastal and marine areas, consistent with national and international law and based on the best available scientific information.

7.3.7.1 Background

Coastal reclamation is an important cause of coastline changes, coastal wetland degradation, and marine pollution. A large number of facts and studies have proved that the negative impacts of coastal reclamation on the coastal zone's environment and ecology are long-term and incalculable. The main hazards include: (1) causing changes to marine tidal, wave, and hydrodynamic conditions; (2) causing changes to the nearshore and offshore sedimentary environment and underwater topography; (3) causing or aggravating the nearshore water environment; (4) causing the loss of tidal flat area and the degradation of ecological functions; (5) causing the loss of nearshore benthic habitats and community destruction; (6) seriously encroaching on and destroying marine fishery resources; (7) adversely affecting the development of aquaculture, the salt industry, tourism, and other marine economic industries; and (8) increasing the risk of natural disasters in coastal zones and inducing economic and social system risks. Therefore, the intensive and economical use of the sea and the control and management of coastal reclamation are related to the realization of SDG 14.5.

The *Notice of the State Council on Strengthening Coastal Wetlands Protection and Strictly Controlling Reclamation* issued in 2018 outlines several conservation policies, including: adherence to the strictest ecological and environmental protection system with a commitment to prioritizing ecology and green development, ending the approach to "land reclamation", strictly controlling new reclamation, strengthening ecological protection and restoration, achieving strict protections, and the effective restoration and intensive use of marine resources. Moreover, the notice aims to promote "blue bays" and the gradual restoration of damaged coastal wetlands by returning enclosures to the sea, returning breeding grounds to tidal flats, and returning reclaimed farmlands.

Coastal reclamation monitoring is an important application of remote sensing research in coastal zones. However, there is a lack of remote sensing research on coastal reclamation management. This case study utilized satellite remote sensing techniques to carry out the monitoring and analysis of the changes in coastal reclamation areas along China's coast from 2010 to 2020. In addition, the case also monitored efforts to return enclosures to the sea and wetlands during the same period, which can provide basic data support for national marine and coastal zone management and scientific research, aiding in the realization of SDG 14.5.

7.3.7.2 Data

- Landsat-5 TM multi-spectral data for 2010, 30 m spatial resolution.
- Landsat-8 OLI multi-spectral data for 2015, 2018, and 2020, 30 m spatial resolution.
- Administrative division data, topographic data, and other reference data.

7.3.7.3 Methods

Definition

The "Comprehensive Investigation and Evaluation of Offshore and Oceans in China" (hereafter referred to as the "908 Special Project") provided by the State Oceanic Administration defines the coastline as the trace line of the boundary between water and land at the average high spring tide. The "908 Special Project" sea area usage classification system defines coastal reclamation as engineering that builds dykes to cut off tidal flats or enclose harbors to reclaim the area as land.

Remote Sensing Mapping of Coastal Reclamation and Returned Enclosures

Coastal reclamation includes two types of sea use, namely sea enclosure and reclamation. A sea enclosure refers to the way to wholly or partially enclose the sea area or tidal flats by building dykes, while sea reclamation refers to the way to fill the sea area or transform the tidal flats to form a coastline, including by direct filling or filling after enclosure. Due to the diverse and complex uses of reclamation areas, there is no effective automatic method for extracting the spatial distribution of various types of reclamation. Suspected reclamation patches can only be screened using satellite images. Therefore, this case adopts a human-machine interactive interpretation method to realize the remote sensing dynamic monitoring of coastal reclamation and further governance measures for returning enclosures to the sea and wetlands.

In the process of the remote sensing interpretation of reclamation, the inner boundary lines of reclamation patches coincide with the coastlines prior to reclamation engineering, while the side and outer boundary lines coincide with the coastlines after reclamation engineering. The study extracted coastal reclamation patches related to human-made coastline dynamics. The independent reclamation patches located on the sea surface or on tidal flats were also supplemented. The usage of reclamation land was further classified using remote sensing images from the updated period. The coastal reclamation land was divided into six types according to the definition of reclamation in the "908 Special Project" and based on the separability of surface features in remote sensing images, and included ports, urban lands, farming, mariculture, salt fields, and others (i.e., under construction or difficult to distinguish in remote sensing images). Since the establishment of the Ministry of Natural Resources of the People's Republic of China in 2018, the supervision of natural resource utilization and protection has been strengthened to an unprecedented level. Therefore, the spatial distribution of major coastal reclamation in three periods, 2010–2015, 2015–2018, and 2018–2020, was successively extracted using remote sensing images and vector data of the mainland coastline in 2010.

In the National Blue Bay Remediation Project, the measures for returning enclosures to the sea and to wetlands were mainly implemented by removing dykes and returning mariculture land to tidal flats and sea areas. Therefore, in the process of remote sensing interpretation, the early remote sensing images of mariculture breeding ponds and other enclosures that were transformed into seas, tidal flats, mangrove wetlands, and other natural terrain in later remote sensing images were classified as measures for returning enclosures to the sea and wetlands (Fig. 7.20).

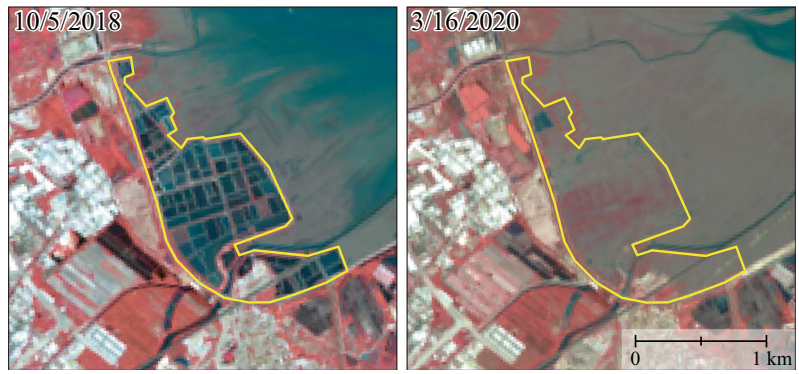

Fig. 7.20 Example of the remote sensing monitoring of measures for returning enclosures to the sea and wetlands

7.3.7.4 Results and Analysis

According to the remote sensing monitoring results, the new reclamation area along China's coast accounted for an area of 2,142.28 km^2 in the period from 2010 to 2020. The reclamation area featured a size of 1,702.47 km^2 from 2010 to 2015, with an annual average of 340.49 km^2, 395.81 km^2 from 2015 to 2018, with an annual average of 131.94 km^2, and 44.00 km^2 from 2018 to 2020, with an annual average of 22.00 km^2 (Fig. 7.21 and Table 7.7). The rate of reclamation from 2018 to 2020 was only 6.46% of that from 2010 to 2015. Therefore, the new coastal reclamation area sharply declined in the second decade of the twenty-first century, and the growth rate of reclamation was effectively controlled in China (Fig. 7.22).

The major types of coastal reclamation areas included mariculture, ports, and others during the period from 2010 to 2020, with their areas accounting for 35.46%, 27.32%, and 25.22%, respectively, and 88.00% of the total new coastal reclamation area during the 10-year period. In terms of the timespan, the growth rate of all types of coastal reclamation continued to decrease, except for the growth rate of others, which was stagnant in the two periods from 2010 to 2015 and 2015 to 2018.

The growth rate of new coastal reclamation decreased nationwide in all sea areas from 2010 to 2020 (Fig. 7.23). The reduction in the new coastal reclamation area was particularly significant in the Bohai Sea. Although the Bohai Sea has a short coastline, it featured the largest

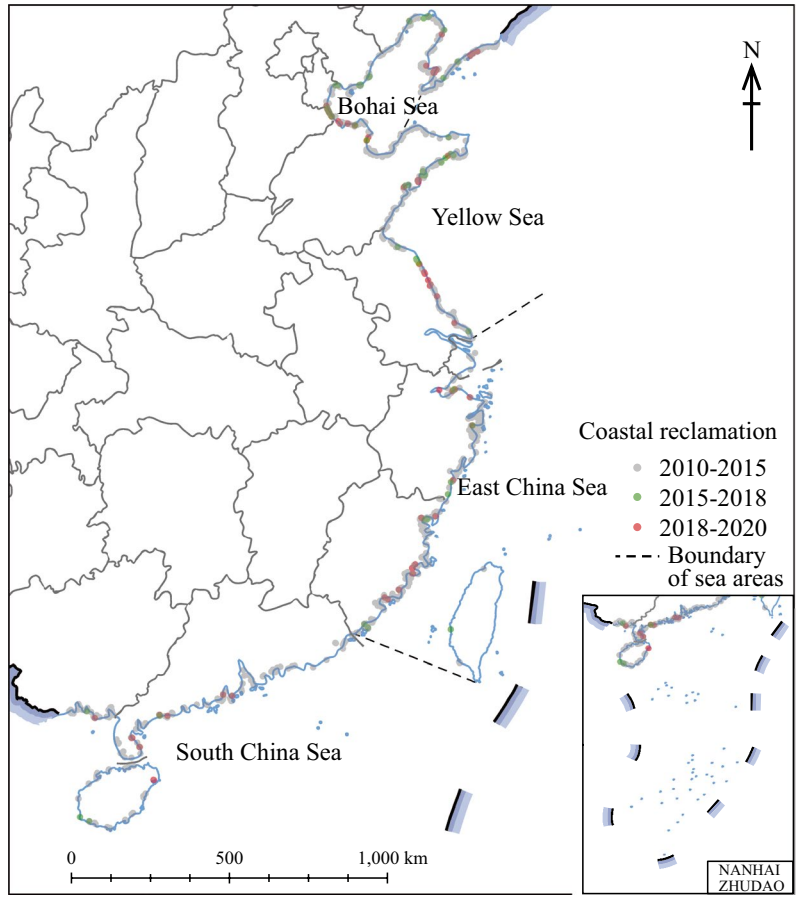

Fig. 7.21 Spatial distribution of major coastal reclamation in China from 2010 to 2020

Table 7.7 Area of major coastal reclamation in China from 2010 to 2020 (Unit: km^2)

Periods	Port	Urban land	Farming	Mariculture	Salt field	Others	Total
2010–2015	447.47	68.91	70.17	654.67	104.99	356.25	1,702.47
2015–2018	79.46	6.42	—	87.12	4.09	218.72	395.81
2018–2020	13.34	2.57	—	17.77	—	10.32	44
Total	540.27	77.89	70.17	759.56	109.08	585.3	2,142.28

Note — indicates that no such type of coastal reclamation occurred during the time period

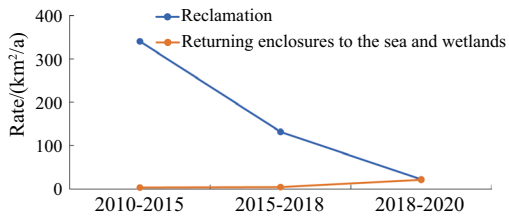

Fig. 7.22 Changes in the rate of major coastal reclamation and the measures to return enclosures to the sea and wetlands in China from 2010 to 2020

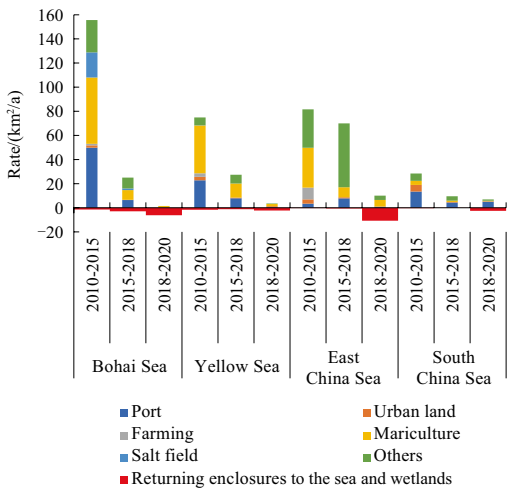

Fig. 7.23 Dynamics of reclamation in China's sea areas from 2010 to 2020

new coastal reclamation area from 2010 to 2015, with an annual average of 155.60 km^2. However, the growth rate of coastal reclamation declined significantly after 2015, with an annual average of 25.04 km^2 from 2015 to 2018 and only 1.48 km^2 from 2018 to 2020, accounting for the least amount of new coastal reclamation of all sea areas in that period. Therefore, the rate of coastal reclamation in the Bohai Sea was completely controlled during the period from 2018 to 2020.

The spatial pattern of new coastal reclamation changed in China after 2015. The coastal reclamation growth rate was relatively fast in the northern sea waters (Bohai Sea and Yellow Sea) and southern sea waters (East China Sea and South China Sea) from 2010 to 2015 and after 2015, respectively. The rate of coastal reclamation in the East China Sea was 69.96 km^2 per year from 2015 to 2018 and 10.03 km^2 per year from 2018 to 2020, which was much lower than the growth rate of 81.62 km^2 per year from 2010 to 2015. Nonetheless, the East China Sea featured the fastest growth rate of coastal reclamation among all sea areas from 2018 to 2020.

The governance measures for returning enclosures to the sea and wetlands were mainly focused on the withdrawal of mariculture ponds, with a total area of 76.16 km^2 from 2010 to 2020. The area of enclosures returned from mariculture ponds was 18.62 km^2 from 2010 to 2015, with an annual average of 3.72 km^2; 14.31 km^2 from 2015 to 2018, with an annual average of 4.77 km^2, and 43.23 km^2 from 2018 to 2020, with an annual average of 21.62 km^2. Figure 7.24 displays the spatial distribution of measures for returning enclosures to the sea and wetlands in China from 2010 to 2020. The rate of the return of enclosures to the sea and wetlands increased abruptly during the period from 2018 to 2020, which was directly related to the implementation of the *Notice of the State Council on Strengthening Coastal Wetlands Protection and Strictly Controlling Reclamation* issued in 2018. During the 2010–2015 and 2015–2018 periods, the Bohai Sea and Yellow Sea registered more

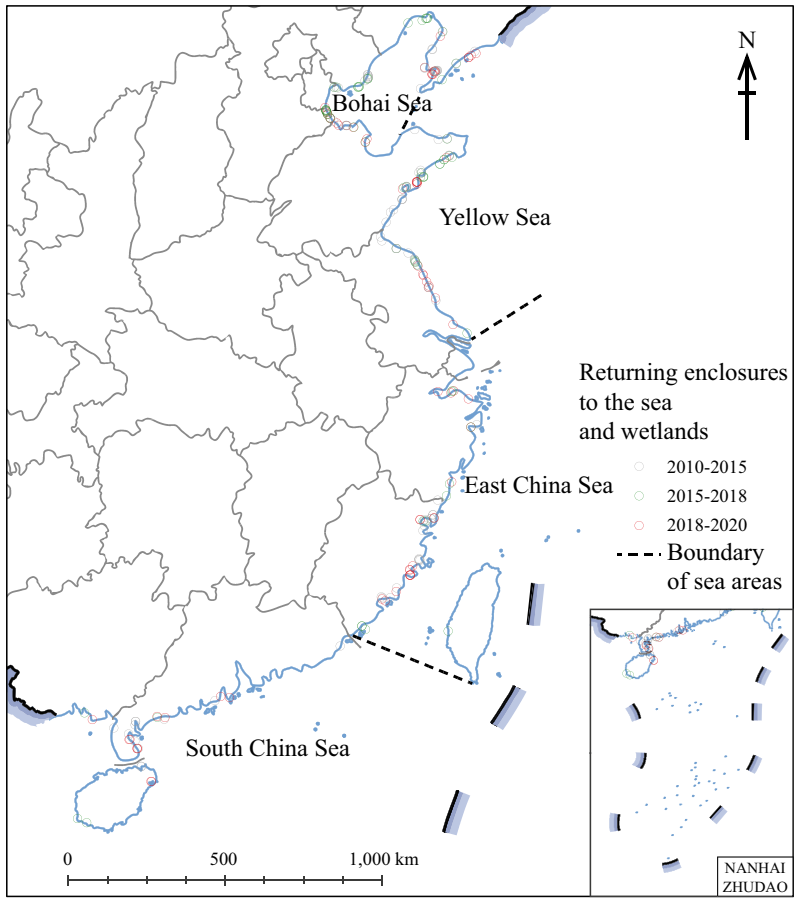

Fig. 7.24 Spatial distribution of the measures for returning enclosures to the sea and wetlands in China from 2010 to 2020

areas returned from mariculture enclosures, together accounting for 83.29% and 85.37% for the two periods, respectively. The area returned from mariculture enclosures increased notably in all seas from 2018 to 2020, with the largest returned area of 21.40 km^2 occurring in the East China Sea, followed by the Bohai Sea at 12.31 km^2, and the South China Sea and Yellow Sea with areas of 5.01 km^2 and 4.51 km^2, respectively. Each sea accounted for 49.49%, 28.48%, 11.58%, and 10.44% of the total returned area in the same period, respectively.

Highlights

- Using time-series Landsat TM/OLI multispectral satellite imagery, this case completed the remote sensing monitoring and analysis of the spatial distribution of major coastal reclamation in China for the three periods in 2010 to 2015, 2015 to 2018, and 2018 to 2020. The results show that the growth rate of coastal reclamation declined sharply, and the rate occurring from 2018 to 2020 was only 6.46% of that in 2010–2015.
- The remote sensing monitoring and analysis of the spatial distribution of coastal governance measures for returning enclosures to the sea and wetlands were also completed for the three periods in 2010–2015, 2015–2018, and 2018–2020. The results show that China strengthened efforts to return enclosures to the sea and wetlands. The returned area from coastal enclosures was almost equal to the

new coastal reclamation area from 2018 to 2020, and accounted for 56.77% of the total returned area from 2010 to 2020.

7.3.7.5 Discussion and Outlook

The growth rate of coastal reclamation decreased nationwide in all sea areas from 2010 to 2020. The growth rate of coastal reclamation was relatively fast in the northern waters (Bohai Sea and Yellow Sea) from 2010 to 2015, and in southern waters (East China Sea and South China Sea) after 2015. The growth rate of new coastal reclamation decreased sharply and the rate of returned mariculture enclosures continued to increase during the second decade of the twenty-first century. The growth rate of coastal reclamation in China decreased sharply from 2018 to 2020 and was basically the same as that of returned enclosures during the same period. The effectiveness of the control and management of coastal reclamation was directly related to the implementation of the *Notice of the State Council on Strengthening Coastal Wetlands Protection and Strictly Controlling Reclamation* issued in 2018.

Coastal reclamation monitoring is an important task in coastal zone management. The complexity and variability of different types of coastal reclamation pose difficulties in automatically monitoring changes using remote sensing technologies. In the future, there is a need to develop suitable methods for the real-time automatic remote sensing monitoring of coastal reclamation with improved frequency to ensure that SDG 14.5.1 and its related objectives can be better implemented in national marine management.

7.4 Summary

This chapter focused on three themes, including preventing and reducing various types of marine pollution, sustainable management and protection of the marine environment, and a comprehensive evaluation of regional SDG 14 progress. The study used Big Earth Data methods to conduct research on the progress of marine resource protection and sustainable utilization to promote sustainable development in China and its surrounding regions. The following products were generated in this chapter, including: datasets for field observations of nutrient concentrations in the coastal waters of Eastern China, spatiotemporal datasets of green tide biomass in the Yellow Sea, datasets for the spatial distribution of China's coastal tidal flats, a dataset containing information on HAB events (commonly referred to as "red tides") in the East China Sea, aggregated typhoon protection value datasets for China's coastal wetlands, remote sensing monitoring data for the development and utilization of spatial resources in China's coastal zones, and datasets for China's coastal reclamation and return of enclosures to the sea and wetlands.

The following recommendations are provided based on the research in this chapter.

1. In pursuit of SDG 14.1 for reducing various types of marine pollution, the high-precision monitoring and evaluation method developed for green tide biomass in China's offshore waters can accurately quantify and finely depict the disaster process caused by large floating algae. In addition, the method can provide technical support and a data reference for the on-site treatment of green tide on the sea surface, analyze responses to marine environmental changes, and aid in sustainable management. In the past decade or so, the concentration of nitrogen and phosphorus in China's offshore waters has mainly decreased due to significant environmental remediation efforts. The influx of large amounts of terrestrial nutrients has significantly decreased over the past decade.
2. In pursuit of SDG 14.2, or the sustainable management and protection of marine ecosystems, the reclamation of coastal tidal flats has been effectively curbed in China. The coastal tidal flats area decreased from 2015 to 2020, mainly since the natural erosion rate was greater than the siltation rate. China's coastal wetlands have played a significant role in reducing disaster losses caused by

typhoons. The total value of typhoon protection provided by China's coastal wetlands continued to rise between 2010 and 2020. The main reasons for this were due to the increase in the number and intensity of typhoons making landfall along China's coast, and the increased protection and restoration received by coastal wetlands.

3. With regard to SDG 14.5, or the protection of coastal and marine areas, the Chinese government has always attached great importance to the control and governance of land reclamation. The speed of land reclamation and the return of enclosures to the sea and wetlands along the Chinese coast continued to increase from 2010 to 2020, fully demonstrating the results that China has achieved in land reclamation control and governance.

The following suggestions are proposed to better promote the sustainable development of the marine environment.

First, coastal wetlands have significant social benefits in typhoon protection and disaster reduction, as well as important ecological functions such as regulating climate and promoting biodiversity. When space conditions permit, it is recommended to consider using more coastal wetlands to achieve typhoon protection.

Second, there is a need to strengthen the policy controls for the development, utilization, and protection of spatial resources in coastal zones. This involves the emphasis on a policy measure system that combines zoning, classification, and hierarchical control. The protection of key types, areas, and targets in coastal zones needs to be strengthened with respect to history and the current situation. In addition, it is necessary to strictly promote and implement ecological red line policies, farmland red line policies, build retreat line systems, and promote the protection and optimization of spatial resources in coastal zones.

Third, satellite remote sensing and other technological means should be fully utilized, so that the measures for the return of coastal enclosures to the sea and wetlands can be effectively tracked and monitored. Such technologies can provide basic information support for national marine and coastal zone management and scientific research. It is recommended that these technologies should be promoted and applied in global coastal protection.

References

908 Special Office of the State Oceanic Administration (2005) Coastal Zone survey technical tegulations. Ocean Press, Beijing (in Chinese)

Anderson DM, Glibert PM, Burkholder JM (2002) Harmful algal blooms and eutrophication: nutrient sources, composition, and consequences. Estuaries 25(4):704–726

Anderson DM, Cembella AD, Hallegraeff GM (2012) Progress in understanding harmful algal blooms: paradigm shifts and new technologies for research, monitoring, and management. Ann Rev Mar Sci 4:143–176

Anderson CR, Moore SK, Tomlinson MC et al (2015) Living with harmful algal blooms in a changing world: strategies for modeling and mitigating their effects in coastal marine ecosystems. In: Shroder JF, Ellis JT, Sherman DJ (eds) Coastal and marine hazards, risks, and disasters. Elsevier, Amsterdam, pp 495–561

Berdalet E, Banas N, Bresnan E et al (2017) GlobalHAB-Global Harmful Algal Blooms. https://hab.whoi.edu/wp-content/uploads/2019/08/GlobalHAB-Science-and-implementation-planfinal5.pdf [2023-08-29]

Cai WJ, Hu XP, Huang WJ et al (2011) Acidification of subsurface coastal waters enhanced by eutrophication. Nat Geosci 4:766–770

CMA Tropical Cyclone Data Center (2022) A brief history of tropical cyclone data in China. https://tcdata.typhoon.org.cn/en/index.html [2023-06-08]

Costanza R, Anderson SJ, Sutton P et al (2021) The global value of coastal wetlands for storm protection. Glob Environ Chang 70:102328

Di XH, Hou XY, Wu L (2014) Land use classification system for China's coastal zone based on remote sensing. Resour Sci 36(3):463–472 (in Chinese)

Du PP, Hou XY, Xu H (2022) Dynamic expansion of urban land in China's coastal zone since 2000. Remote Sens 14(4):916

EDGAR (2019) Emissions database for global atmospheric research. https://edgar.jrc.ec.europa.eu/overview.php?v=431 [2019-12-15]

FAO (2012) Fisheries and aquaculture information and statistics service: capture and aquaculture production 1950–2010, FishStat Plus, 2012. Food and Agriculture Organization of the United Nations, Rome

FAO (2016) Fishery and Aquaculture Statistics 2016. Food and Agriculture Organization of the UN, Roma, Italy

Ferreira JG, Bricker SB, Simas TC (2007) Application and sensitivity testing of a eutrophication assessment method on coastal systems in the United States and European Union. J Environ Manage 82(4):433–445

Garcia RA, Fearns P, Keesing JK et al (2013) Quantification of floating macroalgae blooms using the scaled algae index. J Geophys Res Oceans 118(1):26–42

General Office of the State Council, P. R. China (2017) National comprehensive disaster prevention and reduction plan (2016–2020). http://www.gov.cn/zhengce/content/2017-01/13/content_5159459.htm [2020-09-25] (in Chinese)

Glibert PM, Burkholder JM (2011) Harmful algal blooms and eutrophication: "strategies" for nutrient uptake and growth outside the Redfield comfort zone. Chin J Oceanol Limnol 29(4):724–738

Hou XY, Di XH, Hou W et al (2018a) Accuracy evaluation of land use mapping using remote sensing techniques in coastal zone of China. J Geo-Information Sci 20(10):1478–1488 (in Chinese)

Hu CM (2009) A novel ocean color index to detect floating algae in the global oceans. Remote Sens Environ 113(10):2118–2129

Hu LB, Hu CM, He MX (2017) Remote estimation of biomass of Ulva prolifera macroalgae in the Yellow Sea. Remote Sens Environ 192:217–227

Hu LB, Zeng K, Hu CM et al (2019) On the remote estimation of Ulva prolifera areal coverage and biomass. Remote Sens Environ 223:194–207

Hu CM, Qi L, Hu LB et al (2023) Mapping Ulva prolifera green tides from space: A revisit on algorithm design and data products. Int J Appl Earth Obs Geoinf 116:103173

Jiang TT, Pan JF, Pu XM et al (2015) Current status of coastal wetlands in China: degradation, restoration, and future management. Estuar Coast Shelf Sci 164:265–275

Justić D, Rabalais NN, Turner RE (1995) Stoichiometric nutrient balance and origin of coastal eutrophication. Mar Pollut Bull 30(1):41–46

Keesing JK, Liu DY, Fearns P et al (2011) Inter- and intra-annual patterns of Ulva prolifera green tides in the Yellow Sea during 2007–2009, their origin and relationship to the expansion of coastal seaweed aquaculture in China. Mar Pollut Bull 62(6):1169–1182

Kemp WM, Testa JM, Conley DJ et al (2009) Temporal responses of coastal hypoxia to nutrient loading and physical controls. Biogeosciences 6(12):2985–3008

Li L, Xing QG, Li XR et al (2018) Assessment of the impacts from the world's largest floating macroalgae blooms on the water clarity at the West Yellow Sea using MODIS data (2002–2016). IEEE J Sel Top Appl Earth Obs Remote Sens 11(5):1397–1402

Liu X, Geng R (2022) Assessment of the value of China's coastal wetlands for typhoon protection and disaster reduction. In: Guo HD (ed) Big Earth Data in Support of the Sustainable Development Goals 2022. New York. https://sdgs.un.org/documents/big-earth-data-support-sustainable-development-goals-2022-52847

Liu JY, Zhang ZX, Zhuang DF et al (2003) A study on the spatial-temporal dynamic changes of land-useand driving forces analyses of China in the 1990s. Geogr Res 22(1):1–12 (in Chinese)

Liu DY, Keesing JK, Dong ZJ et al (2010) Recurrence of the world's largest green-tide in 2009 in Yellow Sea, China: Porphyra yezoensis aquaculture rafts confirmed as nursery for macroalgal blooms. Mar Pollut Bull 60(9):1423–1432

Liu X, Wang YB, Costanza R et al (2019) The value of China's coastal wetlands and seawalls for storm protection. Ecosyst Serv 36:100905

Liu JC, Liu JQ, Ding J et al (2022a) A refined imagery algorithm to extract green tide in the Yellow Sea from HY-1C satellite CZI measurements. Haiyang Xuebao 44(5):1–11 (in Chinese)

Liu JQ, Lu YC, Ding J et al (2022b) Oil spills in China Seas revealed by the national ocean color satellites. Chin Sci Bull 67:3997–4008 (in Chinese)

Liu J, Yao QZ, Mi TZ et al (2022c) Change of the long-term nitrogen and phosphorus in the Changjiang (Yangtze) River Estuary. Front Mar Sci 9:885311

Liu JQ, Ye XM, Song QJ et al (2023) Products of HY-1C/D ocean color satellites and their typical applications. Natl Remote Sens Bull 27(1):1–13 (in Chinese)

Ma ZJ, Melville DS, Liu JG et al (2014) Rethinking China's new great wall. Science 346(6212):912–914

Narayan S, Beck MW, Wilson P et al (2017) The value of coastal wetlands for flood damage reduction in the Northeastern USA. Sci Rep 7:9463

Paerl HW (2006) Assessing and managing nutrient-enhanced eutrophication in estuarine and coastal waters: interactive effects of human and climatic perturbations. Ecol Eng 26(1):40–54

Purcell JE (2012) Jellyfish and ctenophore blooms coincide with human proliferations and environmental perturbations. Ann Rev Mar Sci 4:209–235

Qi L, Hu CM, Xing QG et al (2016) Long-term trend of Ulva prolifera blooms in the western Yellow Sea. Harmful Algae 58:35–44

Rabalais NN, Turner RE, Scavia D (2002) Beyond science into policy: Gulf of Mexico Hypoxia and the Mississippi River. Bioscience 52(2):129–142

Rabalais NN, Cai WJ, Carstensen J et al (2014) Eutrophication-driven deoxygenation in the coastal ocean. Oceanography 27(1):172–183

Ren CY, Wang ZM, Zhang YZ et al (2019) Rapid expansion of coastal aquaculture ponds in China from Landsat observations during 1984–2016. Int J Appl Earth Obs Geoinf 82:101902

Seriño MN, Ureta JC, Baldesco J et al (2017) Valuing the protection service provided by Mangroves in Typhoon-hit Areas in the Philippines. https://www.researchgate.net/publication/324363825_Valuing_the_Protection_Service_Provided_by_Mangroves_in_Typhoon-hit_Areas_in_the_Philippines [2023-10-29]

Song JM (2004) Biogeochemistry of China's Marginal Seas. Shandong Science and Technology Press, Jinan (in Chinese)

State Oceanic Administration (2018) 2016 Bulletin of China Marine Disaster. http://gc.mnr.gov.cn/201806/t20180619_1798020.html

Stehfest E, van Vuuren D, Kram T, et al (2014) Integrated assessment of global environmental change with IMAGE 3.0. Model description and policy applications. PBL Netherlands Environmental Assessment Agency, The Hague

Sun S (2012) Regional oceanography of China seas—biological oceanography. China Ocean Press, Beijing (in Chinese)

Tang QS, Zhang XW, Ye NH et al (2010) Review on the research progress on marine green tide. Bull Natl Nat Sci Found China 1:5–9 (in Chinese)

Uye S-I (2008) Blooms of the giant jellyfish Nemopilema nomurai: a threat to the fisheries sustainability of the East Asian Marginal Seas. Plankon Benthos Res 3(Supplement):125–131

van Beek LPH, Wada Y, Bierkens MFP (2011) Global monthly water stress: 1. Water balance and water availability. Water Resour Res 47(7):WO7517

Wang B, Xin M, Wei Q et al (2018) A historical overview of coastal eutrophication in the China Seas. Mar Pollut Bull 136:394–400

Wang JJ, Beusen AHW, Liu XC et al (2020) Spatially explicit inventory of sources of nitrogen inputs to the Yellow Sea, East China Sea, and South China Sea for the period 1970–2010. Earth's Future 8(10):e2020EF001516

Wang K, Wei Q, Jian H et al (2022) Variations of nutrient concentration and composition in Liaodong Bay under long-term human activities. Mar Pollut Bull 182:114016

Wei QS, Yao QZ, Wang BD et al (2015) Long-term variation of nutrients in the southern Yellow Sea. Cont Shelf Res 111:184–196

Xian WW, Kang B, Liu RY (2005) Jellyfish blooms in the Yangtze Estuary. Science 307(5706):41

Xing QG, Hu CM (2016) Mapping macroalgal blooms in the Yellow Sea and East China Sea using HJ-1 and Landsat data: application of a virtual baseline reflectance height technique. Remote Sens Environ 178:113–126

Xing QG, Hu CM, Tang DL et al (2015) World's largest macroalgal blooms altered phytoplankton biomass in summer in the Yellow Sea: satellite observations. Remote Sens 7(9):12297–12313

Xing QG, An DY, Zheng XY et al (2019) Monitoring seaweed aquaculture in the Yellow Sea with multiple sensors for managing the disaster of macroalgal blooms. Remote Sens Environ 231:111279

Xu Q, Zhang HY, Ju L et al (2014) Interannual variability of Ulva prolifera blooms in the Yellow Sea. Int J Remote Sens 35(11/12):4099–4113

Yang H, Ma MG, Thompson JR et al (2017) Protect coastal wetlands in China to save endangered migratory birds. Proc Natl Acad Sci USA 114(28):E5491–E5492

Yang FX, Wei QS, Chen HT et al (2018) Long-term variations and influence factors of nutrients in the western North Yellow Sea, China. Mar Pollut Bull 135:1026–1034

Yunev OA, Carstensen J, Moncheva S et al (2007) Nutrient and phytoplankton trends on the western Black Sea shelf in response to cultural eutrophication and climate changes. Estuar Coast Shelf Sci 74(1/2):63–76

Zhou MJ, Liu DY, Anderson DM, et al (2015) Introduction to the special issue on green tides in the Yellow Sea. Estuar Coast Shelf Sci 163:3–8

SDG 15 Life on Land

8

8.1 Background

China attaches great importance to ecological and environmental issues, upholds the concept that lucid waters and lush mountains are invaluable assets, coordinates the systematic management of mountains, water, forests, fields, lakes, grasses, and sand, and comprehensively promotes the construction of the nature reserve system. These efforts have steadily improved the quality of ecosystems, effectively mitigated the aggravation of biodiversity loss, significantly enhanced the ability to cope with climate change, and made promising progress in the implementation of SDG 15 targets.

In order to promote better implementation of SDG 15 targets in China, it is urgent to improve the scientific and technological content of ecosystem conservation and restoration strategies, and to promote ecological assessments, conservation, and restoration with technological innovation as the driving force to maximize the benefits. Conducting large-scale, spatially explicit assessments of the state of SDG 15 indicators and clarifying the corresponding contributions of climate change and human activity are important to guide the formulation of scientific conservation and restoration policies. However, ecosystem change is influenced by multifactor interactions at multiple scales, and traditional data or analytical methods are clearly beyond their reach. Big Earth Data, with its characteristics of exploring correlations among multidisciplinary data and further discovering new models, rules, and knowledge, already has great potential for research related to SDG 15. In 2022, we focused on four SDG 15 specific objectives, using Big Earth Data as a means to conduct four case studies to better explore the value of Big Earth Data in service of SDG 15.

8.2 Main Contributions

In response to the data and methodological gaps faced when assessing progress toward SDG 15, the case studies in this chapter constructed a technical system for assessing the benefits of natural forest conservation, a fine-scale air-ground monitoring system for biodiversity, a black soil degradation early warning and assessment system, and a methodological system for predicting and assessing the distribution of important invasive agricultural pests. The case studies scientifically identify forest conservation benefits, the current status and risk of the degradation of northeastern black soil, and the damage status and future risk of invasive agricultural pests in China. This chapter can provide important support for the assessment of SDG 15 at the regional and global scales (Table 8.1).

H. Guo, *Big Earth Data in Support of the Sustainable Development Goals (2022) - China*,
Sustainable Development Goals Series, https://doi.org/10.1007/978-981-97-4231-8_8

Table 8.1 Case studies and their main contributions

Corresponding to specific goals/metrics	Cases	Contributions
SDG 15.1 By 2020, ensure the conservation, restoration, and sustainable use of terrestrial and inland freshwater ecosystems and their services, in particular forests, wetlands, mountains, and drylands, in line with obligations under international agreements	Assessment of forest resource dynamics and protection benefits in the Natural Forest Protection Program of China (2000–2020)	**Data products:** Land cover products and vegetation cover products in China's natural forest resources protection program (NFPP) areas from 2000 to 2020 **Decision support:** It was found that since the implementation of the NFPP Program, forest resources in the NFPP Program areas in China have been protected and restored, and the implementation of the NFPP Program has been effective
SDG 15.3 By 2030, combat desertification, restore degraded land and soil, including land affected by desertification, drought, and floods, and strive to achieve a land degradation-neutral world	Early warning and risk assessment of black soil degradation in Northeast China	**Data product:** Spatial distribution map of the degradation degree of black soil in Northeast China **Method and model**: Based on the sequence of soil total organic carbon (TOC) content changes, a new black soil degradation assessment system was constructed by integrating black soil layer thickness, magnetization rate, particle size, erosion rate, and other indicators **Decision support:** Although the degraded black soil area is relatively small, the area of the high-risk zone is more than 10% and the area of the safe zone is only ca. 30%, so it is urgent to take effective measures to carry out scientific protection
SDG 15.5 Take urgent and significant action to reduce the degradation of natural habitats, halt the loss of biodiversity and, by 2020, protect and prevent the extinction of threatened species	Precise Conservation and Management of Biodiversity in Qianjiangyuan National Park	**Method and model:** An accurate big data biodiversity monitoring system was built to estimate the population size and spatial distribution of woody species in Qianjiangyuan National Park **Decision support:** Specific conservation objectives and strategies can be formulated for different species, especially rare and endangered species and endemic species, laying the foundation for precise management and conservation of the national park
SDG 15.8 By 2020, introduce measures to prevent the introduction and significantly reduce the impact of invasive alien species on land and water ecosystems and control or eradicate the priority species	Prediction and assessment of the distribution of critical invasive pests	**Method and model:** The ecological niche model (ENM) was used to predict the potential distribution of invasive agricultural pests, and three indicators were proposed to assess the prevention and control effects of 10 invasive agricultural pests and their potential damage levels in China

8.3 Case Studies

8.3.1 Assessment of Forest Resources Dynamics and Protection Benefits in the Natural Forest Protection Program of China (2000–2020)

Target: SDG 15.1: By 2020, ensure the conservation, restoration, and sustainable use of terrestrial and inland freshwater ecosystems and their services, in particular forests, wetlands, mountains, and drylands, in line with obligations under international agreements.

SDG 15.4: By 2030, ensure the conservation of mountain ecosystems, including their biodiversity, in order to enhance their capacity to provide benefits that are essential for sustainable development.

8.3.1.1 Background

Two significant indicators of SDG 15, which pertains to the protection, restoration, and sustainable use of terrestrial ecosystems, are SDG 15.1.1 "forest area as a proportion of total land area" and SDG 15.4.1 "coverage by protected areas of important sites for mountain biodiversity". The conservation of natural forests is critical, as they are the most stable and biodiverse terrestrial ecosystems on the planet. In October 2000, the State Council officially approved the Implementation Plan for the Protection of Natural Forest Resources in the upper reaches of the Yangtze River and the middle and upper reaches of the Yellow River, as well as the Implementation Plan for the Protection of Natural Forest Resources in the Key State-owned Forest District in Inner Mongolia and Northeastern China. The Natural Forest Protection Program (NFPP) was implemented to address the challenges faced by the forestry sector in China, and it masked a significant shift from timber production to ecological construction. The second phase of the NFPP was completed at the end of 2020, and the monitoring and evaluation of natural forest resources will help to comprehensively and scientifically assess the program's protective effect on forest resources.

The NFPP is faced with the complex challenges of monitoring a vast area with a strong spatial heterogeneity and a large time span. Consequently, generating large area and high-precision forest cover products with strong temporal and spatial consistency remains a challenging task. Despite the abundance of land cover products at the global and national level, discrepancies in forest cover distribution among different products persist. Therefore, there is an urgent need to develop a comprehensive set of data products that can systematically evaluate the dynamic changes in forest cover during the implementation of the NFPP. Similarly, the commonly used MODIS vegetation cover products exhibit limitations such as low accuracy for regions with a strong topographic heterogeneity and unclear applicability in the analysis of trend changes in China's forest areas. Consequently, there is an urgent need for more reliable and accurate datasets based on fractional vegetation coverage (FVC) to analyze the benefits of the NFPP implementation. Failure to address these issues can lead to severe forest landscape fragmentation, particularly in the context of rapid social and economic development. The dynamics in forest connectivity at the landscape scale reflect the impacts of forest protection, and research results can provide decision-making support and a scientific basis for the long-term protection and restoration of natural forests in the future.

8.3.1.2 Data

- National Geomatics Center of China Globeland30 products (http://www.globallandcover.com/) 30 m land cover data in 2000, 2010, and 2020; 30 m land cover data of GLC_FCS30 products (https://data.casearth.cn/) from CAS in 2000, 2015, and 2020;

30 m land cover data of Chinacover products from CAS in 2000, 2010, and 2015; European Space Agency WorldCover product (https://viewer.esa-worldcover.org/worldcover/) 10 m land cover data for 2020.

- Surface reflectance products from 30 m Landsat satellites in China 2000–2020, USGS.
- 250 m per 16 days MODIS vegetation index product MOD13Q1 from 2000 to 2020 (https://modis.gsfc.nasa.gov/), National Aeronautics and Space Administration (NASA).
- 2017–2020 survey sample data of the Chinese Terrain Ecosystem Research Network (CTERN); national continuous forest inventory data, forest resource planning and design survey data; field survey sample data in Northeastern China and Inner Mongolia in 2020.
- Airborne remote sensing data from the Chinese Academy of Forestry (CAF) light detection and ranging (LiDAR), CCD, and Hyperspectral Integrated Airborne Observation System.

8.3.1.3 Methods

A collection of cloud-free remote sensing data was constructed using Landsat surface reflection products during the vegetation growing season. These were achieved by composing time-series remote sensing images with improved pixel evaluation rules. Four sets of land cover classification products were collected, creating a credible classification sample library for the intersection area of similar land cover types from 2000 to 2020. Random classification samples were then selected from the sample library (with no more than 10,000 samples per category) according to the tile-by-tile range ($2.1° \times 2.1°$) for RF classification. Post-processing analysis was carried out using the voting method constrained by rules. Long-term time-series continuous change detection and classification (CCDC) was then employed to calculate the land cover change detection results from 2000 to 2020. The 2000 and 2010 data were consistently analyzed and updated based on the 2020 results. Finally, the products of the NFPP in 2000, 2010, and 2020 were obtained. Using the three-phase land cover products produced in this study, the morphological spatial pattern analysis (MSPA) method was applied to identify the landscape types important for maintaining connectivity, including the forest core area, islet area, and edge area. Furthermore, this study analyzed the dynamics in the forest landscape pattern in the NFPP from 2000 to 2020.

Based on the MODIS vegetation index product and a modified pixel dimidiate model, yearly FVC products were produced. Each MODIS image was divided into 8×8 blocks to obtain the local parameters of the model. Then Theil-Sen median trend analysis and the Mann–Kendall significance test were used to analyze the FVC change trend since the implementation of the NFPP, and the FVC trend was divided into five grades: increasing obviously, increasing slightly, stable, decreasing slightly, and decreasing obviously.

8.3.1.4 Results and Analysis

The forest cover of the NFPP exhibits a spatial heterogeneity, with high density in the northeastern, central, and southwestern regions, and lower coverage in the northwest of China [Fig. 8.1(a)]. The forest cover rate of the entire NFPP area was 35.16% in 2020. Among the different state-owned forest districts, Hainan showed the highest forest cover rate (74.25%), followed by the key state-owned forest district in Inner Mongolia and Northeast China (72.87%), and the upper reaches of the Yangtze River (56.91%). Whereas the middle and upper reaches of the Yellow River exhibited a lower forest cover rate of 15.81%, the state-owned forest district in Xinjiang showed the lowest forest cover rate of 3.78%.

During the period 2000–2020, the forest cover of the NFPP showed a positive trend with an increase in the forest area across the entire project area. Specifically, by the end of the program's second phase, the forest area of the program had grown by 2.09% (as shown in Table 8.2). The upper reaches of the Yangtze River had the highest forest growth, accounting

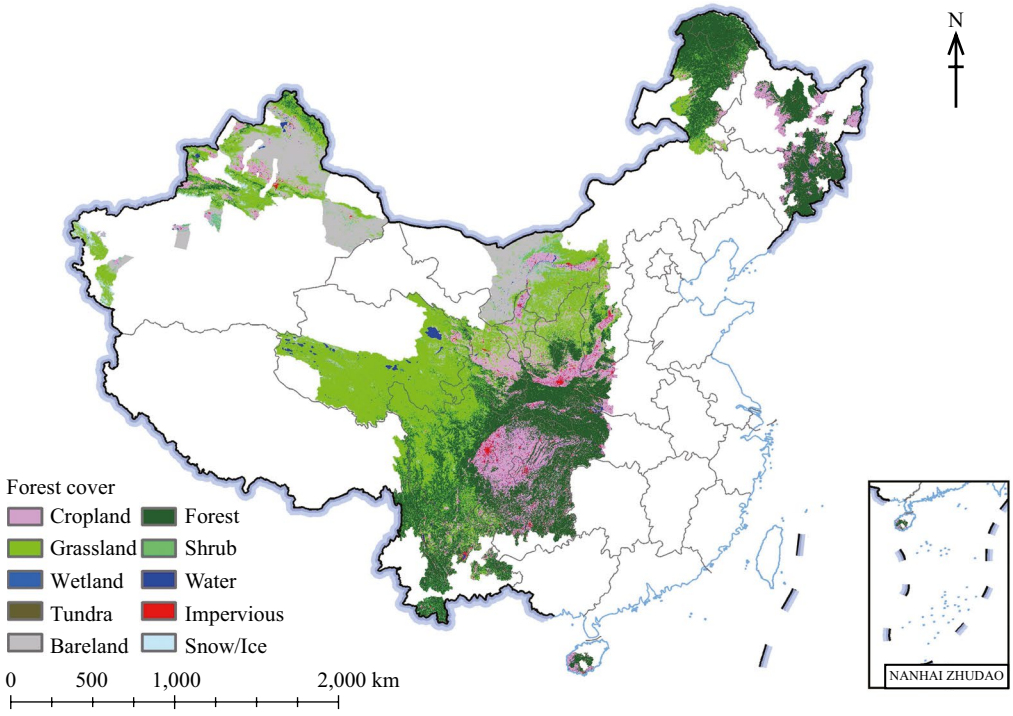

(a) Forest cover map of the NFPP in 2020

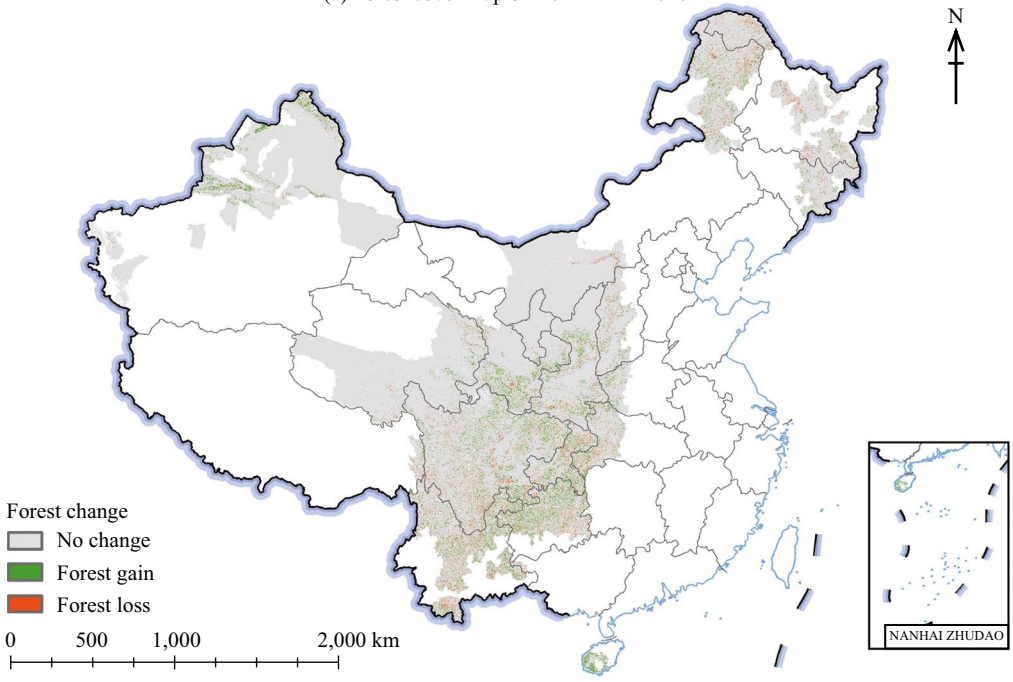

(b) The spatial distribution of forest changes of the NFPP between 2000 and 2020

Fig. 8.1 Spatial distribution of forest cover and forest changes of the NFPP

Table 8.2 Changes in forest cover in the NFPP from 2000 to 2020

Regions	Rate of forest cover /%			Net growth/ Percentage point	Net growth rate/%
	2000	2010	2020	2000–2020	
NFPP	33.07	33.48	35.16	2.09	6.31
Key state-owned forest districts in Inner Mongolia and Northeastern China	71.24	71.69	72.87	1.63	1.65
Upper reaches of the Yangtze River	52.34	53.10	56.91	4.57	8.74
Middle and upper reaches of the Yellow River	14.36	15.04	15.81	1.45	10.03
State-owned forest district in Hainan	70.19	71.03	74.25	4.06	5.46
State-owned forest district in Xinjiang	3.56	3.76	3.78	0.22	6.76

for 62.28% of the total forest growth area in the entire project area. Following this were the middle and upper reaches of the Yellow River (25.55%), the key state-owned forest district in Inner Mongolia and Northeastern China (9.49%), the state-owned forest district in Xinjiang (2.01%), and last, the state-owned forest district in Hainan (0.67%).

During the period 2000–2020, the net growth rate of forests in the NFPP was 6.31%, which represents the proportion of net growth in the total forest area in 2000. The middle and upper reaches of the Yellow River presented the fastest growth rate, with a significant increase of 10.03% in forest cover, followed by the upper reaches of the Yangtze River (8.74%), the state-owned forest district in Xinjiang (6.76%), the state-owned forest district in Hainan (5.46%), and the key state-owned forest district in Inner Mongolia and Northeastern China (1.65%). Concerning spatial distribution [Fig. 8.1(b)], the areas with significant forest growth were mainly concentrated in the south of the Greater Khingan Mountains, the east of the Lesser Xing'an Mountains and the Changbai Mountains, western Shanxi, central Shaanxi and the Qinling region, southern Ningxia, southeastern Gansu, western Sichuan, northern Chongqing, western Guizhou, northern Yunnan, the south of the Tianshan Mountains and Altai Mountains of Xinjiang, and southwestern Hainan. Moreover, the areas of forest loss were mainly distributed in the Greater Khingan Mountains and the Hengduan Mountains.

From 2000 to 2020, the forest core area of the NFPP showed an increasing trend. The islet area and edge area in the key state-owned forest districts in Inner Mongolia and Northeast China, the upper reaches of the Yangtze River, and the state-owned forest district in Xinjiang continued to decrease. The middle and upper reaches of the Yellow River decreased from 2000 to 2010 and then remained stable, while the state-owned forest district in Hainan increased from 2000 to 2010 and fell to the lowest value from 2010 to 2020 (Fig. 8.2). The decrease of the islet and edge areas indicated that the forest landscape fragmentation was decreasing. On the whole, the overall quality of forests in the NFPP has been effectively improved.

In general, since the implementation of the NFPP, the FVC of each region in the NFPP showed an increasing trend (Fig. 8.3). The area with an increasing trend accounted for 78.22% of the total forest area, and the area with a decreasing trend accounted for 9.56% of the total forest area (mainly distributed in western Sichuan and northern Yunnan).

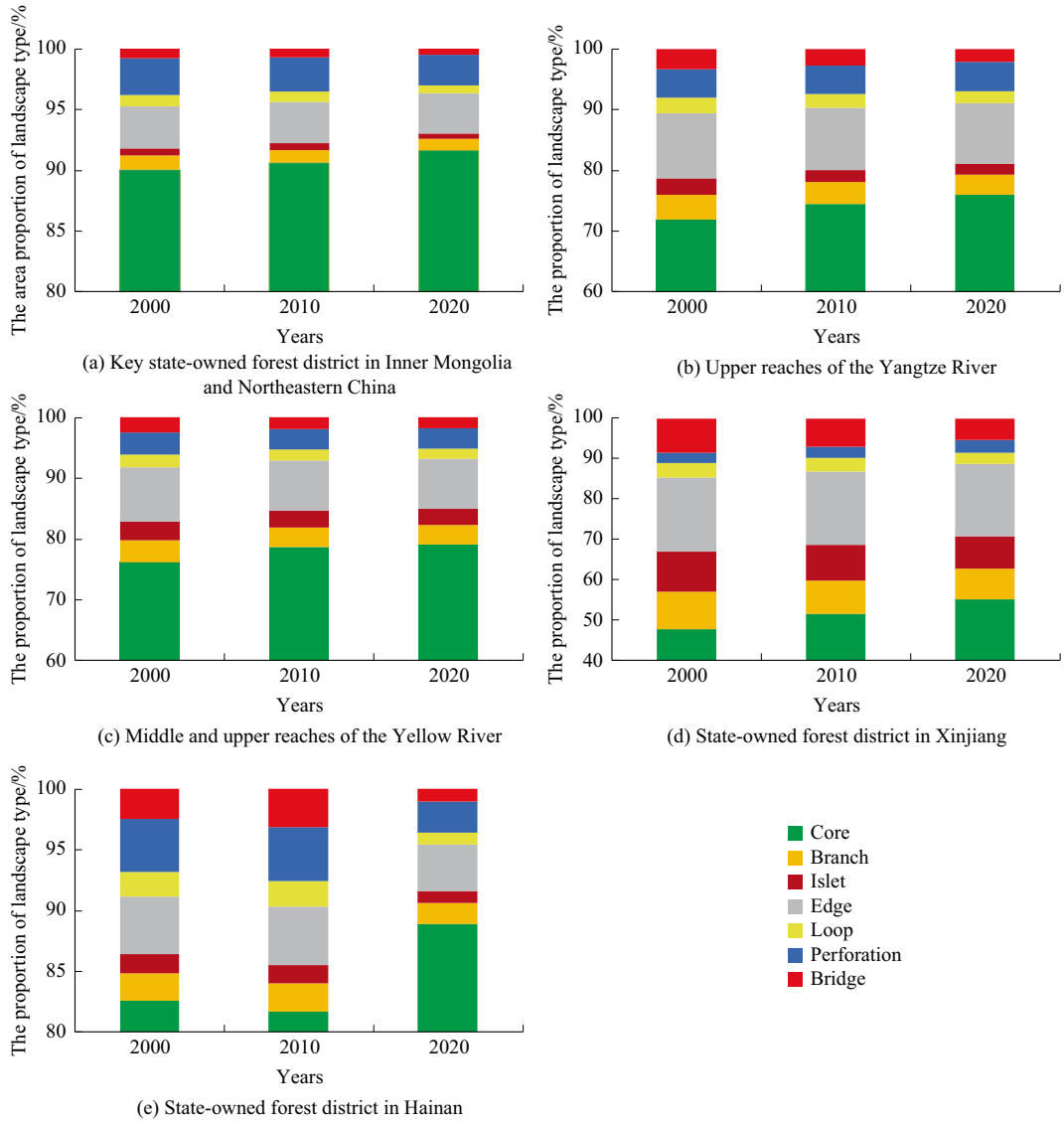

Fig. 8.2 Area proportion of each landscape type in the NFPP

Highlights

- Based on the time-series remote sensing data, land cover products and vegetation cover products were produced in the NFPP in China from 2000 to 2020.
- We used land cover products to characterize the change in the forest cover areas within the NFPP and analyze the landscape patterns within the program implementation areas. Additionally, FVC was used to describe forest quality within the NFPP and to evaluate the protection benefits of the NFPP.
- Since the implementation of the NFPP, China's forest resources within the program area have been effectively protected and restored, and the implementation of the program has yielded significant results.

8.3.1.5 Discussion and Outlook

This study refers to three periods: the beginning of the implementation of the NFPP (2000), the

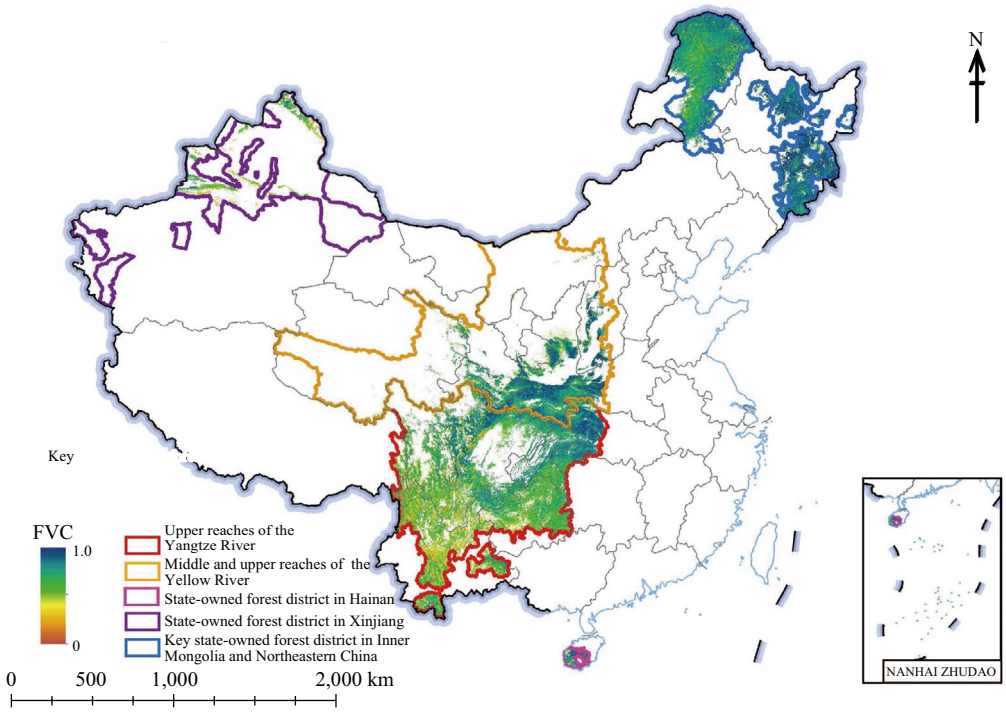

(a) FVC in the NFPP area of China in 2020

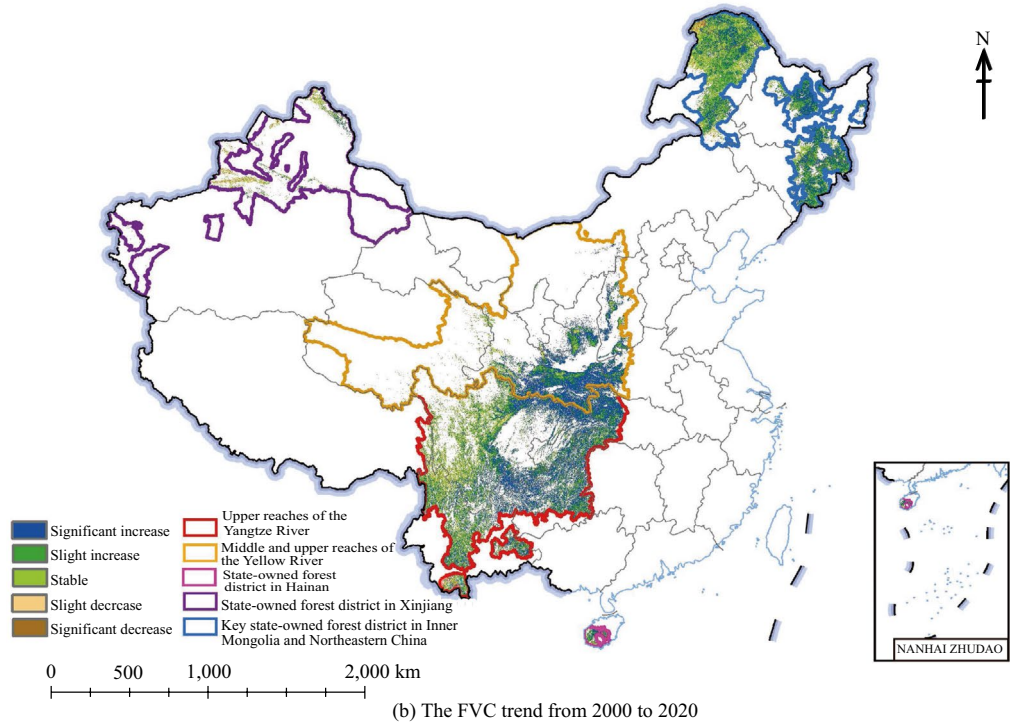

(b) The FVC trend from 2000 to 2020

Fig. 8.3 Fractional vegetation coverage of NFPP in China in 2020 and its trend from 2000 to 2020

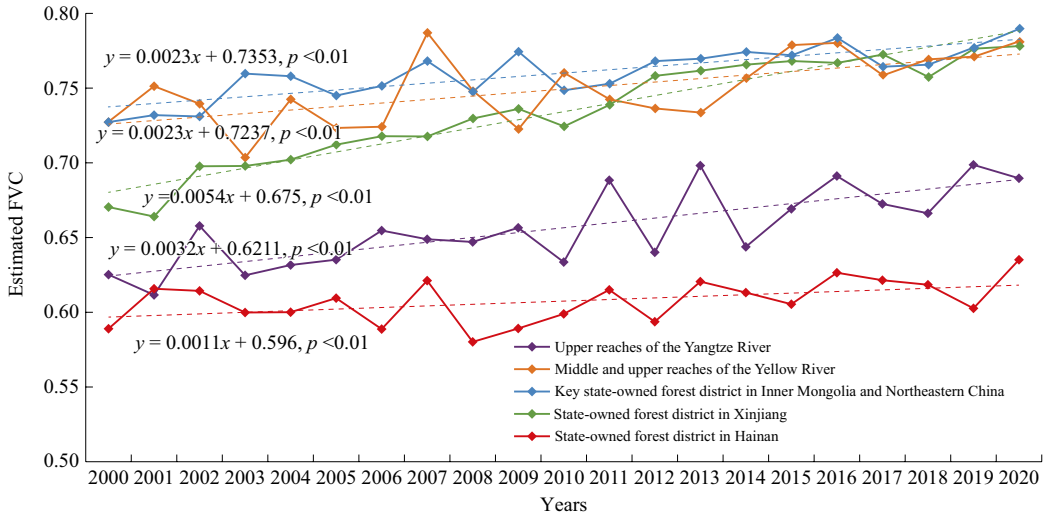

(c) Time series of FVC from 2000 to 2020

(continued)

end of the first phase (2010), and the end of the second phase (2020). The forest cover area and FVC were used as indicators to develop monitoring and evaluation methods for the quantity and quality of forest resources, and the dynamics and protection benefits of forest resources were evaluated.

From 2000 to the end of 2020, the forest cover of the NFPP showed an increasing trend, and the forest cover rate increased by 2.09%. In terms of growth, the upper reaches of the Yangtze River showed the highest forest growth, and the net forest growth accounted for 62.28% of the forest growth area in the NFPP. In terms of the growth rate, forest cover in the middle and upper reaches of the Yellow River increased the fastest, with an increased rate of 10.03%. During the implementation of the NFPP, the core area of the forest in the NFPP showed an increasing trend, and the islet and edge areas decreased, indicating that the forest landscape fragmentation in the NFPP increased from 2000 to 2020, and the forest quality was effectively improved. FVC showed an increasing trend in most of the areas. The area with an increasing trend accounted for 78.22% of the total forest area, and the area with a decreasing trend accounted for 9.56% of the total forest area.

On the whole, the implementation of the NFPP has effectively protected and restored the forest resources in the protected area, the forest cover and FVC have increased steadily, and the implementation of the NFPP has been remarkably effective.

8.3.2 Early Warning and Risk Assessment of Black Soil Degradation in Northeast China

Target: SDG 15.3: By 2030, combat desertification, restore degraded land and soil, including land affected by desertification, drought and floods, and strive to achieve a land degradation-neutral world.

8.3.2.1 Background

Soil degradation was recently suggested to be added as the 10th Earth system process within the planetary boundary framework (Kraamwinkel et al. 2021), because it is a guide for defining a safe operating space in which human development can continue. However, the quantification of soil degradation on a large

scale has proven challenging, partly because of the spatial heterogeneity of soils, the multiple explanations of the degradation index, and the uncertainty of mathematical models.

Black soil, the most fertile and optimally cultivated soil in the world, is a limited and non-renewable resource on the time scale relevant to human welfare, and is therefore often referred to as the "Giant pandas of farmland". Northeast China is one of the four largest black soil regions on Earth, covering an area of approximately 226,000 km^2, and it has become an important grain-producing area both within China and globally. Data from the National Development and Reform Commission indicate that the annual grain output accounts for one-fifth of the total in China, and the output of grain for sale alone accounts for one-third. Unfortunately, loose structure and unsustainable cultivation practices together caused the region's black soil to undergo severe erosion. Consequently, estimating the proportion of land that is degraded over the total land area in Northeast China could make a significant contribution to achieving SDG 15.3, thereby ensuring future food security for China and potentially elsewhere.

8.3.2.2 Data

- Distribution of TOC for surface soil (0–30 cm) in Northeast China (Liu F et al. 2022).
- Data from field investigation and measurement: the thickness of black soil and loess for 185 soil profiles, the erosion rate for 24 typical black soil sites (Wang H et al. 2022), TOC content and magnetic susceptibility and particle size for 14 sandy soil profiles (Guo et al. 2023).
- Data published in China, including the soil erosion rate from Keshan County, the average grain yields over decades across China.

8.3.2.3 Methods

The spatial distribution of the thickness of black soil and its parent material, loess, was obtained through field investigation to evaluate the erosion resistance of black soil. The measured soil TOC content and magnetic susceptibility of the soil profile together with an analysis of the TOC content of soil units were used to examine the relationship between changes in soil properties (e.g., magnetic susceptibility, soil grain size, and soil erosion) and fertility (expressed by the average grain yield across China) and TOC content. Then, a tipping point or critical threshold for soil degradation was determined. By synthesizing TOC content, thickness, and erosion rates for the black soil in Northeast China, a new early warning indicator system for black soil degradation was developed. Ultimately, a risk assessment for black soil degradation in Northeast China was accomplished by analyzing the distribution of TOC for the surface soil (0–30 cm), and both the spatial distribution of the black soil degradation level and the proportion of land that is degraded over the total land area in the region were obtained simultaneously.

8.3.2.4 Results and Analysis

New Early Warning Indicator System of Black Soil Degradation in Northeast China

On the spatial scale, the TOC content and thickness of the black soil in Northeast China exhibit an overall increase from southwest to northeast, with a clear decrease in the erosion rate observed clearly from west (>3 mm/a) to east (0–3 mm/a) across the black soil region. A mean erosion rate of 2.22 mm/a was obtained for the black soil in Northeast China. The correlation of the erosion rates and climatic parameters suggests that wind erosion dominates in the west and water erosion dominates in the east. On the profile scale, the compiled TOC content of soil profiles in the region indicates that soil shifts rapidly into a degraded and infertile state when TOC is less than 0.5% (Fig. 8.4). Further analysis indicates that wind and water erosion are the main causes of the loss of fine PM, leading to increases in the median grain size of the eroded soil and in the regional soil erosion rate. The erosional loss of fine PM, especially carrying strong magnetic minerals, contributes to a

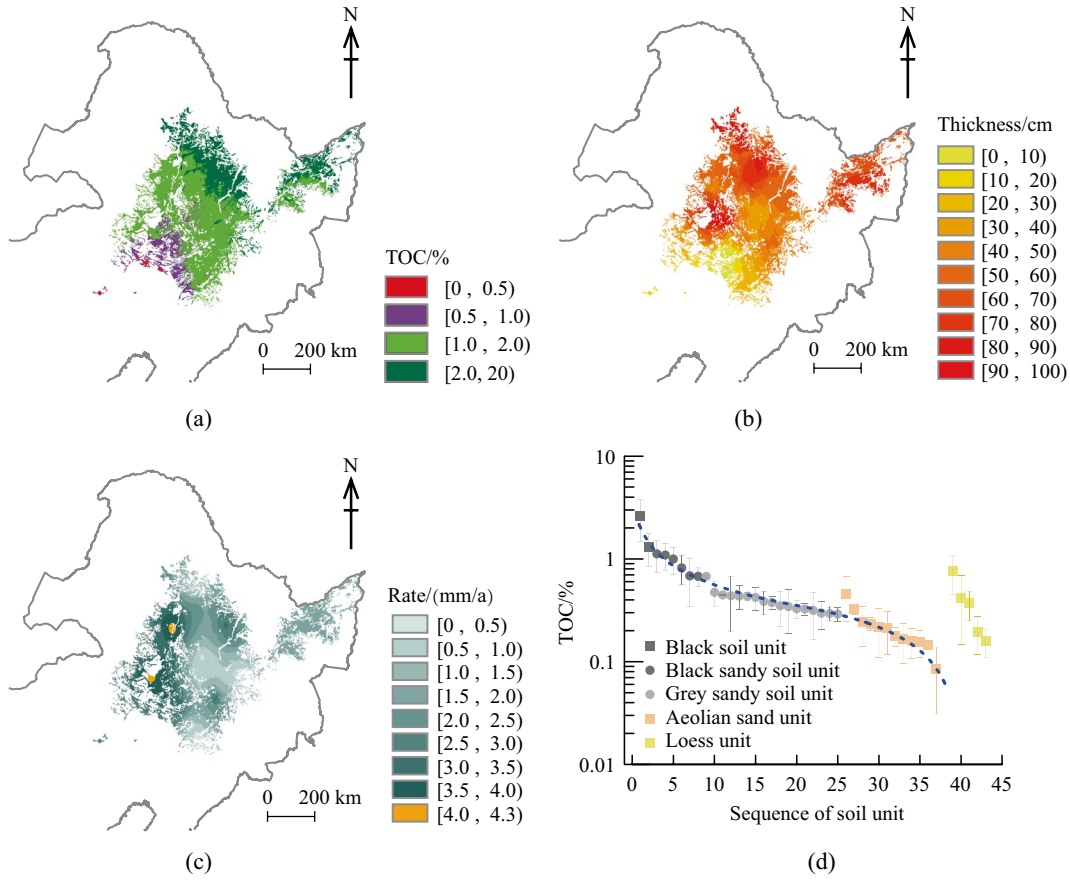

Fig. 8.4 Distribution of the TOC content of topsoil (a) and thickness of black soil layer (b) and erosion rates (c) for the black soil in Northeast China, together with the compiled sequence of soil TOC content from profiles (d) in the region

weaker stage of pedogenesis and a decrease in magnetic susceptibility. Additionally, a compilation of grain yields and corresponding TOC content of soil from 68 experimental sites in cultivated land across China demonstrates that the average grain yield exceeds ca. 2,000 kg/(ha·a) for soil with TOC > 0.5%, but then decreases rapidly for soil with TOC < 0.5%. For soil with TOC < 0.5%, the natural upper limit of soil fertility cannot be raised by human interventions due to the lack of humus. These changes in soil properties and fertility induced by soil degradation, together with our data compilation, suggest that soil TOC can serve as an early warning indicator of soil degradation in Northeast China, where soil remains fertile for TOC > 0.5%, but rapidly shifts into a degraded and infertile state for TOC < 0.5%.

In this study, the authors investigated the relationship between soil TOC content and black soil degradation. The results show that when soil TOC content is between 0.5–1.0%, the black soil degrades slowly and is classified as a high-risk area. Conversely, when soil TOC content is between 1.0 and 2.0%, black soil degradation is limited, resulting in a relatively high level of food production, and is classified as a low-risk area. Furthermore, the black soil with soil TOC content exceeding 2.0% remains in good condition (healthy and fertile), maintaining a stable

level of sustainable food production, and is classified as a safe area. It is worth noting that the thickness of soil required to sustain food production should exceed 10 cm, therefore, black soil with less than 10 cm depth is classified as a high-risk area. Additionally, assuming that soil loss tolerance is 50 t/(ha·a), and that the average bulk density of black soil is 1.25 g/cm, the corresponding erosion rate is 4 mm/a. As a result, the black soil with an erosion rate exceeding 4 mm/a is also classified as a high-risk area.

Spatial Distribution of the Soil Degradation Level for the Black Soil in Northeast China

This study aimed to develop an early warning indicator system for black soil degradation in Northeast China by synthesizing TOC content, thickness, and erosion rates for the black soil in the region. Subsequently, a risk assessment on black soil degradation in Northeast China was conducted based on the distribution of TOC for the surface soil. The results (Fig. 8.5) revealed that degraded black soil areas totaled 2,000 km^2 (0.9%), high-risk and low-risk areas 26,000 km^2 (11.5%) and 131,000 km^2 (58.0%), and safe areas 67,000 km^2 (29.6%) in Northeast China.

Highlights

- Data products with intellectual property rights were produced: spatial distribution of the black soil degradation level, and proportion of land that is degraded over the total land area in Northeast China.
- A contour map depicting the erosion rate of black soil in Northeast China was developed, revealing that wind erosion dominates in the west while water erosion dominates in the east. Using the mean erosion rate of 2.22 mm/a obtained from the contour map as a reference, it is estimated that the black soil will be completely eroded in approximately 113 years.
- The synthesis of TOC content, thickness, and erosion rate for the black soil in Northeast China enabled us to develop the new early warning indicator system for black soil degradation. Subsequently, a risk assessment on black soil degradation in Northeast China was accomplished, revealing that degraded black soil areas totaled 2,000 km^2 (0.9%), high-risk and low-risk areas 26,000 km^2 (11.5%) and 131,000 km^2 (58.0%), and safe areas 67,000 km^2 (29.6%) in Northeast China.

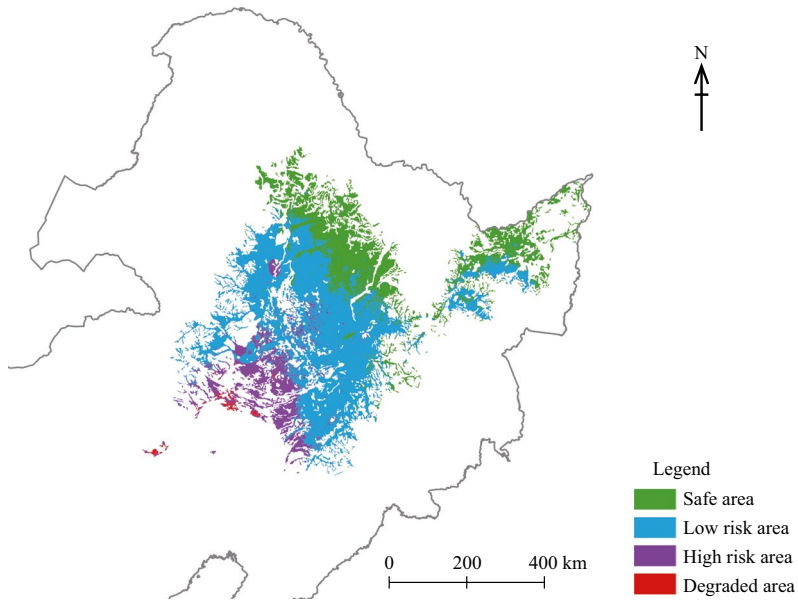

Fig. 8.5 Spatial distribution of the soil degradation level for black soil in Northeast China

8.3.2.5 Discussion and Outlook

Although the degraded black soil areas comprise only 0.9% of the region, the high-risk areas exceed 10%, while safe areas remain at approximately 30%. Using the mean erosion rate (2.22 mm/a) and the typical black soil thickness (average value 25 cm) as a reference, we speculate that the black soil will be entirely eroded in approximately 113 years without any sustainable soil management. Furthermore, the western part of the region exhibits high erosion rates, indicating that complete erosion may occur in a shorter time frame. These findings highlight the severe erosion of the black soil in the region, necessitating the immediate and urgent implementation of sustainable soil management policies to protect soil from further degradation. Given the agricultural importance of the black soil region, we propose a reduction in tillage throughout the region, and the implementation of revegetation by planting herbs in the west and afforestation in the east to control ongoing erosion.

This study comprehensively evaluates the multiple indicators collected from profiles within multiple climatic zones on a large scale, revealing the characteristics and threshold of black soil degradation in Northeast China. Moreover, the estimated proportion of land that is degraded over the total land area in Northeast China can guide decisions and strategies to ensure food security in the black soil and protect it from further degradation. Our findings also contribute significantly to achieving SDG 15.3 and ensuring future food security for China and potentially other regions.

8.3.3 Precise Conservation and Management of Biodiversity in Qianjiangyuan National Park

Target: SDG 15.5: Take urgent and significant action to reduce the degradation of natural habitats, halt the loss of biodiversity and, by 2020, protect and prevent the extinction of threatened species.

8.3.3.1 Background

Biodiversity, as an integral component of nature, has long been recognized as a crucial foundation for human survival and development. As a result, the establishment of a comprehensive system of nature reserves, with national parks as its core, has become a pivotal goal in the pursuit of sustainable development in China. Currently, protected areas in China have reached 18% of the country's total land area (Wang et al. 2020), and this coverage is expected to further expand by 2030. However, it should be noted that the effectiveness of conservation measures cannot be solely determined by the size of the protected areas. A scientific and precise approach to conservation and management within nature reserves is equally critical to effectively guarantee biodiversity conservation and the achievement of the UN SDGs.

Protected areas harbor diverse ecosystems with varying structures and complexities, which are often confronted with numerous environmental pressures such as human activity and climate change. Therefore, the protection and management of nature reserves require a comprehensive approach that includes the determination of protection objectives, formulation of protection strategies, implementation of protection plans, evaluation of protection outcomes, and continuous iterative adaptation of conservation and management measures. However, the present adaptive conservation and management approach is hampered by the lack of adequate scientific data support for setting protection goals, designing plans, and assessing the efficacy of nature reserves. Hence, establishing a long-term, multi-scale biodiversity monitoring system in nature reserves and accurately quantifying the amount and distribution of biodiversity are crucial for the precise protection and management of nature reserves.

Qianjiangyuan National Park, situated in the developed region of the Yangtze River Delta,

holds paramount significance as a national priority area for biodiversity conservation. The park encompasses a broad range of ecosystems, such as large area and continuously distributed mid-subtropical evergreen broadleaf old-growth forests, artificial forests, and secondary forests, forming a complete succession sequence. This study is grounded in the comprehensive datasets of plant diversity and remote sensing monitoring in Qianjiangyuan National Park. This study's primary objectives are to estimate and predict the population size and spatial distribution of plant species, identify biodiversity protection gaps, and finally establish the precise conservation and management of biodiversity, based on biodiversity monitoring data, in the national park. This study could help to form the paradigm of biodiversity conservation and management in the key areas of China, enhance the effectiveness of biodiversity protection and the implementation of the Convention on Biological Diversity, and advance the achievement of the UN SDGs.

8.3.3.2 Methods

A stratified random sampling was taken in Qianjiangyuan National Park. The park was split into 267 grids of 1 km × 1 km, and 1–3 quadrats of 20 m × 20 m with distance ≥ 300 m among quadrats were randomly located in each grid. The number of quadrats in a grid was subsequently determined following the vegetation heterogeneity in the grid. Only one quadrat was established in a grid with highly homogeneous vegetation. All individual trees with a diameter at breast height (DBH) ≥ 1 cm in the quadrat were investigated. A total of 663 quadrats were established.

Airborne LiDAR data were obtained with point density > 4/m^2 in > 90% area in Qianjiangyuan National Park. A high-resolution DEM (1 m) was built from the LiDAR data. The variables characterizing each 20 m × 20 m grid cell and each of the 663 quadrats were extracted from the LiDAR data, the DEM data, and the vegetation map of Qianjiangyuan National Park. These variables include (1) environmental variables: elevation, aspect, slope, and convexity; (2) community structure variables: forest canopy height, leaf area index, and canopy structure complexity (Fig. 8.6); and (3) anthropogenic variables: distance from villages and roads.

Species populations were estimated using species composition data in quadrats with 1 km × 1 km grid cells as a unit. Quadrat-based species, and environmental, community-structural, and human-disturbance data were used to build MaxEnt models for predicting the spatial distribution of 188 species with occurrence in at least 10 quadrats. Finally, conservation gaps in Qianjiangyuan National Park were analyzed.

8.3.3.3 Results and Analysis

Plant Population Size

Populations of 313 woody species observed in Qianjiangyuan National Park followed a log-transformed symmetric distribution (skew = 0.13, $p = 0.32$), with a mean of 625,991 and median of 40,179 [Fig. 8.7 (a)]. Of all those species, *Ligustrum obtusifolium* had the smallest population of ca. 280 individuals (95% confidence interval: 0–559), and *Cunninghamia lanceolata* had the largest population of 21,225,745 individuals (95% confident interval: 15,632,639–27,451,791). *Castanopsis eyrei*, the dominant species in subtropical evergreen broadleaf forests, had 6,238,447 individuals (95% confident interval: 4,003,547–8,808,841).

Spatial Distribution of Woody Species

Woody species occupied, on average, 52.6 km^2 in the areas in Qianjiangyuan National Park, with a mean of 54.6 km^2, standard deviation of 20.9, minimum of 5.1 km^2, and maximum of 97 km^2. The areas showed a negatively skewed unimodal distribution (skew = -0.18, $p = 0.03$), with more species being narrowly distributed in the park [Fig. 8.7 (b)]. Some species were almost exclusively distributed in the core protection areas of the park. Of all the species observed, six species presented > 90% of their distribution areas occurring within the core protection

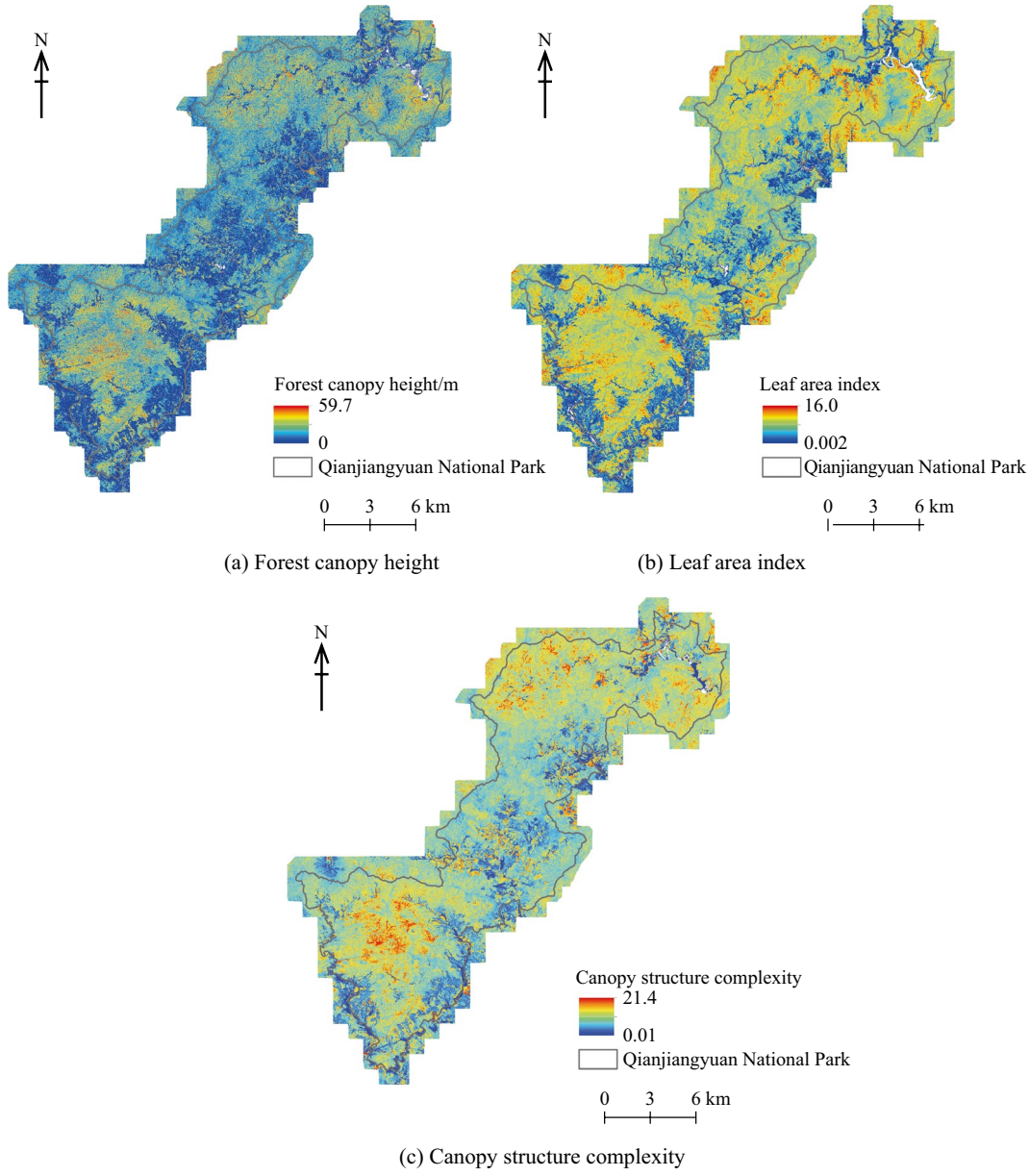

Fig. 8.6 Patterns of forest community structure variables in Qianjiangyuan National Park

areas, for example, *Daphniphyllum macropodum* occupied 12.8 km^2 in the area, 96.5% of which was within the core protection areas [Fig. 8.7 (d)]. Some species were mainly distributed outside the core protection areas, for example, *Cinnamomum camphora* occupied 37.6 km^2, only 40% of which was within the core protection areas [Fig. 8.7 (c)].

Gaps in Biodiversity Protection

Species richness (species number) was higher in the core protection areas (mean: 134) than that in the general control areas (mean: 92) at the resolution of 100 m × 100 m in Qianjiangyuan National Park ($t = 72.2$, $p << 0.001$) [Fig. 8.8 (a)]. The core protection areas covered all 18 rare and endangered woody species, which were richer

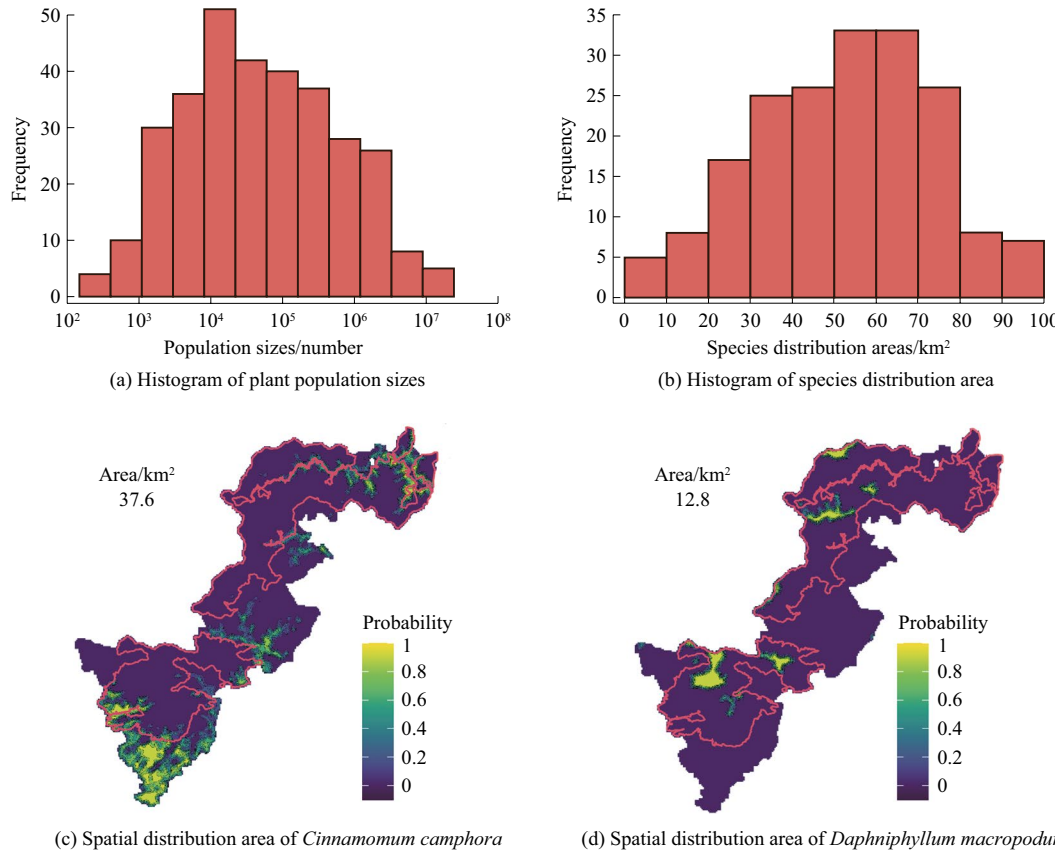

(a) Histogram of plant population sizes

(b) Histogram of species distribution area

(c) Spatial distribution area of *Cinnamomum camphora*

(d) Spatial distribution area of *Daphniphyllum macropodum*

Fig. 8.7 Summaries and illustrations of the spatial distribution of woody species in Qianjiangyuan National Park. *Note* The areas delineated by red lines refer to the core protection areas

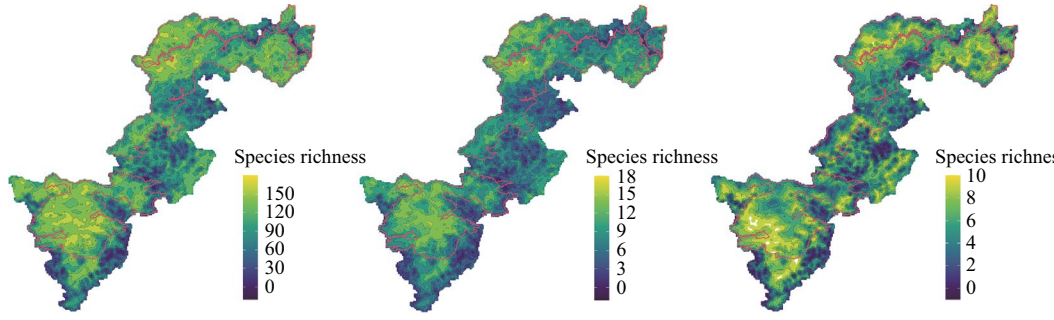

(a) All woody species

(b) Rare and endangered species

(c) Indicator species of typical subtropical evergreen broad-leaved forests

Fig. 8.8 Spatial patterns of species richness for three kinds of species. *Note* The areas delineated by red lines refer to the core protection areas

in the core area (mean:11.3 at the resolution of 100 m × 100 m) than those in the general control areas (mean: 7.4) ($t = 67.8$, $p << 0.001$) [Fig. 8.8 (b)]. The indicator species of typical subtropical evergreen broadleaf forests were richer, being distributed in a huge stretch, in the core

protection areas than those in the general control areas, involving almost all the indicator species [Fig. 8.8 (c)]. Within the core protection areas, the species richness for the three kinds of species above was significantly higher in the Gutianshan subarea (the left-bottom area of the national park map) than that in the other subareas. The species richness for these three kinds of species was very high in some areas abutting on the core protection areas, similar to that in the core protection areas, in Qianjiangyuan National Park.

Highlights

- Based on the data collected from monitored plant plots across the entire Qianjiangyuan National Park, population sizes of the monitored woody species were estimated.
- Based on the data collected from monitored plant plots and the LiDAR data across the entire Qianjiangyuan National Park, spatial distributions of the monitored woody species were estimated.
- Based on spatial patterns of species richness for all monitored woody species, rare and endangered woody species, and indicator species of typical subtropical evergreen broadleaf forests, biodiversity conservation gaps were identified in Qianjiangyuan National Park.

8.3.3.4 Discussion and Outlook

This study used biodiversity monitoring big data to estimate the population size and spatial distribution information of woody species in Qianjiangyuan National Park, which lays the foundation for the management and protection of national parks, allowing for specific conservation goals and strategies for different species, especially rare, endangered, and endemic species.

The highly rich areas of all species, rare and endangered species, and the indicator species of the subtropical evergreen broadleaf forests highly overlap with the core protection area of the national park, indicating the effectiveness of national park planning. There are still large biodiversity-rich areas in the core protection zone outside the Gutianshan subarea, and corresponding adaptive management measures, such as accelerating ecosystem restoration and corridor construction, need to be developed. The large biodiversity-rich areas on the periphery of the core protection zone should be incorporated into the core protection zone to protect the originality and integrity of these typical subtropical evergreen broadleaf forests.

The biodiversity big data of our study provides scientific support for Qianjiangyuan National Park to carry out adaptive conservation and management, and also provides a model case for the conservation and management of other protected areas in China.

8.3.4 Prediction and Assessment of the Distribution of Critical Invasive Pests

Target: SDG 15.8: By 2020, introduce measures to prevent the introduction and significantly reduce the impact of invasive alien species on land and water ecosystems and control or eradicate the priority species.

8.3.4.1 Background

The ecological and socio-economic impacts of insects are closely linked to multiple SDGs (Dangles and Casas 2019). According to statistics, invasive pests cause about $70 billion in direct losses and more than $6.9 billion in associated health costs each year. They are also an important factor in socio-economic problems such as hunger and health crises (Bradshaw et al. 2016). In addition, global warming will further worsen the ecological and socio-economic risks associated with invasive pests (Bradshaw et al. 2016). The Chinese government attached great importance to the risk of invasive pests, especially the early warning and prevention and control of these pests related to agricultural production, and specifically formulated administrative measures for reporting and releasing agricultural plant epidemics. The

important impacts of climate change on invasive organisms and food security have been clearly identified in the China National Climate Change Adaptation Strategy 2035 released in June 2022, and the early warning and prediction of invasive organisms under climate change conditions were also proposed. Modeling the potential distribution of invasive pests and their expansion trends under different climate scenarios based on the existing occurrence data is the basis for assessing their hazards and will strongly support SDG 15.8, controlling invasive alien species, which is also important for ensuring food security and supporting SDG 2.

8.3.4.2 Data

- Occurrence data of 10 invasive pests released by the Ministry of Agriculture and Rural Affairs of the People's Republic of China (fall webworm: 2012–2018, others: 2012–2020).
- Administrative district maps and bio-climatic variables (current scenario/future scenario in 2040) (Fick and Hijmans 2017).
- Maps of rice, potato, and temperate fruit cultivation (International Food Policy Research Institute 2019).

8.3.4.3 Methods

In this case study, we analyzed the current distribution of 10 invasive pests and dynamically simulated the expansion trends of these pests separately. Based on the occurrence data and bio-climatic variables, the ENM was used to predict their potential distribution areas under current and future scenarios. Further overlap analysis on potential distribution maps of invasive pests and cultivation maps of different crops was carried out, and three indicators were proposed to measure the control effectiveness, potential risk, and future expansion trends of these invasive pests as follows: (1) R_1, invaded area as a proportion of the area of potential invasive range; (2) R_2, invaded cultivation area as a proportion of potential invasive cultivation area; and (3) R_3, the proportion of incremental area potentially suitable for an invasive pest in the future climate scenario compared to current scenarios.

8.3.4.4 Results and Analysis

Trends in the Spread of 10 Invasive Pests

Statistics on the distribution of 10 invasive pests over the years (Fig. 8.9) show that the number of counties invaded by rice water weevil (Lissorhoptrus oryzophilus) and red imported fire ant (*Solenopsis invicta*) was increasing rapidly, both exceeding 400 in 2020, and codling moth (*Cydia pomonella*) had invaded nearly 200 counties. The number of counties invaded by Colorado potato beetle (Leptinotarsa decemlineata), grape phylloxera (Daktulosphaira vitifolia), cowpea weevil (Callosobruchus maculatus), and solenopsis mealybug (Phenacoccus solenopsis) was relatively stable, while the number of invaded counties of Japanese orange fly (Bactrocera tsuneonis) decreased. The number of counties invaded by bean weevils (Acanthoscelides obtectus) increased from 2012 to 2013, and then remained stable until 2020. The number of counties invaded by fall webworm (Hyphantria cunea) increased first and then decreased from 2012 to 2018, and it was not listed in the list by the Ministry of Agriculture and Rural Affairs of the People's Republic of China after 2018.

Prediction of Potential Invasive Areas and the Impacts of Climate Change

In this case study, we modeled the potential distribution of all 10 invasive pests to predict where they are potentially at risk of invasion in China, and we also simulated the trends in their potential distribution ranges under future climate change conditions. The results suggested that the potential distribution of rice water weevil [Fig. 8.10(a)], codling moth [Fig. 8.10(c)], Colorado potato beetle [Fig. 8.10(e)], and red imported fire ant was very extensive in China, all exceeding 25% of the national land area, and the potential invasive areas of the remaining pests all accounted for more than 10% of the national land area. Comparing the present

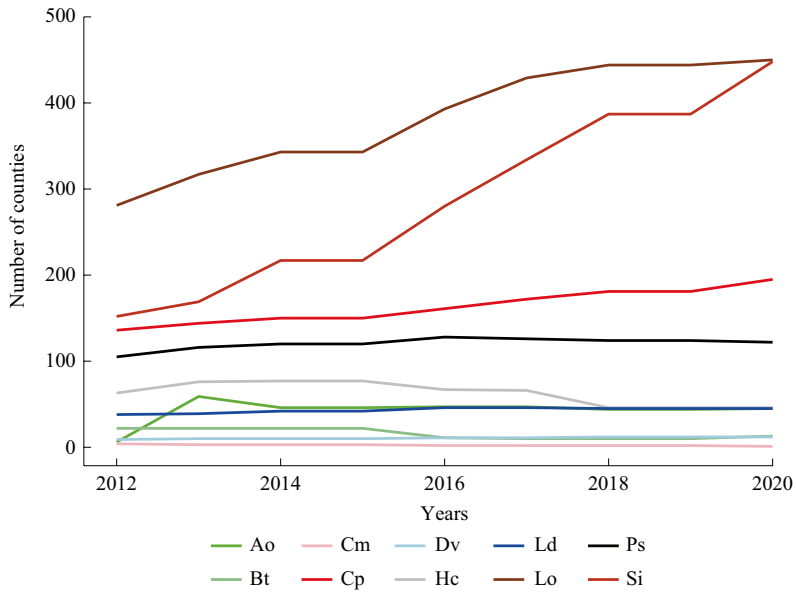

Fig. 8.9 Trends in the number of invaded counties by invasive pests (2012–2020). *Notes* Ao: *Acanthoscelides obtectus*, Bt: *Bactrocera tsuneonis*, Cm: *Callosobruchus maculatus*, Cp: Cydia pomonella, Dv: *Daktulosphaira vitifolia*, Hc: *Hyphantria cunea*, Ld: *Leptinotarsa decemlineata*, Lo: *Lissorhoptrus oryzophilus*, Ps: *Phenacoccus solenopsis*, Si: Solenopsis invicta

potential distribution ranges with the future climate scenario (2040), we found that the potential distribution ranges of seven species were expanded, with rice water weevil adding $R_3 = 7.3\%$ of suitable range [Fig. 8.10(b)], codling moth adding $R_3 = 8.5\%$ [Fig. 8.10(d)], Colorado potato beetle adding $R_3 = 3.5\%$ [Fig. 8.10(f)], and 3.8% for red imported fire ant [Fig. 8.10(h)], while the potential areas of grape phylloxera, Japanese orange fly, and bean weevils were reduced. It is worth noting that the potential distribution areas of all pests have an overall tendency to move to higher latitudes and higher elevations, which will cause more risks to areas originally unsuitable for distribution, such as the expansion of the suitable distribution area of rice water weevil in the northeast and its movement northward, which may further harm the grain-producing base in the northeast.

Assessment on Prevention and Control Effectiveness and Hazard Risk

In this case study, the present range of each species was compared with the potential distribution area predicted by the ENM, and the R_1 index was calculated separately to assess the current prevention and control effectiveness for each species. The results show that more than one-fourth of the potentially suitable distribution area of rice water weevil had been invaded ($R_1 = 0.261$) [Fig. 8.11(a)]; red imported fire ant had also invaded a wide range, and the current distribution area overlapped highly with the potentially suitable distribution area ($R_1 = 0.33$)[Fig. 8.11(g)]; codling moth had invaded most of the potentially suitable distribution area in northwestern and northeastern China ($R_1 = 0.44$), and had a tendency to spread further to the central high suitability areas [Fig. 8.11(c)]. Except for these three species, the R_1 values of other invasive pests were below 0.1, and Colorado potato beetle ($R_1 = 0.098$), which is of great concern, was under effective control.

Three invasive pests, including rice water weevil, codling moth, and Colorado potato beetle, which are more widely damaging to crops, were selected for further evaluation. By overlaying the map of rice cultivation with the

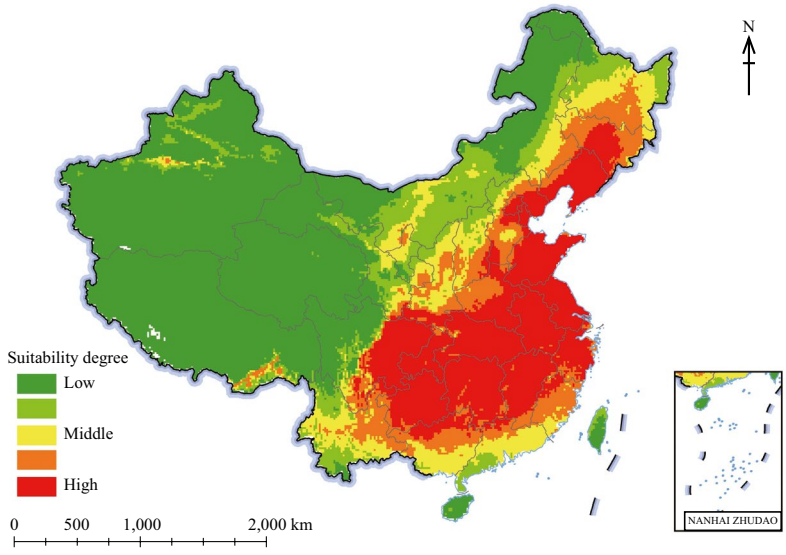

(a) Current potential distribution area of rice water weevil

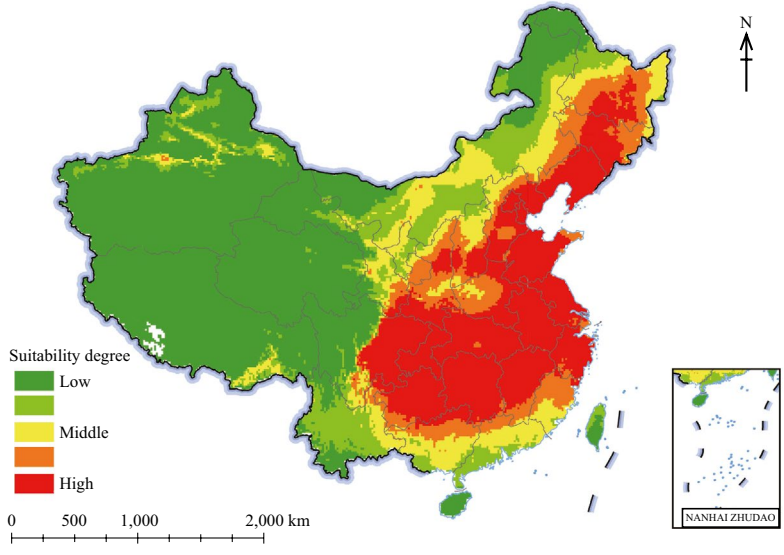

(b) Future potential distribution area of rice water weevil

Fig. 8.10 Potential distribution areas of the invasive pests under current and future climatic conditions

map of potential distribution of rice water weevil, it can be seen that the overlap between the two is very high and the potential suitability is generally high within the rice cultivation area. $R_2 = 0.45$ indicates that a large area of rice cultivation has been invaded, and it can also be seen from Fig. 8.11(b) that rice water weevil has formed a contiguous area of damage. Next is codling moth, which mainly affects temperate fruits such as apples and pears, and $R_2 = 0.22$ also indicates that it has invaded the large areas of temperate fruits [Fig. 8.11(d)], especially affecting the apple industry greatly. Potatoes are widely planted in China, and the potential distribution area of Colorado potato beetle is also very wide. The overlap between the two is

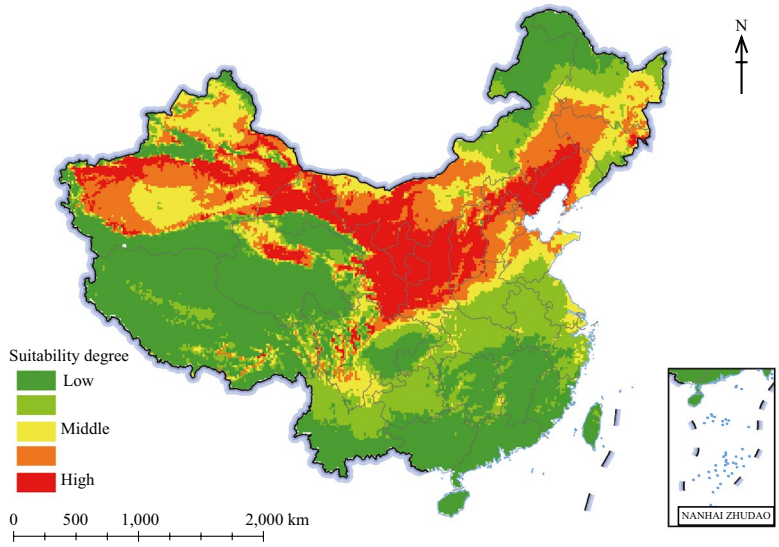

(c) Current potential distribution area of codling moth

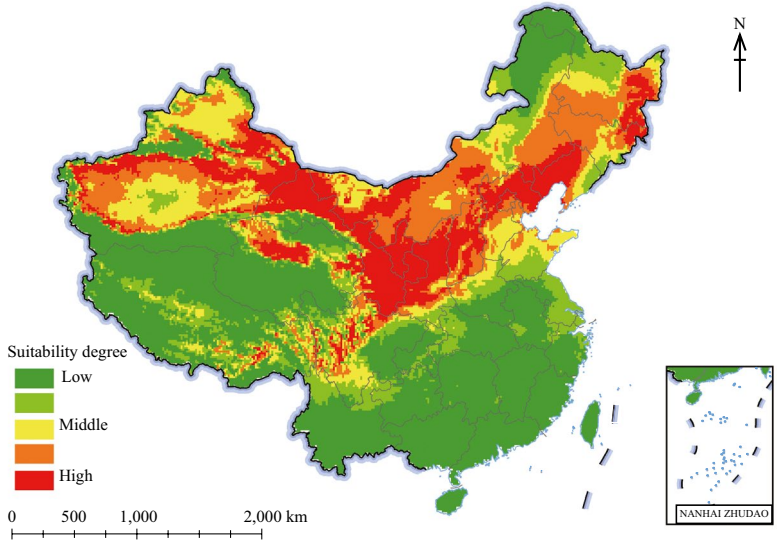

(d) Future potential distribution area of codling moth

(continued)

relatively high [Fig. 8.11(f)], but $R_2 = 0.04$ indicates that the invasion of Colorado potato beetle into the planting area is still in a small range, not yet into the large central and eastern suitable distribution area. The prevention and control of this pest is excellent, playing an important role in the protection of China's potato planting industry.

Highlight

- In this case study, we analyzed the trends in the spread of 10 critical invasive pests, and predicted the potential distribution area for each species at current and future scenarios. The risk of three species, rice water weevil, Colorado potato beetle, and codling moth were further assessed by overlaying crop

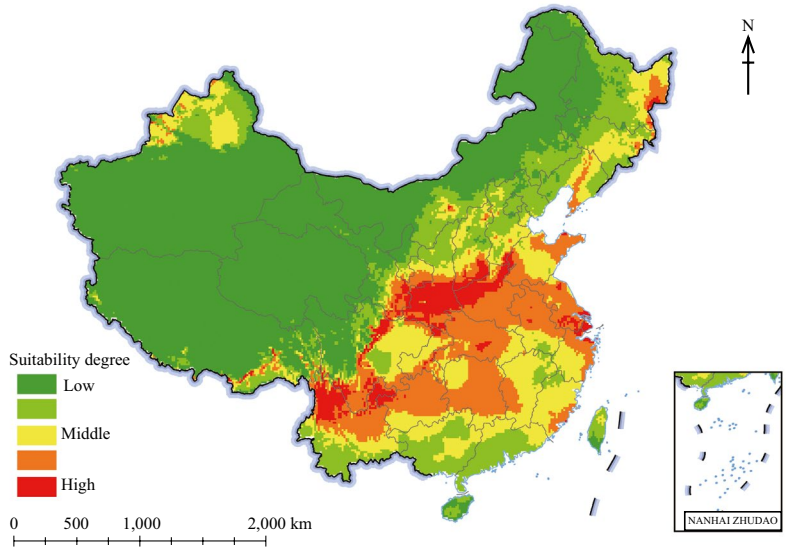

(e) Current potential distribution area of Colorado potato beetle

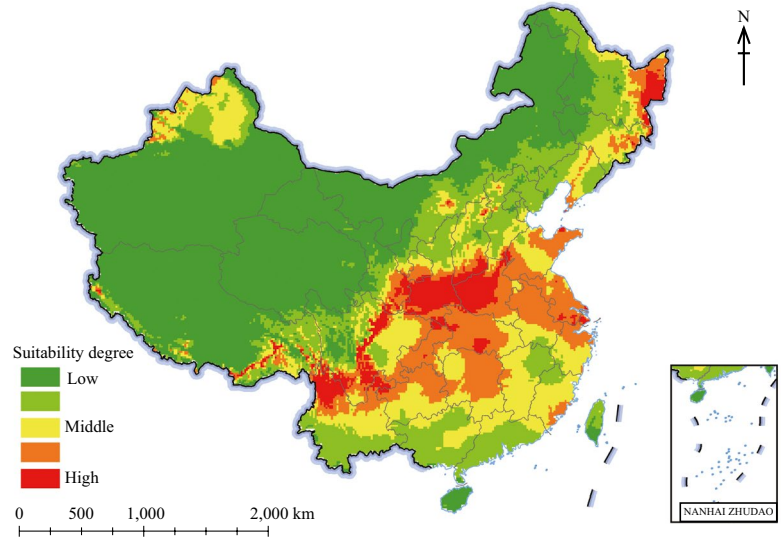

(f) Future potential distribution area of Colorado potato beetle

(continued)

planting maps with their potential distribution maps. The results suggest that seven invasive pests remain relatively stable in their invasive ranges and had been controlled well, while rice water weevil, red imported fire ant, and codling moth are in a rapid expansion stage and need further control. It is recommended to strengthen the early warning and prevention and control of invasive pests under the global climate change conditions.

8.3.4.5 Discussion and Outlook

This case study utilized the ENM to predict the potential distribution of the invasive pests and proposed three indicators to assess the prevention and control of invasive pests and their potential hazard risk in China, which can provide important scientific support at the national scale for achieving SDG 15.8 and SDG 2.

The study reached the following conclusions. (1) Six of the ten invasive pests assessed are in a

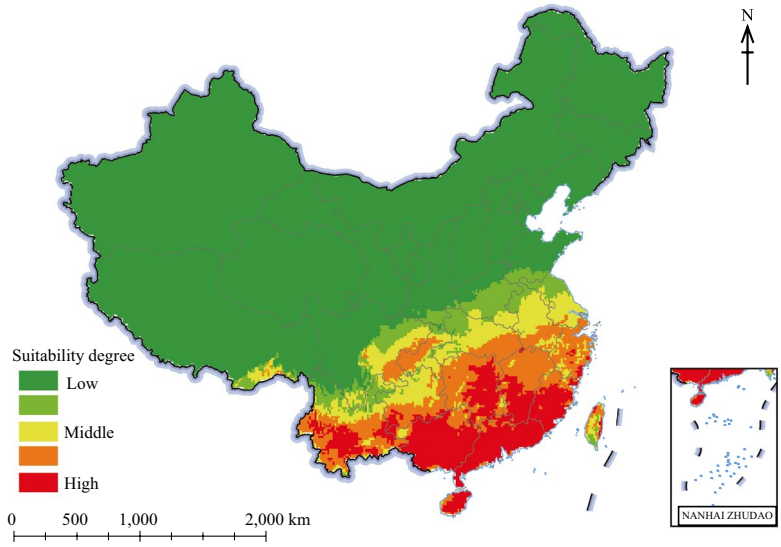

(g) Current potential distribution area of red imported fire ant

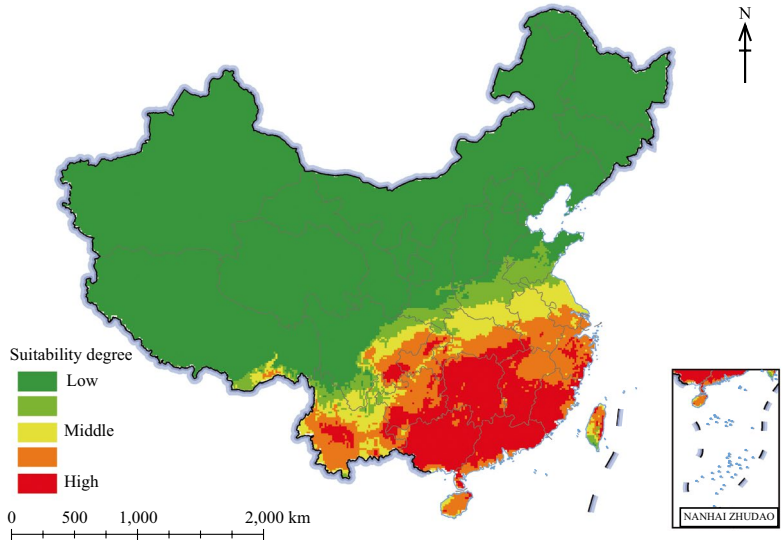

(h) Future potential distribution area of red imported fire ant

(continued)

relatively stable state, and the overall control was effective. In particular, the prevention and control of Colorado potato beetle was effective and has important reference value for controlling other invasive pests and effectively ensuring food security. (2) Rice water weevil and red imported fire ant are in a state of rapid expansion, invading a wide area and causing great risk, and it is urgent to increase efforts to control them. (3) Climate change will cause changes in the distribution areas of invasive pests, and prevention and control efforts will face greater challenges, so early warning forecasts should be strengthened in the future.

8.4 Summary

This chapter made full use of the characteristics of Big Earth Data, and focused on the four themes of forest protection and restoration,

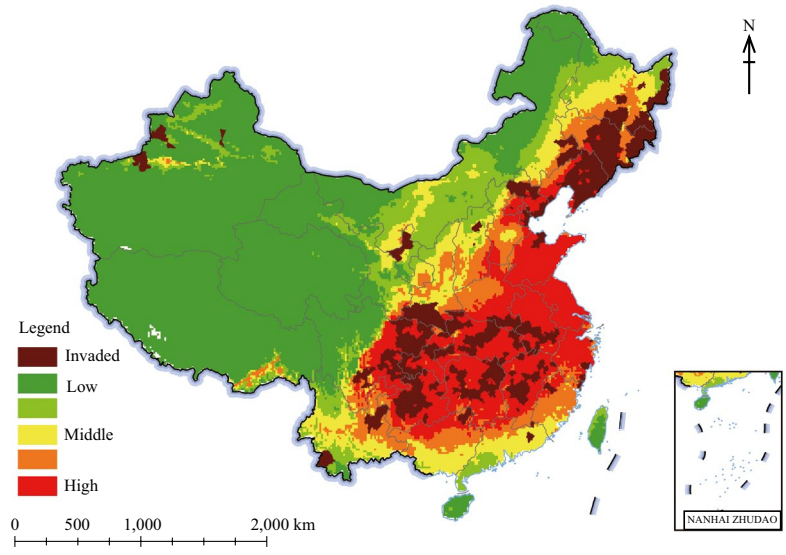

(a) Overlap analysis on invaded areas and potential areas of rice water weevil

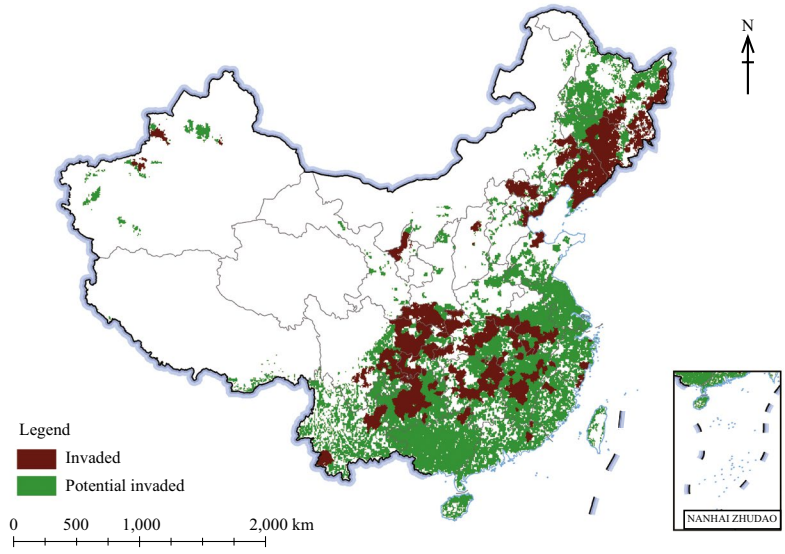

(b) Overlap analysis on invaded planting areas and potential invasive planting areas of rice water weevil

Fig. 8.11 Assessment on prevention and control effectiveness and hazard risk of invasive pests

precise biodiversity protection and management, land degradation and restoration, and invasive alien species at the national scale in China. It identified problems, identified potential, innovated technology and demonstrated applications in the form of case studies to assess the benefits of China's natural forest protection projects, fine-scale monitoring of biodiversity in Qianjiangyuan National Park, and black soil monitoring in Northeast China. The studies provided important support for ecosystem restoration, biodiversity conservation, land degradation management, and invasive alien species control in China.

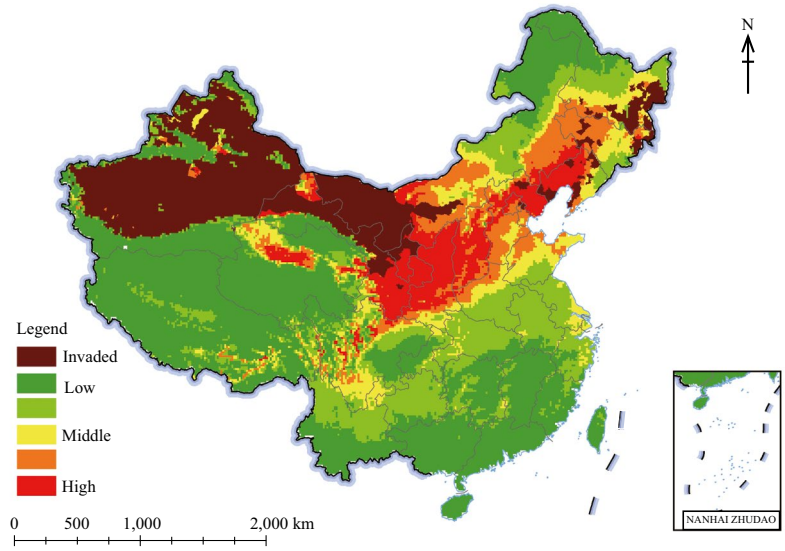

(c) Overlap analysis on invaded areas and potential areas of codling moth

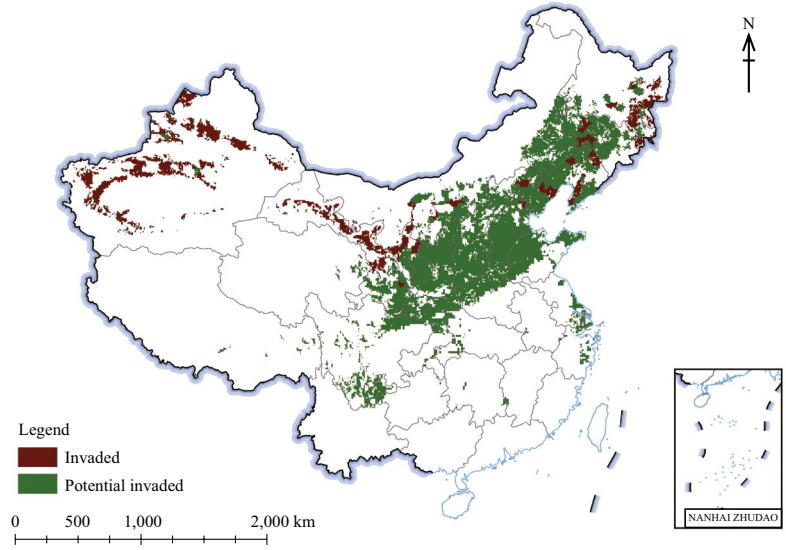

(d) Overlap analysis on invaded planting areas and potential invasive planting areas of codling moth

(continued)

With the attention of the Chinese government, the goal of terrestrial biological sustainability in China continues to develop in a good direction. However, the pressures we face continue unabated. At the same time, the implementation of national strategies such as the Global Development Initiative and the BRI also requires us to export some successful experience and resources to the outside world. Under both internal and external pressures, there is an urgent need to better utilize the value of Big Earth Data to innovatively serve the implementation of SDG 15 from the perspective of science and technology.

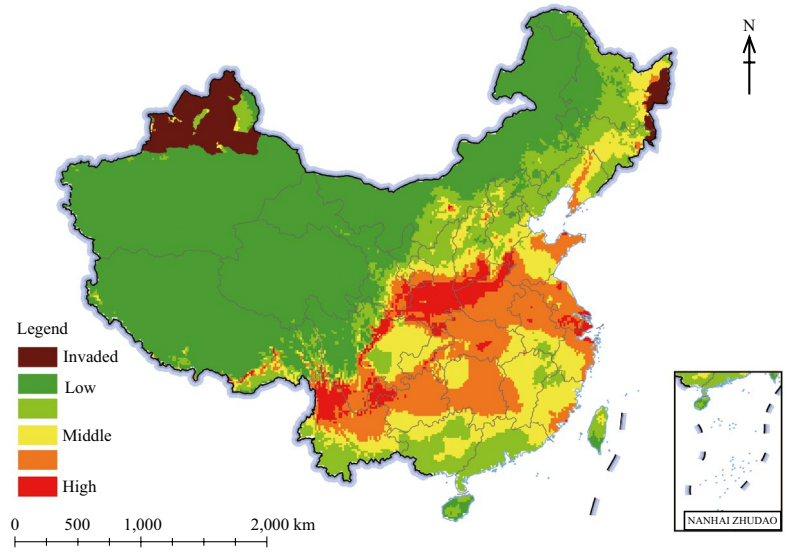

(e) Overlap analysis on invaded areas and potential areas of Colorado potato beetle

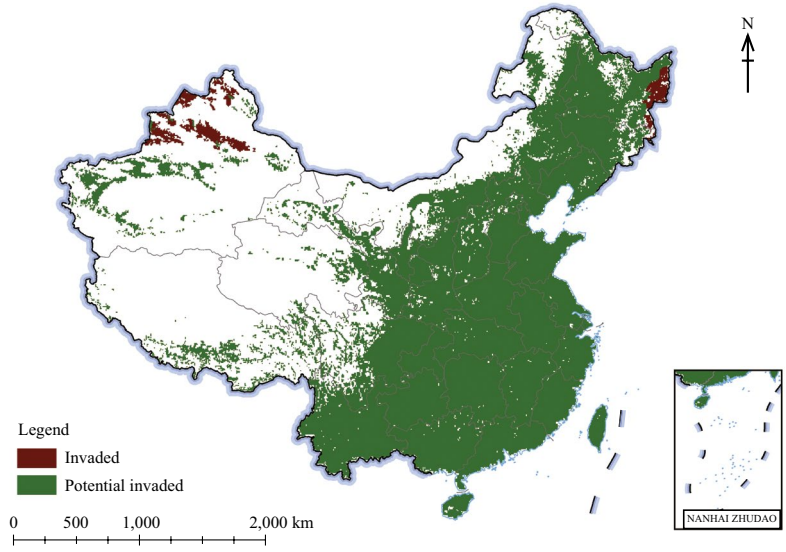

(f) Overlap analysis on invaded planting areas and Potentially invaded planting areas of Colorado potato beetle

(continued)

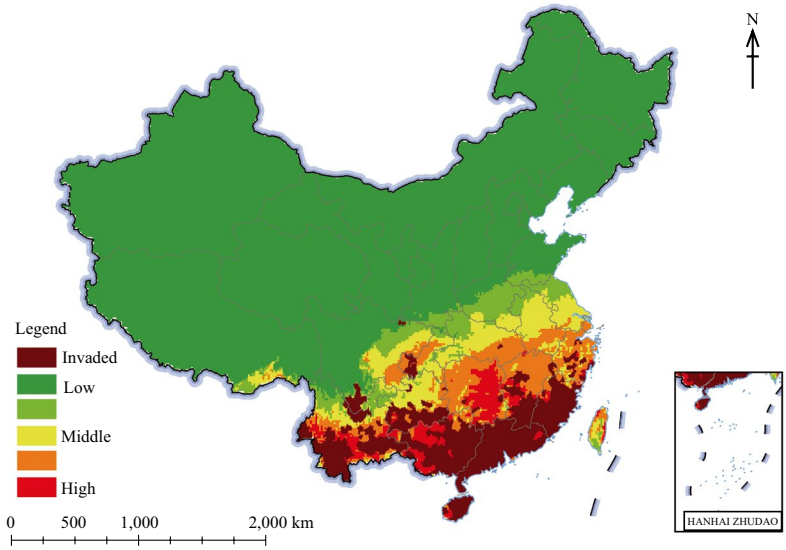

(g) Overlap analysis on invaded areas and potential areas of red imported fire ant

(continued)

References

Bradshaw CJA, Leroy B, Bellard C et al (2016) Massive yet grossly underestimated global costs of invasive insects. Nat Commun 7:12986

Chen C, Park T, Wang XH et al (2019) China and India lead in greening of the world through land-use management. Nat Sustain 2(2):122–129

Dangles O, Casas J (2019) Ecosystem services provided by insects for achieving sustainable development goals. Ecosyst Serv 35:109–115

Fick SE, Hijmans RJ (2017) WorldClim 2: New 1-km spatial resolution climate surfaces for global land areas. Int J Climatol 37(12):4302–4315

Guo LC, Xiong SF, Chen YL et al (2023) Total organic carbon content as an early warning indicator of soil degradation. Science Bulletin 68(2):150–153

International Food Policy Research Institute (2019) Global spatially-disaggregated crop production statistics data for 2010 version 2.0. https://doi.org/10.7910/DVN/PRFF8V[2023-06-08

Kraamwinkel CT, Beaulieu A, Dias T et al (2021) Planetary limits to soil degradation. Communications Earth & Environment 2:249

Liu F, Wu HY, Zhao YG et al (2022) Mapping high resolution National Soil Information Grids of China. Science Bulletin 67(3):328–340

Pang Y, Meng SL, Shi KY et al (2021) Forest coverage monitoring in the natural forest protection project area of China. Acta Ecol Sin 41(13):5080–5092 (in Chinese)

Viña A, McConnell WJ, Yang HB et al (2016) Effects of conservation policy on China's forest recovery. Sci Adv 2(3):e1500965

Wang H, Yang SL, Wang YD et al (2022) Rates and causes of black soil erosion in Northeast China. CATENA 214:106250

Wang W, Feng CT, Liu FZ et al (2020) Biodiversity conservation in China: a review of recent studies and practices. Environmental Science and Ecotechnology 2:100025

Interactions Among the SDGs and Integrated Evaluations

9

9.1 Background

The assessment of a single SDG indicator can track the progress of that indicator, but judging whether the development of a certain region is sustainable requires comprehensive consideration of the impact of different SDG indicators. Due to differences in natural resource endowments, socio-economic development levels, and development paths in different regions, there are complex interactions among the SDGs and related indicators. Research on the intersection of multiple SDG indicators involves the following three aspects: (1) the synergistic and trade-off relationships among multiple SDG indicators in the same time period and same spatial range; (2) the spillover effects of multiple SDG indicators in different spatial ranges but in the same time period; and (3) future scenario simulation of SDGs under the interactions of multiple indicators in the same spatial range. The synergistic indicators promote one another, yet trade-offs emerge when achieving progress at the expense of others. In addition, achieving the SDGs requires the integration of multiple themes, such as SDGs for agriculture, ecological environment, water resources, and urban areas, and balanced and sustainable development across all 17 SDGs. Understanding the intersectional relationships between goals and indicators, and conducting single-theme and regional comprehensive assessments of SDGs, are of great significance for achieving the 2030 Agenda and dynamically adjusting sustainable development paths.

Research on interactions among the SDGs and integrated evaluations has been carried out by organizations and the academic community at different scales since the SDGs were proposed. In terms of SDG interactions, UN-Water analyzed the six targets of SDG 6 and other targets of SDGs with potential interaction relationships, and found that there were 127 pairs with mainly synergistic relationships and 29 pairs with potential trade-off relationships (UN-Water 2016). In 2021, UNEP conducted a progress report on the interaction analysis of environmental indicators and other indicators, analyzing the interaction relationships among the near-nature action indicators, socio-economic development indicators, and natural state indicators in the SDG indicators. Pradhan et al. (2017) used time-series data covering 122 indicators in 227 countries worldwide to quantitatively analyze the synergistic and trade-off relationships within and between all SDG targets at the global and national scales from 1983 to 2016. They concluded that at the global level, most countries in the world exhibit more synergistic relationships than trade-off relationships between SDG targets. Warchold et al. (2021) further analyzed the linear or nonlinear synergistic and trade-off relationships within and between the SDGs at the global and national

H. Guo, *Big Earth Data in Support of the Sustainable Development Goals (2022) - China*,
Sustainable Development Goals Series, https://doi.org/10.1007/978-981-97-4231-8_9

levels using updated and higher coverage data (covering 171 indicators in 247 countries worldwide from 1991 to 2019), and reached the same conclusion. Warchold et al. (2021) also found that the synergistic and trade-off relationships among SDGs vary greatly among different populations, income groups, and regions. In terms of the comprehensive assessment of SDG themes, the FAO evaluated 21 indicators related to food security, and found that progress in global food and agricultural production is still insufficient, making it difficult to achieve the 2030 goals. The latest report from UN-Water indicates that the targets of SDG 6 are currently difficult to achieve at the global level, with 10% of the world's population still unable to access safe drinking water and sanitation facilities, and many water sources drying up or becoming more polluted (UN-Water 2021). In terms of the regional integrated evaluations of the SDGs, the UN Sustainable Development Solutions Network (SDSN) and the Bertelsmann Foundation established an SDG index evaluation system, and developed a set of SDG measurement standards for national levels. The proposed standards aim to help each country identify priority issues, understand the challenges faced in the implementation process, clarify existing gaps, and support the achievement of the 2030 SDGs (Sachs et al. 2018, 2020, 2021, 2022).

However, most of the current studies on SDG interactions and integrated evaluations are based on statistical data, lacking a sufficient consideration of geographical spatiotemporal characteristics. The integration of Big Earth Data, which combines satellite observations, ground-based observations, and ground surveys, has the characteristics of massive volume, multiple sources, and multi-temporal phases, providing important data and technical support for SDG monitoring and evaluation. Earth observation data and geographic information data provide important supplements or replacements for traditional official statistical data. Their continuous spatiotemporal coverage can quickly and frequently capture changes in surface features to help monitor the SDGs, overcoming the problems of inconsistent standards and quality of statistical data in different countries and regions. Furthermore, geographic information modeling and simulation methods based on spatial analysis and other technologies can help sort out the interactions between SDGs, predict future development trends, carry out comprehensive evaluations, and provide a basis for the dynamic adjustment of policy recommendations.

9.2 Main Contributions

To clarify the complex synergies and trade-offs among multiple SDGs, this chapter focuses mainly on the interactions among the SDGs and integrated evaluations of SDG regions. The case studies contribute to the global efforts in supporting the technical advantages of SDG interactions and integration using Big Earth Data, mainly in three aspects: data products, methods and models, and decision support, as shown in Table 9.1.

9.3 Case Studies

9.3.1 Analysis of Synergies and Trade-Offs Among SDGs Indicators in China

Target: SDG 1, SDG 2, SDG 3, SDG 4, SDG 5, SDG 6, SDG 7, SDG 8, SDG 9, SDG 10, SDG 11, SDG 12, SDG 13, SDG 15, SDG 16, SDG 17, total 16 goals, 65 indicators.

9.3.1.1 Background

The UN SDGs, consisting of 17 goals, 169 targets, and over 230 indicators, are a comprehensive framework for achieving sustainability from a system perspective. SDGs are interconnected in a complex network of interactions (Swain and Ranganathan 2021), and ignoring the complex dynamics of interactions between goals can lead to unsustainable SDGs (ICSU 2015). Clarifying the intrinsic correlation between the SDGs has become an important direction for urgent

Table 9.1 Case studies and their main contributions

Themes	Cases	Contributions
Interactions among SDGs	Analysis of synergies and trade-offs among SDGs indicators in China	**Method and model:** Spatiotemporal geographically weighted regression was used to construct complex networks with directions and weights among the SDGs, and to explore their synergistic and trade-off relationships and the variation in interactions **Decision support:** Provides a reference for Chinese provinces in making proper decisions on setting priority development goals and mitigating the SDG trade-offs that exist in development
	Synergetic development of the water–food–air quality nexus over Northeast China	**Method and model:** Based on remote sensing big data and statistical data, this study analyzed the interannual variations in SWA, terrestrial water storage (TWS), grain production, AWU, and air quality indicators, as well as their interactions over Northeast China since 2000 **Decision support:** While the grain yield in Northeast China has been stable or increasing year after year, AWU efficiency has continuously increased, and SWA has significantly increased. The trade-offs between food (SDG 2) and water security (SDG 6) tended to be alleviated. The expansion of corn planting (SDG 2.4) significantly increases the number of fire spots caused by residue burning in spring and autumn, further leading to a significant increase in aerosol optical depth (AOD) and having a certain degree of impact on the local air quality (SDG 11.6)
	Interactions among the SDGs and integrated evaluations in China's transport industry	**Data product:** A dataset was constructed for China's transport industry development under the framework of SDG indicators from 2000 to 2020, which initially solved the problem of the lack of quantitative, comprehensive assessments of the SDGs for China's sustainable transport **Decision support:** After experiencing the rapid development of transport infrastructure construction, China's transport planners are expected to pay more attention to the improvement of green and low-carbon transformation and transportation service quality in the current and future stages, to move from a transport country to a transport power

(continued)

Table 9.1 (continued)

Themes	Cases	Contributions
SDG regional integrated evaluation	SDG integrated evaluation for Lincang, Yunnan Province, China	**Method and model:** A comprehensive evaluation system for the progress of the SDGs in Lincang, Yunnan Province, China, has been constructed from three dimensions: society, economy, and resource-environment, including both UN SDG indicators and localized indicators **Decision support:** Lincang has made significant progress in implementing the 2030 Agenda. In the subsequent development, attention needs to be paid to issues such as the high Engel coefficient of rural residents, relative shortage of rural health and technical personnel, low coverage rate of special education for ethnic minorities, low orientation index of government toward agriculture, low popularity of clean energy, low proportion of government green procurement, increasing wildlife trade, and reducing government revenue due to the impacts of the pandemic
	SDG integrated evaluation for Hainan Island, China	**Method and model:** By integrating and employing the SDG indicator model, knowledge graphs, GIS, and other supporting tools, the knowledge-based representation and spatial visualization of each indicator of the SDGs in Hainan Island, China, were achieved through analysis, calculation, customized assembly, and visualization display technologies **Decision support:** The overall sustainable development progress in Hainan Province is uneven, with differences among cities and counties. Evaluation scores were relatively high in SDG 2 and SDG 15, but relatively low in SDG 6
	SDG integrated evaluation for Guilin, Guangxi Zhuang Autonomous Region, China	**Data product:** Spatial distribution dataset of the sustainable development index of the ecotourism carrying capacity (ECC) of the Lijiang River Basin from 2010 to 2020 in Phase III, spatial distribution dataset of the growth rate of the sustainable development index of the ECC of the Lijiang River Basin from 2010 to 2020 in Phase III, and data products of SDG 11.2.1, SDG 11.3.1, and SDG 11.7.1 were produced for the main functional areas of Guilin City, and the sustainable development process of the main functional areas of Guilin City were evaluated **Decision support:** Based on multi-source CASEarth data such as remote sensing images, ground observation, and socio-economic statistics, a multi-indicator, assessment showed that most areas of the Lijiang River Basin enjoy huge sustainable development potential in the ECC. During the study period, 2010 to 2020, the urban expansion and population growth in Guilin were uneven, the urban expansion rate outpaced PGR, the per capita built-up area continuously increased, the growth rate accelerated, the population served by urban public open spaces decreased, and the distribution and area of those spaces hardly met the needs of citizens

breakthroughs (Fu et al. 2019; Guo et al. 2021). SDG synergy refers to the achievement of one goal that can simultaneously contribute to the improvement of another goal, mutually reinforcing the relationship between goals; SDG trade-off refers to the achievement of one goal at the expense of another goal, creating a conflicting relationship between goals (Barbier and Burgess 2017). Faced with a large and complex SDG system, it is necessary for us to comprehensively grasp the correlations, synergistic effects, and spatial differences among the goals. Only in this way can we seek benefits and avoid harm, as well as safeguard the goals from contradictions and conflicts, thus promoting the implementation process of the SDGs to be comprehensively monitored. The existing studies of synergistic and trade-off relationships among the SDGs are mainly statistically significant positive and negative correlations, often ignoring the spatiotemporal variability of the SDGs and the directionality of interactions among them. To this end, we analyzed the spatial heterogeneity of typical SDG synergy/trade-off goal pairs in each province of China, explored the simple closed loops and their important indicator nodes in the synergy network of each Chinese province, and analyzed the direction of active and passive effects of the SDGs in each Chinese province from 2000 to 2020, so as to provide a scientific basis for formulating sustainable development policies.

9.3.1.2 Data

- Statistics on SDG indicators for 31 provincial-level administrative regions (excluding Hong Kong, Macao, and Taiwan) obtained by the National Bureau of Statistics of China from 2000 to 2020 (http://www.stats.gov.cn/english/).
- $PM_{2.5}$ density data from 2000 to 2020 with the spatial resolution of 1 km (https://acp.copernicus.org/articles/20/3273/2020/).
- CO_2 emission data from 2000 to 2020 with the spatial resolution of 1 km (https://db.cger.nies.go.jp/dataset/ODIAC/).

9.3.1.3 Methods

Based on the data of 65 SDG indicators in 31 provincial-level administrative regions from 2000 to 2020, we constructed an SDG interaction network based on the regression coefficient matrix using the spatiotemporal geographically weighted regression method. The nodes of the SDG interaction network are SDG indicators, the weights of the edges between the nodes are the regression coefficients between the corresponding SDG indicators, and the directions of the edges correspond to the directions of interactions between the indicators. The 31 provincial-level administrative regions in China build both SDG synergistic and trade-off networks year by year, for a total of $31 \times 21 \times 2 = 1302$ complex networks. Combining the edge-mediated centrality of SDG indicator networks, we explored the typical synergistic and trade-off SDG pairs with a strong degree of correlation in each province; explored the typical virtuous circle in each province of China, and preferred important indicators that promote SDG synergy; combined the in/out degree values of network nodes to determine the active and passive changes of the SDGs in each province from 2000 to 2020, and analyzed the important SDGs with large active and passive changes by province.

9.3.1.4 Results and Analysis

There is significant spatial variability in the spatial distribution of SDG multi-indicator synergy and trade-off relationships at the provincial scale in China (Fig. 9.1). SDG 9 (Industry, Innovation, and Infrastructure) in Southwest and Southern China has a synergistic contribution to SDG 11 (Sustainable Cities and Communities), and SDG 11 in Northeast China has a trade-off inhibiting effect on SDG 15 (Life on Land). Most provinces show SDG 6 (Clean Water and Sanitation) and SDG 15 to be more vulnerable to the trade-off effects of other goals. Therefore, the sustainable development process in China needs to improve the refinement of water resources management and strengthen terrestrial ecosystem protection.

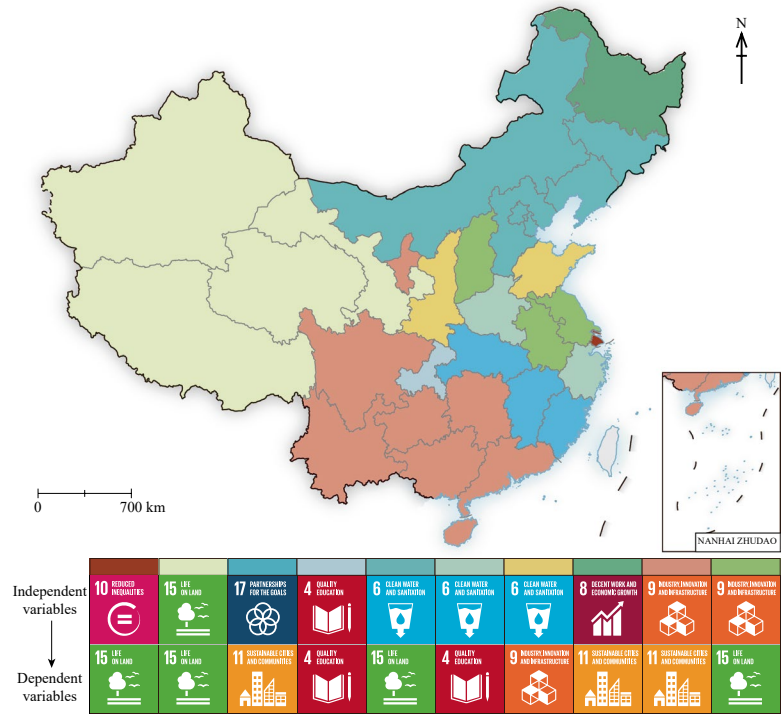

(a) Synergies

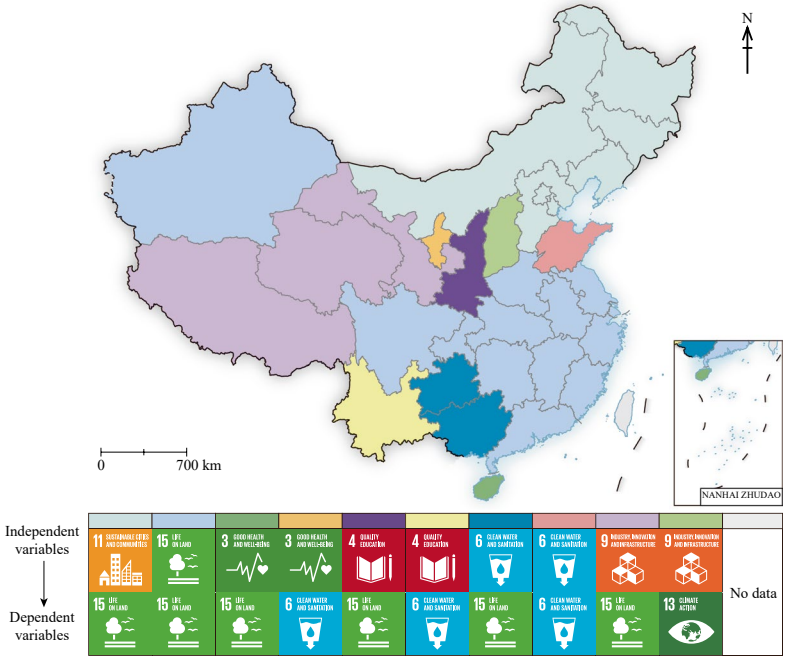

(b) Trade-offs

Fig. 9.1 Spatial distribution of typical synergistic and trade-off SDG pairs in China

From 2000 to 2020, 27.02% of indicator pairs in China's provincial-level administrative regions had their trade-off relationships changed to synergistic relationships, while 18.30% of the intensity of trade-offs between indicator pairs was mitigated. First, among the indicator pairs where trade-offs become synergistic, SDG 3 (Good Health and Well-being) has the widest range of variation to SDG 15, which is mainly due to the implementation of China's air pollution prevention and the popularization of green and low-carbon living awareness. Second, SDG 6 versus SDG 2 (Zero Hunger) changes more significantly in the Yangtze River Delta region, mainly due to measures such as strengthening water management allocation, implementing water-saving irrigation, and increasing the irrigated area of arable land and grain yield in the region in the 20 years. Among the indicator pairs with reduced trade-off intensity, 23 provinces show that SDG 15 is weakened by the trade-off intensity of other goals, such as the implementation of the Action Plan for Water Pollution Prevention and Control, which has led to the basic guarantee of water security in China's major water resources provinces, the good recovery of water ecology, and the obvious improvement of groundwater quality, promoting the synergistic development of SDG 6 to SDG 15 (Fig. 9.2).

The closed loop in the SDG synergistic network is a kind of virtuous circle, and optimizing one indicator in the closed loop can automatically synergize the synergistic development of all other indicators in the closed loop. The analysis results show that this virtuous circle network has spatial aggregation characteristics. SDG indicators such as domestic material consumption (SDG 12.2.2), degree of integrated water resources management (SDG 6.5.1), and increasing investment in education and construction of educational facilities (SDG 4.1.2, SDG 4.b.1, SDG 4.a.1) can promote synergistic SDGs more scientifically and efficiently (Fig. 9.3).

The changes in the active and passive directions of the SDGs from 2000 to 2020 in China's provincial-level administrative regions show significant spatial differences (Table 9.2). In the synergistic network, SDG 13 (Climate Action) is susceptible to active synergistic influence from other SDGs, while SDG 11 and SDG 16 (Peace, Justice, and Strong Institutions) are susceptible to passive synergistic influence from other SDGs. In the trade-off network, there is a significant north–south variation in the active–passive variation in the SDGs across Chinese provinces, with SDG 1 (No Poverty) in the northeastern, northwestern, and northern provinces being susceptible to active trade-offs affecting other SDGs; SDG 7 (Affordable and Clean Energy) in the eastern, central, southern, and southwestern provinces tends to be susceptible to active trade-offs affecting other SDGs; overall, SDG 9, SDG 11, and SDG 16 are vulnerable to the trade-offs of other goals.

Highlights

- Combining the SDG indicator framework system released by the UN and based on statistical data and Big Earth Data, we pioneered the analysis of the directional interactions between SDG indicators/goals at the provincial level in China from a geographical spatiotemporal perspective, explored the typical synergistic and trade-off SDG pairs in each province of China, explored the closed loop of indicators in the SDG synergistic network, and used representative closed loop indicators as an entry point to facilitate the virtuous cycle of the synergistic network. There are significant spatial and temporal differences in the synergistic and trade-off relationships of multiple SDG indicators for provinces in China, with SDG 6 and SDG 15 being more vulnerable to the trade-off effects of other goals in most regions.
- From 2000 to 2020, 27.02% of indicator pairs in Chinese provinces changed from trade-off to synergistic relationships, and 18.30% of the trade-off relationships between indicator pairs were alleviated. The interactions among provincial SDGs were directional, and the change in active and passive directions of the SDGs in the synergistic and trade-off

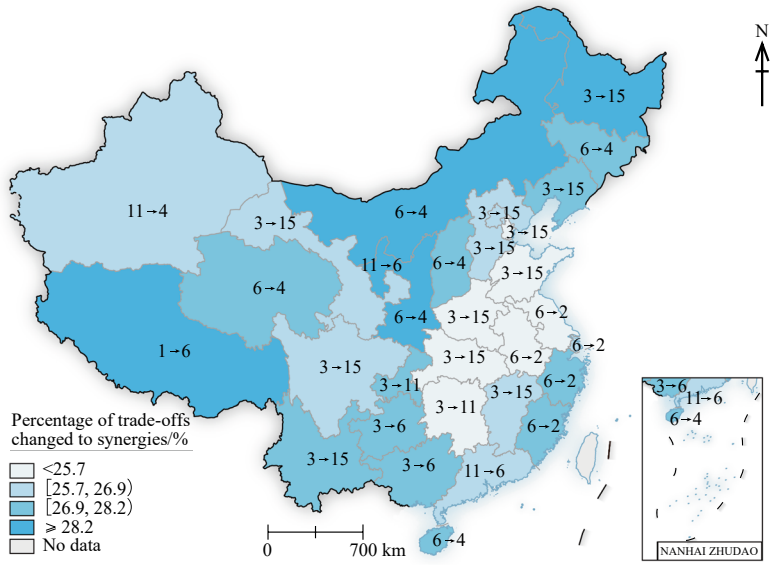

(a) SDG pairs from trade-offs to synergies

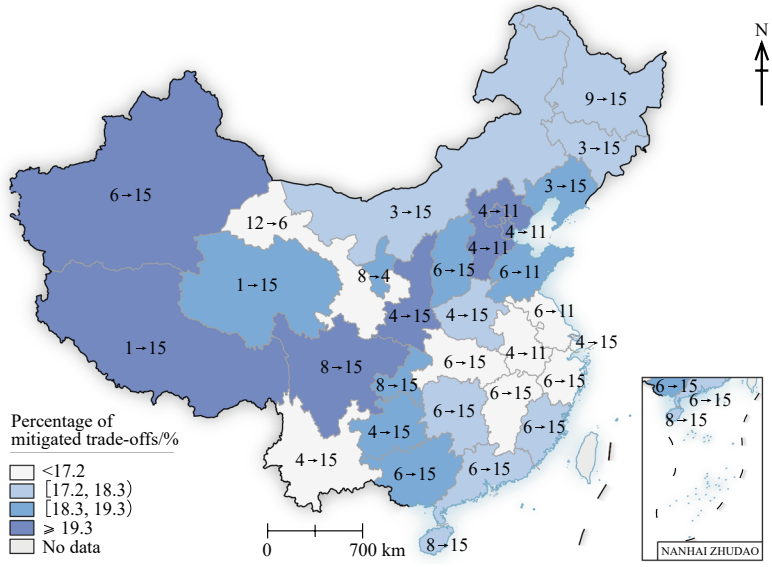

(b) SDG pairs of mitigated trade-offs

Fig. 9.2 The changes of trade-offs in China's provinces. *Note* "→" symbols indicate typical SDG indicator pairs and their directions of action

network in each province was explored. In the trade-off network, SDG 1 and SDG 7 are the main influential SDGs in China with more obvious radiative influence; in the synergistic network, SDG 11 and SDG 16 tend to be passively and synergistically influenced by other SDGs.

- SDG indicators that appear several times in China's synergistic cycle network, such as domestic material consumption (SDG 12.2.2), water management (SDG 6.5.1), and universal primary and secondary education (SDG 4.1.2), are recommended as priority development indicators.

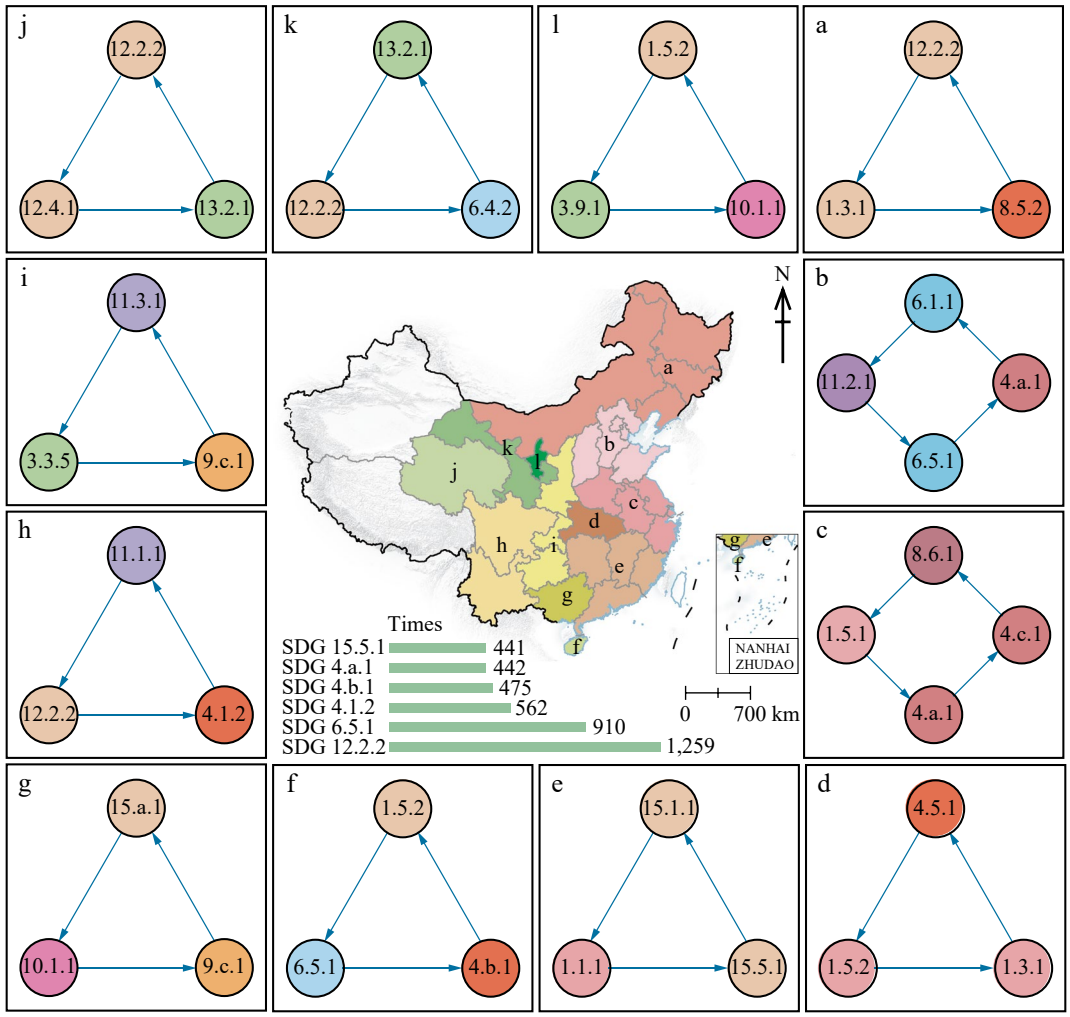

Fig. 9.3 Typical synergy closed loop diagram in China. *Note* No data for Hong Kong, Macao, and Taiwan

- From 2000 to 2020, the changes in the active and passive relationships between the synergistic and trade-off SDG pairs in various provincial-level administrative regions in China showed spatial variability.

9.3.1.5 Discussion and Outlook

This case combines spatiotemporal geographically weighted regression and complex network methods to explore the spatial distribution of typical synergistic and trade-off SDG pairs, a simple closed loop SDG indicator synergistic network, and active–passive directional changes in the SDGs. The analysis covers 31 provincial-level administrative regions of China from 2000 to 2020 and can provide decision support for the achievement of the SDGs. The findings are as follows. (1) SDG 6 and SDG 15 are more vulnerable to the trade-off effects of other goals in most Chinese provinces; (2) From 2000 to 2020, 27.02% of the indicator pairs in China changed from trade-offs to synergies, while 18.30% of the indicator pairs had their strength of trade-offs mitigated. (3) It is recommended that domestic material consumption (SDG 12.2.2), degree of integrated water resources management (SDG 6.5.1), and universal primary and secondary education

Table 9.2 Active–passive changes of the SDGs in China from 2000 to 2020

Regions	Provincial-level administrative regions	Synergy		Trade-off	
		Passive→Active	Active→Passive	Passive→Active	Active→Passive
North China	Beijing	—	SDG 5	**SDG 1**	SDG 4/**SDG 11**
	Tianjin	—	SDG 5	**SDG 1**	SDG 4
	Shanxi	SDG 7	—	**SDG 1**	**SDG 11**/SDG 13
	Hebei	—	—	**SDG 1**	SDG 4/**SDG 11**
	Inner Mongolia	SDG 1	SDG 9	**SDG 1**	—
East China	Shandong	**SDG 13**	**SDG 11**	**SDG 1**	**SDG 11**
	Shanghai	—	**SDG 11**	—	**SDG 11/SDG 16**
	Zhejiang	SDG 4	—	**SDG 7**	**SDG 16**
	Anhui	—	SDG 9	**SDG 7**	**SDG 11/SDG 16**
	Jiangsu	—	**SDG 11**	**SDG 7**	**SDG 9/SDG 11**
	Fujian	—	**SDG 16**	**SDG 7**	**SDG 16**
	Jiangxi	—	—	**SDG 7**	SDG 5/**SDG 16**
Central China	Hubei	—	—	SDG 1	**SDG 9/SDG 16**
	Hunan	**SDG 13**	**SDG 16**	**SDG 7**	SDG 5/**SDG 16**
	Henan	SDG 4	**SDG 11**	**SDG 7**	**SDG 11**
South China	Guangdong	—	**SDG 16**	**SDG 7**	**SDG 9/SDG 16**
	Guangxi	**SDG 13**	**SDG 16**	**SDG 7**	**SDG 16**
	Hainan	SDG 1	**SDG 16**	**SDG 1**	**SDG 16**
Southwest China	Sichuan	—	**SDG 11**	**SDG 7**	SDG 5
	Yunnan	**SDG 13**	**SDG 16**	**SDG 7**	SDG 4/**SDG 16**
	Chongqing	SDG 7	**SDG 16**	**SDG 7**	**SDG 9/SDG 16**
	Guizhou	**SDG 13**	**SDG 16**	**SDG 7**	**SDG 16**
	Xizang	—	**SDG 16**	**SDG 7**	**SDG 16**
Northeast China	Heilongjiang	SDG 4	SDG 5	**SDG 1**	SDG 5
	Jilin	SDG 4	—	**SDG 1**	SDG 4/**SDG 16**
	Liaoning	—	—	**SDG 1**	SDG 4/**SDG 11**
Northwest China	Shaanxi	**SDG 13**	—	**SDG 1**	**SDG 9**
	Xinjiang	SDG 10	SDG 3	—	**SDG 16**
	Qinghai	SDG 7	**SDG 16**	—	**SDG 9**
	Ningxia	SDG 5	—	**SDG 1**	—
	Gansu	SDG 7	—	—	—

Note — indicates no typical SDG was found in the province

(SDG 4.1.2) should be prioritized as development indicators. (4) The active and passive changes in synergistic and trade-off effects of the SDGs show spatial variability in China's provinces from 2000 to 2020.

9.3.2 Synergetic Development of the Water–Food–Air Quality Nexus Over Northeast China

Target: SDG 2.4: By 2030, ensure sustainable food production systems and implement resilient agricultural practices that increase productivity and production, that help maintain ecosystems, that strengthen capacity for adaptation to climate change, extreme weather, drought, flooding, and other disasters, and that progressively improve land and soil quality.
SDG 6.4: By 2030, substantially increase water use efficiency across all sectors and ensure sustainable withdrawals and supply of freshwater to address water scarcity and substantially reduce the number of people suffering from water scarcity.
SDG 11.6: By 2030, reduce the adverse per capita environmental impact of cities, including by paying special attention to air quality and municipal and other waste management.

9.3.2.1 Background

The complex nexus between the SDGs is one of the key challenges encountered in the implementation of each goal. The interrelationships between multiple goals determine that the SDGs cannot be achieved simultaneously. Therefore, tracking and understanding the potential synergies and trade-offs between different pairs of goals is of great significance for implementing the SDGs. For example, previous studies have shown that agricultural irrigation water use has caused severe water scarcity in some typical agricultural production areas around the world, so there is a certain conflict relationship between agricultural irrigation goals and water resources security goals (Aguilar-Rivera et al. 2019; Nilsson et al. 2018).

Northeast China is an important grain base in the country, accounting for 25% of national grain production, and is critical to food security in China (Dong et al. 2016; You et al. 2021), but it has only 7% of the total freshwater resources. In the past few decades, the adjustment of agricultural planting structures in Northeast China, such as the rapid expansion of corn and rice, has led to a continuous increase in AWU, leading to severe groundwater overexploitation. The overexploitation of shallow groundwater in the Songnen Plain and Liaohe Plain is the most severe, with a total area of 480 km^2 of groundwater depletion funnels and a decrease of 30–60 m in the centers of the funnels. Therefore, the water shortage poses a serious threat to sustainable food production in Northeast China.

Since the beginning of the twenty-first century, a series of agricultural management measures, including water-saving irrigation in agriculture, have played an important role in water resources protection (Hu et al. 2010). However, there is currently no consensus on whether measures such as water-saving irrigation have improved the efficiency of AWU. In addition, there is currently no relevant research on whether the adjustment of agricultural planting structures will affect local air quality through straw burning.

With the support of CASEarth, we have comprehensively used various data such as remote sensing and statistics to conduct research on the interactions between SDGs such as water, grain, and air quality in Northeast China. In addition, based on water resources analysis, we have further analyzed the interactions of food–water and food–air quality to provide theoretical and data support for achieving the multi-objective synergetic development of the water–food–air quality nexus over Northeast China.

9.3.2.2 Data

- All available Landsat imagery with a spatial resolution of 30 m in Northeast China (2000–2020).

- Gravity Recovery and Climate Experiment (GRACE) data with a spatial resolution of 1° (2002–2020).
- FIRMS fire and burned area data with a spatial resolution of 1,000 m (2000–2020).
- AOD data (MCD19A2.006) with a spatial resolution of 1,000 m (2000–2020).
- Land use data with a spatial resolution of 100 m in Northeast China (2000–2020).
- Statistical data of AWU, grain production, and agricultural planting area (2000–2020).
- Spatial distribution data of typical kinds of crops, including paddy rice, corn, and soybean (2000–2020).

9.3.2.3 Methods

This study comprehensively utilized remote sensing big data and cloud computing technology to analyze the synergies and trade-offs of water–food–air quality in Northeast China (Fig. 9.4). Based on the remote sensing cloud computing platform and all available Landsat observations, an automated technical process for the continuous monitoring of surface water body changes was built, and surface water body changes were monitored and analyzed on an annual time scale. At the same time, three kinds of GRACE gravity satellite data from 2002 to 2016 were used to analyze the spatiotemporal variation patterns of TWS in Northeast China.

In terms of analyzing the synergies and trade-offs between food and water, the relationship between the interannual changes in AWU and grain production was first analyzed by using statistical yearbook data, and it was found that the two indicators were significantly and negatively correlated with each other. In terms of analyzing the synergies and trade-offs between food and air quality, the spatial pattern consistency between changes in agricultural planting structures and fire and AOD was analyzed by using time-series data on the spatial distribution of major crops and other indicators, such as fire and AOD.

9.3.2.4 Results and Analysis

From 2000 to 2020, while grain production in Northeast China increased year by year, the AWU per km^2 continued to decline at a rate of 9,580

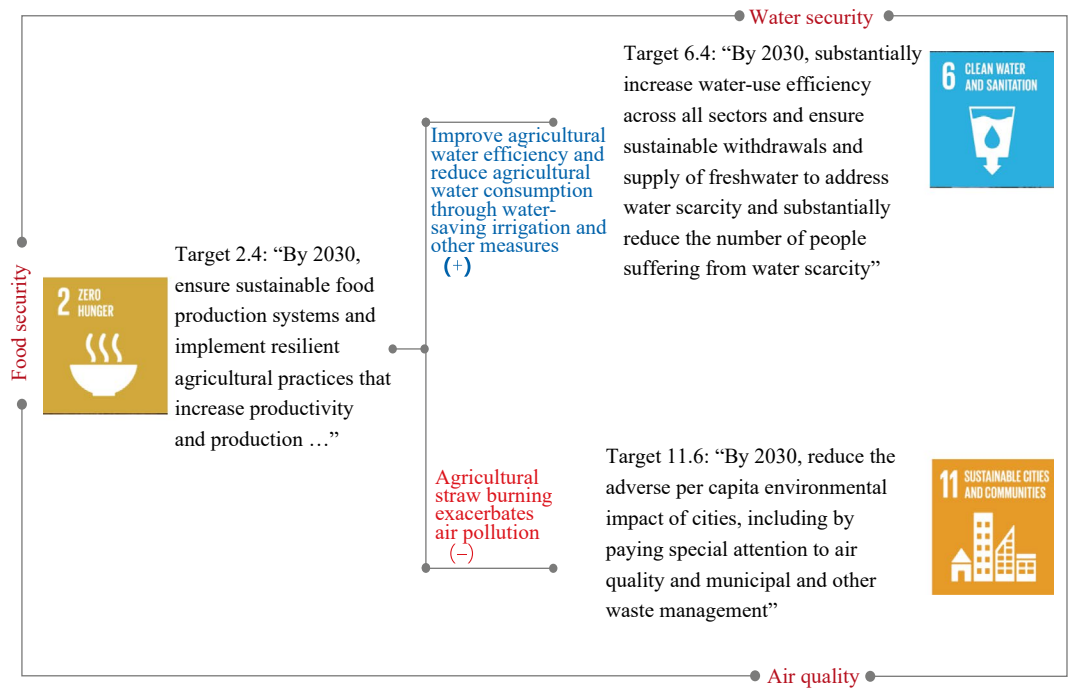

Fig. 9.4 Synergies and trade-offs of water–food–air quality in Northeast China

m^3/a (Fig. 9.5). At the same time, the situation of surface water resources continued to improve, and the SWAs showed a continuously increasing trend at a rate of 82.5 km^2/a, especially in Heilongjiang Province and Jilin Province.

The expansion of the corn planting area is the most rapid in typical areas such as the Songnen Plain and Liaohe Plain. In addition, the spatial pattern of the expansion of the corn planting area is consistent with the increases in the number of fire spots and AOD in spring and autumn (Fig. 9.6), indicating that the expansion of corn planting significantly increases the number of fire spots caused by residue burning in spring and autumn, further leading to a significant increase in AOD and having a certain degree of impact on the local air quality.

In summary, this study found that the contradiction between agricultural production and water shortage in Northeast China has gradually eased from 2000 to 2020. In typical areas such as the Songnen Plain and Liaohe Plain, the expansion of the corn planting area has significantly increased the number of fire points for agricultural straw burning in spring and autumn, exacerbating local air pollution to some extent. Therefore, seeking the synergies of water–food–air quality is crucial for the sustainable development of Northeast China.

Highlights

- Based on remote sensing big data and statistical data, this study analyzed the interannual

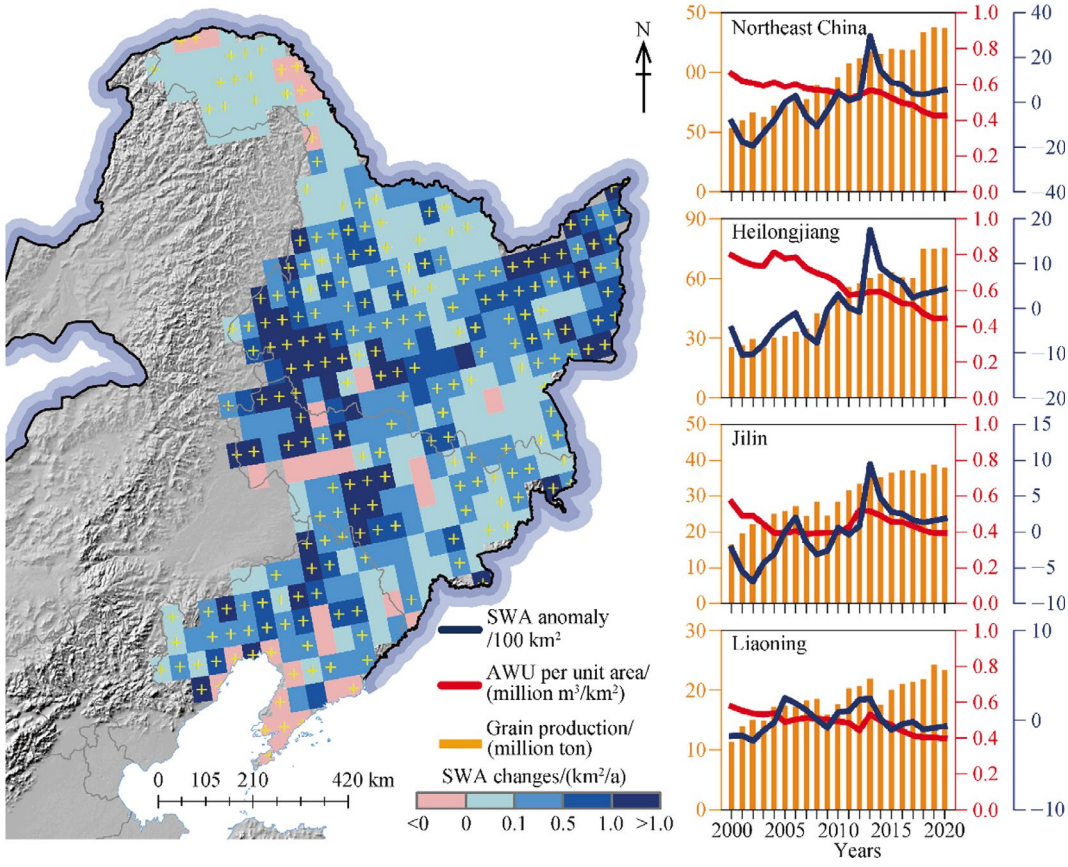

Fig. 9.5 Interannual variations in AWU, grain production, and SWA in Northeast China during 2000–2020. *Note* The symbol "+" in each grid cell indicates a statistically significant trend with a *p*-value <0.05

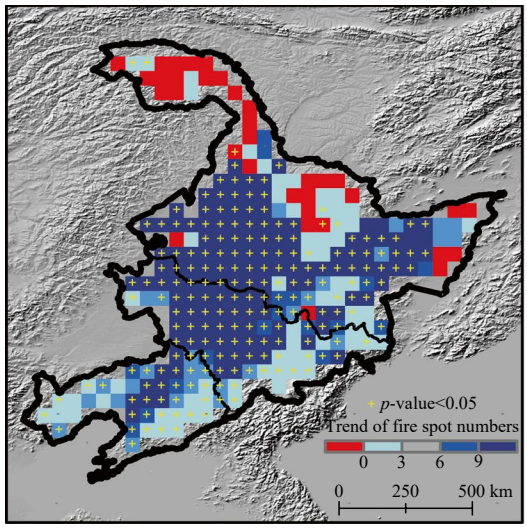

(a) Spatial patterns of linear trends of fire spot numbers in spring

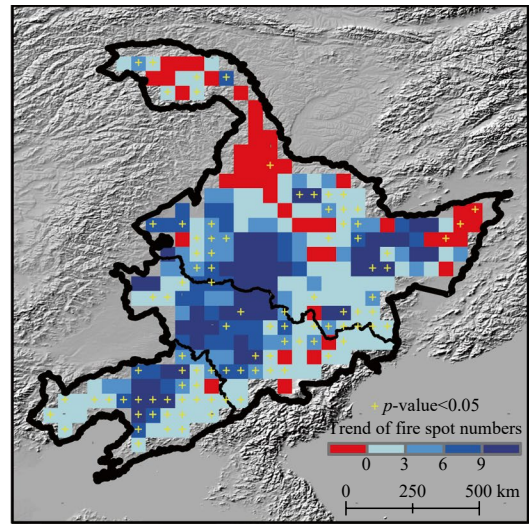

(b) Spatial patterns of linear trends of fire spot numbers in autumn

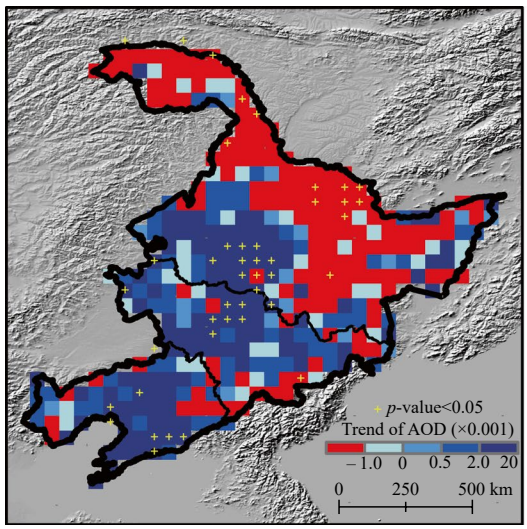

(c) Spatial patterns of linear trends of AOD in spring

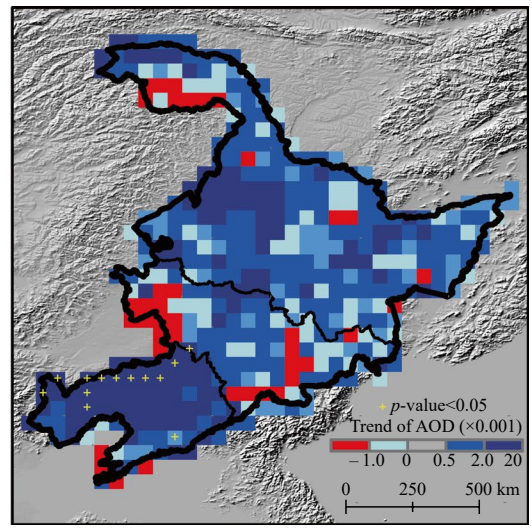

(d) Spatial patterns of linear trends of AOD in autumn

Fig. 9.6 Spatial patterns of linear trends of fire spot numbers and AOD in spring and autumn in Northeast China during 2000–2020

variations in SWA, TWS, grain production, AWU, and air quality indicators, as well as their interactions over Northeast China from 2000 to 2020.

- While the grain yield in Northeast China has been stable or increasing year after year, AWU efficiency has continuously risen, and SWA has significantly increased. The trade-offs between food (SDG 2) and water security (SDG 6) tend to be alleviated.
- The agricultural expansion in Northeast China has not only increased grain production, but also caused a continuous increase in residue burning, exacerbating air pollution.

The effects of agricultural production on air quality in key regions (SDG 11) need to be continuously monitored.

9.3.2.5 Discussion and Outlook

Northeast China accounts for 25% of national grain production and is critical to food security in China, but it has only 7% of the total freshwater resources. The contradiction between food security and water security is prominent. Therefore, achieving the synergetic development of water security and food security in the region is crucial, as well as the key to accelerating the achievement of the UN SDGs. This study found that a series of measures such as water-saving irrigation in agriculture (e.g., sprinkler irrigation, drip irrigation, etc.) have resulted in stable and increased grain production over the years, while the water resources situation continues to improve and SWA continues to expand. However, further research is needed in the future to determine whether surface water expansion will affect local water evaporation, and therefore have a certain impact on TWS. In addition, expansion of corn planting in typical regions such as the Songnen Plain and Liaohe Plain has also led to an increase in fires due to local agricultural straw burning, which has affected local air quality and will require continuous attention in the future.

9.3.3 Interactions Among the SDGs and Integrated Evaluations in China's Transport Industry

Target: SDG 3.6: By 2020, halve the number of global deaths and injuries from road traffic accidents.
SDG 7.2: By 2030, increase substantially the share of renewable energy in the global energy mix.
SDG 8.2: Achieve higher levels of economic productivity through diversification, technological upgrading, and innovation, including through a focus on high-value added and labor-intensive sectors.
SDG 9.1: Develop quality, reliable, sustainable, and resilient infrastructure, including regional and transborder infrastructure, to support economic development and human well-being, with a focus on affordable and equitable access for all.
SDG 11.2: By 2030, provide access to safe, affordable, accessible and sustainable transport systems for all, improving road safety, notably by expanding public transport, with special attention to the needs of those in vulnerable situations, women, children, persons with disabilities, and older persons.
SDG 11.6: By 2030, reduce the adverse per capita environmental impact of cities, including by paying special attention to air quality and municipal and other waste management.
SDG 12.2: By 2030, achieve the sustainable management and efficient use of natural resources.
SDG 13.2: Integrate climate change measures into national policies, strategies, and planning.
SDG 15.1: By 2020, ensure the conservation, restoration, and sustainable use of terrestrial and inland freshwater ecosystems and their services, in particular forests, wetlands, mountains, and drylands, in line with obligations under international agreements.

9.3.3.1 Background

Convenient transport can promote economic development and social welfare, and plays an indispensable role in improving regional economic and social development. However, transport can also have negative impacts on the environment and human safety, such as causing huge carbon emissions (Chen et al. 2021), habitat fragmentation due to road construction (Kang et al. 2020), and traffic death, which is the leading cause of death in developing countries (Sapsirisavat and Mahikul 2021).

Previous studies have focused on the performance of transport on a single SDG, such as the impacts on SDG 9 (Akuraju et al. 2020), SDG 11

(Xu et al. 2019) and SDG 13 (Wenz et al. 2020), and few studies have comprehensively assessed the sustainability of transport and quantitatively explored the trade-offs and synergies between the SDGs. Therefore, this study used Big Earth Data to compare the performance of China's transport industry on different SDGs, and analyzed the interactions between indicators.

9.3.3.2 Data

- Data from the China Statistical Yearbooks.
- OpenStreetMap (national road, provincial road, county road, township road, highway).
- WorldPop.
- China Mobile Source Environmental Management Annual Report.
- Multi-resolution Emission Inventory for China (MEIC) CO_2 database.
- Biological specimen resource sharing platform of China Nature Reserve.
- The time range of the data extraction was from 2000 to 2021.

9.3.3.3 Methods

Quantifiable transport-related indicators from the SDG global indicator framework were selected, and the transport indicators that were consistent with the meaning of the SDGs were constructed (Table 9.3). Based on the five-step decision tree provided by the SDSN, a 100-point target was set as an upper bound for each indicator. For the lower bound, the bottom 2.5% value was used. The scores for each indicator were then converted linearly to 0–100. The Spearman correlation coefficient was used to obtain the correlation between the indicators, and a correlation significance test was carried out. The significant positive correlations with coefficients greater than 0.5 were regarded as "synergy", and significant negative correlations with coefficients less than −0.5 were regarded as "trade-off" (Warchold et al. 2022).

9.3.3.4 Results and Analysis

Scores of SDG Indicators of China's Transport Industry

The results of the indicator scores (Fig. 9.7) showed that China's transport sector performed well in SDG 9.1 to develop quality, reliable, sustainable, and resilient infrastructure. The indicator of the proportion of population covered by roads (SDG 9.1.1) scored high year by year, reaching 77 points in 2020, and the performance of the eastern provinces generally was better (Fig. 9.8a). The overall performance of the growth rate of freight volume was the best [SDG 9.1.2(1)], with a score of 90, and the development of all provinces was balanced (Fig. 9.8b); the score of the passenger volume growth rate was also high [SDG 9.1.2(2)], which was also closer to the target value in the plan, with a score of 87 (Fig. 9.8c). It also scored high on SDG 3.6.1 traffic safety at 78. Furthermore, SDG 12.2.2 had well-balanced development in the sustainable management and efficient use of natural resources, with a high score of 89 for land use efficiency in transport infrastructure. However, in SDG 7.2.1 transport, warehousing, and postal industry use of non-fossil fuels, the overall performance needed to be further improved, despite a 32.9% improvement in 2019 compared to 2018 (Fig. 9.9a). When the national target of reducing CO_2 emissions per unit of GDP by 2020 by 18% compared to 2015 was set for the upper bound, most provinces got high scores on the SDG 13.2.2 CO_2 emission indicator (Fig. 9.8d), with an average score of 89.

Bus ownership per 10,000 people indirectly reflected SDG 11.2.1, the proportion of population with easy access to public transport, which did not score well due to large differences among provinces. SDG 8.2.1, the score of the annual income of employees in transport, warehousing, and the postal industry, increased significantly year by year (Fig. 9.9b), and the annual income score of each province in 2019 was much higher than that of 2006.

After experiencing the rapid development of transport infrastructure construction, China's transport is expected to pay more attention to the improvement of green and low-carbon transformation and transportation service quality in the current and future stages; that is, after meeting the development of SDG 9.1 and SDG 3.6, it should pay more attention to the development of SDG 7.2, SDG 8.2, and other targets, and move from a transport country to a transport power.

Table 9.3 SDG indicators, upper bounds, and data sources

Ranking	SDG targets	SDG indicators	Constructed transport SDG indicators	SDG indicator upper bounds	Data sources and transport sectors included
1	SDG 3.6 By 2020, halve the number of global deaths and injuries from road traffic accidents	SDG 3.6.1 Death rate due to road traffic injuries	Death toll of road traffic accident (person)/resident population at the end of the year	Half of 2015	China Statistical Yearbook 2002–2019
2	SDG 7.2 By 2030, increase substantially the share of renewable energy in the global energy mix	SDG 7.2.1 Renewable energy share in the total final energy consumption	(Heat+electricity+other energy) of transport, warehousing, and postal industries/total energy consumption of this industry	Non-fossil energy accounts for 15% of total energy consumption according to the national plan	China Statistical Yearbook 2000–2019
3	SDG 8.2 Achieve higher levels of economic productivity through diversification, technological upgrading and innovation, including through a focus on high-value added and labor-intensive sectors	SDG 8.2.1 Annual growth rate of real GDP per employed person	Average wage of urban transport, warehousing, and postal industries	The average of the top 5 performers (the higher the wage is, the higher the score is)	China Statistical Yearbook 2006–2019
4	SDG 9.1 Develop quality, reliable, sustainable, and resilient infrastructure, including regional and transborder infrastructure, to support economic development and human well-being, with a focus on affordable and equitable access for all	SDG 9.1.1 Proportion of the rural population who live within 2 km of an all-season road	Proportion of population within 2 km on both sides of Class I-IV roads and highways	100%	Population data were from WorldPop, road data (2014–2020) were from OpenStreetMap Class I–IV road, and highway classification data were from National Catalogue Service for Geographic Information
5		SDG 9.1.2 Passenger and freight volumes, by mode of transport	(1) The annual growth rate of cargo weight transported	The annual growth rate of freight volume is planned to be 2%	China Statistical Yearbook 2001–2020
6			(2) The annual growth rate of the number of passengers transported	The annual growth rate of passenger volume is planned to be 3.2%	

(continued)

Table 9.3 (continued)

Ranking	SDG targets	SDG indicators	Constructed transport SDG indicators	SDG indicator upper bounds	Data sources and transport sectors included
7	SDG 11.2 By 2030, provide access to safe, affordable, accessible, and sustainable transport systems for all, improving road safety, notably by expanding public transport, with special attention to the needs of those in vulnerable situations, women, children, persons with disabilities, and older persons	SDG 11.2.1 Proportion of population that has convenient access to public transport, by sex, age, and persons with disabilities	Bus ownership per 10,000 people, i.e., the number of buses per 10,000 people	The average of the top 5 performers (the more buses, the higher the score)	China Statistical Yearbook 2004–2019
8	SDG 11.6 By 2030, reduce the adverse per capita environmental impact of cities, including by paying special attention to air quality and municipal and other waste management	SDG 11.6.2 Annual mean levels of fine PM (e.g., $PM_{2.5}$ and PM_{10}) in cities (population weighted)	Mobile source PM emission (10,000 tons)/resident population at the end of the year	The average of the top 5 performers (lower PM emission, higher score)	China Mobile Source Environmental Management Annual Report 2010–2019
9	SDG 12.2 By 2030, achieve the sustainable management and efficient use of natural resources	SDG 12.2.2 Domestic material consumption, domestic material consumption per capita, and domestic material consumption per GDP	Land for transport infrastructure (10,000 ha)/(passenger volume+freight volume)	The average of the top 5 performers (lower ratio, higher score)	China Land and Resources Statistical Yearbook 2009–2017
10	SDG 13.2 Integrate climate change measures into national policies, strategies, and planning	SDG 13.2.2 Total greenhouse gas emissions per year	CO_2 emissions from the transport sector/GDP of the province	By 2020, emissions should be 18% less than 2015, according to the Energy Production and Consumption Revolution Strategy (2016–2030)	MEIC database 2015–2017 (CO_2 emissions from mobile sources in MEIC include emissions from trucks, passenger vehicles, construction machinery, agricultural machinery, inland ships, and railway internal combustion engines, excluding energy consumption during construction and road lighting)

(continued)

Table 9.3 (continued)

Ranking	SDG targets	SDG indicators	Constructed transport SDG indicators	SDG indicator upper bounds	Data sources and transport sectors included
11	SDG 15.1 By 2020, ensure the conservation, restoration, and sustainable use of terrestrial and inland freshwater ecosystems and their services, in particular forests, wetlands, mountains, and drylands, in line with obligations under international agreements	SDG 15.1.2 Proportion of important sites for terrestrial and freshwater biodiversity that are covered by protected areas, by ecosystem type	The proportion of 300 m on both sides of Class I-IV roads and highways in the total area of the protected areas	The annual growth rate of the road area as a percentage of the protected area is 0	Protected area data were from the biological specimen resource sharing platform of the China Nature Reserve A buffer zone of 300 m was used according to the guideline of the Specifications for Environmental Impact Assessment of Highways

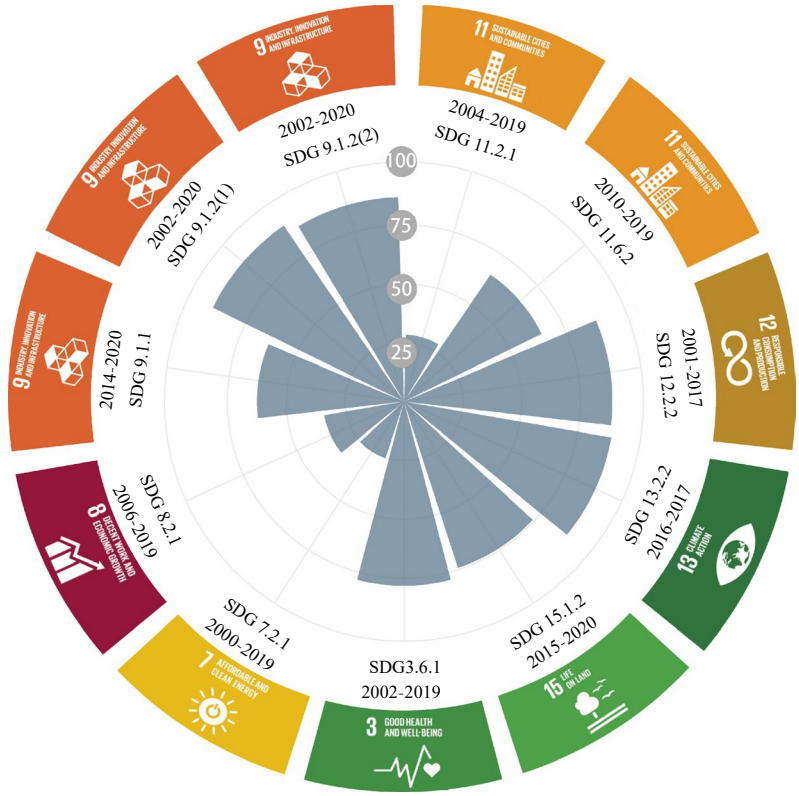

Fig. 9.7 Average performance of 11 transport sustainability indicators. *Note* All scores translate to 0–100 points, with 100 as the best performance. The years under each indicator represent the corresponding year range for the data

Analysis of Interactions Between Indicators

Figure 9.10 showed that among the eleven indicators, fourteen pairs of indicators had significant positive correlations ($p<0.05$), of which three pairs had correlation coefficients greater than 0.5, that is, a synergistic relationship, and eleven pairs of indicators had significant negative correlations ($p<0.05$), but there was no obvious trade-off relationship. SDG 8.2.1 annual income of staff and SDG 9.1.1 road population coverage indicators had the highest number of significant correlations with other indicators, at seven times each. Since these two indicators had the most frequent significant correlations with other indicators and the largest sum of the absolute values of the significant correlation coefficients, these two indicators could be the core indicators and should be prioritized in the path of future development and optimization.

For 2001–2020, through the correlation analysis of eleven indicators, it was found that compared with 2001–2010, the average number of significant, positively correlated pairs to the total pairs from 2011 to 2020 increased by 148.4%, while significant, negatively correlated pairs decreased by 7.2%. At the current stage of development, promoting the coordinated development of the integrated transport system would be the main task of sustainable transport in China.

Highlights

- A dataset of China's transport industry development under the framework of SDG indicators for 2000–2020 was constructed, which initially solved the problem of the lack of quantitative and comprehensive assessment of the SDGs of China's sustainable transport.

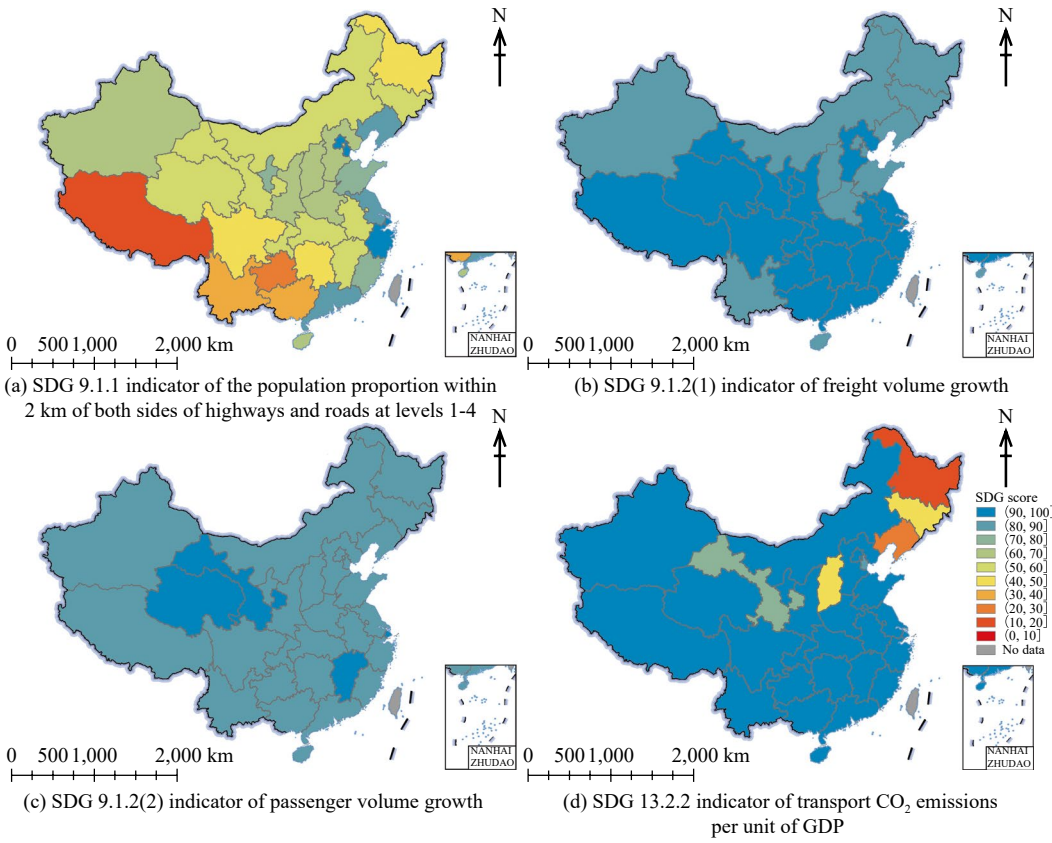

(a) SDG 9.1.1 indicator of the population proportion within 2 km of both sides of highways and roads at levels 1-4

(b) SDG 9.1.2(1) indicator of freight volume growth

(c) SDG 9.1.2(2) indicator of passenger volume growth

(d) SDG 13.2.2 indicator of transport CO_2 emissions per unit of GDP

Fig. 9.8 Average performance of SDG indicators by province

- For SDG 9.1, China's transport sector performed well over 20 years to develop quality, reliable, sustainable, and resilient infrastructure. The growth rate of freight volume was close to the target value of the national plan, with a score of 90; the score of passenger volume growth rate was 87; and the score for the proportion of people within 2 km on both sides of major roads has increased year by year. The transport, warehousing, and postal industry needs to improve their performance in SDG 7.2, clean energy use. In terms of SDG 11.2, accessibility, bus ownership per 10,000 people needs to be developed more evenly among provinces.
- Through the correlation analysis of eleven indicators from 2001 to 2020, it was found that the proportion of indicators with significant, positive correlations in 2011–2020 increased by 148.8% compared with 2001–2010.

9.3.3.5 Discussion and Outlook

Over the 20-year study period, China's proactive fiscal policy revolutionized the transport sector in terms of transport volume, and transport has become the context of the economy and the link of civilization. This study showed that China attached great importance to infrastructure construction and transportation volume, as well as the guarantee of traffic safety and the strict control of land use for transport infrastructure. The analysis of the interactions between indicators indicates that the realization of sustainable transport is a tortuous process, and as the synergies between indicators increase and the trade-offs decrease, the transport industry is gradually achieving the SDGs.

This study analyzed SDG indicators that were directly related to transport itself. However, transport has indirect impacts on many indicators, such as the relationship between transportation and poverty alleviation,

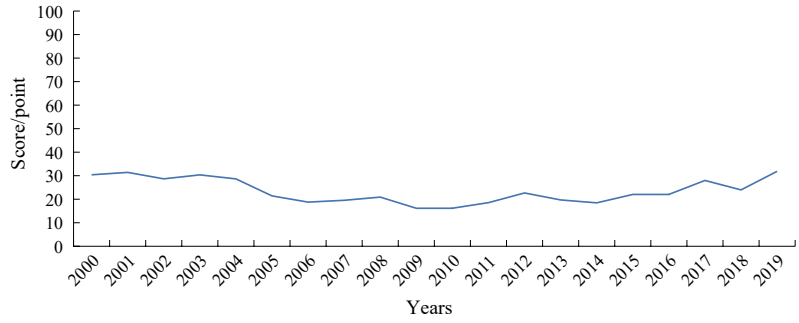

(a) SDG 7.2.1

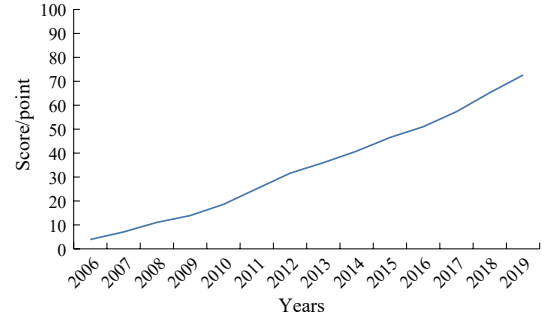

(b) SDG 8.2.1

Fig. 9.9 Line chart of SDG 7.2.1 and SDG 8.2.1 scores

the relationship with food transportation security, and the impacts of China's outbound investment in the Belt and Road region. It is suggested that the future assessment of sustainable transport should include a more quantitative assessment of indirect impact indicators.

9.3.4 SDG Integrated Evaluation for Lincang, Yunnan Province, China

Target: SDG 1, SDG 2, SDG 3, SDG 4, SDG 5, SDG 6, SDG 7, SDG 8, SDG 9, SDG 10, SDG 11, SDG 12, SDG 13, SDG 15, SDG 16, SDG 17, total 16 goals.

9.3.4.1 Background

After the UN proposed the 2030 Agenda in 2015, China released its National Plan on Implementation of the 2030 Agenda for Sustainable Development in September 2016, which clearly outlined specific plans for implementing the 2030 Agenda in China for the foreseeable future. The construction of the "National Innovation Demonstration Zone for Sustainable Development" was identified as an important measure for the Chinese government to comprehensively promote the implementation of the 2030 Agenda and to deepen the implementation of the innovation-driven development strategy. Its goal is to explore and establish several realistic models and typical patterns of sustainable development innovation demonstrations, to drive sustainable development in other areas within China, and to offer China's wisdom to other countries to implement the 2030 Agenda. In May 2019, Lincang City was approved by the State Council as a National Innovation Demonstration Zone for Sustainable Development with the theme of "innovation-driven in multi-ethnic and underdeveloped border areas".

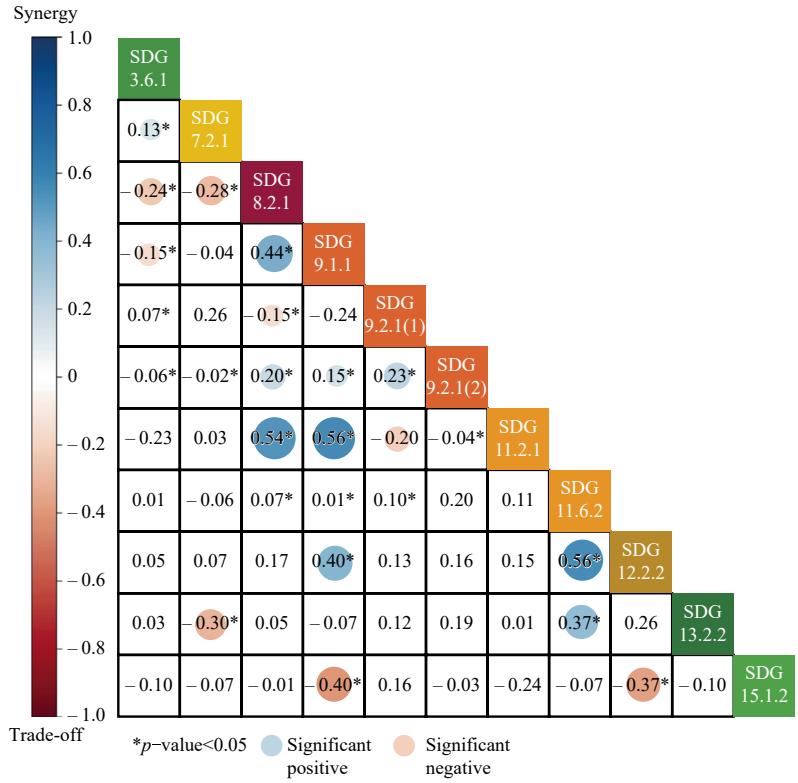

Fig. 9.10 Correlation coefficients between SDGs. *Note* The larger the absolute value of the correlation coefficient is, the bigger and more intensely colored the circle becomes

Currently, scholars in China and abroad have conducted comprehensive assessments of the progress of the SDGs at the global and national levels based on the UN global indicator framework. In terms of methodology, most studies use the equal weighting method proposed by the Bertelsmann Foundation and the SDSN. Fu et al. (2019) proposed employing a systematic approach to promote the comprehensive implementation of the SDGs in all countries globally, avoiding negative impacts from one country's implementation of the SDGs on other countries. However, due to the differences in development among countries, it is difficult to directly apply the global indicator framework of the SDGs, and there is an urgent need for localization. Most existing studies focus on the global or national scale, and there are few comprehensive assessments and localizations of SDG development processes at smaller scales, especially in economically underdeveloped regions. Therefore, based on Big Earth Data, such as statistics, remote sensing, and monitoring, this study takes 2015 as the baseline year and 2020 as the current data year. This case study localized indicators for Lincang City based on the global SDG indicator framework and field surveys, combined with Lincang City's regional characteristics and data acquisition conditions. An indicator system for the comprehensive evaluation of SDG progress was established from three dimensions: society, economy, and resource-environment, including SDG indicators and localized indicators, totaling 16 goals and 70 indicators. Based on this, a comprehensive sustainable development index and social, economic, and resource-environment sustainable development index were calculated for Lincang

City from 2015 to 2020, and the progress trends of the SDGs and indicators were evaluated, providing a reference for achieving the SDGs in underdeveloped mountainous areas.

In addition, the Global Sustainable Development Report 2019 shows that there is insufficient progress in sustainable development at the global, regional, and national levels (Messerli et al. 2019). Experts pointed out that the lack of understanding and handling of the interactions between goals is the primary reason. Identifying and managing the potential interactions among the SDGs can promote the synergistic effects of goals to the greatest extent and minimize trade-offs, which has an important promoting role in achieving the 2030 Agenda (Le Blanc 2015; Stafford-Smith et al. 2017; Hegre et al. 2020). The year 2022 has been designated as the "International Year of Sustainable Mountain Development" by the UN, and the sustainable development issues of mountainous areas, especially underdeveloped ones, are attracting global attention. The region faces various challenges such as No Poverty (SDG 1), Zero Hunger (SDG 2), Good Health and Well-being (SDG 3), Quality Education (SDG 4), Clean Water and Sanitation (SDG 6), Affordable and Clean Energy (SDG 7), Decent Work and Economic Growth (SDG 8), Industry, Innovation and Infrastructure (SDG 9), Climate Action (SDG 13), and Life on Land (SDG 15). There exist complex interactions among the different types of challenges in economy, society, and environment, which directly affect the achievement of the SDGs (Li et al. 2021). Starting from the sustainable development indicators, identifying the interactions between small-scale sustainable development indicators in underdeveloped mountainous areas is beneficial for analyzing the substantive interaction between regional SDGs and formulating corresponding measures (Griggs et al. 2017). Maximizing the synergistic effects of indicators and changing the trade-off roles between indicators are important measures to promote the transformation of ecological resources into ecological capital in underdeveloped mountainous areas, develop a green economy, and help achieve the 2030 Agenda.

9.3.4.2 Data

- Lincang Statistical Yearbook from 2015 to 2020.
- Lincang Water Resources Bulletin from 2015 to 2020.
- Statistical Communiqué of National Economic and Social Development of Lincang City from 2015 to 2020.
- 2015–2020 NDVI data (National Ecosystem Science Data Center, 30 m).
- Land use and land change data, remote sensing data such as forests, grasslands, wetlands, etc.
- National monitoring data of water quality at control sections, monitoring data of meteorological elements, etc.

9.3.4.3 Methods

Localization of Indicators and Dimension Partitioning for Selection

(1) **Localization of Indicators**

The SDG global indicators framework proposed by the UN in September 2015 is designed for national-scale sustainable development assessments. It is not reasonable to use it for assessing subnational regions within a country. Therefore, localizing the SDGs global indicator framework is the primary task for the comprehensive assessment of SDG implementation in a specific region. Taking into account Lincang City's distinct geographic position and ethnic diversity, alongside the specific nuances of SDGs, a meticulous selection and adaptation process was undertaken. This process, guided by considerations of goal comprehensiveness, regional traits, geographical scales, and data accessibility, refined the global SDG indicator framework of 244 metrics down to a tailored set of 70 indicators. This customized set, aimed at effectively assessing Lincang City's sustainable development, incorporates 37 directly utilized indicators and 33 localized indicators (Fig. 9.11).

(2) **Dimension partitioning for selection**

Based on the existing research and data acquisition in Lincang City, 16 goals have been

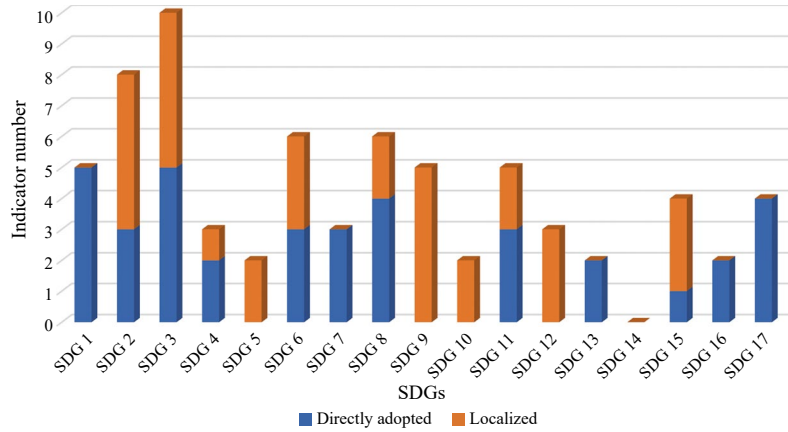

Fig. 9.11 Number of directly adopted indicators and localized indicators for each goal

categorized into three dimensions: society, economy, and resource-environment (Fig. 9.12). SDGs 1, 3, 4, 5, 11, and 16 belong to the social dimension, with a total of 27 indicators. SDGs 8, 9, 10, and 17 belong to the economic dimension, with a total of 17 indicators. SDGs 2, 6, 7, 12, 13, and 15 belong to the resource-environmental dimension, with a total of 26 indicators. As Lincang City is an inland city, there is no data for SDG 14. Please refer to Table 9.4 for specific indicator contents.

Calculation of Sustainable Development Index

(1) **Dimensionless Index**

In order to eliminate the errors caused by different dimensions, variations, or significant differences in the values of various indicators, it is necessary to standardize the data. All indicators were transformed into a dimensionless range from 0 to 1, with 0 indicating poor performance and 1 indicating excellent performance.

$$x_n = \frac{x - \min(x)}{\max(x) - \min(x)} \tag{9.1}$$

(2) **Calculation of Sustainable Development Index**

Following the approach outlined in the Sustainable Development Report by the SDSN (Sachs et al. 2019), which calculates the SDG composite index by using an equal weighting method, we calculated the sustainable development indices for the three dimensions separately. Finally, the sustainable development indices for each dimension were aggregated into a comprehensive sustainable development index using the equal weighting method.

$$I_s = \sum_{j=1}^{N_s} \frac{1}{N_s} \sum_{k=1}^{N_{\mathrm{sj}}} \frac{1}{N_{\mathrm{sj}}} I_{\mathrm{sjk}} \tag{9.2}$$

$$I_e = \sum_{j=1}^{N_e} \frac{1}{N_e} \sum_{k=1}^{N_{\mathrm{ej}}} \frac{1}{N_{\mathrm{ej}}} I_{\mathrm{ejk}} \tag{9.3}$$

$$I_r = \sum_{j=1}^{N_r} \frac{1}{N_r} \sum_{k=1}^{N_{\mathrm{rj}}} \frac{1}{N_{\mathrm{rj}}} I_{\mathrm{rjk}} \tag{9.4}$$

$$\mathrm{SDI} = \frac{1}{3}(I_s + I_e + I_r) \tag{9.5}$$

where I_s, I_e, and I_r represent the sustainable development indices of social, economic, and resource-environmental dimensions respectively; N_s, N_e, and N_r are the number of goals under the social, economic, and resource-environmental dimensions respectively; N_{sj}, N_{ej}, and N_{rj} are the number of indicators for the goals j under the social, economic, and resource-environmental dimensions respectively; I_{sjk}, I_{ejk}, and I_{rjk} are the indicator values for the goals j under the social,

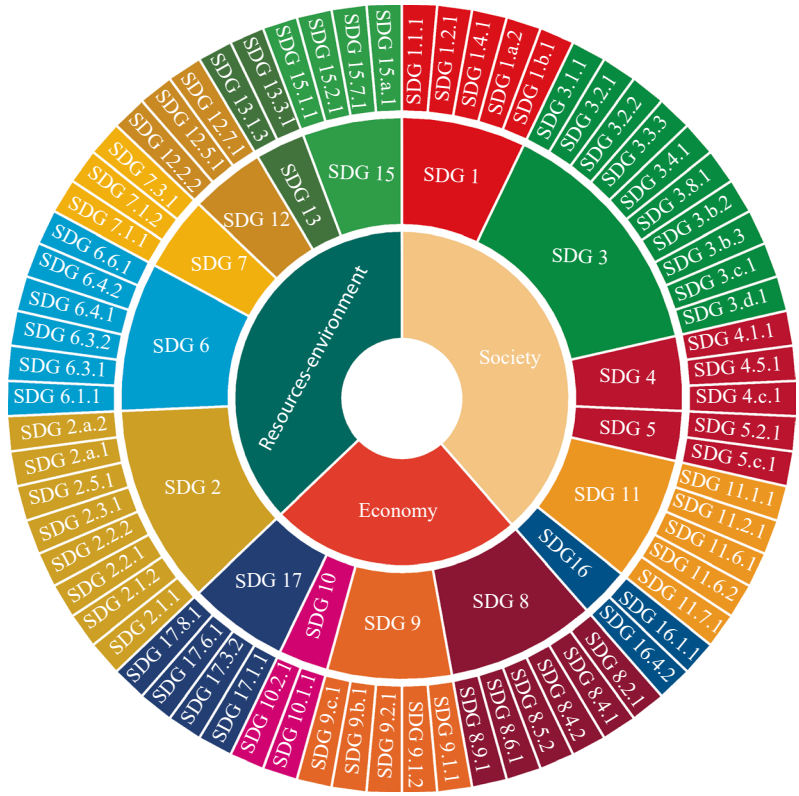

Fig. 9.12 Evaluation of the SDGs and indicators

Table 9.4 Thresholds for sustainable development progress level classification

Categories of development process	Without specific 2030 target values		With specific 2030 target values
	Positive indices	Negative indices	
Achieved or expected to achieve	$x > 0.01$	$x - 0.01$	$x \geq 0.95$
Made progress but needs to be strengthened	$0.005 < x \leq 0.01$	$-0.01 \leq x - 0.005$	$0.50 \leq x 0.95$
No progress	$-0.01 < x \leq 0.005$	$-0.005 \leq x 0.01$	$-0.1 \leq x 0.50$
Negative progress	$x \leq -0.01$	$x \geq 0.01$	$x - 0.1$

economic, and resource-environmental dimensions respectively; and SDI represents the comprehensive sustainable development index.

Quantifying Sustainable Development Progress

(1) Sustainable Development Indicator Construction Process

In order to better implement the 2030 Agenda, we have quantified the development progress of various indicators in Lincang City. First of all, for the indicators that are consistent with the Sustainable Development Report released by the SDSN, when quantifying the development progress, we refer to the threshold in the "SDGs Dashboard", such as annual grain production (SDG 2.1.2) and prevalence of stunting among children under five years of age (SDG 2.2.1). Second, for the indicators that have already developed to 100%, their progress is directly set as "achieved", such as coverage of essential

health services (SDG 3.8.1) and proportion of population with access to electricity (SDG 7.1.1). Finally, except for the above two situations, for the remaining indicators, we adopt the method in the UN Sustainable Development Goals Progress Chart 2020 (UN 2020) to evaluate their development progress from 2015 to 2020, which is divided into two categories.

(1) Indicators without specific 2030 sustainable development target values

$$\mathrm{TR_a} = \left(\frac{x_t}{x_{t_0}} t_0\right)^{\frac{1}{t-t_0}} - 1 \tag{9.6}$$

where, $\mathrm{TR_a}$ denotes the actual annual growth rate, t denotes the current year (2019/2020), t_0 denotes the base year (2015), x_t denotes the index value of the current year, and x_{t_0} denotes the index value of the base year.

(2) Indicators with specific 2030 sustainable development target values

$$\mathrm{TR} = \frac{\mathrm{TR_a}}{\mathrm{TR_r}}$$

$$\mathrm{TR_r} = \left(\frac{x^*}{x_{t_0}}\right)^{\frac{1}{2023-t_0}} - 1 \tag{9.7}$$

where TR stands for the annual growth rate, $\mathrm{TR_r}$ stands for the annual growth rate required to achieve the 2030 target value, and x^* stands for the index value in 2030. According to the above formulas, the development progress is divided into four categories: "achieved or expected to achieve", "made progress but needs to be strengthened", "no progress", and "negative progress" (Table 9.4).

(2) **Construction Process of the SDGs**

In the Sustainable Development Report released by the SDSN, the two indicators with poor performance under each target of every country were selected as the development trend of that goal. This study combined the method in the report and the data characteristics of Lincang City, and took the average value of the corresponding indicator development progress under each goal as the development progress of that goal.

Analysis of Interactions Among Indicators

The interactions of sustainable development indicators were analyzed using the Spearman correlation coefficient and a classification method by Pradhan et al. (2017), which divides the correlation coefficient among the SDGs into the synergistic effect (correlation coefficient >0.6), trade-off effect (correlation coefficient <-0.6), and unclassified type (correlation coefficient between -0.6 and 0.6), with $p<0.05$ considered significant (Pradhan et al. 2017; Sebestyén et al. 2019). The interaction within and between the SDGs was quantified by the percentages of synergistic effects, trade-off effects, and unclassified types of indicator pairs, to avoid bias caused by differences in the number of available indicators between the SDGs (Pradhan et al. 2017).

Social network analysis indicators were introduced based on statistical methods. The interconnection network of sustainable development indicators in Lincang City is an undirected weighted network, and the importance ranking of sustainable development indicators in Lincang City was further clarified using degree, degree centrality, betweenness centrality, closeness centrality, and eigenvector centrality. The interactive relationship between sustainable development indicators in Lincang City was further clarified based on statistical methods and network analysis methods, combined with the progress of corresponding SDG indicators and existing research conclusions.

9.3.4.4 Results and Analysis

Sustainability Index

The sustainability index of Lincang City was calculated from three aspects: society, economy, and resource-environment (Fig. 9.13). Overall, from the trend of change, the comprehensive sustainability index and the society, economy,

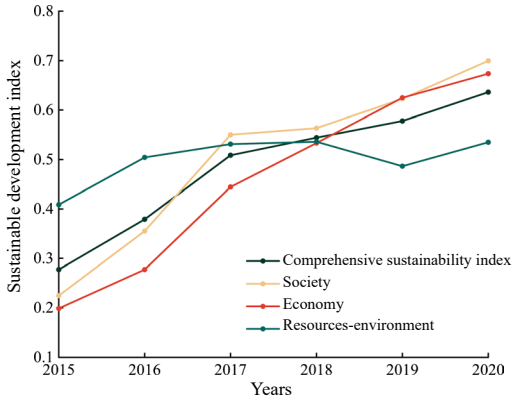

Fig. 9.13 Time-series chart of sustainable development index

and resource-environment sustainability indices of Lincang City all showed an increasing trend from 2015 to 2020. From 2015 to 2020, the comprehensive sustainability index increased from 0.28 to 0.64, with an average annual growth rate of 17.98%; the society sustainability index increased from 0.22 to 0.70, with an average annual growth rate of 26.05%; the economy sustainability index increased from 0.20 to 0.67, with an average annual growth rate of 27.35%; and the resource-environment sustainability index increased from 0.41 to 0.53, with an average annual growth rate of 5.27%. Although the annual average growth rate of the resource-environment sustainability index is relatively small, the index value in the base year is the highest, indicating that the resource-environment sustainability of Lincang City has been in good condition. From a stage-by-stage perspective, the average annual growth rates of the comprehensive sustainability index and society sustainability index in the 2017–2020 stage were slower than those in the 2015–2017 stage. The economy sustainability index had the highest average annual growth rate in the 2015–2017 stage, followed by the 2017–2019 stage, and the smallest in the 2019–2020 stage. The resource-environment sustainability index showed overall small changes, with a decrease in its index value in 2019 and an increase in 2020.

Figure 9.14 shows the scores of various goals in society, economy, and resource-environment dimensions. In the society dimension, the scores of SDG 3, SDG 4, and SDG 11 gradually increased from 2015 to 2020, indicating that these three goals are getting closer to achieving sustainable development. SDG 1 rapidly increased from 2015 to 2019, but decreased by 13.65% in 2020 compared with 2019, which may be mainly due to the impacts of the pandemic, and the decreasing proportion of basic service (education, health, and social security) expenditure to total expenditure by local governments relative to 2019. SDG 5 and SDG 16 showed greater fluctuations in their changes. In the economic dimension, the growth trends of various goals differed greatly. SDG 8 had a three-stage jump growth pattern. SDG 9 was basically stable from 2015 to 2017, with a faster growth rate during 2017–2018 and a slower growth rate from 2018 to 2020. SDG 10 increased at a relatively average rate. SDG 17 had a faster growth rate from 2015 to 2018 and a slight decreasing trend from 2018 to 2020. In the resource-environment dimension, the base year goal scores of various goals were relatively high, and the growth rate was relatively slow. SDG 2 and SDG 15 had lower scores in 2019.

Sustainable Development Process

In order to better monitor the problems that need to be solved in the process of implementing the 2030 Agenda in Lincang City, we have quantified the development process of each indicator (Fig. 9.15). Specifically, each indicator in SDG 5, SDG 6, SDG 8, SDG 10, SDG 13, and SDG 16 has made good progress, while most indicators in other goals have shown good progress, but there are also a few indicators that show no or negative progress. For example, the proportion of the population living below the international poverty line (SDG 1.1.1) and the proportion of total government spending on essential services (education, health, and social protection) (SDG 1.a.2) in SDG 1 show no progress, while the other indicators have a good upward trend. At the same time, against the backdrop of the global economic development being affected by the pandemic, the proportion of total government spending on essential

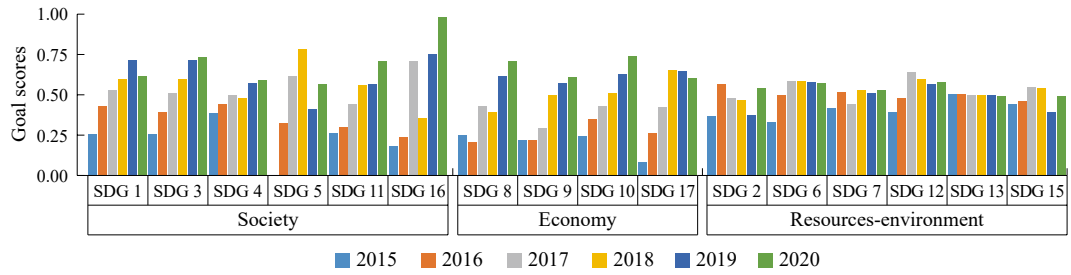

Fig. 9.14 Scores of various goals in society, economy, and resource-environment dimensions

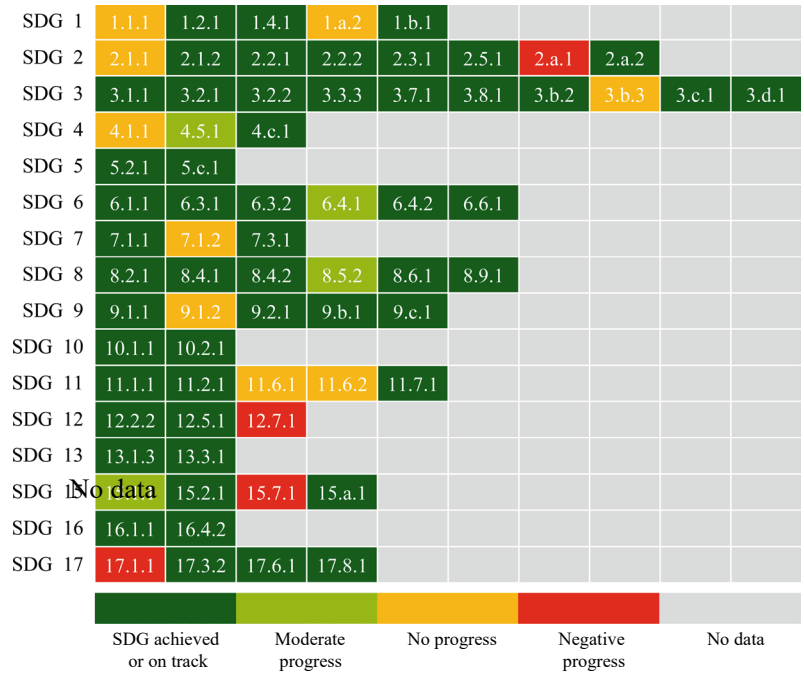

Fig. 9.15 Indicator development process chart

services in SDG 1.a.2 decreased in 2020 compared with 2019. The indicators in SDG 2 have a significant difference in performance. Compared with the progress evaluation threshold in the global "SDGs Dashboard" (Sachs et al. 2019), SDGs 2.1.2, 2.2.1, and 2.2.2 have been achieved. SDGs 2.3.1, 2.5.1, and 2.a.2 have made rapid progress and are expected to achieve their goals by 2030. SDG 2.1.1 (the prevalence of undernourishment) shows no progress, while SDG 2.a.1 (the agriculture orientation index of government spending) shows negative progress. This is because SDG 2.1.1 is a localized indicator expressed by the Engel coefficient of residents, and the Engel coefficient of rural residents in Lincang City has gradually increased, leading to slow progress in this indicator. SDG 2.a.1 represents the ratio of agricultural production input to government total expenditure and the ratio of agricultural added value to GDP. The indices for Lincang City show an overall decreasing trend and are far below the world average. In SDG 3, the average life expectancy (SDG 3.7.1) has achieved its goal compared

with the global "SDGs Dashboard". Coverage of essential health services (SDG 3.8.1) is 100% and has also achieved its goal; the number of health workers per 10,000 population (SDG 3.b.3) shows no progress, while the other indicators have a relatively fast development process. In SDG 4, the average proportion of the education attainment rate (SDG 4.1.1) shows no progress, while the progress of other indicators is good. In SDG 7, the proportion of population with primary reliance on clean fuels and technology (SDG 7.1.2) shows no progress, while the remaining two indicators have relatively fast progress. In SDG 9, the total amount of local passenger and freight volumes (SDG 9.1.2) shows no progress, while the progress of other indicators is good. Due to the impacts of the pandemic, passenger traffic decreased in 2019 and 2020, resulting in the slower overall progress of this indicator. In SDG 11, the urban waste and solid waste treatment rate (SDG 11.6.1) and $PM_{2.5}$ (SDG 11.6.2) show no progress, while the performance of other indicators is good. In SDG 12, the proportion of government green procurement (SDG 12.7.1) shows negative progress, while the other two indicators perform well. The proportion of government green procurement in Lincang City has not reached the national average level. In 2020, the proportion of government green procurement was 1.23%, a decrease of 8.63% compared with 2015. Compared with the national average value of 80%, there is still much room for improvement in the proportion of government green procurement in Lincang City. In SDG 15, the proportion of traded wildlife that was poached or illicitly trafficked (SDG 15.7.1) shows negative progress, while the performance of other indicators is very good. In SDG 17, total government revenue as a proportion of GDP (SDG 17.1.1) shows negative progress, which may be due to the impacts of the pandemic and the significant difference in government total revenue compared with previous years.

Based on this, we aggregated the progress of indicators to the corresponding goals (Fig. 9.16). Overall, all goals have good progress, especially SDG 3, SDG 5, SDG 6, SDG 8, SDG 9, SDG

Fig. 9.16 Development progress chart

10, SDG 13, and SDG 16, which are very likely to achieve the goals by 2030 at the current pace of development. The remaining goals also have some progress, but more efforts are needed to achieve the 2030 Agenda.

Interrelationships Between Indicators

The synergistic effects between sustainable development indicators in Lincang City are significant, with the synergistic effect ratio (39.63%) significantly higher than the trade-off effect ratio (5.49%). Among the goals, the synergistic interaction between SDG 1 (No Poverty) and SDG 3 (Good Health and Well-being) is the most prominent, while the trade-off interaction between SDG 12 (Responsible Consumption and Production) and SDG 13 (Climate Action) is the most obvious, which is consistent with research results from other regions globally (Niessen et al. 2018; Fuso Nerini et al. 2019). Regarding specific indicators, the indicators with higher centrality in the synergistic network include the proportion of total government spending on essential services, the agriculture orientation index for government expenditures, the malaria incidence rate, the proportion of domestic and industrial wastewater flows safely treated, the proportion of population with access to electricity, the proportion of population with primary reliance on clean fuels and technology, tourism direct GDP as a proportion of total GDP, passenger and freight volumes, the proportion of population covered by a mobile network and forest area as a proportion of total land area (SDG 1.a.2, SDG 2.a.1, SDG 3.3.3, SDG 6.3.1, SDG 7.1.1, SDG 7.1.2, SDG 9.1, SDG 8.9.1, and SDG 15.1.1) (Fig. 9.17).

The SDGs generally exhibit synergistic effects, with trade-offs only observed in SDG 15 (Life on Land). The trade-off indicators are for SDG 15.1.1 ("forest area as a proportion of total land area") and SDG 15.7.1 ("proportion of traded wildlife that was poached or illicitly trafficked") (Fig. 9.18).

Among the 70 sustainable development indicators in Lincang City, 28 indicators have been achieved or are expected to be achieved, while 13 indicators have made progress but not enough to achieve the target. The region belongs to an underdeveloped area with low fiscal revenue. Although the government attaches great importance to sustainable development, the total amount of funds available for it is limited. Under the background of funding constraints, it is recommended to prioritize the implementation of relevant policies that help consolidate and expand the achievements of poverty alleviation in mountainous areas and continuously improve the regional medical and health level, in order to promote the early achievement of SDG 1 and SDG 3 (No Poverty and Good Health and Well-being) with higher synergy. At the same time, attention should be paid to the protection of terrestrial and aquatic ecosystems, and efforts should be made to improve the development level of indicators with high coordination centrality, fully exerting the synergistic effect of the above-mentioned goals and indicators, so as to enhance the sustainable development level of Lincang and explore the Lincang model of sustainable development in underdeveloped mountainous areas.

Highlights

- Big Earth Data such as statistics, remote sensing, and monitoring data were applied to the global SDG indicator framework to examine 70 SDG indicators selected through on-site investigations and data acquisition in consideration of the geographical characteristics of Lincang City. An indicator system was constructed from three dimensions (society, economy, and resource-environment) to evaluate the progress of the SDGs in underdeveloped mountainous areas.
- From 2015 to 2020, the comprehensive sustainable development index and the social, economic, and resource-environmental sustainable development indices of Lincang City showed an increasing trend. In terms of the development process of the SDGs, all 16 goals have good development progress, with SDG 5 having the highest average annual growth rate and SDG 13 maintaining a relatively stable trend. In addition, 81% of the SDG indicators have good development progress.

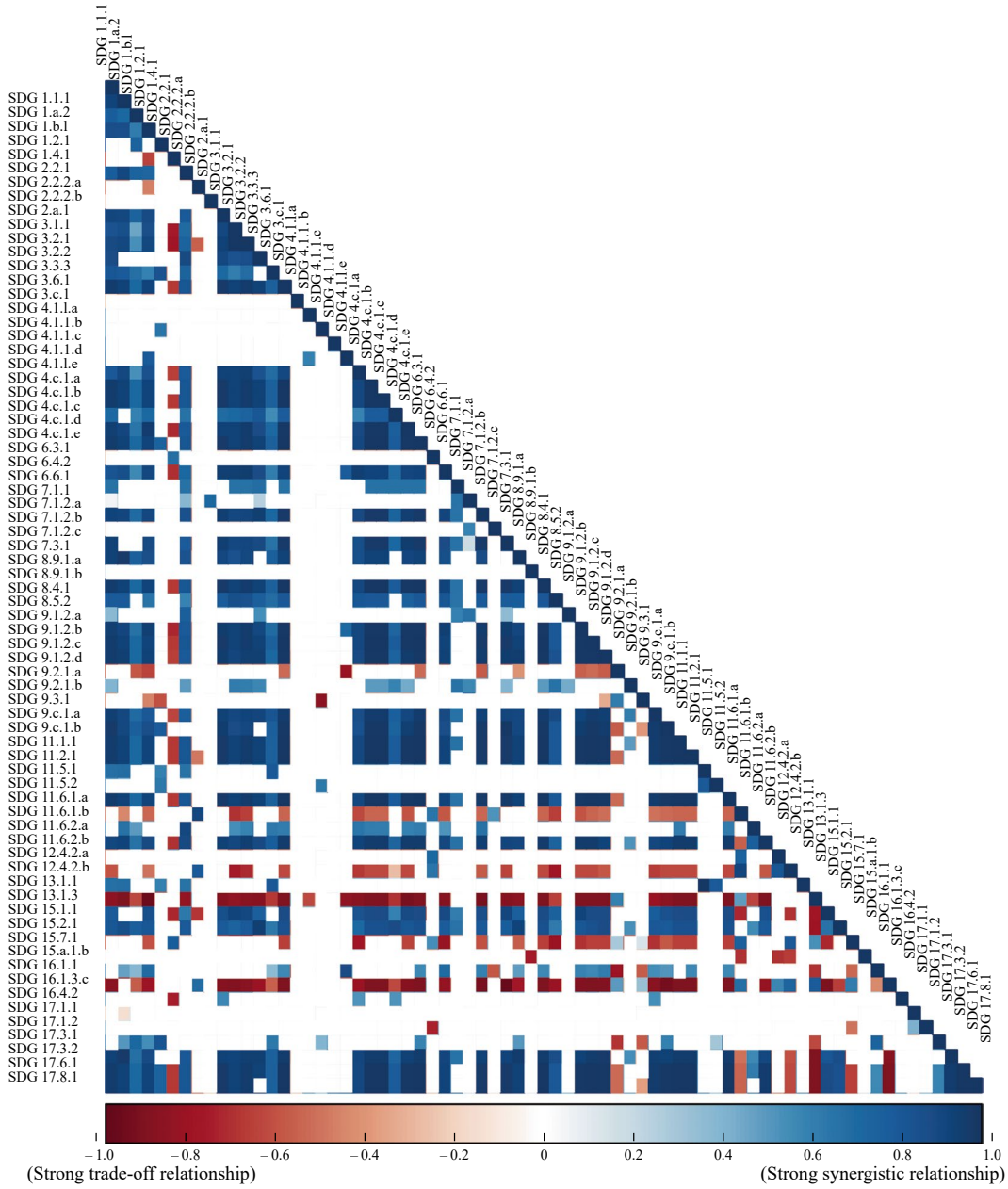

Fig. 9.17 Heatmap of interactions among SDG indicators

- This study can provide a reference for promoting sustainable development in other typical demonstration areas and serve as a good reference for promoting sustainable development in underdeveloped mountainous areas nationwide and even globally.

9.3.4.5 Discussion and Outlook

From 2015 to 2020, Lincang City has made significant progress in implementing the 2030 Agenda. Extreme poverty has been eliminated, and basic economic green development has been achieved. The various undertakings of ethnic

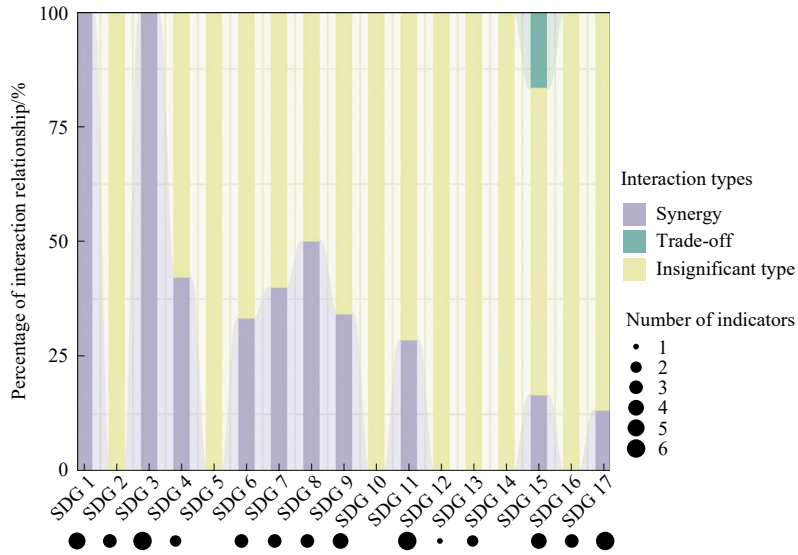

Fig. 9.18 Diagram of interactions among SDGs

minorities have steadily developed. The ability for interconnection and intercommunication has been enhanced. The degree of economic openness has become higher and higher. The environment for foreign investment has steadily improved, and the total volume of import and export of goods and the utilization of foreign capital have increased year by year. Biodiversity has been well protected. However, there are also some shortcomings, such as the high Engel coefficient in rural areas, the relative shortage of rural health technicians, the low penetration rate of special education for ethnic minorities, the government's index for agriculture being relatively small, the low penetration rate of clean energy, the low proportion of government green procurement, increase in illegal wildlife trade, and reduction in government revenue under the impacts of the pandemic. These issues need to be addressed in future development. Lincang City's natural geographical conditions and resource endowments are similar to those of the southwest region of China, as well as South Asia and Southeast Asia. The implementation plan, experience and achievement of Lincang's SDGs can provide a reference for formulating sustainable development action plans for similar underdeveloped mountainous areas.

9.3.5 SDG Integrated Evaluation for Hainan Island, China

Target: SDG 2: End hunger, achieve food security and improved nutrition, and promote sustainable agriculture.
SDG 6: Ensure availability and sustainable management of water and sanitation for all.
SDG 11: Make cities and human settlements inclusive, safe, resilient, and sustainable.
SDG 13: Take urgent action to combat climate change and its impacts.
SDG 14: Conserve and sustainably use the oceans, seas, and marine resources for sustainable development.
SDG 15: Protect, restore, and promote sustainable use of terrestrial ecosystems, sustainably manage forests, combat desertification, and halt and reverse land degradation and halt biodiversity loss.

9.3.5.1 Background

Hainan Island is located in a special economic zone known as the Pilot Free Trade Zone (PFTZ) and is situated at the southernmost tip of China.

It is one of the islands in China with a tropical monsoon climate, and most of the large rivers originate in the central mountains, forming a radial water system. The total land area is about 33,900 km^2. It has adequate sunlight, heat conditions, and abundant water resources, making it a largely tropical agricultural province in China. Hainan has a wide variety of plant species and is home to tropical rainforests and tropical monsoon rainforests. The coastline is 1,944 km long with an exceptional tropical mangrove belt and coral reefs along the eastern coastline. The island has a unique tropical coastal geomorphic landscape possessing robust ornamental value. The rich terrestrial ecology and marine environment make Hainan Island an ideal region to conduct a comprehensive analysis aligned with the UN SDGs.

In recent years, the Chinese government has focused on building the "Districts and One Center" and actively carried out infrastructural megaprojects in Hainan Province titled. "Ecological Province", the "National Ecological Civilization Pilot Zone", and "Beautiful New Hainan", to achieve sustainable development. This study adopted the assessment methodology proposed in the UN report (Sachs et al. 2019), and analyzed the sustainable development of Hainan's cities and counties from multiple perspectives through individual SDG evaluation and integrated SDG evaluation. Hainan Island covers 18 cities and counties with three prefecture-level cities, five county-level cities, four counties, and six autonomous counties of ethnic minorities, excluding Sansha City.

9.3.5.2 Data

- China Statistical Yearbook, Hainan Statistical Yearbook, Trade Bulletin, and statistical data from the National Bureau of Statistics.
- Sentinel-2 and Landsat series from 2016 to 2020.
- Thematic data from the CASEarth thematic data system, including multiple cropping index (MCI) derived from Sentinel-2 (Ye 2022); spatiotemporal data on urbanization development, population, and land-urbanization coupling in Hainan (Guo and Zhang 2023); and a dataset of aquaculture ponds in Hainan based on the Landsat data (1987–2020) (Zhang and Chen 2022).

9.3.5.3 Methods

To evaluate the overall sustainable development of Hainan Province, this study first conducted a comprehensive evaluation of the six SDGs. The individual SDG target evaluation determines the score by thresholding standardized data that have been cleaned and processed, providing a research basis for the current development status of a specific aspect of sustainable development in Hainan Island. The individual SDG evaluation involves an overall analysis of each SDG based on the values of its indicator. The SDG index evaluation, based on the individual SDG target evaluation results, integrates the use of the SDG global indicator framework, knowledge graphs, GIS, and other supporting tools to achieve knowledge-based representation and spatial visualization of Hainan Province's SDG indicators (Sachs et al. 2019). Second, practical research on sustainable development in Hainan was demonstrated, focusing on tropical agriculture (SDG 2), urbanization development (SDG 11), and nearshore aquaculture (SDG 14) in Hainan.

9.3.5.4 Results and Analysis

SDG Evaluations

The evaluations of SDG target scores in 2015 and 2020 are shown in Fig. 9.19. The sustainable development of Hainan Island has continued to improve, but there is still an overall imbalance, with gaps among cities and counties. The overall score is higher for SDG 11 (Sustainable Cities and Communities) and SDG 15 (Life on Land), and lower for SDG 6 (Clean Water and Sanitation). Haikou scores ahead in Hainan on per capita GDP (SDG 8.1), the urban household waste disposal rate and fine PM concentration in air (SDG 11.6), and the mangrove area (SDG 14.2), reflecting the characteristics of equal emphasis on economic development

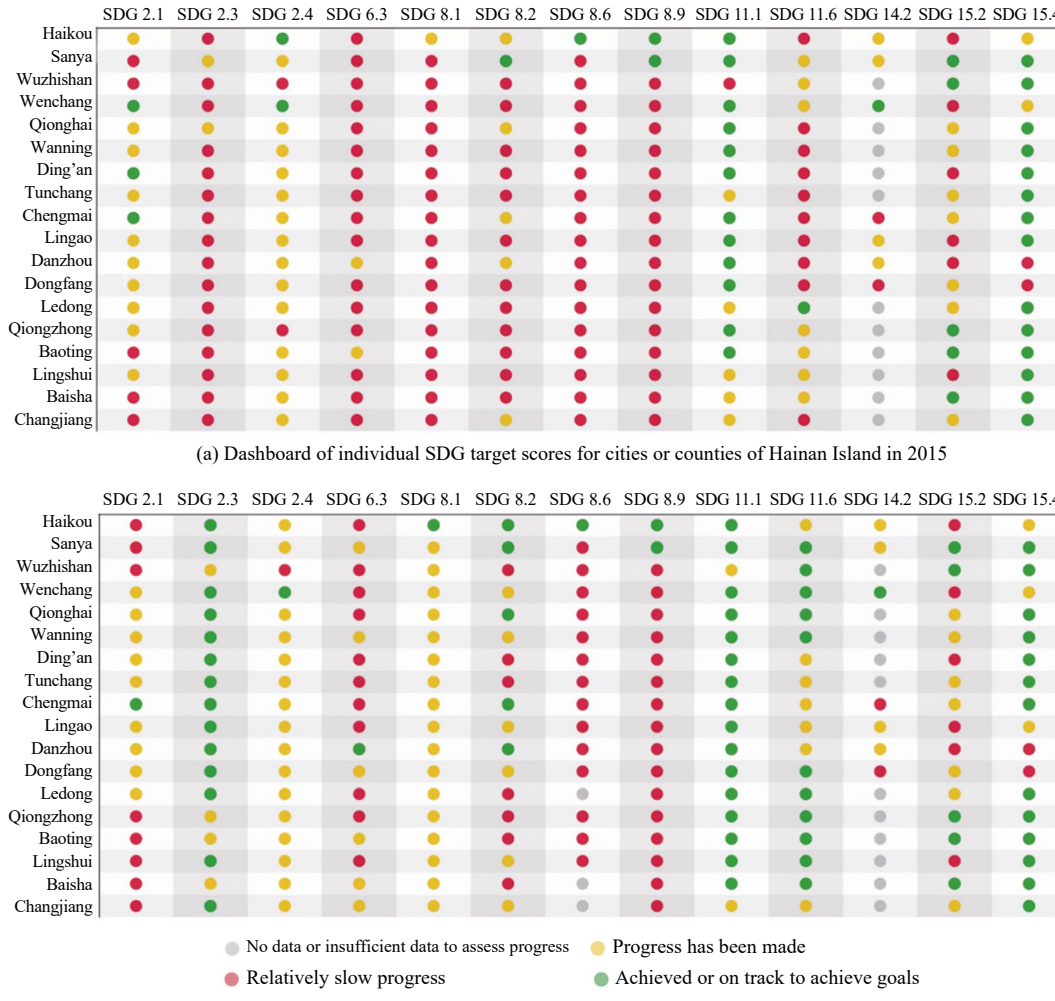

(a) Dashboard of individual SDG target scores for cities or counties of Hainan Island in 2015

(b) Dashboard of individual SDG target scores for cities or counties of Hainan Island in 2020

Fig. 9.19 Dashboards of individual SDG scores for cities or counties of Hainan Island in 2015 and 2020

and ecology in provincial capital cities. Sanya scores higher on indicators such as the proportion of housing security expenditure to fiscal expenditure (SDG 11.1), forest area (SDG 15.2), and mountain vegetation coverage (SDG 15.4), reflecting its advantages in the ecological environment as a tourist city within Hainan.

Between 2015 and 2020, Hainan SDG targets or indicators significantly increased, such as MCI (SDG 2.3), the proportion of good environmental water quality (SDG 6.3), and per capita GDP (SDG 8.1). Urban and ecological environments have also improved while maintaining good scores, especially in the urban household waste disposal rate and fine PM concentration in the air (SDG 11.6). In recent years, Hainan Island has been vigorously promoting the recultivation and replanting of abandoned land, improving land utilization, ensuring agricultural efficiency and farmers' income, and promoting rural revitalization, which have directly contributed to the improvement of the disposable income of rural residents (SDG 2.3) and the annual growth rate of GDP (SDG 8.2). The water and environment quality scores show the characteristics of "Establishing the Province in an Ecological Way in Hainan" and reflect the fact that since 2015, Hainan Island has made

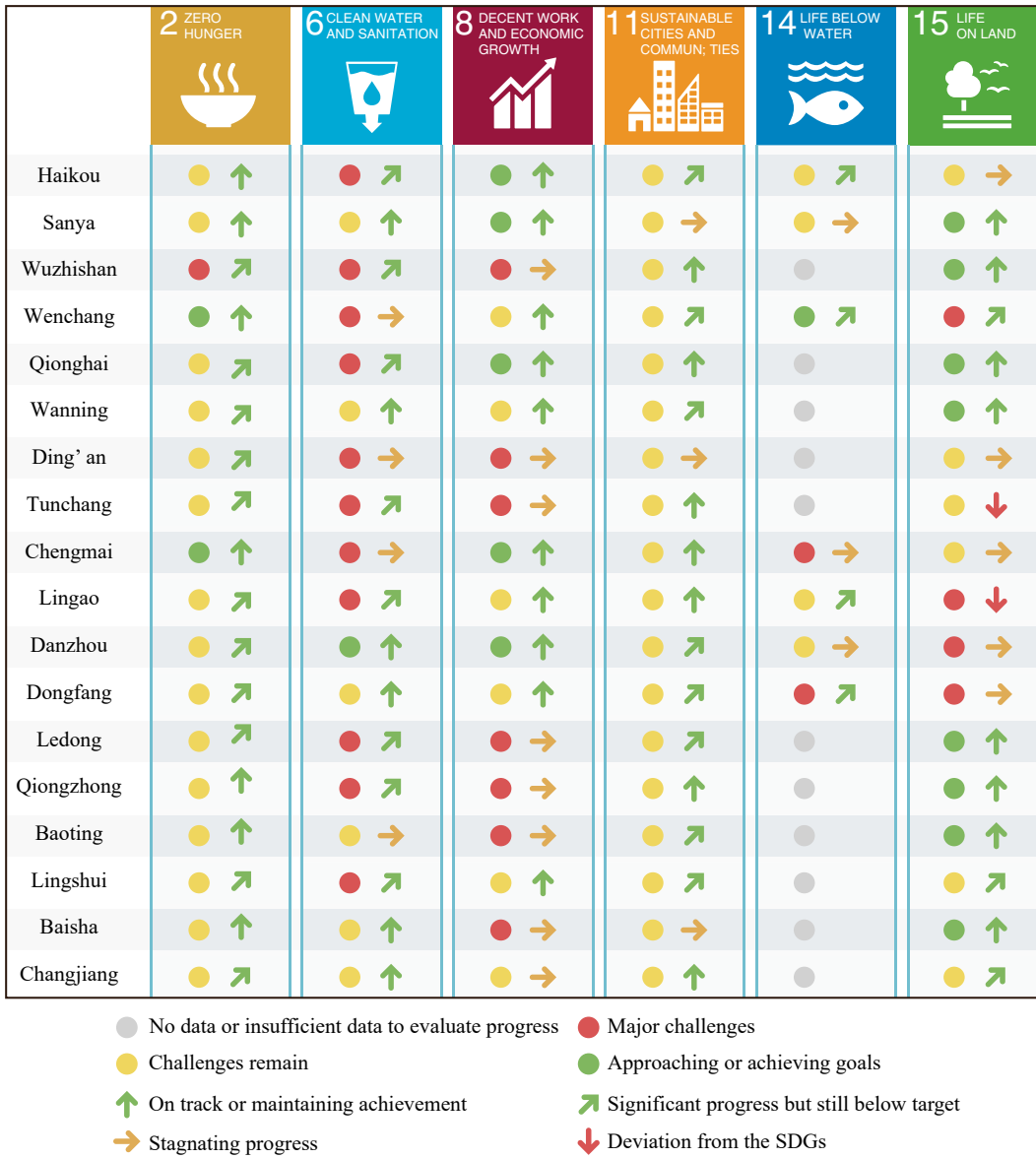

Fig. 9.20 SDG dashboard (levels and trends) for Hainan Island in 2020

ecological protection and sustainable development its "starting point" and "ending point".

The SDG progress scores (Fig. 9.20) show that Hainan has made considerable progress in building an "ecological civilization", with SDG 15 (Life on Land) scoring highest and SDG 2 (Zero Hunger) and SDG 11 (Sustainable Cities and Communities) improving significantly, although there are gaps between counties and cities (Fig. 9.20). Among the 18 cities participating in the assessment (excluding Sansha), there are 14 cities whose scores have significantly improved, two cities (Haikou and Ding'an) have not changed significantly, and two cities (Tunchang and Lingao) have slightly reduced their scores on the individual SDGs. In 2020, SDG 2 (Zero Hunger) generally improved compared to 2015, but still needs improvement.

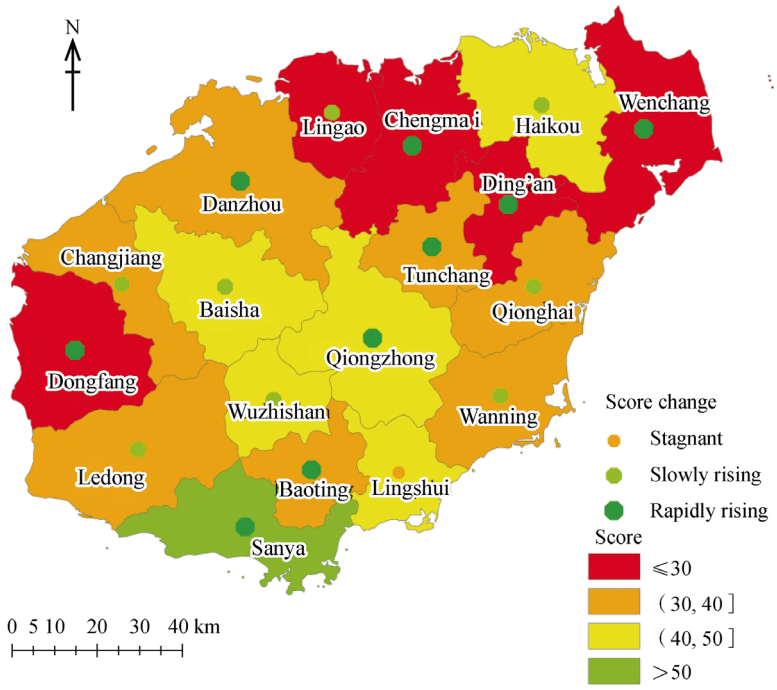

Fig. 9.21 Six-year SDG index scores and trends of score changes from 2015 to 2020

SDG 8 (Decent Work and Economic Growth), SDG 11 (Sustainable Cities and Communities), and SDG 6 (Clean Water and Sanitation) have significantly increased, and SDG 15 (Life on Land) indicators remain at a high level, having preliminarily realized coordinated development between the ecological environment and social economy. Lingao and Tunchang have improved in terms of socio-economic indicators such as the disposable income of rural residents (SDG 2.3), per capita GDP (SDG 8.1), environmental indicators (e.g., $PM_{2.5}$, PM_{10}), and the number of clean days (SDG 11.6). In general, Hainan has achieved good progress in protecting the ecological environment, but it can be better.

While the SDG index evaluation scores for cities in Hainan were generally on the rise between 2015 and 2020, the level of sustainable development in cities and counties in Hainan varied, with a general trend higher in the central part and lower in the west and north of Hainan (Fig. 9.21). In addition, all of Hainan's cities and counties either increased or remained stable in their scores to varying degrees from 2015 to 2020. Sanya's six-year composite score for 2015–2020 was the highest, mainly due to Hainan Province's efforts to develop Sanya's tourism industry and to nurture the city as a key tourism city, with both economic and environmental aspects working in coordination. In 2020, Baisha and Qiongzhong counties were boosted by the influence of Haikou City and the "Haichengwending" integration policy, and the scores of Chengmai, Wenchang, and Ding'an were also on the rise. The assessment of Haikou's score as a catalyst for neighboring cities suggests Hainan's current philosophy of "one city for the entire province and one city for the entire island", which has had a significant positive impact on the comprehensive development of the Qiongbei economic circle with Haikou at its core.

Sustainable Development Applications

(1) Sustainable Development of Tropical Agriculture (SDG 2.4)

Hainan has a unique climatic advantage for the development of tropical agriculture, which makes

it possible to plant multiple crops in a year. However, in the past few years, some areas of Hainan still had a significant amount of underutilized or even abandoned cultivated land. In recent years, with the implementation of "non-grain cultivation" and "non-agriculturalization" of cultivated land and the concentrated restoration of abandoned farmland, the efficient use of farmland resources has been achieved. The multiple cropping index (MCI) refers to the ratio or frequency of two or more crops being planted in the same piece of land in one year. It is an important indicator for measuring the agricultural production efficiency on a plot of land. In this research, the maximum NDVI values of the Sentinel-2 image were used for decadal synthesized data, and the Savitzky-Golay filtering method was applied to smooth the time-series NDVI curve. Then, the number of peak values of the NDVI curve over time was extracted in combination with crop phenology information to calculate the MCI. Finally, the MCI of Hainan Island from 2016 to 2020 was extracted using Sentinel-2 data (Fig. 9.22), and its spatiotemporal variation characteristics were then investigated.

The results show that the MCI in Hainan Island was on an upward trend from 2016 to 2020, increasing from 1.53 to 1.66. There were differences in the MCI among different cities and counties in Hainan Island. From 2016 to 2020, the decrease in the MCI was mainly distributed in the border areas of Haikou, Wenchang, Ding'an, and Qionghai, the border areas of Changjiang, Dongfang, Danzhou, and the northern part of Wanning. The increase in the MCI was mainly concentrated in the northern part of Wenchang, the border areas of Haikou, Chengmai, and Ding'an, the western part of Dongfang, Ledong, and Sanya, and the southern part of Lingao and Danzhou. From 2016 to 2020, the area of abandoned land decreased by 5.6%, the area of single cropland increased by 3.1%, the area of double cropland decreased by 2.6%, and the area of triple cropland increased by 5.1%.

According to the results obtained, the area of abandoned land in Haikou gradually decreased from 2016 to 2020, indicating that the region has been progressing orderly in the renovation and utilization of abandoned land. In order to ensure food security and the sustainable use of cultivated land resources, the following sustainable development-related decision support guidelines are proposed. It is recommended to further strengthen the construction of cultivated land quality. Seasonally abandoned or fallow land should be planted with cover crops, legumes, and other soil-replenishing crops to improve the quality of cultivated land. In addition, the overall increase in land utilization leads to a higher total quantity of chemical inputs such as fertilizers, pesticides, and agricultural films used per unit of arable land, resulting in an increased environmental burden. It is recommended that Hainan should further strengthen comprehensive measures such as protective cultivation, soil testing, fertilizer, straw returning, soil acidification improvement, and heavy metal pollution control, in order to improve and enhance soil fertility and promote sustainable agricultural development.

(2) **Sustainable Development of Urbanization (SDG 11.3)**

Figure 9.23 indicates the average annual growth rates of population urbanization and land urbanization in Hainan Island from 2011 to 2018. It can be observed that the rate of population urbanization in Hainan Island was below the rate of land urbanization from 2011 to 2016, demonstrating that the population urbanization in Hainan Island lagged behind the land urbanization during the period. With the coupling analysis of population urbanization and land urbanization, the coupling coordination level of urbanization across cities and counties showed an overall upward trend from 2011 to 2018. Figure 9.24 indicates the significant spatial pattern differences in the population-land urbanization coupling coordination in 2018. Haikou and Sanya, located in the northern and southern parts of Hainan Island respectively, have played a prominent role in driving growth and development in neighboring Chengmai and Lingshui, benefiting from their effective and mutually beneficial "high coupling-high coordination" state.

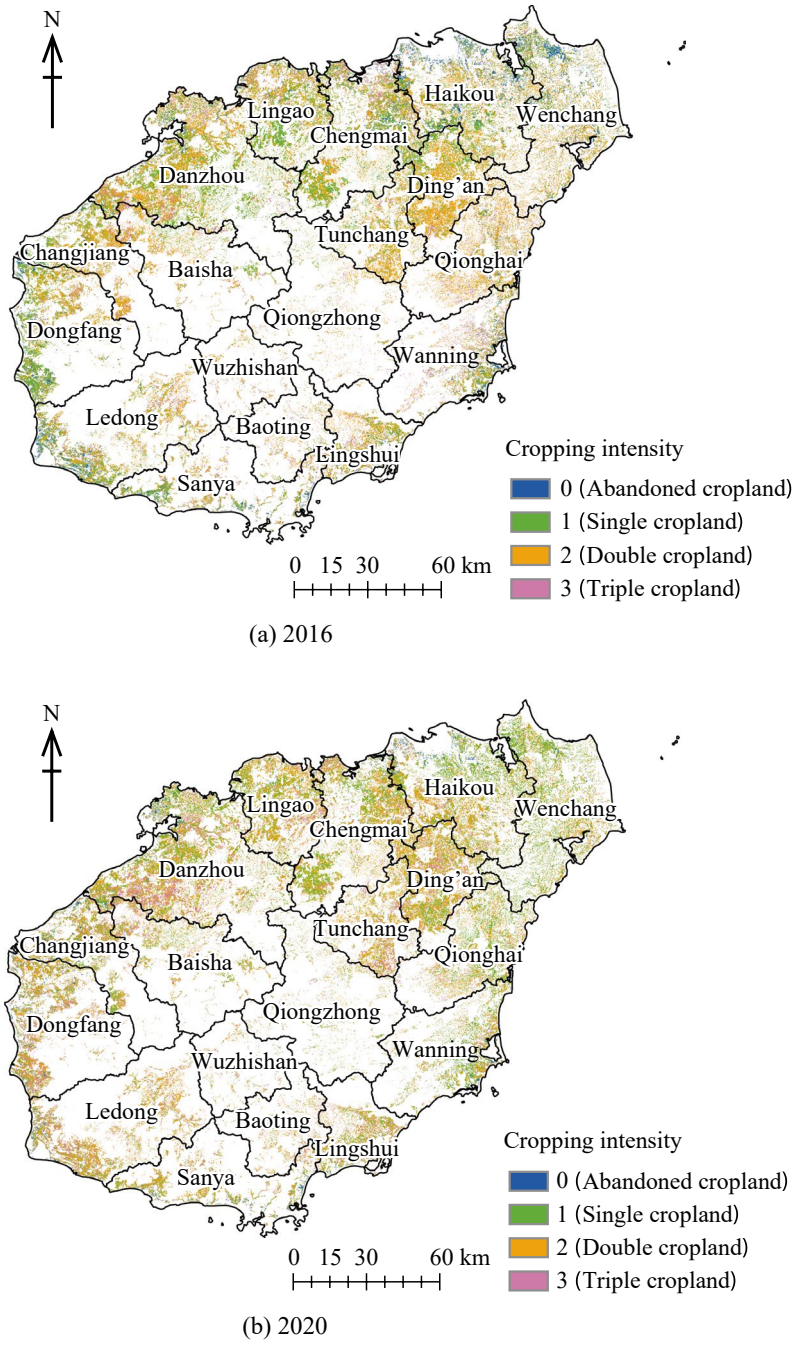

Fig. 9.22 Map of the MCI of cultivated land in Hainan Island in 2016 and 2020

Based on the findings, several recommendations are made for the sustainable development of urbanization in Hainan. First, improving the employment absorption capacity in towns and villages is crucial for promoting local urbanization and coordinating the development of large- and medium-sized cities with small towns and villages while optimizing regional spatial

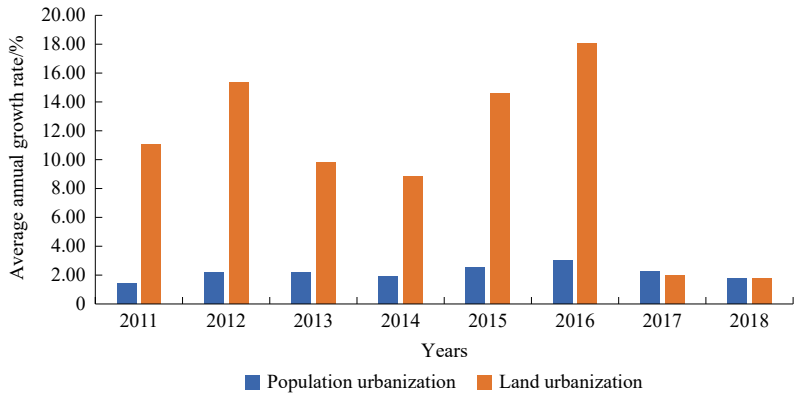

Fig. 9.23 Average annual growth rate of population urbanization and land urbanization in Hainan Island from 2011 to 2018

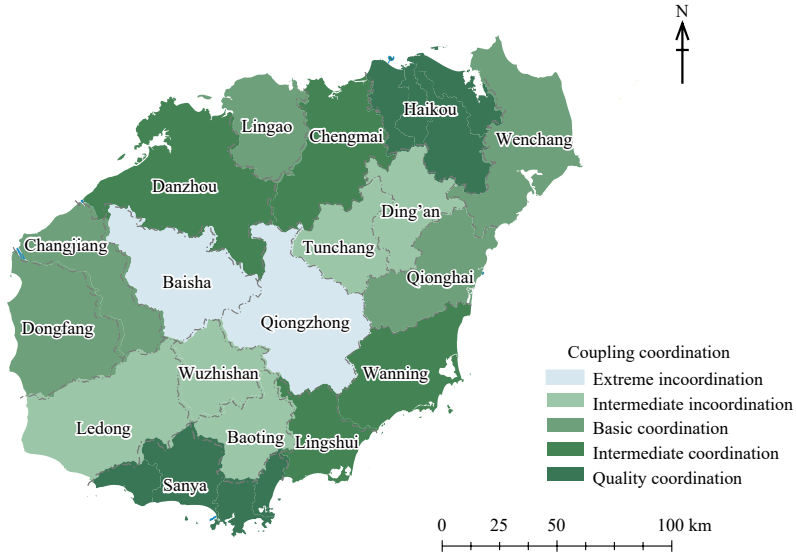

Fig. 9.24 Spatial distribution of population-land urbanization coupling in Hainan Island in 2018

resources. Second, priority should be given to advancing land urbanization in the western part of Hainan, with Danzhou as the center. Moreover, to foster joint development in the "Greater Sanya" Integrated Tourism Economic Circle, it is necessary to enhance the coordinated industrial and demographic development of Ledong and Baoting. Finally, a diversified economic development strategy must be implemented to ensure the sustainable progress of the economic development and urbanization levels of Qiongzhong and Baisha.

(3) **Sustainable Development of Aquaculture**

Based on Landsat imagery from 1987 to 2020, a high-precision map of aquaculture ponds of Hainan was obtained (Fig. 9.25). The aquaculture ponds in Hainan Island showed an overall growth trend during 1987–2020, with a total growth of 23,866 ha during the 33 years, of which the aquaculture area continued to grow from 1987 to 2015, declined from 2015 to 2018, and then changed little afterward. The increasing period of the aquaculture area was concentrated

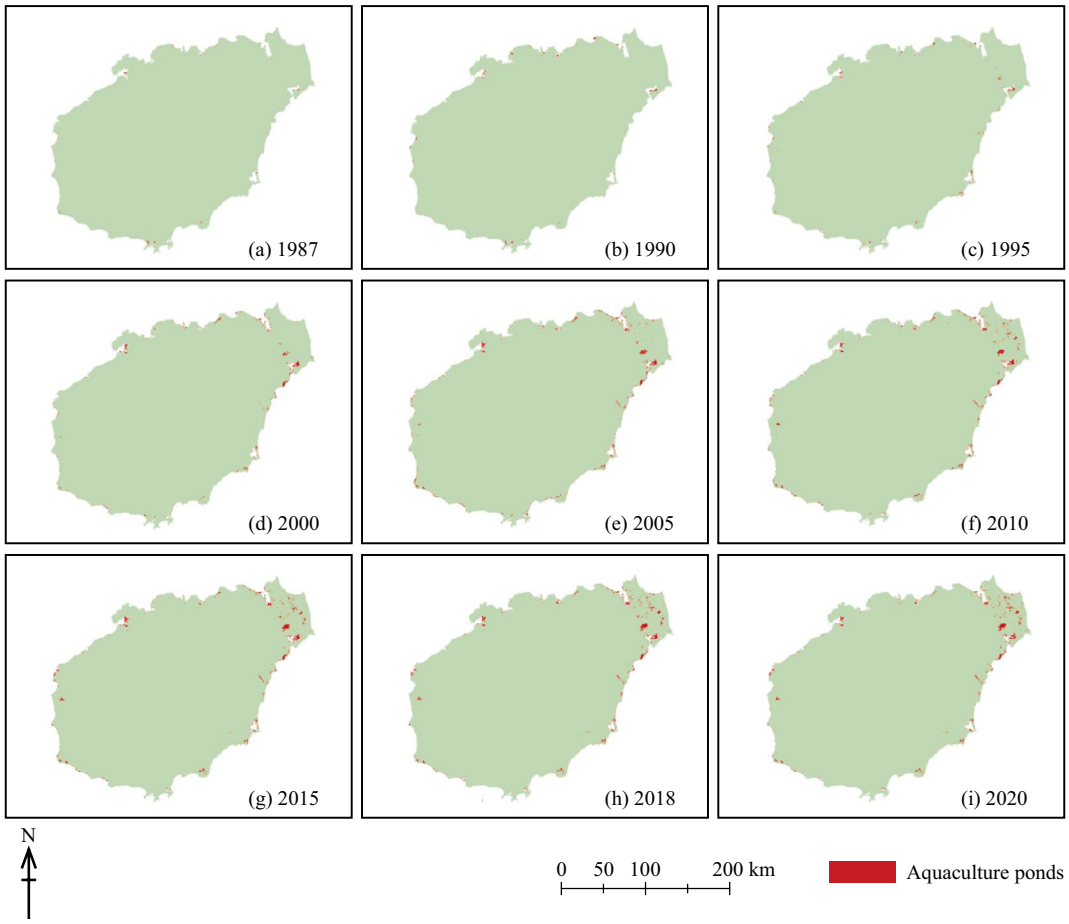

Fig. 9.25 Nearshore aquaculture ponds in Hainan coastal counties based on Landsat satellite data (1987–2020)

from 1995 to 2005, with the fastest growth rate. Aquaculture development was uneven across the region, with the eastern part of Hainan Island developing at a higher rate than the western part.

In recent years, under the influence of ecological restoration policies such as "returning ponds to forests" and "returning ponds to wetlands" advocated by Hainan Province, the ecological restoration work in some areas has shown initial results. In Haikou, Wenchang, and Sanya, some of the privately dug aquaculture ponds have been filled or artificially planted with mangroves. Provisions on the Management of Environmental Protection for Aquaculture Construction Projects in Land Areas of Hainan Province and the local standard Discharge Requirement of Aquaculture Tailwater (DB46/T475—2019) require that governments at all levels must actively push forward the policy of "returning ponds to forests" and "returning ponds to wetlands". In 2017, the Wenchang Government announced the Qinglan Mangrove Provincial Nature Reserve Working Plan for returning ponds to forests and wetlands in Hainan for the Qinglan Mangrove Provincial Nature Reserve, Hainan. The program plans to gradually implement the "returning ponds to forests and wetlands" project for 4159.2 mu (mu, Chinese unit of land measurement that is commonly 666.7 m^2) of shrimp ponds and farms in the core area of the Qinglan Mangrove Provincial Nature Reserve. To strengthen wetland protection and restoration, Hainan Province plans to achieve the project of "returning ponds

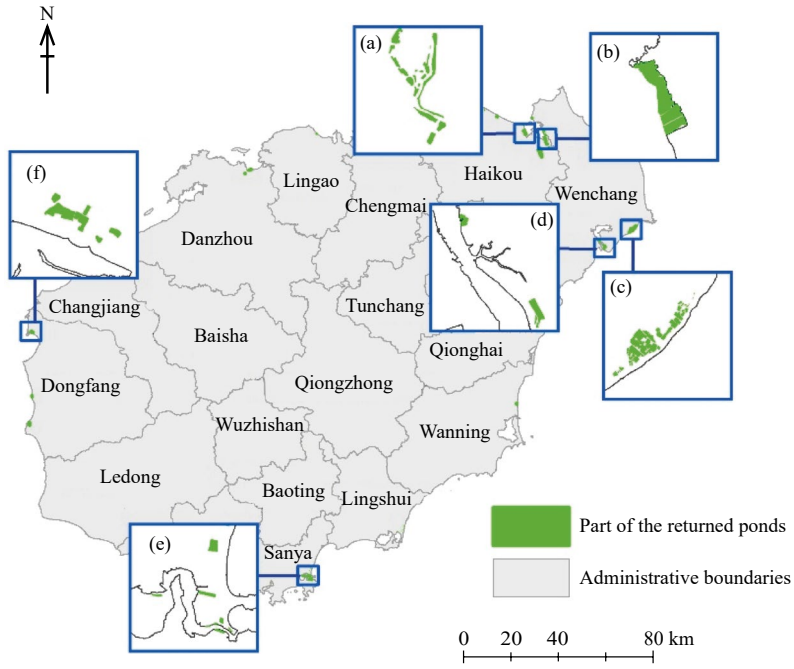

Fig. 9.26 Monitoring of the returned ponds in Hainan's coastal regions based on Gaofen satellite data (2010–2019)

to forests" and "returning ponds to wetlands" for a total of 10,000 mu of ponds within the trunk shelter belt of the coastal protection forest, requiring coastal cities and counties to promulgate local "Layout for beach areas in aquaculture waters", delineate prohibited and restricted breeding areas, and clean up or relocate the breeding facilities in prohibited breeding areas to restore the damaged ecology.

In order to visualize the status of the Hainan farming pond retreat, the retreat of Hainan ponds from 2010 to 2019 was monitored by visual interpretation based on Gaofen-1 and Gaofen-2 satellite images and Google Earth high spatial resolution satellite images. According to the monitoring results, many areas have carried out the work of returning ponds to forests and wetlands, among which the effects of returning ponds, in the Dongzhai Port area of Haikou (Figs. 9.26a and b), southeast coast of Wenchang (Fig. 9.26c), Qinglan Port area (Fig. 9.26d), Tielu Port area of Sanya (Fig. 9.26e), and Sigang Town of Dongfang (Fig. 9.26f) are more significant. Therefore, strictly formulating and implementing aquaculture policies are the key to sustainable, green development of coastal aquaculture. It is suggested that local government departments should decide the development patterns of coastal aquaculture ponds according to the characteristics of local economy, society, and natural resources. For instance, Wenchang can continue to develop aquaculture vigorously; Haikou can appropriately transform coastal aquaculture into wetlands and forests to protect the ecological environment; and Sanya can carry out industrial transformation and develop tourism or other industries to reduce the area of aquaculture. In order to achieve the sustainable development of aquaculture in Hainan without destroying wetlands and other ecological resources, aquaculture ponds should be built in an orderly manner in areas suitable for aquaculture development.

Highlights

- Hainan Island has made great progress in building an "ecological civilization", with SDG 15 (Life on Land) scoring high, and SDG 2 (Zero Hunger) and SDG 11 (Sustainable Cities and Communities)

improving significantly, but there are gaps among cities and counties. Overall, Hainan has achieved good progress in ecological environmental protection, but there is still room for improvement in some aspects.

- On the level of SDG targets, Hainan Island has significantly increased its scores on targets such as SDG 2.3 (MCI), SDG 6.3 (proportion of good environmental water quality), and SDG 8.2 (per capita GDP). The scores of the urban and ecological environment also improved while maintaining good performance, especially the scores on SDG 11.6 (rate of harmless treatment of municipal domestic waste and concentration of fine *PM* in the air) have significantly increased. On the SDG level, urbanization (SDG 11) grows rapidly, most cities and counties show an increasing trend in agriculture (SDG 2), especially a linear increase in water quality (SDG 6), and a better overall protection effect in underwater and terrestrial ecology (SDG 14 and SDG 15).
- Based on the results of the demonstration study: (1) the overall trend of the MCI was on the rise, and the abandoned land area continued to decrease from 2016 to 2020 in Hainan. In recent years, Hainan has actively implemented a series of policies and projects through the adjustment of agricultural planting structures, the construction of high-standard farmland, and comprehensive land improvement to enhance the comprehensive production capacity of arable land and improve the sustainable use of arable land resources. (2) The coupling of urbanization in cities and counties showed an overall increase from 2011 to 2018. The spatiotemporal patterns of the coupled coordination of population urbanization and land urbanization varied significantly. The "North and South Poles" status of Haikou and Sanya is prominent, and both are in the "high coupling-high coordination" type of benign resonance, which has a significant driving effect on neighboring Chengmai County and Lingshui County. (3) The area of coastal aquaculture ponds continued to grow between 1987 and 2015, and then decreased from 2015 to 2018, and the change was not obvious afterwards. In recent years, ecological restoration policies have been achieved, such as "returning ponds to forests", "returning ponds to wetlands", and the protection and restoration of important wetland ecosystems (e.g., mangroves).

9.3.5.5 Discussion and Outlook

This study established a localized sustainable development indicator evaluation system for Hainan. Each city or county in Hainan Province has initially achieved sustainable development, but each has a different degree of development. Due to the limitation of data accessibility, there are limitations to the selected indicators in this study. In the future, we will try to use more Earth observation data to supply the statistical data.

The case study proves that the work of Hainan Province "in re-cultivation of abandoned land", "urbanization of land", and "returning ponds to forests and wetlands" has made outstanding contributions to the sustainable development of Hainan. Meanwhile, it was also found that there are some problems that urgently need to be solved in Hainan Province, such as the decreased MCI of cultivated land, the lower and imbalanced urbanization level, and ecological destruction caused by the development of aquaculture. The problems that need to be addressed are the declining cropland replanting index, the low and uneven urbanization level, and the ecological damage caused by aquaculture. In the future, Hainan Province should strengthen the quality of cultivated land, promote urbanization in the local area, promote the coordinated development of large- and medium-sized cities, small towns and villages, strengthen the intensive management of production space, and ensure the sustainable development of ecological space.

With the initial establishment of the free trade port, its policy institutional system focuses on free and convenient trade, and investment has begun to take shape. At the same time, although Hainan's agriculture has made an important contribution to the province's local economy, in

general, the levels of material life and cultural life and the production conditions of farmers in the province are currently relatively low. Under the influence of tourism promotion and economic development, the construction of an ecological civilization also faces many challenges. With the promotion of sustainable development, ecological environmental protection in the process of development will become a top priority. In the future, with the increasing awareness of ecological protection and the implementation of ecological restoration work, Hainan will be scientifically transformed and upgraded in tropical agriculture, urbanization, and aquaculture, which in turn will continue to promote the sustainable development of Hainan and lead the way for similar regions to follow.

9.3.6 SDG Integrated Evaluation for Guilin, Guangxi Zhuang Autonomous Region, China

Target: SDG 8.9: By 2030, devise and implement policies to promote sustainable tourism that creates jobs and promotes local culture and products.
SDG 11.2: By 2030, provide access to safe, affordable, accessible, and sustainable transport systems for all, improving road safety, notably by expanding public transport, with special attention to the needs of those in vulnerable situations, women, children, persons with disabilities, and older persons.
SDG 11.3: By 2030, enhance inclusive and sustainable urbanization and capacity for participatory, integrated, and sustainable human settlement planning and management in all countries.
SDG 11.7: By 2030, provide universal access to safe, inclusive, and accessible, green and public spaces, in particular for women and children, older persons, and persons with disabilities.
SDG 12.b: Develop and implement tools to monitor sustainable development impacts for sustainable tourism that creates jobs and promotes local culture and products.
SDG 15.1: By 2020, ensure the conservation, restoration and sustainable use of terrestrial and inland freshwater ecosystems and their services, in particular forests, wetlands, mountains, and drylands, in line with obligations under international agreements.
SDG 15.4: By 2030, ensure the conservation of mountain ecosystems, including their biodiversity, in order to enhance their capacity to provide benefits that are essential for sustainable development.

9.3.6.1 Background

Guilin boasts unique ecological and landscape resources along the Lijiang River, making it a national historic and cultural city and a world-class tourist destination. The frequent tourism activity and the livelihoods of a large number of residents have brought great pressure on the ecological environment of the basin. Therefore, a reasonable and scientific assessment of the ECC of the Lijiang River Basin and the sustainable development of Guilin, where tourism is the main productive force, is a major challenge facing the city's sustainable development and is a common problem for similar cities around the world with rich natural resources, fragile ecological environments, and relatively lagging social and economic development. This case uses the platform, data, and technical system of CASEarth to quantitatively evaluate the sustainable development level and potential of the ECC of the Lijiang River Basin in Guilin, and monitors and evaluates SDG 11.2.1, SDG 11.3.1, and SDG 11.7.1 and their dynamic changes in the city's main functional areas. The related data products and analysis conclusions can provide decision-making and support for Guilin's sustainable planning and urban construction.

9.3.6.2 Data

- Gaofen-1/6 satellite image, Sentinel-2 satellite imagery, and SDGSAT-1 satellite imagery with a spatial resolution higher than 10 m from 2010 to 2020.
- Guilin Economic and Social Statistics Yearbook for 2010, 2015, and 2020.
- Statistical and monitoring data from industry sectors in Guilin for 2010, 2015, and 2020.
- Survey questionnaires for residents and tourists in Guilin for 2010, 2015, and 2020.
- Spatial vector maps of the Lijiang River Basin in Guilin and county-level administrative regions in the Lijiang River Basin.
- Road networks in 2020, including highways, national roads, provincial roads, urban main roads, and other roads.
- POI data of bus and train stations in 2015 and 2020.
- Landscan population data in 2013, 2015, and 2020, with a spatial resolution of 1,000 m.

9.3.6.3 Methods

Sustainability Assessment of Tourism Resources in the Lijiang River Basin

A multi-target, comprehensive indicator assessment system for the sustainable development of the ECC in the Lijiang River Basin was established based on a basic time series of 2010, 2015, and 2020. The system starts from the ecological, economic, and social dimensions corresponding to multiple SDG indicators and combines them with the development characteristics of ecotourism in the Lijiang River Basin of Guilin. The coefficient of a variation method was used to assign different weights to multiple assessment indicators, and a weighted composite index model was used to comprehensively evaluate the sustainable development process of the ECC in the Lijiang River Basin using comprehensive CASEarth data, ground observation station data, and social and economic statistical data from multiple sources. County-level administrative units were taken as the smallest assessment units, and a distribution map was obtained of the sustainable development index of ECC in the Lijiang River Basin for the three periods of 2010, 2015, and 2020.

The weighted composite index model is:

$$\mathrm{ECC} = \sum_{i=1}^{n} S_i \times W_i \tag{9.8}$$

where ECC represents the index of the ecotourism carrying capacity; S_i represents the data value of each indicator; W_i represents the weight value of each indicator at different levels; and n represents the number of indicators at each level. A larger index value of ECC indicates better sustainable development of ECC in the area.

Assessment of Urban Sustainable Development in Guilin City

Based on SDG 11.2.1, an accessibility assessment was performed on public transport in Guilin urban functional areas in 2013, 2015, and 2020. Road network and traffic station data were used to check and correct topology errors in the dataset, and a road network model was built. Then, according to the definitions of low-capacity public transportation and high-capacity public transportation, a 500 m service area of bus stations and a 1 km service area of train stations were created through network analysis. The service areas were overlaid with population data to calculate the service population of public transportation stations. Finally, SDG 11.2.1 was calculated. The formula for the SDG 11.2.1 is as follows:

$$\text{Population with convenient access to public transport} = \left[\frac{\text{Population with convenient access to public transport}}{\text{City population}} \right] \times 100\% \tag{9.9}$$

A higher percentage of people served by a convenient public transportation system indicates better accessibility, and vice versa. This method quantifies the proportion of people who have convenient access to public transport and comprehensively reflects the service status of the regional road network and transit stations.

Based on the land use classification results of the study area, the urban functional boundaries were delineated, and the changes in SDG 11.3.1 values were analyzed. The formula for the LCR is as follows:

$$\mathrm{LCR} = \frac{\ln\left(\frac{\mathrm{Urb}_{(t+n)}}{\mathrm{Urb}_t}\right)}{y} \tag{9.10}$$

where Urb_t is the total area covered by the urban area in the initial year t; $\mathrm{Urb}_{(t+n)}$ is the total area covered by the urban area in the final year $t+n$; and y is the number of years between the two measurement periods.

Based on the population grid data, PGR was calculated using the following formula:

$$\mathrm{PGR} = \frac{\ln\left(\frac{\mathrm{Pop}_{(t+n)}}{\mathrm{Pop}_t}\right)}{y} \tag{9.11}$$

where Pop_t is the total population within the urban area in the year t (initial year); $\mathrm{Pop}_{(t+n)}$ is the total population within the urban area in the year $t+n$ (final year); y is the number of years between the two measurement periods.

LCRPGR was calculated based on the change rate of built-up area and population in the urban functional areas:

$$\mathrm{LCRPGR} = \frac{\mathrm{LCR}}{\mathrm{PGR}} \tag{9.12}$$

The proportion of street areas based on the road network data and urban functional area boundaries was calculated. Based on high-resolution remote sensing images, public open spaces were extracted and optimized by using data such as points of interest. The proportion of urban public open spaces was derived. The formulas for calculating the ratio of the sum of streets and urban public open spaces to the urban area (SDG 11.7.1) are as follows:

$$\begin{cases} P_{\mathrm{LAS}} = \frac{S_{\mathrm{streets}}}{S_{\mathrm{city}}} \times 100\% \\ P_{\mathrm{OPS}} = \frac{S_{\mathrm{OPS}}}{S_{\mathrm{city}}} \times 100\% \\ P_{\mathrm{POPS}} = \frac{S_{\mathrm{streets}}+S_{\mathrm{OPS}}}{S_{\mathrm{city}}} \times 100\% \end{cases} \tag{9.13}$$

where P_{LAS} represents the proportion of street areas; S_{streets} represents the area of streets; S_{city} represents the core urban area; P_{OPS} represents the proportion of urban open public spaces; S_{OPS} represents the area of urban public open spaces; and P_{POPS} represents the proportion of the total public open spaces in a city.

A road network model was built, a 400 m service area of public open spaces was generated, and the number and proportion of population in the service area of public open spaces were calculated using the population grid data.

9.3.6.4 Results and Analysis

Sustainability Assessment of Ecotourism Resource Development in the Lijiang River Basin

The spatial distribution map of the sustainable development index of the ECC in the Lijiang River Basin from 2010 to 2020 is shown in Fig. 9.27. During the period from 2015 to 2020, the ECC in most areas reached a sustainable development status. In areas with fewer human activity, the good development of the ecological environment led to a high level of sustainable development of the ECC. Compared with 2010, the ECC of 10 districts and counties was improved in 2015, and the average value of the sustainable development index of the ECC increased from 0.457 to 0.670. Compared with 2015, the indices of four districts and counties improved, and those of four districts and counties decreased in 2020. The average value of the sustainable development index of the ECC increased from 0.670 to 0.711, with Pingle County rising from 0.36 to 0.84.

Figure 9.28 shows the growth rate of the sustainable development index of the ECC in the Lijiang River Basin from 2010 to 2020. Overall, most areas in the Lijiang River Basin experienced sustained growth in the ECC from 2010 to 2020, with highly growing areas mainly

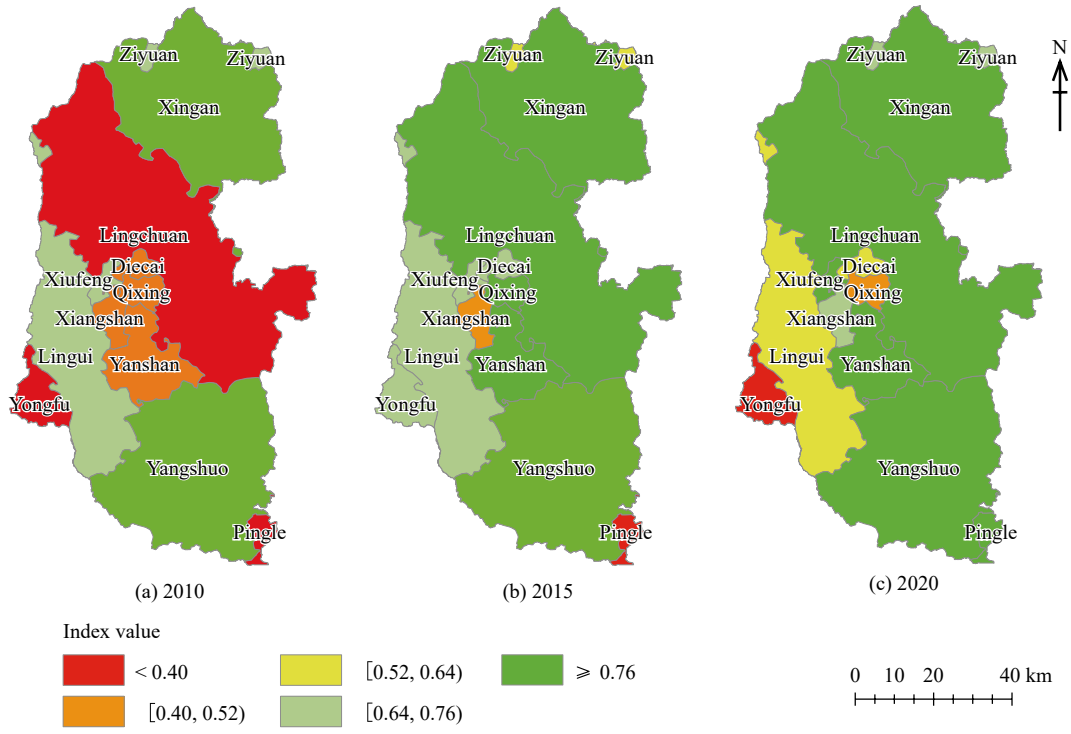

Fig. 9.27 Spatial distribution map of the sustainable development index of the ECC in the Lijiang River Basin from 2010 to 2020

concentrated in Yanshan District, Lingchuan County, and Pingle County, while only Lingui District had negative growth. There were more areas with a high-speed growth in the sustainable development index of the ECC from 2010 to 2015, with huge potential for the ECC, with an average growth rate of 21%; while the average growth rate from 2015 to 2020 was lower, with the growth rate of the sustainable development index of the ECC being only 4% due to the impacts of the pandemic on the tourism economy.

Urban Sustainable Development of Guilin City

The public transport service level continuously improved between 2013 and 2020 (Fig. 9.29). The total population with access to public transport stations increased from 458,861 in 2013 to 489,379 in 2015 and 573,957 in 2020. The value of SDG 11.2.1 increased from 42.08% in 2013 to 52.31% in 2020.

The public transport service areas in Guilin in 2015 and 2020 are shown in Fig. 9.30. The service areas of public transport stations have increased, covering the majority of the population in the main functional areas of the city. However, there are still some densely populated areas that are not covered by the service areas. It is recommended to add bus stations in these areas to optimize the urban transport system.

Table 9.5 shows the changes in LCR, PGR, LCRPGR indicators, and corresponding secondary indicators of SDG 11.3.1 in the study area. The results show that from 2013 to 2020, the urban expansion and population growth in Guilin City were imbalanced, with an urban expansion rate faster than the population growth rate, the per capita construction land area continued to increase, and the growth rate accelerated.

The area of streets within the functional area of Guilin was 16.18 km^2, and P_{LAS} was 5.13%. The area of public open spaces was 160.28 km^2, 123.1 km^2, and 59.32 km^2 in 2013, 2015, and

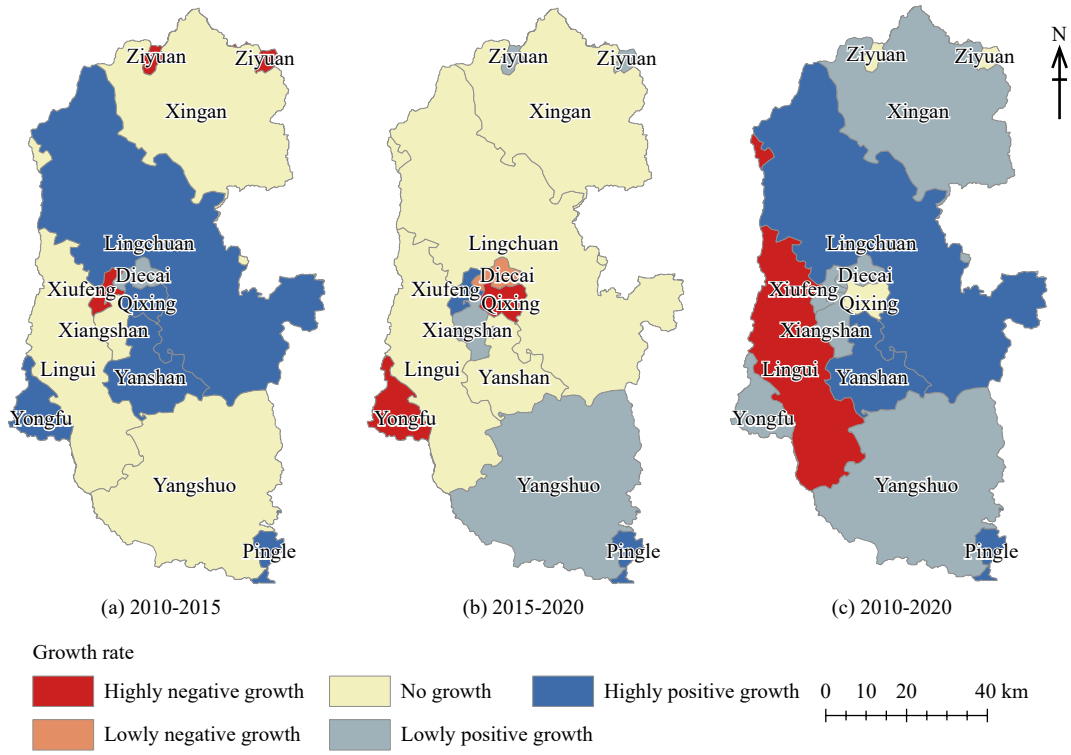

Fig. 9.28 Distribution map of the growth rate of the sustainable development index of the ECC in the Lijiang River Basin from 2010 to 2020

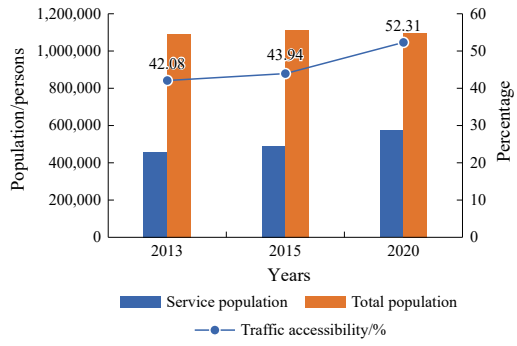

Fig. 9.29 Population and percentage of convenient access to public transport from 2013 to 2020 in Guilin

2020, respectively, which showed a decreasing trend. Corresponding P_{OPS} were 50.83%, 33.91%, and 18.81%, respectively. Overall, the proportion of the total public open spaces, P_{POPS} was 55.97%, 39.04%, and 23.95%, which was gradually decreasing.

The 400 m service areas of public open spaces are shown in Fig. 9.31. The service area in 2013, 2015, and 2020 was 151.34 km^2, 96.09 km^2, and 81.76 km^2, respectively. From 2013 to 2020, the area of urban public open spaces decreased by 100.96 km^2, with most areas being developed for construction purposes, while the service area decreased by 69.57 km^2. The proportion of population in public open spaces service areas was 74.96%, 65.69%, and 60.60% in 2013, 2015, and 2020, respectively. The population served by urban public open spaces was constantly decreasing, and the distribution and area of public open spaces made it difficult to meet the needs of citizens.

Highlights

- Based on the three dimensions of ecology, economy, and society, a quantitative analysis was conducted on the sustainable development process of the ECC in the Lijiang River Basin. The results show that from 2010 to 2020, with the joint efforts of local

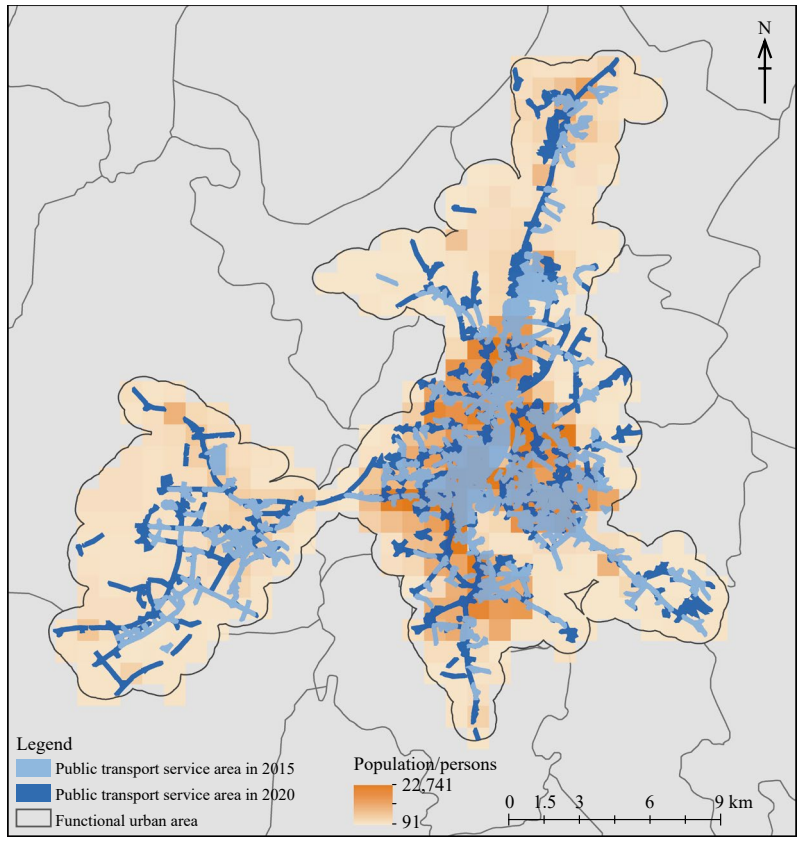

Fig. 9.30 Public transport service areas in 2015 and 2020 in Guilin

Table 9.5 Changes in SDG 11.3.1 from 2013 to 2020

Time	LCR	PGR	Change rate of per capita land consumption (%)	Urban density change rate (%)	Land use efficiency (LCRPGR)
2013–2015	0.0525	0.0179	7.16	4.77	2.9343
2016–2020	0.0320	−0.0007	17.78	23.30	−45.7867

governments and residents in the basin, the ECC of the Lijiang River Basin steadily improved. The specific data showed that the average sustainable development index of the ECC of the Lijiang River Basin increased from 0.457 in 2010 to 0.670 in 2015, and then to 0.711 in 2020.

- From 2013 to 2020, the accessibility of public transport in the functional urban area of Guilin gradually improved, and the values of SDG 11.2.1 increased from 42.08% in 2013 to 52.31% in 2020.
- From 2013 to 2020, the expansion of the built-up area in the urban functional area of Guilin City did not match the growth of the population. The expansion rate of the built-up area was faster than the increase in population, and the per capita built-up area continued to increase with an accelerating growth rate.

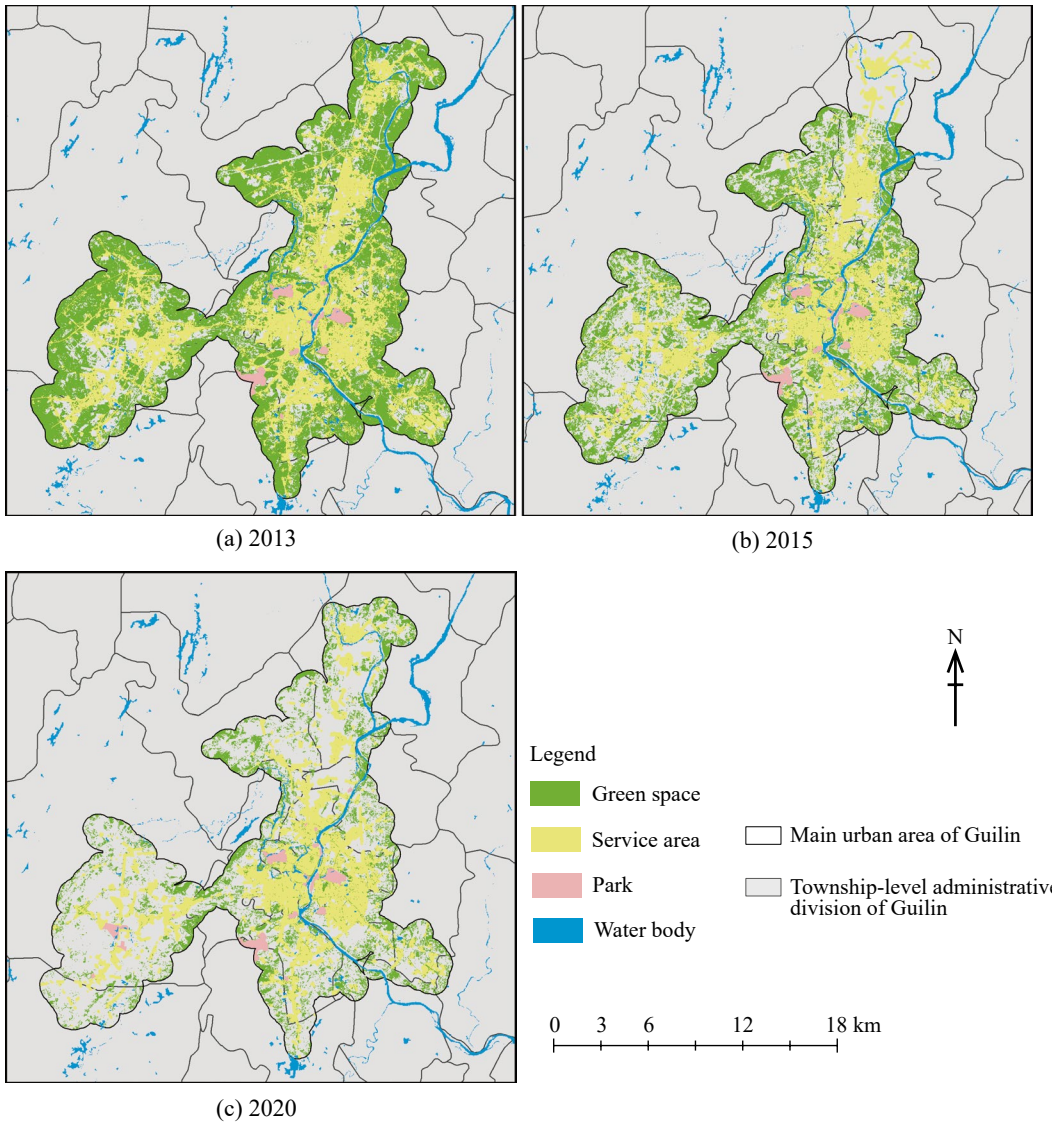

Fig. 9.31 Public open spaces and 400 m service areas from 2013 to 2020 in Guilin

- The proportion of public open spaces in the urban functional area of Guilin City decreased from 55.97% in 2013 to 39.04% in 2015 and 23.95% in 2020, and the proportion of population served by public open spaces decreased from 74.96% to 65.69% and 60.60% correspondingly.

9.3.6.5 Discussion and Outlook

This study conducted a comprehensive assessment of the sustainable development of ecological tourism in the Lijiang River Basin of Guilin and the sustainable development process of Guilin's urban development, based on multiple sources of CASEarth data, such as remote sensing, ground observation, and socio-economic statistics, targeting multiple SDG indicators. From the assessment results, it can be seen that there is great potential for the sustainable development of ecological tourism in most areas of the Lijiang River Basin, and Guilin's ecological tourism has benefited from

the implementation of environmental protection policies by the Guilin Municipal People's Government. In the past decade, the concept of ecological civilization construction has become deeply rooted, enabling a balance between economic development and ecological protection from the perspective of ecological tourism for the sustainable development of the Lijiang River Basin.

In terms of urban sustainable development, this study is based on high-resolution satellite remote sensing images and multi-source Big Earth Data such as population and transportation. The standardized methods recommended by the UN were used to monitor SDG 11.2.1, SDG 11.3.1, and SDG 11.7.1 in Guilin City. Based on the monitoring results in 2013, 2015, and 2020, the dynamic changes in the indicators were analyzed, providing data and information support for the sustainable development, planning, and construction of Guilin City.

Although the best available data were used in the calculation of SDG 11 indicators, indicator calculation for dynamic evaluation can still be improved. The quality of road network data and population data can greatly affect the evaluation results. However, due to the huge amount of road network data and irregular road attributes, it is very difficult to obtain high-quality road network data. In the future, we should develop more effective methods and tools to improve the accuracy of Big Earth Data, in order to obtain more reliable evaluation results.

9.4 Summary

This chapter focused on two themes: interactions among the SDGs and integrated regional evaluations of SDGs. It analyzed the spatial data and methods that Big Earth Data can provide in this regard and presented corresponding case studies in China and representative regions.

In terms of the interaction of multiple SDGs, spatial analysis methods such as spatiotemporal geographically weighted regression were used to explore the synergies, trade-offs, virtuous cycles, and active–passive relationships between SDG indicators. It was found that at the provincial level in China, SDG 6 and SDG 15 are more likely to be balanced against other goals, SDG 1, SDG 7, and SDG 13 are the main influencing SDGs, and SDG 11 and SDG 16 tend to be passively influenced by other SDGs. Prioritizing the development of domestic material consumption (SDG 12.2.2), water resources management (SDG 6.5), and universal primary and secondary education (SDG 4.1) is conducive to promoting the coordinated development of the SDGs more scientifically and efficiently. Through the correlation analysis of long-term time-series data of food–water–air quality in Northeast China based on Big Earth Data, it was found that the trade-offs between food production (SDG 2) and water security (SDG 6) are gradually easing. The expansion of the corn planting area (SDG 2.4) has significantly increased the number of agricultural straw burning fire points in the local area during the spring and autumn seasons, which has, to some extent, exacerbated the local air pollution (SDG 11.6). The comprehensive evaluation of the transportation industry in China over the 20-year study period showed that China has performed well on the transportation facility target (SDG 9.1). In 2019, the score for clean energy transportation, storage, and postal industries for SDG 7.2 increased by 32.9% compared to the previous year.

In terms of integrated SDG evaluation at the regional scale, the examples of Lincang City in Yunnan Province, Hainan Province, and Guilin in the Guangxi Zhuang Autonomous Region demonstrate the support provided by Big Earth Data at various spatial scales, including regional, administrative unit, and pixel levels, for comprehensive regional assessment of SDGs. It was found that from 2015 to 2020, the comprehensive sustainable development index and society, economy, resource-environment sustainable development indices of Lincang City showed an increasing trend. From 2015 to 2020, the sustainable development goal scores of various cities and counties in Hainan Province showed an upward trend. Urbanization (SDG 11) developed rapidly; most cities and counties showed an upward trend in agriculture

(SDG 2), especially the water quality (SDG 6), and the overall protection effect of underwater and land ecology (SDG 14 and SDG 15) was good. From 2010 to 2020, the sustainable development index of the ECC in most areas of the Lijiang River Basin in Guilin continued to rise. There is an imbalance between urban expansion and population growth in Guilin City, with the former expanding faster than the latter. The per capita construction land area is increasing, and the growth rate is accelerating. The population served by urban public open spaces is continuously decreasing, and the number and area of distribution make it difficult to meet the needs of citizens.

References

Aguilar-Rivera N, Michel-Cuello C, Cárdenas-González JF (2019) Green revolution and sustainable development. In: Leal Filho W (ed) Encyclopedia of sustainability in higher education. Springer, Cham, pp 833–850

Akuraju V, Pradhan P, Haase D et al (2020) Relating SDG11 indicators and urban scaling–an exploratory study. Sustain Cities Soc 52:101853

Barbier EB, Burgess JC (2017) The Sustainable Development Goals and the systems approach to sustainability. Economics 11(1):1–22

Chen A, Li Y, Ye K et al (2021) Does transport infrastructure inequality matter for economic growth? Evidence from China. Land 10(8):874

Dong J, Xiao X, Zhang G et al (2016) Northward expansion of paddy rice in Northeastern Asia during 2000–2014. Geophys Res Lett 43(8):3754–3761

Fu BJ, Wang S, Zhang JZ et al (2019) Unravelling the complexity in achieving the 17 sustainable-development goals. Natl Sci Rev 6(3):386–388

Fuso Nerini F, Sovacool B, Hughes N et al (2019) Connecting climate action with other Sustainable Development Goals. Nat Sustain 2:674–680

Griggs DJ, Nilsson M, Stevance A et al (2017) A guide to SDG interactions: from science to implementation. International Council for Science, Paris

Guo HD, Chen F, Sun ZC et al (2021) Big Earth Data: A practice of sustainability science to achieve the Sustainable Development Goals. Science Bulletin 66(11):1050–1053

Guo HD, Zhang L (2023) Remote sensing in Hainan. Science Press, Beijing, pp 352–373 (In Chinese)

Hegre H, Petrova K, von Uexkull N (2020) Synergies and trade-offs in reaching the Sustainable Development Goals. Sustainability 12(20):8729

Hu Y, Moiwo JP, Yang Y et al (2010) Agricultural water-saving and sustainable groundwater management in Shijiazhuang Irrigation District, North China Plain. J Hydrol 393(3–4):219–232

ICSU (2015) Review of the Sustainable Development Goals: the science perspective. ICSU, Paris

Kang DW, Zhao ZJ, Chen XY et al (2020) Evaluating the effects of roads on giant panda habitat at two scales in a typical nature reserve. Sci Total Environ 710:136351

Le Blanc D (2015) Towards integration at last? The sustainable development goals as a network of targets. Sustain Dev 23(3):176–187

Li YR, Zhang XC, Cao Z et al (2021) Towards the progress of ecological restoration and economic development in China's Loess Plateau and strategy for more sustainable development. Sci Total Environ 756:143676

Messerli P, Murniningtyas E, Eloundou-Enyegue P et al (2019) Global Sustainable Development Report 2019: the future is now—science for achieving sustainable development. UN, New York

Nilsson M, Chisholm E, Griggs D et al (2018) Mapping interactions between the sustainable development goals: lessons learned and ways forward. Sustain Sci 13(6):1489–1503

Pradhan P, Costa L, Rybski D et al (2017) A systematic study of Sustainable Development Goal (SDG) interactions. Earth's Future 5(11):1169–1179

Sachs J, Schmidt-Traub G, Kroll C, et al (2018). SDG index and dashboards report 2018. Retrieved from New York: Bertelsmann Stiftung and SDSN. https://www.sustainabledevelopment.report/reports/sdg-index-and-dashboards-2018/ [2018-07-09]

Sachs J, Schmidt-Traub G, Kroll C, et al (2019) Sustainable Development Report 2019. Transformations to achieve the Sustainable Development Goals. https://www.sdgindex.org/reports/sustainable-development-report-2019/ [2019-06-28]

Sachs J, Schmidt-Traub G, Kroll C, et al (2020) The Sustainable Development Goals and COVID-19. Sustainable Development Report 2020. Cambridge University Press, Cambridge

Sachs J, Kroll C, Lafortune G, et al (2021) The decade of action for the Sustainable Development Goals. Sustainable Development Report 2021. Cambridge University Press, Cambridge

Sachs J, Lafortune G, Kroll C, et al (2022) From crisis to Sustainable Development: The SDGs as roadmap to 2030 and beyond. Sustainable Development Report 2022. Cambridge University Press, Cambridge. https://s3.amazonaws.com/sustainabledevelopment.report/2022/2022-sustainable-development-report.pdf [2022-06-02]

Sapsirisavat V, Mahikul W (2021) Drinking and nighttime driving may increase the risk of severe health outcomes: A 5-year retrospective study of traffic injuries among international travelers at a university

hospital emergency center in Thailand. Int J Environ Res Public Health 18(18):9823
Sebestyén V, Bulla M, Rédey Á et al (2019) Network model-based analysis of the goals, targets and indicators of sustainable development for strategic environmental assessment. J Environ Manage 238:126–135
Stafford-Smith M, Griggs D, Gaffney O et al (2017) Integration: the key to implementing the Sustainable Development Goals. Sustain Sci 12(6):911–919
Swain RB, Ranganathan S (2021) Modeling interlinkages between sustainable development goals using network analysis. World Dev 138:105136
UN (2020) Sustainable Development Goals progress chart 2020. https://unstats.un.org/sdgs/report/2020/progress-chart-2020.pdf [2023-06-30]
UN-Water (2016) Water and sanitation interlinkages across the 2030 agenda for sustainable development. https://www.unwater.org/sites/default/files/app/uploads/2016/08/Water-and-Sanitation-Interlinkages.pdf [2016-12-31]
UN-Water (2021). Summary progress update 2021 SDG 6 water and sanitation for all. Version: 1 March 2021. Switzerland, Geneva
Warchold A, Pradhan P, Kropp JP (2021) Variations in sustainable development goal interactions: population, regional, and income disaggregation. Sustain Dev 29(2):285–299
Warchold A, Pradhan P, Thapa P et al (2022) Building a unified sustainable development goal database: Why does sustainable development goal data selection matter? Sustain Dev 30(5):1278–1293
Wenz L, Weddige U, Jakob M et al (2020) Road to glory or highway to hell? Global road access and climate change mitigation. Environ Res Lett 15(7):075010
Xu J, Bai J, Chen J (2019) An improved indicator system for evaluating the progress of Sustainable Development Goals (SDGs) Sub-Target 9.1 in county level. Sustainability, 11(17):4783.
Ye HC (2022) A dataset of multiple cropping index with 10 m spatial resolution in Hainan Island from 2016 to 2020. Int Res Cent. Big Data Sustain Dev Goals. Beijing.https://doi.org/10.12237/casearth.6396cf6c819aec7aa363a687
You NS, Dong JW, Huang JX et al (2021) The 10-m crop type maps in Northeast China during 2017–2019. Scientific Data 8(1):41
Zhang L, Chen B (2022) A dataset of aquaculture ponds with the 30 m spatial resolution in Hainan Island during 1990–2020. Int Res Cent Big Data Sustain Dev Goals. Beijing.https://doi.org/10.12237/casearth.6396cf6c819aec7aa363a691

Summary and Prospects

10

10.1 Summary

This report presents case studies of Big Earth Data supporting the evaluation of SDG indicators for seven SDGs (Zero Hunger, Clean Water and Sanitation, Affordable and Clean Energy, Sustainable Cities and Communities, Climate Action, Life Below Water, and Life on Land) and the interactions among the SDGs. Most of the case studies in this book focus on the national and regional scale in China in concert with the "building a beautiful China" initiative. Experts, scholars, and decision-makers can reference the data products, methods, models, and decision support guidelines provided in this book.

The report presents 30 data products developed for China and its subregions. The datasets have narrowed the data gaps in SDG monitoring; for example, the current status and risk of black soil degradation, the spatial distribution of soil organic carbon density in agricultural fields, changes in groundwater quality, the degree of water stress, and the distribution and risk of important invasive agricultural pests. Other products improve the spatial precision of SDG indicator monitoring and evaluation, such as China's 1 km resolution dataset of WUE for the three major cereal crops, China's 0.5° grid groundwater storage change, China's 10 m resolution spatial distribution of coastal mudflats, and other datasets.

Furthermore, 22 methods and models were developed based on Big Earth Data. Some have closed gaps in terms of how to monitor SDG progress. For example, the evaluation method for WUE is based on multi-source data and crop growth processes, and the cooperative forward modeling method combines gravity satellites and groundwater level data. Some methods and models provide optimized solutions for SDG assessments, such as a monitoring method for the soil salinization level using integrated classification algorithms and machine learning models and a sustainability index for water resources development and protection. In addition, in terms of the cross-cutting and integrated aspects of multiple SDG indicators, the synergistic and trade-off relationships between SDG indicators have been explored using the spatiotemporal geographically weighted regression method. Sustainable development assessment indicator systems for different regions have been constructed, and comprehensive regional assessments of SDGs have been carried out.

The report also presents decision support guidelines and recommendations. Spatiotemporal analyses of sustainable development indicators using the above data and methods led to 32 decision support recommendations for sustainable development for China and globally. Regarding SDG 2, decision support has been provided for the improvement and application of saline-alkali land, sustainable agricultural production,

H. Guo, *Big Earth Data in Support of the Sustainable Development Goals (2022) - China*,
Sustainable Development Goals Series, https://doi.org/10.1007/978-981-97-4231-8_10

agricultural carbon emission reduction policies, and food waste reduction. Regarding SDG 6, decision support has been provided for the evaluation of the effectiveness of the construction and management of drinking water sources, evaluation of surface water and groundwater quality control, policymaking for industrial structure adjustment under the constraints of climate change impacts and water resources, and the evaluation of comprehensive water resources management. Regarding SDG 7, decision support has been provided for China's industrial structure adjustment, and for SDG 11, the report gives suggestions for improving urban land use efficiency, reducing urban disasters, and enhancing urban green space. Decision support for SDG 13 involves reducing losses caused by flooding and constructing disaster reduction systems, while SDG 14 guidelines suggest reducing marine pollution, protecting marine ecosystems, reducing acidification, and protecting marine regions. Regarding SDG 15, decision support has been provided for evaluating the benefits of ecological engineering, the accurate monitoring of biodiversity, the early warning of black soil degradation in Northeast China, and dealing with invasive alien species. Additionally, through the interaction and integrated evaluation of multiple SDG indicators, decision references have been provided for scientifically establishing priority development goals for different regions in China based on their individual characteristics, alleviating the trade-off problems of SDG indicators in development, and optimizing sustainable development paths.

10.2 Prospects

Over the past four years, the Chinese Academy of Sciences has conducted exploratory research in monitoring and evaluating SDG indicators and pinpointed that Big Earth Data had high application potential and promotion value in supporting many SDGs (Guo 2020, 2021, 2022) although many challenges were faced, such as a shortage of spatiotemporal data important for evaluating SDGs, unharmonized data sharing standards, and ineffective data security. Therefore, to facilitate the implementation of the UN 2030 Agenda, we recommend redoubling efforts in the following areas.

10.2.1 Building a Global Collaborative Observation Network for the SDGs

There are more and more satellites launching into space, resulting in the rapid growth of satellite industries and their applications. On November 5, 2021, China successfully launched SDGSAT-1, the world's first sustainable development science satellite, and then committed to sharing its data with the world. Responding to the "leave no one behind" tenet of the 2030 Agenda, we propose to speed up the construction of a collaborative Earth observation network for the SDGs to improve the service capacity of space-based observations, develop a standardized international space-based observation system, and provide joint data support to address unbalanced development and reduce the digital divide.

10.2.2 Improving the Spatiotemporal Dimensions of SDG Progress Assessment

Statistical surveys are among the primary methods of obtaining global SDG monitoring and evaluation data. However, due to the differences in policy and ability in the development of statistical survey systems across the world, survey data often suffer unevenness of quality, insufficient spatiotemporal scales, and a lack of data availability in some developing countries. We therefore propose to make full use of Big Earth Data and other technologies in terms of increasing data acquisition methods and obtaining high-quality and spatiotemporally consistent global SDG data through open access to data

computing and storage facilities and the adoption of advanced data processing methods, with the goal of timely and more accurate SDG progress assessments.

10.2.3 Sharing Public Data Products for SDG Monitoring

Due to the lack of consensus on data sharing policies, and no unified technical standards in terms of data structure and security, many users have no access to the data owned by other institutions or to the data generated by specific statistical agencies excluded from other users. We propose to improve and create new information infrastructure that combines data applications and open services; provide real-time data access, on-demand pooling, integration, open sharing, and analysis services; and provide public data services and products to support the monitoring and evaluation of the SDGs.

10.2.4 Promoting Exemplary Studies on Big Data Supporting the SDGs

Due to the differences in natural resources and socio-economic development, various regions face individual difficulties in their efforts toward sustainable development. Big Earth Data, featuring multiple spatiotemporal scales, can provide important support for implementing and evaluating SDGs in different regions. We propose to promote exemplary studies on Big Earth Data supporting the SDGs, strive to build a sustainable development indicator system with different spatial scales, and develop innovative and comprehensive demonstration systems with regional features to inform the realization of the SDGs around the world.

References

Guo HD (2020) Big earth data in support of the sustainable development goals (2019). Science Press and EDP Sciences, Beijing

Guo HD (2021) Big earth data in support of the sustainable development goals (2020): China. Science Press and EDP Sciences, Beijing

Guo HD (2022) Big earth data in support of the sustainable development goals (2021): China. Science Press and EDP Sciences, Beijing

Index

H. Guo, *Big Earth Data in Support of the Sustainable Development Goals (2022) - China,*
Sustainable Development Goals Series, https://doi.org/10.1007/978-981-97-4231-8